University of California
Santa Barbara

Heat Flows and Entanglement Entropy: Insights From and Into AdS/CFT

A dissertation submitted in partial satisfaction
of the requirements for the degree

Doctor of Philosophy
in
Physics

by

Sebastian Fischetti

Committee in charge:

Professor Donald Marolf, Chair
Professor Gary Horowitz
Professor Benjamin Monreal

September 2015

The Dissertation of Sebastian Fischetti is approved.

Professor Gary Horowitz

Professor Benjamin Monreal

Professor Donald Marolf, Committee Chair

July 2015

Heat Flows and Entanglement Entropy: Insights From and Into AdS/CFT

by

Sebastian Fischetti

Acknowledgements

This dissertation could not have been completed without the assistance and support of many people. My thanks and appreciation go out to:

My advisor, Don Marolf, for his mentoring, support, and encouragement. His creativity, insight, and intuition for physics are remarkable, and I hope in my time as his student I have been able to absorb at least some fraction of them.

My undergraduate advisor Laura Cadonati, whose mentoring, training, and support were crucial ingredients to my success in grad school.

All my other collaborators over my time in graduate school: Tomás Andrade, Netta Engelhardt (thanks to whom I will never cease to laugh at narwhals), William Kelly, David Kastor, Simon Ross, Moshe Rozali, Jorge Santos (whom I will never be able to fully thank for the hours of numerical training he has given me), Jennie Traschen (who was also an excellent undergrad GR instructor!), and Aron Wall. I have learned a ton from working with all of you, and it's been a great experience. Here's to more just like it in the future!

All my friends at UCSB, UMass, and elsewhere, who are too numerous to list here. You've helped to make these past five years lots of fun (despite the lack of winter in Santa Barbara). A special thanks should go to Keith Fratus, with whom I attended undergrad at UMass Amherst and who played a key role in convincing me to attend UCSB. I literally would not be here if not for him.

To all my professors and instructors, from high school (Mr. Lillis, Mrs. Ganz, Mr. Richter, Mrs. Moussa) through college at UMass Amherst (John Donoghue, Lori Goldner, Nikolay Prokof'ev, Chris Santangelo, Boris Svistunov) and here at UCSB (Matthew Fisher, Steve Giddings, Gary Horowitz, Chetan Nayak, Joe

Polchinski, Mark Srednicki). Thanks for the years of knowledge and experience you've attempted to pass on to me, and for making learning so enjoyable. I hope some of it stuck.

To all my students, from physics courses to SIMS, and to those professors for whom I've TAed: thanks for making teaching fun, rather than just a chore to get through!

And finally, thanks to my family. It is thanks to their nurturing of my curiosity (I fondly recall trips to the Liberty Science Center) that I developed a passion for science, and it is thanks to their support that I have been able to feed that passion.

This dissertation was supported by the National Science Foundation under grants PHY08-55415, PHY11-25915, and PHY12-05500, by FQXi grant FRP3-1338, and by funds from the University of California. A special thanks also goes to Gary Horowitz and Benjamin Monreal for serving on my committee.

Curriculum Vitæ

Sebastian Fischetti

Education

2015	Ph.D. in Physics (Expected), University of California, Santa Barbara.
2013	M.S. in Physics, University of California, Santa Barbara.
2010	B.S in Physics, University of Massachusetts, Amherst.
2010	B.S in Astronomy, University of Massachusetts, Amherst.

Publications

1. N. Engelhardt and S. Fischetti, "Covariant Constraints on Hole-ography," arXiv:1507.00354 [hep-th].
2. S. Fischetti, D. Marolf and A. C. Wall, "A paucity of bulk entangling surfaces: AdS wormholes with de Sitter interiors," Class. Quant. Grav. **32**, no. 6, 065011 (2015) [arXiv:1409.6754 [hep-th]].
3. S. Fischetti, D. Kastor and J. Traschen, "Non-Vacuum AdS Cosmologies and the Approach to Equilibrium of Entanglement Entropy," Class. Quant. Grav. **31** 235007 (2014) [arXiv:1407.4299 [hep-th]].
4. S. Fischetti and D. Marolf, "Complex Entangling Surfaces for AdS and Lifshitz Black Holes?," Class. Quant. Grav. **31**, 214005 (2014) [arXiv:1407.2900 [hep-th]].
5. T. Andrade, S. Fischetti, D. Marolf, S. F. Ross and M. Rozali, "Entanglement and correlations near extremality: CFTs dual to Reissner-Nordström AdS_5," JHEP **1404**, 023 (2014) [arXiv:1312.2839 [hep-th]].
6. S. Fischetti and J. E. Santos, "Rotating Black Droplet," JHEP **1307**, 156 (2013) [arXiv:1304.1156 [hep-th]].
7. S. Fischetti, D. Marolf, and J. E. Santos, "AdS flowing black funnels: Stationary AdS black holes with non-Killing horizons and heat transport in the dual CFT," Class. Quant. Grav. **30** 075001, 2013 [arXiv:1212.4820 [hep-th]].
8. S. Fischetti, W. Kelly, and D. Marolf, "Conserved Charges in Asymptotically (Locally) AdS Spacetimes," Chapter 19 of "The Springer Handbook of Spacetime," edited by A. Ashtekar and V. Petkov (Springer-Verlag, 2014). [arXiv:1211.6347 [gr-qc]]

9. S. Fischetti and D. Marolf, "Flowing Funnels: Heat sources for field theories and the AdS_3 dual of CFT_2 Hawking radiation," Class. Quant. Grav. **29**, 105004 (2012) [arXiv:1202.5069 [hep-th]]

10. S. Fischetti, J. Healy, L. Cadonati, L. London, S. R. P. Mohapatra, D. Shoemaker, "Exploring the use of numerical relativity waveforms in burst analysis of precessing black hole mergers," Phys. Rev. D **83**, 044019 (2011) [arXiv:1010.5200 [gr-qc]]

11. R. Sturani, S. Fischetti, L. Cadonati, G. M. Guidi, J. Healy, D. Shoemaker and A. Vicere, "Phenomenological gravitational waveforms from spinning coalescing binaries," [arXiv:1012.5172 [gr-qc]]

12. R. Sturani, S. Fischetti, L. Cadonati, G. M. Guidi, J. Healy, D. Shoemaker, A. Vicere, "Complete Phenomenological gravitational waveforms from spinning coalescing binaries," J. Phys.: Conf. Ser. **243**, 012007 (2010) [arXiv:1005.0551 [gr-qc]]

13. L. Cadonati, S. Chatterji, S. Fischetti, G. Guidi, S. R. P. Mohapatra, R. Sturani and A. Vicere, "Un-modeled search for black hole binary systems in the NINJA project," Class. Quant. Grav. **26**, 204005 (2009) [arXiv:0906.2433 [gr-qc]]

14. B. Aylott *et al.*, "Status of NINJA: the Numerical INJection Analysis project," Class. Quant. Grav. **26**, 114008 (2009) [arXiv:0905.4227 [gr-qc]]

15. B. Aylott *et al.*, "Testing gravitational-wave searches with numerical relativity waveforms: Results from the first Numerical INJection Analysis (NINJA) project," Class. Quant. Grav. **26**, 165008 (2009) [arXiv:0901.4399 [gr-qc]]

Abstract

Heat Flows and Entanglement Entropy: Insights From and Into AdS/CFT

by

Sebastian Fischetti

This dissertation will focus on exploring the AdS/CFT correspondence, both as a tool to probe the behavior of strongly coupled conformal field theories (CFTs) and as a fundamental duality to help us understand the holographic connection between quantum gravity and gauge theories.

We will begin with an overview of this (two-part) dissertation, followed by an introduction to gravity in asymptotically locally AdS spacetimes.

In the first part of the dissertation, we will then discuss the use of AdS/CFT as a tool to probe the dynamics of heat transport in strongly coupled CFTs. We will begin with a simple case in three bulk spacetime dimensions, and then construct a four-dimensional black hole solution which is dual to heat flow in a three-dimensional CFT. This black hole solution is stationary, but its horizon is not a Killing horizon, making it an interesting gravitational solution in its own right. We will then construct the gravitational dual to a CFT on a rotating black hole, and find that the CFT does not carry heat away from the black hole, but rather is confined to a halo around it. This is an artefact of strong coupling, and we comment on possible connections to soft condensed matter phenomena.

In the second part of this dissertation, we probe the AdS/CFT dictionary via entanglement entropy. Specifically, we show that the Hubeny-Rangamani-

Takayanagi (HRT) prescription, which is a prescription for computing CFT entanglement entropy holographically, requires modification. We comment on possible modifications, and explore in depth the possibility of using complexified surfaces in the HRT prescription. Finally, we will approach the issue of bulk reconstruction via hole-ography, which attempts to reconstruct the bulk geometry from the entanglement entropy of regions of the CFT. We put some constraints on when this approach can succeed, and comment on why it might fail when it does.

Contents

Chapter 1

Introduction

General relativity (GR) is one of the most remarkably successful modern theories of physics. Shortly after its birth in 1915 [1], some of its predictions saw confirmation in the precession of the perihelion of Mercury, the deflection of starlight by the sun, and the gravitational redshift of light. Today's tests of GR range from frame dragging and geodetic precession measured by Gravity Probe B [2] to energy loss through gravitational radiation in binary systems like the Hulse-Taylor pulsar [3]. More excitingly, the Laser Interferometer Gravitational-wave Observatory (LIGO) should soon start detecting these gravitational waves directly, which will usher in a new era of astronomical observation [4].

Some modern experiments and observatories like LIGO are designed to probe GR in a strong-field regime. While this regime includes compact astrophysical objects like neutron stars, the more exciting strongly gravitating objects are much simpler (and therefore in a sense more mysterious): *black holes*, objects whose gravity is so strong that even light is not able to escape them. The "surface of

last return" is called the event horizon of the black hole, and (by definition) it can emit no light[1]. While what we recognize today as the first black hole solution of GR was derived by Schwarzschild in 1916 [5], it wasn't recognized as such until the 1960s. Moreover, the astrophysical evidence for black holes is abundant, but somewhat circumstantial: accretion disks emitting energetic X-ray jets like that of Cygnus X-1 [6] are believed to be powered by black holes; there is evidence of a very massive dark object (Sagittarius A*) at the center of our galaxy [7]; and there have been explicit observations of a dark object believed to be a black hole swallowing a red giant star [8]. This evidence has convinced the vast majority of astrophysicists that black holes do in fact exist, but even if this were not the case, direct imaging of a black hole should be provided in the coming years by the Event Horizon Telescope [9].

Black holes are fascinating for a variety of reasons. From an astrophysical standpoint, they are massive objects that play important roles in stellar life cycles and even in galactic dynamics. From a theoretical point of view (and the one that will be taken in this thesis), black holes are simple mathematical objects and thus excellent testing grounds for new physics. Their strong gravity makes GR crucial in their description, but the fact that GR breaks down at the singularity hidden behind the event horizon implies that an observer falling into a black hole must encounter some kind of quantum mechanical corrections to GR at some point. For this reason, black holes have been at the heart of attempts to reconcile general relativity and quantum mechanics into a theory of quantum gravity.

For example, consider the following four "laws of classical black hole mechan-

[1] In a purely classical regime; quantum effects will be discussed shortly.

ics" [10]:

0. The surface gravity κ of any stationary (i.e. time-independent) black hole is constant.

1. Any two vacuum black hole solutions that are infinitesimally related must satisfy
$$dM = \frac{1}{8\pi G}\,\kappa\,dA + \Omega_H\,dJ, \tag{1.1}$$
where dM, dA, and dJ are the differences between the black holes' masses, horizon areas, and angular momenta, and κ and Ω_H are their surface gravity and horizon angular velocity (and G is Newton's constant).

2. It is impossible to decrease the area of a black hole's horizon by any physical process: $\delta A \geq 0$.

3. It is impossible for a black hole's surface gravity to reach zero by any physical process.

The mass M of a black hole is equivalent to its total energy (up to a factor of c^2, which we set to one), so if the surface gravity κ and horizon area A of a black hole are interpreted as a temperature and entropy, respectively (up to constant factors), then the laws of black hole mechanics bear a remarkable similarity to the four laws of thermodynamics. Is this a mathematical coincidence, or is there something deep in this statement? Quantum mechanics says the latter: as Hawking showed in 1974 [11], if quantized fields are placed on a classical black hole spacetime, it

turns out that the black hole will emit radiation with a temperature

$$k_B T_{\text{Hawk}} = \frac{\hbar\kappa}{2\pi}, \tag{1.2}$$

where Boltzmann's constant k_B will from here on be set to one. This calculation, along with arguments by Bekenstein [12, 13], lead us to conclude that black holes really are *bona fide* thermodynamic objects with an entropy given by

$$S_{\text{BH}} = \frac{A}{4G\hbar}. \tag{1.3}$$

Conveniently, the subscript "BH" stands for either "Bekenstein-Hawking" or "black hole".

This behavior is unusual: in most conventional thermodynamic systems (say, an ideal gas), entropy scales like *volume*, not area[2]. But a concrete manifestation of this behavior and insight into its origins came in 1997 with Maldacena's suggestion of the anti-de Sitter/conformal field theory (AdS/CFT) correspondence [19, 20] (often referred to more generally as gauge/gravity duality). The AdS/CFT correspondence has seen remarkable success in the almost twenty years since Maldacena's first paper, and it will be the focus of this dissertation.

[2]This behavior led to some conjectured bounds on the maximum entropy of *any* thermodynamic system, and consequently to the so-called *holographic principle* [14–16]. But in fact, the reasoning that led to these bounds is not sound; see e.g. [17, 18].

1.1 AdS/CFT

In its original formulation, AdS/CFT is the conjecture that Type IIB string theory living on an $\mathrm{AdS}_5 \times S^5$ background is dual to $\mathcal{N} = 4$ super Yang-Mills theory in four dimensions (here AdS_5 is anti-de Sitter space, a particular negatively curved spacetime, and S^5 is the five-dimensional sphere). As we will see later, there is a sense in which the CFT can be said to live "on the boundary" of the space in which the string theory lives; hence we will sometimes refer to the string theory side of the duality as the "bulk", and the CFT side as the "boundary". In this sense, the theory is *holographic*: the CFT lives in fewer dimensions than the string theory. Note, incidentally, that the precise manner in which these two sides are "dual" is an active area of research, but it essentially means that the two apparently different physical systems really describe the same physics.

Maldacena's original conjecture [19] stems from stringy arguments (see also [21–23] for reviews). However, there are certain limits in which the duality simplifies considerably. For example, when the number of flavors (that is, the N of the $SU(N)$ gauge group) and the coupling of the super Yang-Mills are taken to be very large, the string theory side of the duality becomes weakly coupled: it reduces to classical Einstein gravity (i.e. GR) in anti-de Sitter space. Conversely, when the bulk string theory is strongly coupled (and in particular should be exhibiting quantum gravitational effects), the dual CFT is weakly coupled.

AdS/CFT is thus a weak/strong duality: when one side is strongly coupled, the other side becomes weakly coupled. This is both a feature and a bug: it makes it possible to study otherwise untractable strongly coupled systems by simply studying their weakly coupled dual instead, but it also makes it difficult to

give a proof of the conjecture. However, the abundance of evidence supporting it is for many convincing enough to take AdS/CFT for granted, and we will adopt this philosophy in this dissertation.

Because AdS/CFT relates two theories that look drastically different, it has been very successful in yielding insights into systems that would otherwise be very difficult to study directly. For instance, an obvious use of AdS/CFT is to use the boundary CFT to probe the quantum gravity regime of the bulk string theory, specifically in the contexts of cosmology [24–33] and black holes [34–40]. This is an example of the "boundary-to-bulk" direction, wherein the boundary CFT can be used to probe the bulk physics. More common, however, is the "bulk-to-boundary" direction, in which the bulk gravitational theory is used to study strongly coupled CFTs. For instance: the AdS/condensed matter theory (AdS/CMT) correspondence [41–43] has been used to draw insights about condensed matter systems (e.g. superconductors); AdS/CFT can be used to study the thermalization of strongly coupled CFTs, with applications to both quantum quenches [44–46] and even the hydrodynamics of the quark-gluon plasma produced at the Relativistic Heavy Ion Collider [47–53]; turbulence and hydrodynamics has been studied via AdS/CFT [54–56], as well as the related phenomenon of heat transport in strongly coupled CFTs; and AdS/CFT has been used to study the structure of entanglement in strongly coupled CFTs. This list is of course far from exhaustive.

The approaches listed above – the boundary-to-bulk and bulk-to-boundary directions – use AdS/CFT as a tool to probe systems that would otherwise be difficult to study. But the duality *itself* is still not completely understood, and

a complementary avenue of research is to try to understand precisely how the mapping between the two sides works.

This dissertation is divided into two parts. Part I focuses on a bulk-to-boundary direction: we will use AdS/CFT to study Hawking radiation and heat flow in strongly coupled CFTs. A brief overview will be provided in Section 1.2 below. Part II will instead focus on understanding the AdS/CFT duality from the point of view of entanglement, specifically entanglement entropy and reconstructing the bulk geometry from CFT data. We will provide an overview of this part in Section 1.3 below.

Note that in this dissertation we will work exclusively in the limit where the AdS side of the duality is well approximated by classical Einstein gravity, and we will most often be working on the gravity side. In such cases, it is common to consider not just AdS spacetimes, but so-called asymptotically locally AdS spacetimes, which according to AdS/CFT should be dual to some kind of large-N, strongly coupled CFT. For this reason, we give a comprehensive review of asymptotically locally AdS spacetimes in Chapter 2, and briefly conclude that chapter with an explanation of how CFT quantities are extracted from AdS calculations.

1.2 Holographic Heat Flows

Hawking's original derivation of his eponymous radiation considered free fields on a black hole spacetime. While the results are of course of fundamental importance, the field theories that describe our universe are all interacting. An interesting question is therefore how Hawking radiation is affected by the inclusion of

interactions. Unfortunately, studying interacting field theories is notoriously difficult, except in a perturbative regime around weak coupling. As discussed above, however, it is precisely for this reason that AdS/CFT shines: we can use it to study Hawking radiation in strongly-coupled CFTs by performing calculations in Einstein gravity. This will be the goal of Part I of this thesis.

This picture has a nice interpretation in terms of thermodynamics: recall that black holes are thermodynamic objects with corresponding entropies and temperatures. In dynamical gravity, they will lose energy via Hawking radiation and eventually evaporate away. However, in AdS/CFT the boundary spacetime (that is, the spacetime on which the CFT lives) can be imposed at will, and in particular need not satisfy Einstein's equations. This implies that AdS/CFT allows us to consider strongly coupled CFTs on *fixed* black hole backgrounds. Since the black holes may then emit radiation but never evaporate, they can be thought of as objects of finite (Hawking) temperature, but *infinite* entropy. This means that they act as perfect heat sources or heat sinks for heat flow in the CFT. Thus the problem of studying Hawking radiation in the CFT amounts to one of studying properties of heat flow between perfect heat sources and heat sinks, which we will model as black holes or heat baths.

The question of understanding this heat flow from a holographic perspective therefore amounts to finding asymptotically locally AdS spacetimes whose boundaries contain black holes. But note that a given boundary geometry (i.e. putting the CFT on a given black hole spacetime) may admit multiple bulk geometries. These different allowed geometries correspond to different *phases* of the CFT.

As will be reviewed in Chapters 3 and 4, there are roughly two allowed phases

called *black droplets* and *black funnels* [57–62], which are characterized by the geometry of the black hole horizons in the bulk AdS space. From the CFT side, black droplets correspond to a phase in which the CFT is "stuck" around the black hole and unable to radiate; this phase is an artefact of the CFT's strong coupling. The black funnel, on the other hand, corresponds to a CFT phase in which the black hole is radiating, much like in conventional Hawking radiation in free field theories.

Chapter 3 will begin to develop some of these ideas by studying the analytically tractable setup of AdS_3, which admits only black funnel solutions. Chapter 4 will then numerically construct a so-called *flowing black funnel*, which corresponds to a bulk solution whose horizon exhibits a steady-state "flow" of heat (in technical terms, the bulk horizon is stationary but non-Killing). From this solution, we will extract the thermal conductivity of the CFT, and geometric properties of the bulk solution. Finally, in Chapter 5 we will numerically construct a black droplet which is dual to a CFT living on a rotating black hole background.

Before moving on, we should pause to note that the flow of heat behaves much like the flow of a fluid. It so happens that a specific version of gauge/gravity duality, called the fluid/gravity correspondence [63–65], makes this notion precise: it states that Einstein's equations in a certain AdS black hole background can be rewritten as the relativistic Navier-Stokes equations for a conformal fluid. Thus in the limit in which the CFT is well-described by hydrodynamics, the behavior of CFT solutions dual to black droplets and black funnels can be described with the fluid/gravity correspondence. This notion will be briefly developed in Chapter 4, and will be used in future work [66] to study instabilities of flowing black funnels.

1.3 Holographic Entanglement

In Part I of this dissertation, AdS/CFT is used purely as a tool to probe the behavior of the CFT. In Part II, we will instead try to probe the duality itself.

What does this mean? The two sides of the duality look drastically different: one is a theory of (quantum) gravity, the other is a gauge theory. Understanding the duality requires understanding how objects on one side map to the other. The collection of these maps is the "AdS/CFT dictionary", and if AdS/CFT is to give us new insights into either side of the duality, understanding this dictionary is crucial.

In the years since the correspondence was first proposed, the dictionary has grown quite substantially. An early entry, for instance, was the requirement that the Hilbert spaces of the bulk AdS space and boundary CFT be the same (it is in this sense that we mean the two sides "describe the same physics"). One can then match the partition functions of the two sides:

$$Z_{\mathrm{CFT}} = Z_{\mathrm{AdS}}, \tag{1.4}$$

where the boundary conditions on the bulk fields are given by appropriate expectation values and currents in the CFT [21]. This matching allows us to identify thermodynamics quantities on the two sides: for example, a black hole with entropy S and energy M in AdS is dual to a CFT state with the same entropy and energy.

Some of the simplest entries in the dictionary are those that relate *geometric objects* in the bulk to CFT observables. For instance, CFT two-point correlators

are dual to boundary-anchored geodesics in the AdS bulk [67]; CFT Wilson loops are dual to bulk string worldsheets [68]; and the entanglement entropy of a region in the CFT is dual to a bulk extremal-area surface [69, 70]. Besides their simplicity, much of the appeal of these geometric duals is the hope that they may be used to reconstruct the entire bulk geometry (or at least some portion thereof).

We should pause to elaborate on the latter of these. Recall that given a state ρ on some Hilbert space $\mathcal{H}$ which can be factorized as $\mathcal{H} = \mathcal{H}_A \otimes \mathcal{H}_B$, we can trace out the degrees of freedom in B to obtain a reduced density matrix on $\mathcal{H}_A$:

$$\rho_A = \mathrm{Tr}_B \rho. \tag{1.5}$$

We can then compute the usual von Neumann entropy of ρ_A:

$$S_A = \mathrm{Tr}_A \left(\rho_A \ln \rho_A\right). \tag{1.6}$$

This quantity is the entanglement entropy of A; in the case that ρ is a pure state, S_A characterizes the amount of entanglement between the degrees of freedom contained in $\mathcal{H}_A$ and those in $\mathcal{H}_B$. In a field theoretic context, we typically take $\mathcal{H}_A$ to be the Hilbert space associated to some spatial region A of the field theory (that is, $\mathcal{H}_A$ contains those degrees of freedom localized within the region A).

In the holographic context, Ryu and Takayanagi (RT) [69] conjectured that the entanglement entropy of some region of a static holographic CFT is given by the area of a minimal-area bulk surface anchored to the boundary of the bulk spacetime; this conjecture was proven (modulo some details) in [71], and extended to dynamical contexts by Hubeny, Rangamani, and Takayanagi (HRT) [70].

The details of these conjectures, particularly HRT, will be the focus of Part II of this dissertation. In Chapter 6 we will begin with a study of the role of entanglement in a particular class of bulk geometries. In that context, we will use both two-point correlators and entanglement entropy as probes. In Chapter 7 we will construct bulk geometries in which the HRT formula as stated is ill-defined, implying that it will require some modification. We explore one possible modification in Chapter 8, where we explore whether or not one may include *complex* surfaces in the calculation. Chapter 9 will culminate with a discussion on limitations to reconstructing the bulk geometry from entanglement entropy. Finally, Chapter 10 is a slight detour in which we use entanglement entropy to study the equilibration of a CFT in an expanding cosmology.

1.4 Permissions and Attributions

1. The content of Chapter 2 is the result of a collaboration with William Kelly and Donald Marolf, and has been published as Chapter 19 of the "Springer Handbook of Spacetime" [72]. It is reproduced here with the permission of Springer Publishing.

2. The content of Chapter 3 and part of Appendix A is the result of a collaboration with Donald Marolf, and has previously appeared in the journal Classical and Quantum Gravity [73]. It is reproduced here with the permission of the Institute of Physics (IOP): `http://authors.iop.org/atom/help.nsf/LookupJournalSpecific/WebPermissionsFAQ~**`.

3. The content of Chapter 4 and part of Appendix A is the result of a collabora-

tion with Donald Marolf and Jorge E. Santos, and has previously appeared in the journal Classical and Quantum Gravity [74]. It is reproduced here with the permission of the Institute of Physics (IOP): `http://authors.iop.org/atom/help.nsf/LookupJournalSpecific/WebPermissionsFAQ~**`.

4. The content of Chapter 5 and part of Appendix A is the result of a collaboration with Jorge E. Santos, and has previously appeared in the Journal of High Energy Physics [75]. It is reproduced here with the permission of the International School of Advanced Studies (SISSA): `http://jhep.sissa.it/jhep/help/JHEP/CR_OA.pdf`.

5. The content of Chapter 6 and part of Appendix B is the result of a collaboration with Tomás Andrade, Donalf Marolf, Simon F. Ross, and Moshe Rozali, and has previously appeared in the Journal of High Energy Physics [76]. It is reproduced here with the permission of the International School of Advanced Studies (SISSA): `http://jhep.sissa.it/jhep/help/JHEP/CR_OA.pdf`.

6. The content of Chapter 7 and part of Appendix B is the result of a collaboration with Donald Marolf and Aron C. Wall, and has previously appeared in the journal Classical and Quantum Gravity [77]. It is reproduced here with the permission of the Institute of Physics (IOP): `http://authors.iop.org/atom/help.nsf/LookupJournalSpecific/WebPermissionsFAQ~**`.

7. The content of Chapter 8 and part of Appendix B is the result of a collaboration with Donald Marolf, and has previously appeared in the journal Classical and Quantum Gravity [78]. It is reproduced here with the permission of the Institute of Physics (IOP): `http://authors.iop.org/atom/`

help.nsf/LookupJournalSpecific/WebPermissionsFAQ~**.

8. The content of Chapter 9 and part of Appendix B is the result of a collaboration with Netta Engelhardt [79].

9. The content of Chapter 10 is the result of a collaboration with David Kastor and Jennie Traschen, and has previously appeared in the journal Classical and Quantum Gravity [80]. It is reproduced here with the permission of the Institute of Physics (IOP): http://authors.iop.org/atom/help.nsf/LookupJournalSpecific/WebPermissionsFAQ~**.

Chapter 2

A Review of Asymptotically (Locally) AdS Spacetimes

2.1 Introduction

When a physical system is complicated and non-linear, global symmetries and the associated conserved quantities provide some of the most powerful analytic tools to understand its behavior. This is as true in theories with a dynamical spacetime metric as for systems defined on a fixed spacetime background. Chapter 17 of [72] discusses the so-called Arnowitt-Deser-Misner (ADM) conserved quantities for asymptotically flat dynamical spacetimes, exploring in detail certain subtleties related to diffeomorphism invariance. In particular, it shows that the correct notion of global symmetry is given by the so-called asymptotic symmetries; equivalence classes of diffeomorphisms with the same asymptotic behavior at infinity. It also notes that the notion of asymptotic symmetry depends critically

on the choice of boundary conditions. Indeed, it is the imposition of boundary conditions that cause the true gauge symmetries to be only a subset of the full diffeomorphism group and thus allow the existence of non-trivial asymptotic symmetries at all.

This chapter will explore the asymptotic symmetries and corresponding conserved charges of asymptotically anti-de Sitter (AdS) spacetimes (and of the more general asymptotically locally AdS spacetimes). There are three excellent reasons for doing so. The first is simply to gain further insight into asymptotic charges in gravity by investigating a new example. Since empty AdS space is a maximally symmetric solution, asymptotically AdS spacetimes are a natural and simple choice. The second is that the structure one finds in the AdS context is actually much richer than that in asymptotically flat space. At the physical level, this point is deeply connected to the fact (see e.g. [81]) that all multipole moments of a given field in AdS space decay at the same rate at infinity. So while in asymptotically flat space the far field is dominated mostly by monopole terms (with only sub-leading corrections from dipoles and higher multipoles) all terms contribute equally in AdS. It is therefore useful to describe not just global charges (e.g., the total energy) but also the local densities of these charges along the AdS boundary. In fact, it is natural to discuss an entire so-called *boundary stress tensor* $T^{ij}_{\rm bndy}$ rather than just the conserved charges it defines. For this reason, we take a somewhat different path to the construction of conserved AdS charges than is followed in Chapter 17 of [72]. In particular, we will use covariant as opposed to Hamiltonian methods below, though we will show in section 2.4 that the end results for conserved charges are equivalent.

The third reason to study conserved charges in AdS is their fundamental relation to the anti-de Sitter/Conformal Field Theory (AdS/CFT) correspondence [19, 20, 82], which may well be the most common application of general relativity in 21st century physics. While this is not the place for a detailed treatment of either string theory or AdS/CFT, no Handbook of Spacetime would be complete without presenting at least a brief overview of the correspondence. It turns out that this is easy to do once we have become familiar with $T^{ij}_{\rm bndy}$ and its cousins associated with other (non-metric) fields. So at the end of this chapter (section 2.5) we take the opportunity to do so. We will introduce AdS/CFT from the gravity side without using tools from either string theory or conformal field theory.

We will focus on such modern applications below, along with open questions. We make no effort to be either comprehensive or historical. Nevertheless, the reader should be aware that conserved charges for asymptotically AdS spacetimes were first constructed in [83], where the associated energy was also argued to be positive definite.

The plan for this chapter is as follows. After defining and discussing AdS asymptotics in section 2.2, we construct variational principles for asymptotically AdS spacetimes in section 2.3. This allows us to introduce the boundary stress tensor $T^{ij}_{\rm bndy}$ and a similar so-called response function $\Phi_{\rm bndy}$ for a bulk scalar field. The conserved charges $Q[\xi]$ constructed from $T^{ij}_{\rm bndy}$ are discussed in section 2.3.4 and we comment briefly on positivity of the energy in section 2.3.5.

Section 2.4 then provides a general proof that the $Q[\xi]$ do indeed generate canonical transformations corresponding to the desired asymptotic symmetries. As a result, they agree (up to a possible choice of zero-point) with corresponding

ADM-like charges $H[\xi]$ that would be constructed via the AdS-analogues of the Hamiltonian techniques used in Chapter 17 of [72]. The interested reader can find such a Hamiltonian treatment in [84–86]. Below, we generally consider AdS gravity coupled to a simple scalar matter field. More complete treatments allowing more general matter fields can be found in e.g. [87–89]. Section 2.5 then defines the algebra $\mathcal{A}_{\rm bndy}$ of boundary observables and provides the above-mentioned brief introduction to AdS/CFT.

2.2 Asymptotically Locally AdS Spacetimes

This section discusses the notion of asymptotically locally AdS spacetimes. We begin by introducing empty Anti-de Sitter space itself in section 2.2.1 as a maximally-symmetric solution to the Einstein equations. We then explore the asymptotic structure of AdS, and in particular its conformal boundary. This structure is used to define the notions of asymptotically AdS (AAdS) and asymptotically locally AdS (AlAdS) spacetimes in section 2.2.3. Section 2.2.4 then discusses the associated Fefferman-Graham expansion which provides an even more detailed description of the asymptotics and which will play a critical role in constructing variational principles, the boundary stress tensor, and so forth in the rest of this chapter. Finally, section 2.2.5 describes how the above structures transform under diffeomorphisms and introduces the notion of an asymptotic Killing vector field.

2.2.1 Anti-de Sitter Space

Let us begin with a simple geometric description of $(d+1)$-dimensional anti-de Sitter space (AdS_{d+1}) building on the reader's natural intuition for flat geometries. We will, however, need to begin with a flat spacetime $\mathbb{M}^{2,d}$ of signature $(2, d)$ having two time-directions and d spatial directions, so that in natural coordinates $T^1, T^2, X^1, \ldots, X^d$ the line element takes the form

$$ds^2 = -(dT^1)^2 - (dT^2)^2 + (dX^1)^2 + \cdots + (dX^d)^2. \tag{2.1}$$

Consider the $(d+1)$-dimensional hyperboloid $\mathcal{H}$ of events in $\mathbb{M}^{2,d}$ satisfying

$$(T^1)^2 + (T^2)^2 - \sum_{i=1}^{d} \left(X^i\right)^2 = \ell^2, \tag{2.2}$$

and thus which lie at a proper distance ℓ from the origin; see figure 2.1. This hyperboloid is sometimes known as the $d+1$ anti-de Sitter space AdS_{d+1}, though we will follow a more modern tradition and save this name for a closely related (but much improved!) spacetime that we have yet to introduce.

The isometries of $\mathcal{H}$ are given by symmetries of $\mathbb{M}^{2,d}$ preserved by (2.2). Such isometries form the group $SO(d, 2)$, generated by the rotation in the T^1, T^2 plane together with two copies of the Lorentz group $SO(d, 1)$ that act separately on $T^1, X^1, \ldots, X^d$ and $T^2, X^1, \ldots X^d$. This gives $(d+1)(d+2)/2$ independent symmetries so that $\mathcal{H}$ is maximally symmetric.

A simple way to parametrize the hyperboloid is to write $T^1 = \sqrt{\ell^2 + R^2}\, \cos(\tau/\ell)$ and $T^2 = \sqrt{\ell^2 + R^2}\, \sin(\tau/\ell)$, with $R^2 = \sum (X^i)^2$ so that the induced line element

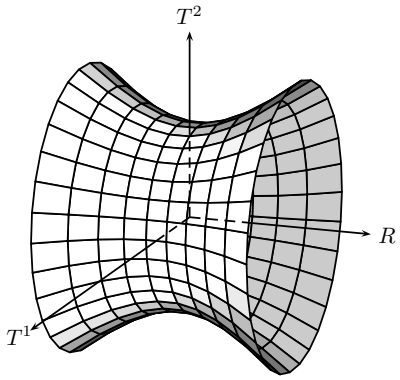

Figure 2.1: The hyperboloid (2.2) embedded in $\mathbb{M}^{2,d}$, defining anti-de Sitter space.

on $\mathcal{H}$ becomes

$$ds^2_{\mathrm{AdS}_{d+1}} = -\left(R^2/\ell^2 + 1\right)\, d\tau^2 + \frac{dR^2}{R^2/\ell^2 + 1} + R^2\, d\Omega^2_{d-1}. \tag{2.3}$$

On $\mathcal{H}$, the coordinate τ is periodic with period 2π. But this makes manifest that $\mathcal{H}$ contains closed timelike curves such as, for example, the worldline $R = 0$. It is thus useful to unwrap this time direction by passing to the universal covering space of $\mathcal{H}$ or, more concretely, by removing the periodic identification of τ (so that τ now lives on $\mathbb{R}$ instead of S^1). We will refer to this covering space as the anti-de Sitter space AdS_{d+1} with scale ℓ. Of course, the line element remains that of (2.3). Since any Killing field of $\mathcal{H}$ lifts readily to the covering space, AdS_{d+1} remains maximally symmetric with isometry group given by (a covering group of) $SO(d, 2)$.

The coordinates used in (2.3) are called global coordinates, since they cover all of AdS. We can introduce another useful set of coordinates, called Poincaré coordinates, by setting $z = \ell^2/\left(T^1 + X^d\right)$, $t = \ell T^2/\left(T^1 + X^d\right)$, and $x^i = \ell X^i/\left(T^1 + X^d\right)$

for $i = 1, \ldots, d-1$. The metric then becomes

$$ds^2_{\mathrm{AdS}_{d+1}} = \frac{\ell^2}{z^2}\left(-dt^2 + \sum_{i=1}^{d-1}\left(dx^i\right)^2 + dz^2\right). \tag{2.4}$$

Poincaré coordinates take their name from the fact that they make manifest a (lower dimensional) Poincaré symmetry associated with the d coordinates t, x^i. As is clear from their definitions, these coordinates cover only the region of AdS where $T^1 + X^d > 0$. This region is called the the Poincaré patch. While we will not make significant use of (2.4) below, we mention these coordinates here since they arise naturally in many discussions of AdS/CFT which the reader may encounter in the future.

Since AdS is maximally symmetric, its Riemann tensor can be written as an appropriately symmetrized combination of metric tensors:

$$R_{\mu\nu\sigma\lambda} = \frac{1}{d(d+1)} R \left(g_{\mu\sigma}g_{\nu\lambda} - g_{\mu\lambda}g_{\nu\sigma}\right). \tag{2.5}$$

A computation shows that the scalar curvature of AdS is $R = -d(d+1)/\ell^2$, and thus that AdS solves the vacuum Einstein field equations with cosmological constant $\Lambda = -d(d-1)/2\ell^2$:

$$R_{\mu\nu} - \frac{1}{2} R g_{\mu\nu} + \Lambda g_{\mu\nu} = 0. \tag{2.6}$$

In this sense, AdS is a generalization of flat space to $\Lambda < 0$.

2.2.2 Conformal Structure and Asymptotic Symmetries of AdS

We now turn to the asymptotic structure of AdS, which was seen in Chapter 17 of [72] to be a crucial ingredient in the construction of conserved charges. It is useful to introduce a new radial coordinate $r_* = \arctan(R/\ell)$, so that the line element becomes

$$ds^2_{\mathrm{AdS}_{d+1}} = \frac{\ell^2}{\cos^2(r_*)}\left[-d\tau^2/\ell^2 + dr_*^2 + \sin^2(r_*)\, d\Omega^2_{d-1}\right]. \tag{2.7}$$

We can immediately identify $r_* = \pi/2$ as a conformal boundary, leading to the conformal diagrams shown in Figure 2.2.2. (For readers not familiar with such diagrams, Chapter 28 will give a brief introduction.)

It is evident from the conformal diagram that AdS is not globally hyperbolic. In order to evolve initial data on some spacelike surface Σ arbitrarily far forward (or backward) in time, one needs to supply additional information in the form of boundary conditions at the conformal boundary. Such boundary conditions will be discussed in detail in section 2.3, where they will play critical roles in our discussion of conserved charged.

Although the line element (2.7) diverges at $r_* = \pi/2$, the rescaled metric

$$\hat{g} = \frac{\cos^2(r_*)}{\ell^2}\, g_{\mathrm{AdS}_{d+1}} \tag{2.8}$$

defines a smooth manifold with boundary. In particular, the metric induced by $\hat{g}$ at $r_* = \pi/2$ is just that of the flat cylinder $\mathbb{R} \times S^{d-1}$, also known as the Einstein

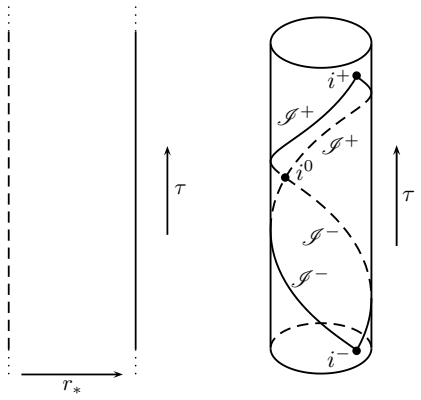

Figure 2.2: Conformal diagrams of AdS_{d+1}, showing both the global spacetime and the region covered by the Poincaré patch. In both figures, the τ direction extends infinitely to the future and to the past. In (a), a full S^{d-1} of symmetry has been suppressed, leaving only the τ, r_* coordinates of (2.7). The dotted line corresponds to $r_* = 0$. In (b), one of the angular directions has been shown explicitly to guide the reader's intuition; the axis of the cylinder corresponds to the dotted line in (a). The Poincaré patch covers a wedge-shaped region of the interior of the cylinder which meets the boundary at the lines marked $\mathscr{I}^{\pm}$ and the points marked $i^{\pm}, i^0$. These loci form the null, timelike, and spacelike infinities of the associated region (conformal to Minkowski space) on the AdS boundary.

static universe (ESU). The manifold with boundary will be called M and the boundary itself (at $r_* = \pi/2$) will be called ∂M. Of course, we could equally well have considered the more general rescaled metric

$$\hat{g}' = \frac{\cos^2(r_*)}{\ell^2}\, e^{2\sigma}\, g_{\mathrm{AdS}_{d+1}}, \tag{2.9}$$

where σ is an arbitrary smooth function on M. This metric is also nonsingular at $r_* = \pi/2$, but the induced geometry on ∂M is now only conformal to $\mathbb{R} \times S^{d-1}$. The choice of a particular rescaled metric (2.9) (or, equivalently, of a particular rescaling factor $\frac{\cos^2(r_*)}{\ell^2}\, e^{2\sigma}$) determines a representative of the corresponding conformal class of boundary metrics. This choice (which still allows great freedom to choose σ away from ∂M) is known as the choice of conformal frame. We shall often call this representative "the boundary metric," where it is understood that the above choices must be made for this term to be well-defined.

Although it is not critical for our discussion below, the reader should be aware of the asymptotic structure of the Poincaré patch and how it relates to that of global AdS as discussed above. From (2.4) we see that the conformal boundary lies at $z = 0$. The rescaled metric

$$\hat{g} = \frac{z^2}{\ell^2}\, g_{\mathrm{AdS}_{d+1}} \tag{2.10}$$

is regular at $z = 0$, where the induced metric is just d-dimensional Minkowski space. Now, it is well known [90] that Minkowski space $\mathbb{M}^{1,d-1}$ is conformally equivalent to a patch of the Einstein static universe $\mathbb{R} \times S^{d-1}$. We conclude that $z = 0$ of the Poincaré patch is a diamond-shaped piece of ∂M, as shown at right

in Figure 2.2.2.

In the interior of AdS the Poincaré patch covers a wedge-shaped region. This can be thought of as follows: future-directed null geodesics fired from i^- in Figure 2.2.2 are focused onto i^0; these geodesics are generators of a null hypersurface which we shall call the past Poincaré horizon $\mathcal{H}^-_{\text{Poincaré}}$. Likewise, future-directed null geodesics fired from i^0 are focused onto i^+, generating the future Poincaré horizon $\mathcal{H}^+_{\text{Poincaré}}$. The Poincaré patch of AdS is the wedge enclosed by these horizons.

2.2.3 A definition of Asymptotically Locally AdS Spacetimes

As was seen in Chapter 17 of [72], when the spacetime metric is dynamical the choice of boundary conditions plays an especially key role in constructions of conserved charges. In this chapter we consider boundary conditions which force the spacetime to behave asymptotically in a manner at least locally similar to (2.3). It turns out to be useful to proceed by using the notion of a conformally rescaled metric $\hat{g}$ which extends sufficiently smoothly to the boundary (see chapter 28 for further discussion of this technique). After imposing the equations of motion, this $\hat{g}$ will allow us to very quickly define both asymptotically AdS (AAdS) and asymptotically local AdS spacetimes (AlAdS). Below, we follow [87, 91–96].

To begin, recall that our discussion of pure AdS above made use of the fact that the unphysical metrics defined in (2.8) and (2.10) could be extended to the conformal boundary ∂M of AdS. We can generalize this notion by considering any manifold M (often called 'the bulk') with boundary ∂M and allowing metrics

g which are singular on ∂M but for which but there exists a smooth function Ω satisfying $\Omega|_{\partial M} = 0$, $(d\Omega)|_{\partial M} \neq 0$ (where $|_{\partial M}$ denotes the pull-back to ∂M), and $\Omega > 0$ on all of M, such that

$$\hat{g} = \Omega^2 g \tag{2.11}$$

can be extended to all of M as a sufficiently smooth non-degenerate metric for which the induced metric on ∂M has Lorentz signature. We will discuss what is meant by sufficiently smooth in more detail in section 2.2.4, but for the purposes of this section one may take $\hat{g}$ to be C^2 (so that its Riemann tensor is well-defined). Note that $\hat{g}$ is not unique; given any allowed Ω one is always free to choose

$$\Omega' = e^{\sigma}\Omega, \tag{2.12}$$

for arbitrary smooth σ on M. Thus, as before, the notion of a particular boundary metric on ∂M is well-defined only after one has chosen some conformal frame. However, the bulk metric g does induce a unique conformal structure on ∂M. The function Ω is termed the defining function of the conformal frame. The above structure is essentially that of Penrose's conformal compactifications [97], except that the Lorentz signature of ∂M forbids M from being fully compact. In particular, future and past infinity are not part of ∂M.

In vacuum Einstein-Hilbert gravity with cosmological constant (2.6), we define an asymptotically locally AdS spacetime to be a spacetime (g, M) as above that solves the Einstein equations (2.6). A key feature of this definition is that it makes no restriction on the conformal structure, or even the topology of the

boundary, save that it be compatible with having a Lorentz signature metric. For an asymptotically locally AdS spacetime to be what we will call asymptotically AdS, the induced boundary metric must be conformal to $\mathbb{R} \times S^{d-1}$. The reader should be aware that in the literature, the term "asymptotically AdS" (AAdS) is sometimes used synonymously with "asymptotically locally AdS" (AlAdS). Here we emphasize the distinction between the two for pedagogical purposes, as only AAdS spacetimes can truly be said to approach global AdS near ∂M.

To show that AlAdS spacetimes do in fact approach (2.5) requires the use of the Einstein equations. By writing $g_{\mu\nu} = \Omega^{-2}\hat{g}_{\mu\nu}$, a straightforward calculation then shows [95] that near ∂M we have

$$R_{\mu\nu\sigma\lambda} = -\left|d\Omega\right|^2_{\hat{g}} \left(g_{\mu\sigma}g_{\nu\lambda} - g_{\nu\sigma}g_{\mu\lambda}\right) + \mathcal{O}\left(\Omega^{-3}\right), \tag{2.13}$$

where

$$\left|d\Omega\right|^2_{\hat{g}} \equiv \hat{g}^{\mu\nu}\partial_\mu\Omega\,\partial_\nu\Omega \tag{2.14}$$

extends smoothly to ∂M. Note that since g has a second-order pole at ∂M, the leading-order term in (2.13) is of order Ω^{-4}. The Einstein field equations then imply that

$$\left|d\Omega\right|^2_{\hat{g}} = \frac{1}{\ell^2} \quad \text{on } \partial M. \tag{2.15}$$

It follows that Riemann tensor (2.13) of an AlAdS spacetime near ∂M looks like that of pure AdS (2.5). Further details of the asymptotic structure (and of the approach to (2.3) for the AAdS case) are elucidated by the Fefferman-Graham expansion near ∂M to which we now turn.

2.2.4 The Fefferman-Graham Expansion

The term asymptotically (locally) AdS suggests that the spacetime metric g should (locally) approach (2.3), at least with a suitable choice of coordinates. This is far from manifest in the definitions above. But it turns out to be a consequence of the Einstein equations. In fact, these equations imply that the asymptotic structure is described by a so-called Fefferman-Graham expansion [98].

The basic idea of this expansion is to first choose a convenient set of coordinates and then to attempt a power-series solution to the Einstein equations. Since the Einstein equations are second order, this leads to a second-order recursion relation for the coefficients of the power series. For, say, simple ordinary differential equations, one would expect the free data in the power series to be parametrized by two of the coefficients. The structure that emerges from the Einstein equations is similar, except for the presence of constraint equations similar to those described in Chapter 17 of [72]. As we briefly describe below, the constraint equations lead to corresponding constraints on the two otherwise free coefficients. We continue to consider the vacuum case (2.6).

Let us begin by introducing the so-called Fefferman-Graham coordinates on some finite neighborhood U of ∂M. To do so, note that since the defining function Ω is not unique it is possible to choose a σ in (2.12) such that the modified defining function $z := \Omega'$ obeys

$$|dz|^2_{\hat{g}} = \frac{1}{\ell^2} \tag{2.16}$$

on U, where $\hat{g} = z^2 g$. In fact, we can do so with $\sigma|_{\partial M} = 1$ so that we need

not change the conformal frame. We can then take the defining function z to be a coordinate near the boundary; the notation z is standard for this so-called "Fefferman-Graham radial coordinate." We choose the other coordinates x^i to be orthogonal to z in U (according to the metric $\hat{g}$). The metric in these so-called Fefferman-Graham coordinates will then take the form

$$ds^2 = \frac{\ell^2}{z^2}\left(dz^2 + \gamma_{ij}(x,z)\,dx^i\,dx^j\right), \tag{2.17}$$

where $i = 0, \ldots, d$. By construction, γ_{ij} can be extended to ∂M, so it should admit an expansion (at least to some order) in non-negative powers of z:

$$\gamma_{ij}(x,z) = \gamma^{(0)}_{ij}(x) + z\gamma^{(1)}_{ij}(x) + \cdots . \tag{2.18}$$

Note that $\gamma^{(0)}_{ij}$ defines the metric $\gamma^{(0)}$ on ∂M in this conformal frame.

Since the Einstein equations are second order partial differential equations, plugging in the ansatz (2.18) leads to a second order recursion relation for the $\gamma^{(n)}$. For odd d this recursion relation admits solutions for all $\gamma^{(n)}$. After specifying $\gamma^{(0)}$, one finds that all $\gamma^{(n)}$ with $n < d$ are uniquely determined (and, in fact $\gamma^{(n)}$ vanishes for all odd $n < d$). For example, for $d > 2$ one finds [96]

$$\gamma^{(2)}_{ij} = \frac{1}{d-2}\left(\mathcal{R}_{ij} - \frac{1}{2(d-1)}\mathcal{R}\gamma^{(0)}_{ij}\right), \tag{2.19}$$

where $\mathcal{R}, \mathcal{R}_{ij}$ are respectively the Ricci tensor and Ricci scalar of $\gamma^{(0)}$.

However, new data enters in $\gamma^{(d)}$. This new data is subject to constraints analogous to those discussed in the Hamiltonian formalism in Chapter 17 of [72].

Indeed, these constraints may be derived by considering the analogues of the Hamiltonian and momentum constraints on surfaces with $z = constant$. They determine the trace and divergence of $\gamma^{(d)}$ (again for d odd) through

$$\left(\gamma^{(0)}\right)^{ij} \gamma^{(d)}_{ij} = 0, \qquad \left(\gamma^{(0)}\right)^{ki} D_k \gamma^{(d)}_{ij} = 0, \tag{2.20}$$

where D_k is the $\gamma^{(0)}$-compatible derivative operator on ∂M (where we think of all $\gamma^{(n)}$ as being defined). We will give a short argument for (2.20) in section 2.3.4. Once we have chosen any $\gamma^{(d)}$ satisfying (2.20), the recursion relation can then be solved order-by-order to express all higher $\gamma^{(n)}$ in terms of $\gamma^{(0)}$ and $\gamma^{(d)}$. Of course, the series (2.17) describes only the asymptotic form of the metric. There is no guarantee that there is in fact a smooth solution in the interior matching this asymptotic data, or that such a smooth interior solution is unique when it exists.

The situation is slightly more complicated for even d, where the recursion relations for the ansatz (2.18) break down at the order at which $\gamma^{(d)}$ would appear. To proceed, one must allow logarithmic terms to arise at this order and use the more general ansatz

$$\gamma_{ij}(x, z) = \gamma^{(0)}_{ij} + z^2 \gamma^{(2)}_{ij} + \cdots + z^d \gamma^{(d)}_{ij} + z^d \bar{\gamma}^{(d)}_{ij} \log z^2 + \cdots , \tag{2.21}$$

where, since the structure is identical for all d up to order $n = d$, we have made manifest that $\gamma^{(n)} = 0$ for all odd $n < d$. The higher order terms represented by $\cdots$ include both higher even powers of z and such terms multiplied by $\log z$. One

finds that $\bar{\gamma}^{(d)}$ is fully determined by $\gamma^{(0)}$ and satisfies

$$\left(\gamma^{(0)}\right)^{ij} \bar{\gamma}^{(d)}_{ij} = 0, \qquad \left(\gamma^{(0)}\right)^{ki} D_k \bar{\gamma}^{(d)}_{ij} = 0. \tag{2.22}$$

For example, for $d = 2$, 4, one obtains [96]

$$\bar{\gamma}^{(2)}_{ij} = 0, \tag{2.23}$$

$$\bar{\gamma}^{(4)}_{ij} = \frac{1}{8}\,\mathcal{R}_{ikjl}\mathcal{R}^{kl} + \frac{1}{48}\,D_i D_j \mathcal{R} - \frac{1}{16}\,D^2\mathcal{R}_{ij} - \frac{1}{24}\,\mathcal{R}\mathcal{R}_{ij} + \left(\frac{1}{96}\,D^2\mathcal{R} + \frac{1}{96}\,\mathcal{R}^2 - \frac{1}{32}\,\mathcal{R}_{kl}\mathcal{R}^{kl}\right)\gamma^{(0)}_{ij}, \tag{2.24}$$

where $\mathcal{R}_{ijkl}$ is the Riemann tensor of $\gamma^{(0)}$, and indices are raised and lowered with $\gamma^{(0)}$. But $\gamma^{(d)}$ may again be chosen freely subject to dimension-dependent conditions that fix its divergence and trace. As examples, one finds [96]

$$d = 2 : \left(\gamma^{(0)}\right)^{ij} \gamma^{(d)}_{ij} = \frac{1}{2}\,\mathcal{R}, \qquad D^i \gamma^{(d)}_{ij} = \frac{1}{2} D_j \mathcal{R}, \tag{2.25}$$

$$d = 4 : \left(\gamma^{(0)}\right)^{ij} \gamma^{(d)}_{ij} = \frac{1}{16}\left(\mathcal{R}_{ij}\mathcal{R}^{ij} - \frac{2}{9}\,\mathcal{R}^2\right), \tag{2.26}$$

$$D^i \gamma^{(d)}_{ij} = \frac{1}{8}\mathcal{R}_i{}^k D^i \mathcal{R}_{kj} - \frac{1}{32} D_j\left(\mathcal{R}^{ik}\mathcal{R}_{ik}\right) + \frac{1}{288}\mathcal{R} D_j \mathcal{R}. \tag{2.27}$$

The higher terms in the series are again uniquely determined by $\gamma^{(0)}$, $\gamma^{(d)}$.

In general, the terms $\gamma^{(n)}$ become more and more complicated at each order. But the expansion simplifies when $\gamma^{(0)}_{ij}$ is conformally flat and $\gamma^{(d)}_{ij} = 0$. In this case one finds [99] that the recursion relation can be solved exactly and terminates at order z^4. In particular, the bulk metric so obtained is also conformally flat,

and is thus locally AdS_{d+1}. For $d = 2$, the Fefferman-Graham expansion can be integrated exactly for any $\gamma^{(0)}$, $\gamma^{(d)}$, and always terminates at order z^4 to define a metric that is locally AdS_3.

2.2.5 Diffeomorphisms and symmetries in AlAdS

The reader of this Handbook is by now well aware of the important roles played by diffeomorphisms in understanding gravitational physics. Let us therefore pause briefly to understand how such transformations affect the structures defined thus far. We are interested in diffeomorphisms of our manifold M with boundary ∂M. By definition, any such diffeomorphism must map ∂M to itself; i.e., it also induces a diffeomorphism of ∂M. As usual in physics, we consider diffeomorphisms (of M) generated by vector fields ξ; the corresponding diffeomorphism of ∂M is generated by some $\hat{\xi}$, which is just the restriction of ξ to ∂M (where by the above it must be tangent to ∂M).

Of course, the metric g transforms as a tensor under this diffeomorphism. But if we think of the diffeomorphism as acting only on dynamical variables of the theory then the defining function $z = \Omega$ does not transform at all, and in particular does not transform like a scalar field. This means that the rescaled metric $\hat{g} = z^2 g$ does *not* transform like a tensor, and neither does the boundary metric $\gamma^{(0)}$. Instead, the diffeomorphism induces an additional conformal transformation on ∂M; i.e., a change of conformal frame.

We can make this explicit by considering diffeomorphisms that preserve the

Fefferman-Graham gauge conditions; i.e., which satisfy

$$\delta g_{zz} = 0 = \delta g_{iz} \tag{2.28}$$

for

$$\delta g_{\mu\nu} = \pounds_\xi g_{\mu\nu} = \nabla_\mu \xi_\nu + \nabla_\nu \xi_\mu, \tag{2.29}$$

where we use $\pounds_\xi$ to denote Lie derivatives along ξ and ∇_μ is the covariant derivative compatible with the metric g on M. Let us decompose the components $\delta g_{\mu\nu}$ into

$$\pounds_\xi g_{zz} = \frac{2\ell}{z}\,\partial_z\left(\frac{\ell}{z}\,\xi^z\right), \tag{2.30}$$

$$\pounds_\xi g_{iz} = \frac{\ell^2}{z^2}\left(\partial_i \xi^z + \gamma_{ij}\partial_z \xi^j\right), \tag{2.31}$$

$$\pounds_\xi g_{ij} = \frac{\ell^2}{z^2}\left(\pounds_{\hat{\xi}}\gamma_{ij} + z^2\,\partial_z\left(z^{-2}\gamma_{ij}\right)\xi^z\right), \tag{2.32}$$

where $\pounds_{\hat{\xi}}$ is the Lie derivative with respect to $\hat{\xi}$ on ∂M. These conditions can be integrated using (2.28) to obtain

$$\xi^z = z\hat{\xi}^z(x), \tag{2.33}$$

$$\xi^i = \hat{\xi}^i(x) - \partial_j\hat{\xi}^z \int_0^z z'\gamma^{ji}(z')\,dz', \tag{2.34}$$

where $\hat{\xi}^z$ and $\hat{\xi}^i$ are an arbitrary function and vector field on ∂M (which we may transport to any $z = \textit{constant}$ surface by using the given coordinates to

temporarily identify that surface with ∂M). In particular, for $\hat{\xi}^i = 0$ we find

$$g_{ij} + \delta g_{ij} = \frac{\ell^2}{z^2}\left(1 - 2\hat{\xi}^z\right)\gamma^{(0)}_{ij} + \mathcal{O}(z^0). \tag{2.35}$$

Thus the boundary metric transforms as $\gamma^{(0)} \to e^{-2\hat{\xi}^z}\gamma^{(0)}_{ij}$. Such transformations are called conformal transformations by relativists and Weyl transformations by particle physicists; we will use the former, but the reader will find both terms in various treatments of AlAdS spacetimes. This is precisely the change of conformal frame mentioned above.

Let us now turn to the notion of symmetry. As in Chapter 17 of [72], we might be interested either in an exact symmetry of some metric g, generated by a Killing vector field (KVF) satisfying $\nabla_{(\nu}\xi_{\mu)} = 0$, or in some notion of asymptotic symmetry. We will save the precise definition of an asymptotic symmetry for section 2.3.3 as, strictly speaking, this first requires the construction an appropriate variational principle and a corresponding choice of boundary conditions. However, we will discuss the closely related (but entirely geometric) notion of an asymptotic Killing field below.

Suppose first that ξ is indeed a KVF of g so that $\pounds_\xi g = 0$. It is clear that there are two cases to consider. Either $\pounds_\xi \Omega = 0$ (in which case we say that ξ is compatible with Ω) or $\pounds_\xi \Omega \neq 0$ (in which case we say that ξ is not compatible with Ω). In the former case we clearly have $\pounds_\xi \hat{g} = \pounds_\xi(\Omega^2 g) = 0$ so that ξ is also a Killing field of $\hat{g}$. But more generally we have seen that the corresponding diffeomorphism changes $\hat{g}$ by a conformal factor. The generators of such diffeomorphisms are called

conformal Killing fields of $\hat{g}$ (see e.g. Appendix C.3 of [90]) and satisfy

$$\pounds_\xi \hat{g}_{\mu\nu} = (\pounds_\xi \ln \Omega^2)\hat{g}_{\mu\nu} \Rightarrow 2\widehat{\nabla}_{(\mu}\xi_{\nu)} = \frac{2}{d+1}\left(\widehat{\nabla}_\sigma \xi^\sigma\right)\hat{g}_{\mu\nu}, \tag{2.36}$$

where $\widehat{\nabla}$ is the covariant derivative compatible with $\hat{g}$, and indices on ξ^μ are lowered with $\hat{g}_{\mu\nu}$. Note that the induced vector field $\hat{\xi}$ on ∂M is again a conformal Killing field of $\gamma^{(0)}$.

This suggests that we define an asymptotic Killing field to be any vector field ξ that satisfies (2.36) to leading order in Ω at ∂M. If we ask that ξ also preserve Fefferman-Graham gauge we may then expand (2.33) and (2.34) and insert into (2.36) to obtain

$$\xi^z = z\hat{\xi}^z(x), \tag{2.37}$$

$$\xi^i = \hat{\xi}^i(x) - \frac{1}{2}z^2\left(\gamma^{(0)}\right)^{ij}\partial_j\hat{\xi}^z + \mathcal{O}(z^4), \tag{2.38}$$

$$\pounds_{\hat{\xi}}\gamma^{(0)}_{ij} - \frac{2}{d+1}\left(D_k\hat{\xi}^k + \hat{\xi}^z\right)\gamma^{(0)}_{ij} = 0. \tag{2.39}$$

Taking the trace of the condition (2.39) shows that $\hat{\xi}^z = \frac{1}{d}D_i\hat{\xi}^i$, so (2.39) is the conformal Killing equation for $\hat{\xi}$ with respect to $\gamma^{(0)}$. In other words, conformal Killing fields $\hat{\xi}$ of $\gamma^{(0)}$ are in one-to-one correspondence with asymptotic Killing fields of g which preserve Fefferman-Graham gauge, where the equivalence relation is given by agreement to the order shown in (2.38).

2.2.6 Gravity with Matter

Our treatment above has focused on vacuum gravity. It is useful to generalize the discussion to include matter fields, both to see how this influences the above result and also to better elucidate the general structure of asymptotically AdS field theory. Indeed, readers new to dynamics in AdS space will gain further insight from section 2.2.4 if they re-read it after studying the treatment of the free scalar field below. We use a single scalar as an illustrative example of matter fields; see [87, 88] for more general discussions.

For simplicity, we first consider a massive scalar field in a fixed AlAdS_{d+1} gravitational background, which we take to be in Fefferman-Graham form (2.17). This set-up is often called the probe approximation as it neglects the back-reaction of the matter on the spacetime. The action is as usual

$$S_\phi^{Bulk} = -\frac{1}{2}\int d^{d+1}x\,\sqrt{|g|}\,\left(g^{\mu\nu}\partial_\mu\phi\partial_\nu\phi + m^2\phi^2\right). \tag{2.40}$$

We study the behavior of solutions near the boundary $z = 0$ by seeking solutions which behave at leading order like z^Δ for some power Δ. The equation of motion

$$\left(-\Box + m^2\right)\phi = 0 \tag{2.41}$$

then requires $(m\ell)^2 = \Delta(\Delta - d)$, yielding two independent small-z behaviors $z^{\Delta_\pm}$. Here we have defined $\Delta_\pm = d/2 \pm \nu$, with $\nu \equiv \sqrt{(d/2)^2 + (m\ell)^2}$. A priori, it seems that we should consider only $\nu \geq \nu_{\min}$ for some $\nu_{\min} > 0$, since one might expect $(m\ell)^2 \geq 0$. However, it can be shown [100] that scalar fields with small tachyonic masses in AdS_{d+1} are stable as long as the mass satisfies the so-

called Breitenlohner-Freedman (BF) bound $(m\ell)^2 \geq -d^2/4 =: m_{BF}^2$; we therefore consider $\nu \geq 0$. The essential points here are: i) It is only for $|(m\ell)^2| \gg 1$ that the flat-space approximation must hold, so for small $|(m\ell)^2|$ the behavior can differ significantly from that of flat space; ii) as noted above, the fact that AdS is not globally hyperbolic means that we must impose boundary conditions at ∂M. These boundary conditions generally require ϕ to vanish on ∂M. So even for $m^2 = 0$ we would exclude the 'zero mode' $\phi =$ constant. For a given boundary condition, the spectrum of modes turns out to be discrete. As a result, we may lower m^2 a finite amount below zero before a true instability develops.

The asymptotic analysis above suggests that we seek a solution of the form

$$\phi(x,z) = z^{\Delta_-}\left(\phi^{(0)} + z^2\phi^{(2)} + \cdots\right) + z^{\Delta_+}\left(\phi^{(2\nu)} + z^2\phi^{(2\nu+2)} + \cdots\right). \qquad (2.42)$$

For non-integer ν the equation of motion can be solved order-by-order in z to uniquely express all coefficients in terms of $\phi^{(0)}$ and $\phi^{(2\nu)}$. But for integer ν the difference $\Delta_+ - \Delta_-$ is an even integer and the two sets of terms in (2.42) overlap. This notational issue is connected to a physical one: keeping only even-integer powers of z (times z^{Δ_-}) does not allow enough freedom to solve the resulting recursion relation; there is no solution at order $d - 2\Delta_-$. To continue further we must introduce a logarithmic term and write:

$$\phi(x,z) = z^{\Delta_-}\left(\phi^{(0)} + z^2\phi^{(2)} + \cdots\right) + z^{\Delta_+}\log z^2\left(\psi^{(2\nu)} + z^2\psi^{(2\nu+2)} + \cdots\right). \qquad (2.43)$$

The recursion relations then uniquely express all coefficients in terms of the free coefficients $\phi^{(0)}$ and $\phi^{(2\nu)}$. As an example, we note for later purposes that (for any

value of ν)

$$\phi^{(2)} = \frac{1}{4(\nu-1)}\Box^{(0)}\phi^{(0)}, \tag{2.44}$$

where $\Box^{(0)}$ is the scalar wave operator defined by $\gamma^{(0)}$ on ∂M. Dimensional analysis shows that the higher coefficients $\phi^{(n)}$ for integer $n < 2\Delta_+ - d$ involve n derivatives of $\phi^{(0)}$.

We now couple our scalar to dynamical gravity using

$$S = S_{\rm grav} + S_\phi^{\rm Bulk}, \tag{2.45}$$

where $S_{\rm grav}$ is the action for gravity. We will postpone a discussion of boundary terms to section 2.3; for now, we simply focus on solving the resulting equations of motion

$$R_{\mu\nu} - \frac{1}{2}\,R g_{\mu\nu} + \Lambda g_{\mu\nu} = 8\pi G T^{(\rm matter)}_{\mu\nu}. \tag{2.46}$$

As in the vacuum case we write the metric in the form (2.17), and as in the solution for nondynamical gravity we write the scalar field as in (2.43). Note that we keep the logarithmic term in (2.21) for all d as, depending on the matter content, it may be necessary even for odd d. (When it is not needed, the equations of motion force its coefficient $\bar{\gamma}_d$ to vanish.) The stress tensor of the scalar field then behaves like

$$T^{(\rm matter)}_{\mu\nu} dx^\mu dx^\nu = \Delta_- z^{2(\Delta_- - 1)} \left[\frac{d}{2} \left(\phi^{(0)}\right)^2 dz^2 + z\phi^{(0)}\partial_i\phi^{(0)}\, dz\, dx^i \right. \\ \left. + \nu \left(\phi^{(0)}\right)^2 \gamma^{(0)}_{ij} dx^i\, dx^j + \cdots \right]. \tag{2.47}$$

For $\Delta_- < 0$ and $\phi^{(0)} \neq 0$, the matter stress tensor turns out to diverge too rapidly at $z = 0$ for the equations of motion to admit an AlAdS solution. So for $\Delta_- < 0$ the only scalar field boundary condition consistent with the desired physics is $\phi^{(0)} = 0$. But for $\Delta_- \geq 0$ the equations of motion *do* admit AlAdS solutions with $\phi^{(0)} \neq 0$ and further input is required to determine the boundary conditions. We will return to this issue in section 2.3.2.

Evidently, the equations of motion admit solutions of the forms (2.17) and (2.43) only if the components of the matter stress tensor in Fefferman-Graham coordinates diverge as $1/z^2$ or slower. This result allows us to generalize our definition of asymptotically locally AdS spacetimes to include matter: an AlAdS spacetime with matter is a manifold M as above with fields satisfying the equations of motion and the requirement that $\Omega^2 T_{\mu\nu}$ admits a continuous limit to ∂M.

2.3 Variational principles and charges

Noether's theorem teaches us that variational principles provide a powerful link between symmetries and conservation laws, allowing the latter to be derived without detailed knowledge of the equations of motion. This procedure works as well for gravitational theories as for systems defined on a fixed spacetime background, though there is one additional subtlety. In more familiar theories, it is often sufficient to consider only variations of compact support so that all boundary terms arising from variations of an action can be discarded. But as shown in Chapter 17 of [72] in the asymptotically flat context, when the gravitational constraints (which are just certain equations of motion!) are satisfied the gravita-

tional charges become pure boundary terms with no contributions from the bulk. Discarding all boundary terms in Noether's theorem would thus lead to trivial charges and we will instead need to treat boundary terms with care. It is in part for this reason that we refer to *variational principles* as opposed to mere actions, the distinction being that all variations of the former vanish when the equations of motion and boundary conditions hold, even including any boundary terms that may arise in computing the variations. Constructing a good variational principle generally requires that we add boundary terms to the familiar bulk action, and that we tailor the choice of such boundary terms to the boundary conditions we wish to impose on ∂M.

2.3.1 A toy model of AdS: Gravity in a box

We have seen that AlAdS spacetimes are conformally equivalent to manifolds with timelike boundaries. This means that (with appropriate boundary conditions) light signals can bounce off of ∂M and return to the interior in finite time, boundary conditions are needed for time evolution, and indeed much of physics in AlAdS spacetimes is indeed like field theory in a finite-sized box. This analogy also turns out to hold for the study of conservation laws in theories with dynamical gravity. It will therefore prove useful to first study conservation laws for gravity on a manifold M with a finite-distance timelike boundary ∂M, which will serve as a toy model for AlAdS gravitational dynamics. This subject, which we call "gravity in a box", was historically studied for its own sake by Brown and York [101]. We largely follow their approach below. For simplicity we will assume that ∂M is globally hyperbolic with compact Cauchy surfaces as shown in figure 2.3,

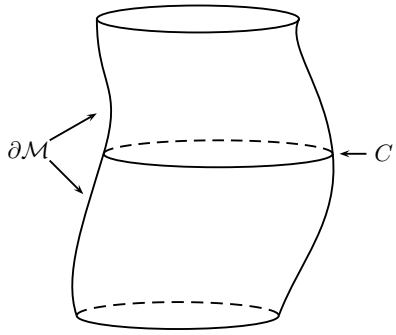

Figure 2.3: A sketch of the spacetime $\mathcal{M}$. The codimension two surface C is a Cauchy surface of the boundary ∂M.

though the more general case can typically be treated by imposing appropriate boundary conditions in the asymptotic regions of ∂M.

Out first task is to construct a good variational principle. But as noted above this will generally require us to add boundary-condition-dependent boundary terms to the bulk action. It is thus useful to have some particular boundary condition (or, at least, a class of such conditions) in mind before we begin. In scalar field theory, familiar classes of boundary conditions include the Dirichlet condition ($\phi|_{\partial M}$ fixed, so $\delta\phi|_{\partial M} = 0$), the Neumann condition (which fixes the normal derivative), or the more general class of Robin conditions (which fix a linear combination of the two). All of these have analogues for our gravity in a box system, but for simplicity we will begin with a Dirichlet-type condition. Recall from chapter 18 that, when discussing the initial value problem, the natural initial data on a Cauchy surface consists of the induced metric and the extrinsic curvature (or, equivalently, the conjugate momentum as described in Chapter 17 of [72]). Since the equations of motion are covariant, the analysis of possible boundary conditions on timelike boundaries turns out to be very similar so that

the natural Dirichlet-type condition is to fix the induced metric h_{ij} on ∂M.

An important piece of our variational principle will of course be the Einstein-Hilbert action $S_{EH} = \frac{1}{2\kappa}\int \sqrt{-g}\ R$ (with $\kappa = 8\pi G$). But S_{EH} is not sufficient by itself as a standard calculation gives

$$\begin{aligned}\delta S_{EH} &= \delta\left(\frac{1}{2\kappa}\int_M \sqrt{-g}R\right) \\ &= \frac{1}{2\kappa}\int_M \sqrt{-g}\left(R^{\mu\nu} - \frac{1}{2}Rg^{\mu\nu}\right)\delta g_{\mu\nu} + \frac{1}{2\kappa}\int_{\partial M}\sqrt{|h|}\hat{r}_\lambda G^{\mu\nu\rho\lambda}\nabla_\rho \delta g_{\mu\nu}\end{aligned} \tag{2.48}$$

where $\hat{r}^\lambda$ is the outward pointing unit normal to ∂M and

$$G^{\mu\nu\rho\lambda} = g^{\mu(\rho}g^{\lambda)\nu} - g^{\mu\nu}g^{\rho\lambda}. \tag{2.49}$$

In (2.48) we have discarded boundary terms not associated with ∂M (i.e., boundary terms in any asymptotic regions of M) as they will play no role in our analysis. Nevertheless, the second term in (2.48) (the boundary term) generally fails to vanish for useful boundary conditions, so that S_{EH} is not fully stationary on solutions.

However, when $\delta h_{ij} = 0$ this problem term turns out to be an exact variation of another boundary term, known as the Gibbons-Hawking term, given by the integral of the trace of the extrinsic curvature of ∂M. (For related reasons the addition of this term is necessary when constructing a gravitational path integral, see [102]). As a result, enforcing the boundary condition $\delta h_{ij} = 0$ guarantees that

all variations of the action

$$S_{\text{Dirichlet in a box}} = S_{EH} + S_{GH} = \frac{1}{2\kappa}\int_{\mathcal{M}} \sqrt{-g}R - \frac{1}{\kappa}\int_{\partial M} \sqrt{|h|}K, \tag{2.50}$$

where $K = h_{ij}K^{ij}$ is the trace of the extrinsic curvature on ∂M, vanish precisely when the bulk equations of motion hold. Thus (2.50) gives a good variational principle for our Dirichlet problem.

Now, Noether's theorem teaches us that every continuous symmetry of our system should lead to a conservation law (though the conservation laws associated with pure gauge transformations are trivial). Gravity in a box is defined by the action (2.50) and by the choice of some Lorentz-signature metric h_{ij} on ∂M. The first ingredient, the action (2.50), is manifestly invariant under any diffeomorphisms of M. Such diffeomorphisms are generated by vector fields ξ on M that are tangent to ∂M at the boundary (so that the diffeomorphism maps ∂M to itself). As before, we use $\hat{\xi}$ to denote the induced vector field on ∂M. The associated diffeomorphism of M will preserve h_{ij} if $\hat{\xi}$ is a Killing field on the boundary. As discussed in Chapter 17 of [72], a diffeomorphism supported away from the boundary should be pure gauge. So it is natural to expect that the asymptotic symmetries of our system are classified by the choice of boundary Killing field $\hat{\xi}$, with the particular choice of a bulk extension ξ being pure gauge.

This set up should remind the reader of (non-gravitational) field theories on fixed spacetime backgrounds. There one finds conservation laws associated with each Killing field of the background metric. Here again the conservation laws are associated with Killing fields of the background structure, though now the only

such structure is the boundary metric h_{ij}.

Pursuing this analogy, let us recall the situation for field theory on a fixed (non-dynamical) spacetime background. There, Noether's theorem for global symmetries (e.g., translations along some Killing field ξ_{KVF}) would instruct us to vary the action under a space-time generalization of the symmetry (e.g., diffeomorphism along $f(x)\xi_{KVF}$ for general smooth functions $f(x)$, or more generally under arbitrary diffeomorphisms). It is clear that the analogue for gravity in a box is just to vary (2.50) under a general diffeomorphism of M.

It turns out to be useful to do so in two steps. Let us first compute an arbitrary variation of (2.50). By construction, it must reduce to a boundary term when the equations of motion hold, and it must vanish when $\delta h_{ij} = 0$. Thus it must be linear in δh_{ij}. A direct calculation (see appendix E of [90]) gives

$$\delta S_{\text{Dirichlet in a box}} = -\frac{1}{2}\int_{\partial M} \sqrt{|h|}\tau^{ij}\delta h_{ij}, \tag{2.51}$$

where $\tau^{ij} = \kappa^{-1}(K^{ij} - Kh^{ij})$. This τ^{ij} is sometimes referred to as the radial conjugate momentum since it has the same form as the (undensitized) conjugate momentum introduced on spacelike surfaces in Chapter 17 of [72]. This agreement of course follows from general principles of Hamilton-Jacobi theory. The reader should recall that for field theory in a fixed spacetime background the functional derivative of the action with respect to the metric defines the field theory stress tensor. By analogy, the object τ^{ij} defined above is often called the boundary stress tensor (or the Brown-York stress tensor) of the gravitational theory.

Let us now specialize to the case where our variation is a diffeomorphism

of M. As we have seen, ξ also induces a diffeomorphism of the boundary ∂M generated by some $\hat{\xi}$. Then $\delta h_{ij} = D_i\hat{\xi}_j + D_j\hat{\xi}_i$, where D_i is the covariant derivative compatible with h_{ij}. Using the symmetry of $\tau^{ij} = \tau^{ji}$ we find

$$\delta S_{\text{Dirichlet in a box}} = -\int_{\partial M} \sqrt{|h|}\tau^{ij} D_i\hat{\xi}_j = \int_{\partial M} \sqrt{|h|}\hat{\xi}_j D_i\tau^{ij}, \tag{2.52}$$

where in the last step we integrate by parts and take $\hat{\xi}$ to have compact support on ∂M so that we may discard any boundary terms. Since $\hat{\xi}$ is otherwise arbitrary, we conclude that

$$D_i\tau^{ij} = 0; \tag{2.53}$$

i.e., τ^{ij} is covariantly conserved on ∂M when the equations of motion hold in the bulk. In fact, since τ^{ij} is the radial conjugate momentum, it should be clear from Chapter 17 of [72] that (2.53) can also be derived directly from the equations of motion by evaluating the radial-version of the diffeomorphism constraint on ∂M. (The radial version of the Hamiltonian constraint imposes another condition on τ^{ij} that can be used to determine the trace $\tau = \tau^{ij}h_{ij}$ in terms of the traceless part of τ^{ij}.)

If we now take $\hat{\xi}$ to be a boundary Killing field, we find $D_i(\tau^{ij}\hat{\xi}_j) = 0$, so that the so-called Brown-York charge

$$Q_{BY}[\xi] := -\int_C \sqrt{q}\, n_i \tau^{ij}\hat{\xi}_j \tag{2.54}$$

is independent of the choice of Cauchy surface C in ∂M. Here n_i is a unit future-pointing normal to C and $\sqrt{q}$ is the volume element induced on C by h_{ij}. Although these charges were defined by methods quite different from the Hamiltonian tech-

niques of Chapter 17 of [72], we will argue in section 2.4 below that the end result is identical up to a possible choice of zero-point. Once again, the argument will turn out to be essentially the same as one would give for field theory in a fixed non-dynamical background.

Before proceeding to the AdS case, let us take a moment to consider other possible boundary conditions. We see from (2.51) that the action (2.50) also defines a valid variational principle for the boundary condition $\tau^{ij} = 0$. Of course, with this choice the charges (2.54) all vanish. But this should be no surprise. Since the condition $\tau^{ij} = 0$ is invariant under *all* diffeomorphisms of M, there is no preferred subset of non-trivial asymptotic symmetries; all diffeomorphisms turn out to generate pure gauge transformations. One may also study more complicated boundary conditions by adding additional boundary terms to the action (2.50), though we will not pursue the details here.

2.3.2 Variational principles for scalar fields in AdS

As the reader might guess, our discussion of AlAdS gravity will follow in direct analogy to the above treatment of gravity in a box. Indeed, the only real difference is that we must work a bit harder to construct a good variational principle. We will first illustrate the relevant techniques below by constructing a variational principle for a scalar field on a fixed AdS background, after which we will apply essentially identical techniques to AdS gravity itself in section 2.3.3.

We will construct our variational principle using the so-called counterterm subtraction approach pioneered in [103, 104] and further developed in [95, 96]. Our discussion below largely follows [95], with minor additions from [89]. We

begin with the bulk action $S_\phi^{\rm Bulk}$ of (2.40) and compute

$$\delta S_\phi^{\rm Bulk} = -\int_{\partial M} \sqrt{|h|}\hat{r}^\mu \partial_\mu \phi \delta\phi, \tag{2.55}$$

where $\hat{r}^\mu$ is the outward-pointing unit normal to ∂M so that $\hat{r}^\mu \partial_\mu = -\frac{z}{\ell}\partial_z$. The form of (2.55) might appear to suggest that $S_\phi^{\rm Bulk}$ defines a good variational principle for any boundary condition that fixes ϕ on ∂M. But the appearance of inverse powers of z means that we must be more careful, and that $S_\phi^{\rm Bulk}$ will suffice only when $\delta\phi$ vanishes sufficiently rapidly.

It is therefore useful to write (2.55) in terms of the finite coefficients $\phi^{(2n)}, \phi^{(2(\nu+n))}$ of (2.42) (or the corresponding coefficients in (2.43)). The exact expression is not particularly enlightening, and for large ν there are many singular terms to keep track of. What is useful to note however is that all of the singular terms turn out to be exact variations. In particular, using (2.44) one may show for non-integer $\nu < 2$ that the action

$$S_\phi = S_\phi^{\rm Bulk} + \int_{\partial M} \sqrt{|h|}\left(-\frac{\Delta_-}{2\ell}\phi^2 + \frac{\ell}{4(\nu-1)} h^{ij}\partial_i\phi\partial_j\phi\right) \tag{2.56}$$

satisfies

$$\delta S_\phi = 2\nu\ell^{d-1}\int_{\partial M}\sqrt{|\gamma^{(0)}|}\phi^{(2\nu)}\delta\phi^{(0)}. \tag{2.57}$$

Since the boundary terms in (2.56) are each divergent in and of themselves, they are known as counterterms in analogy with the counterterms used to cancel ultraviolet divergences in quantum field theory. These divergences cancel against divergences in $S_\phi^{\rm Bulk}$ and the full action S_ϕ is finite for any field of the form (2.42) with non-integer $\nu < 2$. Similar results hold for non-integer $\nu > 2$ if additional

higher-derivative boundary terms are included in (2.56). We will comment on differences for integer ν at the end of this section.

It is clear that S_ϕ provides a good variational principle so long as the boundary conditions either fix $\phi^{(0)}$ or set $\phi^{(2\nu)} = 0$. We may now identify

$$\Phi_{\rm bndy} := 2\nu \ell^{d-1} \phi^{(2\nu)} \tag{2.58}$$

as an AdS scalar response function analogous to the boundary stress tensor τ^{ij} introduced in section 2.3.1. Note that adding an extra boundary term $\int \sqrt{\gamma^{(0)}} W[\phi^{(0)}]$ to S_ϕ allows one to instead use the Robin-like boundary condition

$$\phi^{(2\nu)} = -\frac{\ell}{2\nu} W'[\phi^{(0}], \tag{2.59}$$

where W' denotes the derivative of W with respect to its argument.

Recall from section 2.2.6 that requiring the energy to be bounded below restricts ν to be real (in which case we take ν non-negative). That there are further implications for large ν can also be seen from (2.56). Note that the final term in (2.56) is a kinetic term on ∂M and that for $\nu > 1$ it has a sign *opposite* to that of the bulk kinetic term. Counting powers of z shows that this boundary kinetic term vanishes at ∂M for $\nu < 1$, but contributes for $\nu > 1$. In this case, for any perturbation that excites $\phi^{(0)}$ and which is supported sufficiently close to ∂M, the boundary kinetic term in (2.56) turns out to be more important than the bulk kinetic term. Thus the perturbation has negative kinetic energy. One says that the theory contains ghosts, and any conserved energy is expected to be unbounded below [89]. For this reason, for $\nu > 1$ one typically allows only boundary

conditions that fix $\phi^{(0)}$. Of course, as noted in section 2.3.2, for $\nu > d/2$ coupling the theory to dynamical gravity and requiring the spacetime to be AlAdS will further require $\phi^{(0)} = 0$. On the other hand, for real $0 < \nu < 1$ all of the above boundary conditions lead to ghost-free scalar theories.

The story of non-integer $\nu > 2$ is much the same as that of $\nu \in (1, 2)$. Adding additional higher-derivative boundary terms to (2.56) again leads to an action that satisfies (2.57). While one can find actions compatible with general boundary conditions (2.59), the only ghost-free theories fix $\phi^{(0)}$ on ∂M. The story of integer ν is more subtle; the factors of $\ln z$ arising in that case from (2.43) mean that we can find a good variational principle only by including boundary terms that depend explicitly on the defining function Ω of the chosen conformal frame. Doing so again leads to ghosts unless $\phi^{(0)}$ is fixed as a boundary condition [89].

2.3.3 A variational principle for AlAdS gravity

We are now ready to construct our variational principle for AlAdS gravity. As for the scalar field above, we will start with a familiar bulk action and then add boundary terms. One may note that in the scalar case our final action (2.56) consists essentially of adding boundary terms to $S_\phi^{\rm Bulk}$ which i) are written as integrals of local scalars built from ϕ and its tangential derivatives along ∂M and ii) precisely cancel divergent terms in $S_\phi^{\rm Bulk}$. This motivates us to follow the strategy of [96] for the gravitational case in which we first identify divergent terms in a familiar action and write these terms as local scalars on ∂M. We may then construct a finite so-called renormalized action by adding boundary counterterms on ∂M to cancel the above divergences. At the end of this process

we may check that this renormalized action yields a good variational principle for interesting boundary conditions. In analogy with section 2.3.1, for simplicity in the remainder of this chapter we take the induced (conformal) metric on ∂M to be globally hyperbolic with compact Cauchy surfaces.

Let us begin with an action containing the standard Einstein-Hilbert and cosmological constant terms in the bulk, along with the Gibbons-Hawking term. It will facilitate our discussion of divergent terms to consider a regulated action in which the boundary has effectively been moved in to $z = \epsilon$. For the moment, we choose some $\epsilon_0 > \epsilon$ and impose the Fefferman-Graham gauge (2.17) for all $z < \epsilon_0$, so that this gauge holds in particular at the regulated boundary. This gauge fixing at finite z is merely an intermediate step to simplify the analysis. We will be able to loosen this condition once we have constructed the final action. We let $h_{ij} = (\ell/z)^2 \gamma_{ij}|_{z=\epsilon}$ be the induced metric on this regulated boundary and study the action

$$\begin{aligned} S_{\rm reg} &= \frac{1}{2\kappa}\int_{z\geq\epsilon}\sqrt{|g|}(R+2\Lambda) - \frac{1}{\kappa}\int_{z=\epsilon}\sqrt{|h|}K \qquad (2.60)\\ &= \frac{\ell^{d-1}}{2\kappa}\int_{z=\epsilon}\sqrt{|\gamma^{(0)}|}\left(\epsilon^{-d}a_{(0)} + \epsilon^{-d+2}a_{(2)} + \cdots + \epsilon^{-2}a_{(d-2)} - \log(\epsilon^2)a_{(d)}\right) + (\text{finite}), \end{aligned}$$

where $K = h_{ij}K^{ij}$ is the trace of the extrinsic curvature of the regulated boundary ∂M_ϵ at $z = \epsilon$ and the form of the divergences follows from (2.21). The coefficient $a_{(d)}$ vanishes for odd d. For even d it is called the conformal anomaly for reasons to be explained below.

In analogy with the scalar field results of section 2.3.2, one finds that the coefficients $a_{(n)}$ which characterize the divergent terms are all local scalars built

from $\gamma^{(0)}_{ij}$ and its derivatives along ∂M. This follows directly from the fact that all terms $\gamma^{(n)}$ with $n \leq d$ in the Fefferman-Graham expansion (2.21) are local functions of $\gamma^{(0)}_{ij}$ and its derivatives along ∂M. Dimensional analysis shows that $a_{(n)}$ involves precisely $2n$ derivatives and the detailed coefficients $a_{(n)}$ can be found to any desired order by direct calculation. For example, for $n \neq d$ the $a_{(n)}$ are given by (see e.g. [96])

$$\begin{aligned} a_{(0)} &= -2(d-1), \quad a_{(2)} = -\frac{(d-4)\mathcal{R}}{2(d-2)}, \\ a_{(4)} &= -\frac{d^2-9d+16}{4(d-4)}\left(\frac{d\mathcal{R}^2}{4(d-2)^2(d-1)} - \frac{\mathcal{R}^{ij}\mathcal{R}_{ij}}{(d-2)^2}\right), \quad \ldots, \end{aligned} \tag{2.61}$$

where as in section 2.2.4, $\mathcal{R}$ and $\mathcal{R}_{ij}$ are the Ricci scalar and Ricci tensor of $\gamma^{(0)}$ on ∂M. For $d = 2$, 4, the log terms are given by

$$\begin{aligned} d = 2: \;\; a_{(2)} &= \frac{\mathcal{R}}{2}, \\ d = 4: \;\; a_{(4)} &= \left(\frac{\mathcal{R}^2}{24} - \frac{\mathcal{R}^{ij}\mathcal{R}_{ij}}{8}\right). \end{aligned} \tag{2.62}$$

As foreshadowed above, we now define the renormalized action

$$S_{\text{ren}} = \lim_{\epsilon \to 0} \left(S_{\text{reg}} + S_{\text{ct}}\right), \tag{2.63}$$

where

$$S_{\text{ct}} := -\frac{\ell^{d-1}}{2\kappa} \int_{z=\epsilon} \sqrt{-\gamma^{(0)}} \left(\epsilon^{-d} a_{(0)} + \epsilon^{-d+2} a_{(2)} + \cdots + \epsilon^{-2} a_{(d-2)} - \log(\epsilon^2) a_{(d)}\right) \tag{2.64}$$

is constructed to precisely cancel the divergent terms in $S_{\rm ren}$. The representation (2.64) makes the degree of divergence in each term manifest. But the use of ϵ in defining $S_{\rm ct}$ suggests a stronger dependence on the choice of defining function Ω (and thus, on the choice of conformal frame) than is actually the case. To understand the true dependence, we should use the Fefferman-Graham expansion to instead express $S_{\rm ct}$ directly in terms of the (divergent) metric h induced on ∂M by the unrescaled bulk metric g as was done in [104]. Dimensional analysis and the fact that each $a_{(n)}$ involves precisely $2n$ derivatives shows that this removes all explicit dependence on ϵ save for the logarithmic term in even d. In particular, formally taking ϵ to zero we may write

$$S_{\rm ct} = -\frac{\ell}{2\kappa}\int_{\partial M}\sqrt{|h|}\left[-\frac{2(d-1)}{\ell^2}+\frac{\mathcal{R}_h}{(d-2)}+\cdots-\frac{\epsilon^d\log(\epsilon^2)a_{(d)}}{\ell^2}\right], \qquad (2.65)$$

where the $\mathcal{R}_h$ (Ricci scalar of h) term only appears for $d \geq 3$ and the dots represent additional terms that appear only for $d \geq 5$.

In general, the coefficients in (2.65) differ from those in (2.60) due to sub-leading divergences in a given term in (2.65) contributing to the coefficients of seemingly lower-order terms in (2.60). But the logarithmic term has precisely the same coefficient $a_{(d)}$ in both (2.65) and (2.60). Since the logarithmic term in (2.21) is multiplied by z^d, only the leading $-\frac{2(d-1)}{\ell^2}\sqrt{|h|}$ term in (2.65) could contribute to any discrepancy. But the first variation of a determinant is a trace, and the trace of the logarithmic coefficient $\bar{\gamma}^{(d)}_{ij}$ vanishes by (2.22).

Thus for d odd (where the log term vanishes) the renormalized action $S_{\rm ren}$ can be expressed in a fully covariant form in terms of the physical metric g; all depen-

dence on the defining function Ω (and so on the choice of conformal frame) has disappeared. We therefore now drop the requirement that any Fefferman-Graham gauge be imposed for odd d. But for even d, the appearance of $\log(\epsilon^2)$ in (2.65) indicates that $S_{\rm ren}$ does in fact depend on the choice of defining function Ω (and thus on the choice of conformal frame). In analogy with quantum field theory, this dependence is known as the conformal anomaly. By replacing ϵ with Ω in (2.65), we could again completely drop the requirement of Fefferman-Graham gauge in favor of making explicit the above dependence on Ω. However, an equivalent procedure is to require that the expansion (2.21) hold up through order $\gamma^{(d)}$ and to replace ϵ in (2.65) by the Fefferman-Graham coordinate z. We will follow this latter approach (which is equivalent to imposing Fefferman-Graham gauge only on the stated terms in the asymptotic expansion) as it is more common in the literature.

We are finally ready to explore variations of $S_{\rm ren}$. Since $S_{\rm ren}$ was constructed by adding only boundary terms to the usual bulk action, we know that $\delta S_{\rm ren}$ must be a pure boundary term on solutions. As before, we will discard boundary terms in the far past and future of M and retain only the boundary term at ∂M. Since ∂M is globally hyperbolic with compact Cauchy surfaces, performing integrations by parts on ∂M will yield boundary terms only in the far past and future of ∂M. Discarding these as well allows us to write

$$\delta S_{\rm ren} = \int_{\partial M} S^{\mu\nu} \delta g_{\mu\nu}, \tag{2.66}$$

for some $S^{\mu\nu}$. But let us now return to Fefferman-Graham gauge and use it to

expand $\delta g_{\mu\nu}$ as in (2.21). Since $S_{\rm ren}$ is finite, $\delta S_{\rm ren}$ must be finite as well. But the leading term in $\delta g_{\mu\nu}$ is of order z^{-2}. So the leading term in $S_{\mu\nu}$ must be of order z^2. It follows that only these leading terms can contribute to (2.66). Since the leading term in $\delta g_{\mu\nu}$ involves $\delta\gamma^{(0)}_{ij}$, we may write

$$\delta S_{\rm ren} = \frac{1}{2}\int_{\partial M} \sqrt{|\gamma^0|}\; T^{ij}_{\rm bndy}\delta\gamma^{(0)}_{ij} \tag{2.67}$$

for some finite so-called boundary stress tensor $T^{ij}_{\rm bndy}$ on ∂M. For odd d, the fact that $S_{\rm ren}$ is invariant under arbitrary changes of conformal frame $\delta\gamma^{(0)}_{ij} = e^{-2\sigma}\gamma^{(0)}_{ij}$ immediately implies that the boundary stress tensor is traceless: $T_{\rm bndy} := \gamma^{(0)}_{ij}T^{ij}_{\rm bndy} = 0$. In even dimensions, the trace is determined by the conformal anomaly of $S_{\rm ren}$ (i.e., by the logarithmic term in either (2.60) or (2.65)) and one finds $T_{\rm bndy} = -\ell^{d-1}a_{(d)}/\kappa$. This result may also be derived by considering the radial version of the Hamiltonian constraint from Chapter 17 of [72] and evaluating this constraint at ∂M.

Comparing with section 2.3.1, it is clear that we may write

$$T^{ij}_{\rm bndy} = \lim_{\epsilon\to 0}\left(\frac{\ell}{\epsilon}\right)^{d+2}\left(\tau^{ij} + \tau^{ij}_{ct}\right), \tag{2.68}$$

where again $\tau_{ij} = \kappa^{-1}(K_{ij} - Kh_{ij})$ and the new term $\tau^{ij}_{\rm ct}$ comes from varying $S_{\rm ct}$. In Fefferman-Graham gauge one finds by explicit calculation that for d odd

$$T^{ij}_{\rm bndy} = \frac{d\ell^{d-1}}{2\kappa}\gamma^{(d)\,ij}. \tag{2.69}$$

For d even there are extra contributions associated with the conformal anomaly,

which are thus all determined by $\gamma^{(0)}$; e.g. (see [96])

$$\text{for } d = 2: \quad T^{ij}_{\text{bndy}} = \frac{\ell}{\kappa}\left(\gamma^{(2)ij} - \mathcal{R}\gamma^{(0)ij}\right) \tag{2.70}$$

$$\text{for } d = 4: \quad T^{ij}_{\text{bndy}} = \frac{2\ell^3}{\kappa}\left[\gamma^{(4)ij} - \frac{1}{8}\left((\gamma^{(2)})^2 - \gamma^{(2)kl}\gamma^{(2)}_{kl}\right)\gamma^{(0)ij} - \frac{1}{2}\gamma^{(2)ik}\gamma^{(2)}{}_k{}^j + \frac{1}{4}\gamma^{(2)}\gamma^{(2)ij} + \frac{3}{2}\bar{\gamma}^{(4)ij}\right], \tag{2.71}$$

where $\gamma^{(2)}$, $\bar{\gamma}^{(4)}$ are given by (2.19), (2.23), (2.24). In all cases, we see that we may use $\gamma^{(0)}_{ij}, T^{ij}_{\text{bndy}}$ to parametrize the free data in the Fefferman-Graham expansion.

The reader should note that the particular value of T^{ij}_{bndy} on a given solution depends on the choice of a representative $\gamma^{(0)}$ and thus on the choice of conformal frame. For d odd this dependence is a simple scaling, though it is more complicated for d even.

But this does not diminish the utility of T^{ij}_{bndy}. For example, we see immediately from (2.67) that S_{ren} defines a good variational principle whenever i) $\gamma^{(0)}$ is fixed as a boundary condition or ii) d is odd, so that T^{ij}_{bndy} is traceless, and we fix only the conformal class of $\gamma^{(0)}$.

We close this section with some brief comments on other possible boundary conditions. We see from (2.67) that S_{ren} is also a good variational principle if we fix $T^{ij}_{\text{bndy}} = 0$. As in section 2.3.2, one may obtain variational principles for more complicated boundary conditions by adding further finite boundary terms to (2.65); see [105] for details. However, just as for scalar fields with $\nu > 1$, boundary conditions that allow $\gamma^{(0)}$ to vary generally lead to ghosts [89] (with the exception that, for d odd no ghosts arise from allowing $\gamma^{(0)}$ to vary by a conformal factor). For this reason we consider below only boundary conditions that fix $\gamma^{(0)}$, or at

least its conformal class for d odd.

2.3.4 Conserved Charges for AlAdS gravity

We are now ready to apply the Brown-York-type procedure discussed in section 2.3.1 to construct conserved charges for AlAdS gravity. The key step is again an argument analogous to (2.52) to show conservation of $T^{ij}_{\rm bndy}$ on ∂M. We give the derivation here in full to highlight various subtleties of the AdS case. We also generalize the result slightly by coupling the AlAdS gravity theory of section 2.3.3 to the scalar theory of section 2.3.2. For definiteness we assume that the boundary conditions fix both $\gamma^{(0)}$ and $\phi^{(0)}$ (up to conformal transformations $(\gamma^{(0)}_{ij}, \phi^{(0)}) \to (e^{-2\sigma}\gamma^{(0)}_{ij}, e^{\Delta_- \sigma}\phi^{(0)})$) for odd d, where the transformation of $\phi^{(0)}$ is dictated by (2.42) and we take ν non-integer so that no log terms arise from the scalar field. However, the more general case is quite similar [88, 105].

We thus consider the action $S_{\rm total} = S_{\rm ren} + S_\phi$. The reader should be aware that, because the counterterms in S_ϕ explicitly depend on the boundary metric $\gamma^{(0)}$, this coupling to matter will change certain formulae in section 2.3.3. In particular, if we now make the natural definition

$$T^{ij}_{\rm bndy} = \frac{2}{\sqrt{|\gamma^{(0)}|}} \frac{\delta S_{\rm total}}{\delta \gamma^{(0)}_{ij}}, \tag{2.72}$$

varying the action under a boundary conformal transformation leads to the more general condition

$$T_{\rm bndy} - \Delta_- \Phi_{\rm bndy} \phi^{(0)} = -\frac{\ell^{d-1} a_{(d)}}{\kappa}, \tag{2.73}$$

which reduces to the trace constraint of section 2.3.3 only for $\Phi_{\rm bndy} = 0$, $\phi^{(0)} = 0$,

or $\Delta_- = 0$. Recall that $\Phi_{\rm bndy}$ is given by (2.58).

The coupling to S_ϕ similarly modifies the divergence condition (2.52) of section 2.3.1. Using the definition (2.72), we find

$$\delta S_{\rm total} = \int_{\partial M} \sqrt{|\gamma^{(0)}|} \left(\frac{1}{2} T^{ij}_{\rm bndy} \delta \gamma^{(0)}_{ij} + \Phi_{\rm bndy} \delta \phi^{(0)} \right). \tag{2.74}$$

Let us consider the particular variation associated with a bulk diffeomorphism ξ. It is sufficient here to consider bulk diffeomorphisms compatible with whatever defining function Ω we have used to write (2.74); i.e., for which $\pounds_\xi \Omega = 0$. As described in section 2.2.5, other diffeomorphisms differ only in that they also induce a change of conformal frame. Since we already extracted the information about $T^{ij}_{\rm bndy}$ (and in particular, about its trace) that can be obtained by changing conformal frame in section 2.3.3, we lose nothing by restricting here to vector fields with $\pounds_\xi \Omega = 0$.

As described in section 2.2.5, we then find $\delta \gamma^{(0)} = \pounds_{\hat{\xi}} \gamma^{(0)}$, $\delta \phi^{(0)} = \pounds_{\hat{\xi}} \phi^{(0)}$, where $\hat{\xi}$ is the vector field induced by ξ on ∂M. Thus (2.74) reads

$$\begin{aligned} \delta_\xi S_{\rm ren} = 0 &= \int_{\partial M} \sqrt{|\gamma^{(0)}|} \left(T^{ij} D_i \hat{\xi}_j + \frac{\delta S_{\rm ren}}{\delta \phi^{(0)}} \pounds_{\hat{\xi}} \phi^{(0)} \right) \\ &= - \int_{\partial M} \sqrt{|\gamma^{(0)}|} \hat{\xi}_j \left(D_i T^{ij} - \Phi_{\rm bndy} D^j \phi^{(0)} \right), \end{aligned} \tag{2.75}$$

where D_i is again the covariant derivative on ∂M compatible with with $\gamma^{(0)}$, all indices are raised and lowered with $\gamma^{(0)}$, and we have dropped the usual surface terms in the far past and future of ∂M. Recalling that all $\hat{\xi}^i$ can arise from bulk vector fields ξ compatible with any given Ω, we see that (2.75) must hold for any

$\hat{\xi}_j$. Thus,

$$D_i T^{ij}_{\rm bndy} = \Phi_{\rm bndy} D^j \phi^{(0)}; \tag{2.76}$$

i.e., $T^{ij}_{\rm bndy}$ is conserved on ∂M up to terms that may be interpreted as scalar sources. These sources are analogous to sources for the stress tensor of, say, a scalar field on a fixed spacetime background when the scalar field is also coupled to some background potential. Here the role of the background potential is played by $\phi^{(0)}$, which we have fixed as a boundary condition. As in section 2.3.1, the divergence condition (2.76) may also be derived from the radial version of the diffeomorphism constraint from Chapter 17 of [72] evaluated on ∂M. For $\phi^{(0)} = 0$ and d odd one immediately arrives at (2.20) using (2.76) and (2.69).

We wish to use (2.76) to derive conservation laws for asymptotic symmetries. Here it is natural to say that a diffeomorphism ξ of M is an asymptotic symmetry if the there is *some* conformal frame in which the induced vector field $\hat{\xi}$ on ∂M is i) a Killing field of $\gamma^{(0)}$ and ii) a solution of $\pounds_{\hat{\xi}} \phi^{(0)} = 0$. Due to the transformations of $\gamma^{(0)}, \phi^{(0)}$ under boundary conformal transformations, this is completely equivalent to first choosing an arbitrary conformal frame and then requiring

$$\pounds_{\hat{\xi}} \gamma^{(0)}_{ij} = -2\sigma \gamma^{(0)}_{ij}, \quad \pounds_{\hat{\xi}} \phi^{(0)} = \Delta_- \sigma \phi^{(0)}. \tag{2.77}$$

The first requirement says that $\hat{\xi}$ is a conformal Killing field of $\gamma^{(0)}_{ij}$ with $\frac{1}{d} D_i \hat{\xi}^i = -\sigma$ and the second says that it acts on $\phi^{(0)}$ like the corresponding infinitesimal conformal transformation.

For even d, we must also preserve the boundary condition that $\gamma^{(0)}$ be fixed

(even including the conformal factor) and the requirement of section 2.3.3 that Fefferman-Graham gauge hold to the first few orders in the asymptotic expansion. An analysis similar to that of section 2.2.5 then shows that we must have $\xi^z = \frac{z}{d} D_i \hat{\xi}^i$ to leading order near ∂M. In particular, for $D_i \hat{\xi}^i \neq 0$ an asymptotic symmetry ξ must be non-compatible with Ω is just the right way to leave $\gamma^{(0)}$ invariant.

As a side comment, we mention that the trivial asymptotic symmetries (the pure gauge transformations) are just those with $\hat{\xi} = 0$. This means that they act trivially on both $T^{ij}_{\rm bndy}$ and $\Phi_{\rm bndy}$ of section 2.3.2, so that both both $T^{ij}_{\rm bndy}$ and the $\Phi_{\rm bndy}$ are gauge invariant. This conclusion is obvious in retrospect as these response functions are functional derivatives of the action with respect to the boundary conditions $\gamma^{(0)}_{ij}$ and $\phi^{(0)}$. Since both the action and any boundary conditions are gauge invariant by definition, so too must be the functional derivatives $T^{ij}_{\rm bndy}$ and $\Phi_{\rm bndy}$.

Returning to our construction of charges, note that for any asymptotic symmetries as above we may compute

$$D_i(T^{ij}_{\rm bndy}\hat{\xi}_j) = -\sigma(T_{\rm bndy} - \Delta_- \Phi_{\rm bndy}\phi^{(0)}) = \sigma \frac{\ell^{d-1} a_{(d)}}{\kappa}, \tag{2.78}$$

where in the final step we have used (2.73).

In analogy with section 2.3.1, we now consider the charges

$$Q[\xi] = -\int_C \sqrt{q}\, n_i T^{ij}_{\rm bndy} \xi_j, \tag{2.79}$$

where C is a Cauchy surface of ∂M, $\sqrt{q}$ is the volume element induced on C by

$\gamma^{(0)}$, and n^i is the unit future pointing normal to C with respect to $\gamma^{(0)}$. It follows from (2.78) that these charges can depend on C only through a term built from the conformal anomaly $a_{(d)}$.

It is now straightforward to construct a modified charge $\tilde{Q}[\xi]$ which is completely independent of C. The essential point here is to recall that $a_{(d)}$ depends only on the boundary metric $\gamma^{(0)}$. Since we have fixed $\gamma^{(0)}$ as a boundary condition, the dependence on C is the same for any two allowed solutions. Thus on a given solution s we need only define

$$\tilde{Q}[\xi](s) = Q[\xi](s) - Q[\xi](s_0), \tag{2.80}$$

where s_0 is an arbitrary reference solution satisfying the same boundary condition and which we use to set the zero-point. The construction (2.80) is sufficiently trivial that one often refers to $Q[\xi]$ itself as being conserved.

Our construction of the charges $Q[\xi]$, $\tilde{Q}[\xi]$ depended on the choice of some conformal frame. But it is easy to see that the charges are in fact independent of this choice for d odd. In that case, the factors $\sqrt{q}$, n_i, and $T^{ij}_{\rm bndy}$ all simply scale under a boundary conformal transformation and dimensional analysis shows that the combination (2.79) is invariant. For even d there are additional terms in the transformation of $T^{ij}_{\rm bndy}$. But as usual these depend only on $\gamma^{(0)}$ so that they cancel between the two terms in (2.80). Thus even in this case for fixed s_0 the charges (2.80) are independent of the conformal frame.

To make the above procedure seem more concrete, we now quickly state results

for the AdS_3 and AdS_4 Schwarzschild solutions

$$ds^2 = -\left(1 - \frac{2c_d GM}{\rho^{d-2}} + \frac{\rho^2}{\ell^2}\right) d\tau^2 + \frac{d\rho^2}{1 - \frac{2c_d GM}{\rho^{d-2}} + \frac{\rho^2}{\ell^2}} + \rho^2 d\Omega^2_{(d-2)}, \tag{2.81}$$

where $c_3 = 1$ and $c_4 = \frac{4}{3\pi}$. The boundary stress tensor may be calculated by converting to Fefferman-Graham coordinates, say for the conformal frame defined by $\Omega = \rho^{-1}$. (Note that the Fefferman-Graham radial coordinate z will agree with ρ only at leading order.) One then finds the energy

$$Q[-\partial_\tau] = \begin{cases} M, & d = 3 \\ M + \dfrac{3\pi\ell^2}{32G}, & d = 4, \end{cases} \tag{2.82}$$

where we remind the reader that energies $E = -Q[\partial_\tau] = Q[-\partial_\tau]$ are conventionally defined in this way with an extra minus sign to make them positive. We see that for $d = 3$ we recover the expected result for the energy of the spacetime. For $d = 4$ we also recover the expected energy up to a perhaps unfamiliar choice of zero-point which we will discuss further in section 2.4.4.

2.3.5 Positivity of the energy in AlAdS gravity

Thus far we have treated all charges $Q[\xi]$ on an equal footing. But when $\hat{\xi}$ is everywhere timelike and future-directed on ∂M, it is natural to call $E = Q[-\xi]$ an *energy* and to wonder if E is bounded below. Such a result was established in chapter 20 for the ADM energy of asymptotically flat spacetimes, and the Witten spinor methods [106, 107] discussed there generalize readily to asymptotically

AdS (AAdS) spacetimes so long as the matter fields satisfy the dominant energy condition and decay sufficiently quickly at ∂M [108]. In particular, this decay condition is satisfied for the scalar field of section 2.3.2 with $m^2 \geq m^2_{BF}$ when $\phi^{(0)}$ is fixed as a boundary condition. Extensions to more general scalar boundary conditions can be found in [109–113]. Here the details of the boundary conditions are important, as boundary conditions for which the W of (2.59) diverges sufficiently strongly in the negative direction tend to make any energy unbounded below (see e.g. [114] for examples). This is to be expected from the fact that, as discussed in section 2.3.2, this W represents an addition to the Lagrangian and thus to any Hamiltonian, even if only as a boundary term. As for $\Lambda = 0$, the above AAdS arguments were inspired by earlier arguments based on quantum supergravity (see [115, 116] for the asymptotically flat case and [83] for the AAdS case).

The above paragraph discussed only AAdS spacetimes. While the techniques described there can also be generalized to many AlAdS settings, it is not possible to proceed in this way for truly general choices of M and ∂M. The issue is that the methods of [106, 107] require one to find a spinor field satisfying a Dirac-type equation subject to certain boundary conditions. But for some $M, \partial M$ one can show that no solution exists. In particular, this obstruction arises when $\partial M = S^1 \times \mathbb{R}^{d-1}$ and the S^1 is contractible in M [117].

The same obstruction also arises with zero cosmological constant in the context of Kaluza-Klein theories (where the boundary conditions may again involve an S^1 that is contractible in the bulk). In that case, the existence of so-called bubbles of nothing demonstrates that the energy is in fact unbounded below and that the system is unstable even in vacuum [118, 119]. But what is interesting about

the AlAdS context with $\partial M = S^1 \times \mathbb{R}^{d-1}$ is that there are good reasons [117] to believe that the energy *is* in fact bounded below – even if there are there are some solutions with energy lower than what one might call empty AdS with $\partial M = S^1 \times \mathbb{R}^{d-1}$ (by which we mean the quotient of the Poincaré patch under some translation of the x^i). Perhaps the strongest such argument (which we will not explain here) comes from AdS/CFT. But another is that [120] identified a candidate lowest-energy solution (called the AdS soliton) which was shown [117] to at least locally minimize the energy. Proving that the AdS soliton is the true minimum of the energy, or falsifying the conjecture, remains an interesting open problem whose solution appears to require new techniques.

2.4 Relation to Hamiltonian Charges

We have shown that the charges (2.80) are conserved and motivated their definition in analogy with familiar constructions for field theory in a fixed curved spacetime. But it is natural to ask whether the charges (2.80) in fact agree with more familiar Hamiltonian definitions of asymptotic charges constructed, say, using the AdS generalization of the Hamiltonian approach described in Chapter 17 of [72]. Denoting these latter charges $H[\xi]$, the short answer is that they agree so long as we choose s_0 in (2.80) to satisfy $H[\xi](s_0) = 0$; i.e., they agree so long as we choose the same (in principle arbitrary) zero-point for each notion of charge. We may equivalently say that the difference $Q[\xi] - H[\xi]$ is the same for all solutions in our phase space, though for conformal charges it may depend on the choice of Cauchy surface C for ∂M. As above, for simplicity we take ∂M to be globally

hyperbolic with compact Cauchy surfaces.

This result may be found by direct computation (see [121] for simple cases). But a more elegant, more general, and more enlightening argument can be given [88] using a covariant version of the Poisson bracket known as the Peierls bracket [122]. The essence of the argument is to show that $Q[\xi]$ generates the canonical transformations associated with the diffeomorphisms ξ. This specifies all Poisson brackets of $Q[\xi]$ to be those of $H[\xi]$. Thus $Q[\xi] - H[\xi]$ must be a c-number in the sense that all Poisson brackets vanish. But this means that it is constant over the phase space.

After pausing to introduce the Peierls bracket, we sketch this argument below following [88]. As in section 2.3.4, we suppose for simplicity that the only bulk fields are the metric and a single scalar field with non-integer ν and we impose boundary conditions that fix both $\gamma_{ij}^{(0)}$ and $\phi^{(0)}$. However, the argument for general bulk fields is quite similar [88]. While this material represents a certain aside from our main discussion, it will provide insight into the algebraic properties of conserved charges, the stress tensor itself, and a more general notion of so-called boundary observables that we will shortly discuss.

2.4.1 The Peierls bracket

The Peierls bracket is a Lie bracket operation that acts on gauge-invariant functions on the space of solutions $\mathcal{S}$ of some theory. As shown in the original work [122], this operation is equivalent to the Poisson bracket under the natural identification of the phase space with the space of solutions. However, the Peierls bracket is *manifestly* spacetime covariant. In particular, one may directly define

the Peierls bracket between any two quantities A and B located anywhere in spacetime, whether or not they may be thought of as lying on the same Cauchy surface. In fact, both A and B can be highly non-local, extending over large regions of space and time. These features make the Peierls bracket ideal for studying the boundary stress-tensor, which is well-defined on the space of solutions but is not a local function in the bulk spacetime.

To begin, consider two functions A and B on $\mathcal{S}$, which are in fact defined as functions on a larger space $\mathcal{H}$, which we call the space of histories. This space $\mathcal{H}$ is the one on which the action is defined; i.e., the solution space $\mathcal{S}$ consists of those histories in $\mathcal{H}$ on which the action S is stationary. One may show that the Peierls bracket on $\mathcal{S}$ depends only on A, B on $\mathcal{S}$ and not on their extensions to $\mathcal{H}$.

The Peierls bracket is defined by considering the effect on one gauge invariant function (say, B) when the action is deformed by a term proportional to another such function (A). One defines the advanced ($D_A^+ B$) and retarded ($D_A^- B$) effects of A on B by comparing the original system with a new system given by the action $S_\epsilon = S + \epsilon A$, but associated with the same space of histories $\mathcal{H}$. Here ϵ is a real parameter which will soon be taken to be infinitesimal, and the new action is associated with a new space $\mathcal{S}_\epsilon$ of deformed solutions.

Under retarded (advanced) boundary conditions for which the solutions $s \in \mathcal{S}$ and $s_\epsilon \in \mathcal{S}_\epsilon$ coincide in the past (future) of the support of A, the quantity $B_0 = B(s)$ computed using the undeformed solution s will in general differ from $B_\epsilon^\pm = B(s_\epsilon)$ computed using s_ϵ and retarded ($-$) or advanced ($+$) boundary conditions (see Fig. 2.4). For small epsilon, the difference between these quantities

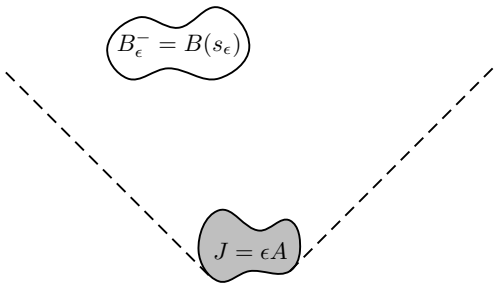

Figure 2.4: An illustration of the definition of B_ϵ^-. A source term $J = \epsilon A$ is added to the action and the gauge invariant function B is calculated for the deformed solution s_ϵ subject to the boundary conditions that s and s_ϵ coincide in the far past. Dashed lines indicate the boundary of the causal future of J. Only functions B which have support in this region can have $B(s_\epsilon) \neq B(s)$. For visual clarity we have chosen our gauge invariant function A and B to have compact support though this is not required.

defines the retarded (advanced) effect $D_A^- B$ ($D_A^+ B$) of A on B through:

$$D_A^\pm B = \lim_{\epsilon \to 0} \frac{1}{\epsilon}(B_\epsilon^\pm - B_0), \tag{2.83}$$

which is a function of the unperturbed solution s. Similarly, one defines $D_B^\pm A$ by reversing the roles of A and B above. Since A, B are gauge invariant, $D_B^\pm A$ is a well-defined (and again gauge-invariant) function on the space $\mathcal{S}$ of solutions so long as both A and B are first-differentiable on $\mathcal{H}$. This requirement may be subtle if the spacetime supports of A and B extend into the far past and future, but is straightforward for objects like $T^{ij}_{\rm bndy}(x)$, $\Phi_{\rm bndy}(x)$ that are well-localized in time.

The Peierls bracket [122] is then defined to be the difference of the advanced and retarded effects:

$$\{A, B\} = D_A^+ B - D_A^- B. \tag{2.84}$$

As shown in [122], this operation agrees with the Poisson bracket (suitably generalized to allow A, B at unequal times). This generalizes the familiar result that the commutator function for a free scalar field is given by the difference between the advanced and retarded Green's functions. In fact, it is enlightening to write the Peierls bracket more generally in terms of such Green's functions. To do so, let us briefly introduce the notation ϕ^I for a complete set of bulk fields (including the components of the bulk metric) and the associated advanced and retarded Green's functions $G^{\pm}_{IJ}(x, x')$. Note that we have

$$D^+_A B = \int dx\ dx' \frac{\delta B}{\delta \Phi^I(x)} G^+_{IJ}(x, x') \frac{\delta A}{\delta \Phi^J(x')} = \int dx\ dx' \frac{\delta B}{\delta \phi^j(x')} G^-_{JI}(x', x) \frac{\delta A}{\delta \phi^j(x)} = D^-_B A, \quad (2.85)$$

where we have used the identity $G^+_{IJ}(x, x') = G^-_{JI}(x', x)$. Thus, the Peierls bracket may also be written in the manifestly antisymmetric form

$$\{A, B\} = D^-_B A - D^-_A B = D^+_A B - D^+_B A. \quad (2.86)$$

The expressions (2.85) in terms of $G^{\pm}_{IJ}(x, x')$ are also useful in order to verify that the Peierls bracket defines a Lie-Poisson algebra. In particular, the derivation property $\{A, BC\} = \{A, B\}C + \{A, C\}B$ follows immediately from the Leibnitz rule for functional derivatives. The Jacobi identity also follows by a straightforward calculation, making use of the fact that functional derivatives of the action commute (see e.g., [123, 124]). If one desires, one may use related Green's function techniques to extend the Peierls bracket to a Lie algebra of gauge dependent

quantities [125].

2.4.2 Main Argument

We wish to show that the charges $Q[\xi]$ generate the appropriate asymptotic symmetry for any asymptotic Killing field ξ. Since this is true by definition for any Hamiltonian charge $H[\xi]$, it will then follow that $Q[\xi] - H[\xi]$ is constant over the space of solutions $\mathcal{S}$. We first address the case where ξ is compatible with Ω, and then proceed to the more general case where $\hat{\xi}$ acts only as a conformal Killing field on the boundary.

Showing that $Q[\xi]$ generates diffeomorphisms along ξ amounts to proving a certain version of Noether's theorem. Recall that the proof of Noether's theorem involves examining the change in the action under a spacetime-dependent generalization of the desired symmetry. The structure of our argument below is similar, where we consider both the action of a given asymptotic symmetry ξ and the spacetime-dependent generalization $f\xi$ defined by choosing an appropriate scalar function f on M. It turns out to be useful to choose f on M (with restriction $\hat{f}$ to ∂M) such that

- $f = 0$ in the far past and $f = 1$ in the far future.
- $\hat{f} = 0$ to the past of some Cauchy surface C_0 of ∂M, and $\hat{f} = 1$ to the future of some Cauchy surface C_1 of ∂M.

Suppose now that ξ is an asymptotic symmetry compatible with Ω. Then the

bulk and boundary fields transform as

$$\delta\phi = \pounds_\xi \phi, \quad \delta g_{\mu\nu} = \pounds_\xi g_{\mu\nu}, \quad \delta\gamma^{(0)}_{ij} = \pounds_{\hat{\xi}} \gamma^{(0)}_{ij} = 0, \quad \text{and} \quad \delta\phi^{(0)} = \pounds_{\hat{\xi}} \phi^{(0)} = 0. \tag{2.87}$$

The key step of the argument is to construct a new transformation $\Delta_{f,\xi}$ on the space of fields such that the associated first order change $\Delta_{f,\xi} S$ in the action generates the asymptotic symmetry $-\xi$. We will first show that the above property turns out to hold for

$$\Delta_{f,\xi} := (\pounds_{f\xi} - f\pounds_\xi), \tag{2.88}$$

and then verify that $\Delta_{f,\xi} S = -Q[\xi]$. The form of $\Delta_{f,\xi} S$ is essentially that suggested in [126] using Hamilton-Jacobi methods, so our argument will also connect $Q[\xi]$ with [126].

An important property of (2.88) is that the changes $\Delta_{f,\xi} g_{\mu\nu}$ and $\Delta_{f,\xi}\phi$ are *algebraic* in ϕ and $g_{\mu\nu}$; i.e., we need not take spacetime derivatives of $g_{\mu\nu}, \phi$ to compute the action of $\Delta_{f,\xi}$. Furthermore, $\Delta_{f,\xi}\phi$ and $\Delta_{f,\xi} g_{\mu\nu}$ are both proportional to $\nabla_a f$, and so vanish in both the far future and the far past. This guarantees that $\Delta_{f,\xi} S$ is a differentiable function on $\mathcal{H}$. In particular, solutions to the equations of motion resulting from the deformed action $S + \epsilon\Delta_{f,\xi} S$ are indeed stationary points of $S + \epsilon\Delta_{f,\xi} S$ under all variations which preserve the conditions and vanish in the far future and past.

It is important to note that the quantity $\Delta_{f,\xi} S$ is gauge-invariant when the equations of motion hold. This is easy to see since by definition on $\mathcal{S}$ all variations of S become pure boundary terms. Boundary terms in the far past and future vanish due to the observations above, and since $\gamma^{(0)}_{ij}, \phi^{(0)}$ are fixed by boundary

conditions the boundary terms on ∂M depend on the bulk fields only through the gauge invariant quantities $T^{ij}_{\rm bndy}$ and $\Phi_{\rm bndy}$. Thus, we may take the Peierls bracket of $\Delta_{f,\xi}S$ with any other observable A.

We proceed by considering the modified action

$$\tilde{S}[\phi, g_{\mu\nu}] = S[\phi, g_{\mu\nu}] + \epsilon\Delta_{f,\xi}S[\phi, g_{\mu\nu}] = S[\phi + \epsilon\Delta_{f,\xi}\phi, g_{\mu\nu} + \epsilon\Delta_{f,\xi}g_{\mu\nu}], \qquad (2.89)$$

where the last equality holds to first order in ϵ (and in fact defines $\Delta_{f,\xi}S[\phi, g_{\mu\nu}]$). Since $\tilde{S}$ is just S with its argument shifted by $\epsilon\Delta_{f,\xi}$, the stationary points s_1 of $\tilde{S}$ are precisely the oppositely-shifted versions of the stationary points s of S; i.e., we may write $s_1 = (1 - \epsilon\Delta_{f,\xi})s$ for some $s \in \mathcal{S}$.

We should of course ask if s_1 satisfies the desired boundary conditions on ∂M. Since ξ is compatible with Ω, the boundary fields shift in the same way as their bulk counterparts; i.e., those of s_1 have been shifted by $-\epsilon\Delta_{f,\xi}$ relative to those of s. Since ξ is an asymptotic symmetry, its action preserves the boundary fields. Now, the reader will note that there is a non-trivial effect from the $\pounds_{f\xi}$ term in $\Delta_{f,\xi}$. But this term is a pure diffeomorphism, and since all boundary terms are covariant on ∂M the action $\tilde{S}$ is invariant under *all* diffeomorphisms compatible with Ω (i.e., which preserve the given conformal frame), even those that act non-trivially on the boundary. So the history

$$s_2 = (1 + \epsilon\pounds_{f\xi})s_1 = (1 + \epsilon f\pounds_{\xi})s \qquad (2.90)$$

has

$$\phi^{(0)}|_{s_2} = \phi^{(0)}|_s, \quad g_{\mu\nu}|_{s_2} = g_{\mu\nu}|_s, \qquad (2.91)$$

and again solves the equations of motion that follow from $\tilde{S}$.

This observation allows a straightforward computation of the advanced and retarded changes $D^{\pm}_{\Delta_{f,\xi}S}A$ for any gauge invariant quantity A. We first consider the retarded change evaluated on a solution s as above. We require a solution s^-_ϵ of the perturbed equations of motion which agrees with s in the far past. Since the infinitesimal transformation $f\pounds_\xi$ vanishes in the far past, we may set $s^-_\epsilon = s_2$ as defined (2.90) above; i.e. $s^-_\epsilon = (1+\epsilon f\pounds_\xi)s$. Thus, the retarded effect on A is just $D^-_{\Delta_{f,\xi}S}A = f\pounds_\xi A$.

To compute the advanced effect, we must find a solution s^+_ϵ of the perturbed equations of motion which agrees with s in the far future. Consider the history $s^+_\epsilon = (1-\epsilon\pounds_\xi)s^-_\epsilon = (1+(f-1)\epsilon\pounds_\xi)s$. Since this differs from s^-_ϵ by the action of a symmetry compatible with Ω, it again solves the desired equations of motion (to first order in ϵ) and induces the required boundary fields (2.91). In addition, s^+_ϵ and s agree in the far future (where $f=1$). Thus, we may use s^+_ϵ to compute the advanced change in any gauge invariant A:

$$D^+_{\Delta_{f,\xi}S}A = (f-1)\pounds_\xi A. \tag{2.92}$$

Finally, we arrive at the Peierls bracket

$$\{\Delta_{f,\xi}S, A\} = D^+_{\Delta_{f,\xi}S}A - D^-_{\Delta_{f,\xi}S}A = -\pounds_\xi A. \tag{2.93}$$

As desired $-\Delta_{f,\xi}S$ generates a diffeomorphism along the asymptotic symmetry ξ as desired.

All that remains is to relate $\Delta_{f,\xi}S$ to $Q[\xi]$. But this is straightforward. Since

f vanishes in the far past and future we have

$$\Delta_{f,\xi} S = \int_M \left(\frac{\delta S}{\delta \phi} \Delta_{f,\xi} \phi + \frac{\delta S}{\delta g_{\mu\nu}} \Delta_{f,\xi} g_{\mu\nu} \right) + \frac{1}{2} \int_{\partial M} \sqrt{\gamma^{(0)}}\, T^{ij}_{\rm bndy} \Delta_{f,\xi} \gamma^{(0)}_{ij} + \int_{\partial M} \sqrt{\gamma^{(0)}}\, \Phi_{\rm bndy} \Delta_{f,\xi} \phi^{(0)}. \quad (2.94)$$

But the bulk term vanishes on solutions $s \in \mathcal{S}$, and from (2.87) we find $\Delta_{f,\xi}\phi^{(0)} = (\pounds_{\hat{f}\hat{\xi}} - \hat{f}\pounds_{\hat{\xi}})\phi^{(0)} = 0$. So only the term containing $T^{ij}_{\rm bndy}$ contributes to (2.94).

To compute the remaining term note that

$$\Delta_{f,\xi} \gamma^{(0)}_{ij} = (\pounds_{\hat{f}\hat{\xi}} - \hat{f}\pounds_{\hat{\xi}})\gamma^{(0)}_{ij} = \hat{\xi}_i \partial_j \hat{f} + \hat{\xi}_j \partial_i \hat{f}. \quad (2.95)$$

Since (2.95) vanishes when f is constant, we may restrict the integral over ∂M to the region V between C_0 and C_1 and use the symmetry $T^{ij}_{\rm bndy} = T^{ji}_{\rm bndy}$ to obtain

$$\begin{aligned} \Delta_{f,\xi} S = &= \int_V \sqrt{|\gamma^{(0)}|} T^{ij}_{\rm bndy} \xi_i \partial_j f \\ &= \int_{C_1} \sqrt{q}\, n_j T^{ij}_{\rm bndy} \xi_i - \int_V \sqrt{|\gamma^{(0)}|} f D_i \left(T^{ij}_{\rm bndy} \xi_j \right) \\ &= -Q_{C_1}[\xi]. \end{aligned} \quad (2.96)$$

Here we used the fact that $\hat{f} = 0$ on C_0 to drop contributions from C_0 and the fact that that $\hat{\xi}$ is a Killing field of the boundary metric along with (2.78) to show that the $\int_V$ term in the second line vanishes.

Thus, $-\Delta_{f,\xi} S$ agrees (on solutions) with the charge $Q[\xi]$ evaluated on the cut C_1. Since $Q[\xi]$ is conserved, this equality also holds on any other cut of ∂M. Having already shown by eq. (2.93) that the variation $\Delta_{f,\xi} S$ generates the action

of the infinitesimal symmetry $-\xi$ on observables, it follows that $Q[\xi]$ generates the action of ξ:

$$\{Q[\xi], A\} = \pounds_\xi A, \tag{2.97}$$

as desired.

2.4.3 Asymptotic Symmetries not compatible with Ω

We now generalize the argument to asymptotic symmetries ξ that are *not* compatible with Ω, so that $\hat{\xi}$ satisfies (2.77). The field content and boundary conditions are the same as above. But the non-trivial action of ξ on Ω means that there are now are additional terms when a diffeomorphism acts on the boundary fields $\phi^{(0)}, \gamma_{ij}^{(0)}$:

$$\delta_{\pounds_{f\xi}}\phi^{(0)} = \pounds_{\hat{f}\hat{\xi}}\phi^{(0)} - \Delta_- \hat{f}\sigma\phi^{(0)}, \quad \delta_{\pounds_{f\xi}}\gamma_{ij}^{(0)} = \pounds_{\hat{f}\hat{\xi}}\gamma_{ij}^{(0)} + 2\hat{f}\sigma\gamma_{ij}^{(0)}. \tag{2.98}$$

Combining (2.77) and (2.98) we see that $\delta_{\pounds_\xi}$ acts trivially on the boundary data $\gamma_{ij}^{(0)}, \phi^{(0)}$, as it must since asymptotic symmetries were defined to leave the boundary conditions invariant. Thus the histories $s_\epsilon^\pm$ identified above (see, e.g., (2.90)) again satisfy the same boundary conditions as s.

In contrast to section 2.4.2 the operation $\pounds_{f\xi}$ now acts non-trivially on Ω and thus on S. But since this is only through the conformal anomaly term $a_{(d)}$ in (2.65), $\pounds_{f\xi}S$ depends only on the boundary metric $\gamma^{(0)}$ and is otherwise constant on $\mathcal{H}$. So the equations of motion are unchanged and the histories $s_\epsilon^\pm$ again solve the equations of motion for $\tilde{S}$.

It remains to repeat the analogue of the calculation (2.96). But here the only change is that the $\int_V$ term on the second line no longer vanishes. Instead, it contributes a term proportional to $a_{(d)}$. Since this term is constant on the space of solutions $\mathcal{S}$, it has vanishing Peierls brackets and we again conclude that $Q_{C_1}[\xi]$ generates the asymptotic symmetry ξ. (This comment corrects a minor error in [125].) And since $Q_C[\xi]$ depends on the Cauchy surface C only through a term that is constant on $\mathcal{S}$, the same result holds for any C. Thus, even when $\hat{\xi}$ is only a conformal symmetry of the boundary, $Q_C[\xi] - H[\xi]$ is constant over the space $\mathcal{S}$ of solutions.

2.4.4 Charge algebras and central charges

We saw above that our charges $Q[\xi]$ generate the desired asymptotic symmetries via the Peierls bracket. This immediately implies what is often called the *representation theorem*, that the algebra of the charges themselves matches that of the associated symmetries up to possible so-called central extensions. This point is really quite simple. Consider three vector field ξ_1, ξ_2, ξ_3 related via the Lie bracket through $\{\xi_1, \xi_2\} = \xi_3$. Now examine the Jacobi identity

$$\{Q[\xi_1], \{Q[\xi_2], A\}\} + \{Q[\xi_2], \{A, Q[\xi_1]\}\} + \{A, \{Q[\xi_1], Q[\xi_2]\}\} = 0 \qquad (2.99)$$

which must hold for any A. Since $\{Q[\xi_i], B\} = \pounds_{\xi_i} B$ for any B, we may use (2.99) to write

$$\pounds_{\xi_3} A = \pounds_{\xi_1} (\pounds_{\xi_2} A) - \pounds_{\xi_2} (\pounds_{\xi_1} A) = \{\{Q[\xi_2], Q[\xi_1]\}, A\}. \tag{2.100}$$

But the left-hand-side is also $\{Q[\xi_3], A\}$. So we conclude that $\{Q[\xi_1], Q[\xi_2]\}$ generates the same transformation as $Q[\xi_3]$. This means that they can differ only by some $K(\xi_1, \xi_2)$ which is constant across the space of solutions (i.e., it is a so-called c-number):

$$\{Q[\xi_1], Q[\xi_2]\} = Q[\{\xi_1, \xi_2\}] + K(\xi_1, \xi_2). \tag{2.101}$$

For some symmetry algebras one can show that any such $K(\xi_i, \xi_j)$ can be removed by shifting the zero-points of the charges $Q[\xi]$. In such cases the $K(\xi_i, \xi_j)$ are said to be trivial. Non-trivial $K(\xi_i, \xi_j)$ are classified by a cohomology problem and are said to represent central extensions of the symmetry algebra.

It is easy to show that $K(\xi_i, \xi_j)$ may be set to zero in this way whenever there is some solution (call it s_0) which is invariant under all symmetries. The fact that it is invariant means that $\{Q[\xi_i], A\}(s_0) = 0$; i.e., the bracket vanishes when evaluated on the particular solution s_0 for any ξ_i and any A. So take $A = Q[\xi_j]$, and set the zero-points of the charges so that $Q[\xi](s_0) = 0$. Evaluating (2.101) on s_0 then gives $K(\xi_i, \xi_j)(s_0) = 0$ for all ξ. But since $K(\xi_i, \xi_j)(s_0)$ is constant over the space of solutions this means that it vanishes identically.

For asymptotically flat spacetimes the asymptotic symmetries generate the Poincaré group, which are just the exact symmetries of Minkowski space. Thus one might expect the asymptotic symmetries of $(d+1)$-dimensional AlAdS space-

times to be (perhaps a subgroup of) $SO(d,2)$ in agreement with the isometries of AdS_{d+1} compatible with the boundary conditions on ∂M. Since (at least when it is allowed by the boundary conditions) empty AdS_{d+1} is a solution invariant under all symmetries one might expect that the corresponding central extensions are trivial.

This turns out to be true for $d > 2$. Indeed, any Killing field of AdS_{d+1} automatically satisfies our definition of an asymptotic symmetry (at least for boundary conditions $\phi^{(0)} = 0$ and $\gamma^{(0)}_{ij}$ the metric on the Einstein static universe). But for $d = 2$ there are additional asymptotic Killing fields that are not Killing fields of empty AdS_3. This is because all $d = 2$ boundary metrics $\gamma^{(0)}_{ij}$ take the form $ds^2 = g_{uv}dudv$ when written in terms of null coordinates, making manifest that any vector field $\hat{\xi}^u = f(u)$, $\hat{\xi}^v = g(v)$ is a conformal Killing field of $\gamma^{(0)}_{ij}$. This leads to an infinite-dimensional asymptotic symmetry group, which is clearly much larger than the group $SO(2,2)$ of isometries of AdS_3.

Thus as first noted in [86] there can be a non-trivial central extension for $d = 2$. In this case, one can show that up to the above-mentioned zero-point shifts all central extensions are parametrized by a single number c called the central charge. (When parity symmetry is broken, there can be separate left and right central charges c_L, c_R.) Ref [86] calculated this central charge using Hamiltonian methods, but we will follow [104] and work directly with the boundary stress tensor.

Since the charges $Q[\xi]$ generate (bulk) diffeomorphisms along ξ, and since the charges themselves are built from T^{ij}_{bndy}, the entire effect is captured by computing the action of a bulk diffeomorphism ξ on T^{ij}_{bndy}. As noted in section 2.2.5, the

action of ξ on boundary quantities generally involves both a diffeomorphism $\hat{\xi}$ along the boundary and a change of conformal frame. And as we have seen, for even d changes of conformal frame act non-trivially on T^{ij}_{bndy}. For $g_{uv} = -1$ a direct calculation gives

$$\begin{aligned} T_{\text{bndy } uu} &\to T_{\text{bndy } uu} + (2T_{\text{bndy } uu}\partial_u\xi^u + \xi^u\partial_u T_{\text{bndy } uu}) - \frac{c}{24\pi}\partial_u^3\xi^u \\ T_{\text{bndy } vv} &\to T_{\text{bndy } vv} + (2T_{\text{bndy } vv}\partial_v\xi^v + \xi^v\partial_v T_{\text{bndy } vv}) - \frac{c}{24\pi}\partial_v^3\xi^v, \end{aligned} \tag{2.102}$$

where $c = 3\ell/2G$. The term in parenthesis is the tensorial part of the transformation while the final (so called anomalous) term is associated with the conformal anomaly $a_{(2)} = -(c/24\pi)\mathcal{R}$.

It is traditional to Fourier transform the above components of the stress tensor to write the charge algebra as the (double) Virasoro algebra

$$i\{L_m, L_n\} = (m-n)L_{m+n} + \frac{c}{12}m(m^2-1)\delta_{m+n,0}, \tag{2.103}$$

$$i\{\bar{L}_m, \bar{L}_n\} = (m-n)\bar{L}_{m+n} + \frac{c}{12}m(m^2-1)\delta_{m+n,0}, \tag{2.104}$$

where $\{L_n, \bar{L}_m\} = 0$ and

$$L_n = -\frac{1}{2\pi}\int_{S^1} e^{iun}T_{\text{bndy } uu}du, \quad \bar{L}_n = -\frac{1}{2\pi}\int_{S^1} e^{ivn}T_{\text{bndy } vv}dv. \tag{2.105}$$

Here we have take $\partial M = S^1 \times \mathbb{R}$ so that the dynamics requires both T_{uu} and T_{vv} to be periodic functions of their arguments. We have taken this period to be 2π.

The anomalous transformation of T^{ij}_{bndy} leads to interesting zero-points for certain charges. Suppose for example we take T^{ij}_{bndy} to vanish for the Poincaré patch

of empty AdS_3 in the conformal frame where the boundary metric is (uncompactified) Minkowski space. Then since $S^1 \times \mathbb{R}$ is (locally) conformal to Minkowski space, we can use the conformal anomaly to calculate T^{ij}_{bndy} for empty AdS_3 with Einstein static universe boundary metric. One finds that the resulting energy does not vanish. Instead, $E_{\text{global AdS}_3} = -c/12\ell = -1/8G$ so that $E = 0$ for the so-called $M = 0$ Bañados-Teitelboim-Zanelli (BTZ) black hole [127, 128]. The offset in (2.82) arises from similarly setting $T^{ij}_{\text{bndy}} = 0$ for empty AdS_5 in the conformal frame where the boundary metric is (uncompactified) Minkowski space.

2.5 The algebra of boundary observables and the AdS/CFT correspondence

We have shown above how the boundary stress tensor can be used to construct charges $Q[\xi]$ associated with any asymptotic symmetry ξ of a theory of asymptotically locally anti-de Sitter spacetimes. The $Q[\xi]$ are conserved (perhaps, up to c-number anomaly terms) and generate the asymptotic symmetry ξ under the action of the Peierls bracket (or equivalently, under the Poisson bracket). Therefore the $Q[\xi]$ are equivalent to the Hamiltonian charges that we could derive using techniques analogous to those described in Chapter 17 of [72] for asymptotically flat spacetimes. Conversely, boundary stress tensor methods can also be applied in the asymptotically flat context [129–131]. Readers interested in direct Hamiltonian approaches to AdS charges should consult [84–86]; see also [83, 91, 92, 132–135] for other covariant approaches.

We chose to use boundary stress tensor methods for two closely related reasons.

The first is that, in addition to its role in constructing conserved charges, the local boundary field $T^{ij}_{\rm bndy}$ turns out to contain useful information on its own. For example, it plays a key role in the hydrodynamic description of large AdS black holes known as the fluid/gravity correspondence [64] (which may be considered a modern incarnation of the so-called membrane paradigm [136]). The extra information in $T^{ij}_{\rm bndy}$ appears at the AdS boundary ∂M due to the fact that all multipole moments of a given field decay near ∂M with the same power law; namely, the one given by the $\gamma^{(d)}$ term in the Fefferman-Graham expansion (2.21). This is in striking contrast with the more familiar situation in asymptotically flat spacetimes where the large r behavior is dominated by the monopole terms, with sub-leading corrections from the dipole and higher order multipoles. Indeed, while as noted above similar boundary stress tensor techniques can be employed in asymptotically flat spacetimes, the asymptotically flat boundary stress tensor contains far less information.

The second reason is that both $T^{ij}_{\rm bndy}$ and $\Phi_{\rm bndy}$ play fundamental roles in the AdS/CFT correspondence [19] (see especially [20]). Any treatment of asymptotic AdS charges would be remiss without at least mentioning this connection, and we take the opportunity below to give a brief introduction to AdS/CFT from the gravity side. This turns out to be straightforward using the machinery described thus far. Indeed, the general framework requires no further input from either string theory or conformal field theory and should be readily accessible to all readers of this volume. As usual, we consider bulk gravity coupled to a single bulk scalar and fix both $\gamma^{(0)}_{ij}$ and $\phi^{(0)}$ as boundary conditions. We refer to $\gamma^{(0)}_{ij}$ and $\phi^{(0)}$ as boundary sources below. More general boundary conditions may be

thought of as being dual to CFTs with additional interactions [137] or coupled to additional dynamical fields [105, 138, 139], though we will not go into the details here.

The only new concept we require is that of the the algebra $\mathcal{A}_{\rm bndy}$ of boundary observables, which is just the algebra generated by $T^{ij}_{\rm bndy}$ and $\Phi_{\rm bndy}$ under the Peierls bracket. Here we mean that we consider the smallest algebra containing both $T^{ij}_{\rm bndy}$ and $\Phi_{\rm bndy}$ which is closed under finite flows; i.e., under the classical analogue of the quantum operation $e^{iA}Be^{-iA}$. A key property of $\mathcal{A}_{\rm bndy}$ follows from the fact that the bulk equations of motion are completely independent of the choice of conformal frame Ω. Thus, up to the usual conformal anomalies, under any change of conformal frame the boundary observables transform only by rescaling with a particular power of $e^{-\sigma}$ known as the conformal dimension (d for $T^{ij}_{\rm bndy}$, and Δ_+ for $\Phi_{\rm bndy}$), with the boundary sources transforming similarly with conformal weights zero for $\gamma^{(0)}_{ij}$ and Δ_- for $\phi^{(0)}$. (In defining the conformal dimension it is conventional not to count the ± 2 powers of $e^{-\sigma}$ associated with the indices on $T^{ij}_{\rm bndy}$ and $\gamma^{(0)}_{ij}$.) In this sense the theory of $\mathcal{A}_{\rm bndy}$ is invariant (or, perhaps better, covariant) under all changes of boundary conformal frame. Of course we have already shown that when the boundary observables admit a conformal Killing field $\hat{\xi}$, the corresponding transformation is generated by the associated $Q[\xi]$ from (2.79). Now since the charges $Q[\xi]$ are built from $T^{ij}_{\rm bndy}$ and $\Phi_{\rm bndy}$ they also lie in the algebra $\mathcal{A}_{\rm bndy}$. When $\hat{\xi}$ can be chosen to be everywhere timelike, this immediately implies that $\mathcal{A}_{\rm bndy}$ is also closed under time evolution. This last property can also be shown much more generally; see e.g. [140].

We now extract one final property of the algebra $\mathcal{A}_{\rm bndy}$. From the expression

(2.85) in terms of Green's functions, it is clear that the Peierls bracket $\{A, B\}$ of two observables vanishes on any solution s for which A, B are outside each other's light cones; i.e., when the regions on which A, B are supported cannot be connected by any causal curve. Furthermore, as shown in [141] the null energy condition implies that two boundary points x, y can be connected by a causal curve through the bulk only when they can also be connected by a causal curve lying entirely in the boundary. It follows that the algebra $\mathcal{A}_{\rm bndy}$ satisfies the usual definition of locality for a field theory on ∂M; namely that Peierls brackets vanish outside the light cones defined by the boundary metric $\gamma^{(0)}_{ij}$.

Though we have so far worked entirely at the classical level, let us now assume that all of the above properties persist in the quantum theory. We then have a conformally covariant algebra of operators $\mathcal{A}_{\rm bndy}$ with closed dynamics, local commutation relations on ∂M, and a stress tensor $T^{ij}_{\rm bndy}$ that generates all conformal symmetries. In other words, we have a local conformal field theory on ∂M.

This is the most basic statement of the AdS/CFT correspondence. *Any* bulk AlAdS quantum gravity theory in which the above classical properties continue to hold defines a conformal field theory (CFT) through its algebra $\mathcal{A}_{\rm bndy}$ of boundary observables. Now, we should remark that the AdS/CFT correspondence as used in string theory goes one step further. For certain specific bulk theories it identifies the so-called dual CFT as a particular known theory defined by its own Lagrangian with a definite field content. For example, when the bulk is type IIB string theory asymptotic to a certain $\mathrm{AdS}_5 \times S^5$ solution, the corresponding CFT is just $\mathcal{N} = 4$ super-Yang-Mills. We will not go into further details here, though the interested reader may consult various reviews such as [21–23].

On the other hand, even without having a separate definition of the CFT, the above observations already have dramatic implications for the bulk quantum gravity theory. In particular, the statement that $\mathcal{A}_{\rm bndy}$ is closed under time evolution runs completely counter to one's usual intuition regarding field theory with a boundary. We usually think that most of the dynamical degrees of freedom live in the bulk spacetime, with perhaps only a small subset visible on the boundary at any time. In particular, we expect any signal present on the boundary at time t_0 to then propagate into the bulk and (at least for some time) to essentially disappear from the algebra of boundary observables. Since $\mathcal{A}_{\rm bndy}$ is closed under time evolution, it is clear that this is simply not the case in our quantum gravity theory. The difference arises precisely from the fact that the gravitational Hamiltonian (and more generally any $Q[\xi]$) is a pure boundary term. This property was called *boundary unitarity* in [140]. See also [142] for further discussion of this point.

The reader should take care to separate boundary unitarity from the possible claim that $\mathcal{A}_{\rm bndy}$ captures the complete set of bulk observables. The two ideas are logically separate, as there can in principle be additional bulk observables $\mathcal{A}_{\rm other}$ so long as they do not mix dynamically with those in $\mathcal{A}_{\rm bndy}$. One says that the possible values of $\mathcal{A}_{\rm other}$ define superselection sectors with respect to $\mathcal{A}_{\rm bndy}$ [143]. But any such additional observables are clearly very special. The requirement that they not affect $\mathcal{A}_{\rm bndy}$ strongly suggests that at least semi-classically such observables have to do only with properties of spacetime hidden from the boundary behind both past and future horizons [144]. In particular, any degrees of freedom that determine whether black holes are connected by (non-traversable) wormholes seem likely to lie in $\mathcal{A}_{\rm other}$. On the other hand, in perturbation theory about empty

AdS (or even about solutions that are empty AdS in the far past) one may show that $\mathcal{A}_{\text{other}}$ is indeed empty [140].

Part I

Holographic Heat Flows

Chapter 3

Flowing Funnels: the AdS_3 Dual of CFT_2 Hawking Radiation

3.1 Introduction

The study of field theories far from equilibrium is a classic problem of long-standing interest. While much can be learned from perturbation theory, more complete results are difficult to obtain. As is by now well known, gauge/gravity duality can be a useful tool to study non-perturbative effects. There has thus been significant interest in using this framework to study plasmas with strong time dependence and the approach to thermalization (see e.g. [145–147] for recent examples and further references), though it has mostly been used to study the equilibrium properties of field theories, or perhaps small perturbations away from equilibrium. Below, we use this duality to study heat transport far from equilibrium in a strongly coupled large N CFT.

We are interested in particular in the response of the field theory when coupled to heat sources or sinks at finite locations. For the purposes of this section, we consider a field theory in d spacetime dimensions. A convenient way to introduce such sources is to place the CFT on a background non-dynamical spacetime containing black holes with surface gravity κ, which have temperatures $T_{BH} = \kappa/2\pi$ due to the Hawking effect. The problem of heat transport then becomes one of computing the expectation value of the stress tensor in the given background. Note that, since gravity is not dynamical in this context, we can choose the metric at will. In particular, we can include as many black holes as we like at locations of our choosing, and we are free to assign their surface gravities as desired. One then seeks states of the field theory which are smooth across all future horizons. Stationary such states are analogues of the Unruh vacuum [148] for black holes in asymptotically flat spacetimes.

Gauge/gravity duality for large N field theories [19] has been used to study related settings in [57–60, 149–165]. Though this exploration involved certain tensions and subtleties, the picture that emerged in [57] (building on [160]) is one with two important phases for each black hole. In the so-called "funnel phase" a given black hole exchanges heat with distant regions much as in a free theory with a similar number of fields. One may say that grey body factors are $\mathcal{O}(1)$ even at large N. But in the contrasting "droplet phase" there is no conduction of heat between a given black hole and the region far away at leading order in large N. In effect, all grey body factors associated with the black hole vanish at this order.[1] While we save a more complete review for section 3.2, we mention that the

[1]To be more precise, the grey body factors are non-zero only for a number of degrees of freedom that scales like $N^0 = 1$.

terms "droplet" and "funnel" refer to the shape of the bulk horizon in the dual gravitational theory; see especially figure 3.1. Additional phases are also possible that conduct heat between subsets of nearby black holes but not to infinity; these are of less concern below. We also mention that 1+1 CFTs (and their 2+1 AdS duals) are a special case in which only the funnel phase is allowed.

The above works have focussed on cases without heat flow; i.e., either droplets (in which heat does not flow at leading order) or on equilibrium funnels. But heat transport is an interesting phenomenon and, moreover, at least for $d \geq 3$ the corresponding solutions of the dual AdS_{d+1} gravitational theory are expected to have novel properties. For example, time-independent such solutions should be black holes which (in some sense) have a temperature that varies along the horizon. But there is no generally accepted definition of horizon temperature which allows the temperature to vary[2]. Indeed, the fact that any definition of temperature should vary implies that the horizon is not a Killing horizon, which is already a novel property for a stationary solution. There is also an interesting question of whether such black holes should have a regular past horizon. On the one hand, from the field theory point of view, the CFT stress tensor must diverge on the past horizon of the (now fixed and non-dynamical) black hole metric in any state with both heat flow and time-translation symmetry. Ref. [57] thus expected the past horizon of the dual bulk solutions to be singular in the presence of (stationary) heat flow. But cases are known where similarly singular stress tensors are described by smooth bulk solutions [168–170]. Perhaps this could be

[2]Except of course within the domain of the gradient expansion, as in the fluid-gravity correspondence [64]; see also [166]. For proposals in more general contexts see e.g. [167] for a recent paper and references. If flowing funnels could be constructed, it might be interesting to apply these proposals and study the results.

the case here as well.

This paper provides a first step in this direction by constructing examples of such 'flowing funnel' solutions in AdS_3, which are then dual to heat transport in a $1+1$ CFT; i.e., for the case $d = 2$. The behavior of the stress tensor (and thus of heat transport) in $1+1$ CFT's is fully determined by conformal invariance, and of course the same is true of the AdS_3 description. This is therefore not an example where one expects gauge/gravity duality to lead to significant new insights for the field theory. In addition, a consequence of this conformal symmetry is that states are characterized by *two* (left- and right-moving) temperatures T_L, T_R, both of which are necessarily constant (independent of spatial position) in a stationary solution. So this is also not a context where we will learn about bulk horizons with non-constant temperature. Nevertheless, it gives a prime opportunity to see how heat transport in the CFT is encoded in the dual bulk solutions. We may also hope that the explicit solutions given below will provide a useful starting point for studying the higher-dimensional case.

We begin with a brief review of black funnels, black droplets, and their dual field theory description in section 3.2. Section 3.3 then constructs flowing funnels from rotating BTZ black holes. We close with some further discussion in section 3.4 and relegate details of the Fefferman-Graham coordinates to Appendix A.1.

3.2 A brief review of droplets and funnels

Studies of the above framework using gauge/gravity duality have led to both surprising phenomena and significant controversy. The first such study appears

to have been [149], which used the AdS_4 C-metric [171] to find a bulk solution describing the dual CFT on an asymptotically flat black hole spacetime. The surprise was that, at leading order in large N, the CFT stress tensor was completely static and described no flow of heat from the (finite temperature) black hole to infinity (where the state approached the vacuum). Indeed, the expectation of finite heat flow was so strong that it motivated predictions [150, 151] (see also [161, 163])) that black holes on Randall-Sundrum brane-worlds [172, 173] could not be stationary even at the classical level[3], in contradiction with the natural intuition based on gravity in the bulk (see [174] for details). The difficulty in finding such stationary solutions with black holes (see e.g. [152–159, 175]) made these arguments seem compelling for some time, though modern numerical techniques have established that these solutions do in fact exist [164, 165]. As in [149], although the field theory contributes a non-trivial stress tensor one finds no transport of energy to infinity at leading order in N; i.e., at $\mathcal{O}(N^2)$ for [164, 165].[4] Indeed, from the bulk viewpoint, heat transport can occur only due to a quantum process (bulk Hawking radiation) which is an effect of order $N^0 = 1$. See also [162].

While intuition from weak coupling may make this tiny heat transport seem surprising, Fitzpatrick, Randall and Wiseman [160] pointed out that similar phe-

[3]The brane in a Randall-Sundrum brane-world spacetime can be thought of as a boundary for an asymptotically AdS spacetime which has been placed at finite distance and given a boundary condition that makes the boundary metric dynamical. At least roughly speaking, this makes the system dual to a field theory coupled to dynamical gravity. Hawking radiation in the dual field theory would therefore cause the brane black hole to shrink. If this effect occurs at leading order in large N, then it would be visible at the classical level from the bulk point of view.

[4]Here and below we will count powers of N as appropriate to a large N $SU(N)$ Yang-Mills theory. This in particular describes theories dual to bulk spacetimes asymptotic to $AdS_5 \times X$ for compact 5-dimensional manifolds X.

nomena are in fact well-known at strong coupling and large N. In particular, they noted that confined phases of large N gauge theories have conductivities of order 1 and not of order N^2. Though the above theories are not strictly confining, we see that an effect of this magnitude would explain the results of [164, 165].

A somewhat more complete picture was constructed in [57] and explored further in [58–60]. The basic approach of [57] was to i) explicitly add a thermal bath at infinity, ii) follow the natural intuition for the bulk gravitating solutions, and iii) translate the results into an explanation[5] of the effect in the gauge theory. The rest of this section briefly summarizes the arguments of [57] with minor additions and clarifications.

Let us take the gauge theory to be conformal, and to be deconfined at all temperatures $T > 0$. We take the theory to live on some asymptotically flat spacetime and imagine coupling the system to a large heat bath (at some temperature T_∞) far from the black hole. It is clear that this heat bath should fill the spacetime with a thermal plasma – at least far from the black hole where the spacetime is nearly flat. In order to discuss the dual gravitational solution, it is useful to introduce two coordinates: r, which parametrizes the distance from the black hole in the gauge theory and z, chosen so that the gauge theory 'lives' on the AdS boundary at $z = 0$ and which parametrizes the distance into the bulk. To be concrete, at least near the boundary one might take these to be part of a Fefferman-Graham type coordinate system[6] in which the bulk metric takes the

[5]Here we mean a self-consistent scenario for the behavior of the strongly-coupled large N gauge theory. A full explanation would of course require the scenario to be derived from first principles, but this remains an open problem.

[6]Though there is no a priori guarrantee that such coordinates are regular across the full bulk horizon. See e.g. the discussion of 2+1 funnels in [57].

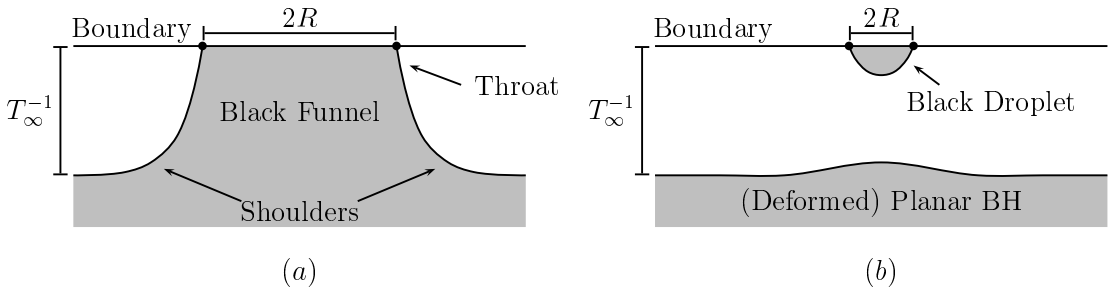

Figure 3.1: A sketch of the relevant solutions: **(a):** black funnel and **(b):** black droplet above a deformed planar black hole. Both describe possible states of dual field theories in contact with heat baths at temperature T_∞ on spacetimes containing black holes of horizon size R. The top line corresponds to the boundary, with the dots denoting the horizon of the boundary black hole. The shaded regions are those inside the bulk horizons.

form

$$ds^2_{d+1} = z^{-2}\left(dz^2 + g_{ij}dx^i dx^j\right), \tag{3.1}$$

with r being one of the boundary coordinates x^i and $ds^2_d = g_{ij}dx^i dx^j$ being the asymptotically-flat black hole spacetime (which we call the 'boundary black hole' or equivalently the 'gauge theory black hole') on which the gauge theory is to be studied. One expects the thermal plasma to be described by a bulk horizon that approximates that of the familiar planar Schwarzschild black hole at large r. On the other hand, one also expects the horizon of the boundary black hole to extend into the bulk. There are then two natural classes of possible bulk solutions. If the above two horizons connect to form a single smooth horizon, the solution is said to describe a "black funnel." If they are instead disconnected, the solution describes a "black droplet, suspended above a (deformed) planar black hole." These two situations are sketched in figure 1.

Taking the gauge theory black hole to have radius R, the product RT_∞ is scale invariant. It is thus natural to expect the basic physics to depend crucially on this product, with the precise details of the gauge theory black hole playing a lesser role. In particular, since depth (z) is related to size (r) on the boundary, for large RT_∞ one expects funnels to exist and to be thermodynamically dominant, while droplets (above planar black holes) should dominate for small RT_∞. See [57] for a more detailed discussion. It is natural to expect that the two phases are connected by a cone transition as occurs in similar settings [176–178] in which dialing a parameter causes two horizons to meet and perhaps merge.[7]

As in [57], let us focus for now on the equilibrium context (where $T_{BH} = T_\infty$). In the funnel case, disturbances of the bulk horizon near $z = 0$ (which describes the region near that boundary black hole) can propagate along the bulk horizon into the region near $r = \infty$ (which describes the thermal plasma). Although any coherent oscillation is highly damped during this propagation, this merely turns the energy of the oscillation into heat which will nevertheless flow along the horizon. In contrast, disturbances of the droplet horizon in figure 3.1 (and the heat they generate) cannot directly propagate to the planar black hole horizon. Instead, they can only couple to the planar black hole horizon via bulk gravity. Since in linear field theory we describe the coupling between asymptotic scattering states and a black hole in terms of grey body factors, it is natural to say that for the dual field theory the boundary black hole has tiny grey body factors (of order

[7]This scenario was proposed and explored in [176] for mergers of horizons with the same temperature. It was shown in [178] that similar behavior can result even when the horizon temperatures differ. We note that the AdS-Schwarzschild black string solution of [174] is such a cone involving a planar black hole of zero temperature. Since there appears to be no nearby stable solution, the full phase diagram is likely to be as complicated and interesting as that of Kaluza-Klein black holes (see e.g. [179]).

$1/N^2$ or smaller).

Of course, the situation is more complicated than this statement might seem to imply as the dual field theory contains many degrees of freedom that interact strongly. A more complete story would note that the $\mathcal{O}(N^0)$ degrees of freedom dual to bulk gravitational waves have more familiar $\mathcal{O}(1)$ grey body factors while the grey body factors for the N^2 degrees of freedom that describe the rest of the plasma near $r = \infty$ appear to vanish exactly to all orders in $1/N$. It is natural to suppose that these latter grey body factors are in fact exponentially small due to tunneling through a potential barrier of height N or N^2. Presumeably this potential barrier is related to the need to change the ways in which flux tubes connect in attempting to move a quasi-particle from a state in which it is attached via flux tubes to the black hole into a plasma state. As noted in [57], the plasma quasi-particles seem to have an effective size which is larger than those of quasi-particles attached to the black hole. Thus one should be able to describe the above potential barrier in terms of an effective potential for the size of a quasi-particle. Again, this is merely a self-consistent interpretation of the bulk gravitational physics. A complete microscopic understanding in terms of the gauge theory remains to be found.

While it is useful to keep the above general context in mind, the discussion degenerates somewhat in the case of 1+1 CFTs (dual to 2+1 AdS solutions). In this context, there is no useful definition of the "size" of a horizon in the CFT. Indeed, all horizons are analogous to planar horizons in higher dimensions and may therefore be considered to have $R = \infty$. In particular, there cannot be any effective potential associated with the size of a quasi-particle. As a result, only

the black funnel phase is allowed.

As a final side comment, we mention that it should be possible to construct an even more general set of droplet-phase solutions. First, note that even in a free field theory, one may consider a thermal state on a black hole background with $T \neq T_{BH}$. Although the correlation functions are then singular at the horizon, a logical possibility is that that our large N CFT in such a state may be described by a smooth bulk gravitational dual which merely fails to be asymptotically AdS in the usual sense at the horizon of the boundary black hole. This was the case in [169, 170], which studied an analogous setting involving de Sitter horizons and found that the field theory temperature T corresponded to the temperature of a smooth *bulk* horizon that attached to the boundary black hole; i.e., $T = T_{\text{bulk } BH} \neq T_{\text{bndy } BH}$. The results of [169, 170] thus suggest that general droplet solutions are labeled by three temperatures: $T_{\text{bndy } BH}$, $T_{\text{bulk droplet}}$, and T_∞. In particular, in contrast to the identification in [164], even for $T_{BH} \neq 0$ the Boulware (ground) state should be described by a smooth bulk solution having only extreme horizons ($T_{\text{bulk droplet}} = T_\infty = 0$).

3.3 Flowing funnels from BTZ black holes

We now turn to the problem of constructing AdS_3 spacetimes which exhibit heat flow in a stationary state. Our particular interest concerns bulk solutions dual to a 1+1 CFT on a black hole background. We refer to such AdS_3 solutions as 2+1 'flowing funnels.'

Note that in 1+1 dimensions a given static region of spacetime can be attached

to no more than two black holes – one on the left, and one on the right. We begin with spacetimes that contain only one black hole (say, on the left) and which approach the Minkowski metric in inertial coordinates on the right; see figure 3.2. Adding the second black hole will be straightforward once this case is under control.

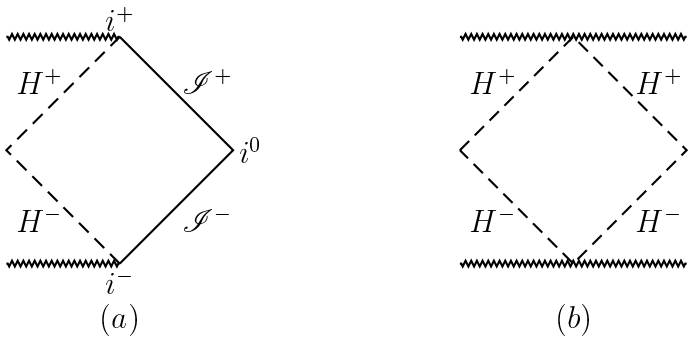

Figure 3.2: Conformal diagrams showing the two types of $1+1$ background spacetimes for our CFTs. **(a):** A single black hole on the left with an asymptotically flat region on the right. **(b):** Two black holes.

In fact, let us first consider the case of no black holes at all. Recall that the stress tensor of stationary CFT states on 1+1 Minkowski space is fully characterized by its right-moving and left-moving temperatures T_R, T_L:

$$ds^2_{CFT} = -dudv, \quad T^{CFT}_{ab}dx^a dx^b = \pi\frac{c}{12}\left(T_R^2 du^2 + T_L^2 dv^2\right), \tag{3.2}$$

where we have introduced null coordinates $u = t-x, v = t+x$, and c is the central charge of the CFT. The system may also be characterized by a temperature $T = 2(T_L^{-1}+T_R^{-1})^{-1}$ and a chemical potential for momentum $\mu = \ell(T_R-T_L)/(T_R+T_L)$. Although 1+1 CFTs are not well-described by perfect fluids, one may nevertheless think of the system as being 'at rest' when $T_L = T_R$, as there is then no net

transport of energy. Boosting to a more general frame, it is natural to define the 'velocity' of the system to be $U^a\partial_a = \frac{1}{\sqrt{T_L T_R}}\left(T_R\partial_v + T_L\partial_u\right)$.

As is well-known, the bulk spacetimes dual to such flowing thermal states are just AdS$_3$ in BTZ coordinates [127, 128]; i.e., they are BTZ black holes with the 'angle' unwrapped so that it runs over $(-\infty,\infty)$ instead of over S^1. In the present context, it is natural to give the would-be BTZ angle the name x and units of length. The bulk metric then takes the form

$$ds^2_{\rm bulk} = -\frac{(\rho^2-\rho_+^2)(\rho^2-\rho_-^2)}{\ell^2\rho^2}\,dt^2 + \frac{\rho^2\ell^2}{(\rho^2-\rho_+^2)(\rho^2-\rho_-^2)}\,d\rho^2 + \frac{\rho^2}{\ell^2}\left(dx - \frac{\rho_+\rho_-}{\rho^2}\,dt\right)^2, \tag{3.3}$$

where ℓ is the usual AdS scale and the temperatures are $T_R = (\rho_+ + \rho_-)/2\pi\ell$ and $T_L = (\rho_+ - \rho_-)/2\pi\ell$. We take $\rho_+ > 0$ so that the sign of ρ_- determines the sign of the BTZ angular momentum J. In (3.3), we have called the usual BTZ radial coordinate ρ in order to reserve r for a radial coordinate along the boundary. The boundary stress tensor [103, 104] of (3.3) is (3.2) with $c = 3\ell/2G$, where G is the bulk gravitational constant.

Now, a general static 1+1 spacetime may be written as $ds^2 = \Omega^2(x)\,(-dt^2 + dx^2)$, and so may be generated from Minkowski space via an appropriate conformal rescaling. In particular, we obtain a black hole of temperature $T_{\text{bndy } BH} = \kappa/2\pi$ by taking $\Omega \to 1$ as $x \to +\infty$ and $\Omega \sim e^{\kappa x}$ as $x \to -\infty$. Under such a conformal rescaling, the CFT stress tensor transforms as [180]

$$T_{ab} \to T_{ab} + \frac{c}{12\pi}\left[\nabla_a\nabla_b\sigma - \nabla_a\sigma\nabla_b\sigma + \frac{1}{2}g_{ab}\left(\nabla\sigma\right)^2 - g_{ab}\nabla^2\sigma\right] \tag{3.4}$$

where $\Omega = e^{\sigma}$. In particular, the stress tensor is unchanged at large positive x (where $\nabla_a \sigma$ vanishes) while at large negative x eqn. (3.2) becomes

$$T_{CFT} = \pi \frac{c}{12} \left[e^{2\kappa u} \left(T_R^2 - \frac{1}{4\pi^2} \kappa^2 \right) dU^2 + e^{-2\kappa v} \left(T_L^2 - \frac{1}{4\pi^2} \kappa^2 \right) dV^2 \right] + \dots \quad (3.5)$$

in terms of the new affinely-parametrized null coordinates U, V (which satisfy $U = -\kappa^{-1} e^{-\kappa u} + \dots$ and $V = \kappa^{-1} e^{\kappa v} + \dots$ where $+\dots$ represents terms that are subleading as $x \to -\infty$). Note that the new stress tensor is regular on the future horizon ($u = \infty$) precisely when we choose $T_R = T_{\text{bndy } BH}$.

For this choice, one may interpret the CFT state as describing heat exchange between a boundary black hole of temperature $T_{\text{bndy } BH} = T_R$ and a heat bath at infinity ($x = +\infty$) with temperature T_L. In particular, suppose that we instead choose the background metric to be time dependent, and to evolve from 1+1 Minkowski space in the far past to the desired boundary black hole spacetime in the far future. Then, by the usual arguments, when the CFT begins in an initial thermal state of temperature T_L the late-time behavior of the CFT is described by our solution above.[8]

Returning to the stationary case, let us remark on several features of our bulk solution:

- The choice $T_L = 0$ is dual to the Unruh state of the CFT. In particular, the Unruh state corresponds to an extreme horizon in the bulk whose properties are fixed by the temperature of the boundary black hole. In contrast, note that the Boulware state is described by an 'unwrapped' $M = 0$ BTZ

[8]Recall that T_L is the temperature of the left-moving part of the CFT. Unfortunately, this is naturally thought of as being sourced by a heat bath on the right (at $x = +\infty$).

black hole with $T_L = T_R = 0 \neq T_{\text{bndy } BH}$, which is just a Poincaré horizon (independent of $T_{\text{bndy } BH}$). As noted in section 3.2, this is a smooth bulk spacetime with a singular boundary stress tensor. In this case, the singular boundary stress tensor is due to a singular choice of conformal frame.

- By construction, on the boundary of our spacetime the stationary Killing field ∂_t of BTZ agrees with the static Killing field of the boundary metric. But BTZ has a second (commuting) Killing field ∂_x. While this is not a Killing field of the boundary black hole, the fact that all 1+1 metrics are conformally flat means that ∂_x acts as a conformal Killing field on the boundary. This is a peculiar feature of our AdS_3 problem that will not be reflected in higher dimensions. Indeed, in higher dimensions it is easy to show that any conformal isometries of boundary metrics describing non-extreme stationary spherically symmetric boundary black holes are in fact boundary Killing fields, so that there can be no such 'accidental' Killing fields in the bulk.[9]

- The bulk solution has a Killing horizon generated by $\chi = \partial_t + \ell^{-1}\mu\partial_x$, where $\mu = \ell(T_R - T_L)/(T_R + T_L)$ as above is related to the angular velocity of the horizon via $\mu = \Omega_H \ell$. Thus we see that μ characterizes the rate at which null generators of the horizon pass from one Killing orbit to another. For $\mu > 0$ we may say that, in this sense, generators 'move' from the boundary down into the bulk and toward positive x, while for $\mu < 0$ the 'motion' is toward negative x and up toward the boundary. As was the case for ∂_x above, χ is

[9] Extreme black holes can have such conformal isometries but do not by themselves lead to heat flow.

an accidental symmetry from the viewpoint of the boundary theory and will have no analogue in higher dimensions; i.e., the black holes that describe flowing funnels dual to $d > 1{+}1$ CFTs will not have Killing horizons.

- For $T_L = T_R$ our solution is precisely the static AdS_3 black funnel constructed in [57].

In many implementations of the AdS/CFT correspondence one may gain insight into the CFT state by displaying the bulk solution in Fefferman-Graham coordinates. This seems to be less useful in the current context as these coordinates are highly singular. We relegate the details of the coordinate transformations and the resulting metrics to the appendix, though we briefly summarize the key points below.

There are three natural sources of coordinate singularities in the Fefferman-Graham coordinates associated with any boundary black hole: i) the past horizon H^- of the boundary black hole, ii) null infinity $\mathscr{I}^{\pm}$ of the boundary spacetime (see figure 3.2), and iii) the singularity of the boundary black hole. The singularity on H^- is associated with the fact that, while we tuned parameters to make the CFT stress tensor smooth across the future horizons, it generally remains singular on H^-. The problem at $\mathscr{I}^{\pm}$ is associated with the fact that these are finite locations when AdS_3 is described in global coordinates[10]. In addition, the singularity of the boundary black hole is clearly a singularity of the transformation between any global coordinates and our Fefferman-Graham coordinates. Since the boundary

[10] The particular global coordinates used in figures 3.3, 3.4, and 3.5 below are the dimensionless τ, R, θ for which

$$ds^2 = \frac{4\ell^2}{(1-R^2)^2}\left[-\frac{1}{4}(1+R^2)^2 d\tau^2 + dR^2 + R^2 d\theta^2\right].$$

metric can be chosen at will (and need not satisfy any equations of motion) we are free to place this singularity anywhere we like inside the boundary horizon. But it is important to note that, when written in conformally flat form, the conformal factor Ω of any boundary black hole metric necessarily has some singular feature associated with the fact that e.g. future-directed null geodesics along $\mathscr{I}^+$ encounter the horizon H^+ only at infinite affine parameter while other left-moving future-directed null geodesics encounter the horizon at finite affine parameter.

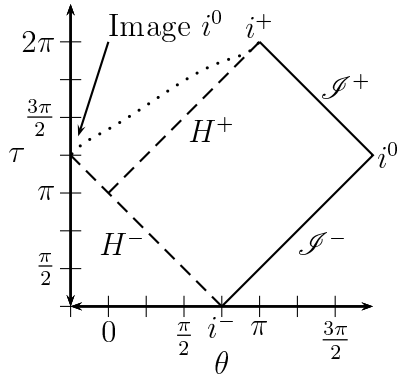

Figure 3.3: The relevant portion of the AdS_3 boundary in global coordinates. The dotted line indicates the singularity of the boundary metric (3.6); i.e., a singularity in the conformal frame associated with (3.6). The boundary past horizon H^- is another such singularity. Since θ has period 2π, the point marked "Image i^0" represents the same event on the boundary of global AdS_3 as does i^0. Due to singularities in the change of conformal frame it nevertheless represents a distinct point of the black hole boundary spacetime (3.6).

It is no surprise that the full singularities of the Fefferman-Graham coordinate system extend into the bulk, connecting to the boundary at the above three locations. One might hope that the singularities remain localized at the the bulk BTZ singularity and at the natural bulk null surfaces associated with (i) and (ii) above. But that turns out not to be the case, and Fefferman-Graham coordinate singularities extend outside the horizons of the BTZ black hole. The situation is

summarized in figures 3.3, 3.5, and 3.4 below for the AdS_3 spacetime dual to the Unruh state of the CFT on the metric

$$ds^2_{CFT} = -\tanh^2 \kappa r \, dt^2 + dr^2 = \frac{-1}{1-\kappa^2 uv} \, dudv, \tag{3.6}$$

where $\kappa = 2\pi T_R$ is again the surface gravity of the boundary black hole. The general case $T_L \neq 0$ is similar. We draw the reader's attention to the branch cut in figures 3.5 and 3.4, which limits the utility of Fefferman-Graham coordinates to a region surprisingly close to the boundary. We also include plots of the Fefferman-Graham z vs. r along the future horizons for various values of T_L/T_R (see figure 3.6).

Finally, let us consider the addition of a 2nd black hole to the 1+1 CFT spacetime. This may be accomplished by performing another conformal rescaling, this time with $\Omega \sim e^{-\kappa_R x}$ at large positive x. It is natural to choose Ω so that $|\partial_t|^2 = -1$ at e.g. $x = 0$. This provides a preferred location with respect to which to normalize notions of temperature and surface gravity. We also rename the above κ as κ_L to refer to the surface gravity of the left black hole. The resulting family of solutions is labeled by four parameters $(T_L, T_R, \kappa_L, \kappa_R)$, and the CFT stress tensor is smooth across both horizons if $T_R = \kappa_L/2\pi$ and $T_L = \kappa_R/2\pi$. Such states describe the asymptotic future of *any* CFT state (with a smooth stress tensor) on a spacetime which evolves from flat Minkowski space in the far past to one containing our two black holes in the far future. The details are in direct analogy to the case of a single black hole above.

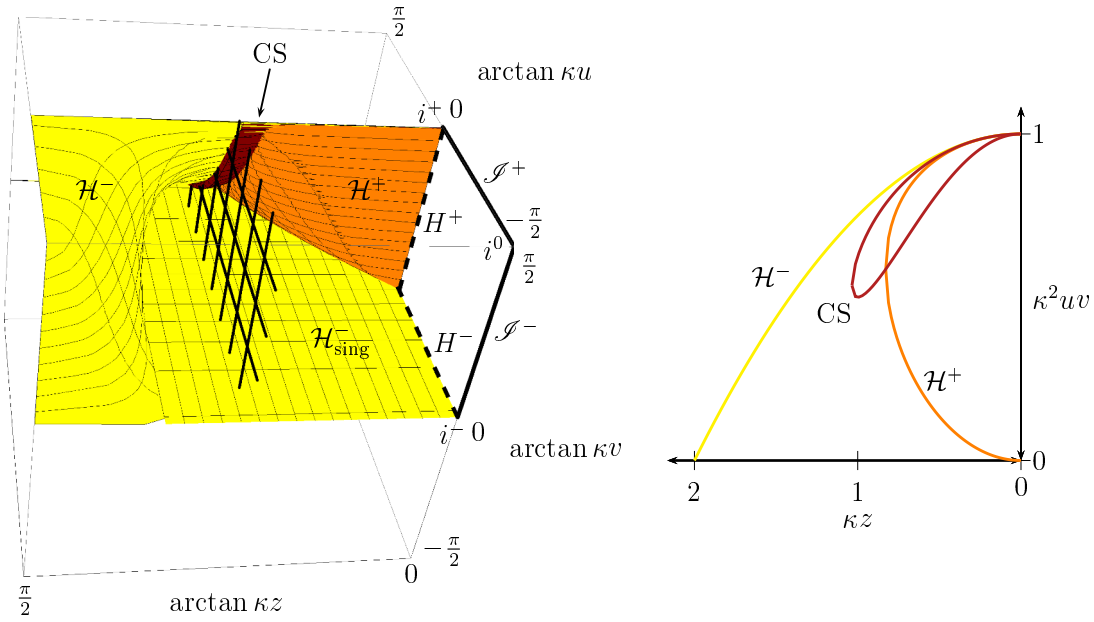

Figure 3.4: **Left:** Notable features of the bulk AdS$_3$ spacetime in Fefferman–Graham (FG) coordinates u, v, z, (compactified to show their full range) for our Unruh state solution ($T_L = 0, \kappa = 2\pi T_R$) and boundary metric (3.6). Past and future bulk horizons $\mathcal{H}^{\pm}$, boundary horizons $H^{\pm}$ and the various pieces $\mathscr{I}^{\pm}$, $i^{0,\pm}$ of infinity for the boundary spacetime (see fig. 3.3) are shown. The surfaces $\mathcal{H}^-_{\text{sing}}$ (at $v = 0$) and CS are FG coordinate singularities. The first ($\mathcal{H}^-_{\text{sing}}$) acts like part of the bulk past horizon from the FG point of view, though its image in global coordinates coincides with that of i^-. The second (CS) is a closed surface from the FG point of view which begins and ends at $z = 0, uv = 1$ (the singularity of the boundary black hole; dotted line in figure 3.3). Parts of the surfaces CS, $\mathcal{H}^{\pm}$ are obscured, as is a third FG coordinate singularity at $\kappa^2 uv = 1$ (for all z). A line on the CS surface near its maximum value of z is a set of branch points. The black grid on the left diagram marks the image of an associated branch cut chosen so that the transformation to FG coordinates is one-to-one in the region bounded by this cut, the CS surface, and the plane $z = 0$. **Right:** The general structure and the relative locations of CS, $\mathcal{H}^{\pm}$ are made clear. These surfaces depend only on the product uv. CS and $\mathcal{H}^+$ intersect along a single line. $\mathcal{H}^+$ and $\mathcal{H}^-$ do not intersect in the bulk but meet only at the singularity of the boundary black hole.

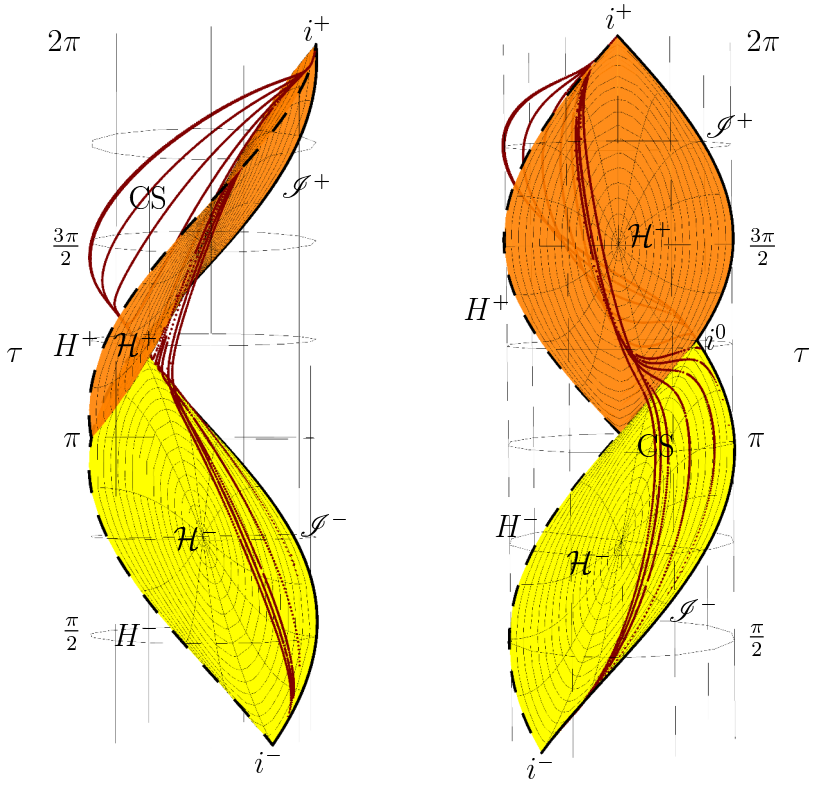

Figure 3.5: Notable features of the bulk AdS$_3$ spacetime in global coordinates associated with the Unruh state ($T_L = 0, \kappa = 2\pi T_R$) and the boundary black hole (3.6). The bulk past and future horizons $\mathcal{H}^\pm$ are labeled, as are $H^\pm$, $\mathscr{I}^\pm$ and $i^{0,\pm}$ describing the horizons and infinity of the boundary metric (see figure 3.3). In global coordinates, the surface $\mathcal{H}^-_{\text{sing}}$ of figure 3.4 coincides with i^-. The lines labeled CS are $uv =$ const. contours of the FG coordinate singularity described by the CS surface of figure 3.4. In Fefferman-Graham coordinates, the CS surface is closed and pinches off as it reaches the boundary singularity at $\kappa^2 uv = 1$. In global coordinates, this behavior gives rise to an open surface with two edges: one edge is at the boundary singularity (seen above behind the bulk horizon $\mathcal{H}^+$; this line is $\kappa^2 uv = 1$ for all values of the FG z coordinate) and $\mathscr{I}^-$. The other edge travels from i^+ to i^- inside the bulk. The associated branch cut shown as a black grid in figure 3.4 is not drawn, but would start near this edge in the bulk and fold back to the right, passing above the CS surface and terminating on $\mathscr{I}^+$ and $\mathscr{I}^-$. One should be aware that the part of the CS surface above the branch cut (near the interior edge) has multiple images in figure 3.3 and is a coordinate singularity only after one has passed through the branch cut.

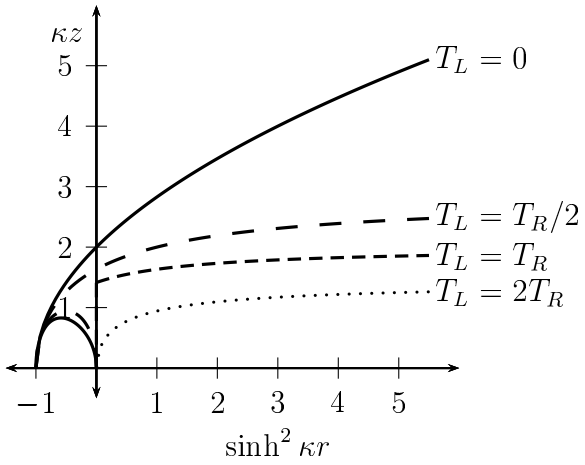

Figure 3.6: The future horizon in Fefferman-Graham coordinates for $T_L/T_R = 2, 1, \frac{1}{2}, 0$ and $\kappa = 2\pi T_R$ (smooth future horizon). The case $T_L = T_R$ describes the Hartle-Hawking state studied in [57]. The case $T_L = 0$ describes the Unruh case studied in detail in this paper. The horizontal axis plots $\sinh^2 \kappa r$ rather than just r in order to reach all the way to the boundary singularity at $\sinh^2 \kappa r = -1$. The curve diverges at large r for $T_L = 0$ but otherwise asymptotes to $\kappa z = 2\sqrt{T_R/T_L}$.

3.4 Discussion

We showed above how AdS_3 solutions dual to stationary CFT_2 states with heat transport between black holes (or between one black hole and a heat bath at infinity) can be constructed by 'unwrapping' the angular coordinate of BTZ black holes and changing conformal frame at infinity. Thus the solutions may also be described as pure AdS_3 in an appropriate conformal frame. An interesting point was that Unruh states of the CFT (living on a spacetime with a single black hole) are dual to extreme horizons in the bulk. But perhaps the notable feature of our solutions is just that they are everywhere smooth, despite the fact that the boundary stress tensor is generally singular on the past horizon of the boundary black hole. This smoothness is similar to the phenomenon seen in

[169, 170] for CFTs on black hole spacetimes in which the CFT was forced to have a temperature different from the Hawking temperature of the boundary black hole ($T_{CFT} \neq T_{\text{bndy } BH}$). See also [168].

In fact, ref. [169, 170] considered AdS_{d+1} solutions for all $d \geq 1{+}1$ and found smooth bulk solutions in all dimensions. But as we now discuss it is difficult to see how this could be possible for higher dimensional flowing funnels. In the AdS_3 case, the 'accidental' Killing fields discussed in section 3.3 meant that our solutions had Killing horizons. As a result, the points along a given null generator were related by a symmetry and nothing interesting can happen as one follows a null generator into the distant past. But section 3.3 noted that there are no accidental symmetries in the higher-dimensional case. Furthermore, as in our AdS_3 case, the flow of heat should make the stationary Killing field ∂_t fail to be null on the horizon[11]. Thus the generators will again move with respect to the stationary Killing orbits.

To understand the implications, let us consider a flowing AdS_{d+1} funnel with $SO(d-1)$ rotational symmetry. Here it is useful to use the size r of the S^{d-2} spheres of symmetry as a coordinate along the horizon. Now, the twist ω_{ab} of the horizon-generating vector field ξ^a is an anti-symmetric tensor on the horizon satisfying $\xi^a \omega_{ab} = 0$; i.e., it effectively has components only in the r-direction and in the angular direction. So by the $SO(d-1)$ symmetry $\omega_{ab} = 0$ and the null generators necessarily focus at finite affine parameter if the expansion or shear is non-zero.

[11] At least near the boundary, one may think of this as due to the fact that non-zero tr components of the boundary stress tensor force ∂_t to be non-hypersurface-othogonal, and thus to differ from the horizon-generating vector field.

Note that the value of r will change as one moves along a null generator of the horizon. This means that one of the eigenvalues of $\nabla_{(a}\xi_{b)}$ must be non-zero and thus that the expansion and shear cannot both vanish. Since horizon generators necessarily extend to infinite affine parameter toward their future, we conclude that they focus at finite affine parameter in the past.

There are now two logical possibilities: 1) that this focusing represents a caustic in a smooth spacetime, or 2) that it represents a spacetime singularity. While we have not completely ruled out the first option, the 2nd seems much more natural. This is just the picture suggested originally in [57]. It remains an interesting challenge to construct such higher-dimensional flowing funnel solutions.

Chapter 4

Stationary AdS Black Holes with non-Killing Horizons

4.1 Introduction

We focus here on the classic problem of heat transport far from equilibrium, and away from the perturbative regime. If the system of interest is an appropriate strongly coupled large N conformal field theory (CFT), we may use gauge/gravity duality to exploit a perhaps-more-tractable description as a semi-classical bulk gravitational system. We will consider the classical limit in cases where the bulk description may be truncated to $\Lambda < 0$ Einstein-Hilbert gravity. Our work complements perturbative computations of heat transport in this regime (e.g. [181]), as well as non-perturbative studies of thermalization (see e.g. [145–147] for recent examples and further references) and holographic shockwaves [182, 183].

Suppose in particular that we couple a CFT in d spacetime dimensions to

heat sources or sinks of finite size and at finite locations. A convenient way to introduce such sources is to place the CFT on a background non-dynamical spacetime containing stationary black holes with surface gravity κ, which have temperatures $\kappa/2\pi$ due to the Hawking effect. As we review in section 4.2 below, this problem may also be generalized so that the field theory temperature at the black hole horizon differs from $\kappa/2\pi$. But since no information can flow outward across the horizon, the choice of a black hole metric is nevertheless useful to decouple our CFT from the details of the heat sources and sinks. The problem of heat transport then becomes one of computing the expectation value of the stress tensor in the given background with the stated boundary conditions. Since the background spacetime is not dynamical, we can choose the metric at will. In particular, we can include as many black holes as we like at locations of our choosing, and we are free to assign their surface gravities as desired. Of course, since we consider CFTs, we may also conformally rescale the background metric to reinterpret our heat sources/sinks as being infinitely large and located at infinite distance; more will be said about this alternate interpretation in section 4.2 below.

Gauge/gravity duality for large N field theories [19] has been used to study related settings in [57–61, 73, 149–165, 184]. In this context, the d-dimensional black hole spacetime on which the CFT lives becomes the conformal boundary of a $(D = d+1)$-dimensional asymptotically locally anti-de Sitter (AlAdS) spacetime and we henceforth refer to our heat sources and sinks as boundary black holes. Though the above explorations in gauge/gravity duality involved certain tensions and subtleties, the picture that emerged in [57] (building on [160]) is one with two important phases for each boundary black hole, even when the CFT state

is assumed to contain a deconfined plasma. See [73] for a condensed review. In the so-called "funnel phase" a given boundary black hole is connected to distant regions of the boundary by a bulk horizon along which heat may be said to flow (say, if unequal temperatures are fixed at the two ends). But there is no such connection in the contrasting "droplet phase." Figure 4.1 depicts both phases for a simple case in which the boundary spacetime is asymptotically flat. In the CFT description, the funnel phase allows a given boundary black hole to exchange heat with distant regions much as in a free theory with a similar number of degrees of freedom. One may say that grey body factors are $\mathcal{O}(1)$ even at large N. But in the droplet phase there is no conduction of heat between a given black hole and the region far away at leading order in large N. In effect, all grey body factors associated with the black hole vanish at this order[1], so that the black hole does not couple efficiently to the surrounding plasma. Additional phases are also possible that conduct heat between subsets of nearby black holes but not to infinity.

Until recently, both funnel and droplet solutions were largely conjectural. Explicit examples were known only in rather contrived settings or in low enough dimensions that all properties were determined by conformal invariance. But numerical methods were used to construct more natural droplets in [164] and more natural funnels in [61]. An interesting detail is that the droplet solutions of [164] contain deformed planar black holes (see figure 4.1) with vanishing temperature. Constructing black droplet solutions that include finite-temperature (deformed) planar black holes remains an open technical challenge, though perturbative arguments give strong indications that they exist.

[1]To be more precise, the grey body factors are non-zero only for a number of degrees of freedom that scales like $N^0 = 1$.

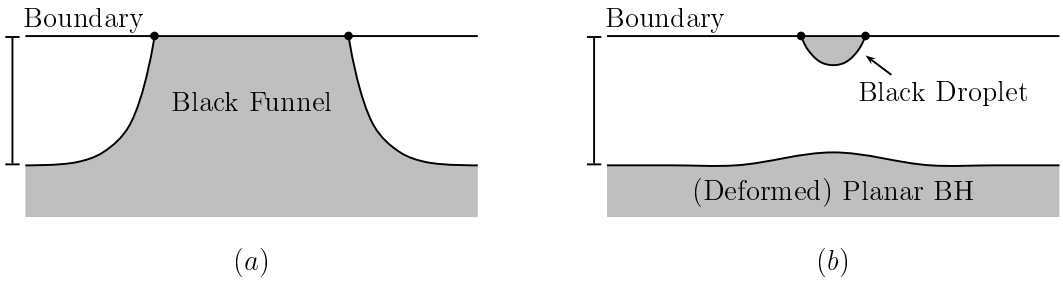

Figure 4.1: A sketch of the relevant solutions: **(a)** a black funnel and **(b)** a black droplet above a deformed planar black hole. For simplicity, we take both solutions to asymptote in the horizontal direction to the so-called planar AdS-Schwarzschild black hole. As a result, both describe possible states of a CFT on an asymptotically flat black hole spacetime filled with a deconfined plasma at constant temperature. In each figure, the top line corresponds to the spacetime on which the CFT lives; i.e., to the conformal boundary of the AlAdS bulk. The dots denote horizons of the boundary black holes. The shading marks regions inside the bulk horizons.

The above funnel and droplet papers largely focussed on cases without heat flow; i.e., either on droplets (in which heat does not flow in the approximation that the bulk is classical) or on equilibrium funnels. The one exception was [73] which showed that, by changing conformal frames, rotating BTZ black holes [127, 128] in AdS_3 can be re-interpreted as describing heat transport in 1+1 CFTs. Here the standard left- and right-moving temperatures T_L, T_R of the BTZ black hole correspond directly to the temperatures of the left- and right-moving components of the CFT. Due to the strong constraints of conformal symmetry in low dimensions these components do not interact and the temperatures T_L, T_R must be constants if the heat flux is stationary. In addition, the flow of heat is necessarily isentropic (having no local generation of entropy).

We refer to black funnels transporting heat as "flowing funnels." Since none of the above special properties should hold for $d > 2$ ($D > 3$), higher dimensional

flowing funnels should be quite different than those found in [73]. For example, a bulk horizon connecting two boundary black holes of different temperatures should (at least in some rough sense) be describable as having a temperature that varies along the horizon. But recall that there is no generally accepted definition of horizon temperature which allows this temperature to vary[2]. Indeed, the fact that any definition of temperature should vary implies that the horizon is not Killing, which is already a novel property for a stationary black hole[3]. This suggests that the horizon generators have positive expansion (though of course tending to zero in the far future), so that they caustic at finite affine parameter in the past. It is natural to expect this caustic to occur at a singular past horizon [57], and section 4.5 confirms this picture for our solutions.

We focus below on what we call $D = 4$ global flowing funnels, by which we mean deformations of the global AdS_4 black string (also known as the Bañados-Teitelboim-Zanelli (BTZ) black string; see e.g. [188] where the solution was obtained as a special case of the AdS C-metric). This reference solution may be constructed by starting with global AdS_4 written in coordinates for which slices of constant radial coordinate z are just AdS_3. One then replaces each such AdS_3 slice with a BTZ metric [127, 128] having the correct z-dependence and which we chose to be nonrotating. The result is an AlAdS Einstein metric which may be

[2]Except of course within the domain of the gradient expansion, as in the fluid-gravity correspondence [64]; see also [166]. For proposals in more general contexts see e.g. [167] for a recent paper and references. Our solutions may therefore provide interesting testbeds for such proposals.

[3]For compactly generated horizons, this behavior is forbidden by the rigidity theorems [185–187]. But our bulk horizon is non-compact since it extends to the conformal boundary.

written

$$ds^2 = \frac{\ell_4^2}{H^2(z)}\left[-f(r)\,dt^2 + \frac{dr^2}{f(r)} + r^2 d\phi^2 + dz^2\right], \tag{4.1}$$

with $H(z) = \ell_3 \cos(z/\ell_3)$ and $f(r) = (r^2 - r_0^2)/\ell_3^2$. The solution is sketched in figure 4.2. Here the horizon of the BTZ string is at $r = r_0$, the parameter ℓ_4 is the AdS_4 length scale, and the AdS_3 length scale ℓ_3 of the BTZ foliations may be set to any desired value by rescaling z, r, r_0. The two boundary black holes (at $z/\ell_3 = \pm\pi/2$) have the same temperature, but we will seek deformations where these temperatures differ and heat flows between the two boundary black holes.

The outline of the paper is as follows. Section 4.2 reviews how static black funnels (i.e., without flow) may be generalized by adding a parameter $\alpha = T_{\text{bndy BH}}/T_{\text{bulk BH}}$ which allows the temperature of bulk and boundary horizons to differ. In the small α limit, the analogous flowing funnels can be described in a derivative expansion; i.e., using the fluid/gravity correspondence of [64]. This correspondence is briefly reviewed and then applied to flowing funnels in section 4.3. Section 4.4 then explains how to formulate the construction of flowing funnels with any α in a manner where one can proceed numerically. The results of such numerics are presented in section 4.5 where they are compared to the fluid approximation of section 4.3. As expected, we find excellent agreement for small α, though for our cases the agreement remains good even for α close to 1. We close with some final discussion in section 4.6.

Note: In the final stages of this work we learned of [189], which also addresses the construction of AdS black holes with non-Killing horizons and may have some overlap with our work.

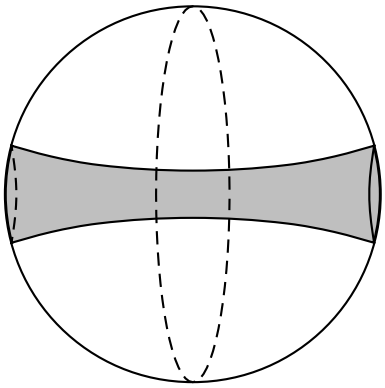

Figure 4.2: A sketch of a $t = const.$ slice of the BTZ string (4.1). The two pieces of the boundary at $z/\ell_3 = \pm\pi/2$ are conformal to two copies of the BTZ black hole, sketched above as the two hemispheres of an S^2. These boundary black holes are joined at infinity (the dashed line around the equator of the sphere), so that the boundary of the BTZ string can be thought of as a sphere with a black hole at either pole. The bulk of the string is the interior of the sphere, where the string stretches from one black hole to the other.

4.2 Detuning the bulk and boundary black hole temperatures

As mentioned in the introduction, even without heat flow the black funnel paradigm may be generalized by adding an extra parameter $\alpha = \frac{T_{\text{bndy BH}}}{T_{\text{bulk BH}}}$ which allows us to detune to the temperatures of the bulk and boundary black holes. In terms of the dual field theory, taking $\alpha \neq 1$ means that one considers a thermal ensemble at some temperature $T_{\text{Field Theory}}$ which differs from the natural temperature $T_{\text{bndy BH}}$ of the (say, static) boundary black hole spacetime on which the field theory lives. One may think of the resulting state as defined by a Euclidean path integral with period $1/T_{\text{Field Theory}} \neq 1/T_{\text{bndy BH}}$ and thus having a conical singularity at the horizon of the boundary black hole. What is interest-

ing about this construction is that the gravitational dual can have a completely smooth Euclidean AlAdS bulk, with the conical singularity of the boundary geometry resulting only from a failure of the standard AlAdS boundary conditions at the singular boundary points [168–170]. Any smooth horizon then clearly has temperature $T_{\text{bulk BH}} = T_{\text{Field Theory}} \neq T_{\text{bndy BH}}$ as determined by the Euclidean period.

The prototypical detuned solution studied in [168–170] is just the general hyperbolic (sometimes referred to as 'topological') black hole of [190–192], whose metric in $D = d + 1$ bulk spacetime dimensions may be written

$$ds^2_{d+1} = -F(r)dt^2 + \frac{dr^2}{F(r)} + r^2 d\Sigma^2_{d-1}, \quad F(r) = \frac{r^2}{\ell^2_{d+1}} - 1 - \frac{r_0^{d-2}}{r^{d-2}}\left(\frac{r_0^2}{\ell^2_{d+1}} - 1\right). \quad (4.2)$$

Here ℓ_{d+1} is the AdS length scale associated with the $(D = d+1)$-dimensional cosmological constant, $d\Sigma^2_{d-1} = d\xi^2 + \sinh^2\xi d\Omega^2_{d-2}$ is the metric on the unit Euclidean hyperboloid, and $r = r_0$ is a smooth horizon of temperature

$$T_{\text{bulk BH}} = \frac{r_0^2 \ell_{d+1}^{-2} d - (d-2)}{4\pi r_0}. \quad (4.3)$$

Note that $F(r)$ approaches r^2/ℓ^2_{d+1} at large r. Making an obvious choice of boundary conformal frame, the boundary metric is just the hyperbolic cylinder $\mathbf{H} \times \mathbb{R}$ with $ds^2_{\mathbf{H}\times\mathbb{R}} = -dt^2 + \ell^2_{d+1} d\Sigma_{d-1}$. But note that we may write

$$ds^2_{\mathbf{H}\times\mathbb{R}} = -dt^2 + \frac{d\rho^2}{(1 - \rho^2/\ell^2_{d+1})^2} + \frac{\rho^2}{1 - \rho^2/\ell^2_{d+1}} d\Omega^2_{d-2}, \quad (4.4)$$

where $\rho/\ell_{d+1} = \tanh\xi$. Multiplying the right-hand side by $(1 - \rho^2/\ell^2_{d+1})$ gives a

metric on the static patch of the d-dimensional de Sitter space dS_d with Hubble constant ℓ_{d+1}^{-1}. So by changing conformal frames in this way we may regard the boundary of (4.2) as having de Sitter horizons with temperature $1/2\pi\ell_{d+1}$. From the perspective of an observer in the static patch, the de Sitter horizon acts just like a black hole horizon with

$$T_{\text{bndy BH}} = \frac{1}{2\pi\ell_{d+1}}. \tag{4.5}$$

For general r_0 this temperature clearly differs from that of the bulk horizon. For the case where they agree, the hyperbolic black hole metric (4.2) is just pure AdS_{d+1} in appropriate hyperbolic coordinates. We recall that even for the tuned case $\alpha = 1$ ref. [61] found the conformal frame (4.4) useful for constructing black funnel solutions numerically.

Since the analysis of temperatures above involves only the horizons, it is clear that detuned bulk and boundary horizons should exist much more generally. Indeed, any static, spherically symmetric boundary metric with a pair of of smooth horizons at $\rho = \pm\ell_{d+1}$ may be written in the form

$$ds^2_{\text{bndy BH}} = \left(1 - \rho^2/\ell^2_{d+1}\right)\left(-\widetilde{F}(\rho)dt^2 + \frac{d\rho^2}{\widetilde{G}(\rho)} + \widetilde{R}^2(\rho)d\Omega^2_{d-2}\right), \tag{4.6}$$

where $\widetilde{F}$, $\widetilde{G}$, and $1/\widetilde{R}^2$ are smooth on some interval including $\rho \in [-\ell_{d+1}, \ell_{d+1}]$, $\widetilde{G}$ has a second order zero at each of $\rho = \pm\ell_{d+1}$, and $1/\tilde{R}^2$ vanishes at $\rho = \pm\ell_{d+1}$. So after a conformal transformation (4.6) agrees with (4.4) to leading order in ρ for each term and in this sense may be said to approach $\mathbf{H} \times \mathbb{R}$ at large ρ. The

ansatz (4.6) can equivalently be written

$$ds^2_{\text{bndy BH}} = e^{-2x/x_0} F(x) \left(-dt^2 + dx^2 + R^2(x) d\Omega^2_{d-2}\right), \tag{4.7}$$

where x_0 is some reference length scale and F and $e^{\mp 2x/x_0} R^2$ are smooth functions of $e^{\mp 2x/x_0}$ at $e^{\mp 2x/x_0} = 0$. In particular, up to the conformal factor $ds^2_{\mathbf{H}\times\mathbb{R}}$ takes this form for $x_0 = \ell_{d+1}$ and $R^2 = \ell^2_{d+1} \sinh^2(x/\ell_{d+1})$. In terms of (4.7) the boundary black holes have temperatures

$$T_\pm^{\text{bndy BH}} = \frac{1}{4\pi} \lim_{x\to\pm\infty} \frac{d}{dx} \ln\left(e^{-2x/x_0} F(x)\right). \tag{4.8}$$

It is therefore sensible to choose any r_0 and seek a smooth bulk solution in which each term approaches that of (4.2) to leading order in $e^{-2|x|/x_0}$ at large $|x|$; see section 4.4 for a more complete analysis of these boundary conditions. Any static such solution will have a bulk horizon with temperature (4.3) and can again be interpreted as being dual to a field theory state of this temperature on a black hole background of temperature (4.5). In the next sections we will seek further generalizations with different values of r_0 (which we then call $r_\pm$) at $x = \pm\infty$. That is to say that for $x \to +\infty$ the bulk solution will asymptote as above to (4.2) with $r_0 = r_+$, while for $x \to -\infty$ it will analogously approach (4.2) with $r_0 = r_-$. The bulk horizon may then be said to approach the temperatures $T_\pm$ given by (4.3) with r_0 replaced $r_\pm$. We will also allow distinct temperatures $T_\pm^{\text{bndy BH}}$ for the $x = \pm\infty$ boundary black holes and introduce the parameters $\alpha_\pm = T_\pm^{\text{bndy BH}}/T_\pm$. In fact, we will always take $\alpha_+ = \alpha_-$.

Of course, we may also consider so-called ultrastatic conformal frames analo-

gous to (4.4). Starting with (4.7) and multiplying by a conformal factor $e^{2x/x_0}/F(x)$, one obtains the boundary metric

$$ds^2 = -dt^2 + dx^2 + R^2(x)d\Omega_{d-2} \tag{4.9}$$

for which ∂_t is a hypersurface-orthogonal Killing field of norm -1. In this frame, the boundary spacetime has two asymptotic regions, each asymptotic to $\mathbf{H} \times \mathbb{R}$ (say, with the same curvature scale ℓ_{d+1}). Furthermore, in the CFT description each region contains an infinite reservoir of deconfined plasma. Such infinite reservoirs may act as heat baths, and indeed the boundary conditions imply that they are in thermal equilibrium at temperature $T_\pm$ in the limits $x \to \pm\infty$.

4.3 The fluid limit

While a general treatment of black funnels remains challenging, it is by now well known that the study of AdS black holes simplifies in the so-called hydrodynamic limit of the fluid/gravity correspondence [64] in which all other parameters vary slowly in comparison with the black hole temperature and the solution can be described using a derivative expansion. For any fixed boundary metric, taking the limit of large temperature (i.e., small $\alpha_\pm$) makes all metric derivatives small in this sense. We may thus expect a good hydrodynamic description if in addition we control temperature gradients by taking $\Delta T = T_+ - T_-$ small.

The key point in the analysis of [64] is that, having chosen a boundary conformal frame with boundary metric $g^{(0)}_{ij}$, every AlAdS_{d+1} solution is associated with a d-dimensional boundary stress tensor T_{ij} which is traceless and conserved on

the boundary:

$$g^{(0)}_{ij} T^{ij} = 0, \quad D_i T^{ij} = 0, \tag{4.10}$$

where D_i is the covariant derivative compatible with $g^{(0)}_{ij}$. Below, we use the boundary metric $g^{(0)}_{ij}$ and its inverse to raise and lower indices $i, j, k, l, \ldots$.

As an example, consider the planar AdS-Schwarzschild black hole

$$ds^2_{\text{AdS}-\text{Schw}} = -\frac{r^2}{\ell^2_{d+1}}\left(1 - \frac{r_0^d}{r^d}\right) dt^2 + \frac{\ell^2_{d+1} dr^2}{r^2\left(1 - r_0^d/r^d\right)} + \frac{r^2}{\ell^2_{d+1}} d\mathbf{x}^2_{d-1}, \tag{4.11}$$

with $r_0 = 4\pi\ell^2_{d+1} T/d$. Taking the boundary metric to be $ds^2_{\text{bndy}} = -dt^2 + d\mathbf{x}^2_{d-1}$, one finds

$$T^{ij} = T^{ij}_{\text{ideal}} = \rho u^i u^j + P\,\mathcal{P}^{ij}, \tag{4.12}$$

which takes the form of an ideal fluid with velocity field $u^i \partial_i = \partial_t$, transverse projector $\mathcal{P}^{ij} = g^{ij} + u^i u^j$, and

$$\rho = (d-1)\frac{\mathcal{T}^d}{16\pi\ell_{d+1} G^{(d+1)}}, \quad P = \frac{\rho}{d-1}, \tag{4.13}$$

which of course satisfies (4.10). In (4.13), we have defined for convenience $\mathcal{T} \equiv 4\pi\ell_{d+1} T/d$. By a simple Lorentz transformation we may obtain corresponding solutions with any constant (normalized) timelike d-velocity u^i.

The main result of [64] was to show that the temperature T and d-velocity u^i may be promoted to slowly-varying functions of the boundary coordinates $\mathbf{x}, t$ (at which point we refer to them collectively as the hydrodynamic fields). Here the term "slowly-varying" is defined with respect to the temperature as measured in the local rest frame selected by u^i. In particular, under these conditions [64]

showed that a smooth bulk solution may be constructed via a gradient expansion so long as u^i is everywhere timelike and the associated boundary stress tensor does indeed satisfy (4.10). They further showed that at each order in this expansion the conditions (4.10) may be expressed as standard hydrodynamic equations for a (conformal) fluid with velocity field u^i, which we take to satisfy $u^i u_i = -1$. This last step essentially just repeats the standard derivation of hydrodynamics from conservation laws.

In particular, ref. [64] showed that the boundary stress tensor takes the form

$$T^{ij} = T^{ij}_{\text{ideal}} + \sum_{n=1} \Pi^{ij}_{(n)}, \tag{4.14}$$

where $\Pi_{(n)}$ are dissipative terms that are n^{th} order in derivatives of the hydrodynamic fields; for example,

$$\Pi^{ij}_{(1)} = -2\eta\sigma^{ij}, \tag{4.15}$$

where

$$\eta = \frac{\mathcal{T}^{d-1}}{16\pi G^{(d+1)}} \tag{4.16}$$

is the shear viscosity, and $\theta = D_i u^i$ and

$$\sigma^{ij} = \mathcal{P}^{ik}\mathcal{P}^{jl} D_{(k}u_{l)} - \frac{\theta}{d-1}\,\mathcal{P}^{ij} \tag{4.17}$$

are respectively the divergence and shear of the velocity field. In writing (4.15) there is a freedom to make certain field redefinitions which, following [64], we have removed by choosing the so-called Landau frame in which the $\Pi^{ij}_{(n)}$ are taken to be purely transverse.

Since by assumption derivatives of the hydrodynamic fields are parametrically small in some parameter ϵ, $\Pi_{(n)}$ is of order ϵ^n. Below, we solve the fluid equations (4.10) at order $n = 0$ and $n = 1$ for the ultrastatic boundary metrics (4.9) and a purely radial velocity field (so that the only non-vanishing components are u^t, u^x). We also assume the flow to be stationary, so that u^i, $\mathcal{T}$ are independent of time.

A new effect at first order is the appearance of dissipation, and thus the production of entropy. At zeroth order, the entropy current J^i_S takes the simple form $(J^i_S)_{\text{ideal}} = su^i$, where $s(x) = \mathcal{T}^{d-1}/4G^{(d+1)}$ is the entropy density. Using the equations of motion and thermodynamic relations, one can show [65] that

$$D_i \left(J^i_S\right)_{\text{ideal}} = 0. \tag{4.18}$$

At first order, the entropy current still takes the form $(J^i_S)_1 = su^i$, but its divergence now becomes [65]

$$D_i \left(J^i_S\right)_1 = \frac{8\pi\ell_{d+1}\eta}{d\mathcal{T}}\,\sigma_{ij}\sigma^{ij} \geq 0, \tag{4.19}$$

showing that entropy is produced unless $\sigma_{ij} = 0$.

4.3.1 Ideal Fluid

We begin at order $n = 0$. We denote the associated fluid quantities $\mathcal{T}_0, u^i_0$ and work in $d = 3$. Following [193], we project the fluid equations into components parallel and perpendicular to the velocity. These yield respectively

$$D_i \left(\mathcal{T}_0^2 u^i_0\right) = 0 \quad \text{and} \quad D^k\mathcal{T}_0 + u^i_0 D_i \left(\mathcal{T}_0 u^k_0\right) = 0, \tag{4.20}$$

or

$$\partial_x \left(\sqrt{-g^{(0)}}\, \mathcal{T}_0^2 u_0^x \right) = 0 \quad \text{and} \quad \partial_x \left(\mathcal{T}_0 \left(u_0 \right)_t \right) = 0. \tag{4.21}$$

Thus

$$\mathcal{T}_0^2 u_0^x = \frac{\mathcal{T}_\infty^2}{2aR}, \quad \mathcal{T}_0 \left(u_0 \right)_t = \mathcal{T}_\infty, \tag{4.22}$$

in terms of integration constants that we have chosen to call $\mathcal{T}_\infty^2/2a$, $\mathcal{T}_\infty$. Since $u^2 = -1$, it remains to solve a quadratic equation for $\mathcal{T}_0, u_0^i$. We of course obtain two solutions labeled by a choice of sign. The solution with finite and nonzero asymptotic temperatures $T_\pm$ has

$$\mathcal{T}_0^2 = \frac{\mathcal{T}_\infty^2}{2} \left[1 + \sqrt{1 - \frac{1}{a^2 R^2}} \right], \tag{4.23a}$$

$$u_0^x = aR \left[1 - \sqrt{1 - \frac{1}{a^2 R^2}} \right]. \tag{4.23b}$$

Note that since R diverges at large x, at this order the asymptotic temperatures $T_\pm$ at $x \to \pm\infty$ agree; i.e., $\Delta T = T_+ - T_- = \mathcal{O}(\epsilon)$. We also find $u_0^x \to 0$ at $x = \pm\infty$.

4.3.2 First Order Corrections

To compute corrections to (4.23a), (4.23b), we choose to solve the fluid equations (4.10) iteratively. Introducing a bookkeeping parameter ϵ to keep track of derivatives, we may write $\mathcal{T} = \mathcal{T}_m + \mathcal{O}(\epsilon^{m+1})$, $u^i = u_m^i + \mathcal{O}(\epsilon^{m+1})$ for each m. We compute $\mathcal{T}_m$, u_m^i by dropping terms with $n > m$ in (4.14) and evaluating the remaining $\Pi_{(n)}^{ij}$ on $\mathcal{T}_{m-n}$, u_{m-n}^i. Thus $\mathcal{T}_m$, u_m^i enter (4.10) only through T_{ideal}^{ij} and the equations to be solved are essentially just (4.20), (4.21) with additional source

terms given by the $\Pi^{ij}_{(n)}$. The integration constants (as well as the sign choices that come from solving quadratic equations) may be fixed by requiring $\mathcal{T}_m$, u^i_m to approximate $\mathcal{T}_{m-1}$, u^i_{m-1} to the desired order as $\epsilon \to 0$.

To first order, one finds

$$\mathcal{T}_1^2 = \frac{1}{2}\left(B(x)+\mathcal{T}_\infty\right)^2\left[1+\sqrt{1-\left(\frac{2(A(x)+\mathcal{T}_\infty^2/2a)}{(B(x)+\mathcal{T}_\infty)^2 R}\right)^2}\right], \tag{4.24a}$$

$$u_1^x = \frac{(B(x)+\mathcal{T}_\infty)^2 R}{2(A(x)+\mathcal{T}_\infty^2/2a)}\left[1-\sqrt{1-\left(\frac{2(A(x)+\mathcal{T}_\infty^2/2a)}{(B(x)+\mathcal{T}_\infty)^2 R}\right)^2}\right], \tag{4.24b}$$

where

$$A(x) = \frac{2\ell_4}{3}\int_0^x R\left[\mathcal{T}\sigma^{ij}\sigma_{ij}\right]^{(0)}\,dx', \tag{4.25a}$$

$$B(x) = \frac{2\ell_4}{3}\int_0^x \left[\frac{\mathcal{T}^{-2}D_i\left(\mathcal{T}^2\sigma^i{}_t\right) - u_t\sigma^{ij}\sigma_{ij}}{u^x}\right]^{(0)}\,dx', \tag{4.25b}$$

and the square brackets $[\cdot]^{(0)}$ indicate that the enclosed quantities are evaluated on the zeroth order solutions (4.23a), (4.23b). At this order, the asymptotic temperatures differ and are given by the (finite) expression

$$\mathcal{T}(\pm\infty) = \mathcal{T}_\infty + B(\pm\infty), \tag{4.26}$$

so that

$$\Delta\mathcal{T} := \mathcal{T}(\infty) - \mathcal{T}(-\infty) = B(\infty) - B(-\infty). \tag{4.27}$$

It is useful to consider the further limit of small $\Delta\mathcal{T}$, which greatly simplifies

the above results. This is equivalent to taking a large. Since

$$B(x) = \frac{2\ell_4}{3}\int_0^x \left[-\frac{R''(x')}{2R^2(x')}\,\frac{1}{a} + \mathcal{O}\left(\frac{1}{a}\right)^2\right] dx', \tag{4.28}$$

we find

$$\Delta\mathcal{T} = \frac{2\ell_4}{3}\int_{-\infty}^{\infty} \left[-\frac{R''(x')}{2R^2(x')}\,\frac{1}{a} + \mathcal{O}\left(\frac{1}{a}\right)^2\right] dx' = -\frac{I}{3a} + \mathcal{O}\left(\frac{1}{a}\right)^2, \tag{4.29}$$

for

$$I := \ell_4 \int_{-\infty}^{\infty} \frac{R''(x)}{R^2(x)}\, dx. \tag{4.30}$$

Noting that $A(x) = \mathcal{O}(1/a)^2$ we then find

$$u_1^t = 1 + \mathcal{O}(\Delta\mathcal{T}^2), \tag{4.31a}$$

$$u_1^x = -\frac{3\Delta\mathcal{T}}{2IR(x)} + \mathcal{O}(\Delta\mathcal{T}^2), \tag{4.31b}$$

$$\mathcal{T}_1 = \mathcal{T}_\infty + \frac{\ell_4\Delta\mathcal{T}}{I}\int_0^x \frac{R''(x')}{R^2(x')}\, dx' + \mathcal{O}(\Delta\mathcal{T}^2), \tag{4.31c}$$

so that the non-zero components of the stress tensor are

$$16\pi\ell_4 G^{(4)} T^t{}_t = -2\mathcal{T}_\infty^3 - \frac{6\ell_4\mathcal{T}_\infty^2\Delta\mathcal{T}}{I}\int_0^x \frac{R''(x')}{R^2(x')}\,dx' + \mathcal{O}(\Delta\mathcal{T}^2), \tag{4.32a}$$

$$16\pi\ell_4 G^{(4)} T^t{}_x = -\frac{9\mathcal{T}_\infty^3\Delta\mathcal{T}}{2IR(x)} + \mathcal{O}(\Delta\mathcal{T}^2), \tag{4.32b}$$

$$16\pi\ell_4 G^{(4)} T^x{}_x = \mathcal{T}_\infty^3 - \frac{3\ell_4\mathcal{T}_\infty^2\Delta\mathcal{T}}{I}\left(\frac{R'(x)}{R^2(x)} - \int_0^x \frac{R''(x')}{R^2(x')}\,dx'\right) + \mathcal{O}(\Delta\mathcal{T}^2), \tag{4.32c}$$

$$16\pi\ell_4 G^{(4)} T^\phi{}_\phi = \mathcal{T}_\infty^3 + \frac{3\ell_4\mathcal{T}_\infty^2\Delta\mathcal{T}}{I}\left(\frac{R'(x)}{R^2(x)} + \int_0^x \frac{R''(x')}{R^2(x')}\,dx'\right) + \mathcal{O}(\Delta\mathcal{T}^2). \tag{4.32d}$$

Note that the lowest order term in the energy flux T^{tx} is linear in $\Delta\mathcal{T}$; this naturally leads to a notion of thermal conductivity. We first calculate the heat flux Φ as the energy flux integrated over a circle of constant x:

$$\Phi = 2\pi R(x) T^{tx} = -\frac{9\mathcal{T}_\infty^3\Delta\mathcal{T}}{16\ell_4 G^{(4)} I} + \mathcal{O}(\Delta\mathcal{T}^2). \tag{4.33}$$

We define the thermal conductivity as $k := -d\Phi/d\Delta T|_{\Delta T=0}$ so that

$$k = \frac{3\pi\mathcal{T}_\infty^3}{4G^{(4)} I}. \tag{4.34}$$

We have also explored the analogous results at second order $n = 2$ in the hydrodynamic approximation. While the general expressions are unenlightening, each quantity above agrees with the $n = 1$ expression up to linear order in $\Delta\mathcal{T}$ for all $\mathcal{T}_\infty$. In particular, the conductivity k is unchanged.

Finally, the entropy current $(J^i_S)_1 = su^i$ for our solutions is

$$4G^{(4)}\left(J^t_S\right)_1 = \frac{(B(x)+\mathcal{T}_\infty)^4 R}{2\sqrt{2}\,(A(x)+\mathcal{T}_\infty^2/2a)}\left[1-\sqrt{1-\left(\frac{2(A(x)+\mathcal{T}_\infty^2/2a)}{(B(x)+\mathcal{T}_\infty)^2 R}\right)^2}\right]^{1/2} \times\left(1+\sqrt{1-\left(\frac{2(A(x)+\mathcal{T}_\infty^2/2a)}{(B(x)+\mathcal{T}_\infty)^2 R}\right)^2}\right), \quad (4.35a)$$

$$4G^{(4)}\left(J^x_S\right)_1 = \frac{1}{R}\left(A(x)+\frac{\mathcal{T}_\infty^2}{2a}\right), \quad (4.35b)$$

which has divergence

$$4G^{(4)} D_i\left(J^i_S\right)_1 = \frac{2\ell_4}{3}\left[\mathcal{T}\sigma_{ij}\sigma^{ij}\right]^{(0)} = \frac{\ell_4\mathcal{T}_\infty}{3\sqrt{2}}\frac{R'^2}{R^2(a^2R^2-1)}\left[1+\sqrt{1-\frac{1}{a^2R^2}}\right]^{1/2}. \quad (4.36)$$

To lowest nonvanishing order in $\Delta\mathcal{T}$, these become

$$4G^{(4)}\left(J^t_S\right)_1 = \mathcal{T}_\infty^2 + \frac{2\ell_4\mathcal{T}_\infty\Delta\mathcal{T}}{I}\int_0^x \frac{R''(x')}{R^2(x')}\,dx' + \mathcal{O}(\Delta\mathcal{T}^2), \quad (4.37a)$$

$$4G^{(4)}\left(J^x_S\right)_1 = -\frac{3\mathcal{T}_\infty^2\Delta\mathcal{T}}{2IR(x)} + \mathcal{O}(\Delta\mathcal{T}^2), \quad (4.37b)$$

$$4G^{(4)} D_i\left(J^i_S\right)_1 = \frac{3\ell_4\mathcal{T}_\infty\Delta\mathcal{T}^2}{I^2}\frac{(R')^2}{R^4} + \mathcal{O}(\Delta\mathcal{T})^3. \quad (4.37c)$$

Note that the divergence of the current is of order $\Delta\mathcal{T}^2$ as expected from (4.19). It turns out that (4.37c) is unchanged when one passes to second order in the hydrodynamic expansion, though the entropy current J^i_S itself changes even at zeroth order in $\Delta\mathcal{T}$.

These expressions may of course be transformed to any other conformal frame.

The ultrastatic frame (4.9) used above had the convenient feature that, at least at small velocity, the local fluid temperature (defined with respect to proper time in the fluid rest frame) coincides with the temperature defined with respect to the static Killing field ∂_t. In a more general conformal frame, these two temperatures do not coincide even at small velocity. Note that we will employ only time-independent conformal transformations below, so that ∂_t remains a Killing field in all frames. We will continue to refer to temperatures normalized (up to a boost to the fluid rest frame) with respect to ∂_t by $\mathcal{T}$, while we denote the local fluid temperature (defined with respect to rest-frame proper time) as $\mathcal{T}_{\rm loc}$. Thus $\mathcal{T}$ is unchanged by the conformal transformation while $\mathcal{T}_{\rm loc}$ is rescaled.

For comparison with our later numerics, appendix A.2 presents the results in the black hole frame for the explicit metric functions and in terms of the particular coordinates used in section 4.5 below. The resulting more explicit expressions are correspondingly more complicated than those above.

4.4 How to flow a more general funnel

Our family of flowing funnels will be labeled by four parameters: the temperatures $T_{\pm}^{\text{bndy BH}}$ of the left- and right- boundary black holes and the temperatures $T_{\pm}$ associated with the left- and right- ends of the bulk black hole. As discussed in section 4.2 these four temperatures are completely independent in principle, though in our simulations we will always set $\alpha_+ = \alpha_-$ which introduces one relation.

The most generic ansatz compatible with our symmetry requirements depends

on seven unknown functions:

$$ds^2 = \frac{\ell_4^2}{(1-w^2)^2(1-y^2)^2}\left\{-M(y)G(w)^2(1-w^2)^2\,y^2\,A\,\left[\ell_4^{-1}d\tilde{t}+Q(w)\frac{\chi_2}{y}dy\right]^2\right.$$
$$\left.+\frac{4(1-w^2)^2\,B\,dy^2}{M(y)}+y_0^2\left[\frac{4\,S_1}{2-w^2}\,\left(dw+\ell_4^{-1}\chi_1\,d\tilde{t}+\frac{F\,dy}{y}\right)^2+S_2 d\phi^2\right]\right\}, \quad (4.38)$$

where A, B, F, S_1, S_2, χ_1 and χ_2 are all functions of y and w. In addition we have defined

$$G(w) = 1+\frac{\beta}{2}w^3(5-3\,w^2), \quad (4.39a)$$
$$M(y) = 2-y^2-\frac{(1-y^2)^2(1-y_0^2)}{y_0^2}, \quad (4.39b)$$
$$Q(w) = 1+\frac{2}{M(0)G(w)}. \quad (4.39c)$$

The insertion of these factors will be justified later, when we will also see that β controls the temperature difference between the two boundary black holes, and y_0 is a parameter that controls the validity of the fluid approximation. Here y ranges over $[0,1]$ and w ranges over $[-1,1]$, with $y=0$ being the bulk horizon and $y=1$ the conformal boundary. At least for $y\neq 0$ regions with $w\sim\pm 1$ are close (in the sense of a conformal diagram) to where either bulk horizon meets either the left or right boundary black hole (compare with figure 4.2). As we will explain below, the symbol $\tilde{t}$ was used in (4.38) in order to save t for another coordinate associated with Fefferman-Graham gauge. However, $\partial_{\tilde{t}}=\partial_t$ so we will refer to the time-translation as simply ∂_t.

4.4.1 Boundary Conditions

At the conformal boundary ($y = 1$) we impose the boundary conditions

$$A(w,1) = B(w,1) = S_1(w,1) = S_2(w,1) = \chi_2(w,1) = 1, \tag{4.40a}$$

$$F(w,1) = \chi_1(w,1) = 0, \tag{4.40b}$$

which ensures a boundary metric conformal to

$$\ell_4^{-2} ds_\partial^2 = -\frac{1}{\ell_4^2 y_0^2}(1-\hat{\rho}^2)^2 G(\hat{\rho})^2\, dt^2 + \frac{4d\hat{\rho}^2}{2-\hat{\rho}^2} + d\phi^2\,, \tag{4.41}$$

where $\hat{\rho} = \rho/\ell_4$. As in section 4.2, we refer to (4.41) as the boundary metric in the black hole conformal frame. In presenting our results in section 4.5 we will describe all boundary quantities, such as the stress energy tensor, with respect to this frame. The boundary metric ds_∂^2 has horizons at $\hat{\rho} = \pm 1$ with Hawking temperatures

$$T_\pm^{\text{bndy BH}} = \frac{G(\pm 1)}{2\pi \ell_4 y_0}\,. \tag{4.42}$$

We will extract the boundary stress tensor following the strategy of [61] and using the results of [96]. The only technical difference with respect to [61] involves the relation between the coordinates $(\tilde{t}, w, y, \phi)$ and Fefferman-Graham coordinates (t, z, ρ, ϕ). Due to the cross term χ_2 in Eq. (4.38) the map between $\tilde{t}$ and t is not trivial, instead it is expressed as a powers series in z of the form:

$$\tilde{t} = t + z\, T_1(\rho) + \mathcal{O}(z^2) \tag{4.43}$$

where for instance $T_1(\rho) = -Q(\rho)y_0/(2(1-\hat{\rho}^2))$.

The left and right boundaries lie at $w = \pm 1$. There we impose

$$A(\pm 1, y) = B(\pm 1, y) = S_1(\pm 1, y) = S_2(\pm 1, y) = \chi_2(\pm 1, y) = 1, \tag{4.44a}$$

$$F(\pm 1, y) = \chi_1(\pm 1, y) = 0, \tag{4.44b}$$

which reduces Eq. (4.38) to

$$ds^2|_{w\to\pm 1} = \frac{\ell_4^2}{(1-y^2)^2}\left\{-M(y)G(\pm 1)^2\, y^2\left[\ell_4^{-1}d\tilde{t} + Q(\pm 1)\frac{dy}{y}\right]^2 + \frac{4\,dy^2}{M(y)} + \frac{y_0^2}{(1\mp w)^2}\left(dw^2 + \frac{d\phi^2}{4}\right)\right\}. \tag{4.45}$$

Under the coordinate transformation:

$$y = \sqrt{1 - \frac{r_0}{r}}, \tag{4.46a}$$

$$\frac{r_0}{\ell_4^2}d\tau = G(\pm 1)\left(\ell_4^{-1}d\tilde{t} + \frac{Q(\pm 1)\,dy}{y}\right), \tag{4.46b}$$

$$w = \pm 1 \mp e^{-\xi}, \quad y_0 \equiv \frac{r_0}{\ell_4}, \tag{4.46c}$$

the line element (4.45) yields the large ξ limit of Eq. (4.2) with $d = 3$. The fact that our ansatz (4.38) reduces to a hyperbolic black hole at $w = \pm 1$ displays the physical meaning of y_0 as an overall scale that controls the bulk horizon temperatures (and thus $\alpha_\pm$). Note that the line element (4.45) also defines $T_\pm = T_\pm^{\text{bndy BH}} M(0)/2$. If $y_0 = 1$, then $T_\pm = T_\pm^{\text{bndy BH}}$, *i.e.* it represents the 'tuned' case $\alpha_\pm = 1$. Thus the fluid approximation becomes more accurate as y_0 increases, or equivalently, as $\alpha_\pm$ decrease.

We have imposed Dirichlet data at each of the above three edges of our computational domain. But it remains to specify boundary conditions at $y = 0$, the flowing funnel horizon. Here we demand that the line element (4.38) be smooth in ingoing Eddington-Finkelstein coordinates (which cover the future horizon). To understand the explicit form of this condition, we introduce local ingoing Eddington-Finkelstein coordinates $(v, \tilde{w}, \tilde{y}, \phi)$ through

$$dv = d\tilde{t} + \ell_4 \frac{d\tilde{y}}{2\tilde{y}} + \mathcal{O}(\tilde{y}^0), \quad d\tilde{w} = \frac{dw}{\chi_1(w,0)} + \ell_4^{-1} dv + \mathcal{O}(\tilde{y}^0)\,, \quad y = \tilde{y}^{1/2}. \quad (4.47)$$

The terms omitted in the above $\tilde{y}$ expansion can be chosen such that a line of constant $(v, \tilde{w}, \phi)$ is an ingoing null geodesic. Note that lines of constant v have $d\tilde{y}/d\tilde{t} < 0$, as required for ingoing coordinates. Furthermore, regularity of the line element (4.38) in the above coordinates requires

$$F(w,0) = \chi_1(w,0), \quad (4.48a)$$

$$B(w,0) = \frac{M(0)^2 G(w)^2 A(w,0)}{4} \left[1 - Q(w)\chi_2(w,0)\right]^2, \quad (4.48b)$$

$$\partial_y A(w,0) = \partial_y S_1(w,0) = \partial_y S_2(w,0) = \partial_y \chi_1(w,0) = \partial_y \chi_2(w,0) = 0. \quad (4.48c)$$

We will find $\chi_1(w,0)$ to be finite and non-zero (at $w \neq \pm 1$), so our original w is already an ingoing coordinate. It will thus be straightforward to read off results associated with the future horizon.

The past horizon is more subtle. It is located at $v \to -\infty$ and can be reached along lines of constant $\tilde{w}$. Depending on the sign of χ_1, this tends to drive w to either ± 1. Below, we consider $T_+ > T_-$ so that the hotter black hole is on the

right. One might therefore expect w to decrease along the horizon generators so their coordinate velocity is toward the cooler black hole; i.e., one might expect $\chi_1(w, 0) > 0$. But for the particular ansatz we have chosen our numerics turn out to give $\chi_1 < 0$ (see section 4.5) so that the past horizon in fact lies at $w = -1$. This appears to be a coordinate artifact, though a full understanding is beyond the scope of this work.

Below, we will solve the Einstein equations (with cosmological constant) in the form

$$E_{ab} := R_{ab} + \frac{3}{\ell_4^2} g_{ab} = 0, \tag{4.49}$$

subject to the boundary conditions detailed above.

4.4.2 The DeTurck Method

The diffeomorphism invariance of (4.49) means that these equations do not lead to a well-posed boundary value problem. While one could attempt to proceed by gauge-fixing, a clever trick known as the DeTurck method was introduced in [184] and in [164, 194] was shown to succeed (under rather general assumptions) when one seeks appropriate stationary equilibrium solutions of the vacuum Einstein equations, with or without a negative cosmological constant. Though our situation turns out to fall outside the bounds of the proof given in [164], we nevertheless employ this method successfully below.

We begin with a brief review. The DeTurck method is based on the so called Einstein-DeTurck equation

$$E^H_{ab} \equiv E_{ab} - \nabla_{(a}\hat{\xi}_{b)} = 0, \tag{4.50}$$

which differs from from Eq. (4.49) by the addition of $-\nabla_{(a}\hat{\xi}_{b)}$. Here $\hat{\xi}^a = g^{cd}[\Gamma^a_{cd}(g) - \Gamma^a_{cd}(\bar{g})]$, $\Gamma(\mathfrak{g})$ is the Levi-Civita connection associated with the metric $\mathfrak{g}$, and $\bar{g}$ is some specified non-dynamical reference metric. Since $\hat{\xi}$ is defined by a difference between two connections, it transforms as a tensor. Hereafter $\bar{g}$ will be chosen to have the same asymptotics and horizon structure as g. In particular, it must satisfy the same Dirichlet boundary conditions as g.

Clearly any solution to $E^H_{ab} = 0$ with $\hat{\xi} = 0$ also solves $E_{ab} = 0$. But one may ask if (4.50) can have additional solutions that do not satisfy $E_{ab} = 0$. Under a variety of circumstances one can show that solutions with $\hat{\xi} \neq 0$, the so called Ricci solitons, cannot exist [164]. However, the assumptions used in [164] seem not to hold for our system of equations. In particular, after reduction along the symmetry directions t, ϕ our system turns out to have a mixed-elliptic hyperbolic nature. This is most easily seen from the fact that, while our system will be elliptic near infinity where ∂_t is timelike, we expect an ergoregion near the horizon where all linear combinations of $\partial_t, \partial_\phi$ are spacelike. So in this region reduction along (t, ϕ) gives a Lorentz-signature metric on the base space. This differs qualitatively from the case of Kerr, where $\partial_t, \partial_\phi$ span a timelike plane everywhere outside the horizon and reduction along (t, ϕ) gives a Euclidean-signature metric on the base space. See [194] for a more detailed discussion. The difference arises from the fact that the Kerr horizon 'flows' only along the Killing field ∂_ϕ while our horizon 'flows' in the w direction, which is not associated with any symmetry. Thus Ricci solitons may well exist in our case. But for any solution to (4.50) one may simply calculate $\hat{\xi}$ to see if it vanishes. For all of our flowing funnel solutions discussed below we find $\hat{\xi} = 0$ to machine precision.

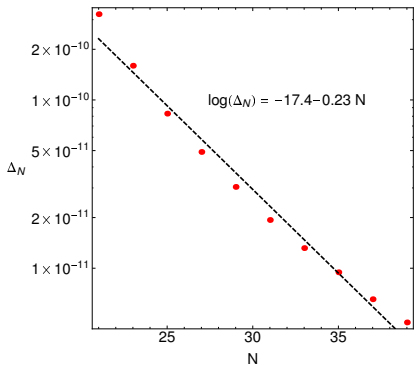

Figure 4.3: Δ_N as a function of the number of grid points N. The vertical scale is logarithmic, and the data is well fit by an exponential decay: $\log(\Delta_N) = -17.4 - 0.23\,N$.

It remains to specify our choice of reference metric $\bar{g}$. We choose $\bar{g}$ to be given by the line element (4.38) with $A = B = S_1 = S_2 = \chi_2 = 1$ and $F = \chi_1 = 0$. This enforces all Dirichlet boundary conditions except those at the horizon, Eq. (4.48). To satisfy these remaining conditions we need only choose $Q(x)$ as in Eq. (4.39).

4.4.3 Numerical Method

We use a standard pseudospectral collocation approximation in w, y and solve the resulting non-linear algebraic equations using a damped Newton method with damping monitoring function $|\hat{\xi}_t|$. This ensures that Newton's method takes a path in the approximate solution space that decreases $|\hat{\xi}_t|$ at each step. This method may also prove useful in solving more general mixed elliptic-hyperbolic systems. We represent the w and y dependence of all functions as a series in Chebyshev polynomials. As explained above, our integration domain lives on a rectangular grid, $(w, y) \in [-1, 1] \times [0, 1]$.

To monitor the convergence of our method we have computed the total heat

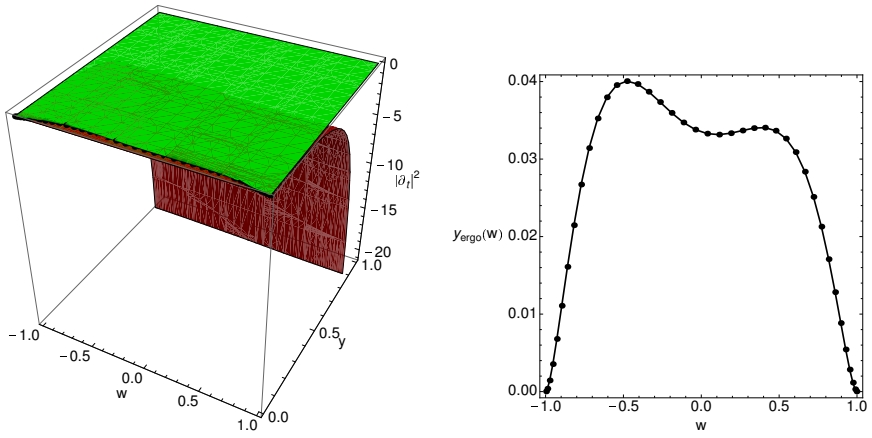

(a) (b)

Figure 4.4: (a): The curved surface shows the norm of ∂_t over our integration domain. To guide the eye, we also draw a flat horizontal surface at zero norm. (b): The ergosurface as a function of w. Both figures use $\alpha_\pm = 1$ and $\Delta T/T_\infty = 0.2$.

flux Φ (defined by the first equality in (4.33)) for several resolutions. We denote the number of grid points in w and y by N and compute $\Delta_N = |1 - \Phi_N/\Phi_{N+1}|$ for several values of N. The results for this procedure are illustrated in Fig. 4.3 for $\beta = 0.1$ and $y_0 = 1$. We find exponential convergence with N, as expected for pseudospectral collocation methods. Furthermore, in order to ensure that we are converging to an Einstein solution rather than a Ricci soliton we monitor all components of $\hat{\xi}$. For all plots shown in this manuscript, each component of $\hat{\xi}_a$ has absolute value smaller than 10^{-10}.

4.5 Results and comparisons

We now present the results of our numerical analysis and compare them with the first-order ($n = 1$) hydrodynamic approximation. The plots below are labeled

by a parameter T_∞ whose definition

$$T_\infty = \frac{\left[256\left(144\sqrt{2}-557\right)\lambda^2 + 105\pi\left(293\lambda^2+128\right)\right]\left(3y_0^2-1\right)}{28\pi\left[15\pi\left(293\lambda^2+128\right)-11008\lambda^2\right]y_0^2} \tag{4.51}$$

was inspired by the first-order hydrodynamic result (4.24a). For small ΔT we have $T_\infty = (T_+ + T_-)/2 + \mathcal{O}(\Delta T)^2$. We note that all the numerical results we will present use units where $\ell_4 = 1$ (so that $\rho = \hat{\rho}$) and $16\pi G^{(4)} = 1$. We also take $T_+ > T_-$ so that the hotter black hole lies on the right.

We begin with the norm $|\partial_t|^2$ of the time translation. Figure 4.4(a) shows a typical plot. To guide the eye we have also plotted a reference surface of constant $|\partial_t|^2 = 0$. The two surfaces intersect at the ergosurface, whose location we display separately in Fig. 4.4(b). Inside the ergoregion $|\partial_t|^2$ becomes positive, changing the character of Eq. (4.50) from elliptic to hyperbolic. This region is at the core of the difficulties in trying to prove that our numerical method ensures $\hat{\xi} = 0$ on solutions of Eq. (4.50) with appropriate boundary conditions. Fig. 4.5 shows $|\partial_t|^2$ and, for comparison and later use, $|\partial_\phi|^2$ as a function of w along the horizon. We remind the reader that ∂_t and ∂_ϕ are precisely orthogonal everywhere in our spacetime, so this describes the full induced metric h_{IJ} (for $I, J = t, \phi$) in the 2-plane spanned by $\partial_t, \partial_\phi$. Both norms are clearly positive everywhere on the horizon, though $|\partial_t|^2$ never becomes very large even with $\Delta T/T_\infty = 0.2$. This may help to explain why our numerical approach succeeded.

Let us now discuss the behavior of the boundary stress tensor. For small $\alpha, \Delta T/T_\infty$, this quantity may also be computed using the hydrodynamic approximation of section 4.3 and provides another good check of our numerics. Fig. 4.6

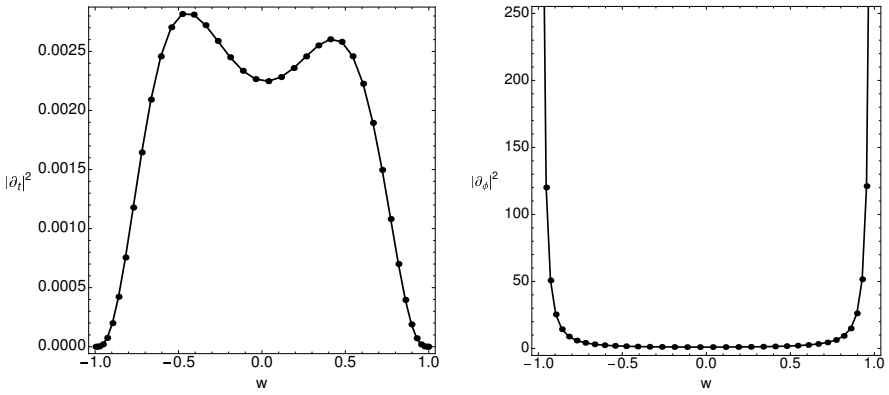

(a) (b)

Figure 4.5: (a): The norm $|\partial_t|^2$ on the future horizon. (b): The norm $|\partial_\phi|^2$ on the future horizon. Both figures use $\alpha_\pm = 1$ and $\Delta T/T_\infty = 0.2$ and are plotted as functions of w.

shows the components of the stress energy tensor as a function of the boundary coordinate ρ for several values of α at fixed β. The lines represent the first order hydrodynamic prediction and the symbols represent data extracted from our numerics. Large stress tensors correspond to larger values of α. We see that at least for small $\Delta T/T_\infty$ the fluid gravity prediction works remarkably well even for for $\alpha \sim 0.8$. The agreement of all of these curves when α is small is a reassuring test of our numerics. However, at larger α qualitative differences from our hydrodynamic approximation begin to appear. For example, we note that while $T^t{}_t$ is always negative (and thus the energy density is positive) in the hydrodynamic regime, for $\alpha \gtrsim 1$ our simulations show $T^t{}_t$ becomes positive near the hotter black hole.

From the standpoint of the dual CFT, the main physical result of our paper is displayed in Fig. 4.7. This plot shows how the total heat flux Φ varies for different values of $\Delta T/T_\infty$ and $\alpha = \alpha_+ = \alpha_-$. We see that it increases in magnitude as

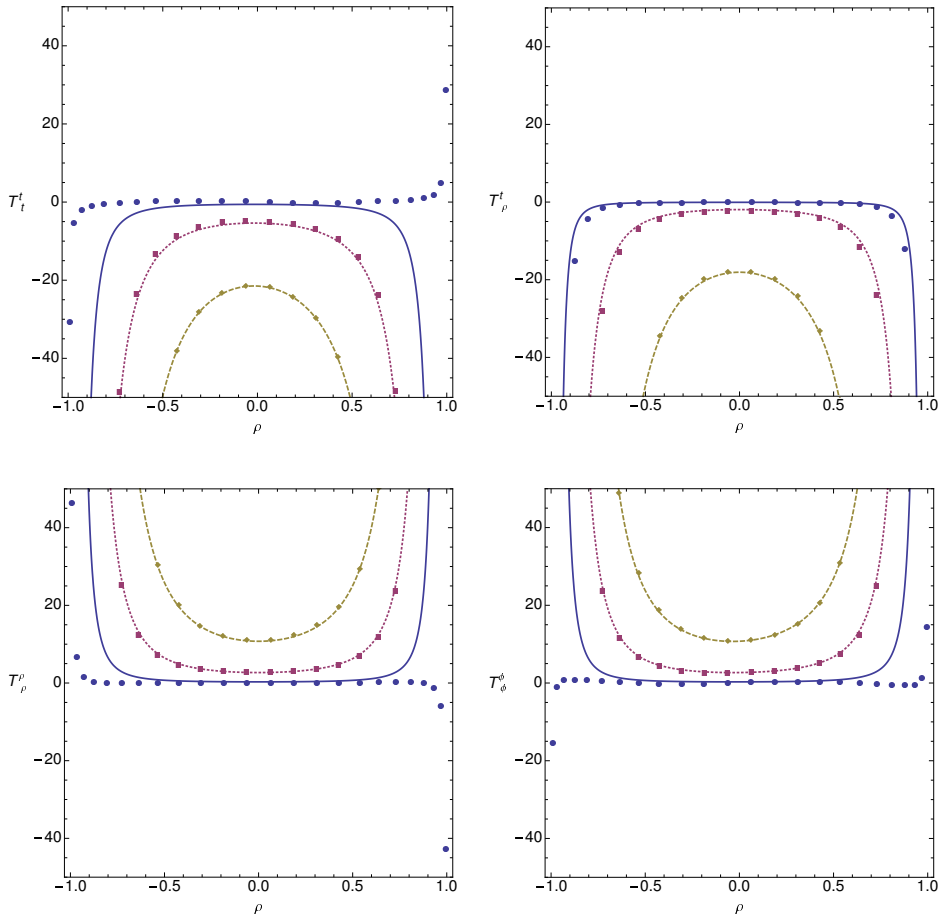

Figure 4.6: Components of the boundary stress energy tensor as a function of ρ for fixed $\beta = 0.04$. Each panel shows the first-order ($n = 1$) hydrodynamic prediction as lines and the exact numerical data as symbols. The disks and solid line show $\alpha_\pm = 1$, the squares and dashed line show $\alpha_\pm = 0.77$ and the diamonds and dotted line show $\alpha_\pm = 0.70$. These corresponds to $\Delta T/T_\infty = 0.080$, $\Delta T/T_\infty = 0.050$ and $\Delta T/T_\infty = 0.034$, respectively. Since $\Delta T/T_\infty$ is small, we have used only the linear results from appendix A.2 to plot the hydrodynamics.

$\Delta T/T_\infty$ increases, and also as α decreases. This computation can be seen as a first principle calculation for the thermal conductivity of a strongly coupled plasma at large N beyond the hydrodynamic regime. Fig. 4.8 compares some $\alpha = $ const. cross-sections of Fig. 4.7 to the the results of first-order ($n = 1$) hydrodynamics at linear order in ΔT; i.e., to (A.9b)-(A.9e). These show good agreement for small α

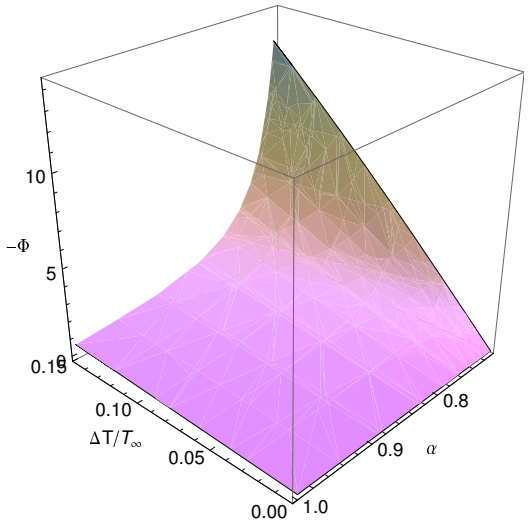

Figure 4.7: Three-dimensional plot of the boundary flux extracted from our numerics as a function of $\Delta T/T_\infty$ and $\alpha = \alpha_+ = \alpha_-$.

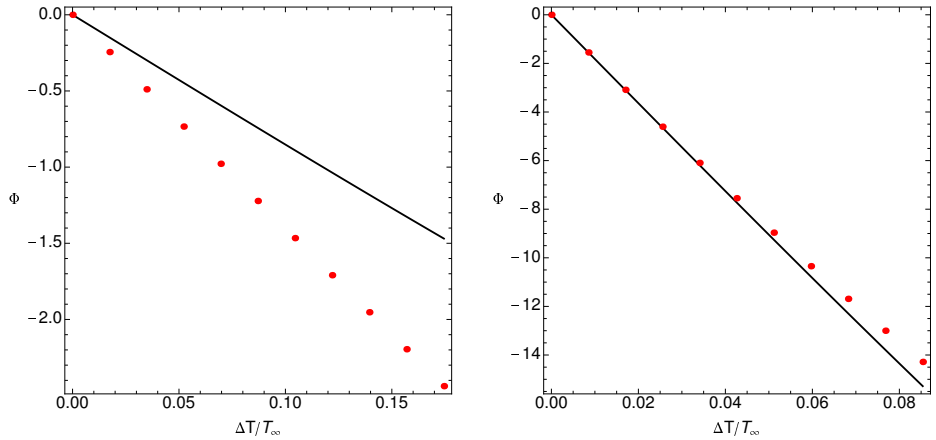

Figure 4.8: The total heat flux Φ as a function of $\Delta T/T_\infty$ for $\alpha = 0.9$ (left) and $\alpha = 0.7$ (right). The solid curves are the first order hydrodynamic results. Since $\Delta T/T_\infty$ is small, we have used only the linear results from appendix A.2. The dots show our numerical data.

and ΔT, but deviate as expected at larger α.

It remains to examine the horizon more closely. Our horizon is a three-dimensional null surface and, since $\partial_t, \partial_\phi$ are both spacelike and tangent to the horizon, any two null geodesics that generate the future horizon generators are

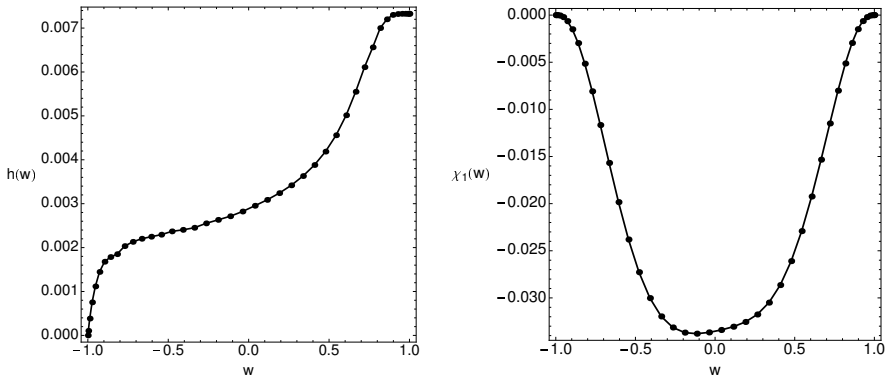

(a) (b)

Figure 4.9: (a): The determinant $h = h_{tt}h_{\phi\phi}$. (b): The metric component χ_1 along the horizon. Both quantities are plotted as functions of w for $\alpha_\pm = 1$ and $\Delta T/T_\infty = 0.2$.

related by some isometry. Thus all generators are equivalent, though it remains to understand the evolution of the spacetime along each generator. We compute the affine parameter, expansion, and shear along each generator using simple expressions in terms of the induced metric h_{IJ} (for $I, J = t, \phi$) on the 2-plane spanned by $\partial_t, \partial_\phi$. These expressions are given in appendix A.3. We study each of these quantities only on the surface $y = 0$.

We begin with h_{IJ} itself. Recall that $w = \pm 1$ are the asymptotic regions of static hyperbolic black holes where the Killing field ∂_t becomes null at the horizon and $|\partial_\phi|^2$ becomes large. These behaviors are clearly shown in figure 4.9(a). But these similarities between $w = \pm 1$ are misleading and the actual behaviors at $w = \pm 1$ are quite different. This may be seen from the plot of $h = \det h_{IJ} = h_{tt}h_{\phi\phi} = |\partial_t|^2|\partial_\phi|^2$ in Fig. 4.9(a). This determinant vanishes at $w = -1$ but approaches a non-zero constant at $w = +1$. Note that h is monotonic along $y = 0$, as it must be along a smooth horizon.

What is perhaps surprising is that h is an increasing function of w. This shows that w increases toward the future along the future horizon, so that the past horizon must lie at $w = -1$. In contrast, in the coordinates of e.g. [63], the coordinate velocity of the horizon generators would be in the direction of heat transport, and thus (since we take the cooler black hole to lie at $w = -1$) toward negative w. Standard coordinates for Kerr also behave like those of [63] and have the equivalent of our χ_1 being positive for positive angular velocity. In contrast, we find χ_1 to be negative at the horizon; see figure 4.9(b). Since χ_1 samples completely different metric components than h, we take this as a strong indication that our solutions are consistent despite the surprising location of the past horizon. Another strong indication of consistency is the above agreement between our boundary stress tensors and those predicted by the hydrodynamic approximation. Indeed, we have tested for various possible errors (such as inverting the sign of ΔT) in our code by examining the effect of various sign changes on Fig. 4.6 and found in each case that such changes would lead to notable discrepancies with hydrodynamics. In particular, we stress that our simulations give the physically correct sign for the heat flux $T^t{}_\rho$.

The apparent proximity of the past horizon to the cooler black hole must thus be a coordinate artifact. We have confirmed this expectation by repeating our simulations in the coordinates defined by Eq. (4.47) and finding that the equivalent of χ_1 is positive for negative heat flux. For comparison, we mention that also note that a similarly surprising sign can be found in the 2+1 flowing funnels of [73]. In that case, writing the horizon generating Killing field in the Fefferman-Graham coordinates of [73] leads to a negative t component on part

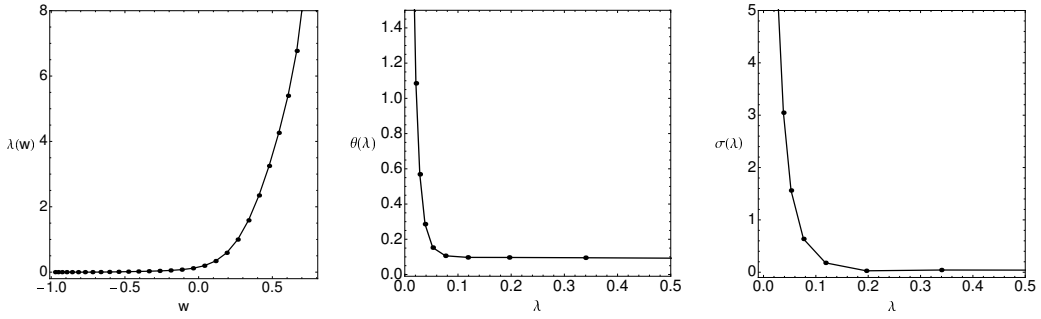

(a) (b) (c)

Figure 4.10: (a): An affine parameter along the horizon as a function of w. (b): The expansion of a future horizon generator as a function of λ. (c): The positive eigenvalue σ of $\hat{\sigma}^I{}_J$ as a function of λ. At small λ we find $\sigma \sim \lambda^{-5/6}$. All figures use $\alpha_\pm = 1$ and $\Delta T/T_\infty = 0.2$.

of the horizon, even though this component is everywhere positive at the AlAdS boundary. It would also be interesting to transform our current 3+1 solutions to the coordinates of [63] (say, for a solution deep within the hydrodynamic regime), though the additional numerics required places such an analysis is beyond the scope of this work.

We may now proceed to investigate various quantities along the horizon. Perhaps the most important quantity is the affine parameter λ, which we show in Fig. 4.10(a) as function of w. Note that λ approaches a constant value at $w = -1$. This is to be expected, as we have already noted that $w = -1$ is the past horizon. Since the affine parameter is only defined up to affine transformations, this constant is arbitrary and we have set $\lambda(w = -1) = 0$ for convenience. In contrast, the affine parameter diverges as we approach $w = 1$.

Figure 4.10(b) shows the expansion θ as a function of λ. As expected on general grounds, θ is everywhere positive with $d\theta/d\lambda < 0$ and θ asymptotes to zero at large λ. We see this as the most solid test of our numerics. Note that

the sign of $d\theta/d\lambda < 0$ is only guaranteed via Raychaudhuri's equation once the equations of motion are used. It is thus far from trivial that the sign comes out right.

The expansion diverges at the past horizon ($\lambda = 0$), indicating the presence of a caustic. In fact, it is easy to see that this caustic is a curvature singularity. To do so, note from 4.5(b) that $|\partial_\phi|$ diverges on the past horizon. But since Killing fields obey a second order differential equation governed by the Riemann tensor (see e.g. (C.3.6) of [90]) they can diverge at finite affine parameter only if R_{abcd} diverges in all orthonormal frames.

We now turn to the shear tensor $\hat{\sigma}_{IJ}$. From (A.14), (A.17) we see that since h_{IJ} is diagonal, the same is true of $\hat{\sigma}_{IJ}$. Since $\hat{\sigma}_{IJ}$ is also symmetric and traceless, it is completely characterized by the positive eigenvalue σ of $\hat{\sigma}^I{}_J$, where the index was raised with the inverse h^{IJ} of h_{IJ}. Note that σ is a spacetime scalar.

This eigenvalue is plotted as a function of λ in figure 4.10(c). As one might expect, it diverges at the caustic. What is interesting is that we find the same divergence structure for all $\alpha, \Delta T$ that we have studied. We quantify this behavior by fitting $\sigma(\lambda)$ to a power law $\mu\,\lambda^\eta$ near $\lambda = 0$. We have extracted η for about 400 flowing funnels spanning the domain $(\alpha, \Delta T/T_\infty) \in (1, 0.7) \times (0, 0.4)$. In all cases we find $\eta = -0.82 \pm 0.03$, where this error is in fact the maximum deviation. We note that this number is remarkably close to $-5/6$. We can then use the Raychaudhuri equation (A.18) and the standard evolution equation for the shear (see (F.34) of [195]) to again show that R_{abcd} diverges on the past horizon. In fact, for $\eta = -5/6$ one may show that some Weyl tensor component $C_{abcd}k^b k^d$ (where k^a is an affinely parametrized tangent to a null generator of the horizon)

must diverge like $\lambda^{-11/6}$. This fact merits an analytic explanation which we are unable to offer at this time.

4.6 Discussion

The above work constructs 'flowing funnel' stationary black hole solutions. Such solutions describe heat flow between reservoirs at unequal temperatures $T_{\pm}$. The particular solutions constructed are global AdS_4 flowing funnels which may be thought of as deformations of the BTZ black string (4.1). Thus each heat reservoir lies just outside a boundary black hole of temperature $\alpha_{\pm}T_{\pm}$. For the case $\alpha_{\pm} = 1$, the CFT_3 duals of our bulk solutions describe heat transfer between two non-dynamical 3-dimensional black holes due to CFT_3 Hawking radiation .

Our solutions display many properties expected on general grounds. There is a connected ergoregion near the horizon where ∂_t becomes spacelike. In fact, all Killing fields are spacelike at the future horizon $\mathcal{H}$, so that $\mathcal{H}$ is not a Killing horizon. This is consistent with the rigidity theorems [185–187] since $\mathcal{H}$ is not compact.

The expansion θ of the null generators is everywhere positive but decreases toward the future along each null generator. The generators extend to infinite affine parameter in the far future (where $\theta \to 0$) but reach a caustic ($\theta \to \infty$) at finite affine parameter toward the past. This caustic occurs on the past horizon, which is a curvature singularity characterized by a universal power law divergences for the shear $\sigma \sim \lambda^{-5/6}$ and for certain components of the Weyl tensor which grow like $\lambda^{-11/6}$ in any orthonormal frame. These exponents were found numerically,

but merit an analytic understanding. It remains an open question whether curvature scalars (e.g. the Kretschmann scalar $R_{abcd}R^{abcd}$) might remain finite[4]. It would also be interesting to study the exponents governing the divergence of the expansion θ, the norm $|\partial_\phi|^2$ and the inverse norm $|\partial_t|^{-2}$, though these have proved to be more difficult to extract from our numerics.

Note that $|\partial_\phi|$ decreases with λ along the early part of the future horizon. But since $\theta > 0$, the shrinkage of the ϕ circle with affine parameter λ is more than compensated by the growth in $|\partial_t|$. This positive expansion is associated with the expected generation of entropy due to the transport of heat from a hot source to a cold sink. In particular, it is the analogue at large $\alpha_\pm, \Delta T/T_\infty$ of the entropy generation term (4.19) seen in the hydrodynamic approximation.

In our coordinate system, the horizon generators appear to flow toward the hotter black hole. While we have confirmed that this is a coordinate artifact, it would nevertheless be desirable to understand the effect in more detail.

We studied the boundary stress tensor of such solutions both numerically and to first order in the hydrodynamic (fluid/gravity) approximation. In particular, we computed the total heat flux Φ for boundary metrics of the form (4.41) as a function of $\alpha, \Delta T/T_\infty$; see figure 4.7. It would clearly be of interest to study more general boundary metrics to understand which parts of this function are universal and which depend on detailed features of the boundary metric.

The hydrodynamic approximation is a derivative expansion which, since we fix all other parameters in the boundary metric, is for us governed by the parameters $\alpha_\pm$ (which control the extent to which the bulk and boundary black hole tempera-

[4]Due to the large number of terms involved, we were not able to reliably calculate $R_{abcd}R^{abcd}$ from our numerics.

tures are detuned) and $\Delta T/(T_+ + T_-)$ (which controls the temperature difference between the heat source and sink). As expected, we find excellent quantitative agreement when these parameters are small. Interestingly, we also find good qualitative agreement when these parameters are close to 1. This gives yet another confirmation of the robust nature of the fluid/gravity correspondence as seen previously in e.g. [146]. Of course, at large enough values of $\alpha_\pm, \Delta T/(T_+ + T_-)$ we find both quantitative and qualitative disagreement. It would be interesting see to what extent agreement might be improved by incorporating higher order hydrodynamic corrections. A particularly notable feature at large α ($\alpha_+ \gtrsim 1$ in our simulations) is that, while $T^t{}_t$ is always negative in the hydrodynamic limit, it becomes positive close to the hotter boundary black hole black hole. It would be interesting to understand this feature analytically.

Chapter 5

A Rotating Black Droplet

5.1 Introduction

Since the revolutionary discovery that black holes radiate with an almost thermal spectrum, much effort has been devoted to gaining a deeper understanding of this process. While considerable advances have been made since Hawking's seminal paper [196], there are still ample open issues that remain to be addressed. In particular, most of the work regarding Hawking radiation has focused on free fields; studying the behavior of *interacting* fields around a black hole is more challenging. Though some progress has been made with weakly interacting fields using perturbative methods [197], strongly interacting fields pose a much more difficult problem.

Fortunately, the AdS/CFT correspondence [19] provides an invaluable tool for tackling this problem. Early applications of holography to studying Hawking radiation coupled the field theory to dynamical gravity, which is holographically dual

to Randall-Sundrum braneworld models [150, 151, 173]. However, if one is not interested in the backreaction of the Hawking radiation on the spacetime, the CFT can be placed on a nondynamical background spacetime $\partial\mathcal{M}$. Then AdS/CFT claims that the CFT is dual to a spacetime $\mathcal{M}$ with conformal boundary $\partial\mathcal{M}$, with $\mathcal{M}$ a solution to classical Einstein gravity with negative cosmological constant. While most applications of the duality place the field theory on ordinary Minkowski space, one may in principle select any conformal boundary structure one desires. In particular, in order to study Hawking radiation in the CFT, [57, 59] considered a CFT living on fixed d-dimensional background containing a black hole of size R and temperature $T_{\rm BH}$. Far away from the black hole, the CFT is in a thermal state with a prescribed temperature T_∞. From the perspective of the CFT, the black hole and the plasma at infinity act as heat sources and sinks, and one can study the exchange of heat between them.

In fact, a complete picture requires the introduction of another parameter T_0, representing the temperature of the CFT plasma near the black hole. Though it might seem natural to take this temperature to be equal to that of the black hole, it is possible to set $T_0 \neq T_{\rm BH}$ at the expense of making the CFT stress tensor singular at the black hole horizon. Details of this so-called "detuning" can be found in [74], though in our solution we will only consider the "tuned" case $T_0 = T_{\rm BH}$ and will therefore never introduce the parameter T_0 explicitly.

Regarding the dual geometry, [57, 59] conjecture two possible families of solutions: so-called "black droplets" and "black funnels," illustrated in Figure 5.1. In the black funnel solutions, the horizon of the boundary black hole is connected to an asymptotically planar horizon in the bulk; this connectedness manifests itself

in the CFT as strong coupling between the boundary black hole and the heat bath at infinity, leading to an exchange of heat between them. In the black droplet solutions, on the other hand, the horizon of the boundary black hole is disconnected from the asymptotically planar horizon in the bulk, implying that the boundary black hole is not coupled to the plasma at infinity (or rather, that the coupling is suppressed by $\mathcal{O}(1/N^2)$ is this large-N picture). From the perspective of the CFT, the transition from funnels to droplets is reminiscent of many soft condensed matter systems which exhibit a transition from a fluid-like behavior to rigid behavior with no flow (e.g. sand in an hourglass, cars on a highway). To borrow from the soft condensed matter nomenclature, we will refer to the the CFT transition from funnels to droplets as a "jamming" phase transition, and will denote the CFT dual of the droplet as a "jammed" phase[1].

The authors of [57, 59] postulate that this jamming transition might occur as the size R of the boundary black hole (or alternatively, as the temperature T_∞ of the heat bath at infinity) is varied. Thus the dimensionless parameter RT_∞ should characterize which phase is thermodynamically preferred.

An analytic construction of black droplets and black funnels has only been performed in select few cases. In [58, 60], black droplets and funnels were constructed from the AdS C-metric, while [73] constructed analytic funnels in $d = 2$ dual to the Unruh state of the CFT (black droplets cannot exist in $d = 2$). However, many of the most interesting cases (notably, asymptotically flat boundary black holes in $d > 2$) do not lend themselves to analytic construction, and one must resort to numerics. To that end, [61] numerically constructed black funnels

[1]We thank Jean Carlson for introducing us to this terminology.

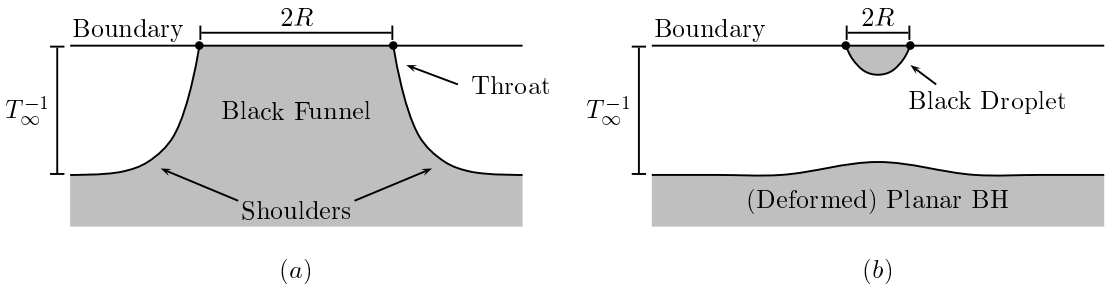

Figure 5.1: A sketch of the relevant solutions: **(a):** black funnel and **(b):** black droplet above a deformed planar black hole. Both describe possible states of dual field theories in contact with heat baths at temperature T_∞ on spacetimes containing black holes of horizon size R. The top line corresponds to the boundary, with the dots denoting the horizon of the boundary black hole. The shaded regions are those inside the bulk horizons.

dual to the Hartle-Hawking state of the CFT, while [74] constructed so-called global funnels to study the exchange of heat between two boundary black holes of different temperatures.

Slightly less effort has been made to construct black droplets, however. Besides those obtained from the AdS C-metric, the only construction to date has been that of [164], which constructed a droplet dual to the Unruh state of a CFT on a $d = 4$ Schwarzschild background (hereafter generally denoted Schw_d). In our notation, this solution sets $T_\infty = 0$, so that the bulk geometry is that of a black droplet suspended above an extremal Poincaré horizon deep in the bulk. The boundary stress tensor contains no flux terms, and the nonzero components of the stress tensor exhibit a $1/r^5$ power-law falloff at large distances from the black hole. This relatively rapid falloff is characteristic of the jammed phase, as it indicates that the CFT plasma is relatively well-localized near the black hole. Interestingly, the stress tensor is regular on both the past and future horizons; the authors speculate that the inclusion of one-loop graviton corrections in the bulk would render the

stress tensor singular on the past horizon, as is typical of Unruh states.

Perhaps some clarifying remarks are in order regarding our nomenclature of CFT states. In free field theory, the distinction between the Unruh, Hartle-Hawking, and Boulware vacua is conventionally based on the behavior of the field theory stress tensor at the horizon and at null infinity. In the Hartle-Hawking state, the stress tensor is regular on both the future and past horizon; in the Unruh state, the stress tensor is empty at past null infinity and regular on the future horizon; and in the Boulware state, the stress tensor is empty at both future and past null infinity. However, one can also understand these behaviors very physically from the point of view of the field theory. The Hartle-Hawking state is one in which the field theory is in thermal equilibrium, with all temperatures equal; in our language, $T_{\rm BH} = T_0 = T_\infty$. The Unruh state is one in which the temperature of the heat bath at infinity is taken to zero (so that for any nonzero T_0, the black hole acts as a source for heat to flow to infinity); $T_\infty = 0$. Finally, the Boulware state is the state of minimum energy, requiring the temperature of the field theory to be zero everywhere; $T_0 = T_\infty = 0$. A crucial point to note is the appearance of the field theory temperature T_0 (rather than the black hole temperature $T_{\rm BH}$) in the above definitions. Thus the regularity properties of the field theory stress tensor in a given state can be thought of as a consequence of how the temperatures T_0 and $T_{\rm BH}$ are tuned, and not as a defining feature of the state itself. For instance, the ubiquitous singularity of the Boulware vacuum on the horizon of a nonextremal black hole is due to the detuning $T_0 = 0 \neq T_{\rm BH}$, whereas the Hartle-Hawking state is generally regular on the black hole horizon because of the requirement that $T_0 = T_{\rm BH}$. When labeling states in strongly

coupled CFTs, we will therefore operate under these latter definitions in terms of the temperatures T_0 and T_∞ of the CFT. For example, we would claim that the CFT dual to the droplet constructed in [164] is in the Unruh state, but not the Boulware state, because $T_\infty = 0$ but $T_0 = T_{\rm BH} \neq 0$. These definitions are also independent of whether the CFT is in the jammed or unjammed phase, so that the categorization of the state and phase of the CFT provide complementary descriptions of its behavior.

Our purpose in this paper is to generalize the result of [164] by adding a new ingredient: rotation. Though [59, 198] compute the stress tensor on a rotating BTZ black hole background, the effect of rotation on a stress tensor in an *asympototically flat* black hole spacetime has not been studied extensively. One might naturally expect that the inclusion of rotation can be accomplished by generalizing the result of [164] to a Kerr spacetime, but because the Kerr metric is cohomogeneity two, this would lead to a cohomogeneity three problem in the bulk. Instead, we take the boundary spacetime to be the $d = 5$ equal-angular-momentum Myers-Perry metric [199] (see also [200] for a review), which is known to be cohomogeneity one and thus leads to a cohomogeneity two problem in the bulk.

The generalization to a non-extremal rotating black droplet should not be expected to exhibit very different behavior from its non-rotating counterpart: the boundary black hole still acts as a heat source at finite and nonzero temperature, and one studies the thermal coupling between the black hole and a zero-temperature heat bath at infinity. However, the presence of rotation provides us with a new parameter to tune, which we can use to take the black hole to

extremality; this will allow us to take T_0 to zero without the need to perform any detuning. For this reason, from this point on we will only refer to $T_{\rm BH}$, with $T_0 = T_{\rm BH}$ understood implicitly.

Taking $T_{\rm BH}$ to zero with T_∞ fixed at zero can be thought of as some limit of an Unruh state. Similarly, the fact that both the extremal black hole and the heat bath at infinity are at zero temperature places the CFT in the Boulware vacuum. Finally, since in the extremal case $T_{\rm BH} = T_\infty$, the CFT can be thought of as being in a Hartle-Hawking state (though perhaps it would be more correct to refer to this as a zero-temperature *limit* of a Hartle-Hawking state). Thus the extremal droplet is in some sense dual to a degenerate state which is a Boulware state and a limit of the Hartle-Hawking and Unruh states.

This paper is organized as follows. In Section 5.2, we review the behavior of stress tensors on black hole spacetimes, and calculate the form our stress tensor must take on a Schw_5 background (i.e. when the angular momentum of the Myers-Perry black hole is taken to zero). In Section 5.3, we briefly review the numerical method used and discuss the numerical construction of our solution. In Section 5.4, we compare our numerically extracted stress tensor to the expectations in Section 5.2, and discuss future directions to pursue.

Note: In the final stages of this work we learned of [201], which also constructs rotating black droplets and may have some overlap with our work. Their paper will appear simultaneously with ours on the arXiv.

5.2 A Review of Stress Tensors in Curved Spacetime

A common difficulty of field theories in curved spacetime is the lack of an unambiguous notion of "particle." This poses no problem, however, if one instead limits oneself only to *currents*. As discussed in [202], when a physical system is probed, the objects that couple to probe fields are currents. In other words, the currents are the objects that appear in the interaction terms in the equations of motion of an interacting field. In addition, a current is a genuinely local object and should retain a well-defined meaning even in the presence of strong external fields (such as spacetime curvature). Thus most of the work devoted to understanding the process of radiation from black holes has focused not on quantum fields themselves, but on the renormalized vacuum expectation value (v.e.v.) of their stress-energy tensor $\langle T^{\mu\nu} \rangle$.

In particular, the stress tensor of quantum fields can exhibit properties that are forbidden of classical stress tensors. For instance, though a classical energy density must be non-negative, it is well-known that even in flat spacetime, the local energy density of a quantum field need not obey this same restriction[2]. Perhaps the most famous example of a negative energy density is the Casimir effect [203], though the existence of negative energy densities in local quantum field theory is in fact quite general [204].

[2]Here, we define the local energy density as measured by an observer with velocity u^μ as

$$\rho = u^\mu u^\nu \langle T_{\mu\nu} \rangle$$

In the context of general relativity, [202] studied the behavior of the energy-momentum tensor of a massless scalar field in a two-dimensional spacetime containing an accelerating mirror. While the total energy radiated by the mirror was positive, a negative energy density and energy flux were present in the region near the mirror, whereas far from the mirror the stress tensor took the classical form of an outward flux of positive energy. A similar result was found by [205], which calculated the renormalized v.e.v. of the stress tensor of a massless scalar field in a two-dimensional model of black hole collapse. As in the case of the radiating mirror, the near-horizon region of the newly-formed black hole was characterized by a negative energy density and a flux of negative energy flowing into the black hole, while far from the black hole the stress tensor again took the form of an outward flux of positive energy. These results are consistent with Hawking's picture of particle-antiparticle creation near the horizon of a black hole, where negative-energy particles flow into the black hole while their positive-energy partners radiate to infinity: by conservation of energy, a positive-energy flux at infinity should be accompanied by a negative-energy flux through the black hole horizon.

These exact results were obtained by exploiting the conformal flatness of two-dimensional spacetimes. Nevertheless, good approximations to thermal stress tensors have been obtained in higher dimensions. Notably, [206] used the Bekenstein-Parker Gaussian path integral approximation [207] to find the approximate form of the stress tensor of a conformally invariant scalar field in the Hartle-Hawking state on the (four-dimensional) Schwarzschild background. The behavior of the stress tensor was similar to the two-dimensional case: at infinity, the stress tensor behaved like a classical thermal stress tensor, while sufficiently near the horizon

(for $r \lesssim 2.34M$) the energy density became negative. These results were consistent with earlier numerical calculations [208] of the stress tensor on the bifurcation two-sphere of Schwarzschild. However, while one naturally expects a negative energy flux near the horizon in an Unruh state, it is not clear whether the ubiquity of negative energy densities near the horizon should extend to Hartle-Hawking states as well.

All of these results focused explicitly on conformally invariant noninteracting massless scalar fields. One might therefore imagine that they have little bearing on the stress tensor we will obtain for our strongly coupled CFT. In fact, the jammed phase dual to the droplet we construct cannot exist in a free field theory, so *a priori* none of the results listed above can even approximately predict the behavior of the stress tensor we will extract. Nevertheless, it is possible (and indeed, quite probable) that the stress tensor of quantum fields on black hole backgrounds should exhibit some kind of universal qualitative behavior. This universal structure was studied in detail by Christensen and Fulling [209], who sought the general behavior of a static, spherically symmetric stress tensor on Schw_4 by solving the conservation equations

$$\nabla_\mu T^{\mu\nu} = 0 \tag{5.1}$$

directly, without restriction to any particular kind of field theory. Their results are particularly useful to our case, because they are also valid in the case of a strongly coupled CFT. In fact, Schw_5 is just the zero-angular momentum limit of the Myers-Perry black holes that we Schwarzschild in higher dimensions.

5.2.1 The General Static Spherically Symmetric Stress Tensor on Schw$_d$

Consider the d-dimensional Schwarzschild metric Schw$_d$ (also called the Tangherlini metric, after its discoverer [210]):

$$ds^2_{\text{Schw}} = -f(r)\,dt^2 + \frac{dr^2}{f(r)} + r^2\,d\Omega^2_{d-2}, \quad f(r) \equiv 1 - \left(\frac{r_0}{r}\right)^{d-3}. \tag{5.2}$$

This spacetime is qualitatively identical to the familiar four-dimensional Schwarzschild, with horizon located at $r = r_0$ and a temperature $T = f'(r_0)/4\pi = (d-3)/4\pi r_0$. Now, a static, spherically symmetric stress tensor must take the form

$$T^{\mu}{}_{\nu} = \begin{pmatrix} T^t{}_t & T^t{}_r & 0 \\ T^r{}_t & T^r{}_r & 0 \\ 0 & 0 & T^{\Omega}{}_{\Omega}\delta^i_j \end{pmatrix}, \tag{5.3}$$

where all components are functions of r only and the indices i, j run over the angular coordinates. Inserting this form into the conservation equations (5.1) and using the metric (5.2), we obtain the following differential equations:

$$0 = \partial_r T^r{}_t + \frac{d-2}{r}\,T^r{}_t, \tag{5.4a}$$

$$0 = \partial_r T^r{}_r + \left(\frac{d-2}{r} - \frac{d-3}{2r_0}\frac{(r_0/r)^{d-2}}{f(r)}\right)T^r{}_r - \frac{d-3}{2r_0}\frac{(r_0/r)^{d-2}}{f(r)}\,T^t{}_t - \frac{d-2}{r}\,T^{\Omega}{}_{\Omega}. \tag{5.4b}$$

Equation (5.4a) can be immediately integrated to yield

$$T^{r}{}_{t} = K\left(\frac{r_0}{r}\right)^{d-2}. \tag{5.5}$$

To integrate equation (5.4b), we first substitute $T^{t}{}_{t} = T^{\mu}{}_{\mu} - T^{r}{}_{r} - (d-2)T^{\Omega}{}_{\Omega}$, and obtain

$$T^{r}{}_{r} = \frac{(r_0/r)^{d-2}}{f(r)}\left[Q - K + \frac{1}{2}\int_{r_0}^{r}\left((d-3)T^{\mu}{}_{\mu}(r') + (d-2)\left(2(r'/r_0)^{d-3} - d + 1\right)T^{\Omega}{}_{\Omega}(r')\right)\frac{dr'}{r_0}\right]. \tag{5.6}$$

Equations (5.5) and (5.6) express the most general static, spherically symmetric stress tensor on Schw_d in terms of two arbitrary constants Q and K and two arbitrary functions $T^{\mu}{}_{\mu}$ and $T^{\Omega}{}_{\Omega}$. In order to study the physical behavior of these solutions, it will prove useful to define

$$\Theta(r) \equiv T^{\Omega}{}_{\Omega}(r) - \frac{1}{2(d-2)}T^{\mu}{}_{\mu}(r), \tag{5.7a}$$

$$G(r) \equiv \frac{d-2}{2}\int_{r_0}^{r}\left(2(r'/r_0)^{d-3} - d + 1\right)\Theta(r')\frac{dr'}{r_0}, \tag{5.7b}$$

$$H(r) \equiv \frac{1}{2}\int_{r_0}^{r}\left(\frac{d-5}{2} + (r'/r_0)^{d-3}\right)T^{\mu}{}_{\mu}(r')\frac{dr'}{r_0}. \tag{5.7c}$$

Converting to the tortoise coordinate $dr_* = dr/f(r)$, the stress tensor can then be expressed as the sum of four pieces:

$$T^{\mu}{}_{\nu} = (T_{(1)})^{\mu}{}_{\nu} + (T_{(2)})^{\mu}{}_{\nu} + (T_{(3)})^{\mu}{}_{\nu} + (T_{(4)})^{\mu}{}_{\nu}, \tag{5.8}$$

where (in t, r_* coordinates)

$$(T_{(1)})^{\mu}{}_{\nu} = \mathrm{diag}\left\{-\frac{(r_0/r)^{d-2}}{f(r)}\,H(r) + \frac{1}{2}\,T^{\mu}{}_{\mu}(r),\ \frac{(r_0/r)^{d-2}}{f(r)}\,H(r),\ \frac{1}{2(d-2)}\,T^{\mu}{}_{\mu}(r)\,\delta^i_j\right\}, \tag{5.9a}$$

$$(T_{(2)})^{\mu}{}_{\nu} = K\,\frac{(r_0/r)^{d-2}}{f(r)}\begin{pmatrix} 1 & 1 & 0 \\ -1 & -1 & 0 \\ 0 & 0 & 0 \end{pmatrix}, \tag{5.9b}$$

$$(T_{(3)})^{\mu}{}_{\nu} = \mathrm{diag}\left\{-\frac{(r_0/r)^{d-2}}{f(r)}\,G(r) - (d-2)\Theta(r),\ \frac{(r_0/r)^{d-2}}{f(r)}\,G(r),\ \Theta(r)\,\delta^i_j\right\}, \tag{5.9c}$$

$$(T_{(4)})^{\mu}{}_{\nu} = Q\,\frac{(r_0/r)^{d-2}}{f(r)}\,\mathrm{diag}\left\{-1,\,1,\,0\right\}. \tag{5.9d}$$

By converting to ingoing Eddington-Finkelstein coordinates $dv = dt + dr_*$, it is straightforward to show that the stress tensor is regular on the future horizon only if Q vanishes[3]. Thus the above decomposition is convenient because each of the $T_{(i)}$ isolates some interesting physical behavior of the stress tensor: $T_{(1)}$ is the only of the $T_{(i)}$ with a nonzero trace (and in fact, it is only a function of the trace $T^{\mu}{}_{\mu}$); $T_{(2)}$ contains nonzero flux terms $T^{r_*}{}_{t}$; $T_{(3)}$ is the only of the $T_{(i)}$ which is both traceless and has nonzero tangential pressure components; and $T_{(4)}$ is singular on the future horizon.

Christensen and Fulling proceed to make use of these results to study the behavior of the stress tensor of fields in the Unruh, Hartle-Hawking, and Boulware vacua on Schw$_4$. Our goal, however, is less broad: we only wish to gain some

[3]Regularity on the past horizon requires $Q = 2K$.

insight on the v.e.v. of the stress tensor of the jammed phase of the CFT. To that end, we make the following observations regarding our droplet:

- The trace anomaly of any odd-dimensional CFT vanishes. Since we work in $d = 5$, we expect $T_{(1)}$ to make no contribution to our stress tensor.

- According to the arguments reviewed briefly at the end of Section 5.1, we expect black droplets to be dual to a jammed phase of the CFT. Such phases are characterized by a suppressed exchange of heat between the black hole and the thermal plasma at infinity, so we should expect our solution to radiate no flux. From (5.5), it is clear that the total flux radiated to infinity from the black hole is a constant proportional to K, so we conclude that $K = 0$ and so $T_{(2)}$ makes no contribution to our stress tensor.

- Unlike the past horizon, which is present only in maximal analytic extensions of black hole spacetimes, the future horizon is a genuine physical location present in any realistic model of gravitational collapse. We thus expect physical quantities to be regular there. In particular, we require the stress tensor of the jammed CFT to be regular there; this implies that $Q = 0$, so that $T_{(4)}$ does not contribute to the stress tensor either (incidentally, since we also have $K = 0$, this means that the stress tensor will be regular at the past horizon as well).

We therefore conclude that only contribution to the stress tensor of the CFT state dual to the Schw_5 droplet should come from (5.9c), and so should only depend on the one function $\Theta(r)$.

In fact, we can go further and make claims about the behavior of $\Theta(r)$. The free field results summarized earlier in this section should not all apply to our stress tensor, but we might draw certain universal behavior from them to make a guess at the behavior of $\Theta(r)$ (which we will then verify with our numerics). First, note that the negative energy density near the horizon present in free field theories is an indication of the highly non-classical nature of the field there; only far from the black hole does the stress tensor of the free fields become classical. But the jammed phase of the CFT is a highly non-classical state, as it consists of a plasma "halo" surrounding the black hole. In analogy with the free field theory results, we might therefore conjecture that the energy density of the strongly coupled CFT becomes negative near the horizon as well. In that case, we expand $(T_{(3)})^t{}_t = -3\Theta(r_0)/2 + \mathcal{O}(r - r_0)$ to see that a negative energy density near the horizon implies that Θ is negative there.

Far from the black hole, one can argue that due to the weak coupling between the black hole and the heat bath at infinity, the components of the stress tensor should fall off "rapidly". This statement can be quantified by following the logic of [164]: there, the authors find that the v.e.v. of a CFT dual to a $d = 4$ Schwarzschild droplet exhibits a $1/r^5$ falloff. In order to explain this falloff, the authors invoke the results of [211], in which the linearized gravitational field created by a point-like source is calculated in the context of the Randall-Sundrum single braneworld model. By using the behavior of the gravitational field far from the source, Einstein's equations

$$R_{\mu\nu} - \frac{1}{2} R g_{\mu\nu} = 8\pi G_N \langle T_{\mu\nu} \rangle \tag{5.10}$$

can be used to obtain the expected large-r behavior of the stress tensor. For the case of a $d = 4$ dimensional spacetime, the predicted falloff of the components $\langle T^{\mu}{}_{\nu} \rangle$ goes like $1/r^5$, consistent with the results of [164]. One can generalize this argument to show that in $d = 5$ dimensions, we expect a $1/r^7$ falloff[4]. This implies that for our solution, we should have $\Theta(r) \sim 1/r^7$ and $G(r) \sim 1/r^4$ at large r.

5.2.2 A Little Spin

Finally, let us consider the effect of giving the boundary black hole a nonzero angular momentum, thus "spinning" the droplet. Unfortunately, an analysis similar to that performed for the nonspinning case is not illuminating, because even with the conservation equations (5.1), there are too many independent functions in the stress tensor for a general solution to be tractable. Nevertheless, we can make some qualitative claims based on physical arguments.

First, we clearly expect there to be angular flux terms as the CFT plasma is dragged around the spinning black hole. This flux density should be maximal near the horizon, and decrease monotonically away from the black hole. Similarly, the fact that the CFT plasma is being forced to rotate around the black hole leads us to expect that a centrifugal barrier forms around the black hole. Indeed, by considering timelike geodesics in the equatorial plane of the five-dimensional equal-angular-momentum Myers-Perry black hole, we can check that the centrifugal barrier of the effective radial potential grows and moves away from the horizon as the spin of the black hole is increased. This barrier may act to confine the plasma

[4]We greatly thank the authors of [201] for finding a mistake in an earlier version of this paper, where we incorrectly claimed a falloff of $1/r^6$ in five dimensions.

near the black hole horizon, effectively acting as a box around the black hole. We might expect that this effect would present itself as an increase in the radial and tangential pressures near the horizon. We should similarly expect an increase in the magnitude of the (negative) energy density near the black hole, as a buildup of negative-energy modes forms in the centrifugal box. This physical reasoning leads us to conjecture that all components of the stress tensor should increase in magnitude as the angular momentum of the black hole is increased.

5.2.3 Extremal Horizons

Our family of solution black holes can be taken all the way to extremality. This limit is particularly interesting, as the causal structure of an extremal black hole is qualitatively very different from its non-extremal relatives. One might therefore imagine that the stress tensor of matter fields on extremal black hole spacetimes exhibits qualitatively different behavior as well. In particular, the fact that the horizon of an extremal black hole is a Cauchy horizon would naïvely lead one to believe that stress tensors should generically be singular on the future horizon of extremal black holes. This question has been addressed by [212–215], who studied the regularity of the v.e.v. of the stress tensor outside an extremal dimensionally reduced two-dimensional Reissner-Nordström (RN) black hole. In short, a static stress tensor (i.e. one sharing the same isometries as the background spacetime) exhibits a mild singularity on the future horizon, whereas the stress tensor of a massive scalar field propagating on an extremal two-dimensional RN geometry forming via gravitational collapse is regular thanks to the presence of decaying (but nonzero) flux terms. As shown in [216], this subtle issue disappears in four

dimensions, as the stress tensor of a scalar field in the zero-temperature vacuum state on the full four-dimensional RN spacetime is regular everywhere without the need for flux terms.

To our knowledge, the stress tensor of a field theory on a *rotating* extremal black hole background has not yet been studied even in free field theory. The four-dimensional RN results might lead us to expect that the stress tensor on extremal rotating black hole spacetimes should similarly be regular on the future horizon, though a key difference between the RN and rotating case is the inherent presence of matter in the RN spacetime. In any case, the fundamental similarity between the causal structures of extremal charged and rotating black holes makes it quite plausible to expect that the CFT stress tensor dual to our rotating droplet will be regular on the future horizon even in the extremal limit.

5.3 Constructing a Spinning Droplet

5.3.1 The DeTurck Method

The standard approach in AdS/CFT is to solve the vacuum Einstein field equations with negative cosmological constant[5]

$$E_{ab} \equiv R_{ab} - \frac{1}{2} R g_{ab} + \Lambda g_{ab} = 0 \tag{5.11}$$

subject to certain boundary conditions. The subleading behavior of the metric g_{ab} near the conformal boundary then contains information about the stress tensor of

[5]Here and below, we will use lower-case Latin letters to denote bulk indices, and lower-case Greek letters to denote boundary indices.

the dual CFT. As is well known, Einstein's equations do not have a well defined character unless a gauge choice is made. Because the solutions we are searching for are stationary, one can hope to choose a clever gauge where the equations (5.11), or a deformation thereof, are manifestly elliptic. This is exactly what the DeTurck trick does for us [164, 184, 217]. In short, one modifies the equations (5.11) by introducing a new vector ξ^a (called the DeTurck vector):

$$E^H_{ab} \equiv E_{ab} - \nabla_{(a}\xi_{b)} = 0, \quad \xi^a = g^{bc}\left(\Gamma^a_{bc} - \bar{\Gamma}^a_{bc}\right), \tag{5.12}$$

where $\bar{\Gamma}^a_{bc}$ is the Levi-Civita connection of some reference metric $\bar{g}$. Equation (5.12) is called the Einstein-DeTurck or harmonic Einstein equation. One can show that for stationary solutions with Killing horizons, the above choice of the DeTurck vector renders the Einstein-DeTurck equation elliptic. Solving the Einstein-deTurck equations then reduces to solving a boundary-value problem. Note, however, that solutions to the Einstein-DeTurck equation are not solutions to the ordinary Einstein equations unless $\xi^a = 0$. To get around this problem, one can show that the quantity $\Phi \equiv \xi_a\xi^a$ must take its maximum value on the boundaries of the domain of integration; thus if the reference metric $\bar{g}$ is chosen with the same boundary conditions as the metric g, Φ is zero on all boundaries of the integration domain, and must therefore be zero everywhere within as well [164]. Then ξ^a is zero as well, and a solution to the Einstein-DeTurck equation is also a solution to the Einstein equations. Indeed, the claim that the Einstein-DeTurck equation automatically takes care of gauge-fixing is justified by thinking of the condition $\xi^a = 0$ as just a choice of gauge, which is a generalized harmonic gauge of the form $\Delta x^a = \bar{\Gamma}^a_{bc}g^{bc}$.

5.3.2 Droplet Ansatz

As mentioned at the end of Section 5.1, the boundary metric we want to impose is the equal-angular-momentum $d = 5$ Myers-Perry solution [199]:

$$ds^2_{\rm MP} = -\frac{g(r)}{h(r)}\,dt^2 + \frac{dr^2}{g(r)} + r^2\left[h(r)\left(d\psi + A_{(1)} + \Omega(r)dt\right)^2 + d\Sigma_2^2\right], \tag{5.13a}$$

$$g(r) \equiv \frac{(r^2 - r_0^2)(r^2 - \beta^2(r^2 + r_0^2))}{(1-\beta^2)r^4}, \tag{5.13b}$$

$$h(r) \equiv \frac{r^4 - \beta^2(r^4 - r_0^4)}{(1-\beta^2)r^4}, \tag{5.13c}$$

$$\Omega(r) \equiv \frac{\beta r_0^3}{r^4 - \beta^2(r^4 - r_0^4)}, \tag{5.13d}$$

where $d\Sigma_2^2$ is the Fubini-Study metric on CP^1, $A_{(1)}$ is the Kähler potential of CP^1, and $\beta = r_0\Omega_H$, with Ω_H the angular velocity of the horizon. Explicit forms for $A_{(1)}$ and $d\Sigma_2^2$ are given by the expressions

$$A_{(1)} = \frac{1}{2}\cos\theta\,d\phi, \quad d\Sigma_2^2 = \frac{1}{4}\left(d\theta^2 + \sin^2\theta\,d\phi^2\right). \tag{5.14}$$

For $\beta = 0$, the metric (5.13) reduces to $d = 5$ Schwarzschild (5.2) with the S^3 written as a Hopf fibration of S^1 over CP^1; setting $\beta^2 = \beta^2_{\rm ext} \equiv 1/2$ yields the extremal solution. The metric is cohomogeneity one owing to its $U(2)$ symmetry, which implies that our bulk solution will be cohomogeneity two.

Let us compactify the range of the radial coordinate r to yield a metric more amenable to our numerical approach. We also rescale $t \to r_0\,t$ and exploit the coordinate freedom $\psi \to \psi + \lambda t$ to shift Ω so that $\Omega(r_0) = 0$, $\Omega(\infty) = -\Omega_H$ (this

will simplify the boundary conditions at the horizon later on). Defining a new radial coordinate $y = 1 - (r_0/r)^2$, we find

$$ds^2_{\rm MP} = r_0^2 \left\{ -y\,\frac{h_1(y)}{h_2(y)}\,dt^2 + \frac{(1-\beta^2)dy^2}{4y\,h_1(y)(1-y)^3} + \frac{1}{1-y}\left[\frac{h_2(y)}{1-\beta^2}\left(d\psi + A_{(1)} - \beta(1-\beta^2)\,\frac{y(2-y)}{h_2(y)}\,dt\right)^2 + d\Sigma_2^2\right]\right\}, \quad (5.15a)$$

$$h_1(y) \equiv 1 - \beta^2(2-y), \quad (5.15b)$$

$$h_2(y) \equiv 1 - \beta^2 y(2-y). \quad (5.15c)$$

Our ansatz will need to have (5.15) as its conformal boundary.

Next, recall that we are considering black droplet solutions with $T_\infty = 0$; this implies that far into the bulk, the solution should approach the near-horizon geometry of pure AdS_6 in Poincaré coordinates. Poincaré AdS_6 in standard coordinates can be written as

$$ds^2_{\rm Poin} = \frac{\ell^2}{z^2}\left[-dt^2 + dz^2 + dr^2 + r^2 d\Omega_3^2\right], \quad (5.16)$$

where ℓ is the AdS_6 length scale, related to the cosmological constant by $\ell^2 = -10/\Lambda_6$. Changing variables to (x, y) defined by

$$z = \frac{1-x^2}{\sqrt{1-y}}, \quad r = x\sqrt{\frac{2-x^2}{1-y}}, \quad (5.17)$$

the Poincaré metric becomes

$$ds^2_{\rm Poin} = \frac{\ell^2}{(1-x^2)^2}\left[-(1-y)\,dt^2 + \frac{dy^2}{4(1-y)^2} + \frac{4\,dx^2}{2-x^2} + x^2(2-x^2)d\Omega_3^2\right]. \tag{5.18}$$

The near-horizon region corresponds to taking y close to 1.

We are now ready to write down an ansatz. Consider

$$\begin{aligned} ds^2 = \frac{\ell^2(1-y)}{(1-x^2)^2}\Bigg\{ & -y\,T\,\frac{h_1(y)}{h_2(y)}\,dt^2 + \frac{A\,dy^2}{4yh_1(y)(1-y)^3} \\ & + \frac{4B}{(1-y)(2-x^2)}\left(dx + F\,\frac{x(1-x^2)}{2(1-y)}\,dy\right)^2 \\ & + \frac{x^2(2-x^2)}{1-y}\left[\tilde{h}_2(x,y)C\left(d\psi + A_{(1)} - G\,\frac{y(2-y)}{h_2(y)}dt\right)^2 + S\,d\Sigma_2^2\right]\Bigg\}, \end{aligned} \tag{5.19}$$

where

$$\tilde{h}_2(x,y) \equiv 1 + x^2\left(\frac{h_2(y)}{1-\beta^2} - 1\right), \tag{5.20}$$

T, A, B, C, S, F, and G are all functions of x and y, and the coordinate range is the rectangle $(x,y) \in (0,1)\times(0,1)$. For the non-extremal case $\beta \neq 1/\sqrt{2}$, our boundary conditions are as follows:

- At the conformal boundary $x \to 1$, we take $T = A/(1-\beta^2) = C = S = r_0^2/\ell^2$, $B = 1$, $G = \beta(1-\beta^2)$, and $F = 0$. Then the metric approaches

$$ds^2 \to \frac{\ell^2}{(1-x)^2}\left(dx^2 + \frac{1-y}{4\ell^2}\,ds^2_{\rm MP}\right) \tag{5.21}$$

  as desired.

- Near the extremal Poincaré horizon $y \to 1$, we take $T = A/(1-\beta^2) = B =$

$C = S = 1$, $G = \text{const.} = \beta(1-\beta^2)$, and $F = 0$ (note that the constant value of G is fixed by requiring consistency with the boundary condition at $x = 1$). Changing to a new coordinate $\psi \to \psi + \beta t$ removes the dt cross-terms, and we recover the $y \to 1$ limit of (5.18).

- At the horizon $y \to 0$, we require regularity of the metric, which imposes a relationship between T and A. In particular, we must have $T/A = (r_0\kappa/(1-2\beta^2))^2$, where $\kappa = (1-2\beta^2)/(r_0\sqrt{1-\beta^2})$ is the surface gravity of the boundary black hole. Thus we find $T/A = 1/(1-\beta^2)$. In addition, expanding the equations of motion and the condition $\xi^a = 0$ order-by-order near $y = 0$ gives Robin conditions on $\partial_y M_i|_{y=0}$ for $M_i = \{T, A, B, C, S, F, G\}$.

- At the fixed point of the $U(2)$ isometry $x = 0$, we require regularity as well. Again, this implies that all metric functions must be smooth functions of x^2, giving the Neumann conditions $\partial_x M_i|_{x=0} = 0$. In addition, note that while the forms $x^2(d\psi + A_{(1)})$ and $x dx$ are regular at $x = 0$, in general the metric components

$$2\,B\,dx^2 + 2\,x^2\left[\tilde{h}_2(x,y)C\left(d\psi + A_{(1)}\right)^2 + S\,d\Sigma_2^2\right] \tag{5.22}$$

are not. In order to make the above expression regular, we must impose that $B = C = S$ at $x = 0$, so that

$$2\,B\,dx^2 + 2\,x^2\left[\tilde{h}_2(x,y)C\left(d\psi + A_{(1)}\right)^2 + S\,d\Sigma_2^2\right] \to 2S(dx^2 + x^2 d\Omega_3^2), \tag{5.23}$$

which is manifestly regular there.

Having understood the boundary conditions on each side of the computational rectangle, we choose the reference metric. Noting from (5.15) that the boundary black hole size r_0 enters only as a conformal factor, we can choose without loss of generality to set $r_0 = \ell$. Then the boundary conditions become consistent, and we take the reference metric to be the ansatz (5.19) with $T = A/(1-\beta^2) = B = C = S = 1$, $G = \beta(1-\beta^2)$, and $F = 0$.

The extremal case ($\beta = \beta_{\text{ext}} \equiv 1/\sqrt{2}$) takes a little more care. Though our ansatz (5.19) still applies, one finds that as extremality is approached the metric function F attains a very large value along $y = 0$ near $x = 0$, leading to large numerical errors. To alleviate the problem, we rewrite (5.19) in terms of a new metric function $\widetilde{F} = yF$; we then find that the numerics are much more well-behaved when written in terms of the new $\widetilde{F}$ rather than the old F. Then the boundary conditions at the conformal boundary, fixed point of the $U(2)$ isometry, and extremal Poincaré horizon remain the same as those discussed above, while at the extremal droplet horizon we require $\tilde{F} = 0$. In addition, converting to Eddington-Finkelstein coordinates and requiring regularity at the extremal droplet horizon imposes the usual regularity condition $A(x,0) = (1-\beta_{\text{ext}}^2)T(x,0) = T(x,0)/2$, as well as the condition $G(x,0) = \text{const.} = \beta_{\text{ext}}(1-\beta_{\text{ext}}^2) = 1/\sqrt{8}$. Boundary conditions on the other metric functions are obtained by expanding the equations of motion order-by-order near $y = 0$ and requiring that they vanish to leading order.

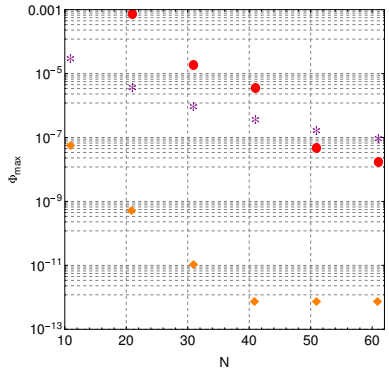

Figure 5.2: The maximum value of the square of the DeTurck vector Φ as a function of N for $\beta = 0$ (circles), 0.6 (diamonds), and $\beta_{\text{ext}} \approx 0.707$ (asterisks).

5.3.3 Numerics

We approximate the Einstein-DeTurck equation (5.12) with the ansatz (5.19) using pseudospectral collocation methods on a Chebyshev grid. The resulting nonlinear algebraic equations are solved using a damped Newton-Raphson method. We monitor the damping with $|E^H_{ab}|$; that is, we ensure that each iteration of the Newton's method decrease the magnitude of E^H_{ab}. Due to the maximum principle that $\Phi \equiv \xi_a \xi^a$ obeys, we can monitor the error in our solutions by monitoring the maximum value of Φ. In Figure 5.2, we plot the maximum value of Φ as a function of the number N of grid points for three different values of the rotation parameter β, showing the expected exponential decrease. Note that we will find later that the accuracy of the extracted of the stress tensor depends strongly on the number of grid points used along the x-direction, so for all results shown in this paper, we use an $N_x \times N_y = 81 \times 41$ grid.

5.3.4 Extraction of the Stress Tensor

In order to extract the boundary stress tensor from our solutions, we follow the approach used in [61]. In short, we first expand the metric functions M_i as a power series in x off of the boundary at $x = 1$:

$$M_i(x, y) = \sum_{n=0} M_i^{(n)}(y)(1-x)^n + \ln(1-x) \sum_{n=0} \widetilde{M}_i^{(n)}(y)(1-x)^n, \tag{5.24}$$

where the logarithmic terms only appear for $\beta \neq 0$ and at no lower order than $n = 5$. Inserting these expansions into (5.12) and in addition imposing $\xi^a = 0$ allows us to solve for the coefficients of the power series order-by-order in $(1-x)$. The expansion is unique up to $n = 4$ for the functions $\{T, A, C, S, F, G\}$ and up to $n = 5$ for the function B. We then change to Fefferman-Graham coordinates $(\tilde{z}, \tilde{y})$ using an expansion of the form

$$1 - x^2 = \sqrt{1-\tilde{y}}\,\tilde{z} + \sum_{n=2} X^{(n)}(\tilde{y})\tilde{z}^n, \tag{5.25a}$$

$$y = \tilde{y} + \sum_{n=1} Y^{(n)}(\tilde{y})\tilde{z}^n, \tag{5.25b}$$

where the $\mathcal{O}(\tilde{z})$ term in the expansion for x fixes the conformal frame, and we have neglected potential logarithms as they do not appear up to the order we need. Requiring that $g_{\tilde{z}\tilde{z}} = \ell^2/\tilde{z}^2$ and $g_{\tilde{z}\tilde{y}} = 0$ order-by-order in $\tilde{z}$ yields a set of algebraic equations that can be solved for the coefficients $X^{(n)}(\tilde{y})$, $Y^{(n)}(\tilde{y})$. Then we find that the metric takes the form

$$ds^2 = \frac{\ell^2}{\tilde{z}^2}\left[d\tilde{z}^2 + \ell^{-2} ds^2_{\mathrm{MP}} + \tilde{z}^5 h_{\mu\nu}\, dx^\mu\, dx^\nu + \mathcal{O}(\tilde{z})^6\right], \tag{5.26}$$

where $h_{\mu\nu}$ is only a function of the boundary coordinates x^μ. According to the prescription of [96], the renormalized v.e.v. of the boundary stress tensor is then

$$\langle T_{\mu\nu} \rangle = \frac{5\ell^4}{16\pi G_N^{(6)}} h_{\mu\nu}. \tag{5.27}$$

The general expressions for the coefficients $M_i^{(n)}$, $\widetilde{M}_i^{(n)}$, $X^{(n)}$, $Y^{(n)}$ and for the stress tensor are too cumbersome to reproduce in this paper, but they become tractable in the nonrotating case $\beta = 0$. In Appendix A.4, we give the $\beta = 0$ expressions for $M_i^{(n)}$, $X^{(n)}$, and $Y^{(n)}$ up to the order we need in order to extract the stress tensor and check its tracelessness and transversality. As expected from our arguments in Section 5.2.1, the stress tensor is given precisely by the expression (5.9c), with[6]

$$\Theta(y) = -\frac{5\ell^4}{16\pi G_N^{(6)}} \frac{(1-y)^{5/2}}{672(1-2y)} \left[14(1-2y)a_5(y) \right.$$
$$\left. +(1-y)(176 - 1712y + 2368y^2 + 14y a_5'(y))\right], \tag{5.28a}$$

$$G(y) = \frac{5\ell^4}{16\pi G_N^{(6)}} \frac{y(1-y)\left(88 - 384y + 296y^2 + 7a_5(y)\right)}{224}, \tag{5.28b}$$

where in an obvious abuse of notation we have written the functions Θ and G in terms of the compactified radial coordinate y rather than the original coordinate r. We will postpone a discussion of this result to Section 5.4.

Now let us return to the general $\beta \neq 0$ case and discuss how to extract the stress tensor from our numerical data. The boundary stress tensor will take the

[6]Note that we drop the tilde on $\tilde{y}$, since y and $\tilde{y}$ agree on the boundary.

form

$$\langle T_{\mu\nu}\rangle dx^\mu d^\nu = T_{tt}\, dt^2 + T_{rr}\, dr^2 + T_{\psi\psi}\left(d\psi + A_{(1)}\right)^2 + 2T_{t\psi}\left(d\psi + A_{(1)}\right) dt + T_{\Sigma\Sigma} d\Sigma_2^2. \quad (5.29)$$

There are thus five functions to solve for, which can be expressed in terms of five of the functions $M_i^{(5)}$ which we will label as $m_i^{(5)} \equiv \{t_5, a_5, c_5, g_5, s_5\}$. In principle, one could extract these functions by taking five x-derivatives of (5.24) at $x = 1$. However, in practice taking such high derivatives numerically gives very poorly behaved results. Instead, we follow a slightly different approach: since we know the coefficients $M_i^{(n)}$ for $n \leq 4$ analytically, we can write

$$\frac{M_i(x,y) - \sum_{n=0}^{4} M_i^{(n)}(y)(1-x)^n}{(1-x)^4} = m_i^{(5)}(y)(1-x) + \mathcal{O}(1-x)^2. \quad (5.30)$$

With the numerically computed values for $M_i(x, y)$, the left-hand side of (5.30) is known numerically, so we perform a fit for the right-hand side to obtain the coefficients $m_i^{(5)}$.

In order to quantify the accuracy of our extracted stress tensor, we proceed as follows. Although the equations of motion don't give unique expressions for the coefficients $m_i^{(5)}$, they do provide two algebraic relations between these coefficients and a_5'[7]. Using one of these relations, we can express t_5 in terms of a_5, c_5, and g_5 in an algebraic expression of the form

$$t_5(y) = \mathcal{T}_5^{\text{exact}}\left(y, a_5(y), c_5(y), s_5(y)\right). \quad (5.31)$$

[7]These relations enforce tracelessness and transversality of the stress tensor, *i.e.* conservation.

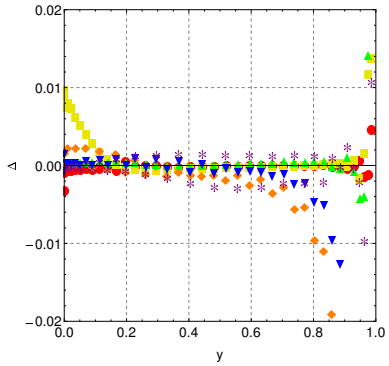

Figure 5.3: The relative error Δ introduced in extracting the coefficients $m_i^{(5)}$ for different values of β. Circles, squares, diamonds, triangles, inverted triangles, and asterisks correspond to $\beta = 0, 0.5, 0.6, 0.65, 0.69$, and β_{ext} respectively. Note that the error remains $\lesssim 0.4\%$ for almost all β and y.

Using the fitted values for the m_i^5, we can therefore use the quantity

$$\Delta(y) \equiv 1 - \frac{t_5(y)}{\mathcal{T}_5^{\text{exact}}\left(y, a_5(y), c_5(y), s_5(y)\right)}, \tag{5.32}$$

as a measure of the error introduced in extracting the $m_i^{(5)}$ (physically, one can think of Δ as a measure of how much the numerically extracted stress tensor fails to be traceless). In Figure 5.3, we plot Δ for the full range of β. We note that the relative error in our extraction is $\lesssim 0.4\%$ for almost all β and y; only for y near 1 does Δ become appreciable. We emphasize that this error is solely due to the difficulty in extracting the $m_i^{(5)}$ from the numerical data, and is not a measure of the accuracy of our numerical solutions themselves.

In Figure 5.4, we plot the components of the stress tensor for various values of β. Recall that to obtain the metric (5.15), we shifted the angular coordinate ψ to make $g_{\psi t} = 0$ at the horizon. As a result, the near-horizon behavior shown in Figure 5.4 physically represents the stress tensor as measured by an observer

co-rotating with the horizon. In addition, in Figure 5.5 we plot the scalar invariant $\langle T_{\mu\nu}\rangle \langle T^{\mu\nu}\rangle$.

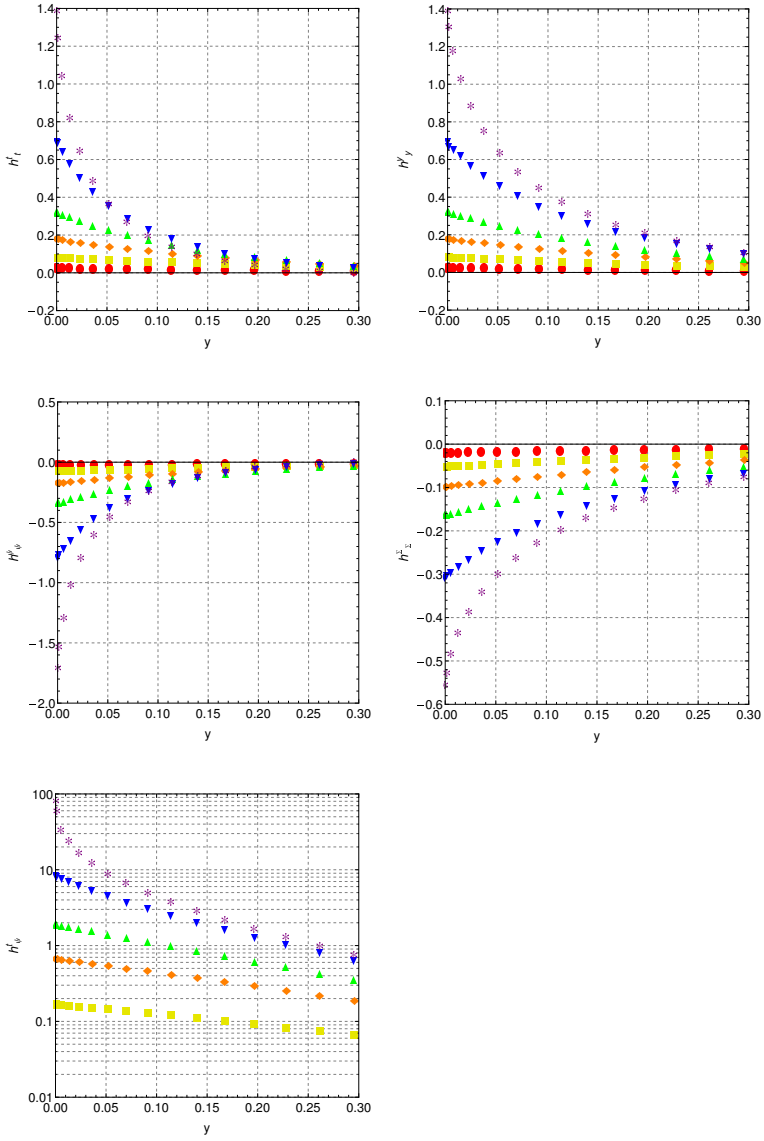

Figure 5.4: The components $h^{\mu}{}_{\nu} = 16\pi G_N^{(6)} \langle T^{\mu}{}_{\nu}\rangle / 5\ell^2$ for the same values of β as Figure 5.3. Note that $h^{t}{}_{\psi} = 0$ for $\beta = 0$. Note that the range of the coordinate y shown corresponds to the range $r_0 \leq r \lesssim 1.2\, r_0$ in the original radial coordinate.

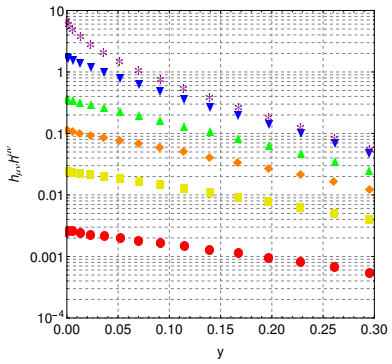

Figure 5.5: The scalar invariant $h_{\mu\nu}h^{\mu\nu}$ for the same values of β as Figure 5.3.

Regularity at Horizon

From the discussion in Section 5.2.1 and the regularity of the functions (5.28), it is clear that in the nonrotating case, the stress tensor of the CFT is regular on the future horizon (and in fact, it is regular on the past horizon as well since $K = Q = 0$). One can similarly examine the behavior of the stress tensor in the rotating case by passing to local ingoing Eddington-Finkelstein coordinates. In the non-extremal case, we change coordinates to

$$dt = dv - \frac{\sqrt{1-\beta^2}}{1-2\beta^2}\frac{dy}{2y}; \tag{5.33}$$

then from (5.29), one finds that the stress tensor is regular on the future horizon only if all the components $\langle T^{\mu}{}_{\nu}\rangle$ are finite and satisfy $\langle T^{t}{}_{t}\rangle = \langle T^{y}{}_{y}\rangle$ on the horizon. We can immediately see from Figure 5.4 that these conditions are satisfied, so the stress tensor is regular on the non-extremal horizon.

Again, the extremal case requires more care. In this case, local ingoing

Eddington-Finkelstein coordinates are given by

$$dt = dv - \frac{1}{\sqrt{2}}\left(\frac{1}{y^2} + \frac{1}{y}\right) dy, \tag{5.34a}$$

$$d\psi = d\psi' - \frac{dy}{2y}. \tag{5.34b}$$

Then one again finds that the stress tensor is regular on the future horizon if it obeys the same conditions as in the non-extremal case, and in addition obeys

$$\sqrt{2}\left\langle T^{t}{}_{\psi}\right\rangle + 2\partial_y\left(\left\langle T^{t}{}_{t}\right\rangle - \left\langle T^{y}{}_{y}\right\rangle\right) = 0 \tag{5.35}$$

on the horizon. It is easy to check that this condition is satisfied to within the expected $\sim 1\%$ accuracy.

5.4 Results and Discussion

Our numerical results exhibit the behavior expected based on our quantitative and heuristic reasoning in Section 5.2. Let us begin with the nonrotating case $\beta = 0$. The expansion of the equations of motion off of the boundary gave us a stress tensor of the form (5.9c) with the functions Θ and G given in (5.28), which is precisely the form expected from the discussion in Section 5.2.1. In particular, we find that the stress tensor is traceless, contains no flux terms, and is regular at the future horizon. Once the numerically extracted functions $m_i^5(y)$ are inserted, we find that the energy density is negative everywhere. The magnitude of the components of the stress tensor increases as the rotation parameter is increased, but otherwise the qualitative behavior of the stress tensor doesn't change

when $\beta \neq 0$ except for the introduction of an angular flux term $T_{t\psi}$.

As shown in Figure 5.3, the error in our extracted stress tensor becomes relatively large near $y = 1$, making it difficult to reliably extract the falloff of the stress tensor components at large r. In fact, these components appear to exhibit a falloff closer to $(1-y)^3 = (r_0/r)^6$ than to the $(1-y)^{7/2} = (r_0/r)^7$ expected from the braneworld arguments of [164]. However, by performing an expansion of the equations of motion about $y = 1$, one can show analytically that the stress tensor components must indeed decay like $(r_0/r)^7$; presumably, the use of higher precision would allow us to extract this behavior numerically. In any case, our results are much more well-behaved in the near-horizon region, where most of the interesting physics lies.

The following physical pictures emerges. As expected, a strongly coupled large-N CFT in a jammed phase forms a halo of negative-energy plasma around a black hole. The stress tensor of the plasma falls off rapidly far from the black hole, indicating that the plasma is well-localized around the black hole. The total energy of the plasma is negative, indicating its highly non-classical nature. When the black hole is made to rotate, the plasma is dragged along with the black hole. The plasma is trapped by the centrifugal barrier created by this rotation, causing the energy density and pressures to increase in magnitude.

The jammed phase is particularly interesting from the point of view of the CFT because it has no analog in a free field theory: a similar static plasma localized around the black hole could not exist in a noninteracting theory, as it would quickly fall into the black hole. The jammed phase is thus an effect of the strongly coupled nature of the CFT.

One might therefore wonder how our droplet phase compares to the corresponding black funnel phases (which *do* admit analogs in free field theory). Black funnels with $T_\infty = 0$ must have a horizon that asymptotes to the extremal Poincaré AdS deep into the bulk; if we require that the bulk horizon also join smoothly to the (non-extremal) boundary horizon, the bulk horizon must have both a non-constant surface gravity and a non-constant angular velocity, and will therefore not be a Killing horizon. We say that such funnel solutions will "flow" in the sense that there exists some notion of a horizon velocity which moves either from the boundary black hole to infinity or vice versa. For non-extremal horizons, these flowing funnels were constructed in [74], but construction of solutions with asymptotically extremal horizons (as is necessary to have the boundary CFT be at zero temperature at infinity) is more difficult.

In fact, it would seem that such funnel solutions might not even be relevant: according to the discussion in Section 5.1, the conjectured jamming transition in the CFT should be parametrized by the parameter RT_∞, with small RT_∞ favoring the jammed phase. If $T_\infty = 0$, we might expect based on this argument that the jammed phase of the CFT will dominate the thermodynamic ensemble for any size of the boundary black hole.

However, recall that one basis for this conjectured phase transition was the potential for Gregory-Laflamme-type instabilies of the bulk horizon [218]: if one starts with a black funnel and lowers the temperature T_∞, the asymptotically planar bulk horizon will sink deeper into the bulk (cf. Figure 5.1). The naïve expectation is that this will narrow the neck of the black funnel and leave it unstable to Gregory-Laflamme instabilities, causing it to collapse into a black

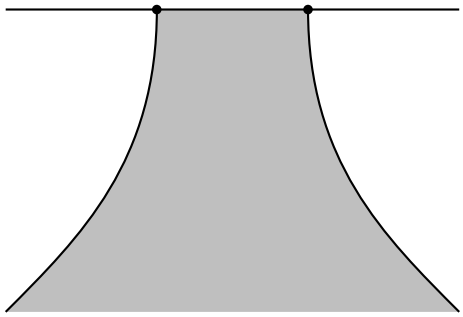

Figure 5.6: A sketch of a black funnel solution with $T_\infty = 0$.

droplet. Taking $T_\infty \to 0$, this argument would lead one to expect that the droplet solution would be the only thermodynamically preferred one.

This potential instability was studied to some extent in [61], which considered funnels dual to a CFT on an asymptoticaly flat black hole spacetime. The size of the boundary black hole was decreased (while keeping the temperature T_∞ fixed) to explore whether such Greogory-Laflamme instabilities would occur. Surprisingly, as the size of the boundary black hole decreased, the neck of the funnel remained wide enough to prevent the formation of such instabilities. Though far from exhaustive, this result implies that it is possible for there to be stable funnels with $T_\infty = 0$ which could compete with the droplet solutions. A sketch of what such a solution might look like is shown in Figure 5.6 (in fact, in [73] such funnels were explicitly constructed in $d = 2$, though the question of their stability is less interesting in that case, since the droplet solutions cannot exist in three bulk dimensions). Clearly, the construction of such solutions would be of much interest. We leave this exploration to future work.

Some words on the extremal limit are also in order. Though this limit is discontinuous from the point of view of the global causal structure of the back-

ground geometry, the line element (5.19) and consequently the stress tensor change smoothly as β approaches β_{ext}. In particular, the stress tensor remains regular on the future horizon, consistent with the result of [216] for the four-dimensional RN spacetime. A natural question is then whether there is some other mechanism that prevents the spacetime from continuing past the Cauchy horizon, analogous to the mass-inflation singularity of black holes with inner horizons [219]; perhaps the inclusion of perturbative corrections at higher order in $1/N$ would resolve the issue.

Indeed, our results may also have implications for the mass-inflation singularity. Ref. [198] computed the stress tensor on a rotating BTZ black hole background and found that it diverged at the inner horizon. This result should be expected in any black hole spacetime with an inner (Cauchy) horizon to preserve the causal structure of the spacetime. Since the spacetime between the inner and outer horizons is dynamical, the numerical approach used in this paper would not be applicable to studying the event horizon in that region. However, obtaining the stress tensor of a field theory on a black hole background all the way to the inner horizon would certainly give some insight into the behavior of the mass inflation singularity there.

Part II

Holographic Entanglement

Chapter 6

Entanglement and Correlations Near Extremality

6.1 Introduction

The entanglement properties of both ground states and thermal states are interesting topics of study in quantum field theory; see e.g. [220, 221]. Here we consider the corresponding structure of so-called thermofield double (TFD) states, which are the natural pure states defined on an (essentially) identical pair of field theories that reduce to thermal density matrices on either theory alone. This entanglement is of particular interest in the holographic context [19, 20, 82] due the existence in the dual bulk solution [222] of a wormhole, or Einstein-Rosen-like bridge, between two asymptotic regions – see figure 6.1 – and the conjectured generalizations of [223–225]. Holography also provides useful tools for such studies, ranging from the minimal area entanglement prescription of Ryu-

Takayangi [69] (recently justified in [71]) to the particle-worldline approximation (a.k.a. the geodesic approximation) of bulk correlators. TFDs also provides a simple laboratory in which to explore more general issues of entanglement in quantum field theory and holography.

We therefore focus on the holographic setting below. TFD entanglement along these lines was explored in great detail for $d = 2$ holographic CFTs in [226] by investigating the dual BTZ black hole, and also earlier in more general contexts through studies of local two-point functions with one operator near each boundary of various two-sided black holes [34, 67, 222, 227–229]. Our interest lies in adding charge via an appropriate chemical potential μ and exploring the behavior at very small temperatures T; see [230–232] for other studies of the small T limit.

Without the chemical potential, taking $T \to 0$ simply drives each theory into its ground state and removes all correlations. But nonzero μ provides an opportunity to maintain finite entanglement even at very small T. The classic gravitational example of such behavior is of course the Reissner-Nordström black hole near extremality. For simplicity we therefore focus on TFD states which are holographically dual to planar Reissner-Nordström AdS (RNAdS). To be concrete, we work with $d = 4$ CFTs dual to 5-dimensional bulks.

The interesting feature of such models is that as $T \to 0$ the bulk geometry develops a throat of finite cross-section but infinite depth. The infinite depth leads many natural probes of entanglement to vanish at $T = 0$. For example, this is the case for two-point functions (with one argument in each CFT) of large-dimension neutral single-trace operators; such correlators decay exponentially with spacelike separation in the bulk. It is also the case for the mutual information between

finite-sized regions of our two CFTs as computed via [69], as the diverging distance through the extreme throat means that at low T the dominant contribution to the von Neumann entropy of any finite region is given by surfaces lying entirely on one side of the black hole.

Nevertheless, the total density of entanglement remains finite. We take some first steps toward probing its structure below, showing in particular that i) the mutual information between one entire CFT and a finite-size strip in the other CFT need not vanish at small T and ii) as suggested in [40], there can be what one may call extremally-charged operators whose two-point functions (with one argument in each CFT) remain finite in the $T \to 0$ limit. The existence of the above extremally-charged operators indicates that the system lies at the threshold of an instability of the extreme RNAdS spacetime associated with Schwinger pair creation[1] [242, 243].

After a brief review of TFDs and the RNAdS geometry in section 6.2, we proceed to study the above mutual information in section 6.3. Section 6.4 then examines the two-point functions of *charged* operators with one argument in each CFT. Some final discussion is given in section 6.5, which in particular connects phenomena described here at small T with similar infrared (IR) effects seen in [45, 46, 229] at large times.

Before beginning, we mention the well-known fact that RNAdS has many potential instabilities that can switch on at low temperature (see e.g. [233, 235, 236, 238–241, 244]), and one certainly does not expect the extreme limit of RNAdS[2] to

[1] Since we consider bosons, this may also be called either a super-radiant instability or an instability to forming a super-conducting phase as in [233–237]. The fermionic analogue would be unstable to forming a Fermi surface as in [238–241].

[2] Or, in fact, any black hole whether extreme or otherwise; see e.g. [228] for a modern

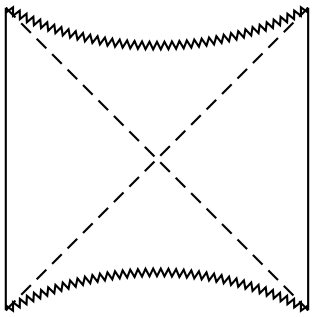

Figure 6.1: A conformal diagram of the maximally extended planar AdS-Schwarzschild black hole. This geometry is the bulk dual to the TFD state of two disconnected CFTs living on the two boundaries of the spacetime.

give an exact description of any microscopic theory with a finite density of states [245–247]. But at any given T/μ, even very close to extremality, models may well exist in which RNAdS remains an accurate description. Furthermore, we expect our results to be typical of those obtained near extreme limits. In particular, at least at first pass one would expect rotating extreme global AdS black holes to behave similarly. In this context one can find black holes that saturate a BPS bound (extreme BTZ [127, 128] for AdS_3 and the solutions of [248] and [249] for AdS_4 and AdS_5), so they are free of the above supergravity instabilities.

6.2 Thermofield Doubles in Bulk and CFT

We begin with a brief review of charged thermofield double states, both in the CFT and in the bulk. In the latter context they become two-sided planar Reissner-Nordström AdS black holes.

statement of this issue.

6.2.1 The Charged Thermofield Double in the CFT

Consider two quantum systems with isomorphic Hilbert spaces $\mathcal{H}_1 = \mathcal{H}_2 = \mathcal{H}$ and identical Hamiltonians $H_1 = H_2 = H$, which for simplicity we take to be invariant under a time-reversal operation[3] $\mathcal{T}$. We will be interested in considering this theory in the TFD state

$$|\psi\rangle = \frac{1}{\sqrt{Z}} \sum_i e^{-\beta E_i/2} |E_i\rangle_1 \otimes |E_i\rangle_2 \,. \tag{6.1}$$

Up to the insertion of possible phases, when the spectrum is non-degenerate this is the unique state on the tensor product $\mathcal{H}_1 \otimes \mathcal{H}_2$ which restricts to the thermal state $\rho = \frac{1}{Z} e^{-\beta H}$ on each factor, where $Z = \mathrm{Tr}_{\mathcal{H}} e^{-\beta H}$ is the usual partition function. The state (6.1) may be constructed by cutting open the thermal path integral with inverse temperature β, where the cut is made along a surface invariant under time-reversal. Equivalently, it may be evaluated by performing the Euclidean path integral in which Euclidean time t_E runs over an interval I of length $\beta/2$. Even in the presence of degeneracies, this Euclidean recipe continues to be well-defined, and implies that the terms in (6.1) take the form $|E\rangle \otimes \mathcal{T}|E\rangle$. Writing the TFD in this form makes clear that constructing (6.1) involves choosing a special time $t = 0$ invariant under $\mathcal{T}$ and furthermore that, once this time has been chosen, the anti-linear nature of $\mathcal{T}$ makes the properly defined (6.1) independent of changes of phase in the basis states $|E\rangle$. We also see that in relativistic theories CPT-invariance implies that the two factors in (6.1) should be taken to have opposite charge .

[3] This will be the case for our system. More generally, when time-reversal is not a symmetry, one takes H_1 and H_2 to be related by time-reversal with corresponding changes in (6.1).

The generalization to the grand canonical ensemble is straightforward: we simply introduce a chemical potential into the Boltzmann weights and define the TFD state to be

$$|\psi\rangle = \frac{1}{\sqrt{\mathcal{Z}}} \sum_i e^{-\beta(E_i+\mu Q_i)/2} |E_i, Q_i\rangle_1 \otimes |E_i, -Q_i\rangle_2 \,, \tag{6.2}$$

where the Q_i are eigenvalues of the conserved $U(1)$ charge conjugate to μ and $\mathcal{Z}$ is now the grand partition function. Again, any ambiguities due to degeneracies are resolved by taking the two states in each term to be CPT conjugates. The state (6.2) arises from a Euclidean path integral as above if we couple the charge Q to a background $U(1)$ gauge field $A = -i\mu\, dt_E$ with the sign in (6.2) requiring us to take system 1 to be associated with the minimum value of t_E in I and system 2 to be associated with the maximum value. Note that the gauge field is imaginary, and that the result is just the TFD state defined by the non-time-reversal invariant deformed Hamiltonians $\tilde{H}_1 = H + \mu Q$, $\tilde{H}_2 = H - \mu Q$; see footnote 3.

The TFD state (6.2) has a well-behaved zero-temperature limit $\beta \to \infty$ only if $\tilde{E}_1 = E + \mu Q$ is bounded below, or equivalently (by applying $\mathcal{T}$) if $\tilde{E}_2 = E - \mu Q$ is bounded below. In the zero-temperature limit, the sum in (6.2) restricts to those terms that minimize $\tilde{E}_1, \tilde{E}_2$. For a general theory one may expect a unique state of minimal $\tilde{E}_1, \tilde{E}_2$. But symmetry can force an exact degeneracy or, alternatively, we may consider a theory with many degrees of freedom (e.g., large N) and an associated approximate degeneracy when β is large but finite. It is this latter option that one expects to apply to the RN-AdS black holes studied below (see e.g. comments in [247]). In either case, up to an irrelevant overall phase the state

becomes effectively independent of time evolutions generated by $\tilde{H}_1, \tilde{H}_2$.

Since any remaining entanglement is associated with excitations of vanishingly small energy above the ground state (in the sense of $\tilde{H}_1, \tilde{H}_2$), one might expect any spatial scale characterizing our TFD entanglement to diverge as $T \to 0$. But this will not quite be the case. Indeed, since we consider RNAdS$_5$, our bulk dual will have an AdS$_2 \times \mathbb{R}^3$ infrared fixed point describing the near-horizon region. Such spacetimes exhibit local criticality, characterized by the limit $z \to \infty$ of dynamical scaling symmetry $(t, x) \to (\lambda^z t, \lambda x)$ which for finite z would give a power law $L \sim T^{-1/z}$. As a result, it is natural to find either that spatial scales L remain constant at small T or that they diverge logarithmically. We will see that both behaviors occur below.

Let us close with a comment on two-point functions. At $\mu = 0$, the uniqueness of the ground states and the resulting lack of TFD entanglement at small T implies that (connected) correlators vanish at $T = 0$. The non-trivial ground-state entropy makes the situation different in principle for $\mu > 0$, though two-point functions with one argument in each CFT can be non-zero at $T = 0$ only if each operator actually has some non-zero matrix element between two ground states of the requisite $\tilde{H}_1, \tilde{H}_2$. The set of operators (if any) for which this occurs will depend on the detailed dynamics of the CFT. The interesting result we will find in section 6.4 is that, at least in the limit of large operator dimensions, this occurs precisely for operators with a certain "extremal" ratio between their U(1) charge and conformal dimension.

6.2.2 Planar Reissner-Nordström AdS

In a holographic field theory the bulk dual of (6.2) is straightforward to construct following [222]. The conserved charge in the field theory will be associated with some $U(1)$ gauge field in the bulk. We thus simply perform the bulk Euclidean path integral with boundary conditions given by the above interval I and gauge field A. Note that the non-trivial gauge field $A = -i\mu dt_E$ on the boundary means that the generator $\tilde{H}$ of bulk time-translations toward the future may be written $\tilde{H} = H \pm \mu Q$, where the $+/-$ signs are respectively appropriate for systems 1 and 2 above. Here H is the generator for $\mu = 0$ given by the standard expression (see e.g. e.g. [95]) for the boundary stress tensor in terms of Fefferman-Graham coefficients of the bulk metric. See [88] for a general discussion of computing time-translation generators by holographic methods for boundary conditions involving vector fields.

In the bulk semi-classical limit our path integral should be dominated by a saddle point. We will consider cases where this saddle point is the planar Reissner-Nordström AdS_{d+1} geometry[4]. We expect this to be the case for $d \geq 3$ holographic field theories on Minkowski space so long as the bulk solution exhibits no instabilities associated with Schwinger pair creation [242, 243] (see also footnote 1). For definiteness we consider only $d = 4$ below. Note that our path integral automatically places quantum fluctuations of bulk fields into a Hartle-Hawking-like state. Below, we use the same symbol $|\psi\rangle$ to denote the CFT state, the state of full bulk quantum gravity, and the Hartle-Hawking-like state of linearized or

[4]While the semi-classical approximation may break down in surprising ways in generic contexts involving black holes (see e.g. [35, 36, 40, 245, 250]), the TFD case is sufficiently special that it is plausibly free of such issues [144].

perturbative bulk quantum fields on the RN-AdS background.

The RN-AdS geometry solves the equations of Einstein-Maxwell gravity with negative cosmological constant. Taking the action to be

$$S = \int d^5x\sqrt{-g}\left[\frac{1}{2\kappa^2}\left(R + \frac{12}{\ell^2}\right) - \frac{1}{4g^2}F^2\right], \tag{6.3}$$

and introducing the dimensionless measure $\gamma^2 \equiv 3g^2\ell^2/2\kappa^2$ of the relative strengths of the gravitational and Maxwell couplings, the solutions for fixed μ may be written in terms of a scale z_0 that will shortly be related to the temperature T. Such solutions take the form

$$ds^2 = \frac{\ell^2}{z^2}\left[-f(z)\,dt^2 + \frac{dz^2}{f(z)} + dx_3^2\right], \tag{6.4a}$$

$$A_\mu dx^\mu = \mu(1-\tilde{z}^2)\,dt, \tag{6.4b}$$

with

$$f(z) = (1-\tilde{z}^2)(1+\tilde{z}^2-\alpha^2\tilde{z}^4), \quad \tilde{z} = \frac{z}{z_0}, \quad \text{and } \alpha^2 \equiv \frac{z_0^2\mu^2}{\gamma^2}. \tag{6.5}$$

The rescaling $z_0 \to z_0/\lambda$ is equivalent to the transformation $(t,z,x) \to (\lambda t, \lambda z, \lambda x)$, $\mu \to \mu/\lambda$, so the physics depends only on the scale-invariant parameter α, or equivalently on μ/T.

The AdS boundary lies at $z = 0$, while $z = z_0$ is a horizon with temperature

$$T = \frac{2-\alpha^2}{2\pi z_0}. \tag{6.6}$$

This expression can be inverted to obtain $z_0(T,\mu)$; we will later need the small

temperature behavior $z_0 = \sqrt{2}\,\gamma/\mu + \mathcal{O}(T/\mu)$. Note that A_t vanishes at the horizon as required by regularity in a static gauge. For nonzero $\alpha^2 < 2$ there is also an inner horizon at $z = z_+$, with

$$z_+^2 = z_0^2 \frac{1 + \sqrt{1 + 4\alpha^2}}{2\alpha^2}. \tag{6.7}$$

The singularity lies at $z = \infty$. The conformal diagram of maximally extended RN-AdS is shown in Figure 6.2.

The above coordinates will be convenient despite the fact that they become singular on horizons. The Schwarzschild-like time coordinate t should be considered to be periodic with period $i\beta$, with β the inverse temperature. Within the real Lorentz-signature solution above, we also take it to change by $\pm i\beta/4$ whenever an outer horizon is crossed[5]. Thus the imaginary part of t determines whether a point lies in region I,II, III, or IV of the conformal diagram (Figure 6.2). In particular, the two asymptotic regions correspond to $\mathrm{Im}(t) = 0$ and $\mathrm{Im}(t) = \beta/2$. Below, it will often be useful to switch to a new radial coordinate $w = \tilde{z}^2$, in terms of which (6.4) becomes

$$ds^2 = \frac{\ell^2}{z_0^2 w}\left[-f\,dt^2 + \frac{z_0^2 dw^2}{4wf} + dx_3^2\right], \tag{6.8a}$$

$$A_\mu dx^\mu = \mu(1 - w)\,dt. \tag{6.8b}$$

We will be most interested in the extreme limit $\alpha^2 \to 2$, where $z_+ \to z_0$ so that $f(z)$ develops a double pole at $z = z_0$. The metric with $\alpha^2 = 2$ has an infinite

[5]Crossing the bifurcation surface counts as crossing two horizons and gives a change of $\pm i\beta/2$. Upon crossing an inner horizon t changes by $i\beta_+/4$ with β_+ the inverse temperature of the inner horizon; see e.g. [227]. We will have no need of this in the following discussion.

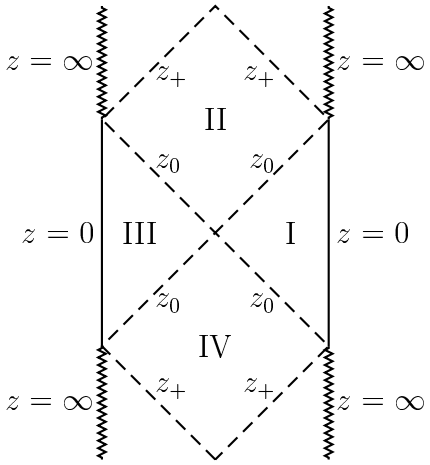

Figure 6.2: The relevant portion of the conformal diagram of RN-AdS. The exterior regions are I and III, with their boundaries at $z = 0$. The singularity is at $z = \infty$, and the spacetime has inner and outer horizons at $z = z_0$ and $z = z_+$, respectively. We take the imaginary part of t in regions I-IV to be 0, $\beta/4$, $\beta/2$, and $-\beta/4$, respectively.

throat, as the horizon at $z = z_0$ is an infinite proper distance away in the slices of constant t, and a Cauchy slice in the maximally extended extremal geometry has only a single boundary. We are interested in following the entanglement between the two boundaries of the non-extremal black hole in this limit, as the length of the Einstein-Rosen bridge connecting the two asymptotic regions diverges. To this end we define $\epsilon \equiv 2 - \alpha^2$ and write $f(z) = (1 - \tilde{z}^2)^2(1 + 2\tilde{z}^2) - \epsilon\tilde{z}^4(1 - \tilde{z}^2)$.

6.3 Mutual Information

A useful probe of the entanglement between our two Hilbert spaces is the mutual information associated with two spacetime regions, with one region in each CFT. In the TFD context it is natural to call this thermo-mutual information (TMI) following [226], which studied the corresponding quantity for holographic

theories with $\mu = 0$ and $d = 2$. After a brief review, we compute TMI for general μ and $d = 4$ for two strips of width L located on a common bulk Killing slice, and also for regions defined by an entire CFT and a single strip of width L in the other CFT. Our main result is that in the former case L must grow as $\ln T$ near extremality in order to have non-zero TMI while it may remain finite in the latter case.

6.3.1 Thermo-Mutual Information

Recall [251, 252] that the mutual information between two non-overlapping regions $\mathcal{A}$ and $\mathcal{B}$ is

$$\mathrm{MI}(\mathcal{A} : \mathcal{B}) = S_{\mathcal{A}} + S_{\mathcal{B}} - S_{\mathcal{A}\cup\mathcal{B}}, \tag{6.9}$$

where $S_X = -\mathrm{tr}(\rho_X \log \rho_X)$ is the von Neumann entropy of the reduced density matrix ρ_X describing the region X. In particular, the mutual information is finite in quantum field theory as all divergences in S_X are local terms at boundaries which explicitly cancel in the combination (6.9). The mutual information is non-negative by virtue of subadditivity $S_{\mathcal{A}} + S_{\mathcal{B}} \geq S_{\mathcal{A}\cup\mathcal{B}}$ for non-overlapping regions; see [253, 254] and also [255] for a holographic derivation.

The term thermo-mutual information (TMI) refers to the case where we consider a thermofield double state and the two regions are associated with different copies of the CFT. We will take $\mathcal{A}$, $\mathcal{B}$ to lie on a single Killing slice of the bulk and compute TMI holographically using the Ryu-Takayanagi prescription [69], which instructs us to identify

$$S_X = \frac{A(\gamma_X)}{4G_N}, \tag{6.10}$$

where G_N is Newton's constant and $A(\gamma_X)$ is the area of the minimal static surface γ_X, which extends into the bulk while being i) homologous to X within the surface of constant Killing time and ii) anchored on the boundary ∂X of X. Since we will apply such recipes to bulk black holes that dominate a Euclidean path integral, this recipe can be justified using the arguments of [71]. The fact that the two regions lie at different Euclidean times $t_E = 0$ and $t_E = i\beta/2$ provides no additional complications.

It is often the case that holographic TMI will vanish identically, saturating the subadditivity condition. This occurs because the disjoint union of two minimal surfaces $\gamma_{\mathcal{A}_1}$ and $\gamma_{\mathcal{A}_2}$ is an extremal surface anchored on the boundary of $\mathcal{A}_1 \cup \mathcal{A}_2$. Holographic TMI vanishes when this is the minimal-area such extremal surface. In the CFT this should be considered an artifact of the large N limit, though one that is unmitigated by $1/N$ corrections. An alternative candidate for $\gamma_{\mathcal{A}_1 \cup \mathcal{A}_2}$ is a surface $\gamma_{\mathcal{A}_1 \mathcal{A}_2}$ that passes through the horizon connecting the boundary of $\mathcal{A}_1$ to the boundary of $\mathcal{A}_2$. Varying the sizes of $\mathcal{A}_{1,2}$ will typically result in a transition where the area of the latter surface becomes smaller than the area of the former and the TMI becomes non-zero. The scale at which this transition occurs provides information about the degrees of freedom entangled between the two CFTs.

6.3.2 Strips

Consider first the case where $\mathcal{A}_1$ and $\mathcal{A}_2$ are strips defined by $0 < x^1 < L$ and extending infinitely far along x^2 and x^3. In this case the extremization problem becomes effectively one dimensional.

It is instructive to first review the case of finite $T = \beta^{-1}$ and $\mu = 0$ [229]. Here

the physics depends only on the dimensionless combination LT. For our strips the connected surface $\gamma_{\mathcal{A}_1\mathcal{A}_2}$ extends straight through the bifurcation surface, connecting $\partial\mathcal{A}_1$ with $\partial\mathcal{A}_2$; see Figure 6.3. Translational invariance implies that its area is independent of LT, while the area of the disconnected surface $\gamma_{\mathcal{A}_1} \cup \gamma_{\mathcal{A}_2}$ vanishes as $LT \to 0$. Thus the disconnected surface dominates $S_{\mathcal{A}_1\cup\mathcal{A}_2}$ for small LT and the TMI vanishes. As we increase LT, the surfaces $\gamma_{\mathcal{A}_1}$ and $\gamma_{\mathcal{A}_2}$ reach further into the bulk but do not cross the horizon. At large LT they lie mostly along the horizon so that their areas grow linearly in L. Thus there exists some critical L_{strips} of order T^{-1} such that for $L > L_{\text{strips}}$, the connected surface dominates in the computation of $S_{\mathcal{A}_1\cup\mathcal{A}_2}$ and the TMI becomes nonzero. This phase transition at $L = L_{\text{strips}}$ is sharp. The TMI grows linearly in L above the phase transition, with the leading behavior at large L given by twice the thermal entropy density times the volume of either region.

We wish to investigate how this picture changes at finite chemical potential. In particular, this allows us to study a meaningful $T \to 0$ limit with finite entanglement density between the two CFTs. For small μ the critical L_{strips} will remain of order T^{-1}, but near extremality we will find that L_{strips} grows as $\ln(1/T)$.

The minimal surfaces may be found by extremizing the area functional

$$A = V_2 \int \frac{\ell^3}{z^3}\sqrt{\frac{dz^2}{f(z)} + dx^2}\,, \tag{6.11}$$

with boundaries at $z = 0$ and $x^1 = 0, L$. Here $V_2 = \int dx^2 dx^3$ is the (infinite) volume in the directions along the strip.

For the connected surface, the extremum of (6.11) is clearly attained when

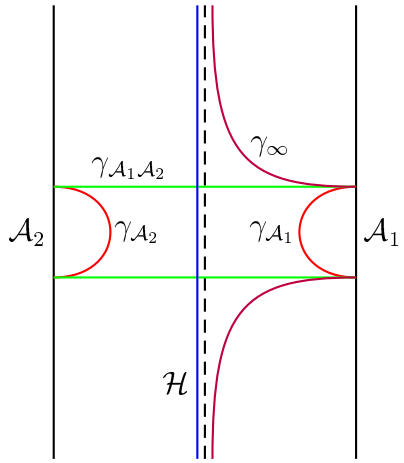

Figure 6.3: Assorted entangling surfaces at $t = 0$. The boundary CFTs live on the solid lines, which show the transverse x^1 direction on which we define the strips $\mathcal{A}_1$ and $\mathcal{A}_2$, which have width L. The dashed line is the bifurcation surface. Here we show five surfaces: $\gamma_{\mathcal{A}_1}$ and $\gamma_{\mathcal{A}_2}$ correspond to the entangling surface of each strip; $\gamma_{\mathcal{A}_1\mathcal{A}_2}$ runs through the bulk from one strip to the other, and can contribute to the entanglement entropy of the two strips; $\mathcal{H}$ is a surface that runs along the horizon and corresponds to the entangling surface of the entire left CFT; and γ_∞ connects $\partial\mathcal{A}_1$ to infinity, and can contribute to the mutual information between $\mathcal{A}_1$ and the left CFT.

$dx = 0$ in (6.11). Thus

$$\frac{A(\gamma_{\mathcal{A}_1\mathcal{A}_2})}{4G_N} = 4z_0 V_2 s \int_{\tilde{z}_{UV}}^1 \frac{d\tilde{z}}{\tilde{z}^3\sqrt{f(z)}}, \tag{6.12}$$

where $s = (1/4G_N)\,(\ell/z_0)^3$ is the thermal entropy density and $\tilde{z}_{UV}$ is a dimensionless ultraviolet (UV) cutoff which we may take to zero after computing the TMI. At extremality f will acquire a double pole at $\tilde{z} = 1$ so the integral (6.12) diverges logarithmically. In order to extract this divergence we make the change of integration variable $u = 1 - \tilde{z} + \epsilon$, where $\epsilon = 2 - \alpha^2$. Expanding the integrand

of (6.12) near $\epsilon = 0$ then gives

$$\frac{A(\gamma_{\mathcal{A}_1\mathcal{A}_2})}{4G_N} = 4z_0 V_2 s \int_\epsilon^{u_{UV}} \frac{du}{u}\left[\frac{1}{(u-1)^3(2-u)\sqrt{2u^2-4u+3}} + O(\epsilon/u)\right], \quad (6.13)$$

where $u_{UV} \equiv 1 - \tilde{z}_{UV} + \epsilon$. For small ϵ and fixed u_{UV}, the integral (6.13) is dominated by the contribution of the first term, which reduces to

$$\frac{A(\gamma_{\mathcal{A}_1\mathcal{A}_2})}{4G_N} \sim \frac{4\gamma V_2 s}{\sqrt{6}\,\mu}\ln(\mu/T), \quad (6.14)$$

where we used (6.6) to express z_0 in terms of μ. One may also derive (6.14) by writing (6.12) in terms of standard elliptic integrals; see appendix B.2 for details.

For the surface $\gamma_{\mathcal{A}_1}$, (6.11) yields

$$\frac{A(\gamma_{\mathcal{A}_1})}{4G_N} = z_0 V_2 s \int_0^{L/z_0} \frac{d\tilde{x}}{\tilde{z}^3}\sqrt{\frac{\tilde{z}'^2}{f(z)}+1}, \quad (6.15)$$

where $\tilde{x} \equiv x/z_0$ and $\tilde{z}' = d\tilde{z}/d\tilde{x}$. The expression for $\gamma_{\mathcal{A}_2}$ is of course identical. The translational symmetry in x implies a conserved quantity

$$\frac{1}{\tilde{z}^3\sqrt{f^{-1}\tilde{z}'^2+1}} \equiv \frac{1}{\tilde{z}_t^3}, \quad (6.16)$$

where $\tilde{z}_t$ is the turning point of $\gamma_{\mathcal{A}_1}$. Since extremal surfaces in static geometries do not penetrate horizons [256], we must have $\tilde{z}_t \leq 1$. The case $\tilde{z}_t = 1$ corresponds to the surface γ_∞ shown in Figure 6.3, which asymptotes to the horizon and never returns to the boundary. For $\tilde{z}_t < 1$ the corresponding boundary length L is given

by

$$\frac{L}{2} = z_0 \int_0^{L/2z_0} d\tilde{x} = z_0 \int_{\tilde{z}_{UV}}^{\tilde{z}_t} \frac{d\tilde{z}}{\tilde{z}'} = z_0 \int_{\tilde{z}_{UV}}^{\tilde{z}_t} \frac{d\tilde{z}}{\sqrt{f(z)}} \left(\frac{\tilde{z}_t^6}{\tilde{z}^6} - 1 \right)^{-1/2} \tag{6.17}$$

and the associated area is

$$\frac{A(\gamma_{\mathcal{A}_1})}{4G_N} = 2z_0 V_2 s \int_{\tilde{z}_{UV}}^{\tilde{z}_t} \frac{d\tilde{z}}{\tilde{z}'} \frac{\sqrt{f^{-1}\tilde{z}'^2 + 1}}{\tilde{z}^3} = 2z_0 V_2 s \int_{\tilde{z}_{UV}}^{\tilde{z}_t} \frac{d\tilde{z}}{\sqrt{f(z)}} \left(\frac{\tilde{z}_t^6}{\tilde{z}^6} - 1 \right)^{-1/2} \frac{\tilde{z}_t^3}{\tilde{z}^6}. \tag{6.18}$$

Since (6.13) grows as $T \to 0$, one can obtain nonzero TMI at small T only when (6.18) is similarly large. This occurs when L is large and $\tilde{z}_t \approx 1$. From (6.17) and (6.18) we find in this regime that $A(\gamma_{\mathcal{A}_1}) = LV_2 s + \mathcal{O}(1)$, describing the extensive thermal entanglement expected for large L. Comparison with (6.14) implies that for small T, the transition to TMI > 0 occurs at

$$L_{\text{strips}} = \frac{\gamma}{\sqrt{6}\,\mu} \ln(\mu/T) + \mathcal{O}(1). \tag{6.19}$$

As advertised, an infinite growth of the entangling regions is required to obtain a non-vanishing TMI near extremality.

6.3.3 A strip and an entire CFT

In contrast to the above, let us now consider the mutual information between a finite strip $\mathcal{A}_1$ in one CFT and the entire second CFT. The calculations are similar to those just performed. Defining a surface γ_∞ that ends on $\partial\mathcal{A}_1$ and

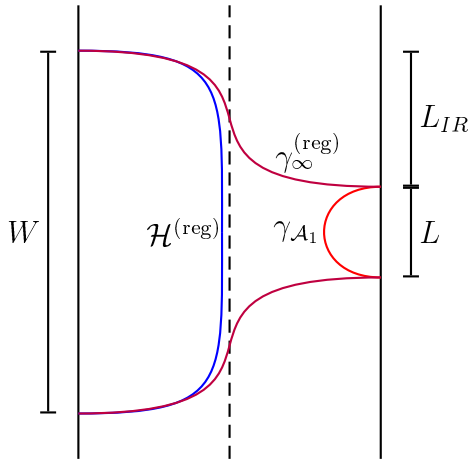

Figure 6.4: Surfaces relevant to the IR regularization used to compute $\mathrm{TMI}(\mathcal{A}_1 : \mathrm{CFT}_2)$.

extends to infinity on the other boundary (as shown in Figure 6.3), we have

$$\mathrm{TMI}(\mathcal{A}_1 : \mathrm{CFT}_2) = \max\left\{0, sV_3 + \frac{A(\gamma_{\mathcal{A}_1}) - A(\gamma_\infty)}{4G_N}\right\}, \tag{6.20}$$

where V_3 is the spatial volume of the CFT. While sV_3 and $A(\gamma_\infty)$ are both IR divergent, one can easily show that these divergences cancel. To do so, first consider the mutual information between the strip $\mathcal{A}_1$ of width L in one CFT and a strip of width W in the other, with W large relative to any other scale; the relevant entangling surfaces $\mathcal{H}^{(\mathrm{reg})}$ and $\gamma_\infty^{(\mathrm{reg})}$ are shown in Figure 6.4. The desired result is obtained in the limit $W \to \infty$, so that W serves as an IR regulator. The length L_{IR} of one of the regulated surfaces $\gamma_\infty^{(\mathrm{reg})}$ (see Figure 6.4) is given by (6.17) with $\tilde{z}_t = \tilde{z}_{\mathrm{IR}} \equiv 1 + \delta$, with δ small and positive[6]. At large W the entropy of the strip of width W will approach $sW + 2S_0 = s(L + 2L_{\mathrm{IR}}) + 2S_0$, where the W-independent correction S_0 is associated with the part of $\mathcal{H}^{(\mathrm{reg})}$ that stretches

[6]In fact, because $\tilde{z}_{\mathrm{IR}} > 1$, the upper bound of the integral in (6.17) should be set to 1.

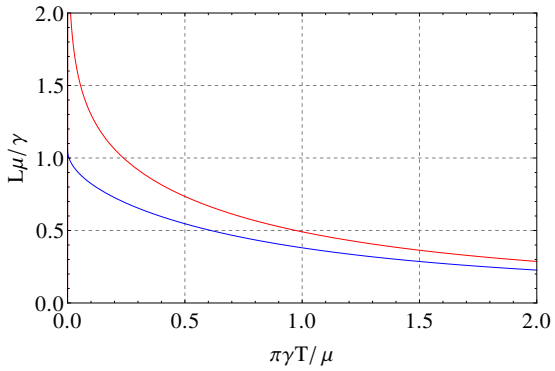

Figure 6.5: The critical lengths L_{strips} (upper curve, red) and $L_{s+\text{CFT}}$ (lower curve, blue) as functions of temperature. L_{strips} diverges logarithmically at small T, whereas $L_{s+\text{CFT}}$ approaches a constant value $\approx 1.05\gamma/\mu$.

from the horizon to the left boundary. Since this same correction appears in the area of $\gamma_\infty^{(\text{reg})}$ we find

$$sV_3 - \frac{A(\gamma_\infty)}{4G_N} = \frac{V_2\ell^3}{G_N z_0^2}\left[\frac{L}{4z_0} - \int_0^1 \frac{1}{\tilde{z}^3}\sqrt{\frac{1-\tilde{z}^6}{f(z)}}\,d\tilde{z}\right] + \mathcal{O}(\delta). \tag{6.21}$$

The divergences have canceled as promised.

Since the UV-regularized value of $A(\gamma_{\mathcal{A}_1})$ is finite and monotonically increasing with L, we see that the regulator-independent quantity

$$sV_3 + \frac{A(\gamma_{\mathcal{A}_1}) - A(\gamma_\infty)}{4G_N} \tag{6.22}$$

relevant to (6.20) grows linearly at large L and diverges to $-\infty$ as $L \to 0$. Thus there is a critical length $L_{s+\text{CFT}}(T/\mu)$ at which (6.20) becomes non-zero, given by requiring (6.22) to vanish. The results are shown in Figure 6.5, and we find numerically that $L_{s+\text{CFT}}|_{T/\mu=0} \approx 1.05\,\gamma/\mu$.

The contrast between L_{strips} and $L_{s+\text{CFT}}$ is striking. A further interesting result

is obtained by considering again two strips $\mathcal{A}_1$ and $\mathcal{A}_2$ of width L, but this time considering the TMI between $\mathcal{A}_1$ and $\mathcal{A}_2^c$, the complement of $\mathcal{A}_2$ in CFT_2. The possible bulk surfaces for computing $S_{\mathcal{A}_1 \cup \mathcal{A}_2^c}$ look much like those studied above (see Figure 6.6).[7] If we take the limit of small T at fixed L, μ, the surface that connects the two boundaries in Figure 6.6(c) will have divergent area, so it cannot dominate the others. But the two remaining surfaces allowed by homology (point (i) below (6.10)) are related by reflection through the horizon and so have equal areas. Since one surface is just $\gamma_{\mathcal{A}_1} \cup \gamma_{\mathcal{A}_2^c}$, we find $\mathrm{TMI}(\mathcal{A}_1 : \mathcal{A}_2^c) = 0$. Thus we have the remarkable result that for finite L the TMI between $\mathcal{A}_1$ and either $\mathcal{A}_2$ or its complement vanish in the limit of small T, but the TMI between $\mathcal{A}_1$ and the entire other copy of the CFT can remain non-zero.

This result is not readily accommodated by the localized-quasiparticle picture of TFD entanglement (see [229], following [257] in the time-dependent case; see also [45, 46] for other features that indicate shortcomings of this model). A quasiparticle picture might suggest that any entanglement between $\mathcal{A}_1$ and CFT_2 should be visible even if we separate CFT_2 into $\mathcal{A}_2$ and $\mathcal{A}_2^c$. That is, a localized-quasiparticle picture would lead us to expect that at least approximately

$$\mathrm{TMI}(\mathcal{A}_1 : \mathrm{CFT}_2) = \mathrm{TMI}(\mathcal{A}_1 : \mathcal{A}_2) + \mathrm{TMI}(\mathcal{A}_1 : \mathcal{A}_2^c). \tag{6.23}$$

This expectation is badly violated in our case at small T, as the former TMI is non-zero, but both of the terms on the other side vanish. This just a particularly striking example of a general failure of (6.23). In the holographic context this

[7] They are also similar to those that might be used to compute $\mathrm{MI}(\mathcal{A}_1 : \mathcal{A}_1^c)$, with both regions in the same CFT. But this is strictly infinite. The UV divergences do not cancel in (6.9) when the regions overlap.

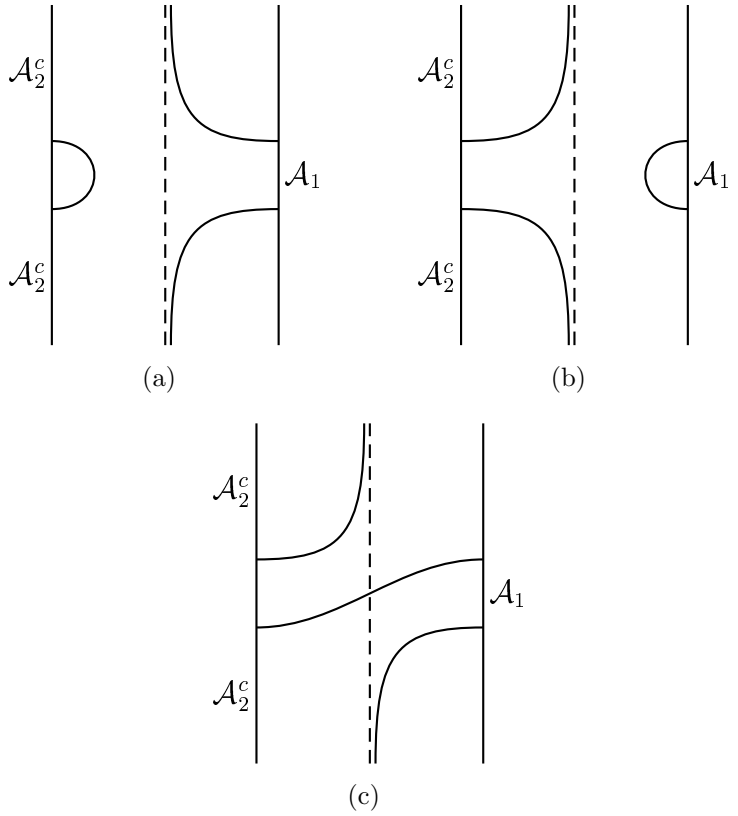

Figure 6.6: Surfaces relevant to the entanglement entropy $S_{\mathcal{A}_1 \cup \mathcal{A}_2^c}$. Note that the surfaces shown in (a) and (b) are reflections of one another across the horizon. Another surface (not shown) is related to (c) by a reflection in the vertical direction; i.e., across $x_1 = 0$.

is because the mutual information between some regions $\mathcal{A}$ and $\mathcal{B}$ on the one hand, and mutual information between $\mathcal{A}$ and subregions $\mathcal{B}_1$, $\mathcal{B}_2$ on the other, will involve different surfaces, and there is no reason to expect their areas to be related in such a way as to make (6.23) valid even approximately. While we offer no better model, it would be interesting to reflect further on what such a model might require, and perhaps to connect it with information-theoretic phenomena such as information locking [258, 259].

6.4 Charged Correlators

We now turn to demonstrating that our TFD entanglement can be seen near extremality in the correlation functions of charged operators, and to extracting features of this entanglement. We work in the approximation of large operator dimension, where the computation of dual bulk two-point correlators amounts to finding appropriate spacelike world lines extending from one boundary to the other. Though this approximation breaks down in certain interesting regimes, it nevertheless provides many useful results. We begin with a detailed discussion of general charged correlators in non-extreme black hole backgrounds and specialize to the near-extreme case only in section 6.4.4.

6.4.1 Holographic Two-Point Functions in the worldline approximation

Let us briefly review the connection between CFT two-point functions and bulk worldlines. In order to probe the entanglement inherent in our charged TFD state, we will be particularly interested in two-point correlation functions involving an operator $\mathcal{O}_1$ acting on one CFT in our TFD and an operator $\mathcal{O}_2$ acting on the other. The construction of (6.2) suggests that we take $\mathcal{O}_2$ to be the time-reverse of $\mathcal{O}_1$. For typical complex scalar fields, this amounts to taking the adjoint: $\mathcal{O}_2 = \mathcal{O}_1^\dagger$.

Recall now that CFT scalar operators $\mathcal{O}$ with conformal dimension Δ are

holographically related to bulk scalar fields ϕ with mass m via

$$\Delta = \frac{d}{2} + \sqrt{\frac{d^2}{4} + m^2\ell^2}, \tag{6.24}$$

with ℓ the AdS radius and d the boundary dimension[8]. At leading order in the bulk semi-classical limit, the CFT two-point function $G_{12} = \langle\psi|\mathcal{O}_2(x_2)\mathcal{O}_1(x_1)|\psi\rangle$ is dual to a certain rescaled limit of the bulk two-point function $\mathcal{G}(x_1, z_1, x_2, z_2) = \langle\psi|\phi^\dagger(x_2, z_2)\phi(x_1, z_1)|\psi\rangle$ as $z_1, z_2 \to 0$. In the former expression $|\psi\rangle$ represents the CFT charged TFD (6.2), while in the latter expression ϕ is an otherwise-free (i.e., linearized) charged field on RN-AdS and $|\psi\rangle$ is the associated Hartle-Hawking state defined by our Euclidean path integral. Here we consider Wightman two-point functions for definiteness, though in both the CFT and bulk our primary interest will be in two-point functions of commuting operators so that the Wightmann and time-ordered two-point functions coincide.

In the limit of large m the bulk two-point function can be studied using the WKB approximation. Since our bulk quantum state was constructed from a Euclidean path integral, for neutral scalars this reduces to the familiar result $\mathcal{G} \sim e^{im\Delta\tau}$, where $\Delta\tau$ is the proper time that elapses along the geodesic connecting (x_1, z_2) to (x_2, z_2); see e.g. [228, 261]. When the geodesic is spacelike it is more natural to write $\mathcal{G}(x_1, x_2) \sim e^{-mL}$, where L is the proper length. Taking $z_1, z_2 \to 0$ and performing the above-mentioned rescaling gives $G_{12} \sim e^{-mL_{\rm reg}}$, where $L_{\rm reg}$ is an appropriately regulated version of the geodesic length L.

It is straightforward to generalize this result to charged operators. If the op-

[8]For m^2 near the Breitenlohner-Freedman bound [100], the bulk field may satisfy alternate boundary conditions in which case we have $\Delta = d/2 - \sqrt{d^2/4 + m^2\ell^2}$ [260]. But this is not relevant for us since we take m^2 large and positive.

erator $\mathcal{O}$ is charged under our global $U(1)$ symmetry, then the dual bulk operator ϕ is charged under the associated bulk Maxwell field. So before integrating over paths, the proper time $\Delta\tau$ above should be replaced with the action S of a charged particle. The relevant saddle points are then extrema of S, which are generally not geodesics, and the Wightman function becomes $\mathcal{G} \sim e^{imS}$. Due to our interest in spacelike separated points at opposite boundaries of the bulk, we write $G_{12} \sim e^{-mI}$ with

$$I = -iS_{\rm reg} = \int \left(\sqrt{g_{\mu\nu} u^\mu u^\nu} - \frac{iq}{m} A_\mu u^\mu \right) d\lambda + I_{\rm ct}, \qquad I_{\rm ct} = -\ell \ln \left(\frac{4}{w_{UV}} \right), \tag{6.25}$$

where q and m are the charge and mass of ϕ, A_μ is the Maxwell field in the bulk solution. In (6.25), the $I_{\rm ct}$ is the appropriate counter-term which that makes the result finite for $z_1 = z_2 = 0$ and thus enacts the above-mentioned rescaling of bulk correlators near the boundaries. This $I_{\rm ct}$ is independent of q and thus identical to the standard counter-term for neutral particles; i.e., it is associated with the divergent length of geodesics near the boundaries. As usual, we understand (6.25) to be defined by first evaluating both $I_{\rm ct}$ and the bulk term with UV cutoffs and then taking the limit where the cutoffs are removed. The detailed justification of the bulk Euclidean action (6.25) is provided in Appendix B.1, in part because this expression corrects certain errors in the literature.

We emphasize that, in our background, the expression (6.25) computes $\mathcal{G}(x_1, x_2)$ with time dependence generated by $\tilde{H}_1 = H + \mu Q$, $\tilde{H}_2 = H - \mu Q$. Recalling that the limit $T \to 0$ with fixed μ restricts (6.2) to terms with a unique value of $\tilde{E}_1 = E_1 + \mu Q_1$, one sees that either time-translation of (6.2) changes the $T = 0$

wavefunction only by an overall phase. So in this limit G_{12} should become time-independent in either argument.

6.4.2 Equations of Motion

The spacelike world lines we seek extremize the action (6.25). We take both end points to have the same spatial coordinates $\vec{x}$ in the directions along the planar black hole. Parity symmetry and momentum conservation then guarantee that $\vec{x}$ is constant along our world line. Without loss of generality we henceforth set $\vec{x} = 0$.

Thus our curves will have tangent vectors $u^\mu = (\dot{t}, \dot{w}, 0, 0, 0)$. We may use the Killing field ∂_t to introduce a conserved (Euclidean) energy E_E

$$(\partial_t)^\mu u_\mu = iE_E + i\frac{q}{m}(\partial_t)^\mu A_\mu. \tag{6.26}$$

Together with the normalization condition $u^\mu u_\mu = 1$, the world lines must satisfy the equations of motion

$$\dot{t} = -\frac{z_0}{\ell} iw \frac{\mathcal{E} + \mathcal{Q}(1-w)}{f(w)}, \tag{6.27a}$$

$$\dot{w}^2 = \left(\frac{2}{\ell}\right)^2 w^2 g(w), \tag{6.27b}$$

where $\mathcal{Q} = z_0 q\mu/m\ell$, $\mathcal{E} = z_0 E_E/\ell$, and

$$g(w) = f(w) - w\left(\mathcal{E} + \mathcal{Q}(1-w)\right)^2. \tag{6.28}$$

We also define $\tilde{q} = qg/m\kappa$ as a dimensionless measure of the charge-to-mass ratio of ϕ.

Recall that we consider theories for which RNAdS_5 remains stable close to extremality. This in turn restricts the possible scalar fields that can exist in the bulk. In particular, we wish to avoid any Schwinger pair creation instability (see again footnote 1) [242, 243]. In the worldline approximation, this instability arises when electrostatic repulsion of the associated particles from the black hole overwhelms the gravitational attraction. This issue is readily analyzed by studying the potential $V(w)$ which controls motion of quasi-static (i.e., non-relativistic) timelike worldlines. For each black hole (with, say, positive charge), there is some critical positive $\tilde{q}_{\rm crit}$ and which $V(w)$ develops a minimum outside the horizon. One finds $\tilde{q}_{\rm crit} > 1$ for all nonextreme black holes and $\tilde{q}_{\rm crit} = 1$ for extreme black holes. For simplicity, we therefore restrict discussion below to the case $\tilde{q} \leq 1$ unless otherwise noted.

We are interested in world lines running from $(t, w) = (t_b, 0)$ to $(t, w) = (-t_b + i\beta/2, 0)$. For fixed t_b there will generally be a finite set of solutions to (6.27a), (6.27b) distinguished by their values of $\mathcal{E}$. These values are generally complex, though (6.27a) implies that one may find solutions with imaginary t_b having real $\mathcal{E}$. Since there are multiple solutions, the full set of solutions for all complex t_b may be associated with a Riemann surface $\mathcal{E}(t_b)$. While we will focus on the curves defined by taking t_b real, the i that accompanies the Maxwell term in (6.25) makes it particularly natural to analytically continue to complex parameters.

It will also be useful to characterize solutions by their turning points w_t in

the complex w-plane. Such turning points are defined by noting that (6.27b) is invariant under changing the sign of the affine parameter λ along the worldline while holding $\mathcal{E}, \mathcal{Q}, \mu$ fixed. Thus one obtains the same curve $w(\lambda)$ whether one integrates (6.27b) starting from $w = 0$ at the right boundary or from the left, and each solution of interest has a Z_2 symmetry mapping $w(\lambda) \to w(-\lambda)$ with a corresponding action on $t(\lambda)$. The turning point is just the value of w at the fixed point, $w_t \equiv w(\lambda = 0)$.

Note that $\dot{w}$ must vanish at this fixed point, so that w_t and $\mathcal{E}$ satisfy a relation given by setting $g(w_t) = 0$. Since g is a cubic polynomial in w, one may take this to define a three-sheeted Riemann surface $w_t(\mathcal{E})$ (see e.g. Figure 6.7) with branch points corresponding in general to double roots of g. This structure will play an important role below. For real α our g has a triple root only for the special case $\mathcal{E} = 0$, $\tilde{q} = 1$ at extremality ($\alpha = \sqrt{2}$), where the root lies at the horizon ($w = 1$).

In general, the term on the right-hand side of (6.27b) acts as an effective (possibly complex) Newtonian potential for w. This understanding allows one to write the total elapsed time $\Delta t = -2t_b + i\beta/2$ and the action I along any solution in the form

$$\Delta t = -\frac{iz_0}{2} \oint \frac{\mathcal{E} + \mathcal{Q}(1-w)}{f(w)\sqrt{g(w)}}\, dw, \tag{6.29a}$$

$$I = \frac{\ell}{2} \oint \frac{f(w) - \mathcal{Q}\, w(1-w)\,(\mathcal{E} + \mathcal{Q}(1-w))}{w f(w)\sqrt{g(w)}}\, dw + I_{\rm ct}, \tag{6.29b}$$

where the integral is over the contour in the complex w-plane defined by our worldline. Expressions (6.29a), (6.29b) use the prescription of [229] for integrating through zeros of f so that crossing any horizon adds $\pm i\beta/4$ to Δt as desired. As

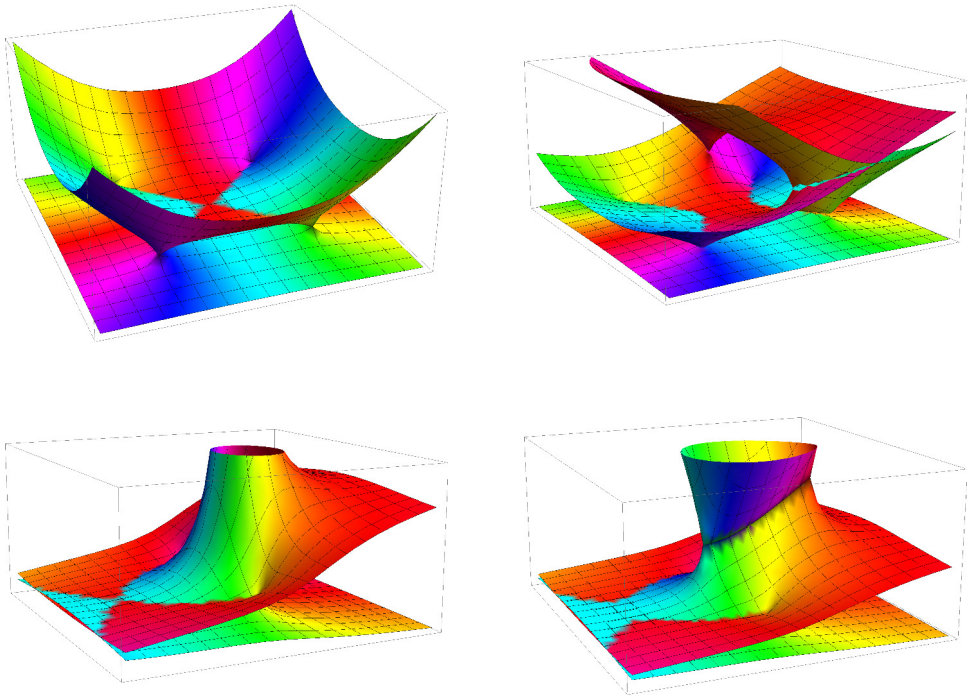

Figure 6.7: Typical Riemann surfaces $w_t(\mathcal{E})$ defined by setting $g(w_t) = 0$ over the complex $\mathcal{E}$ plane. The top left figure displays the Schwarzschild case $\alpha = 0$; the next three show $\alpha = 0.5$, with $\tilde{q} = 0.2$, $\sqrt{2/3}$, and 0.9, from left to right and top to bottom. The height of the sheets corresponds to $|w_t|$, while the hue represents the phase of w_t (with red and turquoise corresponding to positive and negative real w_t, respectively). Along the real axis (parallel to the common plane of symmetry in each figure), the turning point w_t corresponds to the smallest positive real root, which is then analytically continued to the rest of the complex plane. Thus the principal branch of w_t becomes the the lowermost sheet in each figure at large real $\mathcal{E}$.

a technical note we mention that by writing

$$g(w) = \left(\alpha^2 - \mathcal{Q}^2\right)(w_1 - w)(w_2 - w)(w - w_3) \tag{6.30}$$

with $w_t = w_1$, the expressions (6.29) can be evaluated explicitly in terms of standard elliptic integrals. These expressions are functions of w_1, w_2, w_3, α, $\mathcal{Q}$, and $\mathcal{E}$ given in Appendix B.2 and are useful for various asymptotic expansions.

In order to obtain a unique value from (6.29) we must specify $\sqrt{g}$ along this worldline which, as noted above, will necessarily run through a root w_t of g. The correct prescription is determined by taking $\sqrt{g}$ to be continuous along the worldline and requiring the above reflection symmetry $\lambda \to -\lambda$ to change the sign of $\sqrt{g}$; roughly speaking, the sign of $\sqrt{g}$ changes when one passes through the turning point. The remaining sign ambiguity in Δt is fixed by the sign of dw/dt at any point along our worldline, while the sign of the ambiguity in I is fixed by the condition that the divergence at $w = 0$ is canceled by $I_{\rm ct}$. In particular, although there are two solutions for given $\mathcal{E}, w_t$, the action I takes identical values on both.

One would like to think of (6.29a) and (6.29b) as defining I as a function of t_b. But again the multiple geodesics for each t_b mean that $I(t_b)$ is actually a multi-sheeted Riemann surface. A useful way to deal with this complication is to parametrize both I and t_b by the energy $\mathcal{E}$. While the resulting $I(\mathcal{E})$ and $\Delta t(\mathcal{E})$ are again multi-sheeted Riemann surfaces, their structure is closely related to the physics of quasi-normal modes. We review this connection in section 6.4.3 below and use it to extract the most relevant features.

An additional simplifying feature of this perspective is that all branch points in $I(\mathcal{E})$ coincide with those of $w_t(\mathcal{E})$, and thus with w_t being a double root of g. This follows from the above observation that I is uniquely determined once both $\mathcal{E}, w_t$ are specified. Specializing for the moment to non-extreme black holes, we see from (6.28) that f cannot vanish where g has a double root[9]. As a result, the relation (6.28) ensures that no further factors vanish at w_t in either the numerator or denominator of (6.29b) and that double zeros of g give logarithmic branch points. We see that Δt also diverges logarithmically at branch points of w_t and that the only additional branch points in $\Delta t(\mathcal{E})$ are those associated with the overall choice of sign. These play only a very minor role and are not associated with divergences unless they coincide with those above. Thus the branch points of w_t are directly associated with the late time limit $\Delta t \to \infty$.

As a final note, we mention that equations (6.29) and the associated boundary conditions are invariant under the transformation $(t_b, \mathcal{Q}, \mathcal{E}) \to (-t_b, -\mathcal{Q}, -\mathcal{E})$ and also under $(t_b, \mathcal{Q}, \mathcal{E}) \to (-t_b, \mathcal{Q}, \bar{\mathcal{E}})$ where the overbar denotes complex conjugation. Without loss of generality we may thus restrict our analysis to $t_b \geq 0$ and $\mathcal{Q} \geq 0$. We may also restrict ourselves to $\mu \geq 0$ (and thus $\tilde{q} \geq 0$), since the equations are also invariant under $(\mu, q) \to (-\mu, -q)$.

6.4.3 The Late-Time Limit and quasinormal modes

We noted above that our problem is associated with multi-sheeted Riemann surfaces $I(\mathcal{E})$, $t_b(\mathcal{E})$, $w_t(\mathcal{E})$ for which the interesting branch points occur when w_t

[9]Note that $g(w = 0) = 1 \neq 0$. Thus from (6.28) f and g can vanish simultaneously at w_0 only when $\mathcal{E} + \mathcal{Q}(1 - w_0) = 0$. But this forces the second term in (6.28) to have a double root. So if w_0 is a double root of g, would also be a double root of f. And when α is real f can have a double root only at extremality.

is a double zero of $g(w)$. Furthermore, these are precisely the points associated with late-time limits. We now take a moment to understand the structure of these branch points in detail and to more carefully review the connection with late times. In particular, we relate the associated branch cuts with families of quasi-normal modes drawing heavily from [228] and [229].

Note that double roots of g can arise only at special values $\mathcal{E}_c$ of $\mathcal{E}$ at which the discriminant of g vanishes. This discriminant is a sixth order polynomial in $\mathcal{E}$ and, while its explicit form is unilluminating, we plot the associated six roots $\mathcal{E}_c$ in the complex $\mathcal{E}$ plane for representative choices of the parameters α, $\tilde{q}$ in Figure 6.8. Any curve $\mathcal{E}(t_b)$ must approach one of these points as $t_b \to \pm\infty$. There is a special μ-independent value $\tilde{q} = \sqrt{2/3}$ at which two of the $\mathcal{E}_c$ merge on the real axis and disappear. This corresponds to a degenerate case where $g(w)$ becomes quadratic in w, so at this value there are only four $\mathcal{E}_c$. For $\tilde{q} < \sqrt{2/3}$ no $\mathcal{E}_c$ lie on the real axis, while for $\tilde{q} > \sqrt{2/3}$ two of the $\mathcal{E}_c$ always lie on the real axis.

As described in [228], there is a very physical relationship between the critical energies $\mathcal{E}_c$ and the quasi-normal modes (QNMs) of the scalar field probe. In general, the long-time behavior of two-point functions of fields on a black hole background is dominated by the lowest QNM ω_c. This is usually used as an approximation for the two-point function in one static region outside the black hole, but continuing one of the points to the other asymptotic region via $t \to -t + i\beta/2$ one sees that it also provides an approximation to our Wightman function:

$$G_{12}(t_b) \sim e^{-2i\omega_c t_b} \Rightarrow I_{\text{late}} = \frac{2i\omega_c}{m}\, t_b + \cdots , \tag{6.31}$$

where $\cdots$ stand for contributions that are subleading in $1/m$ and $1/t_b$. Working

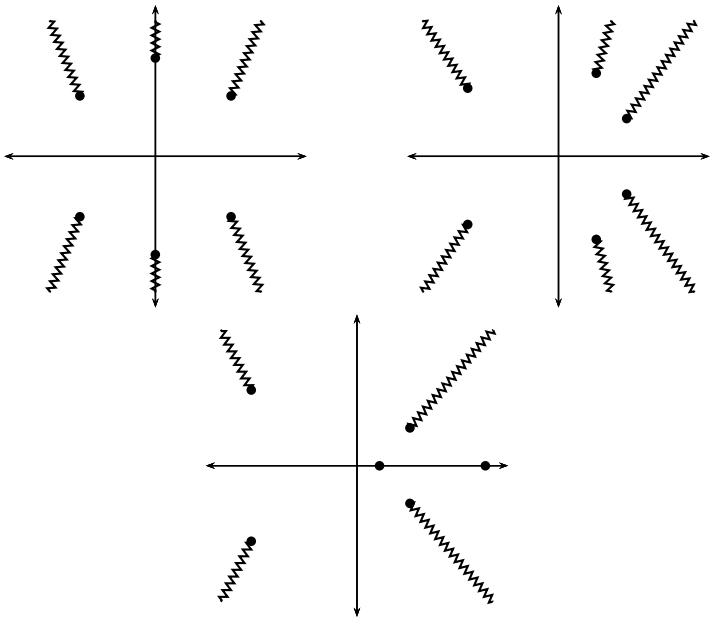

Figure 6.8: Roots of the discriminant of $g(w)$ in the complex $\mathcal{E}$ plane are shown as dots for representative choices of the parameters α, $\tilde{q}$. From left to right, we take $\tilde{q} = 0$, $\tilde{q} < \sqrt{2/3}$, and $\tilde{q} > \sqrt{2/3}$. These indicate possible branch points for $w_t(\mathcal{E}), I(\mathcal{E}), \Delta t(\mathcal{E})$, with the actual branch structure of $I(\mathcal{E}), \Delta t(\mathcal{E})$ being determined by that of $w_t(\mathcal{E})$. On sheets where $\mathcal{E}_c$ is indeed a branch point, both I and Δt diverge logarithmically. As these are the only locations where Δt can diverge, they serve as endpoints for all curves $\mathcal{E}(t_b)$. The jagged lines are rough guesses for the locations of the branch cuts that define the principal sheet of $w_t(\mathcal{E})$, $I(\mathcal{E})$ and $\Delta t(\mathcal{E})$, and should correspond to lines of poles in frequency space correlators for operators of large-but-finite conformal dimension.

in the worldline approximation, this linear behavior at late time can be thought of as corresponding to a world line at fixed (generally complex) w but extended in the t direction [229]. To identify these special values of w (which we denote w_c), we extremize the action obtained from (6.25) by setting $\dot{w}$ to zero. The resulting action is

$$I_{\text{late}} = \frac{i\ell}{z_0} \int V(w)\, dt, \tag{6.32}$$

where

$$V(w) = \sqrt{\frac{f(w)}{w}} - \mathcal{Q}(1-w), \tag{6.33}$$

and its extremization requires solving $V'(w) = 0$. Finding the roots w_c of $V'(w)$ for general α, $\tilde{q}$ amounts to solving the same sextic polynomial. But since from (6.27b) they satisfy $g(w_c) = 0$, the corresponding energies are just the six $\mathcal{E}_c$ defined above:

$$\mathcal{E}_c = V(w_c). \tag{6.34}$$

Thus in the late time limit we may write

$$I_{\text{late}} = -\frac{2i\ell\mathcal{E}_c}{z_0} t_b + \cdots \Rightarrow \omega_c = -m\,(E_E)_c\,, \tag{6.35}$$

where $(E_E)_c = \ell\mathcal{E}_c/z_0$ is again the Euclidean energy from (6.26). Since the large time behavior of a physical probe field is controlled by its lowest QNM, we identify the frequency of this mode as ω_c. Thus, up to a factor of m, the critical energies $(E_E)_c$ are directly related to such frequencies. In particular, for stable situations families of worldlines relevant at late times can have $t_b \to +\infty$ only for $\mathcal{E}_c$ in the upper half-plane.

Not only does the physics of QNMs determine the branch points $\mathcal{E}_c$, it also selects a physically meaningful location at which to place associated branch cuts [228]. This point may be seen by writing the Fourier transform of the worldline-approximation

correlator in the form

$$G_{12}(\omega) \sim \int d\,(\Delta t)\, e^{-i\omega\Delta t} e^{-mI(\Delta t)}, \tag{6.36}$$

$$\sim \int dE_E\, e^{-m(I(E_E)+i(\omega/m)\Delta t(E_E))}. \tag{6.37}$$

For large m, the dominant contribution to this integral comes from those E_E which satisfy the saddle point condition

$$\frac{dI}{dE_E} + \frac{i\omega}{m}\frac{d(\Delta t)}{dE_E} = 0. \tag{6.38}$$

Since I is an action, we have the Hamilton-Jacobi relation

$$dI = iE_E\, d(\Delta t), \tag{6.39}$$

which can also be checked directly from (6.29). Thus (6.38) becomes simply $E_E = -\omega/m$ at all times and the frequency space correlator is

$$G_{12}(\omega) \sim e^{mZ(\omega)}, \quad \text{with } Z(\omega) = (iE_E\Delta t(E_E) - I(E_E))\,\big|_{E_E=-\omega/m}. \tag{6.40}$$

Since $Z(\omega)$ and $I(\Delta t)$ are related by a Legendre transformation, the analytic structure of the functions I and Δt in the complex energy plane is directly related to the analytic structure of the frequency space correlator $G_{12}(\omega)$.

In particular, the only singularities of the exact Green's functions $G_{12}(\omega)$ at finite m computed using field theory should be poles corresponding to quasi-normal modes. In the large m limit these poles organize themselves into closely

spaced families that define curves in the complex ω plane. The endpoints of such curves are (some of) our $\mathcal{E}_c$'s and the associated lines of poles become branch cuts. The most relevant observation is that the actual finite m correlators are free of branch points, so that the parts of our Riemann surfaces $I(\mathcal{E})$ and $\Delta t(\mathcal{E})$ beyond the lines of poles are related much less directly to the physics of finite m. In particular, even at general complex t_b or ω, finite m correlators will never be well-approximated by e^{-mI} for worldlines described by points behind such lines.

We henceforth restrict discussion to what we may call the principal sheets of $w_t(\mathcal{E})$, $I(\mathcal{E})$, and $\Delta t(\mathcal{E})$ defined by introducing branch cuts along the large-m lines of poles in $G_{12}(\omega)$. We also take our principal sheets to include worldlines on which $\mathcal{E}$, w_t, are real and Δt is purely imaginary. While determining the precise location of these cuts would require one to compute the full set of QNMs at large m, it will be enough for our purposes to note that QNMs typically become highly damped away from the lowest QNM. Thus the branch cuts that determine our principal sheet must point away from the real $\mathcal{E}$ axis. A rough guess as to the appearance of these branch cuts is sketched in Figure 6.8. In particular, comparison with Figure 6.10 indicates that while all six values of $\mathcal{E}_c$ define branch points of the principal sheet for small $\tilde{q} < \sqrt{2/3}$, at some point before $\tilde{q} = \sqrt{2/3}$ two of the $\mathcal{E}_c$ move onto a secondary sheet so that only the remaining four define branch points of the principal sheet and correspond to physical low-lying QNMs. As one might expect, for $\tilde{q} > \sqrt{2/3}$ these are the four $\mathcal{E}_c$ with non-vanishing imaginary part.

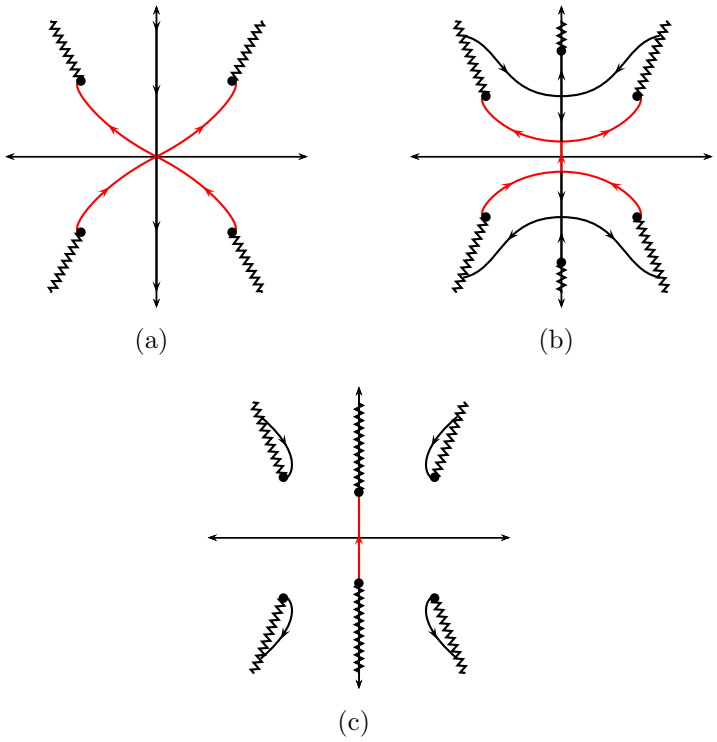

Figure 6.9: Sketches of the $\mathcal{E}(t_b)$ contours corresponding to real values of t_b for a representative sample of α with $\tilde{q} = 0$; arrows on the contours indicate the direction of increasing t_b. Figure (a) is Schwarzschild, with α increasing to the right. Taking $\alpha > 0$ introduces two additional $\mathcal{E}_c$ along the imaginary axis and resolves the bifurcation point at $\mathcal{E} = 0$. Note the presence of new contours that come in from infinity; following these contours to large t_b takes us cross branch cuts (for which our rough guesses are shown as jagged lines) and off the principal sheet. At $\alpha = \alpha_{\text{crit}} \approx 0.406$ the bifurcation points merge and the contour topology changes to that of figure (c). We see that at least parts of some (black) contours move off the principal sheet. Red contours are associated with correlations that decay away from $t_b = 0$ as in comment (ii).

6.4.4 Correlators in the extreme limit

As discussed for the Schwarzschild case in [34], it is generally quite subtle to determine which of the possible complex worldlines connecting our endpoints actually provides a good approximations to finite m correlators via $G_{12} \sim e^{-mI}$.

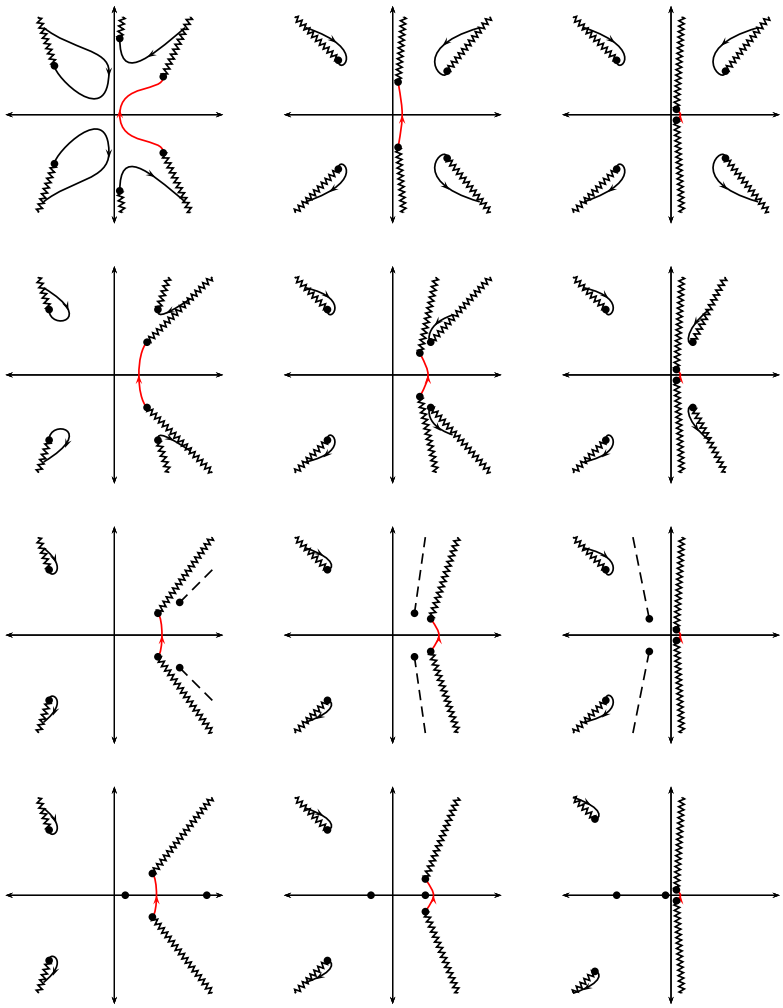

Figure 6.10: Sketches of the $\mathcal{E}(t_b)$ contours corresponding to real values of t_b for a representative sample of α and $\tilde{q}$; arrows on the contours indicate the direction of increasing t_b. Red contours are again associated with correlations that decay away from $t_b = 0$ as in comment (ii). The three columns take $\alpha = \alpha_1$, α_2, α_3, respectively, with $\alpha_1 < \alpha_{\text{crit}} < \alpha_2 < \alpha_3 \approx \alpha_{\text{ext}}$; the rows from top to bottom take $\tilde{q} = \tilde{q}_1$ $\tilde{q}_2$, $\tilde{q}_3$, $\tilde{q}_4$, respectively, with $1 \gg \tilde{q}_1 < \tilde{q}_2 < \tilde{q}_3 < \sqrt{2/3} < \tilde{q}_4$. As $\tilde{q}$ is increased, two of the $\mathcal{E}_c$ in the right-hand plane cross branch cuts (rough guesses for which are again shown as jagged lines), taking their associated contours and branch cuts off the principal branch; this is shown in the third row with such branch cuts indicated by dashed lines (suppressed in the 4th column). At $\tilde{q} = \sqrt{2/3}$, these two $\mathcal{E}_c$ annihilate on the real axis; for $\tilde{q} > \sqrt{2/3}$, these $\mathcal{E}_c$ remain on the real axis and no contours on the principal sheet terminate on them.

The possible Schwarzschild contours $\mathcal{E}(t_b)$ for real t_b are shown in Figure 6.9(a). While the correlator at $t_b = 0$ corresponds to the unique $\mathcal{E} = 0$ geodesic, this splits into three possible branches for nonzero t_b. By writing down a toy model for the path integral, [34] argued that the contours contributing to the path integral are the complex ones terminating at $\mathcal{E}_c = \sqrt{2}\, e^{i\pi/4+k\pi/2}$ for $k = 0, 1, 2, 3$, while the contour along the imaginary $\mathcal{E}$ axis (which only reaches a finite value of t_b as $\mathcal{E} \to i\infty$) does not contribute. This is the case even though the imaginary $\mathcal{E}$ contour represents a smaller action for $t_b > 0$, and so would dominate if it contributed at all. Adding charge ($\alpha > 0$) to the black hole and also to the probe ($\tilde{q} > 0$) leads to even more interesting structure for these contours which may further complicate the analysis. See Figure 6.9 for black holes with neutral probes and Figure 6.10 for charged probes. The captions contain rough explanations of the evolution in $\alpha, \tilde{q}$, though due to our focus on the non-extreme case, we save further commentary for section 6.4.5.

Luckily, an indirect argument suffices to determine the correct contour in the extreme limit. To see this, recall from section 6.2.1 that this limit must make our correlators independent of t_b. Since $\Delta t = -2t_b + i\beta/2$, applying equation (6.39) to any contributing saddles requires $\mathcal{E}(t_b)$ to vanish at extremality for all t_b. Taking the $\epsilon \to 0$ limit of (6.34) shows that that for $\tilde{q} < 1$, precisely two critical energies $\mathcal{E}_c$ vanish at extremality; these are

$$\mathcal{E}_c = \frac{\tilde{q} \pm i\sqrt{1-\tilde{q}^2}}{2\sqrt{3}}\,\epsilon + \mathcal{O}(\epsilon)^2 \quad (\tilde{q} < 1). \tag{6.41}$$

One lies in the lower half plane, and the other lies in the upper half plane. So for

the stable case $\tilde{q} < 1$ there should be a unique contour connecting the two, and which should flow from the former to the latter. This is precisely what one finds numerically; see Figure 6.10. In the extreme limit, consistency thus requires that correlators receive contributions *only* from this contour.

Before analyzing this contour in detail, we remark that it displays several additional pleasing features:

i) At least for $0 \leq \tilde{q} \leq 1$, for all nonextreme black holes with sufficient charge (α^2 close enough to 2) the $\mathcal{E}_c$ values corresponding to endpoints of the chosen contour continue to be the closest $\mathcal{E}_c$ to the real axis; see Figures 6.9 and 6.10. Thus, if they contribute at all, they give the lowest quasi-normal modes.

ii) It is natural to expect $|\tilde{q}| \leq 1$ correlators to be largest at $t_b = 0$ and to decay toward both future and past. From (6.39), this requires any dominant worldline at $t_b = 0$ to have $\mathcal{E}$ real[10], and also requires the contour in its vicinity to flow toward the upper half plane.

   This expectation is trivially satisfied for our chosen contour at $\alpha^2 = 2$, $\tilde{q} = 1$ for which $\mathcal{E} = 0$ identically. But the $t_b = 0$ worldline on this chosen contour admits a unique continuous deformation to general allowed $\alpha, \tilde{q}$. In each case one finds the corresponding $\mathcal{E}(t_b = 0)$ to be real and the contour to flow in the desired direction. This seen from Figures 6.9 and 6.10, recalling that time-reversal symmetry relates the upper and lower half-planes. Thus if any contour crosses the real axis at a single point, this point must be $t_b = 0$. The

[10]Unless it somehow fails to contribute at all to any correlator with $t_b > 0$ (which would allow $\mathrm{Im}(\mathcal{E}) > 0$), or to any correlator with $t_b < 0$ (which would allow $\mathrm{Im}(\mathcal{E}) > 0$). This seems unlikely even at special values of $\alpha, \tilde{q}$, and completely implausible on open sets of these parameters. The real $\mathcal{E}$ requirement applies also to cases where multiple worldlines share dominance at $t_b = 0$.

relevant contour is shown in red for all $\alpha, \tilde{q}$.

iii) The observation that following a branch cut from any $\mathcal{E}_c$ at fixed $\alpha, \tilde{q}$ should take one away from the real axis suggests near extremality that at least a large part of the other contours (for which $\mathcal{E}_c$ does not become small) do indeed move off the principal sheet. See Figures 6.9 and 6.10. It is plausible that at extremality such contours move off the principal sheet for all t_b, though this would require further analysis to determine.

We also mention a further good property of our chosen contour for $\tilde{q} < 1$. Here the behavior near extremality is clear from general considerations even at the quantitative level. The RNAdS$_5$ black hole develops a deep AdS$_2 \times \mathbb{R}^3$ throat and, since this near-horizon region is associated with low energies, the emergent AdS$_2$ isometries define an infrared conformal fixed point that associates each operator with a new effective infrared conformal dimension $\Delta_{\rm IR}$ [233, 234]. As discussed in [235, 236], at finite but very low temperature to good approximation this is just a finite-temperature version of the same AdS$_2$. As a result, if we start with two points at the bifurcation surface and move them radially outward into opposite asymptotic regions then it is clear that $\Delta_{\rm IR}$ also controls the rate of decay of the associated two-point function. Since this decay must continue up to a cutoff controlled by the temperature we arrive at

$$G_{12} \sim T^{2\Delta_{\rm IR}}. \tag{6.42}$$

In particular, the precise condition for a non-vanishing two-point function as $T \to 0$ is $\Delta_{\rm IR} = 0$, which indeed implies that the system sits on the threshold of an

instability as discussed in [241].

Returning to our contour, one can readily see that it provides results consistent with (6.42). Since $\mathcal{E} \sim 0$ and $w_t \sim 1$, the leading-order behavior of I at fixed t_b is

$$I = \ell \int^{1-\epsilon} \sqrt{\frac{1-\tilde{q}^2}{3}} \frac{1}{1-w}\, dw + \mathcal{O}(1) = \ell \sqrt{\frac{1-\tilde{q}^2}{3}} \ln(\mu/T) + \mathcal{O}(1). \tag{6.43}$$

Exponentiating this result gives (6.42) with $\Delta_{\rm IR} = m\ell\sqrt{(1-\tilde{q}^2)/12}$, which as one may easily check is the correct result at large m in 5 bulk dimensions.

We now consider $\tilde{q} = 1$. Since $\Delta_{\rm IR} = 0$ to the approximation with which we work, the correlator will be finite at extremality. But our worldline approximation provides interesting information about time-dependence. To extract this information, we take the extreme limit $\epsilon \to 0$ of (6.34) in which three of the $\mathcal{E}_c$ move to the origin. Two of these correspond to the endpoints of our chosen $\mathcal{E} \to 0$ contour. They are

$$\mathcal{E}_c = \left(\frac{1}{2\sqrt{3}} - \frac{e^{\pm i\pi/3}}{8 \cdot 3^{1/3}}\, \epsilon^{1/3} \right) \epsilon + \mathcal{O}\left(\epsilon^{5/3}\right), \tag{6.44}$$

suggesting that the entire $\mathcal{E}(t_b)$ contour obeys the scaling relation

$$\mathcal{E} = \left(\frac{1}{2\sqrt{3}} - a\, \epsilon^{1/3} \right) \epsilon \tag{6.45}$$

with a a complex number ranging between $e^{\pm i\pi/3}$. Inserting this ansatz into the elliptic integral expressions of appendix B.2 leads to simplified expressions ((B.11)

and (B.12)) which satisfy the relation for all t_b[11]

$$I = \ell \left[-\frac{\pi}{2\sqrt{3}} - 2\sqrt{\frac{2}{3}} \text{arctanh} \sqrt{\frac{2}{3}} - \frac{2\pi i}{\sqrt{3}} T\, t_b + \mathcal{O}\left(T/\mu\right)^{4/3} \right], \tag{6.46}$$

where the $\mathcal{O}(T/\mu)^{4/3}$ term has unspecified time dependence. While this expansion can be continued to higher orders, it is simpler to focus on the late-time behavior and use (6.35) and (6.44). For example, we find

$$\omega_c = m \left[-\frac{\pi}{\sqrt{3}} \ell\, T + \frac{e^{-i\pi/3}}{2^{3/2} \cdot 3^{1/6}} \frac{\ell\mu}{\gamma} \left(\gamma\pi T/\mu\right)^{4/3} + \mathcal{O}(T/\mu)^{5/3} \right]. \tag{6.47}$$

The interesting property of both (6.46) and (6.47) is that, beyond linear order in T, the expansion comes in powers of $(T/\mu)^{1/3}$. This differs markedly from the $\tilde{q} < 1$ expansion which involves only integer powers of T/μ.

6.4.5 Comments on non-extreme contours

We now make some brief remarks on contours for general non-extreme $\alpha, \tilde{q}$ which, while tangential to our analysis of the extreme limit, may nevertheless be of interest.

i) The red contours in Figures 6.9 and 6.10 are associated with correlations that decay away from $t_b = 0$ as in comment (ii). We expect these to dominate for all α near $t_b = 0$, though not necessarily for large t_b. Indeed, there is a regime between Figures 6.9(b) and 6.9(c) where the red contour would reach the imaginary $\mathcal{E}_c$, while the complex $\mathcal{E}_c$ (off the imaginary axis) have smaller

[11] To this order, the time dependent part of this result can also be obtained by using the leading (a-independent) term in (6.45) to integrate (6.39).

imaginary part, potentially corresponding to lower QNMs, and may well still contribute.

ii) The exchange of relevance/dominance of the above $\mathcal{E}_c$ near α_{crit} in Figure 6.9 appears to be related to the massless uncharged scalar results of [262] which found two families of QNMs: purely damped modes, and oscillating damped modes. The latter give the lowest QNM for small α, while the former do so beyond some threshold value. Furthermore, the damping time diverges in the extreme limit. Though [262] studied global RNAdS$_4$, their results persist in the planar (large radius) limit. Note that we find similar behavior for sufficiently small $\tilde{q} > 0$, though this transition disappears at larger $\tilde{q}$.

iii) The location of the bifurcation points in Figure 6.9 corresponds to the location of the maxima and minima of t_b along the imaginary $\mathcal{E}$ axis found by [227], though they did not follow the complex branches.

6.5 Discussion

We have studied the behavior of thermofield double states with chemical potential μ in holographic contexts dual to the two-sided planar Reissner-Nordström AdS$_5$ black hole. One copy of the CFT is associated with each boundary, and we have focused on correlations and entanglement between the two. The deep throat that arises in the extreme limit of RNAdS immediately implies that corresponding two-point functions of neutral operators vanish as $T \to 0$ at fixed μ. For the same reasons, the thermo-mutual information between strips (or other finite-sized regions) of size L in the two CFTs vanishes at small T unless L diverges; see

section 6.3. Such results might at first seem to suggest that all localized measures of entanglement vanish in this limit.

However, we have shown that other localized measures behave differently. One example is the thermo-mutual information (6.20) between a width L strip in one CFT and the full second CFT. As discussed in section 6.3.2, this remains non-zero as $T \to 0$ so long as $L > L_{s+\mathrm{CFT}}|_{T/\mu=0} \approx 1.05\,\gamma/\mu$. Another example is the two-point function of appropriately-tuned charged scalar operators. In the limit of large conformal dimensions, the required tuning in bulk language is $m\kappa = qg$, which in field theory terms at large Δ becomes $\Delta = 2|q|$ for e.g. $N = 4$ SYM when the $U(1)$ charge corresponds to a subgroup of the SO(6) R-symmetry. But as explained in section 6.4.4, a more complete characterization of the requirement is that the effective IR conformal dimension of the operator should vanish, so that the system sits just on the threshold of an instability.

In particular, we saw explicitly in the wordline approximation that CFT two-point functions $G_{12}(x_1, x_2)$ with $\Delta_{\mathrm{IR}} = 0$ remain non-zero at finite arguments and that the correlations they measure do not all shift off to infinitely large scales as $T \to 0$. Since Δ_{IR} controls the scaling of G_{12} at any fixed spatial separation $\vec{x}_1 - \vec{x}_2$, we expect this behavior to continue even for finite-dimension operators; i.e., it is not an artifact of the worldline approximation.

We find the mixture of divergent and finite length scales as $T \to 0$ quite interesting. The $\mathrm{AdS}_2 \times \mathbb{R}^3$ IR fixed point exhibits local criticality, with infinite dynamical scaling exponent z. Since dynamical scaling symmetry at finite z would require length scales $L \propto T^{-1/z}$, both constant (T^0) and logarithmic behaviors ($\ln T$) are natural at $z = \infty$. We see that $\mathrm{AdS}_2 \times \mathbb{R}^3$ fixed points involve a

particular combination of the two – a result one would like to understand from the CFT perspective. Motivated by our results for charged correlators, one would also like to study what one might call the "charged thermo-mutual information" of two finite strips (one in each CFT) defined using the von Neumann version of the charged Rényi entropies of [263]. At least with additional fine-tuning of the new charge parameter, this may well lead to further entanglement measures that remain localized as $T \to 0$.

Understanding the entanglement structure of physically interesting states at various scales is an intriguing and complex problem. Indeed, this is the goal of many studies of tensor network representations of ground states, the multi-scale entanglement renormalization ansatz (MERA), and the like; see e.g. [264–268]. Our parameter T/μ is a dial that one can turn to explore this scale-dependence for TFD states at $t = 0$, just as one may explore the time-dependence of entanglement using the proposal of [70] (see e.g. [45, 46, 70, 229, 257, 269–278]). The two limits are closely related, as both explore the deep infrared. Indeed, our results for TMI at low T have much in common with those of [229] at late times: There again the thermo-mutual information vanished between strips of fixed finite size in opposing CFTs, while – although not actually discussed in [229] – TMI($\mathcal{A}_1$:CFT$_2$) need not vanish since it is in fact independent of time.

As noted earlier, such observations are difficult to reconcile with the quasiparticle picture of TMI entanglement (see [229], following the time-dependent picture of [257]). In particular, as described in section 6.3.3, we find that the TMI between a strip in one CFT and its complement in the other again vanishes at small T, so that one cannot even say that the CFT$_2$ degrees of freedom entangled with

a given strip in CFT_1 have moved off to infinite scales – they remain tied in some essential way to the mirror-strip in CFT_2. The situation is even more dramatic if we compactify space, in which case the analogues of $\mathcal{A}_1$, $\mathcal{A}_2$, $\mathcal{A}_1^c$, $\mathcal{A}_2^2$, all have pairwise vanishing TMI at sufficiently small T. And it is clear that this same behavior will be found at late times using [70]. Assuming this prescription to be correct thus leads to a similarly dramatic late-time failure of the quasiparticle picture for any initial state[12].

A final general feature on which we remark is the sharpness of transitions associated with TMI at large N, in that it strictly vanishes below some threshold. Such sharpness is of course a general feature of transitions involving holographic entanglement [69]. The fact that this behavior is by now well-known should not reduce our desire to understand it at the microscopic level. Indeed, it seems deeply related to the general observation that plasmas in holographic CFTs can strongly *de*couple from short-distance probes. A particularly striking example of such behavior is the funnel/droplet transition described in [57] – see [279] for a review – in which such plasmas suddenly become unable to couple to heat sources smaller than some characteristic size. The funnel/droplet transition was recently linked to color confinement [279], and the resulting circle of ideas may have implications for the present discussion.

Let us now briefly return to two-point functions. In addition to the results summarized above, we also found new phenomena associated with "extremally

[12]Other features of the proposal [70] that are diffcult to reconcile with a free-streaming quasiparticle picture of time-dependence were mentioned in [45, 46]. We comment that CFTs on spaces with compact directions provide yet another. For example, in a $d = 2$ CFT on a circle of radius R, all quantities associated with free-streaming quasiparticles of speed v are periodic with period $2\pi R/v$. But aside from trivial conserved currents at the boundary, holographic duals certainly do not display this periodicity, and neither should more general CFTs.

charged" operators ($\tilde{q} = 1$) at small T. In particular, since all time-dependence of the $T = 0$ TFD is through an overall phase, physical quantities become time-independent. But at least for operators tuned to satisfy $\Delta_{\rm IR} = 0$, the precise way in which they do so seems to be via an unexpected expansion in powers of $T^{1/3}$ that governs corrections beyond the leading linear behavior (see equation (6.47)). While section 6.3 reported TMI results only for $t = 0$, using the proposal of [70] the analysis extends readily to more general times and produces late-time results that agree with [45, 46] and which give only smooth functions of T.

As a final comment, we recall that [34] described how two-point TFD correlators similar to those studied here might be used to probe the classical singularity of the planar Schwarzschild solution ($\mu = 0$), and thus perhaps to study how this singularity is resolved by quantum and/or stringy effects. While already nontrivial at $\mu = 0$, we note that any generalization to $\mu \neq 0$ will involve further subtleties. In particular, for $\mu = 0$ the idea was to study operators of large but finite dimension and to analytically continue t_b until the associated geodesic passes close to the singularity – in our notation, until w becomes very large. As is clear from the upper left diagram in Figure 6.7, for $\mu = 0$ this happens as $\mathcal{E} \to \pm i\infty$ along the principal sheet of the w_t Riemann surface. But as shown in the other diagrams in Figure 6.7, for $\mu \neq 0$ one finds that w_t remains bounded on the principal sheet. Thus finite m correlators are no longer approximated by geodesics passing close to the singularity anywhere in the complex t_b plane. The construction analogous to [34] would thus require first taking the $m \to \infty$ limit of finite-dimension correlators and then analytically continuing to another sheet of the Riemann surface $w_t(\mathcal{E})$. Indeed, from our preliminary numerics it is unclear whether one can even

reach the inner horizon on the principal sheet, so this same complication may well apply to analogous investigations of inner horizon instabilities along the lines of [227].

Chapter 7

AdS Wormholes with de Sitter Interiors

7.1 Introduction

The AdS/CFT correspondence [19, 20] offers a remarkable insight into properties of large-N, strongly coupled conformal field theories (CFTs): Many quantities of interest in the CFT are related to simple geometrical objects in the gravitational bulk. Familiar examples include correlators of scalar fields with large conformal dimension that may be computed from the length of bulk geodesics [67] and Wilson loops given by the areas of bulk string worldsheets [68].

Our interest here concerns the bulk dual of CFT entanglement entropy. Generalizing the Ryu-Takayangi (RT) prescription [69, 280] to time-dependent contexts, the Hubeny-Rangamani-Takayanagi (HRT) proposal [70] states that at leading or-

der in N the entropy of a region A of a holographic CFT is given by

$$S(A) = \frac{\text{Area}(\Xi)}{4G_N}, \tag{7.1}$$

where G_N is the bulk Newton constant and Ξ is the minimal-area (spacelike) extremal surface anchored on the set ∂A. Here we think of both A and ∂A as appropriate subsets of the timelike conformal boundary of an asymptotically locally AdS bulk spacetime. Because Ξ reaches the AdS boundary, the two sides of (7.1) are both infinite; a more meaningful equality of finite quantities follows when the two sides are properly renormalized. As emphasized by Headrick and Takayanagi [255], one should restrict attention to bulk surfaces appropriately homologous to A (viewed as part of the conformal boundary). We therefore use the term HHRT to refer both to the entire framework and to codimension-2 spacelike extremal surfaces homologous to some given A (whether or not the surface has minimal area within this class).

The purpose of this work is to discuss HHRT for a new class of geometries, termed planar AdS-dS-wormholes. These spacetimes describe plane-symmetric black holes with two asymptotically AdS regions connected by a wormhole that in turn contains an inflating region – and in particular a de Sitter-like (spacelike and smooth) region $\mathscr{I}_{\text{dS}}$ of the conformal boundary; see figure 7.1 for an example and section 7.2 for details. We show below that codimension-2 extremal surfaces cannot span any such wormholes, by which we mean that they cannot connect one side to the other. It follows that HHRT predicts the leading-order large-N mutual information $I(A, B)$ to vanish between two finite-sized regions A and B

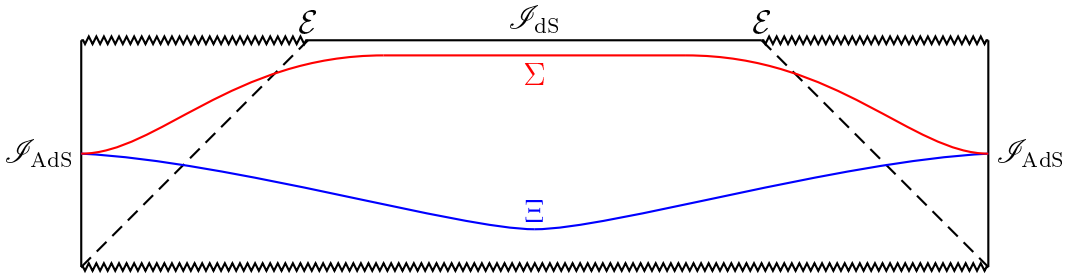

Figure 7.1: A sample conformal diagram for an AdS-dS-wormhole. The surface labeled Ξ (blue in color version) is a putative wormhole-spanning surface (which we will show cannot exist if the spacetime obeys the null energy condition). The surface Σ (red in color version) is an achronal surface that approaches close to $\mathscr{I}_{\rm dS}$ and thus has large volume element. The dashed lines indicate the boundary of the past of the dS-like part $\mathscr{I}_{\rm dS}$ of the conformal boundary. The wormhole shown has a right/left $\mathbb{Z}_2$ reflection symmetry. The explicit wormholes of section 7.2 will share this symmetry, though it is not needed for our general arguments. The edges of $\mathscr{I}_{\rm dS}$ are marked $\mathscr{E}$.

lying on opposite conformal boundaries[1]. This is in sharp contrast to the behavior of thermofield double states studied by Hartman and Maldacena [229].

However, the leading order $I(A, B)$ is non-zero when A and B are the entirety of their respective boundaries since, for that case, the empty set is also homologous to $A \cup B$. Despite the time-dependent nature of our interior geometries, the predicted entanglement is thus similar to that of both generic entangled states (see e.g. [40, 229, 281, 282] for holographic discussions) and a naive interpretation of extreme Reissner-Nordström black holes [76, 282].

At least when interpreted as a suitable large-torus limit of wormholes with toroidal cross sections (see section 7.4.3), we see no inherent inconsistency in this

[1]We remind the reader that this mutual information can be defined in terms of the von Neumann entropies $S(A)$, $S(B)$, and $S(A \cup B)$ as

$$I(A, B) = S(A) + S(B) - S(A \cup B). \tag{7.2}$$

prediction. Indeed, further investigation of this feature may provide insights into the holographic description of inflation (see also [283–286][2]). But the lack of wormhole-spanning codimension-2 surfaces makes our AdS-dS-wormholes a natural context in which to investigate possible corrections to HHRT. In particular, while the two AdS boundaries cannot be connected by any HHRT surface lying in the real Lorentz-signature spacetime, there is no obstacle to finding complex such surfaces in a complexified AdS-dS-wormhole. Indeed, we argue below that such complex extremal surfaces exist, though we leave their detailed analysis for future work. We remind the reader that complex saddle points often dominate the evaluation of integrals along the real axis, so that derivations of RT via saddle-point approximations to Euclidean bulk path integrals [71, 288–291] naturally suggest that complex extremal surfaces be incorporated into HHRT, which would in any case require analytic continuation to make contact with the Euclidean calculation in time-dependent contexts. See [78] for a discussion of these points, some confusions they raise, and a study of complex codimension-2 extremal surfaces in bulk duals of thermofield double states. To leave open the question of whether (7.1) is really the CFT entropy, in what follows we will use the term "HHRT entanglement" to refer to the bulk quantity calculated by (7.2) using real surfaces, without implying any particular interpretation in the dual CFT. The term "HHRT surface" will similarly imply the surface to be real unless explicitly stated otherwise.

[2] These references study time-symmetric spacetimes. Our wormholes cannot be time-symmetric, as a moment of time-symmetry is a totally-geodesic surface. Any wormhole-spanning minimal subsurface would thus be a wormhole-spanning extremal surface of the full spacetime. Indeed, with planar symmetry a Raychaudhuri-equation argument like that of [287] shows that no piece of $\mathscr{I}_{\rm dS}$ on the future boundary can lie to the future of any piece of $\mathscr{I}_{\rm dS}$ on the past boundary.

We begin by constructing examples of planar AdS_{d+1} dS-wormholes in section 7.2. We use a cut-and-paste procedure based on simpler and more familiar geometries. The junctions where the cut-out pieces are sewn together contain distributional sources (null shells) whose stress tensors we compute. For all $d \geq 2$ we identify cases where the result satisfies the null energy condition (NEC), both in the original spacetime from which the pieces were cut and on these null shells.

Section 7.3 then shows that $d \geq 2$ planar AdS_{d+1} dS-wormholes obeying the NEC admit no real wormhole-spanning HHRT surfaces. In fact, the main result is slightly more general: in any asymptotically AdS spacetime respecting the null energy condition, the light cone (boundary of the past or future) from any real codimension-2 spacelike extremal surface Ξ anchored at the AdS boundary can intersect a de Sitter-like region of the conformal boundary only on a set of measure zero. This turns out to forbid wormhole-spanning HHRT surfaces for our planar wormholes. Regulating the geometries by allowing inflation to proceed only to a finite extent can restore theses surfaces, but their area must diverge as the regulator is removed. Either argument leads to the HHRT entanglement properties described above when A, B are finite-sized subsets of opposite boundaries.

The case where A and B are entire boundaries is discussed in section 4, where the associated HHRT surfaces are termed total entropy surfaces. Interestingly, it appears that total entropy surfaces also fail to exist in many AdS-dS-wormholes. We show that there are no plane-symmetric total entropy surfaces in a large class of examples from section 7.2, and we conjecture that less symmetric total entropy surfaces also fail to exist. If so, the HHRT proposal becomes ill-defined and requires improvement. The conceptually-simplest change would replace the HHRT

surfaces with limits of families of surfaces that exist in a regulated geometry. These limiting surfaces can be thought of as living on the conformal completion of the unregulated spacetime, so we refer to this proposal as $\overline{\text{HHRT}}$.

An alternative and tempting modification, discussed in section 7.5, is the inclusion of *complex* codimension-2 extremal surfaces living in complexified wormhole geometries. Unfortunately, our cut-and-paste spacetimes are not analytic, so their complexification is far from unique. We thus save analysis of complex surfaces in actual AdS-dS-wormholes for future work. Instead, we analyze complex surfaces in pure de Sitter space where real surfaces again fail to exist with widely separated anchors and where we may expect a similar structure. With help from appendix B we also note that a sum over complex geodesics accurately reproduces two-point functions of quantum fields in the de Sitter vacuum state. Since the geodesic approximation to two-point functions shares many superficial similarities with HHRT, this provides some partial support for the idea that complex surfaces contribute to holographic entanglement for AdS-dS-wormholes. We close with some final discussion in section 7.6.

7.2 Cut and Paste AdS-dS-wormholes

We define an AdS wormhole to be a connected solution M of the Einstein equations (with a matter source respecting the null energy condition) which has two causally disconnected asymptotically (locally) AdS boundaries[3]. AdS-dS-wormholes are those particular examples which admit a conformal extension $\overline{M}$

[3]With enough assumptions about the nature of these two boundaries their causal disconnection in fact follows from the null energy condition [292, 293].

in which some piece $\mathscr{I}_{\rm dS}$ of the conformal boundary is, smooth, spacelike, and has diverging conformal factor. We require $\mathscr{I}_{\rm dS}$ to contain an open set of the conformal boundary, and smoothness of some part the conformal boundary is taken to mean smoothness there of $\overline{M}$ as defined by an additional conformal factor that vanishes linearly. In the usual way these conditions imply that M is asymptotically de Sitter in the region near $\mathscr{I}_{\rm dS}$. Reasoning as in section 4.1 of [294], one may show that $\mathscr{I}_{\rm dS}$ must be causally inaccessible from (i.e., outside both the past and future of) any region of the AdS boundary $\mathscr{I}_{\rm AdS}$. With enough symmetry – and in particular for planar symmetry as defined below – this follows particularly quickly from the Raychaudhuri equation in parallel with the spherical case studied in [287]; see also [295]. Since such spacetimes cannot be time-symmetric (see footnote 2), we will generally assume that $\mathscr{I}_{\rm dS}$ lies on the future conformal boundary as in figure 7.1.

The goal of this section is to construct simple examples of plane-symmetric AdS-dS-wormholes. This shows that such solutions exist and helps to make the discussion in the remaining sections more concrete; they are of particular use in section 7.4.

We will build planar AdS-dS-wormholes by pasting together regions cut from more familiar spacetimes satisfying the vacuum Einstein equations with cosmological constant, though the value of this cosmological constant will vary from region to region. We will think of each local cosmological constant as set by a distinct extremum in the potential $V(\phi)$ of some scalar field ϕ which is constant in each patch. Each junction will be a null surface, which by the Einstein equations is associated with some thin shell of matter. For appropriate choices of parameters

these null shells satisfy the null energy condition and may be interpreted as shock waves in the scalar field ϕ.

We take each region to admit an additional Killing field ξ beyond those involved in the planar symmetry, though the vector field ξ will generally fail to be continuous across the junctions and, as a result, will not define an isometry of the full wormhole spacetime. Our examples will be built from three such patches, but we impose a $\mathbb{Z}_2$ reflection symmetry exchanging the ends of the wormhole so that these regions are of only two distinct types (called I and II, see figure 7.2).

Region I will be the part of the familiar planar AdS_{d+1}-Schwarzschild black hole (or BTZ for $d = 2$) lying to the past of one AdS boundary, while region II is (part of) an analytic continuation of the planar AdS_{d+1}-Schwarzschild black hole to positive effective cosmological constant (studied in [296]; see (7.3) and (7.4) below). The conformal diagrams of these spacetimes and the indicated regions are shown in figure 7.3. Each patch extends to the relevant part of the future and/or past Killing horizon.

The junctions are two copies of a single null shell (drawn as dotted lines and both labeled A in the figure) which lie on parts of the would-be Killing horizons of ξ. Note that our wormhole has Cauchy horizons H_{Cauchy} along other pieces of the would-be Killing horizons. In analogy with the Reissner-Nordström case [297–299], we expect our Cauchy horizons to be unstable to forming null singularities. They should thus be considered an artefact of our cut-and-paste construction.

We also introduce a coordinate r defined at each point by the scale factor of the corresponding plane of symmetry, and which must be continuous across each shell. This requires the black hole horizon in patch I to have the same "radius"

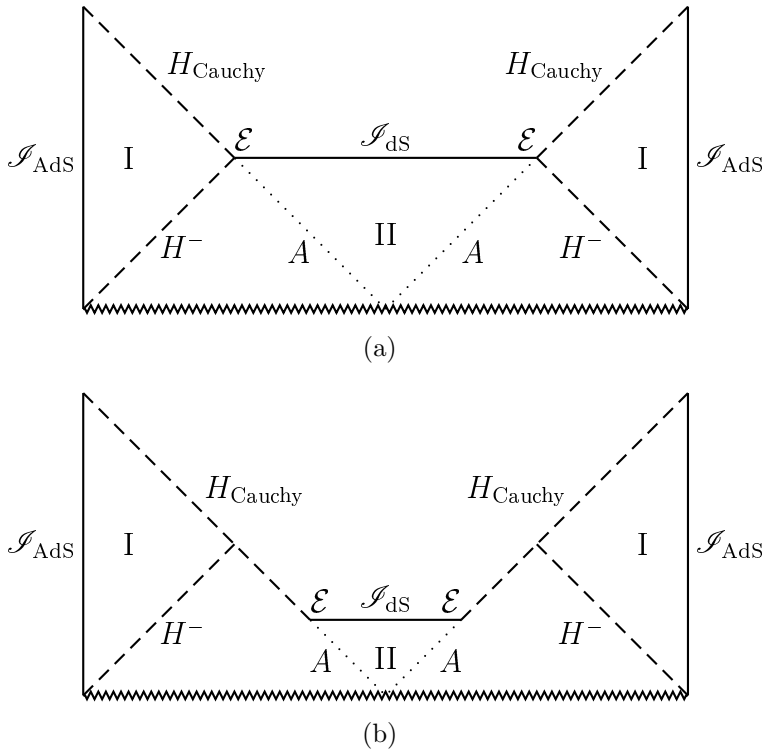

Figure 7.2: Our cut-and-paste AdS-dS-wormholes. The two types of regions are pasted together along null shells, indicated by the dotted lines labeled A, which are taken to lie along (parts of the) Killing horizons of the patches I and II. The dashed lines labeled H_{Cauchy} are Killing horizons of patch I and are Cauchy horizons of the full spacetime; the dashed lines labeled H^- are the past event horizons. The two patches labeled I are isometric under a left/right reflection. (a): A case where the edges $\mathcal{E}$ of $\mathscr{I}_{\text{dS}}$ lie on the past event horizons of $\mathscr{I}_{\text{AdS}}$. (b): A less extreme case where $\mathscr{I}_{\text{dS}}$ lies below the past event horizon.

r_+ as the de Sitter horizon in patch II, though the effective cosmological constant (parametrized by the associated length scales ℓ_I, ℓ_{II}) and black hole mass-density may differ. As noted above, one may think of the associated jumps as modeling gravity coupled to a scalar field whose potential has both AdS and dS extrema.

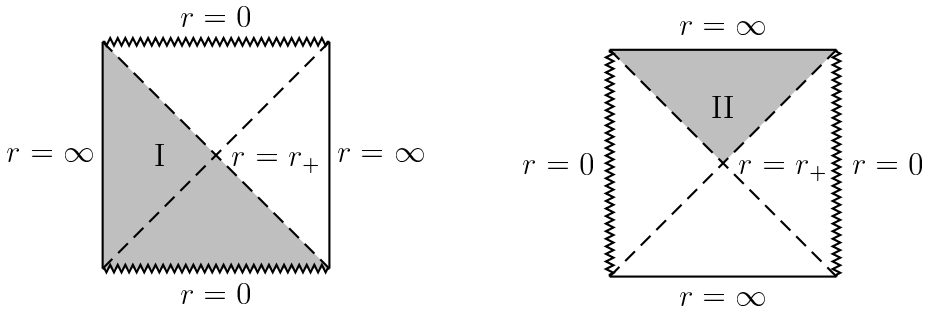

Figure 7.3: Conformal diagrams for the spacetimes from which we cut our (shaded) regions I and II. The dashed lines on both diagrams correspond to the Killing horizons at $r = r_+$. For simplicity we do not show the relative bending between the singularity and boundary.

In both patches the metric thus takes the form

$$ds_n^2 = -f_n(r)dt_n^2 + \frac{dr^2}{f_n(r)} + r^2\, d\vec{x}_{d-1}^2, \tag{7.3}$$

where $n = \mathrm{I}, \mathrm{II}$, each of the f_n have a zero at the same value $r = r_+$, and the coordinates t_n will generally differ from patch to patch. In particular, we take

$$f_I(r) = \frac{r^2}{\ell_I^2}\left(1 - \left(\frac{r_+}{r}\right)^d\right), \tag{7.4a}$$

$$f_{II}(r) = -\frac{r^2}{\ell_{II}^2}\left(1 - \left(\frac{r_+}{r}\right)^d\right). \tag{7.4b}$$

In regions I and II, we have $0 < r < \infty$ and $r_+ < r < \infty$ respectively, as shown in figure 7.3.

Assembling these patches as in figure 7.2 yields a planar AdS_{d+1} dS-wormhole. But the result is far from unique, as we must specify the manner in which each pair of regions is sewn together at the relevant junction. In our context, it is

convenient to do so using Eddington-Finkelstein coordinates

$$du_n = dt_n - \frac{dr}{f_n(r)}, \quad dv_n = dt_n + \frac{dr}{f_n(r)}. \tag{7.5}$$

Recall that the past event horizon in region I is $v_I = -\infty$, with v_I running from ∞ to $-\infty$ below this horizon and then again from $-\infty$ to ∞ above. We sew patch II to the part of patch I below the past horizon using

$$v_{II} = \frac{1}{\kappa_{II}} g_A\left(\kappa_I v_I\right), \tag{7.6}$$

where $g_A(x)$ is an arbitrary continuous monotonic function. The fact that we placed the boundaries of our regions at Killing horizons means that the induced metric is continuous across the junction for any g_A. To construct figure 7.2(a), we choose g_A to map $(-\infty, \infty) \mapsto (-\infty, \infty)$, and in particular take $g_A(-\infty) = -\infty$. This takes the two edges $\mathcal{E}$ of $\mathscr{I}_{\rm dS}$ to lie precisely on the past event horizons H^- of $\mathscr{I}_{\rm AdS}$, as shown in figure 7.2(a). Recall from earlier that, as in [287], the null energy condition prevents $\mathscr{I}_{\rm dS}$ from being to the future of any point of $\mathscr{I}_{\rm AdS}$, so this current case is a threshold case. We may move $\mathscr{I}_{\rm dS}$ lower (as in figure 7.2(b)), but no higher.

That the spacetimes of figure 7.2 obey the NEC is easily verified by calculating the stress tensor of our shells. The key quantities are their energy density μ and pressure p. We wish to find examples satisfying $\mu + p \geq 0$; this condition is equivalent to the NEC in our context. The computations are described in appendix B.3. For the spacetime of figure 7.2(a), we take $g_A(x) = \beta x$; then

using (B.26) the condition $\mu_A + p_A \geq 0$ becomes equivalent to

$$\kappa_{II} \geq \beta \kappa_I \left[1 - \frac{1+\beta}{d-1} \kappa_I r_+ \right]. \tag{7.7}$$

Choosing, for instance,

$$\kappa_I r_+ = \frac{1}{4}, \quad \kappa_{II} r_+ = \frac{1}{4} \left(1 - \frac{1}{2(d-1)} \right), \quad \beta = 1 \tag{7.8}$$

yields $\mu_A + p_A = 0$ for all $d \geq 2$, giving a patched AdS-dS-wormhole that saturates the NEC everywhere.

To construct figure 7.2(b), we instead set $g_A(x) = \ln(e^{dx} - e^{d\kappa_I v_0})$ and take the domain of v_I to be (v_0, ∞); this places the edges $\mathcal{E}$ of $\mathscr{I}_{\rm dS}$ at a finite advanced time $v_I = v_0$ and yields

$$\mu_A + p_A = \frac{1}{8\pi G_N r_+} \left[\frac{2d}{e^{d\kappa_I (v_I - v_0)} - 1} + 2 + \left(1 - e^{-d\kappa_I (v_I - v_0)} \right) \left(1 - \frac{1}{d} \right) \right], \tag{7.9}$$

which is positive[4] for all $v_I > v_0$ and $d \geq 2$.

As noted above, our cut-and-paste construction led to a Cauchy horizon $H_{\rm Cauchy}$. While not a problem for our later discussion and likely unstable, we nevertheless mention that it is easy to shrink this horizon or even remove it entirely by including further simple matter sources. For example, one can fire null dust (obeying the null energy condition) from the AdS boundary, as shown in figure 7.4(a). This

[4]One may ask if in analogy with the threshold case there exists some choice of parameters that saturates the NEC; that is, for arbitrary finite v_0, is there a choice of $\kappa_I > 0$, $\kappa_{II} > 0$, and smooth monotonic $g_A(x)$ with domain (v_0, ∞) that sets $\mu_A + p_A = 0$? The answer is no: using (B.26) the condition $\mu_A + p_A = 0$ becomes a differential equation for g_A, whose only solutions do not obey the monotonicity requirement.

replaces the pure AdS-Schwarzschild metric in the part of patch I above H^- with an ingoing planar AdS-Vaidya metric (i.e., the ingoing planar AdS analogue of [300, 301]) of the form

$$ds_I^2 = -f_I(r, v_I)dv_I^2 + 2\,dv_I\,dr + r^2\,d\vec{x}_{d-1}^2, \text{ where } f_I(r, v_I) = \frac{r^2}{\ell_I^2}\left(1 - \frac{\tilde{r}^d(v_I)}{r^d}\right), \tag{7.10}$$

where $\tilde{r}(v_I)$ is an arbitrary function satisfying $\tilde{r}'(v_I) \geq 0$ and $\tilde{r}(-\infty) = r_+$.

In principle, the Cauchy horizon can be made to disappear entirely by firing in a thin null shell along H^- itself. The spacetime then becomes the one shown in figure 7.4(b). Furthermore, as the new null shell runs along a would-be Killing horizon, each of the (now five) patches Ia, Ib, and II still admits a timelike Killing field ξ. In appendix B.3 we show by explicit construction that the resulting spacetime does indeed obey the null energy condition, though since the new null shell is not pressureless, it is not in any simple sense a limiting case of the Vaidya spacetime[5].

7.3 No localized HHRT entanglement

We turn now to HHRT surfaces and entanglement. The goal of this section is to show for all $d \geq 2$ that, according to HHRT, planar AdS_{d+1}-dS-wormholes describe states defined on two CFTs in which the CFTs are jointly pure at leading order in large N but which have vanishing leading-order mutual information between finite-

[5] That the shell cannot be pressureless follows from the fact that the pressure of the shell is a measure of the discontinuity in the acceleration of its generators across it [302]. Since its generators are future inextendible (extendible) with respect to patch Ia (Ib), this discontinuity must be nonzero and the shell pressure cannot vanish everywhere.

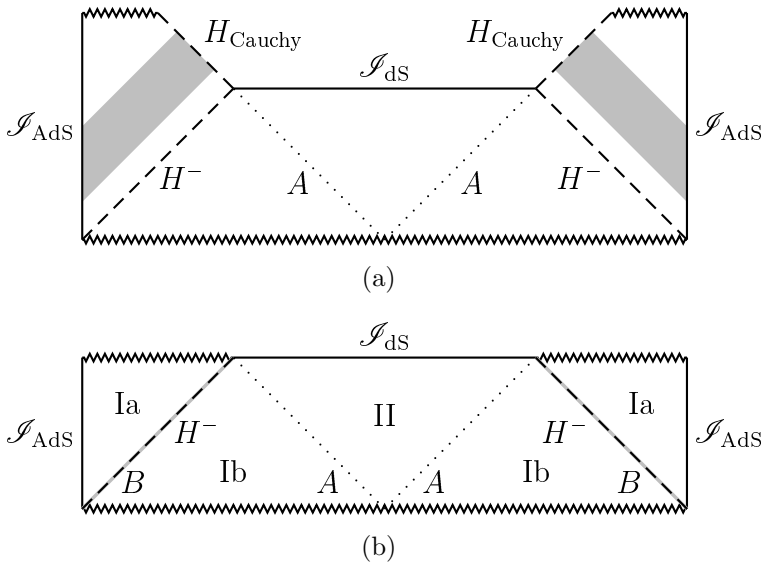

Figure 7.4: Firing in matter from the AdS boundaries modifies the cut-and–paste wormholes of figure 7.2. The spacetimes shown are based on figure 7.2(a), though corresponding results also hold for figure 7.2(b). (a): Patch I is replaced by an AdS-Vaidya metric representing pressureless null dust (shaded) falling in from $\mathscr{I}_{\text{AdS}}$. This adds a future singularity that cuts off part of the Cauchy horizon H_{Cauchy}. (b): One can remove the Cauchy horizon completely by firing in a thin null shell B (light gray lines beneath dashed lines) along H^-. The shell further divides region I into subregions Ia and Ib on either side. This shell cannot be pressureless (see footnote 5) and is not a simple limit of the Vaidya case shown at top.

sized subregions of opposing boundaries. The leading-order purity of the total state is straightforward: the pair of AdS boundaries taken together is homologous to the empty set so that the total leading-order entropy vanishes. And the mutual information (7.2) will vanish between finite-sized subregions A, B if $S(A \cup B) = S(A) + S(B)$.

We show below that AdS-dS-wormholes have no wormhole-spanning codimension-2 extremal surfaces. So when A, B are finite-sized subregions of opposite boundaries, every extremal surface anchored on $\partial(A \cup B)$ is in fact the union of two

disconnected surfaces – one anchored on ∂A and the other on ∂B. A naive application of HHRT thus yields $S(A \cup B) = S(A) + S(B)$ and $I(A, B) = 0$. In order to take a bit more care, we also consider regulated versions of our spacetimes where wormhole-spanning surfaces do exist and show that this behavior is reproduced in the limit where the regulator is removed.

The arguments of this section do not in fact require the full planar symmetry; it is enough to have the translation subgroup. We refer to this as planar-translation symmetry in order to distinguish it from full planar symmetry.

7.3.1 No wormhole-spanning extremal surfaces

We first show that the intersection of de Sitter-like regions of the conformal boundary with the light cone (boundary of the past or future) from any real codimension-2 extremal surface Ξ must have measure zero when the only boundaries of Ξ lie at the AdS boundaries. We will refer to this latter property saying that Ξ is anchored at the AdS boundary. As for $\mathscr{I}_{\rm dS}$ above, we define de Sitter-like regions of the conformal boundary to be those that are smooth and spacelike with divergent conformal factor. We assume the spacetime to satisfy the null convergence condition $R_{ab}k^a k^a \geq 0$, which holds for solutions of the Einstein-Hilbert equations of motion for gravity coupled to matter that respects the null energy condition. The argument is closely related to the methods of [303]. Where not specified, we will use the conventions and definitions of [90].

To begin, consider a real codimension-2 extremal surface Ξ anchored at the AdS boundary whose light cone intersects a de Sitter-like region of the conformal boundary. Since the only boundary of Ξ lies at the AdS boundary, and since any

extremal surface intersects the AdS boundary orthogonally, the light cone of Ξ is generated by a congruence of null geodesics fired orthogonally from Ξ. Furthermore, since Ξ is extremal and codimension-2, the expansion of this congruence vanishes at Ξ. No new generators can join the light cone as one moves away from Ξ, and the null convergence condition implies that the expansion can only decrease. Thus, just as in the proof of the Hawking area theorem [304], the area of the light cone can only decrease as one moves away from Ξ.

On the other hand, any piece of this light cone which intersects a de Sitter-like region of the conformal boundary on a set of non-zero measure has infinite area. If Ξ has finite area this immediately implies that the intersection must have measure zero. If Ξ has infinite area (as in the case of interest), the same conclusion is reached by considering a compact set of null geodesics in our congruence that reach the de Sitter-like infinity; they must have been fired from a compact subset of Ξ with finite area. And if all compact subsets have zero measure then the total measure of the intersection must vanish as well. This argument assumes the light cone to be piecewise C^2 in parallel with Hawking's original derivation [304] of the area theorem, but we expect that this assumption can be dropped using the methods of [305].

One may use the above result to exclude wormhole-spanning HHRT surfaces in an AdS-dS-wormhole with an an everywhere-spacelike freely-acting $\mathbb{R}^{d-1}$ translation symmetry (which we call planar-translation symmetry), or in any quotient of such a spacetime by any subgroup of these translations. For such a translation-planar AdS-dS-wormhole M, it is natural to consider conformal extensions $\overline{M}$ containing $\mathscr{I}_{\rm dS}$ for which the relevant conformal factor and thus $\overline{M}$ are also in-

variant under this planar-translation symmetry. This means that $\overline{M}$ cannot be compact, but we will choose conformal extensions that become so under any quotient by a discrete translation subgroup group that takes $\mathbb{R}^{d-1}$ to the torus T^{d-1}.

The planar-translation symmetry implies that any wormhole-spanning extremal surface Ξ must pass through the region to the past of $\mathscr{I}_{\rm dS}$, see figure 7.1. But the light cone of Ξ can expand only with finite speed in the conformally extended spacetime $\overline{M}$, while $\overline{M}$ remains infinite in the planar directions. Thus the part of $\mathscr{I}_{\rm dS}$ to the future of Ξ can be of only finite extent in the planar directions. Since $\mathscr{I}_{\rm dS}$ is invariant under the full infinite planar-translation symmetry, the future light cone of Ξ (i.e., the boundary of its future) must intersect $\mathscr{I}_{\rm dS}$ along some surface that spans $\mathscr{I}_{\rm dS}$ from one end to the other. And since $\mathscr{I}_{\rm dS}$ is non-trivial, the measure of this intersection is non-zero. This contradicts the result above and shows that Ξ cannot exist. It also follows that wormhole-spanning extremal surfaces cannot exist in any quotient as they would then lift to a wormhole-spanning extremal surface in the covering spacetime M.

We note that this same result can be derived directly using the maximin prescription of [303] (which was shown to be equivalent to HHRT in certain contexts). The maximin construction considers all achronal surfaces Σ satisfying appropriate boundary conditions, such as the one shown in figure 7.1. One then finds the minimal surface on each Σ and then maximizes the area of this surface over all Σ. So the area of the maximin surface is bounded below by the area of the minimal surface on any given Σ. Since $\mathscr{I}_{\rm dS}$ is outside the light cone of any point on any AdS boundary, we may choose Σ to lie arbitrarily close to $\mathscr{I}_{\rm dS}$ over a finite portion of its length as shown in figure 7.1. In the limit where Σ approaches $\mathscr{I}_{\rm dS}$ in

this way the area of the minimal wormhole-spanning surface on Σ grows without bound. We see that the area of any maximin surface must be infinite, and that no actual maximin surface can exist in M. This argument works directly in both translation-planar spacetimes and their quotients.

On the other hand, there is no obstruction to having extremal codimension-2 surfaces outside the horizon. Indeed, we may take the exterior regions of our wormhole to be just planar AdS-Schwarzschild in which extremal surfaces have been extensively studied (e.g. in [69, 280]). Considering finite-sized subregions A and B of opposite boundaries, the lack of wormhole-spanning extremal surfaces means that, when the translation-symmetry is non-compact, a naive application of HHRT finds the minimal area surface computing $S(A \cup B)$ to be disconnected, with each connected component giving just $S(A)$ or $S(B)$ separately[6]. In other words, our result implies $S(A \cup B) \approx S(A) + S(B)$ so that $I(A, B) \approx 0$, where $\approx$ denotes equality at leading order in large N.

We now pause to evaluate this conclusion more carefully. In particular, we consider regulated versions of our AdS-dS-wormholes in which inflation proceeds only for a finite time before the wormhole recollapses to a singularity. Simplified models of such spacetimes are constructed and studied in detail in appendix B.4. Removing $\mathscr{I}_{\rm dS}$ in this way allows wormhole-spanning HHRT surfaces to exist. Indeed, the arguments of [303] tell us that they do, and that they coincide with

[6]The reader may note that $A \cup B$ is homologous to $\bar{A} \cup \bar{B}$ where $\bar{A}, \bar{B}$ are the complements of A, B within their respective boundaries. As a result, there are also disconnected surfaces with each piece separately homologous to $\bar{A}, \bar{B}$. But when the translation symmetry is non-compact and A, B are finite-sized, these latter surfaces will have infinite area and do not contribute. For toroidal wormholes, they will again fail to contribute when A, B are sufficiently small but make the leading-order $I(A, B)$ non-zero for large enough A, B.

maximin surfaces[7].

The maximization step in the maximin procedure suggests that wormhole-spanning extremal surfaces lie near the surface of maximal inflation in the regulated wormhole. More precisely, we argue in appendix B.4 that at late times they approach a surface of maximal effective scale factor in behavior analogous to that found by Hartman and Maldacena in AdS-Schwarzschild [229]. This surface recedes to $\mathscr{I}_{\rm dS}$ and becomes of infinite size in any limit where our regulator is removed. In contrast, the area of disconnected surfaces that lie outside the horizon will remain finite as the regulator is removed. So, as above, when the translation symmetry group is appropriately non-compact, HHRT again predicts $S(A \cup B) \approx S(A) + S(B)$ for AdS-dS-wormholes and $I(A, B) \approx 0$.

7.4 No total entropy surfaces in M, but finite total entropy

We have seen that planar AdS-dS-wormholes have vanishing HHRT entropy between finite-sized subregions of opposite boundaries. This raises the question of taking A and B to be (opposite) boundaries in their entirety. Since $A \cup B$ is then homologous to the empty set, HHRT finds $S(A \cup B) = 0$ and $I(A, B) = S(A) + S(B) = 2S(A)$. But it remains to compute $S(A)$ by finding the associated HHRT surfaces. Such (putative) surfaces are called total entropy surfaces below.

[7] The theorems in [303] address Kasner-like singularities. The singularities of our regulated wormholes are naturally either of Kasner-like or of the 'big crunch' form where all directions shrink to zero size. Since all surfaces near the big crunch are small, it is manifest that the maximization step of the maximin procedure keeps one well away from such singularities. It is thus even easier to apply the arguments of [303] in this case than for Kasner-like singularities.

For a broad class of planar AdS-dS-wormholes from section 7.2, section 7.4.1 will demonstrate that plane-symmetric total entropy surfaces do not exist in the physical spacetime M. This argument uses the full planar symmetry and not just the translation subgroup, though corresponding results follow immediately for toroidal quotients. We conjecture that less-symmetric total entropy surfaces also fail to exist and that the HHRT entropy is ill-defined. More complicated examples similarly suggest that a strict application of HHRT gives physically incorrect results even when a total entropy surface exists in M.

Consideration of regulated spacetimes in section 7.4.2 nevertheless argues that HHRT be extended to assign a finite entropy to each boundary of our AdS-dS-wormholes. The non-zero entropy implies a positive mutual information between the two boundaries. We also locate an effective HHRT surface lying in the conformal boundary at the edge of $\mathscr{I}_{\rm dS}$. The implications for entanglement are summarized in section 7.4.3.

7.4.1 Planar wormholes without planar total entropy surfaces

The example wormholes of section 7.2 have full planar symmetry, including reflections as well as translations in each (spacelike) planar direction. This implies that our wormholes admit unique (future-directed) left- and right-moving null congruences orthogonal to every orbit of the planar symmetry group; i.e., whose velocity field has only r, t components. Since a codimension-2 surface is extremal if and only if the expansion vanishes at the surface for each of the two orthogonal null congruences, plane-symmetric total entropy surfaces arise only when the left-

and right-moving congruences define zero-expansion surfaces ($\theta_L = 0$, $\theta_R = 0$) that intersect.

One can certainly find AdS-dS-wormholes where this intersection exists. For example, this occurs when the wormhole exterior is precisely AdS-Schwarzschild up to and including the bifurcation surface. The left- and right-moving AdS-Schwarzschild Killing horizons have respectively $\theta_L = 0$, $\theta_R = 0$ and intersect at a total entropy surface (i.e. the bifurcation surface). But there are other choices where the zero-expansion surfaces do not intersect.

For planar congruences in planar spacetimes the sign of the expansion is positive when r increases along the congruence and negative when it decreases. So it is straightforward to draw $\theta_L = 0$, $\theta_R = 0$ contours for the simple cases shown in figures 7.2(a) and 7.4(b) in which the matter consists only of thin shells. The results are shown in figure 7.5. Since the expansions are generally not continuous at the junctions, in most cases what we have actually drawn is the boundary between the region of positive expansion (below the indicated lines) and the region of negative expansion (above the indicated lines)[8].

When the matter shells enter along the past event horizons of $\mathscr{I}_{\rm AdS}$ (as in figure 7.5(a)) we find that $\theta_L = 0$, $\theta_R = 0$ surfaces coincide over a finite piece of these horizons near $\mathscr{I}_{\rm dS}$. But this is an artefact of the associated fine tuning. Taking the shell to enter later (as in figure 7.5(b)) displaces the outgoing zero-expansion surface toward the future so that the two surfaces no longer intersect in the physical spacetime M. For appropriate choices, this remains true when we smooth out the thin shell by passing to the Vaiya wormhole shown in figure 7.4(a);

[8]The exception occurs at shell A, where on either side the congruence along this shell has positive expansion that vanishes as the shell is approached.

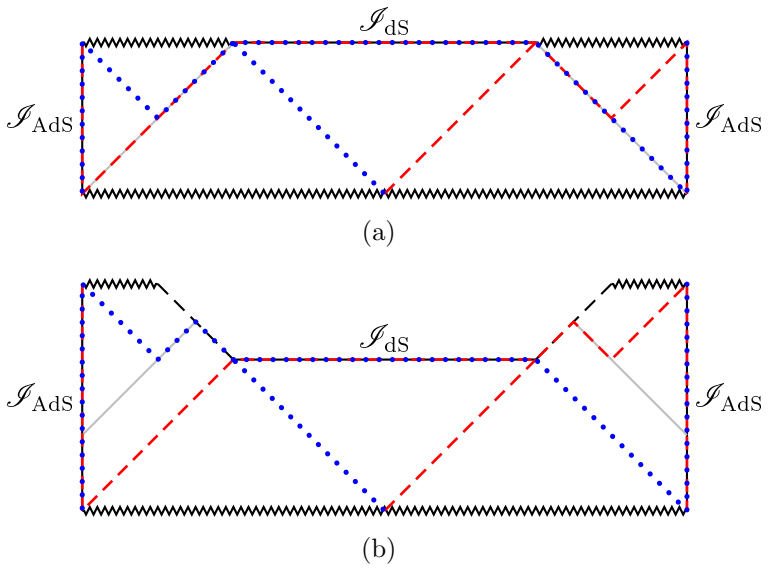

Figure 7.5: Surfaces of $\theta_R = 0$ (dashed lines; red in color version) and $\theta_L = 0$ (dotted lines; blue in color version) for the AdS-dS-wormholes shown in figure 7.4. Note that since affine parameters diverge at $\mathscr{I}_{\rm dS}$ and $\mathscr{I}_{\rm AdS}$, the Raychaudhuri equation guarantees that θ_R, θ_L both vanish on these surfaces. We take the ingoing matter to consist of null shells (solid gray lines). (a): The spacetime of figure 7.4(b). Null shells with non-zero pressure are fired in along the past horizons of $\mathscr{I}_{\rm AdS}$; this fine-tuning leads the $\theta_R = 0$, $\theta_L = 0$ surfaces to overlap along portions of these past horizons. (b): When the incoming shells are displaced to the future the surfaces $\theta_R = 0$, $\theta_L = 0$ no longer intersect in M and total entropy surfaces do not exist in M. Here the shell may be chosen pressureless so that this case is a simple limit of figure 7.4(a). A version in which this new null shell is smoothed out is shown in figure 7.6.

see figure 7.6 for an explicit example which takes $d = 2$ and

$$\tilde{r}(v_I) = r_+ \sqrt{5 + 4\tanh(v_I/\ell_I)}, \tag{7.11}$$

with $\tilde{r}(v)$ defined as in (7.10). The Cauchy horizons in these examples should be unstable and non-generic as described in section 7.2, though we see no reason that such instabilities should restore the missing total entropy surfaces.

In such cases there can be no planar total entropy surface. The same is clearly

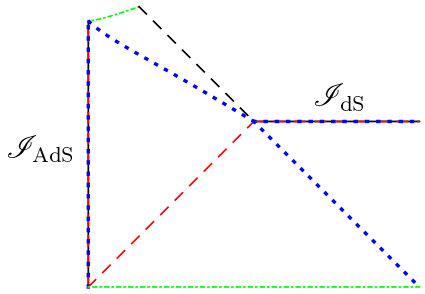

Figure 7.6: Surfaces of zero expansion in the $d = 2$ AdS-Vaidya dS-wormhole with the mass function (7.11). Conventions are the same as in figure 7.5, except that singularities are now drawn as solid lines (green in color version). Note that we only show the left half of the spacetime, and that only surfaces to the future of the past horizon H^- have been calculated and plotted explicitly; the past singularity and $\mathscr{I}_{\rm dS}$ have been drawn as straight lines by hand. The Cauchy horizon intersects the singularity at advanced time $v_0 = -\ell_I \ln\sqrt{3}$. As in figure 7.5, this Cauchy horizon can also be removed by adding a null shell along H^-.

true of toroidal quotients. We expect that less-symmetric total entropy surfaces fail to exist as well[9].

7.4.2 Regulated wormholes

The lack of total entropy surfaces in these cases renders the HHRT entropy of either boundary ill-defined. So this prescription clearly requires modification. When wormhole-spanning extremal surfaces did not exist in section 7.3, we argued that they could equivalently be assigned infinite entropy. But taking the x^i coordinates periodic turns each boundary into a finite torus (at each time). So since the bulk clearly has finite energy, it would be physically incorrect to assign infinite entropy to either CFT. Some other resolution is needed.

[9]In the past domain of dependence of $\mathscr{I}_{\rm dS}$, extremal surfaces that extend in the planar directions will tend to bend toward the singularities. But closed surfaces in M will have points (locally) "closest" to the singularity. So one need only exclude extremal surfaces from other regions of the conformal diagram.

Useful insight can again be obtained by considering the regulated and smoothed-out wormholes of section 7.3; the key point is again that they inflate only to a finite extent before recollapsing to a singularity. Thus all desired extremal surfaces will exist (see footnote 7). Furthermore, in these regulated spacetimes, theorem 16 of [303] guarantees total entropy surfaces to have smaller area $A_{TE}^{\rm reg}$ than the area $A_{\rm bif}$ of the smallest bifurcation surface of either the right or left event horizon. So holding $A_{\rm bif}$ fixed as the regulator is removed gives a regulator-independent upper bound on $A_{TE}^{\rm reg}$. In particular, since the Hawking area theorem guarantees the late-time area of the event horizon to be even larger, the bound on $A_{TE}^{\rm reg}$ is consistent with the expected CFT density of states at the given energy.

This suggests that $A_{TE}^{\rm reg}$ may approach some limit $A_{TE}^{\rm lim}$ as the regulator is removed. Using $A_{TE}^{\rm lim}$ to calculate entropy for AdS-dS-wormholes would be a simple extension of HHRT that we christen $\overline{\rm HHRT}$, though we will not study convergence of this limit in any detail. However, we mention that more complicated variations on the above examples suggest that the original HHRT prescription can assign the wrong entropy even when a total entropy surface does exist. For example, we could modify the spacetimes of figure 7.4 by adding a further AdS-Schwarzschild region with unmolested bifurcation surfaces that introduce new extremal surfaces. If the area $A_{\rm new}$ of this new surfaces exceeds the above $A_{TE}^{\rm lim}$, then HHRT will use a smaller surface to compute our entropy in any regulated spacetime. Strict use of HHRT would then predict the entropy to be discontinuous as the regulator is removed while by construction $\overline{\rm HHRT}$ gives a continuous result. And, as above, in many cases the strict HHRT result will give $A_{\rm new} > A_{\rm bif}$ which will often conflict with the CFT density of states as set by the total energy (while consistency of

$\overline{\text{HHRT}}$ is guaranteed).

It also is useful to discuss the above limit in terms of the maximin prescription of [303], which is equivalent to HHRT in our regulated context (see again footnote 7). We once more recall that a maximin surface is constructed by first studying all achronal surfaces Σ, identifying the minimal surface on each, and maximizing the associated area over all Σ. Now, the proposal that AdS-dS-wormholes have no maximin total entropy surface in the physical spacetime M would mean that this final maximum does not exist. But since [303] guarantees that the minimal surface on any Σ has area smaller than $A_{\rm bif}$, we may still discuss the least upper bound $A_{TE}^{\rm lub}$ of the areas over all achronal surfaces. And for the above toroidal wormholes this $A_{TE}^{\rm lub}$ must be finite, as it is also bounded above by the area of the horizon bifurcation surface.

For simplicity, let us suppose that $\mathscr{I}_{\rm dS}$ lies in the future conformal boundary. Then our regulator deforms the AdS-dS-wormhole only in the far future. In particular, any achronal surface in the AdS-dS-wormhole is also an achronal surface in regulated wormholes with sufficient amounts of inflation. It thus persists as the regulator is removed and gives a lower bound on the limit $A_{TE}^{\rm lim}$. It follows that $A_{TE}^{\rm lim}$ is at least $A_{TE}^{\rm lub}$.

On the other hand, suppose that some regulated spacetime had $A_{TE}^{\rm reg}$ greater than $A_{TE}^{\rm lub}$. Then the achronal surface containing this maximin surface can have no counterpart in the unregulated wormhole. One thus expects to be able to use regulators where $A_{TE}^{\rm reg}$ converges precisely to $A_{TE}^{\rm lub}$ as the regulator is removed; i.e., for which $A_{TE}^{\rm lim} = A_{TE}^{\rm lub}$. It is therefore natural to extend the maximin prescription to our AdS-dS-wormholes by assigning entropy $A_{TE}^{\rm lub}/4G_N$ to each CFT and to

term the associated scheme $\overline{\text{maximin}}$ regardless of the conditions under which this coincides with a limit of A^{reg}_{TE}. We remark that for the spacetimes of figure 7.4 this A^{lub}_{TE} is precisely the area $A_{H^-} = r_+^{d-1} V_{d-1}$ of the past horizon H^- of $\mathscr{I}_{\text{AdS}}$. Here V_{d-1} is the coordinate volume of the x^i directions and we have already argued $A^{\text{lub}}_{TE} \leq A_{H^-}$. Since achronal surfaces close to the future boundary have $r > r_+ - \epsilon$ everywhere for any $\epsilon > 0$ we also have $A^{\text{lub}}_{TE} \geq A_{H^-}$ and thus $A^{\text{lub}}_{TE} = A_{H^-}$.

A useful feature of the original HHRT framework was that it associated the entropy calculation with a specific surface in the bulk. In particular, we recall that this observation has led to proposals [303, 306] for the bulk region dual to subregions of a CFT; see also [307, 308]. It would thus be nice to locate a surface to which we can assign area A^{lub}_{TE}.

There is of course no natural candidate in the physical unregulated spacetime M. But we can ask if the total entropy surfaces of the regulated spacetimes converge in any sense to a surface in the conformal extension $\overline{M}$. Note that, since our regulator deforms the AdS-dS-wormhole only in the far future, removing the regulator must send the total entropy surfaces to the future conformal boundary. And since their area remains bounded, they cannot approach the interior of $\mathscr{I}_{\text{dS}}$. But there is no need to regulate the spacetime far from $\mathscr{I}_{\text{dS}}$, so any limiting surface can have no finite separation from $\mathscr{I}_{\text{dS}}$. The limiting total entropy surface must thus lie at one of the edges $\mathcal{E}$ in figure 7.1 that mark the boundary between $\mathscr{I}_{\text{dS}}$ and the singular part of the future conformal boundary. For similar reasons we expect that studying minimal surfaces on achronal surfaces Σ converging to the future conformal boundary in the unregulated AdS-dS-wormhole will also lead to effective maximin surfaces located at one of the edges $\mathcal{E}$; i.e., that the maximin

procedure naturally defines a surface in the conformal extension $\overline{M}$. In examples with right/left symmetry we should assign two surfaces, one at each edge. In other cases the choice of left edge vs. right[10] will depend on details of the AdS-dS-wormhole, though we expect that it will not depend on the choice of regulator.

7.4.3 Implications for entanglement

Let us now return to the discussion of entanglement. We begin with toroidal AdS-dS-wormholes in which the translation symmetry is compact. We argued above that the corresponding dual CFTs have non-zero leading-order mutual information. We also showed in section 7.3 that $I(A, B) \approx 0$ for regions A, B on opposite boundaries having sizes much smaller than the size of the torus. However, the mutual information can be non-zero at this order for A, B sufficiently large.

To discuss the uncompactified case we take the large-torus limit while holding fixed the size of our regions A, B. The part of the opposite CFT strongly entangled with A then recedes to infinity, while the total mutual information per unit area between the two CFTs remains constant. This suggests that one think of each infinite plane in the non-compact case as the limit of entire tori so that, although finite-sized subregions in opposite CFTs have no leading-order entanglement, the resulting planar CFTs retain finite leading-order mutual information per unit area; i.e., although correlations recede to infinity we do not allow any information to be lost in taking the limit[11]. Repeating this discussion for effective total entropy

[10] Here we assume that $\mathscr{I}_{\rm dS}$ is connected.

[11] A theorem of [309] (Lemma 3, Remark 1) shows that one may successfully approximate any relative entropy defined on a von Neumann algebra by describing this algebra as a limit

surfaces lying in the future conformal boundary of the toroidal wormholes leads us to consider similar effective total entropy surfaces for the planar wormholes, and of course the limit of empty sets remains empty. For the finite tori, the former compute the entropy of each boundary separately while the latter (empty set) surfaces compute the total entropy of both boundaries together. So it is in the above sense that, in the case of non-compact cross-section, our effective HRRT surface and the empty set respectively compute the leading order total entropy of each CFT separately and for the joint state on the pair of CFTs.

While the above notion of limit is essentially unique for finite-sized regions A and B, it should be mentioned that there is an alternate way of interpreting what is meant by the limiting planar CFTs taken as wholes. In this second interpretation, each entire plane is the limit of a family of additional (larger) subregions of the growing tori. These larger regions are taken to grow in size without bound, but at a rate much slower than the size of the torus itself. In other words, one "zooms in" on a smaller and smaller fraction of the torus as the torus grows. Since each resulting plane is built from the limit of "small" regions of the large-but-finite tori, the total leading-order mutual information between the two CFTs must vanish. For a finite torus, the corresponding HHRT surfaces are then anchored to "small" regions of the boundary $\mathscr{I}_{\rm AdS}$ and cannot enter the past of $\mathscr{I}_{\rm dS}$. Moreover, two such regions on opposite boundaries are not homologous and require distinct HHRT surfaces. Taking the large torus limit then implies that we continue to assign the total entropy of each planar CFT a distinct HHRT

of smaller algebras. The same thus holds for mutual information. The above interpretation is consistent with this theorem, as the algebra it assigns to the plane effectively contains many operators "at infinity" which are not limits of operators in finite regions. This "algebra at infinity" corresponds to the distant parts of the finite tori used to take the limit.

surface[12] lying entirely on its side of the wormhole, and that the union of these surfaces describes the total entropy of the two CFTs together. The total leading-order mutual information between the two CFTs then vanishes as desired under the alternate interpretation just described for the limiting planar CFTs.

The highly delocalized entanglement characteristic of toroidal AdS-dS-wormholes thus leads to two physically-distinct notions of the planar limit, both described by the same limiting (planar AdS-dS-wormhole) spacetime. The preceding analysis suggests that non-compact wormholes generally admit at least two correspondingly distinct interpretations of the homology constraint, associated with different possible roles being played by the region "at infinity" in directions transverse to the dimensions displayed in our figures. But we leave further development of this proposal for future work and content ourselves here with the discussions above.

7.5 Complex wormhole-spanning Surfaces?

While we see no inherent inconsistencies in the CFT entropies predicted by $\overline{\text{HHRT}}$, the infinite area of real wormhole-spanning $\overline{\text{HHRT}}$ surfaces makes our AdS-dS-wormholes a natural context in which to investigate further possible improvements. In particular, one might ask if complex extremal surfaces could play a role. This is suggested by the superficial analogy with the geodesic approximation to two-point functions where a lack of real geodesics does indeed indicate the importance of complex ones [34]; see also [67, 228, 310] for more general discussions. It would be very interesting to investigate complex extremal surfaces

[12] This may be only an effective surface in a sense similar to that of the $\overline{\text{HHRT}}$ proposal.

in particular example AdS-dS-wormholes (as done for static planar black holes in [78]) and to see if the results inform any of the conceptual puzzles associated with the use of complex surfaces (see again [78] for discussion). However, since the cut-and-paste spacetimes of section 7.2 are not analytic, it is unclear in what complexification such complex extremal surfaces might live. Indeed, analogy with the geodesic approximation to two-point functions raises the question of whether any HHRT-like prescription can apply to geometries that are not analytic; see e.g. [261].

We thus save analysis of complex surfaces in actual AdS-dS-wormholes for future work and make no attempt to study them here. Instead, we briefly discuss complex codimension-2 surfaces in pure de Sitter space. This section thus represents a slight aside from the main theme of this work and may be skipped without loss of continuity. In pure de Sitter settings analogous to spanning our wormholes, real such surfaces again do not exist. But we shall see that complex surfaces are readily found.

Of course, the existence of complex such surfaces does not immediately imply their relevance to the computations at hand. For example, if they describe complex saddles approximating some path integral, complex surfaces will contribute only if one can appropriately deform the contour of integration to include them. While it is unclear how to analyze this in detail for the entropy problem, it is interesting to consider the superficially-related problem of computing free-field two-point functions in the Bunch-Davies vacuum using the geodesic approximation. Using an expansion of this two-point function from appendix B.5, we show explicitly below how it is given by an infinite set of complex geodesics in dS_3 and

that these geodesics lie on an infinite number of sheets of the associated Riemann surface in the sense of [78].

7.5.1 Complex Extremal Surfaces in dS

It is well known that pure de Sitter space contains pairs of points that cannot be connected by geodesics (see e.g. [186]). Indeed, geodesics tend to bend down and away from future infinity, as shown in figure 7.7. So if the ends of the extremal surface are taken far enough apart, the geodesic becomes null and "bounces" off future infinity in a manner pictorially similar to the bouncing geodesics of AdS-Schwarzschild [34, 78] – though the null limit of bouncing geodesics retains finite length in dS_{d+1} while it vanishes in AdS-Schwarzschild as measured from any finite points in the spacetime. Real geodesics cease to exist when the separation is increased beyond this critical point, leaving only complex ones. This occurs in particular for $d = 2$, where geodesics are codimension-2 extremal surfaces. Extremal surfaces of any codimension turn out to behave similarly for all d, though the area diverges in the null limit for extremal surfaces whose dimension exceeds 1 (i.e., for any case except geodesics).

We now study this phenomenon in detail for a class of codimension-2 extremal surfaces analogous to the would-be wormhole-spanning surfaces of section 7.3. Below we anchor our surfaces at the de Sitter horizon as opposed to at a spacetime boundary. This allows us to work entirely in the dS patch. We study pure de Sitter for simplicity, but analogous results should also hold for patch II as defined in section 7.2.

Consider the inflating spatially-flat patch of pure de Sitter in the familiar

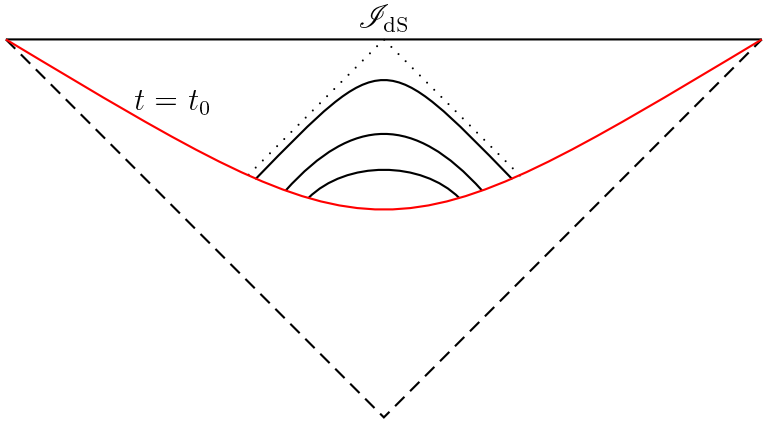

Figure 7.7: The cosmological patch of de Sitter spacetime. The solid black curves are sketches of extremal surfaces ending on a $t = t_0 =$ const slice, shown as a solid red curve. As the endpoints of the surfaces are taken farther apart, the surfaces approach the dotted null curve. At even larger separations real extremal surfaces cease to exist.

coordinates where the metric takes the form

$$ds^2 = -dt^2 + e^{2Ht} d\vec{x}_d^2 \equiv -dt^2 + e^{2Ht}\left(dr^2 + (dx^1)^2 + (d\vec{x}^{\parallel}_{d-2})^2\right). \tag{7.12}$$

We take our surfaces to be anchored on infinite strips defined by $t = t_0$, $r = \pm L/2$, $x^1 =$ const. Conservation of x^1 momentum implies that x^1 remains constant across the entire extremal surface. The surface can thus be parametrized by the coordinates $x^{\parallel}$ and a yet-to-be-specified parameter λ; i.e., $(t, r, x^1, x^{\parallel}) = (t(\lambda), r(\lambda), \text{const.}, x^{\parallel})$. The resulting area functional is

$$A = V_{d-2}\int d\lambda\, e^{(d-2)Ht}\sqrt{e^{2Ht}\dot{r}^2 - \dot{t}^2} \equiv V_{d-2}\int d\lambda\, \mathcal{L}\left(t, r, \dot{t}, \dot{r}\right), \tag{7.13}$$

where $V_{d-2} \equiv \int d^{d-2}x^{\parallel}$ is the volume of the space spanned by the $x^{\parallel}$ coordinates.

Since the effective Lagrangian $\mathcal{L} = e^{(d-2)Ht}\sqrt{e^{2Ht}\dot{r}^2 - \dot{t}^2}$ contains no explicit

dependence on $r(\lambda)$, there is a conserved conjugate momentum

$$p = \frac{\partial \mathcal{L}}{\partial r} = \frac{e^{dHt}\dot{r}}{\sqrt{e^{2Ht}\dot{r}^2 - \dot{t}^2}}. \tag{7.14}$$

Choosing the parameter λ so that $e^{2Ht}\dot{r}^2 - \dot{t}^2 = 1$, we obtain

$$\dot{r} = e^{-Ht_*}e^{-dH(t-t_*)}, \tag{7.15a}$$

$$\dot{t}^2 + V_{\text{eff}}(t) = 0, \tag{7.15b}$$

in terms of an effective Newtonian potential

$$V_{\text{eff}}(t) = 1 - e^{-2(d-1)H(t-t_*)}. \tag{7.16}$$

Here $t_* \equiv \ln p/((d-1)H)$ is the real root of $V_{\text{eff}}(t)$ and describes the turning point of real extremal surfaces. Relating t_* to the coordinate displacement L between the anchor points through

$$2L = 2\int_{t_0}^{t_*} \frac{\dot{r}}{\dot{t}}\, dt \tag{7.17}$$

yields

$$e^{Ht_0}L = \frac{i}{dH}\, e^{-H\Delta t}\left[e^{dH\Delta t}\,{}_2F_1\left(\frac{1}{2}, \frac{d}{2(d-1)}; \frac{3d-2}{2(d-1)}; e^{2(d-1)H\Delta t}\right) - {}_2F_1\left(\frac{1}{2}, \frac{d}{2(d-1)}; \frac{3d-2}{2(d-1)}; 1\right)\right], \tag{7.18}$$

where $\Delta t \equiv t_* - t_0$ and ${}_2F_1$ is the ordinary hypergeometric function written using

standard conventions (e.g. [311]). Likewise, the area (7.13) becomes

$$e^{-(d-2)Ht_0}A = \frac{2iV_{d-2}}{(d-2)H}\left[e^{(d-2)H\Delta t}\,{}_2F_1\left(\frac{1}{2},-\frac{d-2}{2(d-1)};\frac{d}{2(d-1)};1\right)\right.$$
$$\left. - {}_2F_1\left(\frac{1}{2},-\frac{d-2}{2(d-1)};\frac{d}{2(d-1)};e^{2(d-1)H\Delta t}\right)\right]. \quad (7.19)$$

These L and A are plotted in figure 7.8 as functions of Δt. It is clear that L approaches a finite value as $\Delta t \to \infty$. Indeed, expanding (7.18) at large Δt, we obtain

$$e^{Ht_0}L = \frac{1}{H} + \mathcal{O}\left(e^{-H\Delta t}\right). \quad (7.20)$$

As advertised, the surface becomes null in the limit $t_* \to \infty$ ($L \to H^{-1}e^{-Ht_0}$). As shown in figure 7.7, for $L < H^{-1}e^{-Ht_0}$ the entire extremal surface lies within the past light cone of a set on $\mathscr{I}_{\rm dS}$ of vanishing length in the r-direction. This is in fact required by the same reasoning as in section 7.3. Such arguments imply that a null surface fired orthogonally from an extremal surface can intersect $\mathscr{I}_{\rm dS}$ only in some zero-measure set. But continuity requires that the image of our null geodesics on $\mathscr{I}_{\rm dS}$ must span some interval in r. Thus the length of this interval must vanish.

In contrast, for $L > H^{-1}e^{-Ht_0}$ causality would require this interval have non-vanishing length. So real codimension-2 surfaces can no longer exist. But it is straightforward to find complex extremal surfaces in this regime (and indeed for arbitrary L when $d > 2$). One simply analytically continues expressions (7.18) and (7.19) to the entire complex Δt-plane. From (7.18) we see that L is periodic in Δt with period $2\pi i/H$, so it suffices to study L in a finite strip around the real axis. Figure 7.9 shows the complex-valued function $L(\Delta t)$ in this strip for $d =$

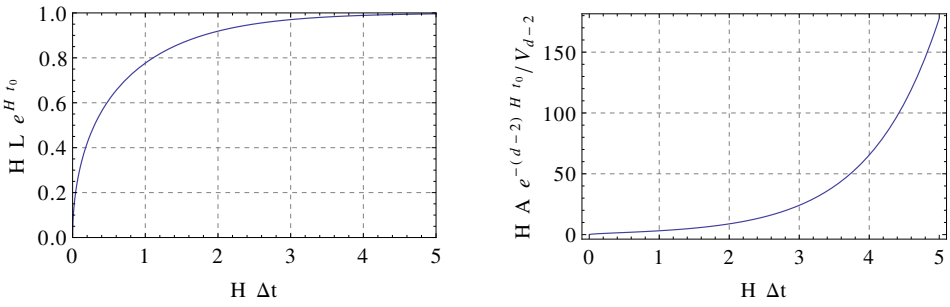

(a) (b)

Figure 7.8: The coordinate displacement L (a, at left) and the area A of codimension-2 extremal surfaces (b, at right) in pure dS as functions of Δt. The plots show results for $d = 3$, though the qualitative behavior is unchanged for $d \geq 3$ (for $d = 2$, the area remains finite at large $H\Delta t$). Note that L approaches a constant e^{-Ht_0}/H at large $H\Delta t$, consistent with the fact that real extremal surfaces do not exist for larger L.

$2, 3, 4, 5, 6, 7$; in particular, we indicate contours along which L is real. One of these runs along the real positive Δt-axis, looping tightly around the branch cut, but the others lie at complex Δt. We see that one may obtain large positive L-values by taking Re Δt large and negative along one of the real L contours in the lower half plane. For $d > 2$ this contour clearly also reaches $L = 0$ (and in fact passes to negative L), providing a complex extremal surface for all physically relevant L.

In parallel with the results of [78] for black holes, we expect additional contours of real L to exist on other sheets of the Riemann surface for $L(\Delta t)$. This function and its Riemann surface is defined by analytic continuation through the branch cuts in figure 7.9. The branch points are of logarithmic type for $d > 2$ where they lead to an infinite number of sheets. The $d = 2$ case is special in that the branch points of $L(\Delta t)$ are only two-sheeted square-root type branches; though in that case there are additional infinite-sheeted logarithmic branchings of the physically-

interesting function $A(L)$ that make the overall structure much the same.

Of course, the mere existence of complex extremal surfaces need not imply that they are relevant to our study of entropy. For bulk spacetimes constructed via some Euclidean path integral, one could plausibly use analytic continuation and the argument of [71] to write the desired entropy in terms of extremal surfaces. But for a given complex extremal surface to appear in this calculation it must be possible to appropriately deform the original contour of integration. A priori, this is far from guaranteed – though since there are no real extremal surfaces for $L > H^{-1}e^{-Ht_0}$, any contours that are allowed must be complex.

For $d = 2$ our codimension-2 surfaces are geodesics and the area becomes a length. As noted earlier, the length of bulk geodesics can also be used to approximate two-point functions of CFT operators with large dimension (so long as it is still small enough to ignore gravitational back-reaction). This is of course closely related to our entropy problem, since entropy can be calculated from the two-point function of twist operators [220]. These twist operators do indeed have large dimension – though, since acting with appropriate twist operators is equivalent to replicating the entire large N CFT in the sense of the replica trick, their dimension is in fact large enough the gravitational back-reaction is generally non-trivial. So while the two calculations are not precisely the same, it is interesting to write the well-known exact two-point functions in dS_3 as a sum over complex geodesics. This result is presented in appendix B.5, which finds this sum to use an infinite number of terms from an infinite number of sheets of the Riemann surface for $A(L)$. The analogue for $d > 2$ would be to use an infinite number of complex geodesics on an infinite number of sheets of the Riemann surface for $L(\Delta t)$. So

at least in this context there is no problem deforming the relevant path integral to take advantage of complex saddles. It is tempting to suggest that related contours will be relevant for studying the entropy of AdS-dS-wormholes, leading to non-zero leading-order mutual information between localized regions on opposite boundaries.

7.6 Discussion

This work considered two-sided AdS-dS-wormholes, which are spacetimes that contain a region of unbounded inflation. In particular, the future conformal boundary of the wormhole interior contains a smooth spacelike piece $\mathscr{I}_{\rm dS}$ as shown in figure 7.1. Explicit examples satisfying the null energy condition were constructed in section 7.2. While our smooth examples contain Cauchy horizons, we expect such solutions to be unstable to decay into a more generic class of AdS-dS-wormholes which otherwise retain all of the properties discussed below.

Our main result is that these geometries fail to admit HHRT surfaces (i.e., possibly non-minimal Hubeny-Rangamani-Takayanagi surfaces with the homology constraint emphasized by Headrick) that would exist in more familiar black hole spacetimes. In particular, section 7.3 showed that no HHRT surface can span the wormhole, connecting one side to the other. Instead, HHRT surfaces for the associated entropy problems must be disconnected, with one piece on each side of the wormhole. Section 7.4 showed that certain of our wormholes have plane-symmetric HHRT surface homologous to an entire boundary – which we termed total entropy surfaces – there is also a large class that do not. We suggested

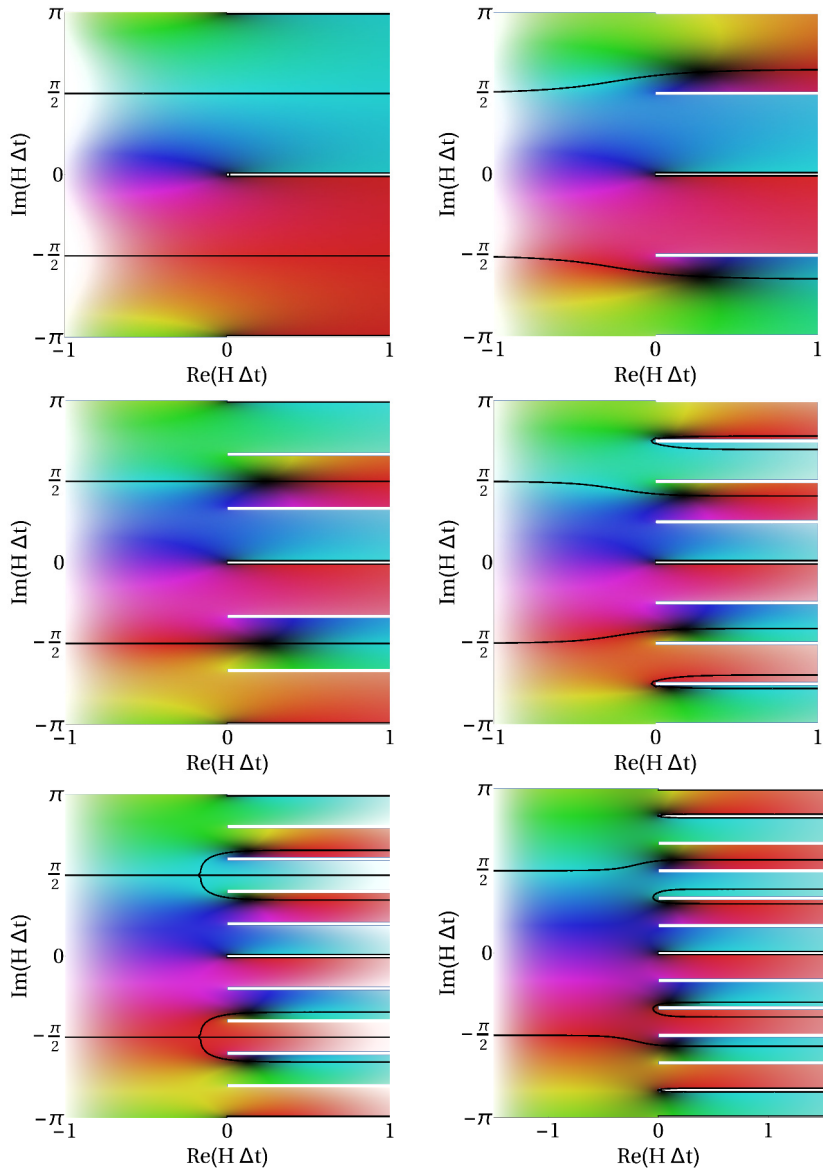

Figure 7.9: L as a function of complex Δt in dS_d. From left to right and top to bottom, the plots show $d = 2, 3, 4, 5, 6, 7$. Hue indicates $\arg(L)$ (with real positive [negative] L in red [turquoise]), while shade indicates the magnitude of $|L|$ (with $|L| = 0$ in black and increasing $|L|$ in lighter shades). The white horizontal strips mark the locations of branch cuts, and the black lines are contours along which L is real. $|L|$ is bounded in the right half-plane, but grows without bound in the left half-plane; thus the only contours that can reach arbitrarily large real L are the two complex ones that run to large negative $\mathrm{Re}(\Delta t)$.

that less-symmetric such surfaces also fail to exist, so that there are no extremal codimension-2 surfaces in the entire homology class. If so, the HHRT proposal becomes ill-defined and requires improvement. We also gave related examples where HHRT surfaces would exist but give physically incorrect results.

The conceptually-simplest possible changes to HHRT were discussed in section 7.4. These involve first regulating the dS-wormhole by allowing only a finite amount of inflation. After the inflating phase, the wormhole is required to collapse to a future singularity; see appendix B.4 for details. We argued that, at least in our examples, the limit in which the regulator is removed gives natural wormhole-spanning and total entropy HRRT surfaces lying in the future conformal boundary; i.e., they lie in the conformally extended spacetime $\overline{M}$ instead of the physical spacetime M. In the wormhole-spanning case this surface has infinite area and so is never the minimal-area surface. But in the total entropy context any limiting surface must have finite entropy density consistent with the CFT density of states. This regulate-and-take-limits approach was called $\overline{\text{HHRT}}$. But we did not investigate the convergence of these limits in detail, so it remains to determine the extent to which they are well-defined.

We also suggested an extended maximim prescription $\overline{\text{maximin}}$ that takes limits directly in the unregulated wormhole spacetime and may give results identical to $\overline{\text{HHRT}}$. The $\overline{\text{maximin}}$ procedure clearly assigns well-defined (though perhaps infinite) area to each entropy problem, and in appropriate cases may also yield a well-defined $\overline{\text{maximin}}$ surface in $\overline{M}$. But we did not analyze precisely when this surface construction succeeds, and it again remains to study when this area will agree with regulate-and-take-limits procedures.

Under either $\overline{\text{HHRT}}$ or $\overline{\text{maximin}}$ one finds that toroidal AdS-dS-wormholes are dual to highly entangled pure states on a pair of CFTs, and that this remains true for planar CFTs obtained through an appropriate large-torus limit[13]. But the associated mutual information is as delocalized as possible. In particular, for CFTs on infinite spacetimes, the leading-order mutual information vanishes between any finite-sized regions A, B of opposite CFTs.

A strictly vanishing mutual information between finite-sized subregions would contradict the non-vanishing correlators $\langle \mathcal{O}_{CFT_1}(x_1, t_1)\mathcal{O}_{CFT_2}(x_2, t_2)\rangle$ associated with taking appropriate boundary limits of bulk two-point functions[14]; see e.g. [252]. But the claim is only that the mutual information vanishes at leading order in large N, so some finite mutual information may remain. Indeed, according to [312] (see also [313]) it is precisely the $O(1)$ correction that is encoded in the state of bulk quantum fields to which the supergravity approximation applies. Such fields are dual to CFT operators whose dimensions are not too large. The implication is thus only that generic operators of large dimension (e.g., of order N^2 in 3+1 $\mathcal{N} = 4$ super Yang-Mills) have vanishing correlators between the two CFTs.

We see no inherent contradiction with this interpretation. Indeed, the physics is quite similar to that naively obtained from the extreme limit of Reissner-

[13]Though there is another large-torus limit where it does not. Both limits are described by the same planar AdS-dS-wormhole but with different notions of the homology constraint. See section 7.4.3.

[14]If our wormhole can be found as the Wick rotation of a saddle that dominates the Euclidean path integral, this integral defines a state in which the correlator can be computed using the geodesic approximation (and where it will be non-zero). But in any case the linearized bulk equation of motion would allow the above CFT correlator to vanish identically only if the corresponding bulk correlator $\langle \phi(x_1, r_1, t_1)\phi(x_2, r_2, t_2)\rangle$ vanishes for all (x_1, r_1, t_1) in the left region I and all (x_2, r_2, t_2) in the right region I. This is a very fine-tuned property and we are free to consider bulk quantum states on our wormhole background for which it does not hold.

Nordström black holes. There the large area of wormhole-spanning surfaces is associated with the infinite throat that develops at zero temperature ($T = 0$). The most apparent difference is that for Reissner-Nordström the two-boundary spacetime becomes disconnected at $T = 0$, making it somewhat more natural to consider quantum states of the linearized bulk fields having vanishing correlators between the two sides. But there are also states with non-vanishing correlators, and for fields with fine-tuned values of the bulk charge and mass such states are in fact naturally constructed by the bulk path integral dual to charged thermofield-double states in the CFT [76]. A more critical difference may be that small T Reissner-Nördstrom black holes tend to be unstable in top-down models, while causality forbids any instability of our exterior (the left and right copies of region I) being activated by starting inflation in the interior of our wormhole.

Intriguingly, the physics is also quite similar to that expected for generic entangled states (see e.g [40, 229, 281, 282] for holographic discussions). This is even more so when one chooses quantum states for the bulk fields where

$$\langle \mathcal{O}_{CFT_1}(x_1, t_1) \mathcal{O}_{CFT_2}(x_2, t_2) \rangle = 0 \tag{7.21}$$

(see again footnote 14). The one point of tension is that [281] predicted wormholes associated with such generic states to have time-independent interiors – though there is no actual contradiction so long as all implications for the CFTs remain time-independent.

It is possible that such physical predictions are correct and will provide insights into the holographic description of inflation. But the paucity of real codimension-

2 surfaces makes our AdS-dS-wormholes a natural context in which to investigate further possible modifications of HHRT. For example, one might ask if our wormholes might have no dual interpretation at all, or more conservatively if dual descriptions might require more than just a pair of CFTs; e.g., despite the HHRT claim that the state on both CFTs is pure at leading order in large N, one might suppose that the natural two CFTs are both highly entangled with some third system. This latter option would be analogous to the mixed-state proposal of [283], and the third system might correspond to the superselection sectors of [143, 144]. The present understanding of gauge/gravity duality is sufficiently coarse that we cannot exclude such suggestions, though as in [283], it is natural to take the constructions of [314] and related work as suggesting that a dual interpretation does in fact exist. And if one can construct our wormholes from (due to the lack of time-symmetry, complex) saddle points for Euclidean path integrals then one should be able to argue as in the thermofield-double discussion of [222] that it is given by a pure state on two CFTs. Indeed, one should then also be able to argue as in [71] that something like HRRT does in fact hold.

The discussion of complex saddles naturally motivates a milder possible modification of HHRT that, at least in analytic spacetimes, would make use of complex extremal surfaces in addition to real ones. For bulk black holes dual to thermofield double states this option was studied in [78], and for AdS-dS-wormholes it was briefly addressed in section 7.5. In particular, noting that HHRT is superficially similar to the the geodesic approximation for two-point functions motivated a study of this latter context. We considered the case of dS_3 – where geodesics are also codimension-2 extremal surfaces – and found complex geodesics to be

critical in constructing a stationary-phase approximation to the exact result. In particular, in the two-point function calculation it appears that one can deform the contour of integration to take advantage of complex geodesics living on an infinite number of sheets of the associated Riemann surface.

It would be very useful to study complex HHRT surfaces in full AdS-dS-wormholes. One would specifically like to understand whether the results might shed light on the confusions surrounding the use of complex surfaces that were discussed in [78]. Unfortunately, since the cut-and-paste examples of section 7.2 are not analytic, the complexification of these particular spacetimes is far from unique and any notion of complex surfaces may be ill-defined. This places a detailed analysis of complex extremal surfaces in any AdS-dS-wormhole beyond the scope of this work, making it an interesting challenge for future investigation.

Chapter 8

Complex Entangling Surfaces for AdS and Lifshitz Black Holes?

8.1 Introduction

The Ryu-Takayanagi proposal [69, 280] for holographic entropy and the covariant generalization [70] by Hubeny, Rangamani, and Takayangi (HRT) relate the area of certain codimension-2 bulk extremal surfaces Σ to corresponding von Neumann entropies $S(\rho_D)$ for the dual CFT. Each entropy involves a reduced density matrix ρ_D defined by restricting the CFT to a globally hyperbolic domain D. The main requirement is that, interpreting D as a region of the conformal boundary of the asymptotically-AdS$_{d+1}$ bulk, the intersection $\Sigma \cap D$ must coincide with the boundary ∂C of a Cauchy surface C in D. In addition, Σ must be homologous to C and there should be no other such surface Σ' of smaller area. In such contexts,

these proposals state

$$S_{\rm ren}(\rho_D) = \frac{{\rm Area}_{\rm ren}(\Sigma)}{4G_N}. \tag{8.1}$$

On both sides, the subscript "ren" indicates that divergent quantities have been renormalized in corresponding ways.

While there is now an impressive amount of data supporting these conjectures (see e.g. [69, 71, 229, 255, 280, 289, 290, 303] and further references in [315]), much of the evidence remains rather qualitative. This is especially true in the time-dependent context. As a result, it leaves open the question of what conditions might be required for (8.1) to hold quantitatively. We focus below on the possibility that analyticity of the bulk spacetime may be important, and on related questions involving complex extremal surfaces. Understanding such issues may be important for properly interpreting recent work using Ryu-Takayanagi and HRT to study the relationship between bulk and boundary notions of localization [306–308] and to derive bulk dynamics from that of the CFT [316–319].

Our study is motivated by two observations. The first is that all attempts [71, 288–291] to provide general derivations of (8.1) make use of both Euclidean path integrals and the bulk saddle-point approximation. This structure inherently relies on some measure of analytic continuation, and suggests that one may find cases where intrinsically complex saddles dominate the path integral. While the arguments in these works (and in particular [71]) are phrased in the static context of the original Ryu-Takayangi proposal [69, 280], the only crucial ingredient appears to be the existence of a well-defined – not necessarily real – asymptotically-Euclidean section. As noted in e.g. [320], for any spacetime with this property analytic continuation to the real Lorenzian section will imply the HRT conjecture

so long as the real Lorentzian extremal surface provides the most relevant saddle point. This suggests that (8.1) might apply only to analytic spacetimes and, furthermore, that even in this case it may generally require the use of complex extremal surfaces.

The second observation is an explicit example of the concerns raised by the first. Recall (see e.g. [67, 321]) that two-point functions of heavy quantum fields may be approximated by e^{-mL}, where L is the proper length of a geodesic connecting the points and m is the relevant mass. Since geodesics are extremal surfaces of codimension d in a $(d+1)$-dimensional spacetime, this geodesic approximation shares formal similarities with the holographic entanglement proposal. Furthermore, it can be derived from the stationary phase approximation to the Euclidean path integral, and the fact [220] that CFT von Neumann entropies may be computed from twist operator correlation functions may provide a tight connection to holographic entanglement for $d = 2$ (with corresponding generalizations from geodesics to other minimal surfaces when $d > 2$). But for the geodesic approximation one can show that analyticity is indeed generally required [261] and that complex geodesics play critical roles in certain contexts [34].

Though this concern has been understood for some time, there is a surprising lack of discussion in the literature. This may be due in part to the lack of known examples. Indeed, to our knowledge no complex codimension-2 surfaces have been previously identified that satisfy appropriate boundary conditions in any spacetime. We overcome this obstacle below by exhibiting families of complex codimension-2 surfaces in standard $(d + 1)$-dimensional planar black holes corresponding as in [222] to thermofield double states in dual CFTs on $\mathbb{R}^d$. We

investigate the Bañados-Teitelboim-Zanelli (BTZ) solution, Schwarzschild-AdS$_{d+1}$ black holes for $3 \leq d \leq 7$, and Schwarzschild-Lifshitz black holes [322]. We work in the maximally analytically extended spacetimes, where the real Lorentzian section has two asymptotic regions. The dual CFT thus lives on two copies of $\mathbb{R}^d$. The surfaces we consider are anchored on both boundaries at some spatial location $x^\perp$ and some time t_b, much as in [229]. They would thus be appropriate for computing the entropy of the CFT on a pair of half $(d-1)$-planes ending at $x_\perp$ at the time t_b, with one half-plane in each copy of $\mathbb{R}^d$. For this case, the globally hyperbolic domain D mentioned in the introduction is just the corresponding pair of Rindler-like wedges with each origin of Rindler coordinates located at $t_b, x^\perp$. In all cases we identify complex extremal surfaces satisfying boundary conditions relevant to the holographic entanglement conjectures. For Schwarzschild-AdS and Schwarzshild-Lifshitz we find families where the real part of the area is smaller than for corresponding real extremal surfaces.

We begin by discussing the status of (8.1) for complex surfaces in section 8.2. The area of a complex surface is generally complex, while entropies must be real. We must therefore modify (8.1) if complex surfaces turn out to be relevant. This issue remains confusing, but for the present work we choose to study a straw-man model that replaces $A_{\rm ren}$ in (8.1) by its real part.

Section 8.3 then explains our general approach to finding the desired complex surfaces and studying their properties. This is largely a transcription of the method used for complex geodesics in [76], which in turn builds on many other works. However, we take the opportunity to make certain improvements and corrections. The technique applies to surfaces of any codimension n, and we

study complex geodesics in Schwarzschild-AdS$_{d+1}$ as an illustration of the general method. The results for $d \neq 4$ appear to be new, and for $d > 4$ indicate that real geodesics in the Lorentz-signature spacetime can fail to dominate even on surfaces invariant under time-reflection symmetry (where analytic continuation between Euclidean and Lorentzian signatures is in some sense trivial). This emphasizes that complex surfaces could be important even in the original Ryu-Takayanagi context of static bulk spacetimes and not just in the more general time-dependent HRT context.

Complex codimension-2 surfaces for planar BTZ, Schwarzschild AdS$_{d+1}$ (with $3 \leq d \leq 7$), and Schwarzschild-Lifshitz are studied in section 8.4. The BTZ case yields a complete analytic solution showing that all complex extremal surfaces are in some sense higher copies of the real HRT surfaces. It follows that the same is true for global AdS$_3$, of which BTZ is just a subset, and also for Poincaré AdS$_3$. Schwarzschild-AdS$_{d+1}$ is more interesting, and exhibits several qualitatively-different families of complex extremal surfaces. We identify two families where the qualitative behavior of Re A_{ren} matches expectations for the dual CFT entropy on our half-planes. For the family called contour C below, Re A_{ren} is notably less than for the corresponding real extremal surfaces. It is thus plausible that the dual CFT entropy is indeed controlled by these complex surfaces. Our brief study of Schwarzschild-Lifshitz indicates results analogous to those for Schwarzschild-AdS.

We close with a summary and some final discussion in section 8.5. In particular, we note that all complex extremal surfaces in our spacetimes lie on what are naturally called secondary sheets of an associated Riemann surfaces. This feature

may make it difficult for the associated saddles to contribute to the stationary phase approximation of the relevant path integrals.

8.2 Entropy from complex areas?

As noted above, if complex surfaces are indeed relevant to the Ryu-Takayanagi or HRT conjectures, the formula (8.1) will require modification. The issue is that the imaginary part of $A_{\rm ren}$ is generally non-zero while the von Neumann entropy is real by definition. Now, since complex numbers enter only by analytic continuation from a real spacetime, complex extremal surfaces must appear in what one might call complex-conjugate pairs satisfying identical boundary conditions with complex-conjugate renormalized areas $A_{\rm ren}$ and $A^*_{\rm ren}$. The two members of each pair are obtained by analytically continuing along corresponding paths but in opposite directions. One might thus hope to combine $A_{\rm ren}$ and $A^*_{\rm ren}$ in some way to give a real entropy S.

The question is just how this should be done. In parallel with the geodesic approximation to two-point functions, it is natural to interpret $A_{\rm ren}/4G_N$ as a saddle-point approximation to the logarithm of a partition function. One might then expect a pair of relevant saddles s_1, s_2 to give

$$S_{\rm ren} = -\ln\left(C(s_1)e^{-A_{\rm ren}(s_1)/4G_N} + C(s_2)e^{-A_{\rm ren}(s_2)/4G_N}\right), \tag{8.2}$$

where the factors $C(s_1), C(s_2)$ represent finite G_N corrections that in particular include fluctuation determinants from quantum fields propagating on the classical spacetimes s_1, s_2.

For $A_{\rm ren}(s_1) = A_{\rm ren}(s_2)^*$ (and presumably $C(s_1) = C(s_2)^*$) the entropy becomes

$$S_{\rm ren} = \frac{\mathrm{Re}\, A_{\rm ren}}{4G_N} - \ln 2|C(s_1)| - \ln\cos\left(-\frac{\mathrm{Im}\, A_{\rm ren}}{4G_N} + \phi\right), \tag{8.3}$$

where the phase ϕ is defined by $C(s_1) = |C(s_1)|e^{i\phi}$. But for small G_N, where the formula (8.1) holds, the cosine oscillates rapidly. This will often give $S_{\rm ren}$ an unphysical imaginary part. It is not a priori clear whether one should think of this imaginary part as being of order $1/G_N$ or instead being bounded but rapidly changing as $G_N \to 0$. In the latter case it would be problematic only at the level of subleading corrections, and we might content ourselves with using

$$S_{\rm ren} \approx \frac{\mathrm{Re}\, A_{\rm ren}}{4G_N} \tag{8.4}$$

at leading order in $1/G_N$.

Interestingly, the actual form of the Lewkowycz-Maldacena argument [71] for (8.1) – or indeed any replica argument with a saddle-point approximation – appears to lead to result somewhat different from (8.2)[1]. This occurs because it is the Renyi entropies $S_n = -\frac{1}{n-1}\ln \mathrm{Tr}\,\rho^n$ (for integer n) that are directly given by partition functions, and for which the saddle-point approximation is then used. The von Neumann entropy is finally computed by analytically continuing to all real n and using

$$S_{\rm ren} = \lim_{n\to 1} S_n = -\lim_{n\to 1}\frac{1}{n-1}\ln \mathrm{Tr}\rho^n, \tag{8.5}$$

renormalizing each expression as needed. In the saddle point approximation we

[1]This point was brought to our attention through a conference presentation by Matt Headrick [323], who in turn learned it from private discussion with Rob Myers [324].

have $\mathrm{Tr}\,\rho^n \approx e^{-I_n/4G_N}$ for some I_n. If the von Neumann entropy is to be finite, I_n must vanish at $n = 1$. So, for fixed G_N, as $n \to 1$ we may write

$$e^{-I_n/4G_N} = 1 - (n-1)\frac{1}{4G_N}\left.\frac{dI_n(s)}{dn}\right|_{n=1} + \cdots, \tag{8.6}$$

where s now denotes a family of saddles with one for each n. If two such families are relevant, we have

$$\begin{aligned} S_n &= -\frac{1}{n-1}\ln\left(C_n(s_1)e^{-I_n(s_1)/4G_N} + C_n(s_2)e^{-I_n(s_2)/4G_N}\right) && \text{(8.7a)} \\ &= -\frac{1}{n-1}\ln\left(C_n(s_1)\left[1-(n-1)\frac{1}{4G_N}\left.\frac{dI_n(s_1)}{dn}\right|_{n=1}+\cdots\right]\right. && \text{(8.7b)} \\ &\quad \left. + C_n(s_2)\left[1-(n-1)\frac{1}{4G_N}\left.\frac{dI_n(s_2)}{dn}\right|_{n=1}+\cdots\right]\right). && \text{(8.7c)} \end{aligned}$$

A finite von Neumann entropy requires the normalization $C(s_1) + C(s_2) = 1$. Taking $n \to 1$ thus yields

$$S_{\mathrm{ren}} = \frac{1}{4G_N}\left.\left(C_1(s_1)\frac{dI_n(s_1)}{dn} + C_1(s_2)\frac{dI_n(s_2)}{dn}\right)\right|_{n=1}, \tag{8.8}$$

where we have neglected a term involving dC_n/dn which is subleading at small G_N.

Furthermore, in any such argument, the saddle at $n = 1$ is taken to be known and fixed; indeed, it should give the bulk dual of the original mixed state ρ. Thus s_1 and s_2 both approach this fixed saddle as $n \to 1$. As a result, if the saddle-point approximation continues to hold as $n \to 1$, the fluctuation contributions $C_1(s_1)$, $C_1(s_2)$ must agree at $n = 1$. The constraint $C_1(s_1)+C_1(s_2) = 1$ then requires both

to be 1/2. Since obtaining (8.1) in the case of a single extremal surface requires $A_{\rm ren} = dI_n(s_1)/dn|_{n=1}$, with two extremal surfaces the argument gives

$$S_{\rm ren} = \frac{A_{\rm ren}(s_1) + A_{\rm ren}(s_2)}{8G_N} \tag{8.9}$$

so long as each surface leads to a corresponding family of saddles for $\mathrm{Tr}\,\rho^n$ for all n. Thus the area in (8.1) has been replaced with the average of the two areas. For $A_{\rm ren}(s_1) = A_{\rm ren}(s_2)^*$ this is equivalent to taking the real part; i.e., the final conclusion is essentially identical to (8.4).

The result (8.9) appears to be physically incorrect. As a concrete example, consider the black hole quotients of AdS_3 described in [325–328] that have a single asymptotically-AdS region (which asymptotes to global AdS_3). Such spacetimes were called AdS geons in [329], which suggested that they are dual to pure CFT states. This was later argued in detail by [222, 330]. This is consistent with the fact that any Cauchy surface for the conformal boundary is homologous in the bulk to the empty set. So minimizing over real extremal surfaces leads to $S = 0$ as desired. But the bifurcation surface of the black hole horizon is another extremal surface, this time of positive area. Averaging the two as in (8.9) would give $S > 0$ and contradict the description as a pure state.

It remains possible that (8.9) might nevertheless be salvaged by including in the average further extremal surfaces not yet identified. Complex extremal surfaces could contribute negatively and cancel the positive contribution from the extremal surface at the horizon. But this seems unlikely and, even if true, would make the entanglement conjectures extremely difficult to use in practice.

One instead expects that the saddle-point phase approximation simply fails near $n = 1$, as this is typically the case when one varies parameters so as to make two saddles coincide.

The above discussion mostly serves to illustrate our ignorance of how (8.1) should be modified to accommodate complex extremal surfaces. While we have discussed the problem at the level of the von Neumann entropy, the replica discussion above makes it clear that the issue is already present at the level of the Renyi entropies. The point is that $\mathrm{Tr}\rho^n$ must be positive definite for any quantum system. But writing

$$\mathrm{Tr}\rho^n = e^{-I_n/4G_N} + e^{-I_n^*/4G_N} \tag{8.10}$$

for a complex conjugate pair of saddles one finds that the sign of the right-hand side oscillates quickly as $G_N \to 0$ when the action I_n is not real. One could choose to take this as an indication that only saddles with real action can contribute to Renyi entropies in the semiclassical limit, and thus that only extremal surfaces with real areas could contribute to von Neumann entropies. But other possibilities may exist. For example, we recall that in some contexts [331] carefully studying contours of integration can show that the correct semi-classical approximation is $e^{-|S|}$. It would be very interesting if a similar conclusion might somehow apply here.

Since we found two arguments above leading us to replace A_{ren} in (8.1) with its real part, we adopt this hypothesis for discussion purposes below. To emphasize the uncertainty in this conclusion, we refer to this suggestion as the straw-man proposal[2]. We will consider each complex conjugate pair separately and not at-

[2] It would be very interesting to understand whether our straw man proposal – or indeed any

tempt to further combine the results from various pairs. We also comment on the relative size of $\mathrm{Re}\, A_{\mathrm{ren}}$ for various such complex pairs, though we refrain from stating whether this means that any such pair necessarily dominates the result. Indeed, given a set of saddles it is typically difficult to determine whether the contour of integration can be deformed to pass through them in such a way that they can actually contribute to the desired saddle-point approximation. We defer further discussion of this issue to section 8.5.

8.3 Method and Analytic Structures

We now outline our general procedure for finding complex extremal surfaces. After a brief introduction to the spacetimes of interest, the basic techniques are presented in section 8.3.1 generalizing methods used to study complex geodesics in [76] (based on e.g. [228, 229, 332]). Relevant analytic structures are discussed in section 8.3.2. We consider extremal surfaces Σ of general codimension n, and we illustrate the method in section 8.3.3 by studying complex geodesics in Schwarzschild AdS_{d+1}.

As noted above, for simplicity we study $(d+1)$-dimensional spacetimes describing planar black holes with AdS-like asymptotics in each of two asymptotic regions. We therefore restrict to spacetimes of the form

$$ds^2 = -f(r)dt^2 + \frac{dr^2}{g(r)} + r^2 dx_{d-1}^2, \tag{8.11}$$

other proposal involving complex extremal surfaces – satisfies well known properties of entropies like strong subadditivity. This property has been shown to hold in [255] and [303] for the original Ryu-Takayanagi and HRT proposals based solely on real extremal surfaces, but it is far from clear that they continue to hold for complex generalizations.

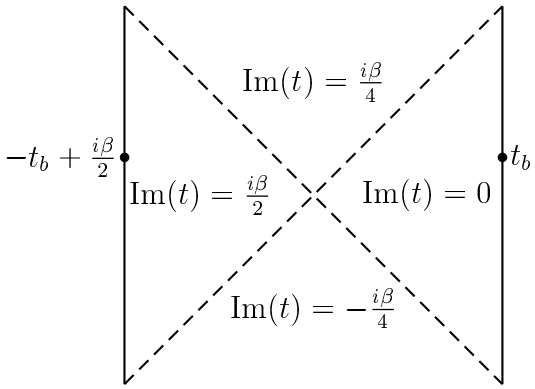

Figure 8.1: A conformal diagram of our spacetimes. The asymptotic regions are located in the left and right regions. The imaginary part of the time coordinate t is constant in each wedge, and t has period $t \sim t + i\beta$. We consider extremal surfaces anchored at the points indicated on each boundary.

where $f(r)$ and $g(r)$ each have a simple zero at some $r = r_h > 0$ corresponding to a horizon with inverse temperature

$$\beta = \frac{4\pi}{\sqrt{f'(r_h)g'(r_h)}}. \tag{8.12}$$

We assume our spacetimes to have timelike conformal boundaries at $r = \infty$, though we make no further assumption about the large r behavior of f and g. In particular, we allow both asymptotically AdS_{d+1} and asymptotically Lifshitz spacetimes [333] restricted to $z \geq 1$ (so that the null energy condition is satisfied [334]). We assume that f, g, and f/g are analytic functions of r everywhere on the complex plane except perhaps at $r = 0$ and ∞. In the Lifshitz case, $r = 0, \infty$ will be branch points so that it is better to say that f, g, and f/g are analytic on appropriate Riemann surfaces.

8.3.1 Extremal Surfaces

To study surfaces Σ of codimension n, it is useful to divide the $(d-1)$ coordinates x into two families

$$\left\{x^{\perp}\right\} = \left\{x^1, \ldots, x^{n-1}\right\}, \tag{8.13a}$$

$$\left\{x^{\parallel}\right\} = \left\{x^n, \ldots, x^{d-1}\right\}. \tag{8.13b}$$

We will require $x^{\perp}$ to be constant on the boundary $\partial\Sigma$ of Σ, and by translation invariance we may take $(x^{\perp})|_{\partial\Sigma} = 0$. This fixes $n-1$ boundary conditions, so it remains only to specify a time coordinate on $\partial\Sigma$.

The horizon at $r = r_h$ divides the spacetime into four wedges, and we can use the Schwarzschild-like coordinates t, r of (8.11) in all four wedges by analytic continuation. This prescription causes the imaginary part of t to shift by $i\beta/4$ every time a horizon is crossed, as shown in figure 8.1, and imposes a periodicity $t \sim t + i\beta$. We thus require Σ to stretch between the two boundaries, with $t|_{\partial\Sigma} = t_b$ on the right and $t|_{\partial\Sigma} = -t_b + i\beta/2$ on the left. We take take t_b to be a real parameter specifying the desired boundary conditions and more generally use Δt to denote the time difference between the two ends of any extremal surface with $(x^{\perp})|_{\partial\Sigma} = 0$. It will sometimes be useful to break Δt into its real and imaginary parts by writing $\Delta t = -2t_R + it_I$ so that surfaces satisfying our boundary conditions have $t_R = t_b$ and $t_I = \beta/2$.

Since our boundary conditions are invariant under translations in $x^{\parallel}$ we assume Σ to share this symmetry. Thus the problem reduces to finding $(t, r, x^{\perp})$ as functions of a single parameter λ which we specify below. In fact, since momen-

tum conservation requires $x^\perp$ to be monotonic in λ, the fact that $x^\perp$ vanishes on both boundaries implies $x^\perp = 0$ on all of Σ so that we need only solve for the two embedding functions $(t, r) = (T(\lambda), R(\lambda))$. The area functional then becomes

$$A = V_{d-n} \int d\lambda \, R^{d-n} \sqrt{-f(R)\dot{T}^2 + \frac{\dot{R}^2}{g(R)}} \equiv V_{d-n} \int d\lambda \, \mathcal{L}, \tag{8.14}$$

where V_{d-n} is the volume of the $x^\parallel$ space and dots denote derivatives with respect to λ.

Since T is cyclic in (8.14), its conjugate momentum (hereafter referred to as energy) is a constant of motion:

$$E = -\frac{\partial \mathcal{L}}{\partial \dot{T}} = \frac{R^{2(d-n)} f(R)}{\mathcal{L}} \dot{T}. \tag{8.15}$$

Note that E may be complex for complex surfaces Σ. Finally, we invoke the reparametrization freedom of (8.14) to choose λ to satisfy $\mathcal{L} = R^{d-n}$. This constraint serves as the remaining equation of motion, which using (8.15) can be written as the Newtonian particle-in-a-potential problem

$$\dot{R}^2 + V_{\text{eff}}(R) = 0, \text{ where } V_{\text{eff}}(R) = -g(R) - \frac{E^2 g(R)}{R^{2(d-n)} f(R)}. \tag{8.16}$$

We have thus reduced the system to quadratures. In particular, since we allow complex R and T, given any contour γ in the complex R plane we can solve (8.16) and (8.15) for dT/dR and integrate to find a $T(R)$ that solves the equations of motion[3]. The only question is whether the associated complex extremal surface

[3] This point was not correctly discussed in [76], which instead claimed that each complex geodesic had a preferred turning point. This is not generally true, but does not affect the final

satisfies our boundary condition. I.e., we must require both ends of the contour γ to approach $R = \infty$ along the real axis and then compare the total elapsed time

$$\Delta t \equiv -2t_R + it_I = \int_\gamma \frac{E}{R^{d-n} f(R) \sqrt{-V_{\text{eff}}(R)}} \, dR \tag{8.17}$$

with $-2t_b + i\beta/2$.

A similar calculation gives the renormalized area of the surface as

$$A_{\text{ren}} = \lim_{\epsilon \to 0} \left(V_{d-n} \int_{\gamma_\epsilon} \frac{R^{d-n}}{\sqrt{-V_{\text{eff}}(R)}} \, dR + A_{\text{ct}}(\epsilon) \right), \tag{8.18}$$

where ϵ is a UV regulator, $A_{\text{ct}}(\epsilon)$ is a counterterm that cancels the ϵ-divergent terms in A, and γ_ϵ is a regulated contour that runs to $R = r_h/\epsilon$ rather than $R \to \infty$. Since the renormalized area is an on-shell action, (8.17) and (8.18) satisfy the Hamilton-Jacobi relation

$$dA_{\text{ren}} = -V_{d-n} E \; d(\Delta t), \tag{8.19}$$

which can also be checked directly. This structure precisely parallels that of complex geodesics; see e.g. [228] and the recent review in [76].

Since $V_{\text{eff}}(R)$ generally vanishes at several values of R, the function $\sqrt{-V_{\text{eff}}(R)}$ defines a non-trivial Riemann surface over the complex R plane. There may also be additional branch points at $R = 0$ and at $R = \infty$ (for the Lifshitz case). The branch points of $\sqrt{-V_{\text{eff}}(R)}$ will be denoted $R_{\text{branch}}(E)$. So long as f and g have no branch points themselves (i.e., except for the Lifshitz case), the Riemann

results of [76].

surface for $\sqrt{-V_{\rm eff}(R)}$ has precisely two sheets.

Because the sign of $\sqrt{-V_{\rm eff}(R)}$ in (8.17) determines the sign of $\dot{R}$, our boundary conditions require it to take opposite values at the two ends of γ. In particular, in the non-Lifshitz case allowed contours γ thus run between endpoints $R = \infty$ on opposite sheets of the Riemann surface for $\sqrt{-V_{\rm eff}(R)}$, and without loss of generality we may take them to run from the negative branch to the positive branch. Examples of such contours are shown in figure 8.2. In the limit where the contour is deformed to tightly circle some branch point, it is natural to think of the branch point as a turning point of the trajectory. This is the case for contours along the real R-axis – such as the one shown in figure 8.2(b)– that describe real extremal surfaces in either Euclidean or Lorentzian signature.

Of course, smooth deformations of the contour γ that preserve the endpoints will not change (8.17) or (8.18). Two contours related in this way will be said to describe equivalent extremal surfaces, with inequivalent surfaces at given E corresponding to homotopically distinct contours on the Riemann surface for $\sqrt{-V_{\rm eff}(R)}$.

8.3.2 Analytic Structure of $\Delta t(E)$ and $A_{\rm ren}(E)$

One would like to use (8.17) and (8.18) to define $A_{\rm ren}$ as a function of t_b. But in general there will be multiple inequivalent extremal surfaces for a given t_b. As a result, $A_{\rm ren}(t_b)$ is in fact properly defined on a multi-sheeted Riemann surface. A useful way to deal with this complication is to work directly with $\Delta t(E)$ and $A_{\rm ren}(E)$ as described by (8.17) and (8.18). While $\Delta t(E)$ and $A_{\rm ren}(E)$ are again defined on non-trivial Riemann surfaces, their structure is closely related to that

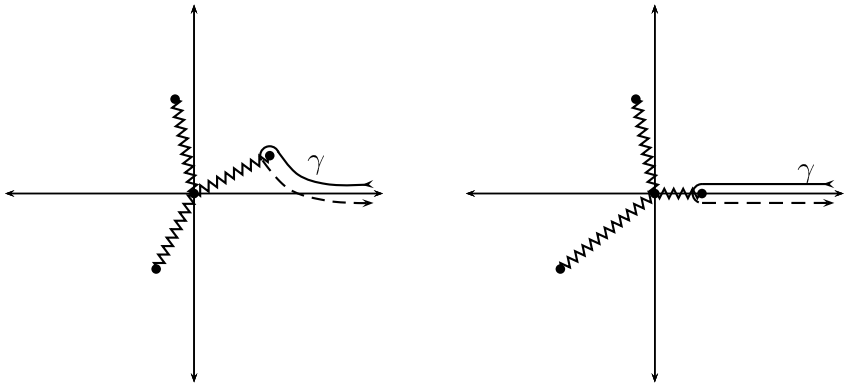

Figure 8.2: The branching structure of the integrands of (8.17) and (8.18) in the complex R-plane, and sample contours of integration γ. The number of branch points depends on the precise form of $V_{\rm eff}$; here we draw four, as for geodesics in $d = 3$ AdS-Schwarzschild. The branch points correspond to zeros of $V_{\rm eff}$ and often an additional branch point at $R = 0$. We introduce branch cuts in order to draw figures; the solid and dashed portions of γ indicate segments that run on different sheets of the associated Riemann surface. For convenience we choose the branch cuts to run radially inward, connecting all other branch points $R_{\rm branch}$ directly to $R = 0$. We adopt this convention even when $R = 0$ is not a branch point – in effect momentarily introducing an artificial branch point whose effects must disappear from the final results. Figure (a) shows the generic (complex E) case in which all the branch points lie at complex R. Figure (b) shows the special case in which E is real, in which case at least one of the branch points lies on the positive R-axis. The extremal surface corresponding to the indicated contour γ is then equivalent to a real extremal surface which may be described as having a turning point at the encircled branch point. The integrand for Δt may also have poles at other values of R, but these are not shown.

of the branch points $R_{\rm branch}(E)$ for $\sqrt{-V_{\rm eff}(R)}$. This structure is again like that of the geodesic case presented in [76], though our discussion below corrects some minor errors in [76] related to footnote 3.

Indeed, the functions (8.17) and (8.18) are analytic in E so long as the contour γ can be deformed to avoid branch points $R_{\rm branch}(E)$ or poles. But at certain critical energies two branch points will merge. Contours γ that run between these

branch points will be said to be pinched as E becomes critical, and can no longer be deformed to avoid them. Mergers of three or more branch points do not occur for the examples considered below.

When the integration contour is pinched we divide the critical energies into two classes, which we denote E_c and E_c'. The former (E_c) are energies where the merging branch points are both simple roots of V_{eff} (with no other coincident singularities[4]), so that V_{eff} develops a double root at E_c. Thus as $E \to E_c$, each integrand becomes structurally similar to $|R - R_{\text{branch}}|^{-1}$ so that the integrals $\Delta t(E)$ and $A_{\text{ren}}(E)$ diverge. Careful examination shows that when the contour γ is pinched at such E_c, the functions $\Delta t(E)$ and $A_{\text{ren}}(E)$ both behave like $C \ln(E - E_c)$ near E_c for some complex coefficient C. So both have logarithmic branch points at E_c. In contrast, the E_c' are energies where roots of V_{eff} moves to $R = 0$ or (for Lifshitz) to $R = \infty$. In general, $\Delta t(E)$ and $A_{\text{ren}}(E)$ do not diverge at such E_c', though they do have branch points there.

When the integration contour is not pinched, $\Delta t(E)$ and $A_{\text{ren}}(E)$ remain analytic even when roots merge; such situations are neither E_c's nor E_c''s and will not be called critical. Since we will see below that different sheets of our Riemann surface are associated with different contours γ, this means that the identification of a given energy E as being critical (or not) will vary as one moves from one sheet to another.

Since $\Delta t(E)$ diverges at the E_c, we expect the large time behavior of at least some families of extremal surfaces to be determined by the E_c. As for the geodesic case [228], for a family of extremal surfaces with $\Delta t \to \infty$ as $E \to E_c$, the

[4]Section 8.4.2 will describe a case where two simple roots of V_{eff} merge with a non-branching singularity (a pole) at $R = 0$.

Hamilton-Jacobi relation (8.19) immediately yields a linear relationship between $\Delta t(E)$ and $A_{\rm ren}(E)$. This can also be seen from the fact that both behave like $\ln(E - E_c)$. In particular, for codimension-2 extremal surfaces (i.e. $n = 2$), one has

$$\frac{A_{\rm ren}}{4G_N} = S_{\rm ren} = -\frac{V_{d-2}E_c}{4G_N}\,\Delta t + \cdots \equiv -\frac{1}{2}svV_{d-2}\Delta t + \cdots\,, \tag{8.20}$$

where $s = r_h^{d-1}/4G_N$ is the thermal entropy density, v is a constant, and $\cdots$ denote subleading terms in Δt. For surfaces of this type that dominate the HRT prescription, the constant v is a speed characterizing the rate of growth of the entanglement entropy; see e.g. [45, 46, 229]. It is interesting that the relation (8.20) is linear for asymptotically Lifshitz spacetimes (and, indeed, for more general asymptotics) as well as for the asymptotically AdS case. This speed was recently computed in [335] along with other properties of Schwarzschild-Lifshitz black holes.

Tracing a closed contour in the complex E-plane around one of the branch points of $\Delta t(E)$ results in movement from one sheet of $\Delta t(E)$ to another. Traveling around such a contour corresponds to swapping two of the roots of $V_{\rm eff}$, so one can think of constructing a secondary sheet of $\Delta t(E)$ by simply changing the contour of integration in (8.17) to a new contour γ', where the new contour is obtained from the original contour γ by exchanging two of the branch points in figure 8.2 without allowing the contour to cross any branch points or poles. Examples of resulting contours are shown in figure 8.3.

In order to draw diagrams, we find it useful to cut the resulting Riemann surfaces into sheets. It is convenient to do so by introducing branch cuts that run radially outward from branch points at any E_c, E_c' to $E = \infty$; see figure 8.4.

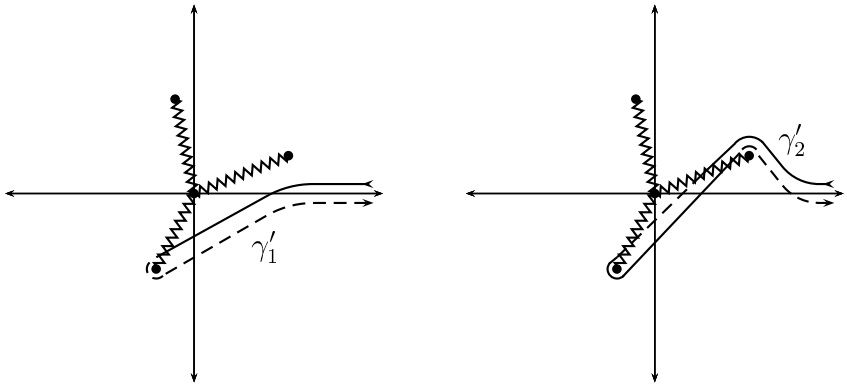

Figure 8.3: Sample integration contours γ_1', γ_2' for (8.17) and (8.18) that define secondary Riemann sheets of $\Delta t(E)$. Both contours are obtained from γ in figure 8.2 by exchanging the branch points in quadrants 1 and 3. For γ_1' the originally-encircled branch point passes below the other during the exchange, while for γ_2' it passes above. At each step, the contour must be deformed to keep it smooth on the associated Riemann surface; it must avoid both branch points and poles, though for simplicity we show only the former.

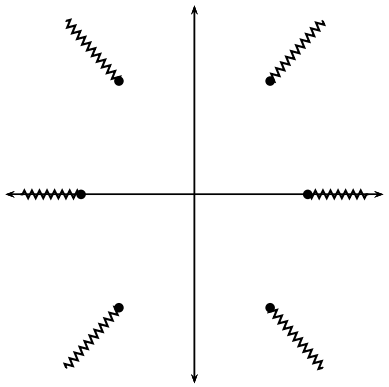

Figure 8.4: A sample choice of branch cut structure used to define a single sheet of Δt and A_{ren} in the complex E-plane; the particular structure shown here is that of e.g. geodesics in Reissner-Nordström AdS_5 or codimension-2 extremal surfaces in Schwarzschild-AdS_7. The branch points shown here correspond to the critical energies E_c at which the contour of integration γ for (8.17) and (8.18) becomes pinched between two roots of V_{eff} that coincide, and are therefore energies at which $|\Delta t|$ and $|A|$ diverge.

It is also convenient to introduce a notion of principal vs. secondary sheets. We take the principal sheet to be the one containing those extremal surfaces that

lie entirely within either the real Lorentzian or real Euclidean sections of the complexified spacetime. For all examples below, it is consistent to take both such families of surfaces to lie on a single sheet. It is natural to ask whether the principal sheet is preferred in any physical sense over the secondary Riemann sheets, but we defer discussion of this question to section 8.5.

The above structure makes the identification of extremal surfaces straightforward. The boundary conditions require that $\Delta t = -2t_b + i\beta/2$, so extremal surfaces satisfying the boundary conditions correspond to the contours $t_I = \beta/2 \pmod{\beta}$ in the complex E-plane. Since $\Delta t(E)$ is analytic (except at branch points and poles), so long as the derivative does not vanish the inverse function $E(\Delta t)$ is also analytic and defines a good conformal map. Thus t_R must change monotonically along these contours when the derivative is non-zero; vanishing derivative is generally signalled by the intersection of multiple contours. The contours $t_I = \beta/2$ may be found by numerically integrating (8.17), for example by using `Mathematica`'s built-in `NIntegrate` command which is capable of performing contour integrals in the complex plane. Below, we use the structure of such contours to probe the associated complex extremal surfaces.

8.3.3 A Cautionary Tale: Geodesics in Schwarzschild-AdS

To illustrate the above techniques, we pause to discuss complex geodesics (the case $n = d$) in Schwarzschild-AdS$_{d+1}$. We have studied only cases with $d \leq 7$, though we expect the results for $d \geq 8$ to resemble those found for $d = 5, 6, 7$. We find interesting distinctions between the cases $d = 3$, $d = 4$, and $d \geq 5$. The case $d = 4$ was discussed in [34], though to our knowledge the results for $d \neq 4$ are

new. In particular, one might have hoped that since the $t = 0$ surface is common to both the Euclidean and Lorentzian sections, geodesics in this surface would always provide good saddle points for path integral with $t_b = 0$. But we will see that Schwarzschild-AdS$_{d+1}$ for $d \geq 5$ provides a counter-example[5].

For definiteness, we first consider $d = 4$ as in [34] so that we have

$$f(r) = g(r) = \frac{r^2}{\ell^2}\left(1 - \frac{r_h^4}{r^4}\right). \tag{8.21}$$

The function V_{eff} is as in (8.24a), and one finds [34]

$$\Delta t(E) = \frac{\beta}{2\pi}\left[\ln\left(\frac{\mathcal{E}^2/2 - \mathcal{E} + 1}{\sqrt{1 + \mathcal{E}^4/4}}\right) - i\,\ln\left(\frac{-\mathcal{E}^2/2 + i\mathcal{E} + 1}{\sqrt{1 + \mathcal{E}^4/4}}\right)\right], \tag{8.22}$$

where $\mathcal{E} \equiv E\ell/r_h$ and $\beta = \pi\ell^2/r_h$. Note that Δt has branch points at $\mathcal{E}^4 = -4$. Sketching the contours of $t_I = \beta/2$ in the center panel of figure 8.5, one finds a contour along the real E-axis corresponding to real geodesics, and two complex contours that start and end on the branch points[6]. Taking again (8.25) for the area regulator, one finds that the regulated length diverges as the contours approach the branch points.

The presence of complex contours is generic and independent of dimension. In figure 8.5 we sketch the contours on the principal sheet for the three cases $d = 3$, $d = 4$, and $d \geq 5$. Note that there are always two sets of contours: a contour along the real E-axis corresponding to real geodesics, and a set of complex contours

[5]This might be expected from the analysis of [34], which argued that perturbing the $d = 4$ case would produce this result. Changing $d = 4$ to $d = 5$ is such a perturbation, though so is changing $d = 4$ to $d = 3$ (which yields very different results as shown in figure 8.5).

[6]In fact, these contours spiral infinitely many times around the branch points, so they actually move off of the principal sheet of $\Delta t(E)$.

that end at the branch points.

For $d \geq 5$ the real geodesics have properties very similar to those found in [34] for $d = 4$. In particular, the renormalized action diverges to $-\infty$ at finite t_b. If these were the relevant saddle points for the path integral, this would imply a boundary to boundary two-point function $e^{-m\mathcal{L}_{\rm ren}}$ that diverges at finite t_b. This cannot happen in a good field theory, and even the small t_b behavior is suspicious. The fact that the arrow on the real contour runs to the left in the right panel of figure 8.5 means that t_b increases in that direction and thus by the Hamilton-Jacobi relation (8.19) that $t_b = 0$ would be a local *minimum* of the resulting two-point function. But on physical grounds it should be a local maximum; see e.g. [40, 228, 229, 332]. We conclude that there must be some obstacle to deforming the path integral contour of integration to make use of the real Lorentz-signature geodesics. Instead, it is the complex geodesics shown in the right-most panel of figure 8.5 that give physically reasonable behavior, and which in particular end at branch points for which $\mathcal{L}_{\rm ren}$ diverges to positive infinity as $t_b \to \pm\infty$. The story is similar to that in [34] for $d = 4$ except that the complex $t_I = \beta/2$ contours do not pass through $E = 0$, and the correct complex geodesics now differ in action from the real Lorentzian geodesic even at $t_b = 0$. Indeed, we find that the complex geodesics with $t_b = 0$ have smaller action[7].

[7] We stress, however, that the real $t_b = 0$ geodesic appears not to provide even a subdominant contribution. If the path integral contour could be deformed to use this geodesic in the saddle point approximation, then by continuity the same should be true of real geodesics with $t_b \neq 0$. But the action of the real geodesics clearly has smaller real part in the limit where it approaches $-\infty$, so in that limit the real geodesics would become the dominant saddles.

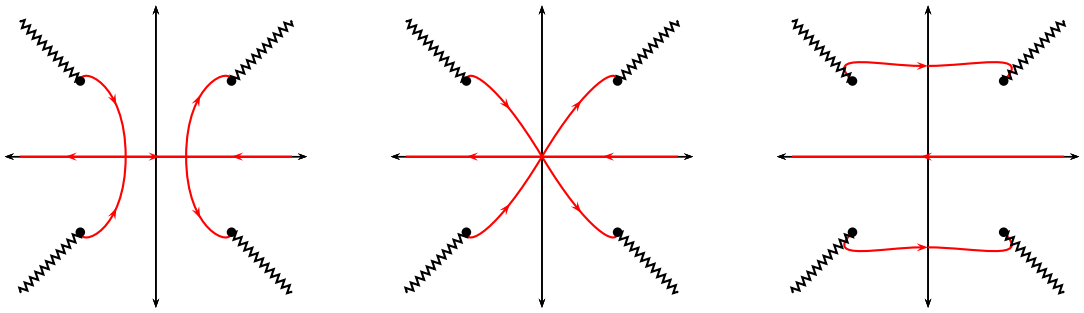

Figure 8.5: The structure of the $t_I = \beta/2$ contours for geodesics in Schwarzschild-AdS$_{d+1}$; arrows denote the direction of increasing t_b. From left to right, the figures show $d = 3$, $d = 4$, and $d \geq 5$. Note that there is always a contour along the real E-axis, which for $d \geq 5$ is disconnected from the two complex ones. The complex contours spiral into the branch points.

8.4 HRT Surfaces in Planar Black Holes

We now turn to codimension-2 extremal surfaces ($n = 2$), which are our primary interest. In particular, we apply the above methods to identify and study such surfaces in the maximally-extended planar BTZ, Schwarzschild-AdS$_{d+1}$, and Schwarzschild-Lifshitz spacetimes, each of which is dual to a thermofield double state on $\mathbb{R}^d$ in parallel with the discussion in [222]. In all cases, we consider the class of surfaces described in section 8.3 which satisfy boundary conditions appropriate to computing the entropy of a pair of half $(d-1)$-planes in opposite components of the thermofield double state. These are bulk surfaces that stretch from one of the two conformal boundaries to the other as shown in figure 8.1. We are mostly interested in the Schwarzschild-AdS$_{d+1}$ case (section 8.4.2), but study BTZ as an analytically-solvable warm-up in section 8.4.1. We also use Schwarzschild-Lifshitz to probe possible dependence on boundary conditions in section 8.4.3. Of course, since $d = 2$ for BTZ, geodesics and codimension-2

surfaces coincide in that context.

8.4.1 HRT in BTZ

A planar version of the BTZ spacetime [127] may be defined by taking $d = n = 2$ and

$$f(r) = g(r) = \frac{r^2}{\ell^2}\left(1 - \frac{r_h^2}{r^2}\right). \tag{8.23}$$

The metric (8.11) then describes a region of global AdS_3 and contains no singularities. One might thus argue that a better name for this region is AdS_3-Rindler, but we use the term planar BTZ to emphasize that it is the unique 3-dimensional analogue of planar Schwarzschild-AdS_{d+1} for $d \geq 3$.

For this case one finds

$$V_{\text{eff}}(R) = -f(R) - E^2, \tag{8.24a}$$

$$\Delta t = \beta\left[-\frac{1}{\pi}\operatorname{arctanh}\mathcal{E} + \frac{i}{2}\right], \tag{8.24b}$$

where again $\mathcal{E} \equiv E\ell/r_h$ and now $\beta = 2\pi\ell^2/r_h$. Taking the area regulator to be

$$A_{\text{ct}} = -2\ell \ln\left(\frac{1}{\epsilon}\right), \tag{8.25}$$

we obtain

$$A_{\text{ren}} = \ell \ln\left(\frac{4}{1-\mathcal{E}^2}\right). \tag{8.26}$$

The simple form of the expressions (8.24b) and (8.26) allows one to write A_{ren} as an explicit function of Δt. But in order to illustrate the general procedure,

we continue to treat $A_{\rm ren}$ and Δt as separate functions parametrized by $\mathcal{E}$. In order to find geodesics connecting the two boundaries of the BTZ black hole, we require $t_I = \beta/2 \pmod{\beta}$. This condition will clearly be satisfied for real $\mathcal{E} \in (-1, 1)$. These energies correspond to the usual real geodesics, so we will call this the principal $t_I = \beta/2$ contour. At the endpoints $\mathcal{E} \to \pm 1$ we find $t_b \to \pm\infty$. Moreover, $A_{\rm ren}$ is real and diverges to $+\infty$ at the endpoints. Indeed, on the principal $t_I = \beta/2$ contour $A_{\rm ren}$ has a global minimum at $t_b = 0$. It then increases monotonically as one moves away from this value. This agrees with the expected behavior of the entanglement entropy at large times. One can also check that certain results are quantitatively correct [229]. Since these surfaces are geodesics it is also natural to compare $e^{-m\mathcal{L}_{\rm ren}}$ with two-point functions, and one finds corresponding agreement [228].

However, we may also consider the full Riemann surfaces defined by Δt and $A_{\rm ren}$. These are obtained by a simple analytic continuation of the arctanh and logarithm, so that each of the resulting sheets can be labeled by an integer m:

$$\Delta t_m = \beta \left[-\frac{1}{\pi} \operatorname{arctanh} \mathcal{E} + \frac{(2m+1)i}{2} \right], \tag{8.27a}$$

$$A_{{\rm ren},m'} = \ell \ln \left(\frac{4}{1-\mathcal{E}^2} \right) + 2m'\pi i \ell. \tag{8.27b}$$

The union of all such sheets yields the full Riemann surface. There are now many contours for which $t_I = \beta/2 \pmod{\beta}$. These contours are labeled by m and all project to the interval $\mathcal{E} \in (-1, 1)$ along the real line in the complex E plane. We see that $t_b(E)$ is independent of m, while $A_{\rm ren}(E)$ (and thus $A_{\rm ren}(t_b)$) differs from its values on the principal ($m' = 0$) contour only by a t_b-independent purely-

imaginary constant. So all choices of m' would lead to the same entropies under the straw-man proposal of section 8.2.

As noted above, the spacetime we called planar BTZ is really just a subset of global AdS_3 (described in Rindler-like coordinates). Thus our surfaces immediately define complex extremal surfaces in AdS_3. If (t, r, θ) are the usual global coordinates, these surfaces intersect the boundary at $(t, \theta = 0)$ and $(t, \theta = \pi)$. For given m above, they are all related by global time translations; the nontrivial time-dependence of the area in (8.27b) is entirely due to the transformation between the global AdS_3 and BTZ conformal frames. One may also describe these surfaces in the Poincaré patch.

8.4.2 HRT in Schwarzschild-AdS

We now turn to the more interesting case of Schwarzschild-AdS_{d+1}. We again set $n = 2$ and take

$$f(r) = g(r) = \frac{r^2}{\ell^2}\left(1 - \frac{r_h^d}{r^d}\right). \tag{8.28}$$

We identify the critical E_c and the corresponding coincident branch points R_{branch} by requiring $V_{\text{eff}}(R_{\text{branch}}) = 0 = V'_{\text{eff}}(R_{\text{branch}})$, which gives

$$E_c = \pm e^{2\pi i m/d}\sqrt{\frac{d}{d-2}}\left(\frac{d-2}{2(d-1)}\right)^{(d-1)/d}\frac{r_h^{d-1}}{\ell} \tag{8.29}$$

for $m = 1, \ldots, d$. By numerically integrating (8.17), we find for all $3 \leq d \leq 7$ that the only E_c on the principal sheet of $\Delta t(E)$ are the two real ones, which form a pair of points on the real axis with opposite signs. We also find that the only $t_I = \beta/2$ contour on this sheet connects these E_c by running along the real

axis, as shown in figure 8.6(a) for $d = 4$. This contour corresponds to the real surfaces studied in [229]. As in that work, taking

$$A_{\rm ct} = -\frac{2\ell r_h^{d-2} V_{d-2}}{d-2} \frac{1}{\epsilon^{d-2}} \tag{8.30}$$

shows that $A_{\rm ren}$ increases as one moves along this contour away from $t_b = 0$ and diverges to positive infinity as the branch points are approached (where $t_b \to \pm\infty$). Though we have studied only $d \leq 7$, we expect similar behavior for larger values of d.

The secondary sheets turn out to contain much more structure. For simplicity, we will focus in detail on the case $d = 4$, though we will briefly comment on the cases $d = 3$ and $d = 6$ as well[8]. In Appendix B.6, we express the integrals (8.17) and (8.18) for $d = 4$ in terms of standard elliptic integrals, which we will use to obtain various approximations.

For $d = 4$, we see from (8.29) that there are only four critical energies E_c. These E_c lie on the real and imaginary axes, and are related to one another by multiples of the phase $e^{i\pi/2}$. In addition, there is another critical energy $E_c' = 0$ at which two roots of $V_{\rm eff}(R)$ coincide at $R = 0$. Though $R = 0$ is not a branch point of the integrands of (8.17) and (8.18) for $d = 4$, it remains a singularity; in this case a pole for $E \neq 0$. Thus the functions $\Delta t(E)$ and $A_{\rm ren}(E)$ will generally have branch points at $E = 0$ though they will not diverge there.

Let us now analytically continue off the principal sheet through one of the branch cuts shown in figure 8.6(a) onto what we now call sheet #2. As shown in

[8]For even d the analysis is simplified by working in terms of a new variable $w = (r_h/r)^2$; thus is $d = 6$ more tractable than $d = 5, 7$.

figure 8.6(b), we find a sheet with branch points at all four of the E_c as well as at $E_c' = 0$. The choice of direction is arbitrary for the branch cut ending at $E_c' = 0$; we find the choice shown in the figure convenient.

The new purely imaginary E_c lead to interesting behavior. This is perhaps best studied by using expression (B.53) to show that near $E_c = -i\sqrt{2}/3^{3/4}\, r_h^3/\ell$,

$$\Delta t = -\frac{i\beta}{2^{3/2} \cdot 3^{1/4}\, \pi} \ln\left(\mathcal{E} - \mathcal{E}_c\right) + C + \mathcal{O}\left(\mathcal{E} - \mathcal{E}_c\right), \tag{8.31}$$

where $\beta \equiv \pi \ell^2 / r_h$, $\mathcal{E} \equiv \ell E / r_h^3$, and C is a (complex) constant. In particular, we see that taking $|E - E_c|$ arbitrarily small makes t_I arbitrarily large and that and t_R increases uniformly as one travels around this E_c. Thus there are an infinite number of contours satisfying $t_I = \beta/2 \pmod{\beta}$ circling near these E_c, crossing to higher and higher sheets with each cycle; these contours thus form an infinite family of "helical contours". Some examples are shown in figure 8.6.

Returning to sheet #2, we also find the additional contours shown in figure 8.6(b). Two contours start at the branch point on the negative real axis and leave through branch cuts, while the contour in the first quadrant enters and exits through branch cuts. Tracking this contour through a branch cut onto a third sheet (#3), we find that it continues and crosses yet another branch cut. On this third sheet, we also find a variety of new contours. We will focus on the contour labeled B in figure 8.6, which starts at the branch point E_c' and ends at the branch point on the positive real axis. This contour resembles a deformed version of the original real contour, and we expect additonal such deformed contours to appear as one probes more of the Riemann surface.

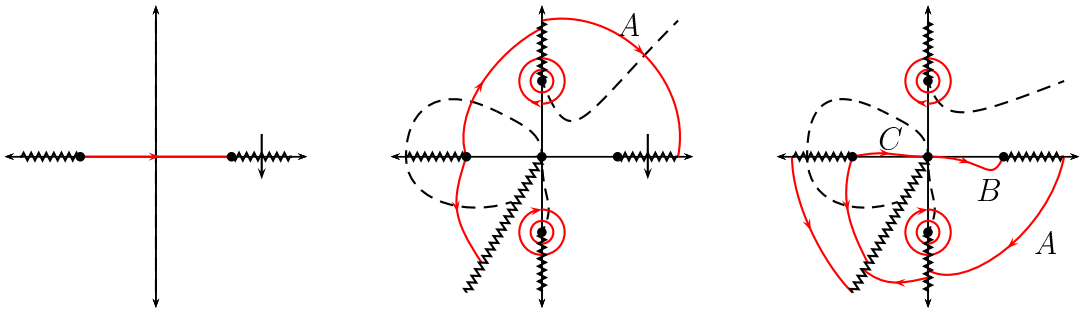

Figure 8.6: Schematic drawings where solid lines with arrows (red in color version) show contours with $t_I = \beta/2 \pmod{\beta}$ for codimension-2 extremal surfaces on various sheets of $\Delta t(E)$ for Schwarzschild-AdS$_5$. Arrows on the contours show directions of increasing t_b and dashed lines indicate loci where $t_b = 0$. Panel (a) shows the principal sheet. Here the only contour lies along the real E-axis, so on this sheet only the familiar real extremal surfaces satisfy our boundary conditions. Analytically continuing through the right-hand branch cut in the direction indicated by the vertical arrow takes us to sheet #2, shown in (b). Note the infinite family of helical contours that circle the branch points on the imaginary axis, as well as new contours and branch points. Analytically continuing through the right-hand branch cut takes us to sheet #3, shown in (c). The contour labeled A on sheet #2 continues through this cut onto sheet #3. Aside from the real contour on the principal sheet, only the two contours marked B and C on sheet #3 are physically acceptable near $t_b = 0$ under the straw-man proposal of section 8.2. All other segments of complex contours shown above cross $t_b = 0$ when Re $E \neq 0$. In addition, on helical contours Re $A_{\rm ren}$ remains unphysically bounded at large t_b.

For the $d = 3$ case, the only contour on the principal sheet is again the real one. In this case there are no contours on sheet #2 with $t_I = \beta/2 \pmod{\beta}$, and in particular no analogue of the helical contours in figure 8.6(b). However, we expect that new contours could be found on higher sheets. For $d = 6$, we once more find that the only contour on the principal sheet is the real one. On sheet #2 there are analogues of the helical contours for $d = 4$ that now spiral into the the complex E_c of (8.29). We also find an analogue of the contour in the upper

left quadrant of figure 8.6(b), again terminating at an E_c on the negative real axis. We have not examined higher sheets.

It is clearly of interest to investigate the areas of the extremal surfaces along our contours. For simplicity we limit this discussion to $d = 4$. Following the straw-man hypothesis of section 8.2, we focus on the real part Re $A_{\rm ren}(E)$. Were this real part to describe the CFT entropy on our pair of half-planes, the time-reflection symmetry of the dual CFT thermofield-double state would require a corresponding symmetry of the relevant Re $A_{\rm ren}$'s. In particular, if a single smooth contour is to provide the relevant surfaces near $t_b = 0$, then the derivative with respect to t_b must vanish there. The Hamilton-Jacobi relation (8.19) then requires that Re E vanish as well; i.e., t_b could vanish only on the imaginary E axis. Of the complex contours shown in figure 8.6, only the two marked B and C have vanishing Re E at $t_b = 0$.

Of course, the symmetry of the spacetime under time-reversal implies that any contour must have a time-reversed image somewhere on the Riemann surface – though this will generically lie on some yet-unexplored Riemann sheet. One can clearly combine the $t_b > 0$ part of one contour with the $t_b < 0$ part of its image to define time-symmetric Re $A_{\rm ren}$. But with non-vanishing Re E at $t_b = 0$, the time-derivative is discontinuous at $t_b = 0$; one would then need to rely on surprising sub-leading corrections in $1/G_N$ to match the physically expected vanishing of $dS_{\rm ren}/dt_b$ in the CFT. Furthermore, choosing to keep the surfaces with smallest Re $A_{\rm ren}$ would necessarily force Re $A_{\rm ren}$ to have a local maximum at $t_b = 0$; see figure 8.7.

In contrast, as discussed in e.g. [229] the thermofield-double nature of the CFT

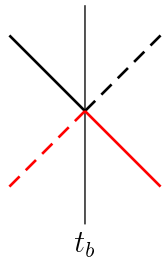

Figure 8.7: The small t_b part of a generic smooth real function (solid) with non-vanishing slope at $t_b = 0$ and its time-reversed image (dashed). Taking the minimum of the two (red parts in color version) defines a function with a local maximum at $t_b = 0$ where the derivative is discontinuous.

state strongly suggests that the entropy should be a mininum at $t_b = 0$ followed by monotonic increase with $|t_b|$ to diverge as $t_b \to \pm\infty$. From the Hamilton-Jacobi relation (8.19) and the arrows in figure 8.6, we see that this correctly describes the behavior of Re $A_{\rm ren}$ along contours B and C. But it fails at various points along other contours. In particular, for helical contours (8.31) and (8.19) imply that Re $A_{\rm ren}(E)$ oscillates with each cycle and remains bounded as $t_b \to \pm\infty$. The large t_b regimes of these contours are particularly problematic, as there Re $A_{\rm ren}(E)$ is clearly smaller than for any physically acceptable contour. Under suitable extensions of the straw man proposal, the comments in footnote 7 about the implications of such behavior for the geodesic approximation would thus apply here as well and indicate that even finite t_b pieces of these contours cannot be relevant to the dual CFT entropy.

For the above reasons we discuss only contours B and C in detail. These contours are defined only for $t_b > 0$ and $t_b < 0$ respectively, and since at $t_b = 0$ they reach the $E = 0$ branch point there is no simple notion of an extension through $t_b = 0$. But each must have a time-reversed copy as discussed above, and this copy will also reach the $E = 0$ branch point at $t_b = 0$. So it is natural to

glue B and C at $t_b = 0$ to their respective time-reversed copies. Since $E(t_b) = 0$, extending B and C in this way defines contours where $A_{\rm ren}$ is at least C^1, which continue to meet the above physical expectations.

We begin with B. As shown in figure 8.8 (left), to good accuracy the function Re $A_{\rm ren}(t_b)$ along B agrees with that along the real contour on the principal sheet. It would be interesting to understand whether the tiny discrepancy near $t_b/\beta \sim 0.1$ is a numerical artifact. While this is beyond the scope of the present work, it is straightforward to study the small- and late-time regimes perturbatively at leading order. In particular, the Hamilton-Jacobi relation (or alternatively, (8.20)) guarantees that the late-time growth of $A_{\rm ren}(t_b)$ will be identical along the two contours since both approach the same E_c. At small E we can expand the elliptic integrals (B.53) and (B.57) to find

$$t_b = \frac{\beta}{2\pi}\,\mathcal{E} + \mathcal{O}(\mathcal{E})^3, \tag{8.32}$$

$$\mathrm{Re}\, A_{\rm ren} = \frac{\ell r_h^2 V_2}{2}\,\mathcal{E}^2 + \mathcal{O}(\mathcal{E})^4, \tag{8.33}$$

so that

$$\mathrm{Re}\, A_{\rm ren} = \frac{2 r_h^4 V_2}{\ell^3}\, t_b^2 + \mathcal{O}(t_b)^4 \tag{8.34}$$

along both contours. Thus B agrees with the real contour to this order.

Contour C is even more interesting. The Hamilton-Jacobi relation again guarantees the late-time growth to be identical to those above, and (B.53) and (B.57) again yield (8.32), (8.4.2), and (8.34). But for $t_b \neq 0$ figure 8.8 clearly shows the associated Re $A_{\rm ren}(t_b)$ to be smaller than for real extremal surfaces. It is thus plausible that the associated entropy of the dual CFT is controlled by the complex

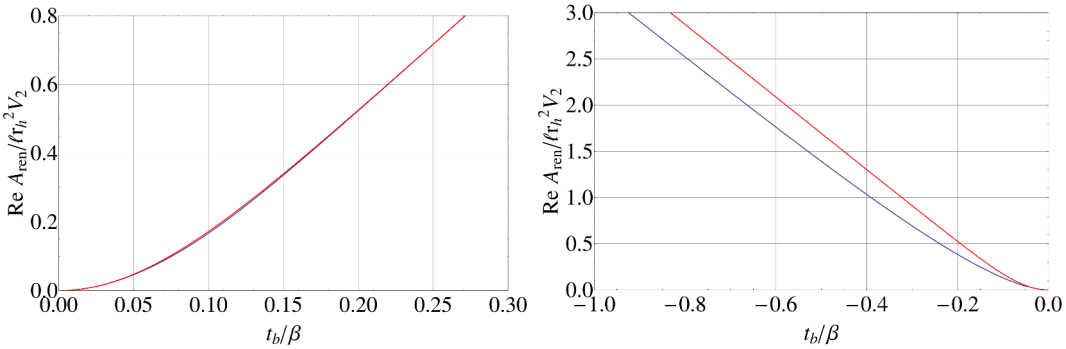

Figure 8.8: The plots show Re $A_{\rm ren}(t_b)$ for contour B (lower curve in left panel, blue in color version) and contour C (lower curve in right panel, blue in color version) in comparison with that on the real contour (upper curve in both panels, red in color version). Contour C clearly has smallest Re $A_{\rm ren}$. Near $t_b/\beta = 0.1$ contour B also appears to have Re $A_{\rm ren}$ slightly smaller than for the real contour, though a more careful analysis would be required to show that this is not an artifact of our numerics.

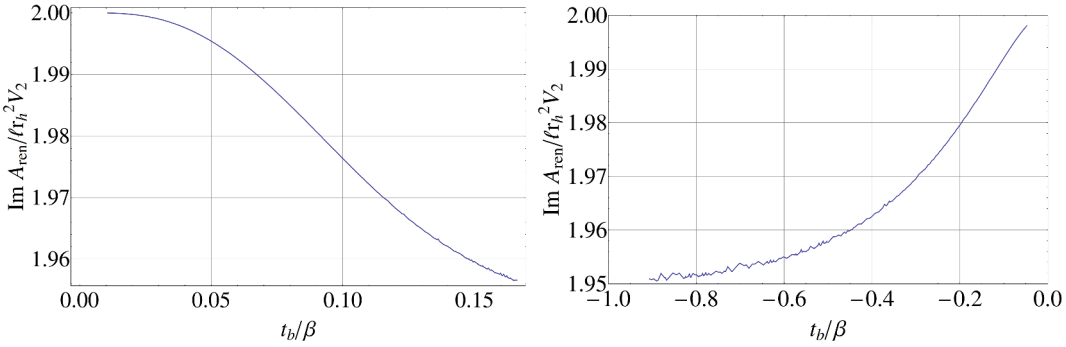

Figure 8.9: The imaginary parts Im $A_{\rm ren}(t_b)$ along contours B (left) and C (right). The noise at larger values of t_b is a numerical artifact, likely due the failure of Im $A_{\rm ren}(E)$ to be continuous at E_c. The function Im $A_{\rm ren}(E)$ does admit direction-dependent limits at E_c that make Im $A_{\rm ren}(t_b)$ continuous there for real t_b, but a small error in the location of our contour near E_c can translate into a large error in Im $A_{\rm ren}$. We have also excised portions near $t_b = 0$ which exhibit numerical noise.

surfaces contour C, and not by the original real extremal surfaces.

For completeness we also include plots of the imaginary part of $A_{\rm ren}$ along B and C in figure 8.9. Expansions analogous to those above show that Im $A_{\rm ren}$ =

$2+\mathcal{O}(t_b^4)$ near $t_b = 0$ for both contours, and since they end at real E_c the imaginary parts are again much smaller than $\mathrm{Re}\, A_{\mathrm{ren}}$ at large $|t_b|$. As a result, for large t_b we have $|A_{\mathrm{ren}}| \sim \mathrm{Re}\, A_{\mathrm{ren}}$ and using $|A_{\mathrm{ren}}| \sim \mathrm{Re}\, A_{\mathrm{ren}}$ gives the same result as taking the absolute value.

8.4.3 Lifshitz

In order to investigate possible dependence on boundary conditions, we now briefly consider the Schwarzschild-Lifhshitz black holes of [322]. The spacetimes are characterized by the spacetime dimension $d+1$, a choice of dynamical scaling exponent z, and a horizon radius r_h. Since $z = 1$ is just the Schwarzschild-AdS case already studied in section 8.4.2, we assume $z \neq 1$ below. In order to respect the null energy condition we consider only $z > 1$ [334]. We also restrict to rational z.

We will find that these spacetimes follow the same pattern seen above. The only $t_I = \beta/2$ contour on the principal sheet describes real extremal surfaces, but complex contours appear on secondary sheets. We refer to the contour on the principal sheet as the real contour below. For an infinite class of special cases, an analytic argument allows us to identify contours on certain secondary sheets that are simply related to the real contour: the associated extremal surfaces satisfy the same boundary conditions (i.e., they have same Δt) while A_{ren} differs from that on the real contour by a phase. For appropriate choices, such families satisfy our qualitative physical expectations (minimum at $t_b = 0$ and monotonic increase to infinity with $|t_b|$) for use as an HRT surface. However, in such cases $\mathrm{Re}\, A_{\mathrm{ren}}(t_b)$ is always smaller than for the corresponding real extremal surface.

We now begin the calculations. From [322] one sees that the desired spacetimes satisfy

$$f(r) = \left(\frac{r}{\ell}\right)^{2z}\left(1-\left(\frac{r_h}{r}\right)^{d+z-1}\right), \quad g(r) = \left(\frac{r}{\ell}\right)^{2}\left(1-\left(\frac{r_h}{r}\right)^{d+z-1}\right). \tag{8.35}$$

We therefore find

$$\Delta t = \frac{\alpha\beta}{4\pi}\int_\gamma \frac{\mathcal{E}}{\rho^{z-1}\left(\rho^\alpha-1\right)\sqrt{-\widetilde{V}_{\text{eff}}(\rho)}}\,d\rho, \tag{8.36a}$$

$$A = V_{d-2}\ell\, r_h^{d-2}\int_\gamma \frac{\rho^{d-2}}{\sqrt{-\widetilde{V}_{\text{eff}}(\rho)}}\,d\rho, \tag{8.36b}$$

where $\alpha \equiv d+z-1$, $\beta = 4\pi\ell^{z+1}/\alpha r_h^z$, $\rho \equiv R/r_h$, $\mathcal{E} \equiv \ell^z E/r_h^{\alpha-1}$, and

$$\widetilde{V}_{\text{eff}}(\rho) = -\frac{1}{\rho^{2(\alpha-2)}}\left(\rho^{2(\alpha-1)}-\rho^{\alpha-2}+\mathcal{E}^2\right). \tag{8.37}$$

We regulate the area with

$$A_{\text{ct}} = -\frac{2V_{d-2}\ell r_h^{d-2}}{(d-2)\epsilon^{d-2}}. \tag{8.38}$$

The critical energies are

$$\mathcal{E}_c = \pm(1)_n^{1/\alpha}\sqrt{\frac{\alpha}{\alpha-2}}\left(\frac{\alpha-2}{2(\alpha-1)}\right)^{(\alpha-1)/\alpha}, \tag{8.39}$$

where $(1)_n^{1/\alpha}$ is the n^{th} root of $x^\alpha = 1$. If α is irrational, there are an infinite number of such roots and the critical energies are dense in a circle in the complex E-plane. We therefore restrict our analysis to rational α or, equivalently, rational z.

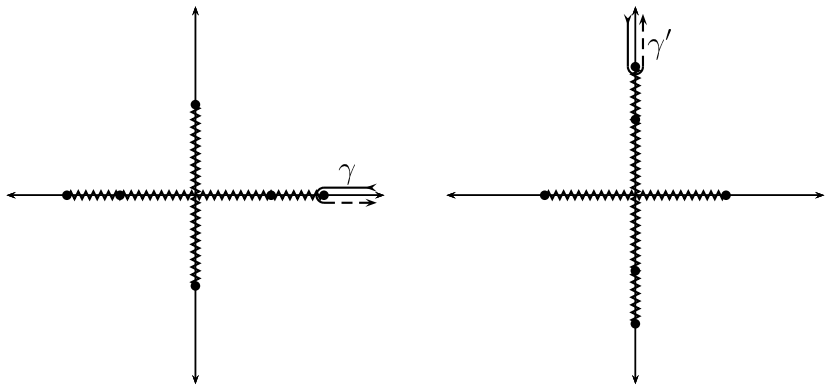

Figure 8.10: Sample integration contours γ, γ' in the complex ρ plane for Schwarzschild-Lifshitz with $d = 3$, $z = 2$. The left panels shows the contour γ which defines a real extremal surface for real E. There are 4 real and two imaginary branch points, with γ encircling only the largest real branch point. The right panel is obtained from the left by (8.40). The new contour contour γ' defines a complex extremal surface that lies on a secondary sheet of Δt and $A_{\rm ren}$.

We have examined the principal sheet numerically for $(d, z) = (3, 2)$, $(3, 3)$, $(4, 2)$, and $(4, 3)$. In each of these cases we find only the real contour. Turning now to secondary sheets, we will show that certain z exhibit a special symmetry relating the principal sheet to a class of secondary sheets. This may be seen by choosing an integer m and noting that the phase rotations

$$\rho \to e^{2\pi i m/\alpha}\rho, \quad \mathcal{E} \to e^{-2\pi i m/\alpha}\mathcal{E}, \tag{8.40}$$

act on the effective potential as $\widetilde{V}_{\rm eff} \to e^{4\pi i m/\alpha}\widetilde{V}_{\rm eff}$. Thus if ρ^* is a root of $\widetilde{V}_{\rm eff}$ at energy $\mathcal{E}$, then $e^{2\pi i m/\alpha}\rho^*$ is also a root of $\widetilde{V}_{\rm eff}$ at energy $e^{-2\pi i m/\alpha}\mathcal{E}$.

Consider then any contour γ in the complex ρ plane that defines a real extremal surface. The contour γ then runs along the real ρ axis, coming in from $\rho = \infty$ before turning around the largest real branch point $\rho_{\rm turn}$ and returning to $\rho = \infty$.

The expressions for Δt and $A_{\rm ren}$ can be written as

$$\Delta t = \frac{\alpha\beta}{2\pi}\int_{\rho_{\rm turn}}^{\infty} \frac{\mathcal{E}}{\rho^{z-1}\left(\rho^{\alpha}-1\right)\sqrt{-\widetilde{V}_{\rm eff}(\rho)}}\,d\rho, \tag{8.41a}$$

$$A_{\rm ren} = 2V_{d-2}\ell\, r_h^{d-2}\lim_{\epsilon\to 0}\left(\int_{\rho_{\rm turn}}^{1/\epsilon}\frac{\rho^{d-2}}{\sqrt{-\widetilde{V}_{\rm eff}(\rho)}}\,d\rho - \frac{1}{(d-2)\epsilon^{d-2}}\right), \tag{8.41b}$$

$$= 2V_{d-2}\ell\, r_h^{d-2}\left[\int_{\rho_{\rm turn}}^{\infty}\left(\frac{\rho^{d-2}}{\sqrt{-\widetilde{V}_{\rm eff}(\rho)}} - \rho^{d-3}\right)d\rho - \frac{\rho_{\rm turn}^{d-2}}{(d-2)}\right], \tag{8.41c}$$

where we have conveniently reabsorbed the counterterm $A_{\rm ct}$ into the integral expression for $A_{\rm ren}$ in order to extend the integration out to $\rho=\infty$.

Acting with (8.40) takes the (real) turning point $\rho_{\rm turn}$ to $\rho'_{\rm turn} = e^{2\pi i m/\alpha}\rho_{\rm turn}$. Consequently, the original contour γ is taken to a new contour γ' that runs from infinity to $\rho'_{\rm turn}$ along a line of constant $\arg(\rho) = 2\pi i m/\alpha$. In particular, the contour γ' does not approach $\rho=\infty$ along the positive real axis, as we require of our allowed contours. But because both of the integrands in (8.41) die off sufficiently fast at infinity, γ' can be deformed to approach $\rho=\infty$ along the positive real axis without changing Δt and $A_{\rm ren}$. As a result, the new contour γ' defines a secondary sheet of the Riemann surfaces for Δt and $A_{\rm ren}$ which is related to the principal sheet by the transformations (8.40). Examples of γ' for the special case $d=3$, $z=2$ are shown in figure 8.10.

If (8.40) preserve the condition $t_I = \beta/2 \pmod\beta$, then they will map the real $t_I = \beta/2 \pmod\beta$ contour to another on the secondary sheet defined by γ'; examples of these contours for the special case $d=4$, $z=3$ are shown in figure 8.11.

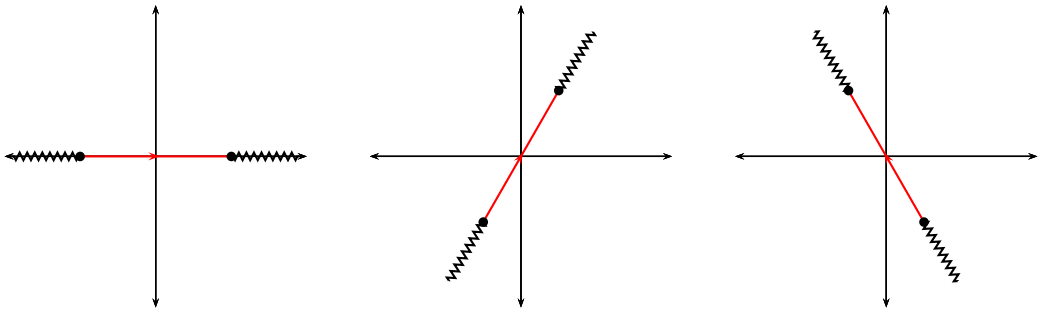

Figure 8.11: Three sheets of the Riemann surface for Δt in $d = 4$, $z = 3$ Lifshitz. The left panel shows the principal sheet (generated by the contour γ in figure 8.10) and the contour $t_I = \beta/2$ corresponding to real extremal surfaces. The middle and right panels show the secondary sheets that are obtained from the principal sheet by acting with the transformations (8.40); each of these contains an image of the real contour.

Setting $\rho = e^{\pi i m/\alpha}\rho'$, $\mathcal{E} = e^{-\pi i m/\alpha}\mathcal{E}'$, we find

$$\Delta t_\gamma(\mathcal{E}) = e^{\pi i(d-1)m/\alpha}\frac{\alpha\beta}{2\pi}\int_{\rho'_{\rm turn}}^{\infty}\frac{\mathcal{E}'}{(\rho')^{z-1}\left((\rho')^\alpha-1\right)\sqrt{-\widetilde{V}_{\rm eff}(\rho')}}\,d\rho' \tag{8.42a}$$

$$= e^{\pi i m(d-1)/\alpha}\Delta t_{\gamma'}(\mathcal{E}'). \tag{8.42b}$$

So $t_I = \beta/2 \pmod\beta$ is preserved when $(d-1)m/\alpha$ is an integer.

Examining the area, we find

$$A_{{\rm ren},\gamma}(\mathcal{E}) = e^{\pi i m(d-2)/\alpha}2V_{d-2}\ell\, r_h^{d-2}\left[\int_{\rho'_{\rm turn}}^{\infty}\left(\frac{(\rho')^{d-2}}{\sqrt{-\widetilde{V}_{\rm eff}(\rho')}}-(\rho')^{d-3}\right)d\rho' - \frac{(\rho'_{\rm turn})^{d-2}}{(d-2)}\right], \tag{8.43a}$$

$$= e^{\pi i m(d-1)/\alpha}e^{-\pi i m/\alpha}A_{{\rm ren},\gamma'}(\mathcal{E}'). \tag{8.43b}$$

Thus if $e^{\pi i m(d-1)/\alpha} = \pm 1$ the behavior of $A_{\rm ren}$ on the secondary sheet will be related to its behavior on the principal branch by a rotation $e^{\pi i m/\alpha}$ in the complex $\mathcal{E}$-plane,

and by a change of phase $e^{-\pi i m/\alpha}$. So since $A_{\rm ren}$ is real along the real contour, it acquires an imaginary part along these secondary contours. And since $\cos\theta \leq 1$, the real part Re $A_{\rm ren}$ is clearly smaller for the surfaces defined by γ' than for the original real extremal surfaces. However, if $\mathrm{Re}\, e^{\pi i m(d-1)/\alpha} e^{-\pi i m/\alpha} < 0$, the real part of A along these secondary contours becomes large and *negative* at large times, in contrast with the physical behavior expected of the entanglement entropy. Thus the straw-man hypothesis of section 8.2 is inconsistent with the use of extremal surfaces on certain secondary contours though it is consistent with others.

We can be a bit more explicit as to when this occurs. Let us write $\alpha = p/q$ with $(p,q) = 1$, where (p,q) denotes the greatest common divisor of two integers p, q. We must satisfy the constraint $m(d-1)q/p \in \mathbb{Z}$ for the above symmetry to preserve $t_I = \beta/2 \pmod{\beta}$. But the map becomes trivial when mq/p is an even integer. If p is a divisor of m, one can show that non-trivial solutions occur for any odd q and that Re $A_{\rm ren}$ behaves as desired for even d, while for odd d it has a global maximum at $t = 0$ and is unbounded below at large $|t_b|$. When p is not a divisor of m, non-trivial solutions occur when $(p, d-1) > 1$ and one can choose m so that $A_{\rm ren}$ behaves as desired for $(p, d-1) > 2$; for $(p, d-1) = 2$ one can choose m so that $A_{\rm ren}$ is purely imaginary. We thus find many cases where the dual CFT entropy may plausibly be controlled by complex surfaces instead of real extremal surfaces.

8.5 Discussion

The above work considered the possible significance of complex extremal surfaces for the Ryu-Takayanagi and Hubeny-Rangamani-Takayanagi (HRT) holographic entanglement conjectures. As emphasized by the study of complex geodesics in $d > 4$ Schwarzschild-AdS$_{d+1}$ (section 8.3.3), this issue could in principle be as important for the static setting as for the time-dependent context. We began by discussing how the formula (8.1) might be modified if complex surfaces are indeed relevant. We reached no firm conclusions, but noted that a straw-man model replacing the renormalized area $A_{\rm ren}$ by its real part is not without motivation.

Given the confusion surrounding how holographic entanglement conjectures might be extended to include codimension-2 surfaces with complex areas, one might have hoped that no such surfaces would meet the real conformal boundary in the manner that these conjectures require. But we showed that they do. Such complex surfaces exist in complexified spacetimes defined by analytic continuation of simple real solutions. For planar BTZ, or equivalently global AdS$_3$, they are somewhat trivial copies of the real surfaces in which $A_{\rm ren}$ differs from the real case only by a quantized purely imaginary offset. One might expect similar behavior for global AdS$_{d+1}$ for $d \geq 3$. But for Schwarzschild-AdS$_5$ we find many distinct families of surfaces with a rich structure; we suspect that this is the case in other dimensions as well. We also found interesting families for Schwarzschild-Lifshitz.

Given the existence of complex extremal surfaces, one might next have hoped that they would exhibit clearly pathological behavior so as to be excluded on physical grounds. But in all cases studied in depth we identified families of complex extremal surfaces consistent under the above straw-man proposal with basic

physical expectations for the time-dependence of the entropy. Furthermore, these complex surfaces have Re $A_{\rm ren}$ smaller than (or sometimes equal to) that of corresponding real extremal surfaces. It is thus plausible at this level that the dual CFT entropy is indeed determined by such complex extremal surfaces and not by the real ones.

Nevertheless, one may contrast the situation here with that concerning the geodesic approximation for 2-point functions in Schwarzschild-AdS$_{d+1}$ for $d \geq 3$. As shown in [34] for $d = 4$ (and more generally in section 8.3.3 for other $3 \leq d \leq 7$), use of the real geodesics in such cases would imply unphysical behavior for the two-point function. It is then clear that, if a geodesic approximation is to be maintained at all, the geodesics involved must be complex. On the other hand, at least in cases studied here the real codimension-2 extremal surfaces lead to no obvious unphysical behavior. Furthermore, one knows that entropies based on the real surfaces will satisfy strong subadditivity [255, 303] – a property we are unable to test using the complex surfaces found above since we considered only the entropy of a single boundary region at each time; see also related comments in footnote 2. On a similar note, recall that for Schwarzschild-AdS and Schwarzschild-Lifshitz we also find families where the behavior of Re $A_{\rm ren}$ does not match expectations for entropy in the dual CFT; this may indicate that the relevant path integral cannot generally be deformed to take advantage of such complex surfaces. So while the relevance of complex extremal surfaces is plausible, it is by no means assured.

Our work studied planar black hole spacetimes and looked for surfaces as shown in figure 8.1, running from the left boundary to the right and intersecting

each boundary on a plane (also of codimension-2 with respect to the boundary) at some given time t_b in analogy with those studied in [229][9]. For extremal surfaces of this form the time difference Δt between the left and right ends defines an infinite-sheeted Riemann surface when expressed in terms of the conserved energy E. The same is true of the renormalized area $A_{\rm ren}$. By definition, extremal surfaces in the real Lorentzian spacetime live on the principal sheet of this Riemann surface. In all cases studied, numerical investigation indicated that there are no further extremal surfaces on this sheet; all complex extremal surfaces mentioned above lie on secondary sheets. In addition to the spacetimes addressed in the main text, we have also checked that the hyperbolic AdS black hole[10] [190–192] and planar Reissner-Nordström-AdS$_5$ are free of complex extremal surfaces on their primary sheets. In the latter case, the particular cases checked were $T/\gamma\mu \approx 0.56$ and 0.16, where T and μ are the temperature and chemical potential of the black hole, and $\gamma \equiv \sqrt{3/2}\, g\ell/\kappa$ is a dimensionless ratio of the Maxwell and gravitational couplings as in [76].

The above discussion brings to the fore the issue of which extremal surfaces should actually contribute to (8.1) and the associated entanglement conjectures. Thinking of our surfaces as representing saddle points of a path integral suggests that the general answer may be difficult to determine. We refer the reader to the classic discussion of [34] in the perhaps-related context of geodesics in Schwarzschild-AdS$_5$. But in typical cases one might expect saddles on the the

[9] If complex surfaces in the bulk do determine the dual CFT entropy, this would affect the detailed results of [229]. But the most plausible families of complex surfaces found above behave sufficiently similar to the real surfaces that this change would not alter their main conclusions.

[10] In the hyperbolic black hole, the planar line element dx_{d-1}^2 in (8.11) is replaced by a metric of constant negative curvature, but otherwise the procedure is identical.

principal sheet of our Riemann surface to be more accessible than those on secondary sheets. We therefore again remind the reader that, for codimension-2, the principal sheets studied here admit only real extremal surfaces. This may suggest that only such real surfaces are relevant to the entropies we consider.

For the geodesic approximation to the two-point function one can give a stronger argument [76] to exclude secondary sheets. The point is that, in that context, branch cuts are a clear artifact of taking what from the dual CFT perspective is the large-dimension limit of the operators involved. For any finite operator dimension, the actual two-point function resolves the branch cut into a discrete series of poles associated with bulk quasi-normal modes [228, 332]. It follows that the geodesic approximation to two-point functions must break down whenever it involves geodesics on secondary sheets.

This last argument might perhaps be adapted to the present context using the fact that the Renyi entropies S_n are given by correlators of twist operators [220]. In particular, one might argue that such correlators must again involve only poles (say, in the energy plane) and that branch cuts must be absent. But it is unclear what this would imply for the analytic structure of the von Neumann entropy whose construction requires the analytic continuation to general n and taking the limit (8.5) as $n \to 1$.

It would be interesting to determine whether the principal sheet remains free of complex extremal surfaces when one studies the entropy of other regions on the boundaries of these spacetimes (i.e., not just for the pair of half $(d-1)$-planes considered here). One might hope that the appearance of complex contours on the principal sheet is in fact forbidden by the null energy condition (NEC) so

that this argument could be extended to truly general settings. However, in a forthcoming work [77] we describe spacetimes satisfying the NEC where complex extreme surfaces do indeed arise on the principal sheet.

Our discussion of complex codimension-2 surfaces was in part motivated by analogy with the case of larger codimension $n > 2$. But comparison of figures 8.5 and 8.6 shows that, at least in practice, the $n = 2$ setting behaves very differently. This is perhaps most clear on the principal sheet. While this may at first come as a surprise, one sees from e.g. [303] that codimension-2 surfaces are subject to much tighter constraints than for $n > 2$. This occurs because $n = 2$ surfaces define a pair of orthogonal null congruences (see e.g. [90, 195]) and the extremality condition requires both to have vanishing expansions. The result is that properties of such extremal surfaces are dictated much more directly by the null energy condition than for $n > 2$. Some of the associated implications for real $n = 2$ extremal surfaces were discussed in [303, 336]. It could be very useful to understand any ramifications for complex $n = 2$ surfaces as well.

We conclude that there remain many open questions, and that the possible relevance of complex extremal surfaces to CFT entanglement remains mysterious. But the existence of physically-plausible contours for Schwarzschild-AdS and analogous results for Schwarzschild-Lifshitz makes it critical to understand this issue in detail. One would in particular like to find an independent calculation of the corresponding CFT entropy allowing quantitative comparison with figure 8.8. At least for this case such an analysis would definitively answer whether the CFT entropy is determined by real extremal surfaces, or instead by the complex surfaces found in this work.

Chapter 9

Constraints on Hole-ography

9.1 Introduction

The deep connection between entanglement and geometry has the potential to provide profound insights into the inner workings of a nonperturbative theory of quantum gravity. This connection has been made especially manifest in the AdS/CFT duality, which states that certain conformal field theories (CFT) without gravitational dynamics are dual to string theory on asymptotically (locally) anti-de Sitter (AdS) backgrounds [19, 20]. In this correspondence, the CFT lives on a representative of the conformal class of boundary metrics of the AdS space; we colloquially say that the CFT "lives on the boundary of AdS". In the limit where the string theory is well approximated by classical gravity, the dual CFT is strongly coupled (large λ) with a large number of colors (large N). Numerous observables in the CFT are dual in this limit to geometric objects in the (now classical) AdS space.

In this context, an issue of considerable interest is that of bulk reconstruction. That is, given some CFT data, how much of the bulk data can be reconstructed, and how is this reconstruction performed? Understanding how this reconstruction works in the limit where the AdS bulk is classical may offer insights into how to reconstruct the bulk gravitational theory perturbatively in $1/N$, and even potentially in a nonperturbative regime (*i.e.* finite N).

Because many CFT quantities are dual to geometric bulk objects in the large N limit, a fundamental bulk quantity to reconstruct is the geometry itself. A promising approach has focused on reconstructing the bulk using extremal codimension-two surfaces anchored to the boundary: according to the Ryu-Takayanagi (RT) and Hubeny-Rangamani-Takayanagi (HRT) conjectures [69, 70], such extremal surfaces are dual to the entanglement entropy of regions of the CFT. In fact, the general arguments of [306] suggest that the density matrix of a subregion of the CFT should be sufficient to reconstruct a portion of the bulk geometry: the so-called "entanglement wedge"[1]. Indeed, [337, 338] explicitly offer such a construction for the spatial slices of AdS_3 by using the hole-ographic approach [339, 340] of reconstructing bulk surfaces from boundary-anchored extremal surfaces (see also [341–343] for related constructions).

The appeal of this approach stems from its simplicity: it relates (*a priori*) any bulk surface to computable CFT quantities. Specifically, the area of an arbitrary bulk surface γ is dual to the so-called differential entropy of a family of boundary intervals. The full range of validity of hole-ography remains unclear, though substantial headway in this direction was made in [342]. In this paper, we continue

[1]Although [306] made use of the bulk equations of motion, which are unknown when the bulk theory is no longer classical.

this exploration: specifically, in any 2+1-dimensional spacetime (or in any higher dimensional spacetime with a sufficient degree of symmetry), we will state and prove general theorems that constrain how well surfaces in the bulk spacetime can be reconstructed from extremal surfaces anchored to the AdS boundary, and we interpret these constraints in terms of bulk surfaces that play a special role: the so-called holographic screens introduced in [344]. We emphasize that while our strongest theorems only apply to systems that are "effectively" 2+1-dimensional, they are otherwise covariant. In particular, while our results are constrained in more than two spatial dimensions to these symmetric setups, in 2+1-dimensional bulks, we impose no restrictions except a generic condition ad a condition on the Ricci tensor (the null curvature condition), which amounts to positivity of the stress tensor for a bulk obeying the Einstein Equations.

To give these statements some context, recall that the Hubeny-Rangamani-Takayangi (HRT) conjecture [70] states that in the large-N limit, the entanglement entropy of a region $\mathcal{R}$ in the CFT can be constructed as follows. Consider all bulk codimension-two extremal surfaces Ξ homologous to the region $\mathcal{R}$ on the AdS boundary[2]. Then the entanglement entropy of $\mathcal{R}$ is

$$S(\mathcal{R}) = \min_{\Xi \sim \mathcal{R}} \frac{\text{Area}(\Xi)}{4G_N\hbar}, \tag{9.1}$$

where G_N is the bulk Newton's constant and $\sim$ means "homologous to". Both the left- and right-hand sides of the above equation are naïvely divergent, and are understood to be regulated appropriately. A generalization of this prescription

[2]Note that the homology constraint (see *e.g.* [255]) implies that Ξ must be anchored to the AdS boundary on $\partial\mathcal{R}$.

exists for perturbatively quantum bulks [312, 313].

The key insight of hole-ography is that the HRT formula (9.1) can be utilized to compute the area of arbitrary bulk surfaces. In the pure AdS_3 context, consider an arbitrary curve γ lying on a static time slice, as shown in Figure 9.1. At each point p on γ, there is a unique geodesic tangent to γ at p anchored at the ends of some boundary interval $I_\theta = (\theta - \alpha(\theta), \theta + \alpha(\theta))$. By the RT (and HRT) conjectures, the length of this geodesic computes the entanglement entropy $S(\alpha)$ of the interval I_θ. The result of [340] is that the length of γ can be computed from the boundary entanglement entropies as

$$\frac{\text{length}(\gamma)}{4G_N\hbar} = \frac{1}{2}\int_0^{2\pi} d\theta \left.\frac{dS(\alpha)}{d\alpha}\right|_{\alpha=\alpha(\theta)}. \tag{9.2}$$

This construction has been generalized to non-static contexts and higher dimensions (admitting a sufficient degree of symmetry) in [341, 342].

In order to use the hole-ographic approach for bulk reconstruction, [337] noted that points in the bulk spacetime can be identified by effectively shrinking γ to arbitrarily small size around a point p, so that the geodesics tangent to it all intersect at p; see 9.2(a). The resulting region function $\alpha_p(\theta)$ is an extremum of a boundary action constructed only from $S(\alpha)$, and thus yields a construction of bulk points from boundary data. Similarly, to compute the geodesic distance between two points p and q, the curve γ is shrunk to a thin convex[3] curve that encircles p and q, as shown in 9.2(b). The region function for such a curve can be constructed from those that define the points p and q, $\alpha_p(\theta)$ and $\alpha_q(\theta)$, and is

[3]In this context, a closed curve γ is convex if any geodesic connecting two points on γ lies entirely inside γ.

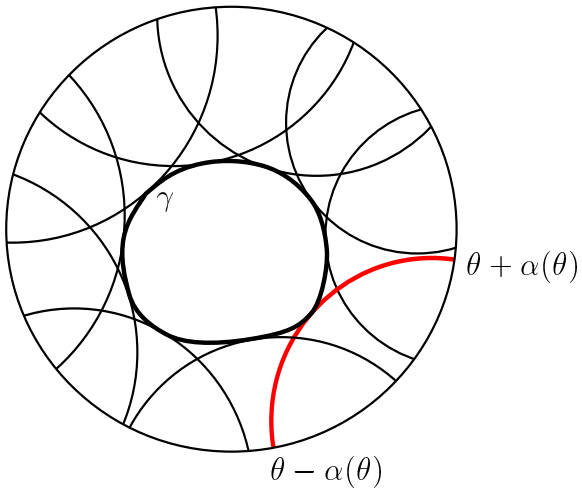

Figure 9.1: An arbitrary closed curve γ on a static time slice of global AdS_3. The set of all geodesics tangent to γ define a family of regions on the boundary parametrized by a (possibly multi-valued) function $\alpha(\theta)$. The differential entropy of these regions gives the length of γ.

therefore also constructed purely from boundary data.

This approach is clean and elegant, and has close ties to integral geometry [338] and to tensor networks and MERA [345, 346]. It is therefore quite natural to ask how much it can be generalized, and how much of the bulk it can reconstruct.

One obvious impediment to this reconstruction is the presence of extremal surface barriers (or relatedly, bulk regions that cannot be reached by any HRT surfaces – "entanglement shadows" [347]). These are surfaces that split the bulk spacetime in two such that no codimension-two extremal surface (such as those used in the hole-ographic reconstruction of bulk surfaces) can cross them [336]. Then anything behind the barrier cannot be probed via boundary entanglement entropy. Interestingly, it was found in [256] that event horizons of static black holes cannot be probed by extremal surfaces anchored to one asymptotic boundary, as long as we consider only families of extremal surfaces that can be deformed

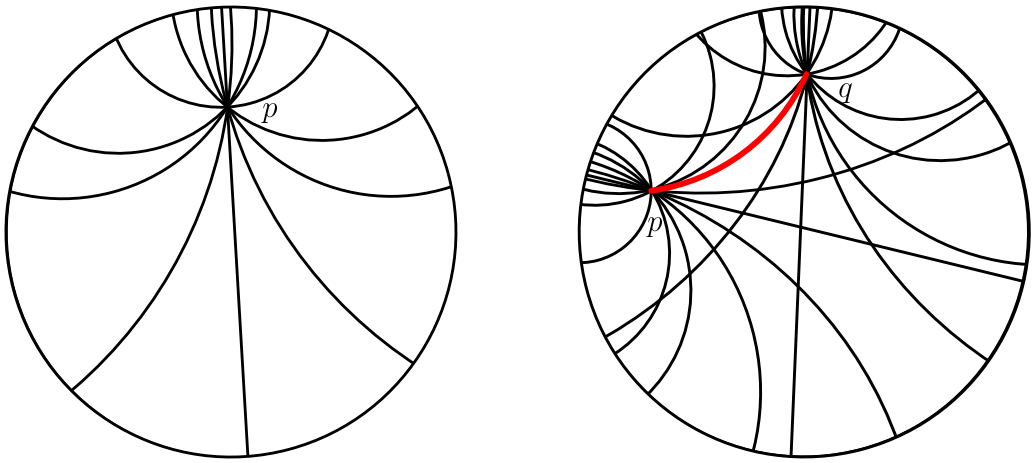

(a) (b)

Figure 9.2: (a): reconstruction of bulk points via hole-ography. The curve γ is shrunk to be arbitrarily small and centered at p, so that p is identified by the common intersection of all the geodesics generated by $\alpha(\theta)$. (b): reconstruction of geodesic distances via hole-ography. The curve γ is shrunk to be an arbitrarily thin convex curve (thick red line) encircling two points p and q. The geodesic distance between p and q is then given by the differential entropy of the resulting boundary intervals.

back to that boundary. This barrier phenomenon was characterized for arbitrary spacetimes in [336]; in particular, such barriers do not include the event horizons of dynamical black holes. Thus generically, an event horizon is a barrier only in stationary setting.

This is not so surprising: in a dynamical context, an event horizon is a global object, but from a local perspective, its only special property is the fact that its area is non-decreasing. Since extremal surfaces are not sensitive to the global structure of the spacetime, there is no reason to expect the event horizon to generically play a special role in constraining their behavior. A much more promising alternative is that of *local* analogues of the event horizon: it is common to consider dynamical horizons [348] or trapping horizons [349], but we will instead consider

more general objects called holographic screens. These will be defined precisely in Section 9.2 below, but they should roughly be thought of as objects that can be foliated by marginally trapped (or anti-trapped) surfaces. Holographic screens can be constructed from an arbitrary foliation of a spacetime[4]; we will illustrate such a construction in Section 9.2 (see Figure 9.5).

Our motivation for focusing on these screens is fourfold. First, there is a sense in which they are analogues of event horizons that are local in time and defined independenly of an asymptotic boundary. Second, it was shown in [350, 351] that under certain (fairly generic) assumptions, they obey an area law much like that obeyed by event horizons. These first two points make it quite appealing to think of holographic screens as local versions of event horizons. Third, they have a holographic interpretation by the Bousso bound [352]: their area places an upper bound on the total entropy lying on one of the null surfaces orthogonal to them. The fourth and last point is a technical one: holographic screens can be constructed from a null foliation of spacetime, and null congruences are very useful in constraining the behavior of codimension-two extremal surfaces. Thus it should be relatively straightforward to derive constraints on such surfaces in the presence of holographic screens.

Interestingly, our results show that while there are indeed such constraints, they are subtle. Holographic screens need not be barriers: codimension-two extremal surfaces may enter them. However, we prove that when they do, the extremal surfaces must move through achronal[5] subregions of a holographic screen

[4]This means a given spacetime may generally admit infinitely many holographic screens: one per null foliation.

[5]In the special case where the extremal surfaces are anchored on a connected boundary region, we can drop the achronality requirement.

monotonically. That is, they may never become tangent to one of the leaves of the null foliation that was used to construct the screen. This puts a limit on hole-ographic approaches to reconstructing surfaces and geometry in the interior of a holographic screen, for any (sufficiently smooth) codimension-two spacelike surface γ lying inside the screen must be tangent to at least two of the null foliation surfaces. This implies that there are points on γ that cannot be tangent to any boundary-anchored codimension-two extremal surface.

Thus hole-ography (or at least, those hole-ographic approaches of which we are aware) cannot be used to reconstruct arbitrary surfaces contained in the interiors of holographic screens. At best, it can reconstruct only portions of them, yielding some "coarse-grained" form of reconstruction.

The outline of this paper is as follows. We develop and state our main theorems in Section 9.2. In the interest of readability, we will defer the lengthier of our proofs to Appendix B.7. In Section 9.3 we present some examples illustrating the ideas used in our construction, and highlighting previous instances in the literature where hints of our results first appeared. Finally, in Section 9.4 we discuss the potential relevance of our results to bulk reconstruction, as well as some possible generalizations, and conclude.

9.2 Constraints on the Behavior of Extremal Surfaces

In this section, we will prove the theorems discussed in Section 9.1. To make for a more streamlined presentation, our theorems will be stated for (2+1)-

dimensional spacetimes. However, we emphasize here that in higher dimensions, all of our results remain true as stated with the same proofs as long as the spacetime has a sufficient degree of symmetry; this will be made precise in Section 9.2.4, where we will also make some comments about what can be shown for less symmetric setups in higher dimensions. For this reason, we will continue to discuss "codimension-two surfaces" rather than "curves", so the generalization to higher dimensions is natural.

Furthermore, while we will narrate the development of the theorems for purposes of pedagogy and clarity, we will leave a discussion and interpretation of their consequences to Sections 9.3 and 9.4. Terms in quotation marks are intended to provide intuition, and will be made precise in due course.

Preliminaries We will always consider a spacetime M that obeys the null curvature condition: $R_{ab}k^a k^b \geq 0$ everywhere for any null vector k^a. Unless otherwise specified, we take all null vectors to be future-directed. The term *extremal surface* will always be used to refer to spacelike, C^2, codimension-two extremal surfaces. A null hypersurface and the null geodesic congruence that generates it will be given the same name (*e.g.* N). The expansion of a congruence N will be denoted $\theta(N)$, while the expansion of a spacetime-filling family of congruences $\{N_s\}$ will be denoted $\theta(\{N_s\})$. All unspecified conventions and definitions are as in [90].

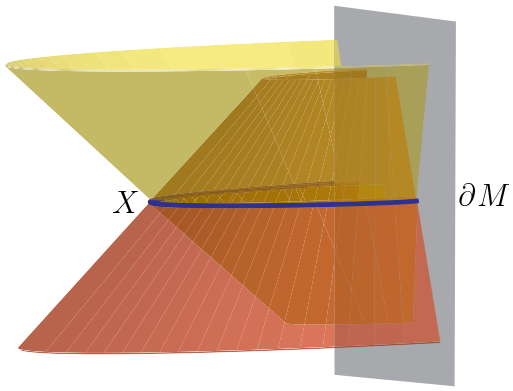

Figure 9.3: The two null congruences of an extremal surface X of codimension two anchored to a timelike boundary ∂M.

9.2.1 General Behavior of Null Hypersurfaces and Extremal Surfaces

First, we introduce a null foliation $\{N_s\}$ of M into null hypersurfaces N_s which we shall call *leaves*[6]. The leaves are permitted to have cusps, but only at intersections of their generators; a generator leaves a leaf if and only if it encounters an intersection with another generator of the same congruence. Next, recall that any extremal surface X has two null normals, each of which generates a null congruence (as shown in Figure 9.3), and the extremality condition is simply the requirement that the expansions of the null geodesic congruences tangent to these normals vanish on X. The sign of the expansion on leaves of the null foliation $\{N_s\}$ yields a constraint on the behavior of extremal surfaces in the neighborhood of a null hypersurface:

Lemma 1. Let N be a null hypersurface in M and let X be a codimension-two

[6]Recall that the leaves $\{N_s\}$ form a foliation of M if for every $p \in M$, p lies on precisely one leaf N_s. Also, note that this foliation is arbitrary; any spacetime admits infinitely many such foliations.

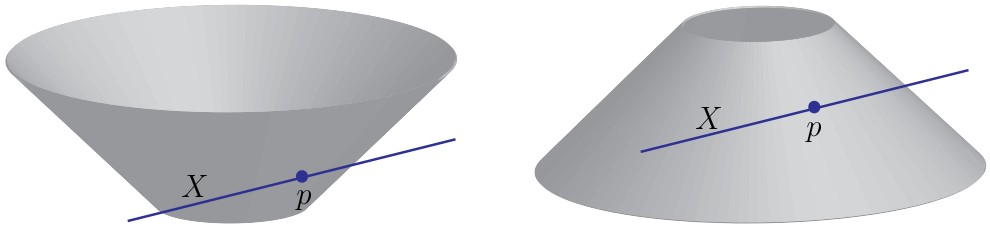

Figure 9.4: An illustration for Lemma 1. In Minkowski space, an extremal surface X is just a plane (drawn here as a straight line). If X is tangent to an expanding light cone, it lies nowhere to the cone's future, and the cone has positive expansion. If X is tangent to a shrinking light cone, it lies nowhere to the cone's past, and thus the shrinking light cone has negative expansion.

spacelike extremal surface which is tangent to N at a point p; let $\mathcal{O}_p$ be an open neighborhood of p. Then:

- If $X \cap \mathcal{O}_p$ is nowhere to the past of N, then $\theta(N)|_p \leq 0$;
- If $X \cap \mathcal{O}_p$ is nowhere to the future of N, then $\theta(N)|_p \geq 0$.

Proof. As explained in [351], this follows directly from Theorem 4 of [303] or Theorem 1 of [294]. □

As a useful illustration of this lemma, consider extremal surfaces and null hypersurfaces N in flat space, as shown in Figure 9.4.

The converse of Lemma 1 is in general not true[7]. However, in the restricted case of a (2+1)-dimensional spacetime, we can indeed prove its converse (see Section 9.2.4 for a generalization to higher dimensions):

Lemma 2. Let N be a null hypersurface in a (2+1)-dimensional spacetime M and let X be a codimension-two spacelike extremal surface which is tangent to N at a point p. Then there exists a small neighborhood $\mathcal{O}_p$ of p such that

[7]We thank Aron Wall for pointing this out to us.

- If $\theta(N)\big|_p > 0$, then $X \cap \mathcal{O}_p$ is nowhere to the future of N;
- If $\theta(N)\big|_p < 0$, then $X \cap \mathcal{O}_p$ is nowhere to the past of N.

Proof. Consider the first case, where the expansion of N is positive. At p, the null generator of N agrees with a null normal of X; call this vector k^a. Also let v^a be the unit vector tangent to X at p (which will also be tangent to N, since X is), and let ℓ^a be the other null normal to X at p normalized so $k \cdot \ell = -1$. Then the metric at p can be decomposed as

$$g_{ab}|_p = -2k_{(a}\ell_{b)} + v_a v_b. \tag{9.3}$$

The expansion of N at p can then be written as

$$0 < \theta(N)\big|_p = \nabla_a k^a\big|_p = \ {}^N K_{ab} v^a v^b\big|_p , \tag{9.4}$$

where ${}^N K_{ab}$ is the extrinsic curvature of N[8]. Next, consider a spacelike surface Σ containing X. Recall that ${}^N K_{ab} v^a v^b|_p$ is a measure of how much $N \cap \Sigma$ bends away from its tangent plane (*i.e.* the plane spanned by k^a and v^a) with motion away from p in the v^a direction. By extremality, the trace of the extrinsic curvature of X vanishes: ${}^X K^c{}_{ab} v^a v^b|_p = 0$, so X must curve away from its tangent plane less than $N \cap \Sigma$ on a small open neighborhood of p. But this immediately implies

[8]Recall that the extrinsic curvature of a null codimension-one hypersurface with normal k^a is given (up to scaling) by

$$K_{ab} = \frac{1}{2} \pounds_k g_{ab}. \tag{9.5}$$

For a codimension-two surface with null normals k^a and ℓ^a, the extrinsic curvature gets an extra index:

$$K^a{}_{bc} = \frac{1}{2} \left(\ell^a \pounds_k g_{bc} + k^a \pounds_\ell g_{bc} \right). \tag{9.6}$$

that $X \cap \mathcal{O}_p$ cannot lie in the future of N. The proof proceeds identically for the second case. □

Lemmata 1 and 2 give conditions on how extremal surfaces are allowed to be tangent to null hypersurfaces. Crucially, these conditions do not impose any restrictions on the global structure of the null hypersurface – it may be a hypersurface of non-constant expansion on a global scale, but as long as it has definite expansion on an open set that contains p, both lemmata are applicable. This means that in any region of the spacetime with constant sign of $\theta(\{N_s\})$ – a scalar function on the spacetime – an extremal surface can "turn around" at most once with respect to the foliation $\{N_s\}$ (this notion will be made precise below). In order to understand the general behavior of extremal surfaces, it is therefore useful to divide the spacetime into those regions where $\theta(\{N_s\})$ is positive, and those where $\theta(\{N_s\})$ is negative. Note that we will assume a generic condition, to be made precise in Definition 2, which will not allow $\theta(\{N_s\})$ to vanish on an open set.

9.2.2 Holographic Screens

The division between regions of positive and negative $\theta(\{N_s\})$ is provided quite naturally by so-called *preferred* holographic screens, first defined in [344]. The idea is the following: given a spacetime foliation $\{N_s\}$, move along each leaf N_s until its expansion changes sign. By the focusing theorems (see *e.g.* [90]), this sign change can happen at most once (since the expansion of N_s is non-increasing). Thus to each leaf N_s, this procedure associates at most one codimension-two surface σ_s

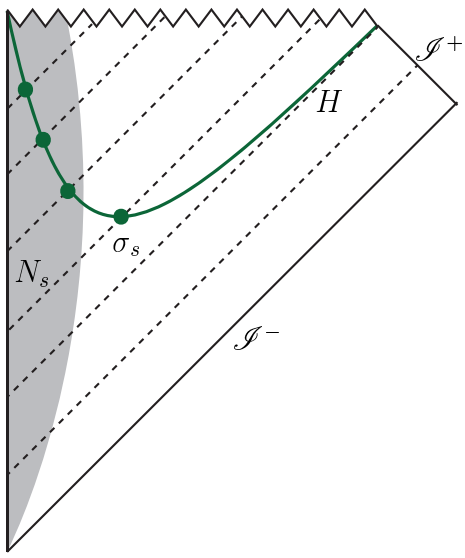

Figure 9.5: Constructing a preferred holographic screen from a null foliation of a spacetime. The dashed diagonal lines are the leaves of the foliation; the dot on each leaf marks the leaflets σ_s where the expansion of the leaf changes sign. The union of all the leaflets is a preferred holographic screen.

called a *leaflet*[9]; see Figure 9.5 for an example of this construction. The union of all such leaflets is a preferred holographic screen, and provides the division we were looking for. The term holographic screen is derived from the Bousso bound, which postulates that the leaflet is holographic: its area provides a bound on the entropy of N_s [344, 352].

Note that each leaflet σ_s has two null normal directions, each tangent to an associated null congruence. By construction, one of these congruences has zero expansion. We can use the sign of the expansion of the other congruence to label the "type" of holographic screen: in analogy with event and dynamical horizons, a screen will be called "future" ("past") if it is foliated by marginally (anti-)trapped surfaces [350, 351]. This notion is made precise by the following definition:

[9]Note that this terminology goes against convention: typically the σ_s are referred to as "leaves". Here we reserve the term "leaves" for the null hypersurfaces of the spacetime foliation.

Definition 1. *Preferred future holographic screen.* A preferred future holographic screen H associated to a null spacetime foliation $\{N_s\}$ is a smooth hypersurface such that for each leaf N_s, the intersection $H \cap N_s$ is either empty or a codimension-two achronal surface σ_s such that the two orthogonal null directions k_s^a and ℓ_s^a to σ_s obey:

$$\theta_{k_s} = 0, \tag{9.7}$$

$$\theta_{\ell_s} < 0, \tag{9.8}$$

where θ_{k_s,ℓ_s} are the expansions of the null geodesic congruences fired off of σ_s in the k_s^a and ℓ_s^a directions. The intersections σ_s are called *leaflets* of H, and the null normals k_s^a and ℓ_s^a to all the leaflets define null vector fields k^a and ℓ^a everywhere on H.

Past holographic screens are defined analogously, except that $\theta_\ell > 0$, *i.e.* the leaflets are marginally *anti*-trapped. All discussions and proofs for past holographic screens proceed identically to future holographic screens via time reversal (all future constructs become past-directed), so for the rest of this section we will refer only to future holographic screens.

The above definition of holographic screens is too weak to guarantee that they be sufficiently well-behaved for our purposes. But by further imposing some mild conditions, it is possible to ensure that the screens obey certain "nice" properties. For this reason, we include the requisite technical assumptions in the definition of a regular holographic screen:

Definition 2. *Regular future holographic screen.* A preferred future holographic

screen is *regular* if the following are true [351]:

- The null expansion of leaflets in the k^a direction immediately decreases away from H: $k_s^a \nabla_a \theta_{k_s}|_{\sigma_s} < 0$;
- The boundary of all spacelike subsets of H within H is the boundary of all timelike subsets of H within H (*i.e.* the only null portions of H are junctions between spacelike and timelike pieces);
- Every inextendible portion of H with indefinite sign is either timelike or contains a complete leaflet; and
- Every leaflet is compact and splits a Cauchy surface containing it into two disjoint subsets.

The first two assumptions can be viewed as types of generic conditions[10]. We will not have occasion to explicitly use the last two assumptions in this section, but they are required for certain properties of regular holographic screens to hold. Also note that we will occasionally use the word "screen" to refer to a regular holographic screen when it will cause no ambiguity.

The screens on which we will focus must divide the spacetime into two disjoint regions so that we can sensibly refer to their "interior" and "exterior". Such screens will be referred to as *splitting screens*; the holographic screen shown in Figure 9.5 is an example. Moreover, if the screen is regular, we can unambiguously define its interior and exterior: [350, 351] showed that a regular holographic screen is never tangent to k^a, implying that k^a must always point to the same

[10]However, these do not reduce to the usual generic condition used in the singularity theorems, see *e.g.* [90].

side of the screen. Thus we will call the interior $\mathrm{Int}(H)$ of a splitting future holographic screen H the region towards which the null vector field k^a points[11]. The exterior $\mathrm{Ext}(H)$ will be the complement in M.

We are now equipped to make statements about the behavior of extremal surfaces in general spacetimes in the presence of holographic screens. We need one more definition to make precise what we mean by an extremal surface "turning around":

Definition 3. *Turning and inflection points.* We say that an extremal surface X has a *pivot point* at a point p if it is tangent to a leaf N_s at p. X is said to have a *turning point* at p if in a small neighborhood of p, X lies nowhere to the past or nowhere to the future of N_s. Otherwise, X is said to have an *inflection point* at p. Moreover, if an extremal surface X has a turning point in some region $R \subset M$, then we say X *turns around* in R.

See Figure 9.6 for an illustration. Note that turning points and the notion of turning around are dependent on the foliation $\{N_s\}$. Also note that by definition, if N is any null splitting hypersurface, then any surface Q which has a turning point on N is (in some small neighborhood) in its past or future. In the former case, we will say Q is *tangent to N from the past*, and in the latter we will say Q is *tangent to N from the future*.

[11]This definition may seem backwards, since we typically think of the "interior" of a surface as the direction in which the expansion of its null normals is more negative. However, note that since marginally trapped surfaces must always lie behind (or possibly on) the future event horizon of the spacetime M, $\mathrm{Int}(H)$ can never have any intersection with the asymptotic region of M. It is in this sense that this definition agrees with intuition.

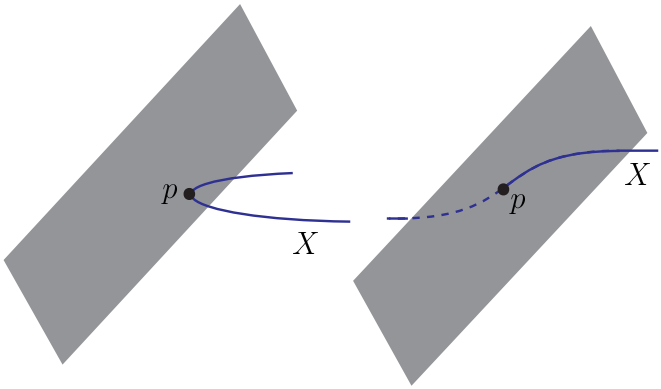

Figure 9.6: An extremal surface tangent to a foliation leaf has a pivot point which can either be a turning point (left) or an inflection point (right).

9.2.3 Theorems

We can now state our first theorem, which is simply a precise rephrasing of the heuristic discussion above:

Theorem 1. Let R be a region such that $\theta(\{N_s\})$ has a definite sign everywhere in R, and let X be an extremal surface. Then any connected portion of X in R can turn around at most once, and has no inflection points if M is (2+1)-dimensional. In particular, if H is a regular splitting future holographic screen, any connected portion of X in $\mathrm{Int}(H)$ can turn around at most once.

For a detailed proof, see Appendix B.7. For a pictoral proof, see Figure 9.7: if a connected portion of X in R has more than one turning point, at least one such turning point must violate Lemmata 1 and 2.

Theorem 1 and the lemmata make local statements: they make no use of the global structure of the spacetime M. We now focus on the asymptotically locally AdS case[12], where M has a timelike boundary ∂M to which the extremal surfaces

[12]See [353] for the definition of asymptotically locally AdS spacetimes.

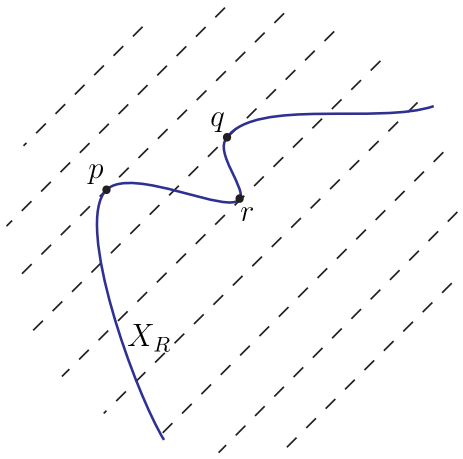

Figure 9.7: X_R is any connected portion of X in R. It cannot have multiple turning points without violating Lemma 1 or 2.

are anchored. We will find that Theorem 1 can be strengthened significantly: under the appropriate conditions, boundary-anchored extremal surfaces can *never* turn around in the interior of a holographic screen.

Before we state and prove the theorem, we will need to develop some notions that take into account the global structure of the extremal surface and of the holographic screen. First, we will restrict our analysis to so-called *H-deformable* extremal surfaces [336]: these are surfaces that can be deformed to lie entirely in the exterior of a screen H while still being kept extremal (for a precise definition, see Appendix B.7). Next, we will need to impose some constraints on the global causal structure of a splitting screen:

Definition 4. *Future achronal screen.* Let H be a regular splitting future holographic screen. Consider the null congruences $\{L_s\}$ generated from each leaflet by firing null geodesics in the ℓ^a direction[13]. If the $\{L_s\}$ foliate Int(H) (as they

[13]As with the N_s, we will take the generators of L_s to leave L_s at local and non-local intersections.

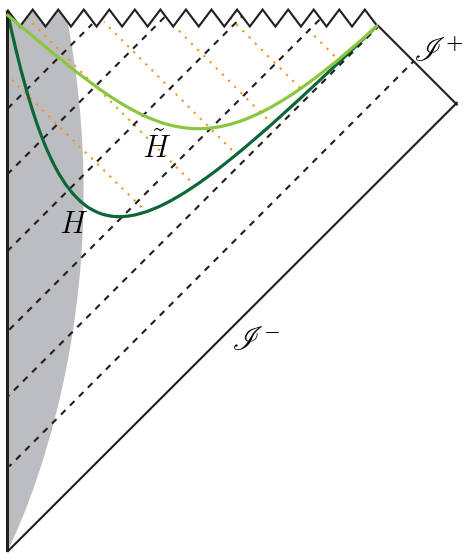

Figure 9.8: A future achronal screen in a collapsing star geometry. The future holographic screen H (solid dark green) has indefinite signature. The future achronal screen $\tilde{H}$ (solid light green) is generated by intersections of the N_s (dashed black) with the L_S (dotted orange) in the interior of H.

generally will, since they form the boundaries of the futures of the leaflets σ_s), then we may construct a modified holographic screen as follows: consider deforming each leaflet σ_s of H into $\mathrm{Int}(H)$ along the associated N_s leaf, to define a new leaflet $\tilde{\sigma}_s$ which is a complete intersection with a member of the $\{L_s\}$ foliation. For each leaf N_s, choose the new leaflet $\tilde{\sigma}_s$ such that the hypersurface $\tilde{H} = \bigcup_s \tilde{\sigma}_s$ is smooth. If $\tilde{H}$ is achronal, we will call it a *future achronal screen* of H. Note that by construction, the leaflets $\tilde{\sigma}_s$ of an achronal screen are trapped surfaces. See Figure 9.8 for an illustration.

We now state our main theorem:

Theorem 2. Let H be a regular splitting future holographic screen in a (2+1)-dimensional asymptotically locally AdS spacetime M. Then no H-deformable boundary-anchored extremal surface can have a pivot point in the interior of any

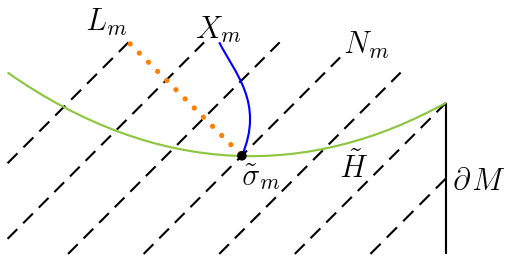

Figure 9.9: If an extremal surface X_m (solid blue) is tangent to a leaflet $\tilde{\sigma}_m$ of an achronal screen $\tilde{H}$, it must lie entirely in the future of $\tilde{\sigma}_m$ (bounded by L_m, dotted orange, and N_m, dashed black) and therefore cannot be boundary-anchored. Note that we have suppressed a spatial direction in this figure, which is why X_m appears timelike and ends at $\tilde{\sigma}_m$. It is actually spacelike everywhere and tangent to $\tilde{\sigma}_m$ in the suppressed direction.

future achronal screen of H. Moreover, if H is itself achronal, no such extremal surfaces can have a pivot point in $\mathrm{Int}(H)$.

For a detailed proof, see Appendix B.7. For a sketch of part of the proof, consider an extremal surface X_1 with a turning point in the interior of an achronal screen $\tilde{H}$. We should be able to deform X_1 to an extremal surface X_m with a turning point on $\tilde{H}$ itself. If this turning point is tangent to a leaflet $\tilde{\sigma}_m$, then Lemma 2 implies that X_m must lie to the future of the null congruences normal to $\tilde{\sigma}_m$, and therefore in the future of $\tilde{\sigma}_m$; see Figure 9.9. But since $\tilde{H}$ is achronal, this implies that X_m must live entirely in the interior of $\tilde{H}$ and therefore cannot be boundary-anchored. The case when X_m is not tangent to a leaflet is more complicated, but similar in spirit.

One of the remarkable properties of regular future holographic screens found in [350] was that they obey an area law even when they have indefinite signature. It may therefore seem somewhat odd that our theorem applies only to achronal screens, and not to those of indefinite signature. It well may be the case that it also holds for such screens (we have checked some easy cases and have not found

any violations of it), but the approach used in the proof above cannot also be used for non-achronal screens. To see a potential pitfall, consider Figure 9.10. As an H-deformable surface X_0 in the exterior of H is deformed into a surface X_3 in its interior, the midway surface X_m may develop an inflection point on H, allowing X_3 to develop a turning point in $\mathrm{Int}(H)$. This is not ruled out by the proof above: X_m can in this case exit the future of σ_m through the timelike portion of the screen.

Theorem 2 may still be true for regular future holographic screens of indefinite signature, but it is not clear to us how a proof of such a statement would proceed. However, some progress can be made in higher dimensions, as we will now discuss.

9.2.4 Higher Dimensions

Theorem 2 relies heavily on Lemma 2, which is only valid in (2+1)-dimensional spacetimes. If we were to attempt a naïve extension of it to higher dimensions, we would encounter a problem: equation (9.4) and the extremality condition would become

$$0 < {}^{N}K_{ab}\left(v^a v^b + \sum_i \xi^a_{(i)}\xi^b_{(i)}\right)\Bigg|_p, \tag{9.9a}$$

$$0 = {}^{X}K^{a}{}_{bc}\left(v^b v^c + \sum_i \xi^b_{(i)}\xi^c_{(i)}\right)\Bigg|_p, \tag{9.9b}$$

where the sum runs over an additional $(d-2)$ orthonormal spatial vectors $\xi^a_{(i)}$ that are orthogonal to v^a and tangent to X and N at p (so that the term in parentheses is the induced metric on X and N at p). These summed expressions do not allow

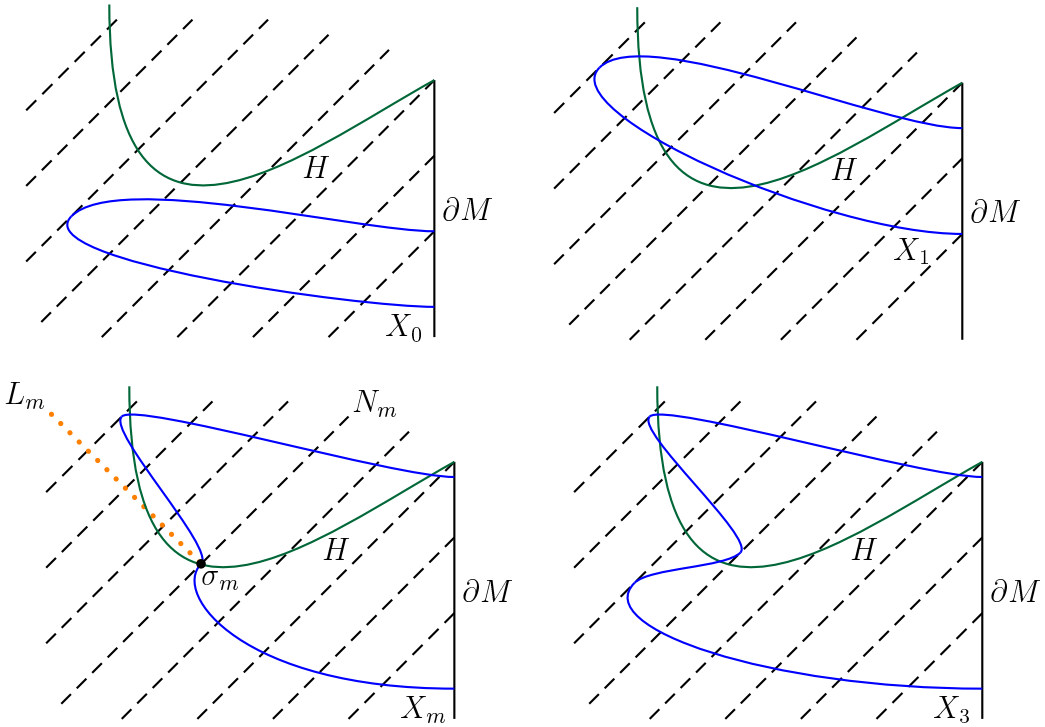

Figure 9.10: Here we show a potential H-deformable family that would allow an H-deformable extremal surface X_3 (solid blue) to have a turning point in the interior of a regular future holographic screen of indefinite signature. From top left to bottom right: a surface X_0 starts out entirely outside the screen H (solid green). It is then deformed into a surface X_1 which passes through $\mathrm{Int}(H)$, though with no turning points. It then deforms into a surface X_m with an inflection point on some leaflet σ_m, but which is able to leave the future of σ_m (the wedge bounded by L_m, dotted orange, and N_m, dashed black) because it can exit the interior of H. Finally, X_3 is obtained by deforming the inflection point into two turning points, one inside and the other outside H. Note that the X_α are everywhere spacelike; the apparent mixed signature here is only due to the suppression of the extra spatial dimension in these diagrams.

us to separately compare the bending of X and N in different directions, so the proof does not go through as it did before.

Tt is clear from the above considerations, however, that a version of Lemma 2 will remain true in higher dimensions if we require that all of the $\xi^a_{(i)}$ have trivial contraction with the extrinsic curvatures of X and N. In such a case, only

the v^a terms in equations (9.9) remain, and the proof of the lemma proceeds as in the (2+1)-dimensional case. We therefore define:

Definition 5. *Reducibility to (2+1) dimensions.* Let S be a surface of codimension at most two in a spacetime M. We will say that S is *reducible to (2+1) dimensions* (or *reducible* for short) if there exist $(d-2)$ vector fields $\xi^a_{(i)}$, $i = 1, \ldots, d-2$ in M that are everywhere spacelike[14] such that S is tangent to the $\xi^a_{(i)}$ everywhere, and for each i

$$ {}^S K^a{}_{bc}\, \xi^b_{(i)}\, \xi^c_{(i)} = 0, \tag{9.10} $$

where ${}^S K^a{}_{bc}$ is the extrinsic curvature of S.

For an arbitrary surface S, the reducibility condition is simply a constraint on its allowed behavior. However, we will specifically require that our H-deformable extremal surfaces X be reducible: this will in general only be the case when the spacetime exhibits a sufficient amount of symmetry. In particular, note that in spacetimes obeying the generalized planar symmetry of [342] (see their Section 3.3 for a full definition), extremal surfaces that have this symmetry are reducible[15]. For example, spacetimes with planar or spherical symmetry provide a simple setup admitting reducible extremal surfaces. Most significantly, Lemma 2 still holds for reducible extremal surfaces and foliations, and therefore so does Theorem 2.

We have therefore shown that *the results outlined in the previous section will still hold in any (d+1)-dimensional spacetime if the foliations $\{N_s\}$ and all extremal surfaces X under consideration are reducible to (2+1) dimensions.*

As mentioned at the end of the previous section, we can actually do more in

[14] The $\xi^a_{(i)}$ may be singular on a set of measure zero.

[15] To our knowledge, this is the most general system in which hole-ography has been shown to hold.

higher dimensions: in more than two spatial dimension, it is possible for extremal surfaces to "cap off" (for example, where the size of spheres spanned by the $\xi^a_{(i)}$ shrinks to zero). We therefore have the following theorem, which holds for holographic screens of arbitrary signature (*i.e.* it does not require the screen to be achronal):

Theorem 3. Let M be an asymptotically locally AdS spacetime, and let H be a regular splitting future holographic screen constructed from a reducible foliation $\{N_s\}$. Assume further that that there exists a foliation of the future of H with L_s congruences. Let X be a boundary-anchored, codimension-two spacelike extremal surface such that:

1. X is reducible to (2+1) dimensions;
2. ∂X is connected; and
3. X intersects $\mathrm{Ext}(H)$ only on regions with $\theta(\{N_s\}) > 0$.

Assume further that there exists an H-deformation of X that obeys the above conditions as well. Then X cannot have a pivot point in $\mathrm{Int}(H)$.

Note that condition (2) rules out geodesics, so this theorem is only nontrivial in greater than three bulk spacetime dimensions. Also, condition (3) requires that there exist at least one family of deformations from X to the boundary that does not intersect another holographic screen somewhere else in the spacetime.

For a detailed proof of this theorem, see Appendix B.7. For a rough picture, consider Figure 9.10: the only way for an extremal surface X_3 to have a turning point inside the screen is to be anchored on the boundary at two places, *i.e.* to have

disconnected ∂X. If it did not, it would have an illegal turning point somewhere, either with respect to the foliation $\{N_s\}$ or $\{L_s\}$.

It is worth making some remarks about potential pitfalls in higher dimensional spacetimes in which the extremal surfaces and/or null foliations are not reducible. As noted above, Lemma 2 will then generally be false, and cannot be used to rule out inflection points. We suspect it should be possible to use only Lemma 1 to prove weaker versions of Theorems 2 and 3 that do not exclude inflection points. However, such constraints have minimal relevance for hole-ography.

We should also note that while our proofs do not hold in non-reducible settings, we can think of no counterexamples to the statements of the theorems. It is possible that they hold in more generality, but if that is the case, they would need to be proven using a different approach than that taken here.

9.3 Examples

Here we present examples illustrating the application and consequences of the theorems discussed in the previous section.

9.3.1 dS and AdS Spacetimes

As an example of Theorem 1 (which states that connected components of extremal surfaces can have no more than one turning point in a region of constant $\theta(\{N_s\})$), consider the simplest cases of pure de Sitter (dS) or anti-de Sitter (AdS) spacetimes, whose conformal diagrams are shown in Figure 9.11 (the analysis of Minkowski space is similar to that of AdS, so we will not discuss it sepa-

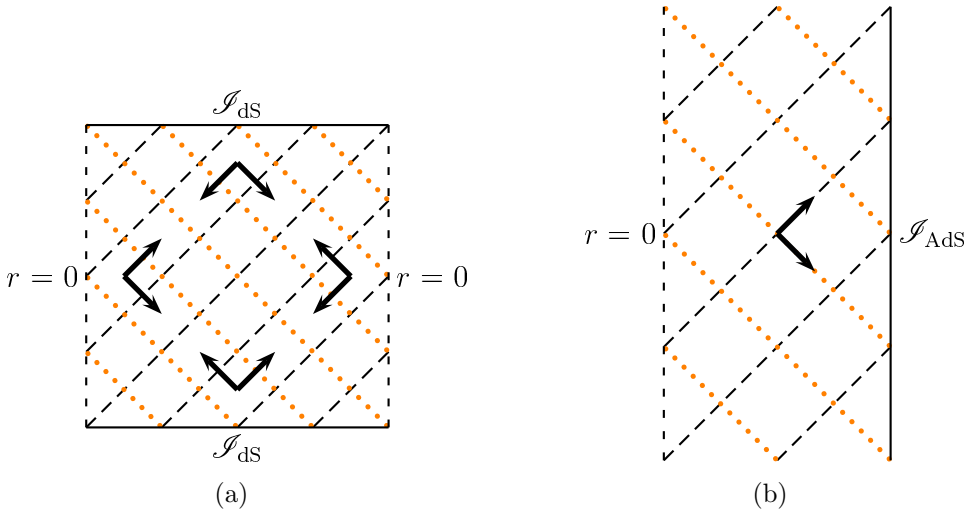

Figure 9.11: The conformal diagrams of de Sitter (a) and anti-de Sitter (b) space. Each point on these diagrams corresponds to a suppressed sphere S^{d-1} whose area is parametrized by a radial coordinate r. The null foliations shown are generated by light rays fired from $r = 0$, *i.e.* the north and south poles of dS and the origin of AdS. The black arrows indicate the directions in which extremal surface are allowed to turn around (*e.g.* an arrow pointing down and to the right indicates that extremal surfaces may only be tangent to the dashed foliation from the past). They imply that extremal surfaces must bend away from $\mathscr{I}_{\rm dS}$, but towards $\mathscr{I}_{\rm AdS}$.

rately). Both dS and AdS have a spherical isometry to which we have adapted the conformal diagrams; we introduce a coordinate r which parametrizes the areas of the spheres of symmetry[16].

In each spacetime we introduce two null foliations which we take to be adapted to its spherical isometry: these foliations are generated by light cones fired from $r = 0$ towards the boundary $r = \infty$. It is then easy to use Theorem 1 to understand

[16]Specifically, r is the usual radial coordinate that appears in the slicing

$$ds^2 = -\left(1 \pm r^2/\ell^2\right) dt^2 + \frac{dr^2}{1 \pm r^2/\ell^2} + r^2 d\Omega_{d-1}^2, \tag{9.11}$$

with the positive (negative) sign for the global (static) slicing of AdS (dS).

how extremal surfaces must behave. The cross-sectional area of the null foliations increases with r, so the expansion along each foliation is positive in the direction of increasing r. It then follows that the expansion along each sheet of the foliations never changes sign. This allows us to draw on Figure 9.11 the directions in which extremal surfaces are allowed to turn with respect to these foliations. In particular, note that extremal surfaces in AdS must bend *towards* the conformal boundary $\mathscr{I}_{\text{AdS}}$, while extremal surfaces in dS sufficiently near the boundary $\mathscr{I}_{\text{dS}}$ must bend *away* from it.

In principle, these claims only constrain the behavior of extremal surfaces with respect to the two null foliations introduced here. However, the high degree of symmetry of both dS and AdS allows us to conclude that *all* extremal surfaces in AdS must bend towards $\mathscr{I}_{\text{AdS}}$, while *all* extremal surfaces in dS that lie entirely in the future and past wedges marked on Figure 9.11 must bend away from $\mathscr{I}_{\text{dS}}$. The former point is, of course, well-known: extremal surfaces anchored to the boundary of AdS come up frequently in holographic contexts, and necessarily bend towards the boundary. The latter point was made generally in [77] using similar considerations to the ones used here. In particular, it follows that no boundary-anchored extremal surfaces exist in dS, since they would necessarily need to bend towards the boundary.

9.3.2 AdS Spherical Collapse

The above simple examples of dS and AdS illustrate how Theorem 1 puts constraints on the general behavior of extremal surfaces in arbitrary spacetimes, even those not containing splitting holographic screens. Our focus, however, is

on applications to AdS/CFT and bulk reconstruction. To that end, let us now discuss how Theorem 2 (which states that bounday-anchored extremal surfaces in the interior of achronal screens cannot have pivot points) explains some of the observations of [45, 46, 354] in the context of null collapse in AdS.

To briefly review, consider the formation of a black hole in Poincaré AdS by infalling null dust. In the holographic context, this process is dual to the thermalization of the boundary field theory following a perturbation (typically a form of a quantum quench). The bulk solution consists of two pieces: to the past of the null dust, the solution is a vacuum solution and therefore just (the Poincaré patch of) pure AdS. The portion of the bulk containing the dust and to the future of it is AdS-Vaidya:

$$ds^2 = -f(r,v)dv^2 + 2\,dv\,dr + \frac{r^2}{\ell^2}d\vec{x}_{d-1}^2, \tag{9.12}$$

where

$$f(r,v) = \frac{r^2}{\ell^2}\left(1 - \frac{\mu(v)}{r^d}\right), \tag{9.13}$$

where d is the boundary spacetime dimension, and we can think of compactifying the planar directions $\vec{x}$ into a torus to make them compact (it is the planar symmetry of these directions that allows us to apply Theorem 2 here). Here the mass function $\mu(v)$ characterizes the profile of the dust; the null energy condition is satisfied when $\mu'(v) \geq 0$. The full solution is shown in Figure 9.12(a).

Let us now consider the plane symmetric foliation of this spacetime generated by light cones fired from $r = 0$. The cross-sectional areas of these sheets go like $A \propto r^{d-1}$, so the expansion is positive in the direction of increasing r. In

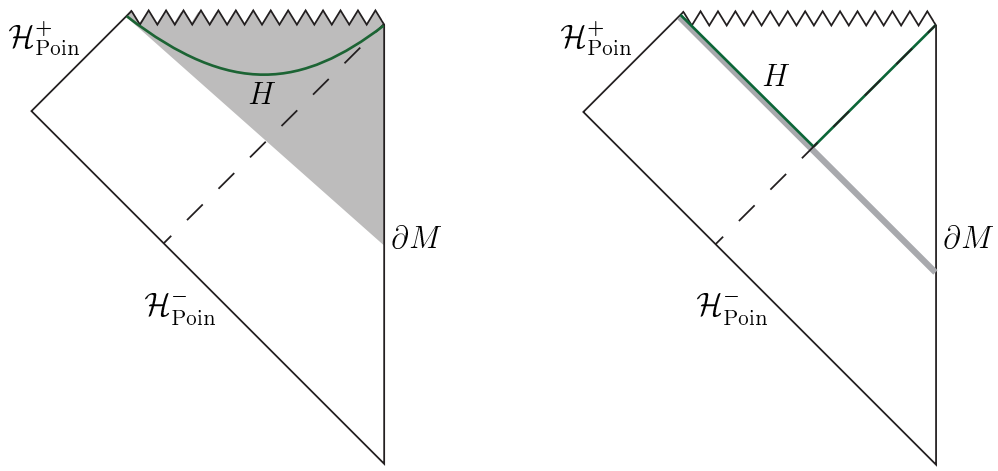

Figure 9.12: The formation of a black hole in pure AdS by infalling null dust (the shaded gray regions). To the past of the dust, the solution is pure AdS; the portion of the spacetime containing the dust is AdS-Vaidya. (a): for continuously infalling null dust, the spacetime contains an achronal future holographic screen (solid green curve). (b): if the dust is taken to be a thin shell, the screen approaches two null pieces, with one lying on the event horizon and the other on the shell. However, if the shell has an arbitrarily small but nonzero thickness, and if an arbitrarily small but nonzero amount of matter continues to fall in after the shell, the screen will be achronal (and arbitrarily close to being null). Note that here, the null boundaries are really the Poincaré horizons $\mathcal{H}^{\pm}_{\text{Poin}}$.

particular, this means that the expansion of the right-moving null sheets to the future of the event horizon changes sign, giving rise to a future holographic screen. This screen coincides with the dynamical horizon at $f(r, v) = 0$.

In the context of holographic quantum quenches, [45, 46] considered such a collapse scenario where the infalling null matter was taken to be a thin shell. The resulting holographic screen technically violates the assumptions of our theorems, since it is null and therefore not regular. However, it is easy to consider a regulated solution in which the null shell is smeared out slightly and given a rapidly decaying tail all the way into the far future. The screen will then be slightly deformed into

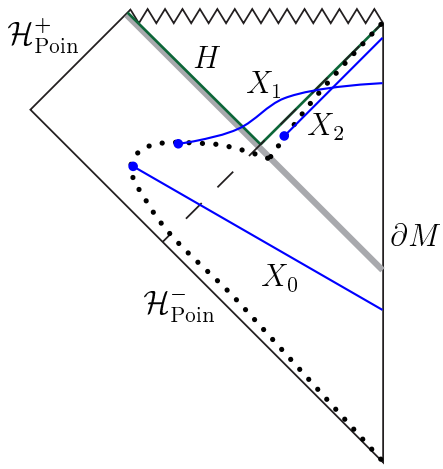

Figure 9.13: A family of extremal surfaces (solid blue lines) anchored to the boundary of AdS in thin shell Vaidya-AdS, as found in [45, 46]. The dot at the end of each surface indicates the location of its turning point; the dotted black line follows the path of this turning point as time at which the surface is anchored to ∂M is varied. Note that some surfaces in this family do enter the holographic screen H, but the turning points never do.

a regular achronal screen, as illustrated in Figure 9.12(b). Then our theorems can be applied to the regulated collapse geometry. By taking the limit where the regulator goes to zero, we may expect our theorems to apply to the thin shell solution as well.

Theorem 2 asserts that any reducible boundary-anchored extremal surface cannot turn around inside the screen. This is precisely what [45, 46] found, as shown in Figure 9.13. Extremal surfaces anchored to strips on the boundary sometimes penetrate the screen, but the turning point never does. In particular, as the boundary strips are taken to later times, the turning point of the corresponding extremal surfaces tracks out a curve which never enters the screen. Thus the interesting behavior of the turning point shown in Figure 9.13 is simply a consequence of our theorem.

Ref. [354] considered a similar problem, but in global AdS. In that case, the generalized planar symmetry is (a subset of) the full spherical symmetry. They too found extremal surfaces anchored to spherical boundary regions that penetrated the holographic screen, but never any that turned around in it.

9.4 Discussion

The key questions of hole-ography are: does there exist an object in the CFT which is dual to the area of an arbitrary spacelike codimension-two bulk surface? If so, what are the limitations of this duality? The former question has been partially answered in [339–343]; in this paper, we have proven theorems that give a partial answer to the latter.

9.4.1 Incomplete Reconstruction Inside Screens

Recall that [342] showed that under an appropriate set of assumptions (including generalized planar symmetry), if a given bulk spacelike codimension-two surface γ can be reconstructed from boundary-anchored extremal surfaces tangent to it, then the area of γ is given by the differential entropy of the boundary regions selected by the extremal surfaces. This direction was referred to as the "bulk-to-boundary" direction. Conversely, given a set of intervals on the boundary, the extremal surfaces anchored to them can be used to define at least one bulk surface γ whose area is equal to the differential entropy of the intervals; this is the "boundary-to-bulk" direction.

We pause here to note an important subtlety: to get a good correspondence

between the area of γ and the CFT differential entropy, the extremal surfaces must be the minimal ones that are picked out by the HRT formula. More generally, if the extremal surfaces used to reconstruct γ are not minimal, they may be related to other CFT quantities such as entwinement [355] (for example, minimal surfaces alone cannot be used to reconstruct the AdS_3 conical defect geometry or BTZ [337]). Here we will show that surfaces inside holographic screens cannot be fully reconstructed from *any* boundary-anchored extremal surfaces, be they minimal or not.

For example, consider the consequences of our results for a bulk-to-boundary construction: let γ be a sufficiently smooth spacelike closed curve[17] that lies entirely in the interior of some regular holographic screen H. Since γ is smooth, there must be some points at which γ is tangent to leaves of the null foliation used to construct H. We have illustrated this in Figure 9.14(a), where we have shown a spatial slice containing γ and its intersection with H and some leaves of the null foliation. Theorem 2 implies that there cannot exist boundary-anchored geodesics tangent to γ at the marked points. Moreover, if we slightly deform the null foliation, these points will shift slightly along γ, so we find that there are open regions of γ to which no boundary-anchored geodesics are tangent.

This is our main result: γ cannot be entirely reconstructed from any set of boundary-anchored geodesics, minimal or not. Generically, however, there will be regions of γ that *can* be. Thus in this bulk-to-boundary approach, γ can only be *partially* reconstructed from boundary-anchored geodesics (and therefore from CFT entanglement entropy, if these geodesics are the minimal-length ones

[17]Here we will restrict the discussion to three bulk dimensions (so γ is just a curve), though our statements also hold in reducible setups.

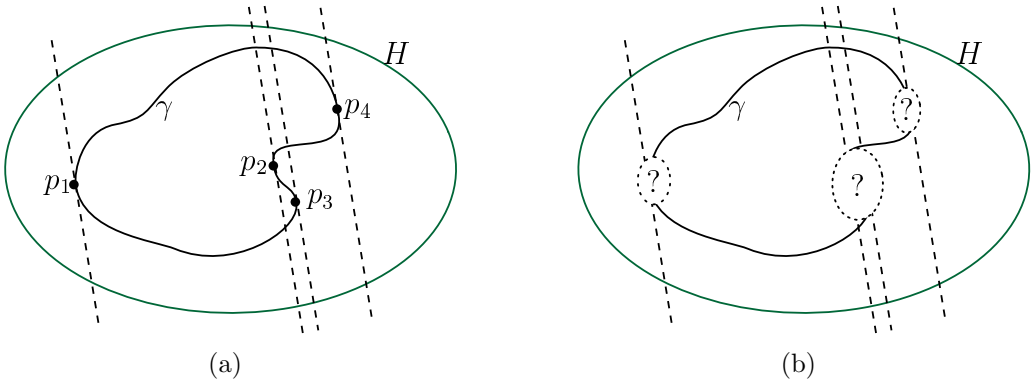

Figure 9.14: The plane of the page is a time slice containing a spacelike curve γ (solid black line) in the interior of a holographic screen H; the green oval shows the intersection of H with this particular time slice. (a): the curve γ will always be tangent to at least two leaves of the foliation (dotted black lines); in this particular case, it is tangent to four of them at the marked points. (b): by our theorem, boundary-anchored extremal surfaces cannot be tangent to γ at the marked points, so portions of γ in a neighborhood of these points cannot be reconstructed from them.

that are picked up in the HRT formula). This is a form of coarse-graining: the boundary data simply does not know how to reconstruct some pieces of γ. This coarse-grained reconstruction is illustrated in Figure 9.14(b).

Recall, however, that the boundary-to-bulk approach of [342] is slightly different: in order to reconstruct (the area of) a bulk curve γ from a set of boundary intervals, we do not need the corresponding geodesics to be tangent to γ. Rather, we only require what [342] call the "null alignment condition": where a geodesics meets γ, their tangent vectors need not agree, but may simply span a null plane. This is a weaker constraint, and it is therefore natural to wonder if the boundary-to-bulk construction fares any better in this case.

The answer is no. Suppose a smooth bulk curve γ constructed via the boundary-to-bulk approach is contained entirely inside H. Consider the two null planes gen-

erated by congruences fired off of γ in its two orthogonal null directions[18]. The null alignment condition says that γ may be constructed from boundary-anchored geodesics that intersect γ and are tangent to one of these planes when they do. But since γ is smooth, by the same argument given above there must exist some points at which this null plane is tangent to a leaf of the foliation. Then proceeding as we did in the bulk-to-boundary construction, we conclude that γ must contain segments that cannot be constructed from boundary-anchored geodesics.

The conclusion is that whether one takes the bulk-to-boundary or boundary-to-bulk approach, it is not possible to reconstruct an entire smooth[19] curve γ contained inside a holographic screen from boundary-anchored geodesics. In fact, it is very plausible that there are curves of which only an arbitrarily small portion can be reconstructed.

Of course, there is nothing preventing either approach from reconstructing a bulk curve that is only partly contained inside the holographic screen. However, a promising approach of hole-ography was to be able to reconstruct the bulk geometry itself via the integral geometry approach of [337, 338]. In order to use this approach to reconstruct the spacetime inside a holographic screen, one would need to reconstruct arbitrary curves entirely contained within it. It would thus appear that a naïve hole-ographic approach to reconstructing the interior of a holographic screen will not succeed.

[18]We fire the congruences in both future and past directions so that these two null planes contain γ.

[19]There may still be reconstruction issues even if γ has cusps, but we will not consider this case here.

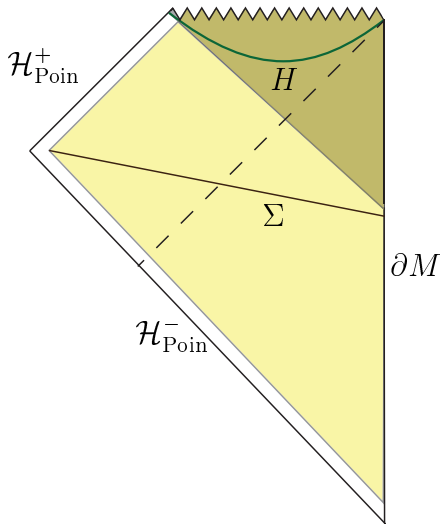

Figure 9.15: Attempting to reconstruct the interior of a holographic screen by evolving forward from an initial time slice Σ. The shaded yellow region shows the domain of dependence $D(\Sigma)$ of Σ; in principle, if we knew the equations of motion everywhere, we could reconstruct this entire domain just from data on Σ. In particular, this can include the interior of a holographic screen H (green).

9.4.2 Quantum Effects

A possible objection to our conclusion is the following: why not use boundary-anchored extremal surfaces to reconstruct the geometry of a portion of a Cauchy slice Σ to the past of the screen, and then use the bulk equations of motion to evolve forward from Σ to reconstruct its entire causal development? In particular, this may include the interior of a holographic screen; such an example is shown in Figure 9.15.

In principle this is possible, but only if we know the equations of motion *a priori*. Specifically, there is a sense in which a "full" bulk reconstruction should reconstruct the equations of motion as well as the geometry. The interiors of holographic screens, however, tend to contain singularities, that is, regions where

quantum gravitational effects become important. As soon as quantum fluctuations are introduced into the metric, even perturbatively, the possibility of reconstructing the bulk from its equations of motion is lost, particularly in near-singularity regions. For this reason, we find it more natural to seek a way of reconstructing the bulk *directly* from CFT data, without recourse to any equations of motion.

While our work has hithero been entirely classical, the appearance of quantum effects motivates the following observations:

- Recall that the interior of a holographic screen has a holographic interpretation in terms of bulk entropy via the Bousso bound [344, 352]. The area of a leaflet of a future or past holographic screen gives a bound on the entropy of the leaf generating it:

$$S(N_s) \leq \frac{\text{Area}(\sigma_s)}{2G_N\hbar}. \tag{9.14}$$

  This raises an interesting question: can the holographic screen itself be reconstructed from boundary observables? More precisely, what is the CFT dual of a holographic screen, and how is it linked to bulk entropy? As discussed in the previous subsection, the holographic screen is an obstacle to complete hole-ographic reconstruction of its interior; perhaps the information that is lost in the "coarse-graining" discussed above is stored in extra degrees of freedom associated with the screen (similar to *e.g.* the superselection sectors of [144]).

- Even in the presence of quantum effects, the option of direct reconstruction from boundary observables remains: for a semiclassical bulk (*i.e.* working

to first order in $G_N\hbar/\Lambda^{d-1}$ where Λ is a characteristic length scale of the quantum fields in the theory), [312] found that the *generalized entropy* of extremal surfaces yields the dual CFT entanglement entropy. More precisely, the generalized entropy of a spacelike codimension-two surface X is given by [13]:

$$S_{\text{gen}}(X) = \frac{\text{Area}(X)}{4G_N\hbar} + S_{\text{ent}} + \text{counterterms}, \tag{9.15}$$

where S_{ent} is the von Neumann entropy of the exterior of X on some Cauchy surface. It was later conjectured by [313] that, at any finite order in perturbation theory in $G_N\hbar/\Lambda^{d-1}$ in the bulk, there exists a quantum analogue of a classical extremal surface, obtained by replacing the area by the generalized entropy in the extremization procedure. The quantum extremal surface is obtained by extremizing S_{gen} with respect to variations along a null surface fired from X. The entanglement entropy of the boundary region enclosed by ∂X is conjectured to be dual to the generalized entropy of X [313]. The extension of the hole-ographic construction to semiclassical and perturbatively quantum gravity has not been discussed, as it is yet to be well-understood even at the classical level. However, it is very tempting to hope that a similar construction can be made using quantum extremal surfaces.

Since quantum fields may violate the null energy condition (which was assumed for all of the proofs in this paper), it may *prima facie* appear that our results are applicable exclusively to the classical case, where reconstruction may be undertaken via the bulk equations of motion. However, by replacing

all surfaces with their quantum analogues, relinquishing the null energy condition in favor of the recent quantum focussing conjecture of [356], which asserts that the variation of the generalized entropy (rather than the area) is nonpositive, and an analogous generic condition, to be introduced in [357], we may hope to prove similar statements about bulk reconstruction from "quantum hole-ography". In other words, quantum extremal surfaces cannot be used to reconstruct holes in spacetime regions foliated by leaves with decreasing generalized entropy.

Chapter 10

Non-Vacuum AdS Cosmologies

10.1 Introduction

A large class of interesting and useful asymptotically locally anti-de Sitter (AlAdS) spacetimes have been constructed by starting with AdS in Poincaré coordinates, in which the spacetime is foliated by slices on which the metric is conformal to the Minkowski metric η_{ab}, and replacing η_{ab} with any Ricci-flat metric γ_{ab}. Thus $(D-1)$-dimensional vacuum solutions to Einstein's equations straightforwardly give rise to new D-dimensional solutions to Einstein's equation with a negative cosmological constant. For example, taking γ_{ab} to be the Schwarzchild black hole yields a black cigar [174], and γ_{ab} was taken to be a vacuum *pp*-wave in [358] to construct a wave in the far field of an AdS-brane spacetime. Furthermore, the AlAdS solutions so generated are of particular interest in light of the AdS/CFT correspondence [19, 20, 82], since they are dual to a large-N, strongly coupled conformal field theory (CFT) that lives on the spacetime γ_{ab} (or a confor-

mally rescaled version thereof). For instance, [32, 359] took γ_{ab} to be a vacuum Kasner metric in order to study a cosmological singularity by computing the entanglement entropy and Wightman functions of the CFT[1].

In this paper we generalize this construction and show how non-vacuum $(D-1)$-dimensional spacetimes can be used to give AlAdS spacetimes with nonzero stress-energy. Specifically, if γ_{ab} is a solution to the Einstein equations in $(D-1)$-dimensions with stress-energy tensor $\widehat{T}_{ab}$, we show that replacing η_{ab} on the Poincaré slices with γ_{ab} gives a D-dimensional AdS solution with stress-energy T_{ab} that satisfies

$$T_{\mu\nu} = \widehat{T}_{\mu\nu}, \tag{10.1}$$

where $\mu, \nu = 0, \ldots, D-1$. By appropriate choice of $\widehat{T}_{ab}$, we use this construction to find new AlAdS spacetimes that have a physically sensible stress-energy. We also show that these spacetimes can be "solitonized" [360] by adding a compact dimension that shrinks smoothly to zero in the AdS bulk. A variation of this non-vacuum construction was performed in [361–363], which studied getting supergravity gauge fields "on the brane" by doing a Kaluza-Klein reduction of a supergravity theory in the higher dimensional AdS spacetime. A related construction starting with supergravity fields in ten dimensions was used to explore properties of time dependent boundaries in references [30, 31, 364, 365]. The relation between their higher and lower dimensional matter theories differs from what we find here, as will be clarified in Section 10.2.

As a special example, we will take γ_{ab} to be a Friedman-Robertson-Walker

[1]In fact, in [32] the CFT lived on a singularity-free conformally rescaled version of Kasner.

(FRW) cosmology[2]. The cosmological stress-energy is an isotropic perfect fluid with energy density $\tilde{\rho}(t)$ and pressure $\tilde{p}(t)$, which are related by an equation of state $\tilde{p}(t) = w\tilde{\rho}(t)$. We will show that in the AdS spacetime, the fluid is still isotropic on the cosmological slices with the same equation of state $p = w\rho$ and that the pressure in the AdS radial direction is given by $p_y = (3w-1)\rho/2$. The pressures and density decay towards the AdS boundary as well as in time as the universe expands. A case of special interest is a free, massless scalar field which in a $(D-1)$-dimensional FRW spacetime has the equation of state $\tilde{p} = \tilde{\rho}$, that is, $w = 1$. Hence the scalar field generates a D-dimensional AdS cosmology which is isotropic in all spatial directions and has corresponding equation of state $p = \rho$. According to the AdS/CFT prescription, such a scalar field in the bulk AdS is dual to to a scalar operator in the CFT with vanishing expectation value but nonzero source.

We will focus on FRW metrics with negatively curved spatial slices, in which case γ_{ab} approaches the future Milne wedge of Minkowski space at late time, so long as $w > -1/3$. The resulting AlAdS solution therefore approaches either the Poincaré patch of AdS or the AdS soliton at late times, which we interpret as an approach to equilibrium. We use these solutions to perturbatively study the approach to equilibrium of the boundary stress tensor and the ADM charges. Interestingly, we find that the latter *decrease* to their equilibrium values at late times, with the time dependent correction proportional to the dimensionless density parameter of the universe Ω. For example, the mass of the solitonized cosmology

[2]From the CFT side, such solutions can be thought of as a generalization of those in [366], which took the boundary metric to be a conformally flat FRW geometry.

decays as

$$\mathcal{M} = \left(1 - \frac{1}{2}\Omega\right) \mathcal{M}^{(0)} + \cdots , \tag{10.2}$$

where $\mathcal{M}^{(0)}$ is the mass of the static soliton and $\cdots$ stands for subleading terms at late times. In the context of spacetimes approaching the AdS soliton, this result is consistent with the energy conjecture of [117] that the AdS soliton is the lowest energy spacetime with the prescribed asymptotic structure.

A second application of our cosmological AdS solutions will be to compute the behavior of the entanglement entropy S of a spherical region in the CFT as the spacetime evolves to equilibrium. We use the covariant prescription of [70], which is a generalization of the static prescription [280]. This states that the entanglement entropy $S_{\mathcal{R}}$ of a region $\mathcal{R}$ of a holographic CFT is related to the area of a special bulk surface Σ. In general, $S_{\mathcal{R}}$ is UV-divergent, but it can be regulated and the behavior of this regulated entropy S_{reg} is studied. We find that at late times, the correction δS_{reg} to this quantity decays as a power law in the proper time of an asymptotically static observer.

Our results add to and complement the substantial body of work in the literature on vacuum AlAdS spacetimes in which the metric on the AdS boundary is time dependent. For instance, [367] constructed an elegant solution in which the metric on each Poincaré slice is a de Sitter cosmology. Several studies in the general category of holographic cosmology apply coordinate transformations to AdS black holes to produce cosmological boundaries [105, 368–374], and resulting metrics have been analyzed as describing an expanding boost-invariant plasma [47, 375–378]. Significant analytical work has also been done on out of equilibrium thermal properties of field theories using various AdS black hole spacetimes,

including [73, 74, 146, 379–383]. Discussion and further references can be found in [279]. Our work adds a set of new non-vacuum AlAdS spacetimes which allow a wide range of boundary metrics.

This paper is organized as follows. Section 10.2 contains the derivation of the new AlAdS solutions, as well as an analysis of the scalar field and perfect fluid cases. In section 10.3, the leading time dependent corrections to the boundary stress tensor and the ADM charges for a solitonic cosmology in an open universe are found. In section 10.4 the perturbation to the entanglement entropy is calculated, and section 10.5 contains discussion and concluding remarks. Unless otherwise specified, we take Newton's constant $G_N = 1$.

10.2 AdS and AdS Soliton Cosmologies

We start by considering AlAdS spacetimes of the general form

$$ds_D^2 = dy^2 + e^{2y/l}\gamma_{\mu\nu}(x^\alpha)dx^\mu dx^\nu, \tag{10.3}$$

where l is the AdS length and as before $\mu, \nu = 0, 1, \ldots, D-1$. For $\gamma_{\mu\nu} = \eta_{\mu\nu}$ this is AdS in Poincaré coordinates with cosmological constant given by

$$\Lambda = -\frac{(D-1)(D-2)}{2l^2}, \tag{10.4}$$

so we will refer to hypersurfaces $y =$ const. as "Poincaré slices". As mentioned above, it is well known that the Einstein equations with cosmological constant Λ are still satisfied for any Ricci-flat $\gamma_{\mu\nu}(x^\rho)$. In the particular case where $\gamma_{\mu\nu}$ is a

cosmological metric, we refer to (10.3) as an AdS cosmology.

In general, spacetimes of the form (10.3) with $\gamma_{\mu\nu} \neq \eta_{\mu\nu}$ suffer from a singularity at the Poincaré horizon $y \to -\infty$. This singularity can be resolved by introducing an additional compact direction v:

$$ds_D^2 = \frac{dy^2}{F(y)} + e^{2y/l}\left(F(y)dv^2 + \gamma_{\mu\nu}(x^\rho)dx^\mu dx^\nu\right), \tag{10.5}$$

where $F(y) = 1 - e^{-(D-1)(y-y_+)/l}$, and now $\mu, \nu = 0, 1, \ldots, D-2$. The metric (10.5) is capped off at $y = y_+$, so that the Poincaré horizon (and its possibly singular behavior) is removed. Regularity at this cap fixes the period of v to be

$$v \sim v + \frac{4\pi l e^{-y_+/l}}{D-1}. \tag{10.6}$$

Now, if $\gamma_{\mu\nu} = \eta_{\mu\nu}$, then (10.5) is the usual AdS soliton metric [117][3]. However, it was noted in [360] that the Einstein equations with negative cosmological constant Λ will still be satisfied for any Ricci-flat $\gamma_{\mu\nu}$. In analogy with (10.3), if $\gamma_{\mu\nu}$ is a cosmological metric, we will refer to (10.5) as an AdS soliton cosmology.

The solutions (10.3) and (10.5) provide a simple construction of AlAdS spacetimes with any desired Ricci-flat boundary metric $\gamma_{\mu\nu}$[4]. Our goal is to generalize the above results to isotropic FRW cosmological metrics $\gamma_{\mu\nu}$; as such cosmologies are not (in general) Ricci-flat, we will require the introduction of matter fields.

[3] Although this is no longer Poincaré AdS, we will continue to call surfaces of $y = \text{const.}$, $v = \text{const.}$ Poincaré slices.

[4] Technically, the boundary of (10.5) is $\gamma_{\mu\nu}$ cross the circle direction v.

10.2.1 Massless Scalar Field

We obtain a direct analogue of the results for vacuum metrics by considering a free massless scalar field ϕ in the AdS and AdS soliton spacetimes above. The full D-dimensional Einstein-massless scalar equations are

$$G_{ab} = -\Lambda g_{ab} + 8\pi T_{ab}, \qquad \nabla^2 \phi = 0, \tag{10.7}$$

where G_{ab} is the Einstein tensor and

$$T_{ab} = \frac{1}{8\pi}[(\nabla_a \phi)(\nabla_b \phi) - \frac{1}{2} g_{ab} g^{cd} (\nabla_c \phi)(\nabla_d \phi)] \tag{10.8}$$

is the stress-energy of a free massless scalar field in any dimension. Consider a lower-dimensional metric $\gamma_{\mu\nu}(x^\rho)$ and scalar field configuration $\phi(x^\mu)$ that solve the Einstein-scalar equations

$$\widehat{G}_{\mu\nu} = 8\pi \widehat{T}_{\mu\nu}, \qquad \widehat{\nabla}^2 \phi = 0, \tag{10.9}$$

where hatted objects are computed with respect to the metric $\gamma_{\mu\nu}$. Furthermore, let

$$s_{\mu\nu} = e^{2y/l} \gamma_{\mu\nu} \tag{10.10}$$

be the induced metric on a Poincaré slice. Finally, we pause to note that the scalar field stress energy satisfies the important property that from the full D-dimensional point of view, the induced stress tensor on each Poincaré slice is

equal to the lower-dimensional stress tensor of the scalar field on $\gamma_{\mu\nu}$:

$$T_{\mu\nu} = \widehat{T}_{\mu\nu}. \tag{10.11}$$

Now, consider first the metric (10.3). The D-dimensional Ricci tensor for g_{ab} is related to the Ricci tensor of $s_{\mu\nu}$ by

$$R_{\mu\nu}[g] = R_{\mu\nu}[s] - \frac{D-1}{l^2}\, s_{\mu\nu}, \quad R_{yy} = \frac{D-1}{l^2}. \tag{10.12}$$

When these components are assembled into the D-dimensional Einstein tensor and substituted into the left hand side of the Einstein field equation (10.7), one sees that the terms which do not involve the curvature of $s_{\mu\nu}$ are equal to the cosmological constant term on the right hand side. If $\gamma_{\mu\nu}$ is Ricci flat, then the metric (10.3) is a solution with $T_{ab} = 0$. If instead $\gamma_{\mu\nu}$ is a solution to (10.9) with nonzero $\widehat{T}_{\mu\nu}$, then it is then straightforward to show that the metric (10.3) constructed from $\gamma_{\mu\nu}$ will satisfy the full equations of motion (10.7), with the full bulk scalar field taken to be $\phi(x^\mu)$ (which, in particular, is independent of y). The additional nonzero component of the stress-energy tensor is $8\pi T_{yy} = -\frac{1}{2} s^{\mu\nu}\nabla_\mu\phi\nabla_\nu\phi$. The construction with the solitonized metric (10.5) proceeds in a similar way, and one finds that T_{yy} is the same and $T_{vv} = g_{vv}T_{yy}$.

One may naturally ask if such a straightforward foliation can be extended to other types of matter as well. For instance, one might hope to replace the scalar field with a Maxwell field and obtain multi-black hole solutions analogous to those of [384]. This is not the case: a key ingredient in the proof was the property (10.11) of the scalar field stress-energy. This property holds for the massless scalar field

stress tensor but not *e.g.* for Maxwell fields, or even for a scalar field with nonzero potential $V(\phi)$.

A massless scalar field that depends only on time can serve as the source for an FRW cosmology on the Poincaré slices of either (10.3) or the soliton metric (10.5). For instance, setting $d\hat{s}^2 = \gamma_{\mu\nu}dx^\mu dx^\nu$ and specializing to 4-dimensional cosmologies with flat spatial sections we have

$$d\hat{s}^2 = -dt^2 + \left(\frac{t}{t_0}\right)^{2/3}(dx^2+dy^2+dz^2), \quad \phi = -\sqrt{\frac{2}{3}}\,\ln\left(\frac{t}{t_0}\right), \tag{10.13}$$

with corresponding stress tensor equal to that of a perfect fluid obeying the stiff matter equation of state $\tilde{p} = \tilde{\rho}$. From the holographic perspective, the AdS/CFT dictionary tells us that the bulk scalar field is dual to a scalar operator in the CFT. To be specific, the near-boundary behavior of a massless scalar field in AdS takes the form

$$\phi(y) = (\phi_0 + \cdots) + e^{-(D-1)y/l}\left(\phi_{(D-1)} + \cdots\right), \tag{10.14}$$

where ϕ_0 and $\phi_{(D-1)}$ are independent parameters that are fixed by the boundary conditions, and $\cdots$ represent subleading terms in $e^{-y/l}$. The coefficient ϕ_0 should be interpreted as the source of a scalar operator $\mathcal{O}$ of dimension $D-1$, whose expectation value is $\langle\mathcal{O}\rangle = \phi_{(D-1)}$. Our solutions correspond to the special case $\phi_{(D-1)} = 0$. Note that this is unconventional: the operator $\mathcal{O}$ is being sourced, but nevertheless has a zero expectation value.

10.2.2 Perfect Fluid Matter

Noting that property (10.11) of the scalar field stress tensor was the key element in the above construction, we may extend the range of AdS and AdS soliton cosmologies by considering more general types of stress-energy that satisfy this condition. We will shortly focus on perfect fluids, but we begin by assuming just that the metric $\gamma_{\mu\nu}$ satisfies Einstein's equation on a Poincaré slice with some stress-energy $\widehat{T}_{\mu\nu}$. We can then analyze the content of the full D dimensional Einstein equations, beginning with the AdS type metrics (10.3), in the following way.

Using the relations between the components of the Ricci tensor (10.12) as in the previous subsection, we find that the AdS-type metric (10.3) solves the Einstein equation (10.7) with stress-energy given by

$$T_{\mu\nu} = \widehat{T}_{\mu\nu}, \qquad T_{yy} = \frac{1}{D-3}\, T, \tag{10.15}$$

where $T = s^{\mu\nu}\, T_{\mu\nu}$. A similar analysis for the AdS soliton-type metric (10.5) shows that the Einstein equation (10.7) is solved with stress-energy given by

$$T_{\mu\nu} = \widehat{T}_{\mu\nu}, \qquad T_{yy} = \frac{1}{D-4}\, g_{yy} T, \qquad T_{vv} = \frac{1}{D-4}\, g_{vv} T. \tag{10.16}$$

For example, one could embed a textbook example of a four-dimensional spherical static star into AdS. According to (10.16) the pressures in the radial AdS and compact soliton directions of this cigar-star will be equal to each other, but different from the radial pressure in the Poincaré plane.

We now specialize to the case of AdS and AdS soliton cosmologies, taking the metric $\gamma_{\mu\nu}$ to have the FRW form

$$d\hat{s}^2 = -dt^2 + a^2(t)\, d\Sigma_k^2, \tag{10.17}$$

where $d\Sigma_k^2$ is a metric on a space with constant curvature $k = 0, \pm 1$. We also restrict our attention to 4-dimensional Poincaré slices, so that the AdS cosmologies (10.3) have overall dimension $D = 5$ and the AdS soliton cosmologies (10.5) have dimension $D = 6$. Finally, we assume that the stress-energy $\widehat{T}_{\mu\nu}$ on the slice has the perfect fluid form

$$\widehat{T}_{\mu\nu} = (\hat{\rho} + \hat{p})\hat{u}_\mu \hat{u}_\nu + \hat{p}\gamma_{\mu\nu}, \tag{10.18}$$

with $\gamma^{\mu\nu}\hat{u}_\mu\hat{u}_\nu = -1$ and equation of state $\hat{p} = w\hat{\rho}$. Note that the strong energy condition requires $w \geq -1/3$. Important special cases are $w = 0$ for dust, $w = 1/3$ for radiation, and $w = 1$ for the massless free scalar field; indeed, note that such a stress tensor obeys the condition (10.11)[5].

The cosmological scale factor on the Poincaré slices evolves according to the Friedmann equations

$$d(\hat{\rho}\, a^3) = -\hat{p}\, d(a^3), \qquad \left(\frac{\dot{a}}{a}\right)^2 = \frac{8\pi\hat{\rho}}{3} - \frac{k}{a^2}. \tag{10.19}$$

The full stress energy tensor T_{ab} for AdS cosmologies, given by (10.15), now has the form of an anisotropic fluid, with a distinct equation of state parameter for the

[5]Values of w different from 1 could be obtained from an interacting scalar field, but as such interactions would require the introduction of a scalar potential, they are not compatible with our ansatz. We will keep w general, with the understanding that this is a bulk, hydrodynamic description.

pressure in the y-direction. Moreover, the energy density and pressures depend on the radial coordinate y, as well as on time. One finds that the energy density is given by $\rho = e^{-2y/l}\hat{\rho}$, while the pressures tangent to the Poincaré slices satisfy an equation of state in the D-dimensions of the same form as in $(D-1)$, namely $p = w\rho$. In the y-direction one finds that $p_y = w_y\rho$ with

$$w_y = \frac{(3w-1)}{2}. \tag{10.20}$$

With a soliton, equation (10.16) implies that the pressure in the compact v-direction is equal to p_y, so also $p_v = w_y\rho$. To summarize, the stress-energy for the AdS soliton cosmology is

$$\rho = e^{-2y/l}\hat{\rho}(t), \quad p = w\rho, \quad p_y = p_v = \frac{(3w-1)}{2}\,\rho. \tag{10.21}$$

Some observations are as follows. For $w = 1$, which corresponds to the massless scalar field discussed above, $w_y = 1$ as well so the pressure in the full spacetime is isotropic. For radiation ($w = 1/3$), the stress-energy on the Poincaré slices is traceless and the pressure orthogonal to the slices vanishes, so the stress tensor remains traceless. For $w < 1/3$, the orthogonal pressure is negative.

10.2.3 Open AdS and AdS Soliton Cosmologies

We will be particularly interested in AdS and AdS soliton cosmologies with open ($k = -1$) FRW universes on the Poincaré slices. In this case, provided that the equation of state parameter is in the range $w > -1/3$ (that is, that the strong energy condition holds), the energy density $\hat{\rho}$ will fall off faster than $1/a^2$ and at

late times the scale factor will grow linearly in time. At sufficiently late times, the metric $\gamma_{\mu\nu}$ on the Poincare slices then approaches

$$d\hat{s}^2_{\text{late}} = -dt^2 + t^2\, d\Sigma^2_{-1}, \tag{10.22}$$

which is flat spacetime in Milne coordinates. The full AdS and AdS soliton cosmological metrics (10.3) and (10.5) then respectively approach the AdS or AdS soliton metrics at late times. The late-time behavior of these cosmologies can therefore be thought of as an approach to equilibrium; in particular, the CFT dual can be thought of as an expanding isotropic plasma equilibrating at late time. The solutions (10.3) and (10.5) correspond to the plasma being in a deconfined or confined phase, respectively.

10.3 ADM Mass and Boundary Stress Tensor for AdS Soliton Cosmologies

As a first examination of the properties of these AdS cosmologies, we look at how the cosmological expansion impacts the boundary stress tensor and the ADM mass and tensions of the AdS soliton (which corresponds to the confined phase of the dual field theory; see e.g. [385]). In general we lack a definition of the ADM charges that will apply at the boundary $y = \infty$ with a time dependent boundary metric. However, as we will see the special case of an open cosmology with matter obeying the strong energy condition $w > -1/3$ allows for a perturbative computation of how the ADM charges of the soliton approach their static values

at late times.

The static AdS soliton has negative ADM mass, reflecting the negative Casimir energy of the boundary field theory with a compact direction, and is conjectured to be the lowest energy solution among spacetimes with these asymptotics [117]. In addition to its mass, the AdS soliton has nonzero ADM tensions [386, 387]. The tension along the compact v-direction in (10.5) is found to be large and positive, while the other three spatial tensions have negative values, such that the trace of the ADM charges (sum of the mass and the tensions) vanishes. One can think of the static soliton solution as an equilibrium configuration. In this section we will compute the approach to equilibrium of the boundary stress tensor, as well as the mass and tensions for an open AdS soliton cosmology. We will see that the mass decreases to the static soliton value, a result that is consistent with the minimum mass conjecture with matter obeying the strong energy condition.

As noted above, the FRW boundary metric does not have a time-translation symmetry and therefore the ADM mass is not defined in the usual sense. However, at late times the FRW cosmologies with negatively curved spatial slices approach Minkowski spacetime. We can then define a time dependent ADM mass in this late time limit by writing the metric as static AdS plus time dependent perturbations that decay to zero. These perturbations to the metric determine the late time corrections to the asymptotic constant value of the mass of the soliton.

Consider an AdS soliton cosmology (10.5) with an open FRW metric

$$d\hat{s}^2 = -dt^2 + a^2(t)\left(d\chi^2 + \sinh^2\chi\, d\Omega_{(2)}^2\right) \tag{10.23}$$

on the Poincaré slices. We assume that $w > -1/3$, so that in the late time limit $a(t) \simeq t$. Define new coordinates on the slices according to

$$T = a(t)\cosh\chi, \quad R = a(t)\sinh\chi. \tag{10.24}$$

Note that since $R/T = \tanh\chi$ it follows that $R/T \leq 1$ with equality when $\chi \to \infty$. In terms of these new coordinates the AdS soliton cosmology has the form

$$ds^2 = \frac{dy^2}{F(y)} + e^{2y/l}\left[\, F(y)\,dv^2 - (1-\delta\tilde{g}_{TT})dT^2 + (1+\delta\tilde{g}_{RR})dR^2 \right. \\ \left. +2\,\delta\tilde{g}_{TR}\,dR\,dT + R^2 d\Omega^2_{(2)}\right] \tag{10.25}$$

where $F(y)$ is given in (10.5) and the functions $\delta\tilde{g}_{TT}$, $\delta\tilde{g}_{RR}$ and $\delta\tilde{g}_{TR}$, which give the deviance of the metric on the Poincaré slices from flat, may be written as

$$\delta\tilde{g}_{TT} = \Omega\,\frac{1}{1-(R/T)^2}, \quad \delta\tilde{g}_{RR} = \Omega\,\frac{(R/T)^2}{1-(R/T)^2}, \quad \delta\tilde{g}_{TR} = \Omega\,\frac{R/T}{1-(R/T)^2}. \tag{10.26}$$

Here Ω is the dimensionless density parameter of the open FRW metric,

$$\Omega = \frac{8\pi\hat{\rho}}{3H^2} = \left(1 - \frac{1}{\dot{a}^2}\right), \tag{10.27}$$

and $H = \dot{a}/a$ is the Hubble parameter. For an open universe $\Omega < 1$ and approaches zero in the far future. Hence, the metric (10.25) approaches the AdS soliton at late times. We emphasize that the expressions in (10.26) are exact up to this point.

To proceed further, the density parameter Ω must be expressed in terms of

the asymptotically Minkowski coordinates (T, R), which requires the expression for the scale factor $a(t)$ at late times. To obtain this expression, first we substitute the equation of state $p = w\rho$ into the Friedman equations (10.19), which allows the energy density to be solved for in terms of the scale factor, giving

$$\hat{\rho}(t) = \frac{3\bar{\Omega}_* H_*^2}{8\pi (H_* a(t))^{3(1+w)}} \ , \ \text{where } \bar{\Omega}_* \equiv \frac{\Omega_*}{(1-\Omega_*)^{3(w+1)/2}} \tag{10.28}$$

and H_* and Ω_* are the Hubble and density parameters evaluated at a fiducial time $t = t_*$. The density and scale factor evaluated at t_* are given by $\hat{\rho}_* = 3\Omega_* H_*^2/8\pi$ and $a_* = 1/(H_*\sqrt{1-\Omega_*})$ respectively. The equation for the scale factor then reduces to

$$\dot{a}^2 = 1 + \frac{\bar{\Omega}_* H_*^2 a_*^{3(1+w)}}{a^{1+3w}}. \tag{10.29}$$

For $w > -1/3$, this reduces in the limit of large scale factor to $\dot{a}^2 \simeq 1$, giving $a(t) \simeq t$ in the late time limit. Including a subleading correction of the form $a(t) \simeq t + \alpha t^\beta$ yields

$$a(t) \simeq t - \frac{\bar{\Omega}_*}{6wH_*(H_* t)^{3w}}, \quad w \neq 0, \tag{10.30a}$$

$$a(t) \simeq t + \frac{\bar{\Omega}_*}{2H_*} \ln\left(\frac{t}{H_*}\right), \quad w = 0, \tag{10.30b}$$

which by (10.27) yield

$$\Omega(t) \simeq \frac{\bar{\Omega}_*}{(H_* t)^{(1+3w)}}. \tag{10.31}$$

The expressions (10.30) can be inverted and combined with the transformation to (R, T) coordinates to yield the coordinate transformation from t to (R, T), valid

at late times, including terms up to order R^2/T^2,

$$t \simeq T + \frac{\bar{\Omega}_*}{6wH_*(H_*T)^{3w}} - \frac{R^2}{2T}, \qquad w \neq 0, \tag{10.32a}$$

$$t \simeq T - \frac{\bar{\Omega}_*}{2H_*}\ln\left(\frac{T}{H_*}\right) - \frac{R^2}{2T}, \qquad w = 0, \tag{10.32b}$$

which then give Ω as a function of T and R:

$$\Omega \simeq \frac{\bar{\Omega}_*}{(H_*T)^{3w+1}}\left(1 - \frac{(1+3w)\bar{\Omega}_*}{6w(H_*T)^{3w+1}} + \frac{(1+3w)R^2}{2T^2}\right), \quad w \neq 0, \tag{10.33a}$$

$$\Omega \simeq \frac{\bar{\Omega}_*}{H_*T}\left(1 + \frac{\hat{\Omega}_*}{2H_*T}\ln\left(\frac{T}{H_*}\right) + \frac{R^2}{2T^2}\right), \quad w = 0. \tag{10.33b}$$

This is our desired result.

We are now prepared to compute the leading late time corrections to the boundary stress tensor density, which we will denote by $\tau_{\mu\nu}$. Let $K_{\mu\nu}$ be the extrinsic curvature of the AdS boundary. In the boundary stress tensor formalism a boundary action is defined that includes an integral over K plus geometrical counterterms that are constructed from the metric on the boundary $s_{\mu\nu}$, defined in equation (10.10). These terms include a cosmological constant, the scalar curvature of $s_{\mu\nu}$, and potentially higher derivative counter terms as needed. The stress tensor density results from varying the boundary action with respect to $s^{\mu\nu}$. The coefficients of the counter terms are chosen to cancel divergences that occur in $\tau_{\mu\nu}$ and are dimension dependent. One finds the result [96, 104, 388]

$$8\pi\tau_{\mu\nu} = \sqrt{-s}\left(K_{\mu\nu} - Ks_{\mu\nu} + \frac{D-2}{l}s_{\mu\nu} + \frac{1}{D-3}G_{\mu\nu}[s] + \cdots\right), \tag{10.34}$$

where the $\cdots$ indicate higher derivative terms in the Riemann tensor of $s_{\mu\nu}$, which we will show are subdominant at late times. We work with the boundary stress tensor density because the volume element of the late time metric changes at leading order, and also because this is the appropriate quantity to integrate to get the ADM charges.

In the case of the static AdS soliton, the metric on the boundary is flat and the terms in (10.34) depending on the curvature of $s_{\mu\nu}$ all vanish. This is no longer true for the cosmological AdS spacetimes. The Einstein tensor term in (10.34) contributes a time-dependent piece to $\tau_{\mu\nu}$ which goes to zero at late times like the energy density $\hat{\rho}$ in (10.28). Additional time dependence in $\tau_{\mu\nu}$ comes from the volume element in (10.34) which goes like

$$\sqrt{-s} = \left(1 - \frac{1}{2}\,\Omega\right)\sqrt{-s_{(0)}}, \tag{10.35}$$

where $\sqrt{-s_{(0)}}$ denotes the volume element in the static AdS soliton, and the late time behavior of the density parameter Ω is given in (10.31). Comparing the decay rates of $\hat{\rho}$ and Ω, one finds that the contribution of $G_{\mu\nu}$ to the boundary stress tensor density is subdominant at late times compared to that of the volume element. The contributions of higher derivative terms in (10.34) will decay even more rapidly. The leading contributions to the boundary stress tensor density are then readily found by combining the results for the static AdS soliton in [386] with equation (10.35) giving

$$\tau_{\mu\nu} = \frac{e^{5y_+/l}}{16\pi l}\left(1 - \frac{1}{2}\,\Omega\right)\mathrm{diag}(-1, 1, 1, 1, -4), \tag{10.36}$$

where the coordinates are ordered according to (t, x_1, x_2, x_3, v). Hence the decaying time dependent corrections to the static values of $\tau_{\mu\nu}$ are simply proportional to Ω, the density parameter of the cosmology.

We now use the results above to determine the ADM mass and tensions for the AdS soliton cosmologies. Comparison with [386] shows that the integrands of the ADM charges in AdS coincide with the first three terms in the boundary stress tensor in equation (10.34), and the components of $\tau_{\mu\nu}$ above then just need to be integrated to obtain the ADM charges. In the static coordinates, the density parameter Ω depends on R as well as T, so the integrand is not a constant. This does not mean that $R = 0$ is a special point, since any location in the homogeneous open cosmology could equally well be chosen as the origin. For the static AdS soliton, the ADM charges are made finite by taking the planar geometry to be periodically identified, with $-L_j/2 \leq x^j \leq L_j/2$. For notational brevity let the asymptotic volume be $V = L_1 L_2 L_3 L_v$ where L_v is the range of compact coordinate v given in (10.6). In the limit that the plane is infinite, the relevant energy is the mass per unit volume obtained by dividing the total mass by V, and similarly for the spatial tensions.

Finally, it is important to note that the static radial coordinate R has the range $0 \leq R \leq T$, with the upper limit corresponding to $\chi \to \infty$ in the coordinate transformation (10.24). The integrals for the ADM charges are then over a box of length $L < T$, and at the end we divide out the volume of the box. Define the spatial average of the density parameter Ω at time T by

$$\langle \Omega \rangle = \frac{\bar{\Omega}_*}{V(H_* T)^{3w+1}} \int dx_1 dx_2 dx_3 dv \, \Omega(R, T). \tag{10.37}$$

In the late time limit, we substitute the approximate expression for Ω given in (10.33). For the general case $w \neq 0$, this yields

$$\langle \Omega \rangle = \frac{\bar{\Omega}_*}{V(H_* T)^{3w+1}} \left(1 - \frac{c_1}{T^{3w+1}} + \frac{c_2 L^2}{T^2} \right), \tag{10.38}$$

where the coefficients c_1, c_2 can be read off of the expansion of Ω in equation (10.33). One sees that the terms proportional to c_1 and c_2 make increasingly small contributions and so will be dropped in subsequent formulae. This also allows us to treat the cases $w = 0$, $w \neq 0$ simultaneously, since the leading-order term in (10.38) is identical to that obtained in the special case $w = 0$.

Following the conventions of past work (*e.g.* [386]), we give the ADM tension rather than a pressure, where tension is simply minus the pressure[6]. Assembling the pieces, at late times the mass and tensions of the soliton in the metric (10.25) are

$$\mathcal{M} = \mathcal{T}_j = -\frac{V}{16\pi l} e^{5y_+/l} \left(1 - \frac{1}{2} \langle \Omega \rangle \right) \ , \quad j = 1, 2, 3, \tag{10.39a}$$

$$\mathcal{T}_v = \frac{4V}{16\pi l} e^{5y_+/l} \left(1 - \frac{1}{2} \langle \Omega \rangle \right). \tag{10.39b}$$

The expressions for the ADM charges have the same structure as the components of the boundary stress tensor, relaxing to the equilibrium values like $\langle \Omega \rangle$. Since $\langle \Omega \rangle > 0$, the mass of the AdS soliton cosmology decreases as $\langle \Omega \rangle$ goes to zero, approaching its negative static value at late times, consistent with the energy bound conjectured in [117]. The tension $\mathcal{T}_v$ around the compact dimension

[6]This convention is natural in asymptotically flat static spacetimes where the gravitational tension can be shown to be positive [389].

increases to its static positive value, while the trace $\mathcal{M} + \mathcal{T}_v + \Sigma_j \mathcal{T}_j$ vanishes throughout the relaxation process.

10.4 Entanglement Entropy

The new AdS cosmological solutions allow us to compute how the entanglement entropy of a region in the dual CFT approaches equilibrium. To perform the computation, we use the holographic prescription [70, 280], which proposes that the entanglement entropy of a region $\mathcal{R}$ (called the entangling region) in the boundary CFT is equal to

$$S_{\mathcal{R}} = \frac{\text{Area}\,[\Sigma]}{4G_N}, \tag{10.40}$$

where Σ (referred to as the entangling surface) is the minimal-area extremal surface in the bulk spacetime anchored to $\partial\mathcal{R}$ and homologous to $\mathcal{R}$. Note that in this section we have restored Newton's constant G_N. We will also keep w general, though we emphasize that only the case $w = 1$ (wherein the bulk matter is a scalar field) has a well-understood CFT dual.

Parametrizing Σ as $X^a(\sigma^i)$, with σ^i coordinates on Σ, $i = 1, ..., D-2$, the area functional is

$$A = \int \sqrt{h}\, d^{D-2}\sigma, \tag{10.41}$$

where h is the determinant of the induced metric on the surface

$$h_{ij} = g_{ab}\partial_i X^a \partial_j X^b. \tag{10.42}$$

In general, extremizing (10.41) to obtain the entangling surface is difficult

to accomplish analytically, and the AdS soliton cosmologies are no exception. However, we can make progress by working in the non-solitonized AdS cosmology (10.3) and noting that the calculations performed there should approximate those in the AdS soliton cosmology, as long as the relevant surfaces do not extend too deeply into the spacetime. The boundary metric is then

$$ds_\partial^2 = -(1-\delta\tilde{g}_{TT})dT^2 + (1+\delta\tilde{g}_{RR})dR^2 - 2\delta\tilde{g}_{TR}\,dR\,dT + R^2 d\Omega_{(2)}^2, \qquad (10.43)$$

and the full metric is given in (10.3) with $\gamma_{\mu\nu}$ equal to ds_∂^2. Working in pure AdS has the significant advantage that the extremal surface is known for a spherical entangling region on the boundary [280]. This allows us to use perturbative techniques to compute the time dependent correction to the area as the metric approaches the static AdS spacetime in the future.

In order to compute the late-time behavior of the entanglement entropy we work to first order in powers of R/T in $\delta\tilde{g}_{TT}$, $\delta\tilde{g}_{RR}$, and $\delta\tilde{g}_{TR}$, given in equations (10.26) and (10.33). We take the boundary of the entangling region to be a sphere of radius R_0 at some time T_0; the corresponding entangling surface Σ in pure AdS was found in [280]. We may then perturb off of this solution to compute the leading correction to the area. There are two natural options for how this sphere should evolve in time: (i) the sphere can be of fixed proper size in the asymptotically static coordinates so that R_0 is held constant as T_0 advances; or (ii) the sphere can be comoving, so that fluid elements on the boundary of the sphere follow geodesics, and R_0 grows like $a(t)$. We will discuss both choices below.

10.4.1 Zeroth Order Solutions

At zeroth order, the boundary metric (10.43) is just Minkowski space. Parametrizing the surface by $z \equiv le^{-y/l}$ and the coordinates on the sphere, the area functional (10.41) is

$$A = 4\pi l^3 \int_\epsilon^1 dx \, \frac{(1-x^2)^{1/2}}{x^3}, \tag{10.44}$$

where $\epsilon = z_{\rm cut}/R_0$ and $z_{\rm cut}$ is a UV cutoff to regulate the integral. The corresponding entangling surfaces were calculated in [280] and are given by

$$\Sigma_0 : \quad z^2 + R^2 = R_0^2 \ , \quad T = T_0, \tag{10.45}$$

with area

$$A^{(0)} = l^3 \left[\frac{A_{\rm static}}{2z_{\rm cut}^2} - \pi \ln\left(\frac{A_{\rm static}}{\pi z_{\rm cut}^2} \right) - \pi \right], \tag{10.46}$$

where $A_{\rm static} = 4\pi R_0^2$ is the area of $\partial\Sigma_0$. The first term in the above expression denotes the usual area law growth of the entanglement entropy, while the coefficient of the logarithmically divergent term provides a UV-independent measure of the entanglement entropy.

10.4.2 First Order Corrections: Approach to Equilibrium

Now, consider corrections to (10.46) which arise both from perturbations to the metric and to the surface X^a. Write each as a zeroth order piece plus a perturbation,

$$g_{ab} = g_{ab}^{(0)} + \delta g_{ab} \ , \qquad X^a(\sigma_i) = X^a_{(0)} + \delta X^a. \tag{10.47}$$

To first order the volume element on the surface becomes

$$h = h^{(0)} \left(1 + \mathrm{Tr}\left[\delta g_{ab} \partial_i X^a_{(0)} \partial_j X^b_{(0)} + 2 g^{(0)}_{ab} \partial_i \delta X^a \partial_j X^b_{(0)}\right]\right). \tag{10.48}$$

However, the second term in the trace is a variation of the surface in the background metric, and so this integrates to zero since the background surface is extremal. Thus the first-order change in the area is governed by the perturbation to the metric:

$$\delta A = \frac{1}{2} \int \sqrt{h^{(0)}}\, \mathrm{Tr}\left[\delta g_{ab} \partial_i X^a_{(0)} \partial_j X^b_{(0)}\right]\, d^{d-1}\sigma. \tag{10.49}$$

The final step is to substitute the expressions for the metric perturbations (10.26) into the metric equations (10.3), (10.43). Using $R'(z) = -z/R$ on the zeroth order surface (10.45), the induced metric in the perturbed spacetime is given by

$$(g^{(0)}_{ab} + \delta g_{ab}) \partial_i X^a_{(0)} \partial_j X^b_{(0)} d\sigma^i d\sigma^j|_{\Sigma_0} = \frac{l^2}{z^2} \left\{ \left(\frac{R_0^2}{R^2} + \frac{z^2 \Omega}{T_0^2} \right) dz^2 + R^2 d\Omega^2_{(2)} \right\}, \tag{10.50}$$

where $R = \sqrt{R_0^2 - z^2}$. Using this expression in (10.49) and substituting Ω from (10.33) gives the first-order correction to the area of the entangling surface

$$\delta A = \frac{4\pi l^3 \bar{\Omega}_*}{(H_* T_0)^{3w+1}} \left(\frac{R_0^2}{2T_0^2} \right) \int_\epsilon^1 dx \frac{(1-x^2)^{3/2}}{x} \tag{10.51}$$

$$= \frac{l^3 \bar{\Omega}_*}{4(H_* T_0)^{3w+3}} H_*^2 A_{\mathrm{static}} \left(\ln\left(\frac{A_{\mathrm{static}}}{\pi z_{\mathrm{cut}}^2} \right) - \frac{4}{3} \right). \tag{10.52}$$

This result is valid at sufficiently late times such that $H_* T_0 \gg 1$ and $T_0 \gg R_0$.

The entanglement entropy, including the leading late time contribution, fol-

lows from substituting (10.51) and (10.46) into the entropy-area relation in equation (10.40). The conversion from area to entropy contains the prefactor $l^3/G_N^{(5)}$, which can be translated into the parameters of the dual CFT. According to the AdS/CFT correspondence, the solutions (10.3) in $D = 5$ are dual to an $\mathcal{N} = 4$ supersymmetric Yang-Mills theory on the FRW spacetime (10.17). Following the discussion in [280], we consider $\mathcal{N} = 4$ $SU(N)$ SYM theory on $\mathrm{AdS}_5 \times S^5$, in which case the AdS radius, the ten dimensional Newton's constant, and the five dimensional Newton's constant are identified with the string coupling, string tension, and N according to $l^4 = 4\pi g_s(\alpha')^2 N$, $G_N^{(10)} = 8\pi^6 g_s^2(\alpha')^4$, and $G_N^{(5)} = G_N^{(10)}/l^5$. This gives $l^3/G_N^{(5)} = 2N^2/\pi$, and the entanglement entropy is then

$$S = \frac{N^2}{2\pi}\left[\frac{A_{\mathrm{static}}}{2z_{\mathrm{cut}}^2} - \pi \ln\left(\frac{A_{\mathrm{static}}}{\pi z_{\mathrm{cut}}^2}\right) - \pi + \frac{\bar{\Omega}_* H_*^2 A_{\mathrm{static}}}{4(H_* T)^{3w+3}}\left(\ln\left(\frac{2A_{\mathrm{static}}}{\pi z_{\mathrm{cut}}^2}\right) - \frac{4}{3}\right) + \cdots\right], \tag{10.53}$$

where $\cdots$ denotes terms that are subleading at late time, and the subscript on T has been dropped for simplicity. The coefficient of the logarithmic term is invariant under rescalings of the cutoff, so this term serves as a regularized measure S_{reg} of the entanglement entropy. We see that the correction to this term is given by

$$\delta S_{\mathrm{reg}} \simeq \frac{N^2}{8\pi}\frac{\bar{\Omega}_* H_*^2 A_{\mathrm{static}}}{(H_* T)^{3w+3}} \ln\left(\frac{2A_{\mathrm{static}}}{\pi z_{\mathrm{cut}}^2}\right). \tag{10.54}$$

Note that this is positive, which means that S *decreases* to its equilibrium value. This behavior differs markedly from that of quenches in CFTs [221, 269–271, 335, 390, 391], wherein the entanglement entropy grows until is saturates. There is a temptingly simple and compelling physical reason for the decrease of S found in this calculation: in the Cartesian coordinates T, R there is a nonzero radial

flux proportional to g_{TR}, so the decrease of the entropy in the ball $R \leq R_0$ can be interpreted as due to an energy flow out of the ball. In particular, in the quasi-particle picture of entanglement entropy propagation [221], entanglement is carried by entangled particle pairs; a new flow of such particles out of the entangling ball $R \leq R_0$ leading to a decrease in entanglement entropy is consistent with this picture. Alternatively, note that at late time, our bulk solution approach the Minkowski vacuum, and therefore the CFT evolves from an excited state to the zero-temperature vacuum state. We would therefore naturally expect probes of correlation (such as entanglement entropy) to decay in the late time limit[7].

The time dependent contribution decays as a power law, and the time scale for the decay is set by the Hubble parameter H_*. The power depends on the equation of state. For example, for dust the correction goes to zero like T^{-3}, and for a free massless scalar field like T^{-6}. The time dependence in δS is analogous to the result of [359], in which the entropy of a strip in a vacuum-Kasner AdS spacetime was found to have a power law behavior, in both cases a reflection of the time evolution of the cosmology.

Turning to the amplitude of $\delta S_{\rm ren}$, we see that this is set by an interesting combination of factors. At sufficiently late times $t_*\Omega_* \ll 1$, so that $H_*^2\bar{\Omega}_* \simeq 8\pi G_N^{(5)}\hat{\rho}_*/3$. Hence the dimensionless combination $H_*^2\bar{\Omega}_* A_{\rm static}$ has the interpretation of the non-vacuum energy, measured in Planck units, that is contained in a shell of width the Planck length that surrounds the sphere. That is, the entangling modes of the perturbation act like they are concentrated on the boundary of the sphere. This is a reflection of the fact that the change in the area of the extremal

[7]We thank Juan Pedraza for this observation.

surface comes from the metric perturbations near the surface.

10.4.3 The Cosmological View

An alternative way to interpret the time evolution of the entanglement entropy is to take the boundary sphere to be comoving, so that points on the boundary sphere follow geodesics. In the cosmological coordinates (10.23) this means that the sphere is at a fixed coordinate $\chi = \chi_0$. The extremal surface Σ_0 does not lie within a slice of constant cosmological time, but it does intersect the boundary at a constant time, as can be seen by evaluating (10.24) at $z = 0$. Transforming the zeroth order surface (10.45) to the cosmological coordinates gives

$$\Sigma_0 : \quad a(t)\cosh\chi = a(t_b)\cosh\chi_0 \ , \quad z^2 + \cosh^2\chi_0 \tanh^2\chi = a(t_b)^2\sinh^2\chi_0. \tag{10.55}$$

Let

$$A_{\rm geod}(t_b) = 4\pi a(t_b)^2 \sinh^2\chi_0 \tag{10.56}$$

be the proper area of the comoving sphere on the boundary at t_b. Then in terms of the cosmological coordinates the zeroth order area (10.46) becomes

$$A^{(0)}(t_b) = l^3\left[\frac{A_{\rm geod}}{2z_{\rm cut}^2} - \pi\ln\left(\frac{A_{\rm geod}}{\pi z_{\rm cut}^2}\right) - \pi\right] \tag{10.57}$$

and the time dependent correction (10.51) is

$$\delta A = l^3\bar{\Omega}_* H_*^2 (4\pi a_*^2 \sinh^2\chi_0)\left(\frac{a_*}{a(t_b)}\right)^{3w+1}\left(\ln\left(\frac{A_{\rm geod}}{2\pi z_{\rm cut}^2}\right) - \frac{2}{3}\right). \tag{10.58}$$

Hence the time dependent piece redshifts to zero as $(1+z_{\rm b})^{-(3w+1)}$ where $1+z_b = a(t_b)/a_*$ is the cosmological redshift. The power in the decaying term is different than for the static sphere (10.51) because $A_{\rm geod}$ increases as a^2.

So far the expressions for the area (10.57) and (10.58) are just translations from the asymptotically static coordinates to the cosmological coordinates. The difference from the previous section, in which the area of the boundary sphere is held constant, comes when one follows the time evolution by considering increasing values of the boundary time t_b. The area of the boundary co-moving sphere increases like $a^2(t_b)$, so although (the UV-independent part of) δA is positive and decreasing to zero, the total entropy increases with t_b. This brings up the important issue of the range of validity of the expressions in cosmological time. As discussed in section 10.4, if the results are to be good approximations to the results in a solitonized spacetime, one needs to restrict to surfaces that do not penetrate too deeply into the bulk, which precludes taking $R \sim t_b \sinh\chi_0$ too large. This means that the validity of (10.51) is restricted to times that are not so large that the proper radius of the boundary sphere approaches the length scale set by the soliton, that is, we need $t_b \sinh\chi_0 \ll l e^{-y_+/l}$. The situation here is similar to that in [32].

10.5 Discussion

In this paper, we have shown how to construct AdS cosmologies that satisfy the Einstein equations with a nonzero stress tensor and negative cosmological constant. Our solutions were built as foliations of lower-dimensional solutions;

the induced metric on each of these hypersurfaces itself satisfies Einstein's equations with a nonzero stress tensor. This construction has the advantage that the boundary metric of the AlAdS solution is just (conformal to) the induced metric on each hypersurface. Therefore, this construction offers us significant freedom in constructing AlAdS spacetimes with a boundary metric of our choosing.

The particular AdS cosmologies that we have constructed take the stress tensor to be that of a perfect fluid obeying the strong energy condition; for the equation of state $w = 1$, the fluid is sourced by a massless noninteracting scalar field. Moreover, we have focused on the specific case in which the spatial slices of the FRW cosmologies are negatively curved, as such FRW cosmologies then approach the Milne patch of Minkowski space at late times. The AdS cosmology constructed from these slices therefore approaches the Poincaré patch of AdS at late times, while the AdS soliton cosmology approaches the static AdS soliton.

Such solutions are especially interesting because they allow us to perturbatively calculate the behavior of physically relevant quantities at late times. For instance, we have calculated the late-time perturbation to the ADM mass of the AdS soliton cosmology, and have found this perturbation to be

$$\delta\mathcal{M} = -\frac{\Omega\mathcal{M}}{2}, \tag{10.59}$$

where $\mathcal{M}$ is the unperturbed mass and Ω is the dimensionless density parameter of the FRW cosmology, which goes to zero at late times in the solutions we are interested in. Since $\mathcal{M}$ is negative for the soliton this implies that the mass *decreases* to the mass of the static AdS soliton. Hence this result is consistent

with the energy conjecture of [117] that the AdS soliton is the lowest energy spacetime with the prescribed asymptotic structure. We found the ADM tensions to be modified in a similar manner to $\mathcal{M}$.

Moreover, our solutions also have immediate applicability to large-N, strongly coupled CFTs via the AdS/CFT correspondence. Indeed, our AdS cosmologies are dual to CFTs living on an FRW cosmology, while the massless, noninteracting scalar field in the bulk is dual to a scalar operator in the CFT with zero expectation value but nonzero source. This atypical behavior can be tied to the fact that our AdS cosmologies are singular at the Poincaré horizon. This singularity is removed by "solitonizing": introducing a compactified direction in the bulk that caps off the geometry. This cap amounts to putting the CFT in a confined phase.

As a probe of the behavior of the CFT on these FRW spacetimes, we study the entanglement entropy S of a sphere of constant radius. Using perturbative techniques to find the leading time dependent correction to the entropy, we find that the regulated entanglement entropy S_{ren} decays as a power law to its equilibrium value. The power depends on the equation of state of the fluid. Note that this decay to equilibrium is starkly different from the behavior of entanglement entropy after a quench, when the entanglement entropy *grows* to its equilibrium (thermal) value. However, note that our solutions at late time approach Poincaré AdS, which has zero temperature; this is drastically different from the end state of a quench, which in the bulk is usually modelled by the injection of energy, forming a black hole of finite temperature.

Several issues and questions are raised by these examples. First, can these solutions be generalized to include planar black holes in the bulk spacetimes?

Such solutions could conceivably be used to model the approach of a CFT on an FRW cosmology to thermal equilibrium with a nonzero temperature T, much as here we have modeled the approach to equilibrium at $T = 0$. Second, for reasons of tractability our entropy calculations have been perturbative analyses in the AdS cosmology. It would also be interesting to study the entanglement entropy of the CFT at all times, in both the AdS cosmologies and especially in the AdS soliton cosmologies, to see if there is any behavior that was not captured by our perturbative methods. Such calculations would most likely be numerical, so we leave them for the future.

Chapter 11

Conclusions and Future Directions

The AdS/CFT correspondence is the most precisely formulated manifestation of holography we have to date. In its strongest form, it states that string theory on an asymptotically (locally) AdS spacetime is equivalent to a conformal field theory that lives on (a representative of) the conformal boundary of the AdS spacetime.

In the first part of this dissertation, we used AdS/CFT as a tool to probe the behavior of heat flow in strongly coupled conformal field theories. We considered a CFT living on a background containing two black holes, which serve as heat sources and sinks. By numerically constructing the AdS bulk duals to this CFT state, we were able to compute the thermal conductivity of the CFT. We taking the CFT into a hydrodynamic regime, we found excellent agreement with the hydrodynamics approximation obtained from the fluid/gravity correspondence.

Incidentally, the bulk dual geometry consists of a black hole whose horizon is

stationary but non-Killing; such black holes are unusual objects and worthy of further study. In particular, the fluid/gravity correspondence implies that there is a regime in which these horizons are described by hydrodynamics. But it is well known that stationary fluid flows can be unstable to instabilities, which can either lead to new stationary-state flows, quasi-stationary flows, or fully developed turbulence. Thus studying the instabilities of these stationary non-Killing horizons may offer new insights into novel gravitational solutions or instabilities. We leave these results to future work.

We have also numerically constructed black droplets dual to CFTs on rotating black hole backgrounds. The CFT state exhibits no Hawking radiation to infinity; rather, the CFT is "stuck" around the black hole. This is an artefact of the strong coupling, and we have tentatively interpreted this behavior in terms of the jamming transition studied in soft condensed matter physics. It would be interesting to study this phenomenon further; with the success that AdS/CFT has had in making connections to (hard) condensed matter, it would be quite remarkable to be able to draw ties to soft condensed matter phenomena as well.

In the second part of this dissertation, we have instead probed the structure of the duality itself. Our focus was entanglement, particularly the RT and HRT formulas for entanglement entropy. We showed that there exist bulk geometries in which the HRT formula as it currently stands is ill-defined, and therefore requires modifications. We suggested some possible modifications, and explored whether or not the solutions might be to include complex extremal surfaces. We concluded that all of our suggested modifications are plausible, but in order to understand which (if any) is correct, we would need to better understand the origins of HRT.

We then turned to the question of bulk reconstruction from entanglement entropy: how much of the bulk can be reconstructed from the extremal surfaces that contribute to the HRT formula? A promising approach to bulk reconstruction is that of hole-ography, which allows us to reconstruct bulk surfaces from CFT entanglement entropy. However, we proved some general results showing that in 2+1 dimensions (or in higher dimensions with enough symmetry), the regions inside holographic screens can only be partly reconstructed via a hole-ographic approach. We interpreted the result in terms of some kind of coarse-graining, which may be related to additional degrees of freedom living on the holographic screen. It would be interesting to understand whether this interpretation is correct, and if so, precisely how the missing information is encoded on the screen. We leave this to future work.

Part III

Appendices

Appendix A

Funnels and Droplets

A.1 Flowing Funnels in Fefferman-Graham coordinates

The goal of this appendix is to describe the solutions of section 3.3 in Fefferman-Graham coordinates associated with the boundary metric (3.6). This boils down to computing the relevant coordinate transformation between these new coordinates and e.g. the BTZ coordinates t, ρ, x of (3.3). We will in fact use null Fefferman-Graham coordinates u, v, z with $u = -\kappa^{-1} e^{-\kappa t} \sinh \kappa r$, $v = \kappa^{-1} e^{\kappa t} \sinh \kappa r$ so that (using the Fefferman-Graham gauge conditions) the bulk metric takes the form

$$ds^2 = \frac{\ell^2}{z^2}\left[-\left(\frac{1}{1-\kappa^2 uv} + \mathcal{O}(\kappa^2 z^2)\right) du\, dv + \mathcal{O}(\kappa^2 z^2)\, du^2 + \mathcal{O}(\kappa^2 z^2)\, dv^2 + dz^2\right]. \tag{A.1}$$

While it is in principle possible to compute this transformation directly, we

find it simpler to use Poincaré coordinates U_P, V_P, Z_P on AdS_3, for which the AdS_3 metric is $ds^2 = \ell^2(-dU_P\, dV_P + dZ_P^2)/Z_P^2$, as an intermediate step. The point here is that the transformation from (ρ, t, x) to (U_P, V_P, Z_P) is known explicitly. We may then change conformal frame and solve for (u, v, z) in terms of (U_P, V_P, Z_P) as a power series in z and, due to the relative simplicity of the Poincaré patch metric, the result is a geometric series that is easily summed and written in closed form. Combining the two transformations then gives the desired result. In contrast, summing the series solution to go directly from (ρ, t, x) to (u, v, z) is more difficult.

Let us look for Fefferman-Graham coordinates in which the boundary metric takes the form (A.1) by making the ansatz that U_P, V_P, Z_P have a series expansion in (integer) powers of z and that the leading $\mathcal{O}(z^0)$ terms in U_P, V_P are respectively $\ell(\kappa u)^{\gamma_R}$, $\ell(\kappa v)^{\gamma_L}$, while the leading term in Z_P is $\ell\sqrt{\gamma_R\gamma_L(\kappa u)^{\gamma_L-1}(\kappa v)^{\gamma_R-1}(1-\kappa^2 uv)}\,\kappa z$. Then as stated above one finds that the result is a geometric series. Summing the series yields

$$U_P(u,v,z) = \ell(\kappa u)^{\gamma_R}\left[1 - 2\gamma_R \frac{(1-\kappa^2 uv)[1-\gamma_L(1-\kappa^2 uv)](\kappa z)^2}{4\kappa^2 uv(1-\kappa^2 uv) - [1-\gamma_L(1-\kappa^2 uv)][1-\gamma_R(1-\kappa^2 uv)](\kappa z)^2}\right], \quad \text{(A.2a)}$$

$$V_P(u,v,z) = \ell(\kappa v)^{\gamma_L}\left[1 - 2\gamma_L \frac{(1-\kappa^2 uv)[1-\gamma_R(1-\kappa^2 uv)](\kappa z)^2}{4\kappa^2 uv(1-\kappa^2 uv) - [1-\gamma_L(1-\kappa^2 uv)][1-\gamma_R(1-\kappa^2 uv)](\kappa z)^2}\right], \quad \text{(A.2b)}$$

$$Z_P(u,v,z) = \ell\sqrt{\gamma_L\gamma_R}\times \\ \frac{4(\kappa u)^{(\gamma_L+1)/2}(\kappa v)^{(\gamma_R+1)/2}(1-\kappa^2uv)^{3/2}\kappa z}{4\kappa^2uv(1-\kappa^2uv)-[1-\gamma_L(1-\kappa^2uv)][1-\gamma_R(1-\kappa^2uv)](\kappa z)^2}. \quad \text{(A.2c)}$$

It is then straightforward to read off the boundary stress tensor [103, 104] to obtain

$$T_{uu} = \frac{c}{12\pi}\kappa^2\left[\frac{\kappa^2v^2}{4(1-\kappa^2uv)^2}+\frac{\gamma_R^2-1}{4\kappa^2u^2}\right], \quad \text{(A.3a)}$$

$$T_{vv} = \frac{c}{12\pi}\kappa^2\left[\frac{\kappa^2u^2}{4(1-\kappa^2uv)^2}+\frac{\gamma_L^2-1}{4\kappa^2v^2}\right], \quad \text{(A.3b)}$$

$$T_{uv} = -\frac{c}{12\pi}\,\frac{\kappa^2}{2(1-\kappa^2uv)^2}, \quad \text{(A.3c)}$$

where as usual $c = 3\ell/2G$. Note that regularity of T_{ab} on the future horizon ($u = 0$) would require $\gamma_R = 1$, while a vanishing incoming flux at $\mathscr{I}^-$ ($u = -\infty$) would require $\gamma_L = 0$. Thus the transformations (A.2) degenerate in the Unruh state, as they suggest that V_P is independent of (u, v, z).

This subtlety disappears when one instead transforms to BTZ coordinates. The transformation from (U_p, V_p, Z_p) to (t, ρ, x) is given for $\rho > \rho_+$ by equations (2.9) of [392] and takes a simple form in terms of the null Fefferman-Graham coordinates $U = -\ell e^{-\kappa(t-x)}$, $V = \ell e^{\kappa(t+x)}$, and Z given by the implicit relation

$$\rho = \frac{\ell^2}{Z}\sqrt{1+(\Delta^2+\Sigma^2)\,(Z/\ell)^2+\Delta^2\Sigma^2(Z/\ell)^4}, \quad \text{(A.4)}$$

for $\Delta = (\rho_+ - \rho_-)/2\ell$ and $\Sigma = (\rho_+ - \rho_-)/2\ell$. We mention that the metric in

(U, V, Z) coordinates is

$$ds^2 = \frac{\ell^2}{Z^2}\left[\frac{\ell^2}{UV}\left(1+\Delta^2\Sigma^2(Z/\ell)^4\right)\,dU\,dV \right. \\ \left. +Z^2\left(\frac{\Sigma^2}{U^2}\,dU^2+\frac{\Delta^2}{V^2}\,dV^2\right)+dZ^2\right]. \quad \text{(A.5)}$$

The transformation from (U_P, V_P, Z_P) to (U, V, Z) is then

$$U_P = -\ell\frac{1-\Sigma\Delta(Z/\ell)^2}{1+\Sigma\Delta(Z/\ell)^2}\,(-U/\ell)^{2\Sigma}\,, \quad \text{(A.6a)}$$

$$V_P = \ell\frac{1-\Sigma\Delta(Z/\ell)^2}{1+\Sigma\Delta(Z/\ell)^2}\,(V/\ell)^{2\Delta}\,, \quad \text{(A.6b)}$$

$$Z_P = \frac{2\sqrt{\Sigma\Delta}\,Z}{1+\Sigma\Delta(Z/\ell)^2}\,(-U/\ell)^{\Sigma}\,(V/\ell)^{\Delta}\,. \quad \text{(A.6c)}$$

Combining (A.6) with (A.2) and using the identifications $\Delta = 2\gamma_L$ and $\Sigma = 2\gamma_R$ yields the transformation between the BTZ coordinates U, V, Z and (u, v, z). In particular, the result is well-behaved in the extremal limit $\Delta = 0$, $\Sigma = 1/2$, where it becomes

$$U(u,v,z) = \ell\kappa u\left[1-\frac{2(1-\kappa^2uv)(\kappa z)^2}{4\kappa^2uv(1-\kappa^2uv)-\kappa^2uv(\kappa z)^2}\right], \quad \text{(A.7a)}$$

$$V(u,v,z) = \ell\kappa v\,\exp\left[-(\kappa z)^2\,\times \right. \\ \left. \frac{8(1-\kappa^2uv)^2-2(2-\kappa^2uv)(1-\kappa^2uv)(\kappa z)^2}{(4(1-\kappa^2uv)-(\kappa z)^2)(4\kappa^2uv(1-\kappa^2uv)-(2-\kappa^2uv)(\kappa z)^2)}\right], \quad \text{(A.7b)}$$

$$Z(u,v,z) = \ell\sqrt{\frac{-16(1-\kappa^2uv)^3(\kappa z)^2}{(4(1-\kappa^2uv)-(\kappa z)^2)(4\kappa^2uv(1-\kappa^2uv)-(2-\kappa^2uv)(\kappa z)^2)}}. \tag{A.7c}$$

A non-degenerate (but rather implicit) transformation from Fefferman-Graham coordinates u, v, z to the global coordinates τ, R, θ of footnote 10 may then be obtained by combining eqns (A.7) with the transformation

$$U(\tau,R,\theta) = -\ell\,\frac{2R\cos\theta + (1+R^2)\cos\tau}{2R(\cos\theta-\sin\theta)+(1+R^2)(\cos\tau+\sin\tau)}, \tag{A.8a}$$

$$V(\tau,R,\theta) = \ell\exp\left[\frac{1}{2} + \frac{2R\sin\theta+(1+R^2)\sin\tau}{4R\cos\theta+2(1+R^2)\cos\tau} + \frac{2R\sin\theta-(1+R^2)\cos\tau}{2R(\cos\theta-\sin\theta)+(1+R^2)(\cos\tau+\sin\tau)}\right], \tag{A.8b}$$

$$Z(\tau,R,\theta) = \ell\frac{1-R^2}{\sqrt{[2R\cos\theta+(1+R^2)\cos\tau][2R(\cos\theta-\sin\theta)+(1+R^2)(\cos\tau+\sin\tau)]}}. \tag{A.8c}$$

which relates the BTZ coordinates U, V, Z to global coordinates τ, R, θ. We have used this procedure to generate figures 3.5 and 3.4. In particular, we were able to identify the bulk horizons $H^{\pm}$ in Fefferman-Graham coordinates from (A.7) and the known horizons in BTZ coordinates. We also identified singular surfaces of the transformation by examining the Jacobian; these are the plane $v = 0$ and the dark surface labeled CS in figure 3.4. The CS surface was numerically mapped to

the global coordinates by using equations (A.8) and is shown in figure 3.5 as a set of lines, each of which is a contour of constant uv. Note that the surface defined by these lines ends abruptly in the middle of the spacetime. This edge corresponds to the boundary singularity at $\kappa^2 uv = 1$. Further examination reveals that the CS surface contains a set of branch points in the transformation to Fefferman-Graham coordinates. To make the coordinate transformation one-to-one, we must introduce an appropriate branch cut. Our choice is indicated in figure 3.4. The transformation is one-to-one in the region between the cut, the boundary, and the CS surface. In terms of our global coordinates (figure 3.5), the cut is a surface that starts near the internal edge of the CS surface, runs to the right above the CS surface, and terminates at $\mathscr{I}^{\pm}$.

A.2 Fluid results in the black hole frame

We may transform the hydrodynamic results of section 4.3.2 to the black hole frame associated with the metric (4.41) by implementing a boundary conformal transformation and an appropriate change of coordinates. Setting $\ell_4 = 1$ the

result is

$$\mathcal{T}_{\rm loc} = \frac{y_0}{(1-\rho^2)G(\rho)}\left[\mathcal{T}_\infty + \frac{\Delta\mathcal{T}}{I}f(\rho) + \mathcal{O}(\Delta\mathcal{T}^2)\right], \tag{A.9a}$$

$$16\pi G^{(4)}T^t{}_t = \frac{y_0^3}{(1-\rho^2)^3G^3(\rho)}\left[-2\mathcal{T}_\infty^3 - \frac{6\mathcal{T}_\infty^2\Delta\mathcal{T}}{I}\,f(\rho) + \mathcal{O}(\Delta\mathcal{T}^2)\right], \tag{A.9b}$$

$$16\pi G^{(4)}T^t{}_\rho = -\frac{9\mathcal{T}_\infty^3\Delta\mathcal{T}}{I}\,\frac{y_0^3}{\sqrt{2-\rho^2}\,(1-\rho^2)^3G^3(\rho)} + \mathcal{O}(\Delta\mathcal{T}^2), \tag{A.9c}$$

$$16\pi G^{(4)}T^\rho{}_\rho = \frac{y_0^3}{(1-\rho^2)^3G^3(\rho)}\left[\mathcal{T}_\infty^3 + \frac{3\mathcal{T}_\infty^2\Delta\mathcal{T}}{I}\,(h(\rho)+f(\rho)) + \mathcal{O}(\Delta\mathcal{T}^2)\right], \tag{A.9d}$$

$$16\pi G^{(4)}T^\phi{}_\phi = \frac{y_0^3}{(1-\rho^2)^3G^3(\rho)}\left[\mathcal{T}_\infty^3 + \frac{3\mathcal{T}_\infty^2\Delta\mathcal{T}}{I}\,(-h(\rho)+f(\rho)) + \mathcal{O}(\Delta\mathcal{T}^2)\right], \tag{A.9e}$$

where $\Delta\mathcal{T}$ is again defined with respect to ∂_t, $\mathcal{T}_{\rm loc}$ is the local temperature with respect to proper time in the fluid rest frame, and setting $H(\rho) := (1-\rho^2)G(\rho)/y_0$ we have defined

$$h(\rho) = \frac{1}{2}\sqrt{2-\rho^2}\,H(\rho)H'(\rho), \tag{A.10a}$$

$$f(\rho) = \int_0^\rho \frac{1}{2\sqrt{2-\rho^2}}\left[\rho H(\rho)H'(\rho) + (2-\rho^2)\left((H'(\rho))^2 - H(\rho)H''(\rho)\right)\right]d\rho, \tag{A.10b}$$

$$I = f(1) - f(-1). \tag{A.10c}$$

A.3 The horizon-generating null congruence

We wish to study the expansion and the shear tensor associated with the null geodesic congruence that generates the future bulk horizon. Instead of solving

the geodesic equation and taking derivatives of deviation vectors, we take advantage of the fact that our system is co-homogeneity 2 to compute these quantities directly (up to a position-dependent scale factor) from the induced metric h_{IJ} on 2-dimensional surfaces tangent to the Killing fields $\partial_t, \partial_\phi$. We then compute the affine parameter λ along these geodesics from the Raychaudhuri equation as explained below.

Recall that we consider a future event horizon $\mathcal{H}$ of an AlAdS_4 spacetime with two commuting KVFs ∂_t and ∂_ϕ. The horizon is 3-dimensional, with a two-dimensional space of generators. So long as the horizon is not itself Killing, we see that any two generators are related by the actions of ∂_t and ∂_ϕ.

Choose one horizon generator with affine parameter λ. We can extend λ to a scalar function on $\mathcal{H}$ by requiring it to be invariant under $\partial_t, \partial_\phi$. In our case we can take $\lambda = \lambda(w)$ since w is indeed invariant under both KVFs and is a good coordinate on $\mathcal{H}$.

Let k^a be the tangent to our generator associated with affine parameter λ. Note that since $\partial_t, \partial_\phi$ are also tangent to the horizon we have $k \perp \partial_t, \partial_\phi$. We also choose any ℓ^a satisfying $\ell^a k_a = -1$ and $\ell \perp \partial_t, \partial_\phi$. We then extend k, ℓ to vector fields defined across all of $\mathcal{H}$ by requiring them to be invariant under $\partial_t, \partial_\phi$. We then define a 'deformation tensor' $\hat{B}_{ab}$ associated with flow along the horizon generators by projecting $B_{ab} = \nabla_b k_a$ onto the space orthogonal to k, ℓ. See e.g. appendix F of [195].

Let us note that since $\partial_t, \partial_\phi$ commute they are surface-forming, and k is orthogonal to this surface. So k is hypersurface orthogonal and the twist $\hat{\omega}_{ab} = \hat{B}_{[ab]}$ vanishes. Thus $\hat{B}_{ab} = \hat{B}_{ba}$. We will use this symmetry below.

Deviation vector fields for the horizon-generating null congruence are defined by the property that, when evaluated on a given horizon generator γ, they point to the same horizon generator γ' for all λ. Let us consider a deviation vector field η orthogonal to both k and ℓ. Then (see e.g. appendix F of [195]) η satisfies

$$\eta^c \hat{B}^a_c = k^c \nabla_c \eta^a. \tag{A.11}$$

Since translations along $\partial_t, \partial_\phi$ map one geodesic to another, both ∂_t and ∂_ϕ are deviation vectors. And both are orthogonal to k, ℓ. So we may choose $\eta_I = \partial_I$ for $I = t, \phi$. Here the η_I are two spacetime vectors, not the components of a single vector.

Let us now consider the set of associated inner products

$$h_{IJ} = \eta_I \cdot \eta_J := \eta^a_I g_{ab} \eta^b_J. \tag{A.12}$$

In any coordinate system, $\eta^a_t = \partial_t x^a$ and $\eta^a_\phi = \partial_\phi x^a$. So in particular in the coordinate system $y, w, \tilde{t}, \phi$ we have (since $\partial_{\tilde{t}} = \partial_t$)

$$h_{IJ} = g_{IJ}; \tag{A.13}$$

i.e., this is just the induced metric on the 2-plane generated by $\partial_t, \partial_\phi$ in coordinates $(\tilde{t}, \phi)$ or, equivalently for this purpose, coordinates (t, ϕ). So it is easy to read off from our numerics. But note that h_{IJ} was defined to be a set of scalars, so covariant derivatives of h_{IJ} are just coordinate derivatives.

The evolution of h_{IJ} (with respect to λ, or equivalently with respect to w) is

governed by (A.11). Using (A.11) we compute

$$\begin{aligned}\frac{d}{d\lambda}h_{IJ} = & \qquad\qquad k^c\nabla_c h_{IJ} = k^c\nabla_c\left(\eta_I\cdot\eta_J\right)\\ &= \hat{B}^a_c\eta^c_I\eta_{Ja} + \eta^a_I\hat{B}^c_a\eta_{Jc}\\ &= 2\hat{B}_{ac}\eta^a_I\eta^c_J = 2\hat{B}_{IJ}, \qquad\qquad (A.14)\end{aligned}$$

where in the last step as for (A.13) above we have used $\hat{B}_{IJ}$ to denote the $\tilde{t},\phi$ components of $\hat{B}_{ac}$ in the particular coordinate system $y, w, \tilde{t}, \phi$ (or equivalently the t,ϕ components).

The deformation tensor $\hat{B}^{ab}$ is by construction orthogonal to k,ℓ. Thus we may write $\hat{B}^{ab}\partial_a\partial_b = \hat{B}^{IJ}\partial_I\partial_J$. Furthermore, from (A.13) we have

$$\hat{B}_{IJ} = g_{Ia}\hat{B}^{ab}g_{Jb} = g_{IK}\hat{B}^{KL}g_{LJ} = h_{IK}\hat{B}^{KL}h_{LJ}, \qquad (A.15)$$

where K, L also range over ϕ, t. Thus we may safely use h_{IJ} and its inverse h^{IJ} to raise and lower indices I, J on $\hat{B}_{IJ}$.

Now, the components $\hat{B}_{IJ}$ are essentially exponentials of integrated versions of the expansion and shear. In particular, introducing the projector $Q^a{}_b$ onto the subspace orthogonal to k,ℓ (i.e., onto the space spanned by $\partial_t, \partial_\phi$) we have

$$\theta = Q_{ab}\hat{B}^{ab} = h_{IJ}\hat{B}^{IJ} = h^{IJ}\hat{B}_{IJ}, \qquad (A.16)$$

and

$$\hat{\sigma}_{IJ} = \hat{B}_{IJ} - \frac{1}{D-2}\theta h_{IJ}, \qquad (A.17)$$

where $D = 4$ for AdS_4.

Of course, it remains to actually find the affine parameter λ used in the above definitions. We choose to calculate λ from Raychaudhuri's equation which, in the present context, may be written

$$\frac{d\theta}{d\lambda} = -\hat{B}_{ab}\hat{B}^{ab} - Q^{ab}R_{acbd}k^c k^d. \tag{A.18}$$

As usual, the symmetries of the Riemann tensor imply that $Q^{ab}R_{acbd}k^c k^d = g^{ab}R_{acbd}k^c k^d$, which is proportional to $R_{cd}k^c k^d$. But $R_{ab} \propto g_{ab}$ by the equations of motion, so the final term in (A.18) vanishes. Since $\hat{B}^{ab}$ is orthogonal to both k and ℓ we may then write

$$\frac{d\theta}{d\lambda} = -\hat{B}_{IJ}\hat{B}^{IJ}. \tag{A.19}$$

In terms of a general coordinate w along the generators, (A.19) may be rearranged to yield

$$\lambda'' = \lambda'\left(h^{IJ}h'_{IJ}\right)^{-1}\left[\frac{1}{2}h^{I_1I_2}h^{J_1J_2}h'_{I_1J_1}h'_{I_2J_2} + \frac{d}{dw}\left(h^{IJ}h'_{IJ}\right)\right] := \lambda' Z(w), \tag{A.20}$$

where $'$ denotes the coordinate derivative d/dw and the last equality defines $Z(w)$. This equation is then easily solved for λ in terms $Z(w)$, which is relatively straightforward to extract from the numerics.

A.4 Near-Boundary Expansion for the Nonrotating Droplet

In this appendix, we list the expansions of the metric functions near the conformal boundary $x = 1$ for the nonrotating ($\beta = 0$) droplet, as well as the form of the Fefferman-Graham expansion (5.26). For the metric functions, we have

$$T(x,y) = 1 + (1-y)\left(-6(1-x)^2 + 6(1-x)^3 + \frac{67-408y^2}{14}(1-x)^4\right) + t_5(y)(1-x)^5 + \mathcal{O}(1-x)^6, \quad \text{(A.21a)}$$

$$A(x,y) = 1 + (1-y)\left(-6(1-x)^2 + 6(1-x)^3 + \frac{67-296y^2}{14}(1-x)^4\right) + a_5(y)(1-x)^5 + \mathcal{O}(1-x)^6, \quad \text{(A.21b)}$$

$$S(x,y) = C(x,y) = 1 + (1-y)\left(2(1-x)^2 - 2(1-x)^3 + \frac{5(19+8y^2)}{14}(1-x)^4\right) + s_5(y)(1-x)^5 + \mathcal{O}(1-x)^6, \quad \text{(A.21c)}$$

$$B(x,y) = 1 + \frac{4}{7}(1-y)(5+y)\left((1-x)^4 - 2(1-x)^5\right) + \mathcal{O}(1-x)^6, \tag{A.21d}$$

$$F(x,y) = -(1-y)(1-x)^2\left[1 + (1-x) + \frac{211-192y}{28}(1-x)^2 + \mathcal{O}(1-x)^3\right], \tag{A.21e}$$

$$G(x,y) = 0. \tag{A.21f}$$

The coefficients $t_5(y)$, $a_5(y)$, and $s_5(y)$ cannot be determined uniquely, but must satisfy the relationships

$$t_5(y) = \frac{7(1-2y)a_5(y) - (1-y)(656y - 960y^2 - 14ya_5'(y))}{7(1-2y)}, \tag{A.22a}$$

$$s_5(y) = -\frac{14(1-2y)a_5(y) + (1-y)(8(55 - 265y + 266y^2) + 14ya_5'(y))}{21(1-2y)}. \tag{A.22b}$$

For the transformation to Fefferman-Graham coordinates, we have

$$1 - x^2 = \tilde{z}\sqrt{1-\tilde{y}}\left[1 - \frac{1-\tilde{y}^2}{4}\tilde{z}^2 + \frac{3(1-\tilde{y})^2(3+6\tilde{y}+19\tilde{y}^2)}{224}\tilde{z}^4 + \mathcal{O}(\tilde{z})^6\right], \tag{A.23a}$$

$$y = \tilde{y}\left[1 + (1-\tilde{y})^2\tilde{z}^2 + \frac{(1-\tilde{y})^3(1-3\tilde{y})}{2}\tilde{z}^4 - \frac{(1-\tilde{y})^4(4+19\tilde{y}-44\tilde{y}^2)}{21}\tilde{z}^6 + \mathcal{O}(\tilde{z})^7\right]. \tag{A.23b}$$

Appendix B

Holographic Entanglement

B.1 Geodesic Approximation for Charged Operators

Here we derive the form of the action (6.25) in the limit of large m, following [261]. The Green's function for the field ϕ with mass and charge m and q should be a Green's function of the Klein-Gordon operator $H = (-i\partial - qA)^2 + m^2 = (p - qA)^2 + m^2$; we can represent this Green's function as

$$\frac{-i}{H} = \int_0^\infty e^{-iNH}\, dN, \tag{B.1}$$

so that using the standard path integral construction, we get

$$\left\langle x \left| \frac{-i}{H} \right| y \right\rangle = \int_0^\infty dN \int \mathcal{D}x\, \mathcal{D}p \, \exp\left\{ i \int_0^1 \left[\dot{x}p - N((p - qA)^2 + m^2) \right] d\lambda \right\}. \tag{B.2}$$

We can interpret N as a field in some appropriate gauge-fixing; we can make this explicit by introducing the gauge-fixing condition and determinant. Then we obtain

$$\left\langle x\left|\frac{-i}{H}\right|y\right\rangle = \int \mathcal{D}N\,\mathcal{D}x\,\mathcal{D}p\,\Delta(x)\,\exp\left\{i\int_0^1 \left[\dot{x}p - N((p-qA)^2+m^2)\right]d\lambda\right\}, \tag{B.3}$$

where now N is a field to be integrated over. Now, in the WKB approximation, we can integrate out the fields N and p by replacing them in the action with their on-shell values. Their equations of motion are

$$(p-qA)^2 + m^2 = 0, \tag{B.4a}$$

$$\dot{x} - 2N(p-qA) = 0, \tag{B.4b}$$

so their on-shell values are

$$p = \frac{m\dot{x}}{\sqrt{-\dot{x}^2}} + qA, \tag{B.5a}$$

$$N = \frac{\sqrt{-\dot{x}^2}}{2m}. \tag{B.5b}$$

The correlator then becomes

$$\left\langle x\left|\frac{-i}{H}\right|y\right\rangle = \int \mathcal{D}x\,(\cdots)\exp\left\{-\int_0^1 \left[m\sqrt{\dot{x}^2} - iqA\dot{x}\right]d\lambda\right\}, \tag{B.6}$$

where $(\cdots)$ represents functional determinants that we can neglect at leading order in the WKB approximation. Approximating the path integral over x using

the saddle point method, we get

$$\left\langle x\left|\frac{-i}{H}\right|y\right\rangle \sim e^{-mI[x_{\rm cl}]}, \tag{B.7}$$

where $x_{\rm cl}$ is a solution to the equations of motion that come from the action

$$I[x] = \int \left[\sqrt{\dot{x}^2} - \frac{iq}{m}A\dot{x}\right] d\lambda. \tag{B.8}$$

This last expression is precisely (6.25) used in the text. Note that it differs from the action used in [227] by a crucial factor of i in the second term.

B.2 Evaluation of the Elliptic Integrals

Our notation in this appendix follows [393]. The expressions for Δt and I in terms of elliptic integrals are

$$\begin{aligned}\Delta t = \frac{2z_0\mathcal{Q}}{\alpha^2\sqrt{\alpha^2-\mathcal{Q}^2}}\frac{1}{\sqrt{\Delta_{21}}}\Bigg\{&\frac{\Delta_{20}}{(w_2-1)\Delta_{2-}\Delta_{2+}}\left[F(\psi|m)-K(m)\right]\\ &+\frac{1-w_0}{(1-w_-)(w_+-1)(w_2-1)}\left[\Pi\left(\frac{w_2-1}{\Delta_{21}};\psi\middle|m\right)-\Pi\left(\frac{w_2-1}{\Delta_{21}}\middle|m\right)\right]\\ &+\frac{\Delta_{0-}}{(1-w_-)\Delta_{+-}\Delta_{2-}}\left[\Pi\left(\frac{\Delta_{2-}}{\Delta_{21}};\psi\middle|m\right)-\Pi\left(\frac{\Delta_{2-}}{\Delta_{21}}\middle|m\right)\right]\\ &+\frac{\Delta_{0+}}{(w_+-1)\Delta_{+-}\Delta_{2+}}\left[\Pi\left(\frac{\Delta_{2+}}{\Delta_{21}};\psi\middle|m\right)-\Pi\left(\frac{\Delta_{2+}}{\Delta_{21}}\middle|m\right)\right]\Bigg\},\end{aligned} \tag{B.9a}$$

$$I = \frac{2i}{\sqrt{\Delta_{21}}}\Bigg\{-\frac{h(w_2)}{w_2\Delta_{2-}\Delta_{2+}}\left[K(m)-F(\psi|m)\right] - \frac{h(w_-)}{w_-\Delta_{2-}\Delta_{+-}}\left[\Pi\left(\frac{\Delta_{2-}}{\Delta_{21}}\middle|m\right)-\Pi\left(\frac{\Delta_{2-}}{\Delta_{21}};\psi\middle|m\right)\right] + \frac{h(w_+)}{w_+\Delta_{2+}\Delta_{+-}}\left[\Pi\left(\frac{\Delta_{2+}}{\Delta_{21}}\middle|m\right)-\Pi\left(\frac{\Delta_{2+}}{\Delta_{21}};\psi\middle|m\right)\right] + \frac{h(0)}{w_2w_+w_-}\Pi\left(\frac{w_2}{\Delta_{21}}\middle|m\right)\Bigg\} + \frac{2ih(0)}{\sqrt{\Delta_{21}}\,w_2w_+w_-}\Pi\left(\frac{w_2}{\Delta_{21}};\arctan\sqrt{\frac{\Delta_{21}}{w_1-w_{\rm UV}}}\middle|m\right) + I_{\rm ct}, \quad \text{(B.9b)}$$

where

$$\tan\psi \equiv \sqrt{\frac{\Delta_{21}}{w_1}}, \quad \text{(B.10a)}$$

$$m \equiv \frac{\Delta_{23}}{\Delta_{21}}, \quad \text{(B.10b)}$$

$$\Delta_{ij} \equiv w_i - w_j, \quad \text{(B.10c)}$$

$$w_0 \equiv 1 + \frac{\mathcal{E}}{\mathcal{Q}}, \quad \text{(B.10d)}$$

$$h(w) \equiv \frac{\ell}{\alpha^2\sqrt{\alpha^2-\mathcal{Q}^2}}\left[1+w-\alpha^2w^2-\mathcal{Q}w(\mathcal{E}+\mathcal{Q}(1-w))\right]. \quad \text{(B.10e)}$$

These expressions have branch points wherever $m = 1$ or ∞, corresponding to points where $w_1 = w_2$ or $w_1 = w_3$.

In the scaling limit (6.45) with $\tilde{q} = 1$, the above expressions reduce to

$$\frac{2\Delta t}{\beta} = -\frac{8\cdot 3^{1/4}\,i\,b^{2/3}\left[K(\widetilde{m})-\Pi(n|\widetilde{m})\right]}{\pi\left(8\cdot 3^{2/3}e^{i\pi/3}a-\sqrt{3}\,e^{-i\pi/3}b^{2/3}\right)\sqrt{16\cdot 3^{1/6}e^{-5i\pi/6}\,a\,b^{1/3}+2e^{-i\pi/6}b}}, \quad \text{(B.11)}$$

$$I = \ell \left\{ \frac{4\, b^{2/3}\, [K(\widetilde{m}) - \Pi(n|\widetilde{m})]}{3^{1/4} \left(8 \cdot 3^{2/3} e^{i\pi/3} a - \sqrt{3}\, e^{-i\pi/3} b^{2/3}\right) \sqrt{16 \cdot 3^{1/6} e^{-5i\pi/6}\, a\, b^{1/3} + 2 e^{-i\pi/6} b}} \right.$$
$$\left. -2\sqrt{\frac{2}{3}} \operatorname{arctanh} \sqrt{\frac{2}{3}} \right\}, \quad \text{(B.12)}$$

where

$$b = 1 + \sqrt{1 + 512\sqrt{3}\, a^3}, \quad \text{(B.13a)}$$

$$\widetilde{m} = \frac{\sqrt{3}(8 \cdot 3^{1/6} a + b^{2/3})}{8 \cdot 3^{2/3} e^{-i\pi/3} a + \sqrt{3}\, e^{i\pi/3} b^{2/3}}, \quad \text{(B.13b)}$$

$$n = \frac{8 \cdot 3^{1/6} e^{-i\pi/6} a + e^{i\pi/6} b^{2/3}}{8 \cdot 3^{2/3} e^{-i\pi/3} a + \sqrt{3}\, e^{i\pi/3} b^{2/3}}. \quad \text{(B.13c)}$$

Next, consider the indefinite version of the integral (6.12),

$$\mathcal{I}_\alpha(w) = \frac{i}{2\alpha} \int \frac{dw}{w^2 [(1-w)(w-w_+)(w-w_-)]^{1/2}}. \quad \text{(B.14)}$$

We are interested in the logarithmic divergence that comes from $w = 1$ for small $\epsilon = 2 - \alpha^2$. We can extract it by noting that (B.14) can be written in terms of Elliptic integrals as

$$\frac{2\alpha}{i} \mathcal{I}_\alpha(w) = -\frac{1}{w w_-} \left(\frac{(1-w)(w-w_-)}{w - w_+} \right)^{1/2} - \frac{(w_+ - 1)^{1/2}}{w_+ w_-} E(\hat{\psi}|\hat{m})$$
$$+ \frac{(w_+ + 1)}{w_+^2 (w_+ - 1)^{1/2}} F(\hat{\psi}|\hat{m}) + \frac{[w_- + w_+(w_- + 1)]}{w_- w_+^2 (w_+ - 1)^{1/2}} \Pi(\hat{n}; \hat{\psi}|\hat{m}), \quad \text{(B.15)}$$

where

$$\tan\hat{\psi} = \left(\frac{w_+ - 1}{1 - w} \right)^{1/2}, \qquad \hat{m} = \frac{w_+ - w_-}{w_+ - 1}, \qquad \hat{n} = \frac{w_+}{w_+ - 1}. \quad \text{(B.16)}$$

For small ϵ, the dominant contribution to the integral comes from $w = 1$, so we can drop the first term in (B.15) and let $\hat{\psi} = \pi/2$ for all $w_+ > 1$. Then the incomplete Elliptic integrals reduce to complete ones, i.e. $F(\pi/2|x) = K(x)$, $E(\pi/2|x) = E(x)$, $\Pi(x; \pi/2|y) = \Pi(x|y)$. Using the asymptotics for small z

$$E\left(\frac{a}{z}\right) = i\frac{a^{1/2}}{z^{1/2}} + O(z^{1/2}), \tag{B.17}$$

$$K\left(\frac{a}{z}\right) = -i\frac{z^{1/2}}{2a^{1/2}}\log\left(-\frac{16a}{z}\right) + O(z^{3/2}), \tag{B.18}$$

$$\Pi\left(\frac{b}{z}\middle|\frac{1}{z}\right) = \frac{z^{1/2}}{2(b-1)^{1/2}}\left[\log\left(\frac{\sqrt{b-1}+i}{\sqrt{b-1}-i}\right) - i\pi\right], \tag{B.19}$$

we arrive at (6.14).

B.3 Shell Stress Tensors

We now compute the stress tensors on the null shells of section 7.2. Following [302], we embed each shell in each associated patch of the spacetime via parametric relation $x^\alpha = X^\alpha(y^a)$, where the y^a are a set of d coordinates on the shell and the x^α are the spacetime coordinates of the patch in which the shell is to be embedded. We take $d-1$ of the y^a to be the transverse coordinates x^i associated with the $\mathbb{R}^{d-1}$ translation symmetry and the remaining coordinate to be some parameter η along the null direction. The parameter η is arbitrary and need not be affine; indeed, for a non-trivial null shell the affine parameter is discontinuous across the shell and one cannot take η to be affine on both sides.

We also introduce tangent vectors

$$e_i^\alpha \equiv \frac{\partial X^\alpha}{\partial x^i}, \quad k^\alpha \equiv e_\eta^\alpha \equiv \frac{\partial X^\alpha}{\partial \eta}, \tag{B.20}$$

and an auxiliary null vector N^α which satisfies $N_\alpha k^\alpha = -1$. Note that both k^α and N^α are orthogonal to the transverse tangent vectors e_i^α.

The relevant results from [302] are as follows. The induced metric on a shell is

$$\sigma_{ij} = g_{\alpha\beta}\left(X^\alpha\right) e_i^\alpha e_j^\beta, \tag{B.21}$$

which for regularity is required to be the same when calculated from either side of a given shell. The transverse extrinsic curvature of a shell is

$$C_{ab} \equiv -N_\alpha e_a^\beta \nabla_\beta e_b^\alpha, \tag{B.22}$$

which need not be the same on the two sides. The difference in transverse curvature across the shell gives the shell stress tensor. It is convenient to decompose this tensor into a surface energy density μ, energy current j^i, and pressure p:

$$\mu = -\frac{1}{8\pi G_N}\sigma^{ij}\left(C_{ij}^+ - C_{ij}^-\right), \tag{B.23a}$$

$$j^i = \frac{1}{8\pi G_N}\sigma^{ij}\left(C_{j\eta}^+ - C_{j\eta}^-\right), \tag{B.23b}$$

$$p = -\frac{1}{8\pi G_N}\left(C_{\eta\eta}^+ - C_{\eta\eta}^-\right), \tag{B.23c}$$

where the $+(-)$ superscripts imply that the quantity is calculated on the side of the shell into (away from) which k^α points, and G is the full $(d+1)$-dimensional

Newton's constant.

Since our shells lie on horizons $r = r_+$, the induced metric on each shell is just

$$ds^2_{\text{shell}} = r_+^2 \, d\vec{x}^2_{d-1}. \tag{B.24}$$

To construct the single-shell spacetime of figure 7.2 with the edges $\mathcal{E}$ of $\mathscr{I}_{\text{dS}}$ at advanced time $v_I = v_0$, we use the embeddings

$$r = r_+, \quad v_I = \eta_A, \quad v_{II} = \frac{1}{\kappa_{II}} \, g_A \left(\kappa_I \eta_A \right), \tag{B.25}$$

where $\kappa_n \equiv |f_n'(r_+)|/2$ are the surface gravities of each horizon, η_A is a parameter along the generators of the shell, and as stated in the main text $g_A(x)$ is an arbitrary continuous and monotonically increasing function with range $(-\infty, \infty)$ and domain (v_0, ∞). The density, current, and pressure of shell A are then

$$\mu_A = \frac{d-1}{8\pi G_N r_+} \left[\frac{\kappa_{II}}{\kappa_I g_A'(\kappa_I \, \eta_A)} - 1 \right], \tag{B.26a}$$

$$j_A^i = 0, \tag{B.26b}$$

$$p_A = \frac{\kappa_I}{8\pi G_N} \left[1 + g_A'(\kappa_I \eta_A) - \frac{g_A''(\kappa_I \eta_A)}{g_A'(\kappa_I \eta_A)} \right]. \tag{B.26c}$$

To instead construct the doubly-patched spacetime shown in the lower panel of figure 7.4, we leave patches Ib and II and shell A untouched (that is, patch Ib is just the corresponding piece of the original patch I with $\ell_{Ib} = \ell_I$), and we take patch Ia to be the exterior of a Schwarzschild-AdS black hole with horizon size r_+ and AdS radius ℓ_{Ia}. The three patches we stitch together are shown in figure B.1,

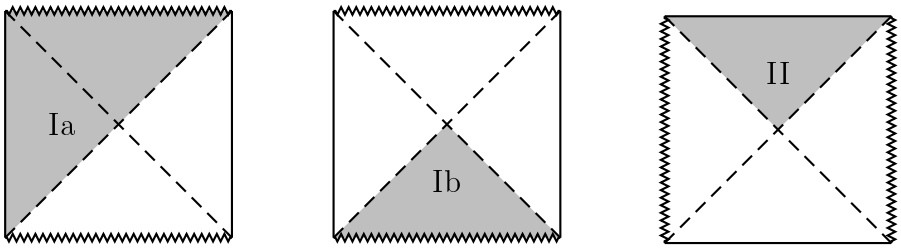

Figure B.1: Conformal diagrams from which we cut our (shaded) regions Ia, Ib, and II.

and their metrics are as in (7.3) with

$$f_{Ia}(r) = \frac{r^2}{\ell_{Ia}^2}\left(1 - \left(\frac{r_+}{r}\right)^d\right), \tag{B.27a}$$

$$f_{Ib}(r) = -\frac{r^2}{\ell_{Ib}^2}\left(\left(\frac{r_+}{r}\right)^d - 1\right), \tag{B.27b}$$

$$f_{II}(r) = -\frac{r^2}{\ell_{II}^2}\left(1 - \left(\frac{r_+}{r}\right)^d\right). \tag{B.27c}$$

In terms of the Eddington-Finkelstein coordinates (7.5), the embeddings of shell B in patches Ia and Ib are

$$r = r_+, \quad u_{Ia} = -\frac{1}{\kappa_{Ia}} \ln\left(-\kappa_{Ia}\eta_B\right), \quad u_{Ib} = \frac{1}{\kappa_{Ib}} g_B\left(\kappa_{Ia}\eta_B\right), \tag{B.28}$$

where as for shell A, $g_B(x)$ is an arbitrary continuous and monotonically increasing function that maps $(-\infty, \infty) \mapsto (-\infty, \infty)$. Note that with this embedding, η_B is an affine parameter along the shell with respect to the metric of patch Ia. The

density, current, and pressure of shell B are then

$$\mu_B = \frac{d-1}{8\pi G_N r_+}\left[\kappa_{Ia}\eta_B + \frac{\kappa_{Ib}}{\kappa_{Ia}\, g_B'(\kappa_{Ia}\eta_B)}\right], \tag{B.29a}$$

$$j_B^i = 0, \tag{B.29b}$$

$$p_B = \frac{\kappa_{Ia}}{8\pi G_N}\left[\frac{g_B''(\kappa_{Ia}\eta_B)}{g_B'(\kappa_{Ia}\eta_B)} - g_B'(\kappa_{Ia}\eta_B)\right]. \tag{B.29c}$$

Note that p_B vanishes only if $g_B(x) = \text{const.}$ or $g_B(x) = -\ln(x+c)$, neither of which is compatible with the continuity and monotonicity of g_B. So as claimed in footnote 5, shell B cannot be pressureless, and this spacetime is not a limiting case of AdS-Vaidya.

Nevertheless, the null energy condition can be satisfied for an appropriate choice of parameters. Indeed, for any $d \geq 2$, let

$$\kappa_{Ia} r_+ = 1, \quad \kappa_{Ib} r_+ = 1, \quad g_B(x) = \operatorname{arcsinh}(x). \tag{B.30}$$

Then we find that

$$\mu_B + p_B = \frac{d}{8\pi G_N r_+} P(\kappa_{Ia}\eta_B)\left(1 - \frac{\Delta(\kappa_{Ia}\eta_B)}{d}\right), \tag{B.31}$$

where

$$P(x) = x + \sqrt{1+x^2} \quad \text{and} \quad \Delta(x) = 1 + \frac{1}{1+x^2} \tag{B.32}$$

satisfy $P(x) > 0$ and $\Delta(x) \leq 2$ everywhere. It then follows that $\mu_B + p_B \geq 0$ for all $d \geq 2$.

B.4 Regulated Wormholes

This appendix considers simple models of the regulated wormholes mentioned in sections 7.3 and 7.4 in which inflation ends on a finite surface, after which the wormhole collapses to a singularity. The simplification made here is that sections 7.3 and 7.4 required this singularity to be everywhere of Kasner or of big crunch type (see footnote 7), but the examples below will violate this condition at the regulated analogues of the edges $\mathcal{E}$ of $\mathscr{I}_{\rm dS}$. The point is that it is convenient to retain symmetry of patch II under the Killing field ξ of section 7.2. But since the orbits of ξ approach $\mathcal{E}$, this means that surfaces of constant scale factor will also approach $\mathcal{E}$ in the regulated spacetimes. The singularity of our regulated spacetimes thus fails to be either Kasner-like or of big crunch type at $\mathcal{E}$.

Retaining symmetry along ξ takes the above singularity to lie at a proper time τ along the worldline of any freely falling observer chosen to start at $\tau = 0$ from the point labeled $\mathcal{C}$ on the past boundary of figure B.2. In the limit $\tau \to \infty$, we recover the original AdS-dS-wormhole.

Such regulated wormholes can be constructed as in Section 7.2 above by replacing the metric in patch II with

$$ds^2 = -d\rho^2 + R^2(\rho)dt^2 + X^2(\rho)d\vec{x}^2_{d-1}, \tag{B.33}$$

where $\rho \in [0, \tau)$ is the proper time along worldlines of freely falling observers with constant t, x^i. Near $\rho = 0$, we impose that $X = r_+ + \cdots$ and $R = \kappa_{II}\rho + \cdots$ where $\cdots$ represent terms that vanish as $\rho \to 0$. Then to good approximation $\rho = 0$ remains a horizon with surface gravity κ_{II}, and in particular the regulated

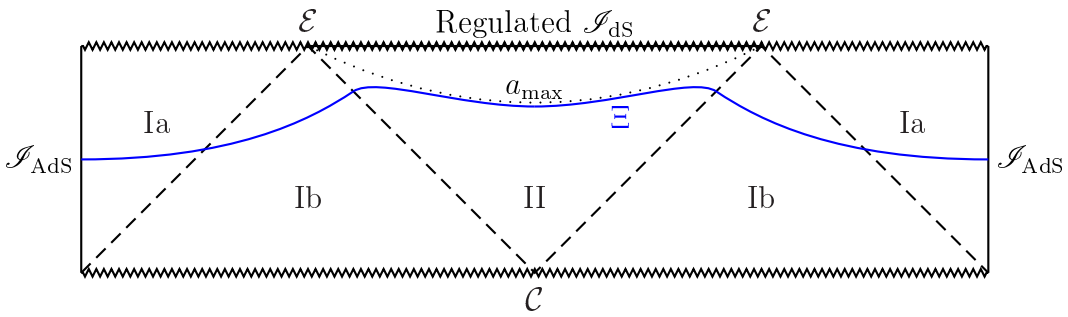

Figure B.2: A regulated AdS-dS-wormhole with a finite amount of inflation followed by collapse to a singularity. The dotted line labeled $a_{\rm max}$ indicates the surface on which the effective scale factor (B.35) in patch II reaches a maximum; this slice serves as an accumulation surface for wormhole-spanning extremal surfaces. In the cut-and-paste geometry, the proper distance between any point in patch II and either of the boundary points $\mathcal{E}$ is infinite; this is an artefact of the cut-and-paste construction, and will no longer be true for appropriately smoothed out null shells. Such smoothed cases lead to the existence of finite-area HHRT surfaces such as the one labeled Ξ (solid line, blue in color version).

spacetime (B.33) can be patched into the wormhole using the same null shells (with precisely the same stress tensor) as in section 7.2. In these coordinates, the patch II metric (7.3) of the original unregulated spacetime corresponds to

$$R(\rho) = \frac{r_+}{\ell} \tanh\left(\frac{d\rho}{2\ell}\right) \cosh^{2/d}\left(\frac{d\rho}{2\ell}\right), \quad X(\rho) = r_+ \cosh^{2/d}\left(\frac{d\rho}{2\ell}\right). \tag{B.34}$$

It is straightforward to identify extremal surfaces for which t and $d-2$ of the $\vec{x}_{d-1}$ are constant. These are the analogue in region II of surfaces found by Hartman and Maldacena [229] to be attractors for more generic extremal surfaces in the two-sided planar AdS-Schwarzschild black hole in the limit where both boundaries of the extremal surface are anchored to very late times on the two AdS boundaries. The area of our highly symmetric surfaces is governed in region

II by the effective scale factor

$$a_{\text{eff}}(\rho) = R(\rho)X^{d-2}(\rho), \tag{B.35}$$

and extremal such surfaces lie at extrema of $a_{\text{eff}}(\rho)$. In parallel with [229], in the fully-regulated case we expect one of these extrema to be a late-time attractor with the actual wormhole-spanning extremal surface staying very close to one of these surfaces across most of region II, as shown in figure B.2. The maximin argument of section 7.3 suggests that the desired extremal surfaces in fact accumulate along the global maximum of $a_{\text{eff}}(\rho) = a_{\max}$. In fact, note that our cut-and-paste construction renders the area of the attractor surface $a_{\max}$ infinite, since any point in patch II is an infinite distance from either of the boundary points marked $\mathcal{E}$. As a result, the wormhole-spanning extremal surfaces in this geometry still have infinite area. However, it is clear that this is simply an artefact of our patching procedure, which causes $\mathcal{E}$ to violate the conditions of footnote 7. By smoothing out the null shells, the distance to any $\mathcal{E}$ from patch II becomes finite, and thus so does the area of the $a_{\max}$. These smoothed-out regulated AdS-dS-wormholes thus have HHRT surfaces with finite areas that grow without bound as we increase $a_{\max}$.

We now construct explicit examples of the above (unsmoothed) regulated wormholes and verify the above conjecture concerning wormhole-spanning extremal surfaces. To do so we couple gravity to a scalar field ϕ, so that the action

is

$$S = \frac{1}{16\pi G_N}\int d^dx\sqrt{-g}\,R - \int d^dx\sqrt{-g}\left(\frac{1}{2}\,g^{\mu\nu}\nabla_\mu\phi\nabla_\nu\phi + V(\phi)\right). \tag{B.36}$$

We set $\phi = \phi(\rho)$ and take the metric to be (B.33), in which the coordinate ρ plays the role of a proper time. The equations of motion obtained from the action (B.36) can be rearranged into

$$\frac{2X'R'}{XR} + (d-2)\left(\frac{X'}{X}\right)^2 - \frac{8\pi G_N}{d-1}\left((\phi')^2 + 2V(\phi)\right) = 0, \tag{B.37a}$$

$$\frac{X''}{X} - \frac{X'R'}{XR} + \frac{8\pi G_N}{d-1}(\phi')^2 = 0, \tag{B.37b}$$

$$\frac{R''}{R} + (d-3)\frac{X'R'}{XR} - (d-2)\left(\frac{X'}{X}\right)^2 + \frac{8\pi G_N}{d-1}(\phi')^2 = 0, \tag{B.37c}$$

$$\phi'' + \left(\frac{R'}{R} + (d-1)\frac{X'}{X}\right)\phi' + V'(\phi) = 0. \tag{B.37d}$$

Note that (B.37a) is a constraint equation, while the other three are dynamical. As usual, the constraint is conserved by the dynamical equations, so that there are only three independent equations that must be solved.

Solutions to (B.37) will be characterized by some ρ at which X, R, and ϕ become singular; without loss of generality we take this time to be $\rho = 0$. Then one can show that for polynomial $V(\phi)$, the solutions near such singular points

behave like

$$X(\rho) = \rho^r \left[X_{00} + \sum_{n=1}^{\infty} \sum_{m=0}^{nN} X_{n,m} \rho^{2n} \left(\ln \rho/\rho_0 \right)^m \right], \tag{B.38a}$$

$$R(\rho) = \rho^{1-3r} \left[R_{00} + \sum_{n=1}^{\infty} \sum_{m=0}^{nN} R_{n,m} \rho^{2n} \left(\ln \rho/\rho_0 \right)^m \right], \tag{B.38b}$$

$$\phi(\rho) = \phi_{00} + \phi_{01} \ln \rho/\rho_0 + \sum_{n=1}^{\infty} \sum_{m=0}^{nN} \phi_{n,m} \rho^{2n} \left(\ln \rho/\rho_0 \right)^m, \tag{B.38c}$$

where ρ_0 is some arbitrary scale, the integer N is the highest power of ϕ appearing in $V(\phi)$, and r, X_{00}, R_{00}, ϕ_{00}, and ϕ_{01} are free parameters subject to the constraint $8\pi G_N \phi_{01}^2 = 6r(1-2r)$.

The near-horizon behavior requires $r = 0$ (and therefore $\phi_{01} = 0$) as well as $X_{00} = r_+$ and $R_{00} = \kappa_{II}$. The condition $\phi_{01} = 0$ can be interpreted as the statement that the energy density of the scalar field must be finite at the horizon, or else backreaction would destroy the near-horizon geometry. Furthermore, $r = 0$ implies that $\phi'(0) = 0$, so that the scalar field starts at rest at the horizon and evolves according to the form of $V(\phi)$.

By choosing $V(\phi) = \text{const.} > 0$ and $\phi'(0) = 0$, we obtain the unregulated solution (B.34). In order to obtain a regulated solution that crunches in finite proper time, we require a potential $V(\phi)$ with extrema at both $V(\phi) > 0$ and $V(\phi) < 0$. We therefore consider a potential of the form shown in figure B.3; explicitly, we take

$$V(\phi) = h^2 \left[\frac{1}{20} - \frac{3}{16} \left(\frac{\phi}{\phi_*} \right)^2 + \frac{7}{5} \left(\frac{\phi}{\phi_*} \right)^4 - 4 \left(\frac{\phi}{\phi_*} \right)^6 + 3 \left(\frac{\phi}{\phi_*} \right)^8 \right], \tag{B.39}$$

where h is an overall scale that sets the height of the potential and ϕ_* is a reference scale. This potential has local maxima at the origin and some ϕ_2, and local minima at some ϕ_1 and ϕ_3. In particular, it satisfies $V(0) > 0$, $V(\phi_1) > 0$, $V(\phi_2) > 0$, but $V(\phi_3) < 0$.

To construct a solution, the scalar field is released at some initial value ϕ_0 at which $V(\phi_0) > 0$. If ϕ_0 is smaller than some critical value $\phi_{\rm crit}$, the scalar field rolls past the extrema ϕ_1 and ϕ_2 and into the AdS extremum ϕ_3, where $V(\phi_3) < 0$. This produces a negative effective cosmological constant, causing the solution to become singular in finite ρ. As ϕ_0 is increased closer to $\phi_{\rm crit}$, the scalar field spends more and more time near the maximum ϕ_2, yielding a spacetime with a longer and longer expanding region before the singularity. Eventually, when $\phi_0 = \phi_{\rm crit}$, the initial conditions are tuned such that the scalar field remains at ϕ_2 indefinitely, yielding a version of the unregulated AdS-dS-wormhole[1]. Thus the regulator τ can be made arbitrarily large by taking ϕ_0 arbitrarily close to $\phi_{\rm crit}$.

Finally we consider wormhole-spanning extremal surfaces in smoothed, regulated wormholes that satisfy the conditions of footnote 7 everywhere. Note that any wormhole-spanning surface Ξ must pass through patch II, entering and leaving this patch through the de Sitter horizon $\rho = 0$. For our unsmoothed cut-and-paste geometries, Ξ will cross the de Sitter horizon in the far future in order to run along the entire (infinite) length of the accumulation surface $a_{\rm max}$. Smoothing out the null shells to obtain a finite-area Ξ will keep these anchors at a finite place. The exact point of crossing is determined by balancing the tendency to maximize the area in patch I (which tends to flatten Ξ in this region) with the tendency to run

[1]For $\phi_{\rm crit} < \phi_0 < \phi_2$, the scalar field comes to rest at ϕ_1, again producing an unregulated AdS-dS-wormhole.

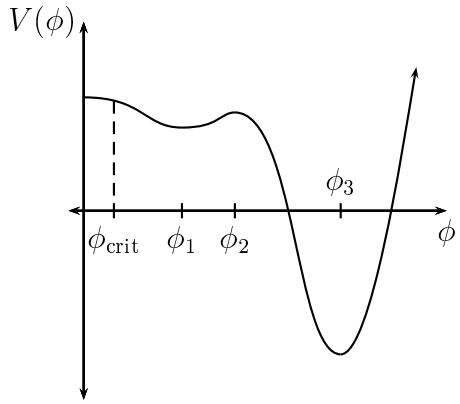

Figure B.3: A sketch of the potential we consider. At the horizon, the scalar field is at rest at some ϕ_0 and is then allowed to roll down the potential. If $\phi_0 < \phi_{\rm crit}$, the scalar field falls into the minimum at ϕ_3; if $\phi_0 = \phi_{\rm crit}$, the scalar field stops at ϕ_2, and if $\phi_{\rm crit} < \phi_0 < \phi_2$, the scalar field falls into the minimum at ϕ_1.

along the $a_{\max}$ surface in patch II. So as the anchors on $\mathscr{I}_{\rm AdS}$ move to the far future, so does the intersection of Ξ with the dS horizon. It is thus sufficient to study codimension-2 extremal surfaces anchored at $\rho = 0$ in the limit where these anchors are taken to the far future. Sample such surfaces are plotted numerically[2] in figure B.4 for $d = 4$ in comparison with surfaces on which $a_{\rm eff}(\rho)$ (defined in (B.35)) attains its maximum. We find $\phi_{\rm crit} \approx 0.21\,\phi_*$.

B.5 Correlators in dS_3

We now show how the geodesic approximation in dS_3 reproduces the large-mass behavior of the Wightman function of a free massive scalar field in the Hadamard de Sitter-invariant (Bunch-Davies) vacuum. As is well known (see e.g. [394, 395]

[2]These solutions were found by integrating the equations of motion (B.37) using `Mathematica`'s built-in `NDSolve` command, which is more than sufficient for generating the desired figures.

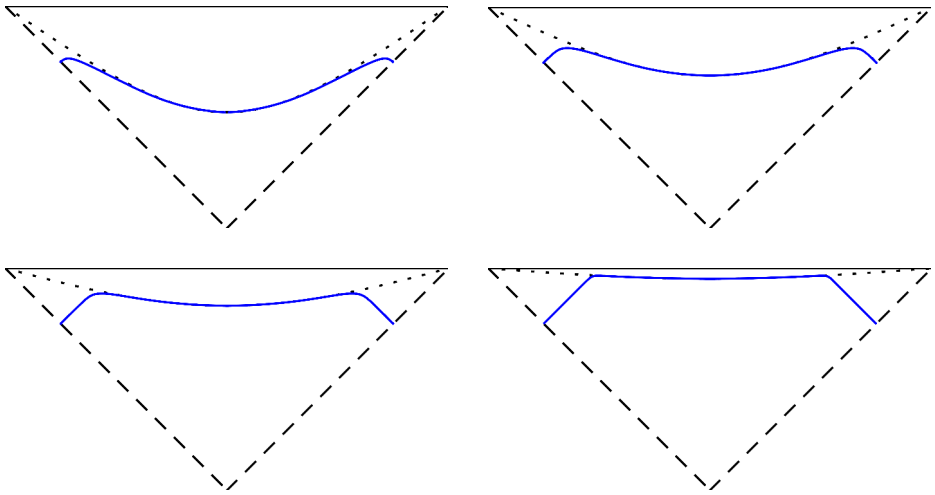

Figure B.4: The regulated asymptotically dS patch for $d = 4$ and various values of ϕ_0; from left to right, top to bottom, the figures have $(\phi_{\rm crit} - \phi_0)/\phi_* = 10^{-1}, 10^{-2}, 10^{-3}, 10^{-5}$, corresponding to $\sqrt{8\pi G_N}\, h\tau \approx 2.5, 3.2, 3.9, 5.5$. The dotted lines mark the maxima $a_{\rm max}$ of $a_{\rm eff}$, while the solid curves (blue in color version) show extremal surfaces that enter through the horizon. The solid horizontal lines are singularities, which the extremal surfaces are prevented from reaching. For $\phi_0 = \phi_{\rm crit}$, $\tau = \infty$ and $a_{\rm max}$ merges with the singularity to create future dS infinity $\mathscr{I}_{\rm dS}$. The extremal surfaces then cease to exist in the Lorentzian section.

for $d = 1, 3$), for dS_{d+1} this two-point function is

$$G(x, x') = \frac{H^{d-1}}{(4\pi)^{(d+1)/2}} \frac{\Gamma(-c)\Gamma(c+d)}{\Gamma((d+1)/2)} {}_2F_1\left(-c, c+d; \frac{d+1}{2}; \frac{1+Z}{2}\right), \tag{B.40}$$

where

$$c = -\frac{d}{2} + \sqrt{\frac{d^2}{4} - \frac{m^2}{H^2}}, \tag{B.41}$$

H is the Hubble constant, m is the mass of ϕ, and Z is the de Sitter invariant given by the inner product of unit vectors associated with the standard embedding

of dS_{d+1} into $d+2$ Minkowski space. In the coordinates of (7.12) we have

$$Z(x,x') = 1 + \frac{(e^{-Ht} - e^{-Ht'})^2 - H^2(\vec{x}-\vec{x}')^2}{2e^{-Ht}e^{-Ht'}}. \tag{B.42}$$

We wish to study (B.40) for $d=2$ and $m/H \gg 1$. Using the identities [311]

$$\Gamma(1+z)\Gamma(1-z) = \frac{\pi z}{\sin(\pi z)}, \tag{B.43a}$$

$$\begin{aligned} &{}_2F_1\left(a, 2-a; \frac{3}{2}; -z^2\right) = \\ &\quad \frac{1}{4(a-1)z\sqrt{1+z^2}}\left[\left(\sqrt{1+z^2}+z\right)^{2(a-1)} - \left(\sqrt{1+z^2}-z\right)^{2(a-1)}\right], \end{aligned} \tag{B.43b}$$

for $d=2$ we find

$$G(t_0,\vec{x};t_0,\vec{x}') = \frac{H}{4\pi}\frac{1}{\widetilde{L}\sin(\pi\nu)}\begin{cases} \frac{1}{\sqrt{1-\widetilde{L}^2/4}}\sin(2\nu\arccos(\widetilde{L}/2)), & \widetilde{L}<2, \\ \frac{1}{\sqrt{\widetilde{L}^2/4-1}}\sinh(2\nu\,\mathrm{arccosh}(\widetilde{L}/2)), & \widetilde{L}>2, \end{cases} \tag{B.44}$$

where $\nu \equiv \sqrt{1-m^2/H^2}$ and $\widetilde{L} \equiv He^{Ht_0}|\vec{x}-\vec{x}'|$. For large m/H we have $\nu \approx im/H$ and thus

$$G(t_0,\vec{x};t_0,\vec{x}') \sim \frac{e^{-\pi m/H}}{1-e^{-2\pi m/H}}\begin{cases} e^{(2m/H)\arccos(\widetilde{L}/2)} - e^{-(2m/H)\arccos(\widetilde{L}/2)}, & \widetilde{L}<2, \\ e^{(2im/H)\mathrm{arccosh}(\widetilde{L}/2)} - e^{-(2im/H)\mathrm{arccosh}(\widetilde{L}/2)}, & \widetilde{L}>2, \end{cases} \tag{B.45}$$

where the $\sim$ indicates that we have dropped polynomial corrections to exponentials in m; i.e., we have kept terms that in a saddle point approximation can come

from a sum over saddles. The remaining terms may well come from fluctuations around these saddles, though we will not consider this in detail. Note that since the factor $1 - e^{2\pi m/H}$ lies in the denominator of (B.45), it in fact leads to an infinite number of terms exponential in m.

We now make explicit that spacelike geodesics can reproduce the exponential terms in (B.45). For $d = 2$, expressions (7.18) and (7.19) simplify to

$$\widetilde{L} = 2e^{-H\Delta t}\sqrt{e^{2H\Delta t} - 1}, \tag{B.46a}$$

$$A_n^{\pm} = \frac{2}{H}\left[\pm \arctan\sqrt{e^{2H\Delta t} - 1} + n\pi\right], \tag{B.46b}$$

where now $\widetilde{L} = 2He^{Ht_0}L$. The $\pm$ sign and the integer n that appear in $A_n^{\pm}$ represent the analytic continuation to all sheets of the square root and inverse tangent, respectively. Writing $A_n^{\pm}$ in the form

$$A_n^{\pm} = \frac{1}{H}\begin{cases} (2n \pm 1)\pi \mp 2\arccos\left(\widetilde{L}/2\right), & \widetilde{L} < 2, \\ (2n \pm 1)\pi \mp 2i\,\mathrm{arccosh}\left(\widetilde{L}/2\right), & \widetilde{L} > 2, \end{cases} \tag{B.47}$$

one may interpret each term as the length of a distinct (possibly complex) geodesic. Comparing with the exact expression (B.45) shows that

$$G(t_0, \vec{x}; t_0, \vec{x}') \sim \sum_{2n\pm 1 \geq -1} c_n^{\pm} e^{-mA_n^{\pm}} \tag{B.48}$$

for appropriate order-1 phases $c_n^{\pm}$ (which in the saddle-point approximation are higher order effects determined by fluctuations around each saddle). Since the sum is over precisely those n and signs $\pm$ with $2n \pm 1 \geq -1$, we conclude that these

are the saddles that contribute to the desired path integral. It is interesting that this represents a sum over both all sheets in the Riemann surface for $\widetilde{L}(\Delta t)$ and an infinite number of sheets in the Riemann surface for $A(\widetilde{L})$, though sufficiently "negative" sheets are not included. We note that $d = 2$ is a special case where $A(\widetilde{L})$ (understood as a map from the Riemann surface for $\widetilde{L}(\Delta t)$ to the Riemann surface for $A(\Delta t)$) is multi-valued; in higher dimensions we expect that as in [78] one can take $A(\widetilde{L})$ to be single valued, since the Riemann surface for $\widetilde{L}(\Delta t)$ has an infinite number of sheets for $d > 2$.

B.6 Integration in Terms of Elliptic Integrals

In this appendix, we give the expressions for Δt and A_{ren} for codimension-2 extremal surfaces in Schwarzschild-AdS$_5$ ($d = 4$). First, note that the integrals for Δt and A_{ren} take the form

$$\Delta t = \frac{\beta}{\pi} \int_\gamma \frac{\rho^2 \mathcal{E}}{(\rho^4 - 1)\sqrt{\rho^6 - \rho^2 + \mathcal{E}^2}}\, d\rho, \tag{B.49a}$$

$$A_{\text{ren}} = \ell r_h^2 V_2 \lim_{\epsilon \to 0} \left(\int_{\gamma_\epsilon} \frac{\rho^2}{\sqrt{\rho^6 - \rho^2 + \mathcal{E}^2}}\, d\rho - \frac{1}{\epsilon^2} \right), \tag{B.49b}$$

where $\rho \equiv R/r_h$, $\mathcal{E} \equiv E\ell/r_h^3$, and $\beta = \pi \ell^2 / r_h$. It will be convenient to convert to a new variable $w = 1/\rho^2$ in terms of which these become

$$\Delta t = \frac{\beta}{2\pi} \int_\gamma \frac{w \mathcal{E}}{(1 - w^2)\sqrt{1 - w^2 + \mathcal{E}^2 w^3}}\, dw, \tag{B.50a}$$

$$A_{\text{ren}} = \ell r_h^2 V_2 \lim_{\epsilon \to 0} \left(\frac{1}{2} \int_{\gamma_\epsilon} \frac{dw}{w^2 \sqrt{1 - w^2 + \mathcal{E}^2 w^3}} - \frac{1}{\epsilon^2} \right), \tag{B.50b}$$

with the contours γ and γ_ϵ modified accordingly.

We now use $w_1(\mathcal{E}), w_2(\mathcal{E}), w_3(\mathcal{E})$ to label the three roots of the cubic $h(w) = 1 - w^2 + \mathcal{E}^2 w^3$ as follows. For real extremal surfaces, we take w_1 to be the turning point. We then extend this this definition by continuity to the region near the principal contour in the complex $\mathcal{E}$ plane. We similarly specify $w_2(\mathcal{E})$ by requiring that it diverge at $\mathcal{E} = 0$ (as some root must since $h(w)$ becomes a quadratic at $\mathcal{E} = 0$) and that it be continuous in the same region. The remaining root is w_3. Defined in this way, $w_1(\mathcal{E}), w_2(\mathcal{E}), w_3(\mathcal{E})$ are single-valued functions which can be used directly in all expressions below whether evaluated on the principal contour, contour B, or contour C.

We also define a function

$$I(z_1, z_2) = \int_{z_1}^{z_2} \frac{w\mathcal{E}}{(1-w^2)\sqrt{1 - w^2 + \mathcal{E}^2 w^3}}\, dw. \tag{B.51}$$

By tracking the behavior of the contour γ as one moves in the complex $\mathcal{E}$-plane, it is possible to show that Δt near the principal (real) contour and near contours B and C can be written[3]

$$\Delta t_{\text{principal}} = \frac{\beta}{\pi} I(0, w_1), \tag{B.52a}$$

$$\Delta t_B = \frac{\beta}{\pi} \left(I(0, w_2) + I(w_1, w_2) \right), \tag{B.52b}$$

$$\Delta t_C = \frac{\beta}{\pi} \left(I(0, w_1) - 2I(w_1, w_3) - 2I(w_2, w_3) \right). \tag{B.52c}$$

The integral $I(z_1, z_2)$ can be expressed in terms of standard elliptic integrals; one

[3]One does need to be careful in order to avoid having the contour γ cross the poles at $w = \pm 1$; luckily, these add a constant contribution of $\pm i\beta$ or $\pm\beta$, so we find it convenient to allow γ to cross the poles, and then compensate by subtracting off the corresponding residue.

obtains

$$I(0,w_1)=\frac{1}{(1-w_2^2)\sqrt{w_1-w_2}}\left\{2w_2\left(F(\psi|m)-K(m)\right)\right.$$
$$-(w_2-1)\left[\Pi\left(\frac{w_2+1}{w_2-w_1};\psi\middle|m\right)-\Pi\left(\frac{w_2+1}{w_2-w_1}\middle|m\right)\right]$$
$$\left.-(w_2+1)\left[\Pi\left(\frac{w_2-1}{w_2-w_1};\psi\middle|m\right)-\Pi\left(\frac{w_2-1}{w_2-w_1}\middle|m\right)\right]\right\}, \quad \text{(B.53)}$$

where

$$\psi=\arctan\sqrt{\frac{w_2-w_1}{w_1}}, \quad m=\frac{w_2-w_3}{w_2-w_1}. \quad \text{(B.54)}$$

$I(0,w_2)$ and $I(0,w_3)$ are obtained from $I(0,w_1)$ by the exchanges $w_1\leftrightarrow w_2$ and $w_1\leftrightarrow w_2$, and $I(w_i,w_j)=I(0,w_j)-I(0,w_i)$.

For the area, we proceed similarly. We define

$$J(z_1,z_2)=\int_{z_1}^{z_2}\frac{1}{w^2\sqrt{1-w^2+\mathcal{E}^2w^3}}\,dw. \quad \text{(B.55)}$$

The renormalized area on the above sheets is then

$$A_{\text{ren,principal}}=\ell r_h^2V_2\lim_{\epsilon\to0}\left(J(\epsilon^2,w_1)-\frac{1}{\epsilon^2}\right), \quad \text{(B.56a)}$$
$$A_{\text{ren,B}}=\ell r_h^2V_2\lim_{\epsilon\to0}\left(J(\epsilon^2,w_2)-\frac{1}{\epsilon^2}+J(w_1,w_2)\right), \quad \text{(B.56b)}$$
$$A_{\text{ren,C}}=\ell r_h^2V_2\lim_{\epsilon\to0}\left(J(\epsilon^2,w_1)-\frac{1}{\epsilon^2}-2J(w_1,w_3)-2J(w_2,w_3)\right). \quad \text{(B.56c)}$$

Again evaluating J in terms of elliptic integrals, we obtain

$$J(\epsilon^2, w_1) = \frac{1}{\epsilon^2} + \frac{1}{w_2} - \frac{\mathcal{E}}{\sqrt{w_1 - w_2}} \left[(w_2 - w_1) \left(E(m) - E(\psi|m) \right) \right.$$
$$\left. + w_1 \left(K(m) - F(\psi|m) \right) \right] + \mathcal{O}(\epsilon^2), \quad \text{(B.57)}$$

where ψ and m are as before. Then $J(\epsilon^2, w_2)$ and $J(\epsilon^2, w_3)$ are obtained from $J(\epsilon^2, w_1)$ by the exchanges $w_1 \leftrightarrow w_2$ and $w_1 \leftrightarrow w_3$, and $J(w_i, w_j) = \lim_{\epsilon \to 0}(J(\epsilon^2, w_j) - J(\epsilon^2, w_i))$.

B.7 Proofs

In this Appendix, we prove the theorems stated in the main text and provide some more technical details.

B.7.1 Theorem 1

Theorem 1. Let R be a region such that $\theta(\{N_s\})$ has a definite sign everywhere in R, and let X be an extremal surface. Then any connected portion of X in R can turn around at most once, and has no inflection points if M is (2+1)-dimensional. In particular, if H is a regular splitting future holographic screen, any connected portion of X in $\mathrm{Int}(H)$ can turn around at most once.

Proof. First, let us index the leaves of the foliation $\{N_s\}$ by a parameter s which runs to the future along the foliation, *i.e.* N_s is nowhere to the past of $N_{s'}$ if and only if $s > s'$, which we will also denote by $N_s > N_{s'}$.

Now, we prove the theorem by contradiction. Let $\theta(\{N_s\}) < 0$ everywhere in R; the opposite case proceeds analogously. Let X_R be a connected component of X in R, and suppose X_R has a pivot point at $p \in R$. Let $N_{s(p)}$ be the leaf containing p. By Lemma 2, p cannot be an inflection point if M is (2+1)-dimensional.

Now suppose p is a turning point. Suppose also that X_R has another turning point $q \in R$; *i.e.* X_R is tangent to another leaf $N_{s(q)}$, and it must be tangent to it either from the past or from the future. By Lemma 1, X_R must be tangent to $N_{s(q)}$ from the future. This immediately requires X_R to have another turning point r such that $N_{s(r)} > N_{\max(s(p),s(q))}$, and X_R must be tangent to $N_{s(r)}$ from the past at r, as shown in Figure 9.7. But if $r \in R$, then by construction $\theta(N_{s(r)}) < 0$, and X_R cannot be tangent to $N_{s(r)}$ from the past. Therefore $r \notin R$, and $X_R \nsubseteq R$, in contradiction with the definition of X_R.

To prove the last statement of the theorem, we simply note that by construction, $\theta(\{N_s\})$ has the same sign everywhere in $\mathrm{Int}(H)$. □

B.7.2 H-deformability

Definition 6. *H-deformability.* Let $\{X_\alpha\}$ be a family of boundary-anchored extremal surfaces such that every surface in $\{X_\alpha\}$ can be continuously deformed via other surfaces in $\{X_\alpha\}$ to some initial surface X_0 that lies entirely in $\mathrm{Ext}(H)$. Then every surface in $\{X_\alpha\}$ is said to be *H-deformable*, and $\{X_\alpha\}$ is an *H-deformable family.*

B.7.3 Theorem 2

Theorem 2. Let H be a regular splitting future holographic screen in a (2+1)-dimensional asymptotically locally AdS spacetime M. Then no H-deformable boundary-anchored extremal surface can have a pivot point in the interior of any future achronal screen of H. Moreover, if H is itself achronal, no such extremal surfaces can have a pivot point in $\mathrm{Int}(H)$.

Proof. By contradiction. Let $\tilde{H}$ be an achronal screen of H, and let X_1 be an H-deformable extremal surface. Suppose X_1 has at least one pivot point p_1 in $\mathrm{Int}(\tilde{H})$, and let N_1 be the leaf containing p_1. Consider a deformation parametrized by α along an H-deformable family $\{X_\alpha\}$ to a surface $X_0 \in \mathrm{Ext}(H)$. Note that X_0 exists by definition of H-deformability.

Next, let X_m be the last surface in the deformation which is tangent to a leaf N_m at some point $p_m \in \mathrm{Int}(\tilde{H}) \cup \tilde{H}$ (it may be the case that $X_m = X_0$). Because the expansion is negative on all leaves in $\tilde{H}$, by Lemma 2, in a sufficiently small neighborhood $\mathcal{O}_{p_m}$ of p_m, $X_m \cap \mathcal{O}_{p_m} \subset J^+(N_m)$; thus p_m is a turning point. If $p_m \in \mathrm{Int}(\tilde{H})$, then evolving backward along the deformation from X_1 to X_0, there exists some $\epsilon > 0$ such that the surface $X_{m-\epsilon}$ must also be tangent to a leaf in $\mathrm{Int}(\tilde{H})$ (since $\mathrm{Int}(\tilde{H})$ is open). But this contradicts the definition of X_m. So $p_m \notin \mathrm{Int}(\tilde{H})$, and thus $p_m \in \tilde{H}$. Then there are two cases: (1) X_m is tangent to $\tilde{H}$ at p_m, or (2) X_m is not tangent to $\tilde{H}$ at p_m. We consider the two cases separately.

Case 1: If X_m is tangent to $\tilde{H}$ at p_m, then X_m is also tangent to the intersection $\tilde{H} \cap N_m$, which is a leaflet $\tilde{\sigma}_m$. This immediately implies that X_m is also tangent to L_m, the member of the $\{L_s\}$ foliation whose intersection with N_m defines

$\tilde{\sigma}_m$. By Lemma 2, $\mathcal{O}_{p_m} \cap X_m \subset J^+(L_m)$. We also have that $\mathcal{O}_{p_m} \cap X_m \subset J^+(N_m)$, and thus since L_m and N_m are boundaries of the future of $\tilde{\sigma}_m$, $\mathcal{O}_{p_m} \cap X_m \subset J^+(\tilde{\sigma}_m)$. Because $\tilde{H}$ is by assumption achronal, $J^+(\tilde{\sigma}_m)$ has no intersection with $\mathrm{Ext}(H)$, implying that it is foliated by N_s leaves with negative expansion. Therefore $I^+(\tilde{\sigma}_m) \cap X_m$ can never be tangent to N_s or L_s, since if it were, it would be tangent to them from the past (see the proof of Theorem 1), in violation of Lemma 1. Thus $X_m \subset J^+(\tilde{\sigma}_m)$. But because trapped and marginally-trapped surfaces always lie to the future of the future event horizon $\partial I^-(\partial M)$, $J^+(\tilde{\sigma}_m) \cap \partial M = \varnothing$. This would imply that X_m cannot be boundary-anchored, in contradiction with its definition.

Case 2: Suppose X_m is not tangent to $\tilde{H}$ at the pivot point p_m. Then X_m is not tangent to L_m at p_m. Since X_m intersects L_m at p_m and is not tangent to it at p_m, there exists a small neighborhood of p_m on which X_m intersects both $I^+(L_m)$ and $I^-(L_m)$. This immediately implies that there is a small open subset of X_m which lies in $J^+(\tilde{\sigma}_m)$. By assumption, $\partial X \subset \partial M$, and so $\partial X \cap J^+(\tilde{\sigma}_m) = \varnothing$. Therefore, there must exist some point $q \in \mathrm{Int}(\tilde{H})$ at which X is tangent from the past to either a null hypersurface $L \in \{L_s\}$ or a leaf N (for if there were not, X would need to have a boundary in $J^+(\tilde{\sigma}_m)$). But in $\mathrm{Int}(H)$, the expansion of all of the L_s and the N_s leaves are negative, so an extremal surface can only be tangent to them from the future. We have therefore arrived at a contradiction.

This proves the first portion of the theorem. To prove the last statement, consider an achronal regular future holographic screen H. Each of its leaflets may be deformed an arbitrarily small amount forward along the leaves N_s to produce an achronal screen $\tilde{H} \subset \mathrm{Int}(H)$ arbitrarily close to H. Then the proof above

implies that no H-deformable extremal surface can have a pivot point in $\mathrm{Int}(\tilde{H})$. But in the limit that $\tilde{H}$ is taken to be arbitrarily close to H, $\mathrm{Int}(\tilde{H})$ coincides with $\mathrm{Int}(H)$, and thus we conclude that no H-deformable extremal surface can have a pivot point in $\mathrm{Int}(H)$ as well. □

B.7.4 Theorem 3

Theorem 3. Let M be an asymptotically locally AdS spacetime, and let H be a regular splitting future holographic screen constructed from a reducible foliation $\{N_s\}$. Assume further that that there exists a foliation of the future of H with L_s congruences. Let X be a boundary-anchored, codimension-two spacelike extremal surface such that:

1. X is reducible to (2+1) dimensions;
2. ∂X is connected; and
3. X intersects $\mathrm{Ext}(H)$ only on regions with $\theta(\{N_s\}) > 0$.

Assume further that there exists an H-deformation of X that obeys the above conditions as well. Then X cannot have a pivot point in $\mathrm{Int}(H)$.

Proof. The first part of the proof is identical to that of Theorem 2: we consider an H-deformable family of extremal surfaces, except that the members of this family are required to have connected ∂X. We then consider the last deformation surface X_m tangent to a leaf N_m at a point p_m, and by the same reasoning as above we conclude that $p_m \in H$. Again, we are faced with two cases: either (1) X_m is tangent to H at p_m, or (2) it is not.

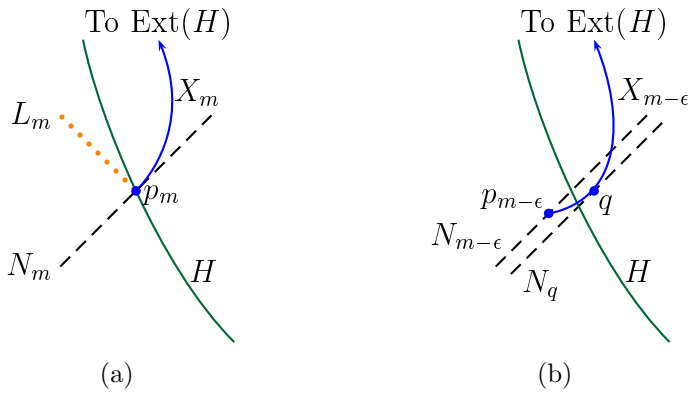

Figure B.5: (a): the behavior of the midway surface X_m (solid blue) when it is tangent to N_m and H (solid green) at a point p_m on H. Note here that the surface caps off smoothly in the suppressed spatial directions at p; in this sketch, this is shown as the surface ending there. (b): after a small perturbation through the H-deformable family, the turning point p_m moves out to $p_{m-\epsilon}$. This requires the surface to develop a new turning point q, as shown. But q is not allowed to exist. (Note that here we show H as timelike in a neighborhood of p_m, but this behavior remains unchanged for other signatures).

Case 1: As before, if X_m is tangent to H at p_m, then X_m is also tangent to a leaflet σ_m, and therefore to L_m. By Lemma 2, $\mathcal{O}_{p_m} \cap X_m \subset J^+(L_m)$. But the expansion of the portion of N_m to the future of L_m is negative: $\theta(N_m \cap J^+(L_m)) < 0$, even if $\theta(N_m)|_{p_m} = 0$. Thus although X_m is tangent to N_m at a point where $\theta(N_m) = 0$, with motion away from p along X_m is into the region of $\theta(\{N_s\})$; see Figure B.5(a). Then by the same reasoning that led to Lemma 2, it must also bend into $J^+(N_m)$, and therefore $\mathcal{O}_{p_m} \cap X_m \subset J^+(\sigma_m)$.

If $X_m \cap J^+(\sigma_m)$ has no intersection with H, then we obtain a contradiction as we did for Theorem 2. If $X_m \cap J^+(\sigma_m)$ does have an intersection with H, X_m must exit $\mathrm{Int}(H)$ through that intersection. But now consider a slight deformation to $X_{m-\epsilon}$ along the H-deformable family. Then the pivot point p_m must deform to a new pivot point $p_{m-\epsilon} \in \mathcal{O}_{p_m}$ of $X_{m-\epsilon}$ which lies in $\mathrm{Ext}(H)$ (since by assump-

tion X_m was the last extremal surface in this family with a turning point in or on H). Because $\text{Int}(H)$ is open, we can always find a sufficiently small deformation from X_m to $X_{m-\epsilon}$ such that $X_{m-\epsilon}$ must still enter $\text{Int}(H)$ before exiting, as shown in Figure B.5(b). This implies that there must exist another pivot point $q \in \mathcal{O}_{p_m}$ where $X_{m-\epsilon}$ is tangent to a leaf N_q from the future. Now, this pivot point cannot lie in $\text{Ext}(H)$, since there $\theta(N_q) > 0$. But this point also cannot lie in $\text{Int}(H) \cup H$, since by assumption X_m was the last surface with a pivot point in $\text{Int}(H) \cup H$. We therefore have a contradiction.

Case 2: Next, suppose X_m is not tangent to H at p_m. Then as in the proof of Theorem 2, there is a small open subset $\mathcal{O}_{p_m} \cap X_m^+$ of X_m which lies in $I^+(L_m)$. Likewise, there is a small open subset $\mathcal{O}_{p_m} \cap X_m^-$ of X_m which lies in $I^-(L_m)$. By the arguments made in Case 1, we have that $\mathcal{O}_{p_m} \cap X_m^+ \subset J^+(\sigma_m)$, and $\mathcal{O}_{p_m} \cap X_m^- \subset J^-(\sigma_m)$. Thus $\mathcal{O}_{p_m} \cap X_m^+$ and $\mathcal{O}_{p_m} \cap X_m^-$ can meet only on $\sigma_m \subset N_m$. In particular, σ_m divides X_m into two pieces X_m^+ and X_m^-.

Near p_m, X_m^- lies to the past of N_m. Therefore, if it were to be tangent to any other leaf N_s, it would have to be tangent from the future. This is not allowed in $\text{Ext}(H)$, since there only turning points from the past are allowed, nor is it allowed in $\text{Int}(H)$ (by assumption). Therefore X_m^- must reach the boundary.

Similarly, near p_m, X_m^+ lies to the future of L_m. By assumption, the $\{L_s\}$ foliate $J^+(H)$, so X_m^+ can only have a turning point with respect to $\{L_s\}$ outside of $J^+(H)$. But the fact that near p_m X_m^+ also lies to the future of N_m implies that X^+ can only leave $J^+(H)$ if it turns around with respect to $\{N_s\}$ on some leaf $N_s > N_m$ (and if it does, it will be tangent to N_s from the past). But then it can have no further turning points with respect to $\{N_s\}$: if it did, these would be

from the future. Such turning points cannot occur in $\mathrm{Ext}(H)$ by Lemma 2 and are not allowed in $\mathrm{Int}(H)$ by the assumption that X_m is the last surface to have a turning point in $\mathrm{Int}(H) \cup H$. Thus X_m^+ must also reach the boundary.

But if each of X_m^+ and X_m^- reach the boundary, and they join only at σ_m, then ∂X must consist of (at least) two disconnected pieces, in contradiction with the assumption that it be connected. $\square$

Bibliography

[1] A. Einstein, *Die Grundlage der allgemeinen Relativitätstheorie*, *Annalen der Physik* **49** (1916) 769822.

[2] C. Everitt, D. DeBra, B. Parkinson, J. Turneaure, J. Conklin, *et. al.*, *Gravity Probe B: Final Results of a Space Experiment to Test General Relativity*, *Phys.Rev.Lett.* **106** (2011) 221101, [arXiv:1105.3456].

[3] R. Hulse and J. Taylor, *Discovery of a pulsar in a binary system*, *Astrophys.J.* **195** (1975) L51–L53.

[4] **LIGO Scientific** Collaboration, J. Aasi *et. al.*, *Advanced LIGO*, *Class.Quant.Grav.* **32** (2015) 074001, [arXiv:1411.4547].

[5] K. Schwarzschild, *Über das Gravitations-feld eines Massenpunktes nach der Einsteinschen Theorie*, *Sitzungsberichte der Königlich Preussischen Akademie der Wissenschaften zu Berlin* **7** (1916) 189196.

[6] S. Bowyer, E. T. Byram, T. A. Chubb, and H. Friedman, *Cosmic x-ray sources*, *Science* **147** (1965), no. 3656 394–398, [http://www.sciencemag.org/content/147/3656/394.full.pdf].

[7] B. Balick and R. L. Brown, *Intense sub-arcsecond structure in the galactic center*, *Astrophysical Journal* **194** (Dec., 1974) 265–270.

[8] S. Gezari, R. Chornock, A. Rest, M. Huber, K. Forster, *et. al.*, *An ultraviolet-optical flare from the tidal disruption of a helium-rich stellar core*, *Nature* **485** (2012) 217, [arXiv:1205.0252].

[9] H. Falcke, F. Melia, and E. Agol, *Viewing the shadow of the black hole at the galactic center*, *Astrophys.J.* **528** (2000) L13, [astro-ph/9912263].

[10] J. M. Bardeen, B. Carter, and S. W. Hawking, *The four laws of black hole mechanics*, *Comm. Math. Phys.* **31** (1973), no. 2 161–170.

[11] S. Hawking, *Black hole explosions*, *Nature* **248** (1974) 30–31.

[12] J. Bekenstein, *Black holes and the second law*, *Lett.Nuovo Cim.* **4** (1972) 737–740.

[13] J. D. Bekenstein, *Black holes and entropy*, *Phys.Rev.* **D7** (1973) 2333–2346.

[14] J. D. Bekenstein, *Generalized second law of thermodynamics in black hole physics*, *Phys.Rev.* **D9** (1974) 3292–3300.

[15] G. 't Hooft, *Dimensional reduction in quantum gravity*, gr-qc/9310026.

[16] L. Susskind, *The World as a hologram*, *J.Math.Phys.* **36** (1995) 6377–6396, [hep-th/9409089].

[17] D. Marolf and R. D. Sorkin, *On the status of highly entropic objects*, *Phys.Rev.* **D69** (2004) 024014, [hep-th/0309218].

[18] D. Marolf, D. Minic, and S. F. Ross, *Notes on space-time thermodynamics and the observer dependence of entropy*, *Phys.Rev.* **D69** (2004) 064006, [hep-th/0310022].

[19] J. M. Maldacena, *The Large N limit of superconformal field theories and supergravity*, *Adv.Theor.Math.Phys.* **2** (1998) 231–252, [hep-th/9711200].

[20] E. Witten, *Anti-de Sitter space and holography*, *Adv.Theor.Math.Phys.* **2** (1998) 253–291, [hep-th/9802150].

[21] O. Aharony, S. S. Gubser, J. M. Maldacena, H. Ooguri, and Y. Oz, *Large N field theories, string theory and gravity*, *Phys.Rept.* **323** (2000) 183–386, [hep-th/9905111].

[22] E. D'Hoker and D. Z. Freedman, *Supersymmetric gauge theories and the AdS / CFT correspondence*, hep-th/0201253.

[23] J. Polchinski, *Introduction to Gauge/Gravity Duality*, arXiv:1010.6134.

[24] T. Hertog and G. T. Horowitz, *Towards a big crunch dual*, *JHEP* **0407** (2004) 073, [hep-th/0406134].

[25] T. Hertog and G. T. Horowitz, *Holographic description of AdS cosmologies*, *JHEP* **0504** (2005) 005, [hep-th/0503071].

[26] N. Turok, B. Craps, and T. Hertog, *From big crunch to big bang with AdS/CFT*, arXiv:0711.1824.

[27] B. Craps, T. Hertog, and N. Turok, *On the Quantum Resolution of Cosmological Singularities using AdS/CFT*, *Phys.Rev.* **D86** (2012) 043513, [arXiv:0712.4180].

[28] J. Barbon and E. Rabinovici, *AdS Crunches, CFT Falls And Cosmological Complementarity*, *JHEP* **1104** (2011) 044, [arXiv:1102.3015].

[29] B. Craps, A. Rajaraman, and S. Sethi, *Effective dynamics of the matrix big bang*, *Phys.Rev.* **D73** (2006) 106005, [hep-th/0601062].

[30] S. R. Das, J. Michelson, K. Narayan, and S. P. Trivedi, *Time dependent cosmologies and their duals*, *Phys.Rev.* **D74** (2006) 026002, [hep-th/0602107].

[31] A. Awad, S. R. Das, S. Nampuri, K. Narayan, and S. P. Trivedi, *Gauge Theories with Time Dependent Couplings and their Cosmological Duals*, *Phys.Rev.* **D79** (2009) 046004, [arXiv:0807.1517].

[32] N. Engelhardt, T. Hertog, and G. T. Horowitz, *Holographic Signatures of Cosmological Singularities*, *Phys.Rev.Lett.* **113** (2014) 121602, [arXiv:1404.2309].

[33] N. Engelhardt, T. Hertog, and G. T. Horowitz, *Further Holographic Investigations of Big Bang Singularities*, arXiv:1503.0883.

[34] L. Fidkowski, V. Hubeny, M. Kleban, and S. Shenker, *The Black hole singularity in AdS / CFT*, *JHEP* **0402** (2004) 014, [hep-th/0306170].

[35] A. Almheiri, D. Marolf, J. Polchinski, and J. Sully, *Black Holes: Complementarity or Firewalls?*, *JHEP* **1302** (2013) 062, [arXiv:1207.3123].

[36] A. Almheiri, D. Marolf, J. Polchinski, D. Stanford, and J. Sully, *An Apologia for Firewalls*, *JHEP* **1309** (2013) 018, [arXiv:1304.6483].

[37] K. Papadodimas and S. Raju, *An Infalling Observer in AdS/CFT*, *JHEP* **1310** (2013) 212, [arXiv:1211.6767].

[38] K. Papadodimas and S. Raju, *State-Dependent Bulk-Boundary Maps and Black Hole Complementarity*, *Phys.Rev.* **D89** (2014), no. 8 086010, [arXiv:1310.6335].

[39] K. Papadodimas and S. Raju, *Black Hole Interior in the Holographic Correspondence and the Information Paradox*, *Phys.Rev.Lett.* **112** (2014), no. 5 051301, [arXiv:1310.6334].

[40] D. Marolf and J. Polchinski, *Gauge/Gravity Duality and the Black Hole Interior*, *Phys.Rev.Lett.* **111** (2013) 171301, [arXiv:1307.4706].

[41] S. A. Hartnoll, *Lectures on holographic methods for condensed matter physics*, *Class.Quant.Grav.* **26** (2009) 224002, [arXiv:0903.3246].

[42] G. T. Horowitz, *Introduction to Holographic Superconductors*, *Lect.Notes Phys.* **828** (2011) 313–347, [arXiv:1002.1722].

[43] S. A. Hartnoll, *Horizons, holography and condensed matter*, arXiv:1106.4324.

[44] S. R. Das, *Holographic Quantum Quench*, *J.Phys.Conf.Ser.* **343** (2012) 012027, [arXiv:1111.7275].

[45] H. Liu and S. J. Suh, *Entanglement Tsunami: Universal Scaling in Holographic Thermalization*, arXiv:1305.7244.

[46] H. Liu and S. J. Suh, *Entanglement growth during thermalization in holographic systems*, arXiv:1311.1200.

[47] R. A. Janik and R. B. Peschanski, *Asymptotic perfect fluid dynamics as a consequence of Ads/CFT*, *Phys.Rev.* **D73** (2006) 045013, [hep-th/0512162].

[48] H. Nastase, *The RHIC fireball as a dual black hole*, hep-th/0501068.

[49] E. Shuryak, S.-J. Sin, and I. Zahed, *A Gravity dual of RHIC collisions*, *J.Korean Phys.Soc.* **50** (2007) 384–397, [hep-th/0511199].

[50] R. B. Peschanski, *Quark-gluon plasma/black hole duality from gauge/gravity correspondence*, *J.Phys.Conf.Ser.* **110** (2008) 032014, [arXiv:0710.0756].

[51] V. Schomerus, *Strings for Quantumchromodynamics*, *Int.J.Mod.Phys.* **A22** (2007) 5561–5571, [arXiv:0706.1209].

[52] S. S. Gubser, *Comparing the drag force on heavy quarks in N=4 super-Yang-Mills theory and QCD*, *Phys.Rev.* **D76** (2007) 126003, [hep-th/0611272].

[53] C. Herzog, A. Karch, P. Kovtun, C. Kozcaz, and L. Yaffe, *Energy loss of a heavy quark moving through N=4 supersymmetric Yang-Mills plasma*, *JHEP* **0607** (2006) 013, [hep-th/0605158].

[54] F. Carrasco, L. Lehner, R. C. Myers, O. Reula, and A. Singh, *Turbulent flows for relativistic conformal fluids in 2+1 dimensions*, *Phys.Rev.* **D86** (2012) 126006, [arXiv:1210.6702].

[55] A. Adams, P. M. Chesler, and H. Liu, *Holographic turbulence*, *Phys.Rev.Lett.* **112** (2014), no. 15 151602, [arXiv:1307.7267].

[56] S. R. Green, F. Carrasco, and L. Lehner, *Holographic Path to the Turbulent Side of Gravity*, *Phys.Rev.* **X4** (2014), no. 1 011001, [arXiv:1309.7940].

[57] V. E. Hubeny, D. Marolf, and M. Rangamani, *Hawking radiation in large N strongly-coupled field theories*, *Class.Quant.Grav.* **27** (2010) 095015, [arXiv:0908.2270].

[58] V. E. Hubeny, D. Marolf, and M. Rangamani, *Black funnels and droplets from the AdS C-metrics*, *Class.Quant.Grav.* **27** (2010) 025001, [arXiv:0909.0005].

[59] V. E. Hubeny, D. Marolf, and M. Rangamani, *Hawking radiation from AdS black holes*, *Class.Quant.Grav.* **27** (2010) 095018, [arXiv:0911.4144].

[60] M. M. Caldarelli, O. J. Dias, R. Monteiro, and J. E. Santos, *Black funnels and droplets in thermal equilibrium*, *JHEP* **1105** (2011) 116, [arXiv:1102.4337].

[61] J. E. Santos and B. Way, *Black Funnels*, *JHEP* **1212** (2012) 060, [arXiv:1208.6291].

[62] J. E. Santos and B. Way, *Black Droplets*, *JHEP* **1408** (2014) 072, [arXiv:1405.2078].

[63] S. Bhattacharyya, V. E. Hubeny, R. Loganayagam, G. Mandal, S. Minwalla, *et. al.*, *Local Fluid Dynamical Entropy from Gravity*, *JHEP* **0806** (2008) 055, [arXiv:0803.2526].

[64] S. Bhattacharyya, V. E. Hubeny, S. Minwalla, and M. Rangamani, *Nonlinear Fluid Dynamics from Gravity*, *JHEP* **0802** (2008) 045, [arXiv:0712.2456].

[65] M. Rangamani, *Gravity and Hydrodynamics: Lectures on the fluid-gravity correspondence*, *Class.Quant.Grav.* **26** (2009) 224003, [arXiv:0905.4352].

[66] S. Fischetti and B. Way. To appear.

[67] P. Kraus, H. Ooguri, and S. Shenker, *Inside the horizon with AdS / CFT*, *Phys.Rev.* **D67** (2003) 124022, [hep-th/0212277].

[68] J. M. Maldacena, *Wilson loops in large N field theories*, *Phys.Rev.Lett.* **80** (1998) 4859–4862, [hep-th/9803002].

[69] S. Ryu and T. Takayanagi, *Holographic derivation of entanglement entropy from AdS/CFT*, *Phys.Rev.Lett.* **96** (2006) 181602, [hep-th/0603001].

[70] V. E. Hubeny, M. Rangamani, and T. Takayanagi, *A Covariant holographic entanglement entropy proposal*, *JHEP* **0707** (2007) 062, [arXiv:0705.0016].

[71] A. Lewkowycz and J. Maldacena, *Generalized gravitational entropy*, *JHEP* **1308** (2013) 090, [arXiv:1304.4926].

[72] A. Ashtekar and V. Petkov, eds., *Springer Handbook of Spacetime*. Springer, 2014.

[73] S. Fischetti and D. Marolf, *Flowing Funnels: Heat sources for field theories and the AdS_3 dual of CFT_2 Hawking radiation*, *Class.Quant.Grav.* **29** (2012) 105004, [arXiv:1202.5069].

[74] S. Fischetti, D. Marolf, and J. E. Santos, *AdS flowing black funnels: Stationary AdS black holes with non-Killing horizons and heat transport in the dual CFT*, *Class.Quant.Grav.* **30** (2013) 075001, [arXiv:1212.4820].

[75] S. Fischetti and J. E. Santos, *Rotating Black Droplet*, *JHEP* **1307** (2013) 156, [arXiv:1304.1156].

[76] T. Andrade, S. Fischetti, D. Marolf, S. F. Ross, and M. Rozali, *Entanglement and correlations near extremality: CFTs dual to Reissner-Nordstrm AdS_5*, *JHEP* **1404** (2014) 023, [arXiv:1312.2839].

[77] S. Fischetti, D. Marolf, and A. C. Wall, *A paucity of bulk entangling surfaces: AdS wormholes with de Sitter interiors*, *Class.Quant.Grav.* **32** (2015), no. 6 065011, [arXiv:1409.6754].

[78] S. Fischetti and D. Marolf, *Complex Entangling Surfaces for AdS and Lifshitz Black Holes?*, *Class.Quant.Grav.* **31** (2014), no. 21 214005, [arXiv:1407.2900].

[79] N. Engelhardt and S. Fischetti, *Covariant Constraints on Hole-ography*, arXiv:1507.0035.

[80] S. Fischetti, D. Kastor, and J. Traschen, *Non-Vacuum AdS Cosmologies and the Approach to Equilibrium of Entanglement Entropy*, *Class.Quant.Grav.* **31** (2014), no. 23 235007, [arXiv:1407.4299].

[81] G. T. Horowitz and V. E. Hubeny, *CFT description of small objects in AdS*, *JHEP* **0010** (2000) 027, [hep-th/0009051].

[82] S. Gubser, I. R. Klebanov, and A. M. Polyakov, *Gauge theory correlators from noncritical string theory*, *Phys.Lett.* **B428** (1998) 105–114, [hep-th/9802109].

[83] L. Abbott and S. Deser, *Stability of Gravity with a Cosmological Constant*, *Nucl.Phys.* **B195** (1982) 76.

[84] M. Henneaux and C. Teitelboim, *Hamiltonian Treatment of Asymptotically anti-de Sitter Spaces*, *Phys.Lett.* **B142** (1984) 355–358.

[85] M. Henneaux and C. Teitelboim, *Asymptotically anti-De Sitter Spaces*, *Commun.Math.Phys.* **98** (1985) 391–424.

[86] J. D. Brown and M. Henneaux, *Central Charges in the Canonical Realization of Asymptotic Symmetries: An Example from Three-Dimensional Gravity*, *Commun.Math.Phys.* **104** (1986) 207–226.

[87] I. Papadimitriou and K. Skenderis, *Thermodynamics of asymptotically locally AdS spacetimes*, *JHEP* **0508** (2005) 004, [hep-th/0505190].

[88] S. Hollands, A. Ishibashi, and D. Marolf, *Counter-term charges generate bulk symmetries*, *Phys.Rev.* **D72** (2005) 104025, [hep-th/0503105].

[89] T. Andrade and D. Marolf, *AdS/CFT beyond the unitarity bound*, *JHEP* **1201** (2012) 049, [arXiv:1105.6337].

[90] R. M. Wald, *General Relativity*. Chicago University Press, Chicago, USA, 1984.

[91] A. Ashtekar and A. Magnon, *Asymptotically anti-de Sitter space-times*, *Class.Quant.Grav.* **1** (1984) L39–L44.

[92] A. Ashtekar and S. Das, *Asymptotically Anti-de Sitter space-times: Conserved quantities*, *Class.Quant.Grav.* **17** (2000) L17–L30, [hep-th/9911230].

[93] M. C. Cheng and K. Skenderis, *Positivity of energy for asymptotically locally AdS spacetimes*, *JHEP* **0508** (2005) 107, [hep-th/0506123].

[94] K. Skenderis, *Asymptotically Anti-de Sitter space-times and their stress energy tensor*, *Int.J.Mod.Phys.* **A16** (2001) 740–749, [hep-th/0010138].

[95] K. Skenderis, *Lecture notes on holographic renormalization*, *Class.Quant.Grav.* **19** (2002) 5849–5876, [hep-th/0209067].

[96] S. de Haro, S. N. Solodukhin, and K. Skenderis, *Holographic reconstruction of space-time and renormalization in the AdS / CFT correspondence*, *Commun.Math.Phys.* **217** (2001) 595–622, [hep-th/0002230].

[97] R. Penrose and W. Rindler, *Spinors and Space-Time*, vol. 2. Cambridge University Press, 1984.

[98] C. Fefferman and C. R. Graham, *Conformal invariants*, in *Elie Cartan et les Mathématiques d'aujourd'hui*, Astérisque, p. 95, 1985.

[99] K. Skenderis and S. N. Solodukhin, *Quantum effective action from the AdS / CFT correspondence*, *Phys.Lett.* **B472** (2000) 316–322, [hep-th/9910023].

[100] P. Breitenlohner and D. Z. Freedman, *Positive Energy in anti-De Sitter Backgrounds and Gauged Extended Supergravity*, *Phys.Lett.* **B115** (1982) 197.

[101] J. D. Brown and J. York, James W., *Quasilocal energy and conserved charges derived from the gravitational action*, *Phys.Rev.* **D47** (1993) 1407–1419, [gr-qc/9209012].

[102] S. Hawking, *The path-integral approach to quantum gravity*, in *General Relativity: An Einstein Centenary Survey* (S. Hawking and W. Israel, eds.), vol. 1, pp. 746–789. Cambridge University Press, Cambridge; New York, 1979.

[103] M. Henningson and K. Skenderis, *The Holographic Weyl anomaly*, *JHEP* **9807** (1998) 023, [hep-th/9806087].

[104] V. Balasubramanian and P. Kraus, *A Stress tensor for Anti-de Sitter gravity*, *Commun.Math.Phys.* **208** (1999) 413–428, [hep-th/9902121].

[105] G. Compere and D. Marolf, *Setting the boundary free in AdS/CFT*, *Class.Quant.Grav.* **25** (2008) 195014, [arXiv:0805.1902].

[106] E. Witten, *A Simple Proof of the Positive Energy Theorem*, *Commun.Math.Phys.* **80** (1981) 381.

[107] J. A. Nester, *A New gravitational energy expression with a simple positivity proof*, *Phys.Lett.* **A83** (1981) 241.

[108] P. Townsend, *Positive energy and the scalar potential in higher dimensional (super)gravity theories*, *Phys.Lett.* **B148** (1984) 55.

[109] T. Hertog and S. Hollands, *Stability in designer gravity*, *Class.Quant.Grav.* **22** (2005) 5323–5342, [hep-th/0508181].

[110] A. J. Amsel and D. Marolf, *Energy Bounds in Designer Gravity*, *Phys.Rev.* **D74** (2006) 064006, [hep-th/0605101].

[111] A. J. Amsel, T. Hertog, S. Hollands, and D. Marolf, *A Tale of two superpotentials: Stability and instability in designer gravity*, *Phys.Rev.* **D75** (2007) 084008, [hep-th/0701038].

[112] T. Faulkner, G. T. Horowitz, and M. M. Roberts, *New stability results for Einstein scalar gravity*, *Class.Quant.Grav.* **27** (2010) 205007, [arXiv:1006.2387].

[113] A. J. Amsel and M. M. Roberts, *Stability in Einstein-Scalar Gravity with a Logarithmic Branch*, *Phys.Rev.* **D85** (2012) 106011, [arXiv:1112.3964].

[114] T. Hertog, *Violation of Energy Bounds in Designer Gravity*, *Class.Quant.Grav.* **24** (2007) 141–154, [hep-th/0607171].

[115] S. Deser and C. Teitelboim, *Supergravity Has Positive Energy*, *Phys.Rev.Lett.* **39** (1977) 249.

[116] M. T. Grisaru, *Positivity of the Energy in Einstein Theory*, *Phys.Lett.* **B73** (1978) 207.

[117] G. T. Horowitz and R. C. Myers, *The AdS / CFT correspondence and a new positive energy conjecture for general relativity*, *Phys.Rev.* **D59** (1998) 026005, [hep-th/9808079].

[118] E. Witten, *Instability of the Kaluza-Klein Vacuum*, *Nucl.Phys.* **B195** (1982) 481.

[119] D. Brill and H. Pfister, *STATES OF NEGATIVE TOTAL ENERGY IN KALUZA-KLEIN THEORY*, *Phys.Lett.* **B228** (1989) 359–362.

[120] E. Witten, *Anti-de Sitter space, thermal phase transition, and confinement in gauge theories*, *Adv.Theor.Math.Phys.* **2** (1998) 505–532, [hep-th/9803131].

[121] S. Hollands, A. Ishibashi, and D. Marolf, *Comparison between various notions of conserved charges in asymptotically AdS-spacetimes*, *Class.Quant.Grav.* **22** (2005) 2881–2920, [hep-th/0503045].

[122] R. E. Peierls, *The commutation laws of relativistic field theory*, *Proc. Roy. Soc. (London)* **214** (1952) 143.

[123] B. S. DeWitt, *Dynamical Theory of Groups and Fields.* Gordon and Breach, 1965.

[124] B. S. DeWitt, *The spacetime approach to quantum field theory*, in *Relativity, Groups, and Topology II: Les Houches, part 2* (B. S. Dewitt and R. Stora, eds.), p. 381. North-Holland, 1984.

[125] D. M. Marolf, *The Generalized Peierls bracket*, *Annals Phys.* **236** (1994) 392–412, [hep-th/9308150].

[126] R. D. Sorkin, *Conserved Quantities as Action Variations*, .

[127] M. Banados, C. Teitelboim, and J. Zanelli, *The Black hole in three-dimensional space-time*, *Phys.Rev.Lett.* **69** (1992) 1849–1851, [hep-th/9204099].

[128] M. Banados, M. Henneaux, C. Teitelboim, and J. Zanelli, *Geometry of the (2+1) black hole*, *Phys.Rev.* **D48** (1993) 1506–1525, [gr-qc/9302012].

[129] R. B. Mann and D. Marolf, *Holographic renormalization of asymptotically flat spacetimes*, *Class.Quant.Grav.* **23** (2006) 2927–2950, [hep-th/0511096].

[130] R. B. Mann, D. Marolf, and A. Virmani, *Covariant Counterterms and Conserved Charges in Asymptotically Flat Spacetimes*, *Class.Quant.Grav.* **23** (2006) 6357–6378, [gr-qc/0607041].

[131] R. B. Mann, D. Marolf, R. McNees, and A. Virmani, *On the Stress Tensor for Asymptotically Flat Gravity*, *Class.Quant.Grav.* **25** (2008) 225019, [arXiv:0804.2079].

[132] G. Gibbons, S. Hawking, G. T. Horowitz, and M. J. Perry, *Positive Mass Theorems for Black Holes*, *Commun.Math.Phys.* **88** (1983) 295.

[133] G. Gibbons, C. Hull, and N. Warner, *The Stability of Gauged Supergravity*, *Nucl.Phys.* **B218** (1983) 173.

[134] J. Katz, J. Bicak, and D. Lynden-Bell, *Relativistic conservation laws and integral constraints for large cosmological perturbations*, *Phys.Rev.* **D55** (1997) 5957–5969, [gr-qc/0504041].

[135] N. Deruelle and J. Katz, *On the mass of a Kerr-anti-de Sitter spacetime in D dimensions*, *Class.Quant.Grav.* **22** (2005) 421–424, [gr-qc/0410135].

[136] E. Thorne, Kip S., E. Price, R.H., and E. Macdonald, D.A., *Black Holes: The Membrane Paradigm*, .

[137] E. Witten, *Multitrace operators, boundary conditions, and AdS / CFT correspondence*, hep-th/0112258.

[138] S. S. Gubser and I. Mitra, *Double trace operators and one loop vacuum energy in AdS / CFT*, *Phys.Rev.* **D67** (2003) 064018, [hep-th/0210093].

[139] E. Witten, *SL(2,Z) action on three-dimensional conformal field theories with Abelian symmetry*, hep-th/0307041.

[140] D. Marolf, *Unitarity and Holography in Gravitational Physics*, *Phys.Rev.* **D79** (2009) 044010, [arXiv:0808.2842].

[141] S. Gao and R. M. Wald, *Theorems on gravitational time delay and related issues*, *Class.Quant.Grav.* **17** (2000) 4999–5008, [gr-qc/0007021].

[142] D. Marolf, *Holographic Thought Experiments*, *Phys.Rev.* **D79** (2009) 024029, [arXiv:0808.2845].

[143] D. Marolf, *Black Holes, AdS, and CFTs*, *Gen.Rel.Grav.* **41** (2009) 903–917, [arXiv:0810.4886].

[144] D. Marolf and A. C. Wall, *Eternal Black Holes and Superselection in AdS/CFT*, *Class.Quant.Grav.* **30** (2013) 025001, [arXiv:1210.3590].

[145] P. M. Chesler and L. G. Yaffe, *Holography and colliding gravitational shock waves in asymptotically AdS_5 spacetime*, *Phys.Rev.Lett.* **106** (2011) 021601, [arXiv:1011.3562].

[146] M. P. Heller, R. A. Janik, and P. Witaszczyk, *The characteristics of thermalization of boost-invariant plasma from holography*, *Phys.Rev.Lett.* **108** (2012) 201602, [arXiv:1103.3452].

[147] H. Bantilan, F. Pretorius, and S. S. Gubser, *Simulation of Asymptotically AdS5 Spacetimes with a Generalized Harmonic Evolution Scheme*, *Phys.Rev.* **D85** (2012) 084038, [arXiv:1201.2132].

[148] W. G. Unruh, *Notes on black hole evaporation*, *Phys. Rev. D* **614** (1976) 870.

[149] D. Astefanesei and R. C. Myers, "Boundary black holes and ads/cft correspondence." Talk presented by R.C. Myers at Black Holes IV: Theory and Mathematical Aspects, at Honey Harbor, Ontario, May 25-28, 2003.

[150] T. Tanaka, *Classical black hole evaporation in Randall-Sundrum infinite braneworld*, *Prog. Theor. Phys. Suppl.* **148** (2003) 307–316, [gr-qc/0203082].

[151] R. Emparan, A. Fabbri, and N. Kaloper, *Quantum black holes as holograms in AdS brane worlds*, *JHEP* **0208** (2002) 043, [hep-th/0206155].

[152] T. Wiseman, *Relativistic stars in Randall-Sundrum gravity*, *Phys.Rev.* **D65** (2002) 124007, [hep-th/0111057].

[153] T. Wiseman, *Static axisymmetric vacuum solutions and nonuniform black strings*, *Class.Quant.Grav.* **20** (2003) 1137–1176, [hep-th/0209051].

[154] R. Casadio and L. Mazzacurati, *Bulk shape of brane world black holes*, *Mod.Phys.Lett.* **A18** (2003) 651–660, [gr-qc/0205129].

[155] D. Karasik, C. Sahabandu, P. Suranyi, and L. Wijewardhana, *Small black holes in Randall-Sundrum I scenario*, *Phys.Rev.* **D69** (2004) 064022, [gr-qc/0309076].

[156] H. Kudoh, T. Tanaka, and T. Nakamura, *Small localized black holes in brane world: Formulation and numerical method*, *Phys.Rev.* **D68** (2003) 024035, [gr-qc/0301089].

[157] H. Kudoh, *Thermodynamical properties of small localized black hole*, *Prog.Theor.Phys.* **110** (2004) 1059–1069, [hep-th/0306067].

[158] H. Kudoh, *Six-dimensional localized black holes: Numerical solutions*, *Phys.Rev.* **D69** (2004) 104019, [hep-th/0401229].

[159] D. Karasik, C. Sahabandu, P. Suranyi, and L. Wijewardhana, *Small black holes on branes: Is the horizon regular or singular?*, *Phys.Rev.* **D70** (2004) 064007, [gr-qc/0404015].

[160] A. L. Fitzpatrick, L. Randall, and T. Wiseman, *On the existence and dynamics of braneworld black holes*, *JHEP* **0611** (2006) 033, [hep-th/0608208].

[161] H. Yoshino, *On the existence of a static black hole on a brane*, *JHEP* **0901** (2009) 068, [arXiv:0812.0465].

[162] R. Gregory, S. F. Ross, and R. Zegers, *Classical and quantum gravity of brane black holes*, *JHEP* **0809** (2008) 029, [arXiv:0802.2037].

[163] B. Kleihaus, J. Kunz, E. Radu, and D. Senkbeil, *Electric charge on the brane?*, *Phys.Rev.* **D83** (2011) 104050, [arXiv:1103.4758].

[164] P. Figueras, J. Lucietti, and T. Wiseman, *Ricci solitons, Ricci flow, and strongly coupled CFT in the Schwarzschild Unruh or Boulware vacua*, *Class.Quant.Grav.* **28** (2011) 215018, [arXiv:1104.4489]. Temporary entry.

[165] P. Figueras and T. Wiseman, *Gravity and large black holes in Randall-Sundrum II braneworlds*, *Phys.Rev.Lett.* **107** (2011) 081101, [arXiv:1105.2558]. Temporary entry.

[166] S. Kinoshita and N. Tanahashi, *Hawking temperature for near-equilibrium black holes*, *Phys.Rev.* **D85** (2012) 024050, [arXiv:1111.2684].

[167] G. Abreu and M. Visser, *Kodama time: Geometrically preferred foliations of spherically symmetric spacetimes*, *Phys.Rev.* **D82** (2010) 044027, [arXiv:1004.1456].

[168] M. Headrick, *Entanglement Renyi entropies in holographic theories*, *Phys.Rev.* **D82** (2010) 126010, [arXiv:1006.0047].

[169] D. Marolf, M. Rangamani, and M. Van Raamsdonk, *Holographic models of de Sitter QFTs*, *Class.Quant.Grav.* **28** (2011) 105015, [arXiv:1007.3996].

[170] L.-Y. Hung, R. C. Myers, M. Smolkin, and A. Yale, *Holographic Calculations of Renyi Entropy*, *JHEP* **1112** (2011) 047, [arXiv:1110.1084].

[171] J. Plebanski and M. Demianski, *Rotating, charged, and uniformly accelerating mass in general relativity*, *Annals Phys.* **98** (1976) 98–127.

[172] L. Randall and R. Sundrum, *A large mass hierarchy from a small extra dimension*, *Phys. Rev. Lett.* **83** (1999) 3370–3373, [hep-ph/9905221].

[173] L. Randall and R. Sundrum, *An alternative to compactification*, *Phys. Rev. Lett.* **83** (1999) 4690–4693, [hep-th/9906064].

[174] A. Chamblin, S. Hawking, and H. Reall, *Brane world black holes*, *Phys.Rev.* **D61** (2000) 065007, [hep-th/9909205].

[175] A. Chamblin, H. S. Reall, H.-a. Shinkai, and T. Shiromizu, *Charged brane world black holes*, *Phys.Rev.* **D63** (2001) 064015, [hep-th/0008177].

[176] B. Kol, *Topology change in general relativity, and the black hole black string transition*, *JHEP* **0510** (2005) 049, [hep-th/0206220].

[177] B. Kol and T. Wiseman, *Evidence that highly nonuniform black strings have a conical waist*, *Class.Quant.Grav.* **20** (2003) 3493–3504, [hep-th/0304070].

[178] R. Emparan and N. Haddad, *Self-similar critical geometries at horizon intersections and mergers*, arXiv:1109.1983.

[179] G. T. Horowitz and T. Wiseman, *General black holes in Kaluza-Klein theory*, arXiv:1107.5563.

[180] P. Di Francesco, P. Mathieu, and D. Sénéchal, *Conformal Field Theory*. Springer, New York, 1997.

[181] D. T. Son and A. O. Starinets, *Hydrodynamics of r-charged black holes*, *JHEP* **0603** (2006) 052, [hep-th/0601157].

[182] S. Khlebnikov, M. Kruczenski, and G. Michalogiorgakis, *Shock waves in strongly coupled plasmas*, *Phys.Rev.* **D82** (2010) 125003, [arXiv:1004.3803].

[183] S. Khlebnikov, M. Kruczenski, and G. Michalogiorgakis, *Shock waves in strongly coupled plasmas II*, *JHEP* **1107** (2011) 097, [arXiv:1105.1355].

[184] M. Headrick, S. Kitchen, and T. Wiseman, *A New approach to static numerical relativity, and its application to Kaluza-Klein black holes*, *Class.Quant.Grav.* **27** (2010) 035002, [arXiv:0905.1822].

[185] S. W. Hawking, *Black holes in general relativity*, *Commun. Math. Phys.* **25** (1972) 152–166.

[186] S. Hawking and G. Ellis, *The Large scale structure of space-time*. Cambridge University Press, 1973.

[187] S. Hollands, A. Ishibashi, and R. M. Wald, *A Higher dimensional stationary rotating black hole must be axisymmetric*, *Commun.Math.Phys.* **271** (2007) 699–722, [gr-qc/0605106].

[188] R. Emparan, G. T. Horowitz, and R. C. Myers, *Exact description of black holes on branes. 2. Comparison with BTZ black holes and black strings*, *JHEP* **0001** (2000) 021, [hep-th/9912135].

[189] P. Figueras and T. Wiseman, *Stationary holographic plasma quenches and numerical methods for non-Killing horizons*, *Phys.Rev.Lett.* **110** (2013) 171602, [arXiv:1212.4498].

[190] R. Emparan, *AdS membranes wrapped on surfaces of arbitrary genus*, *Phys.Lett.* **B432** (1998) 74–82, [hep-th/9804031].

[191] D. Birmingham, *Topological black holes in Anti-de Sitter space*, *Class.Quant.Grav.* **16** (1999) 1197–1205, [hep-th/9808032].

[192] R. Emparan, *AdS / CFT duals of topological black holes and the entropy of zero energy states*, *JHEP* **9906** (1999) 036, [hep-th/9906040].

[193] S. R. Das, A. Ghosh, J.-H. Oh, and A. D. Shapere, *On Dumb Holes and their Gravity Duals*, *JHEP* **1104** (2011) 030, [arXiv:1011.3822].

[194] A. Adam, S. Kitchen, and T. Wiseman, *A numerical approach to finding general stationary vacuum black holes*, *Class.Quant.Grav.* **29** (2012) 165002, [arXiv:1105.6347].

[195] S. M. Carroll, *Spacetime and geometry: An introduction to general relativity*. Addison-Wesley, San Francisco, USA, 2004.

[196] S. W. Hawking, *Black hole explosions?*, *Nature* **248** (1974) 30–31.

[197] N. D. Birrell and P. C. W. Davies, *Quantum fields in curved space*. Cambridge University Press, 1982.

[198] A. R. Steif, *The Quantum stress tensor in the three-dimensional black hole*, *Phys.Rev.* **D49** (1994) 585–589, [gr-qc/9308032].

[199] R. Myers and M. Perry, *Black holes in higher dimensional space-times*, *Annals of Physics* **172** (1986), no. 2 304 – 347.

[200] R. C. Myers, *Myers-Perry black holes*, arXiv:1111.1903.

[201] P. Figueras and S. Tunyasuvunakool, *CFTs in rotating black hole backgrounds*, *Class.Quant.Grav.* **30** (2013) 125015, [arXiv:1304.1162].

[202] S. A. Fulling and P. C. W. Davies, *Radiation from a moving mirror in two dimensional space-time: Conformal anomaly*, *Proc.R.Soc.Lond.A.* **348** (1976) 393–414.

[203] H. Casimir, *On the Attraction Between Two Perfectly Conducting Plates*, *Indag.Math.* **10** (1948) 261–263.

[204] H. Epstein, V. Glaser, and A. Jaffe, *Nonpositivity of the energy density in quantized field theories*, *Il Nuovo Cimento Series 10* **36** (1965) 1016–1022.

[205] P. C. W. Davies, S. A. Fulling, and W. G. Unruh, *Energy-momentum tensor near an evaporating black hole*, *Phys. Rev. D* **13** (May, 1976) 2720–2723.

[206] D. N. Page, *Thermal stress tensors in static einstein spaces*, *Phys. Rev. D* **25** (Mar, 1982) 1499–1509.

[207] J. D. Bekenstein and L. Parker, *Path-integral evaluation of feynman propagator in curved spacetime*, *Phys. Rev. D* **23** (Jun, 1981) 2850–2869.

[208] P. Candelas, *Vacuum polarization in schwarzschild spacetime*, *Phys. Rev. D* **21** (Apr, 1980) 2185–2202.

[209] S. M. Christensen and S. A. Fulling, *Trace anomalies and the hawking effect*, *Phys. Rev. D* **15** (Apr, 1977) 2088–2104.

[210] F. Tangherlini, *Schwarzschild field in n dimensions and the dimensionality of space problem*, *Nuovo Cim.* **27** (1963) 636–651.

[211] S. B. Giddings, E. Katz, and L. Randall, *Linearized gravity in brane backgrounds*, *JHEP* **0003** (2000) 023, [hep-th/0002091].

[212] S. P. Trivedi, *Semiclassical extremal black holes*, *Phys. Rev. D* **47** (May, 1993) 4233–4238.

[213] D. J. Loranz, W. A. Hiscock, and P. R. Anderson, *Thermal divergences on the event horizons of two-dimensional black holes*, *Phys. Rev. D* **52** (Oct, 1995) 4554–4558.

[214] R. Balbinot, S. Fagnocchi, A. Fabbri, S. Farese, and J. Navarro-Salas, *On the quantum stress tensor for extreme 2-D Reissner-Nordstrom black holes*, *Phys.Rev.* **D70** (2004) 064031, [hep-th/0405263].

[215] S. Farese, *Regularity of the stress-energy tensor for extremal Reissner-Nordstrom black holes*, *J.Phys.Conf.Ser.* **33** (2006) 451–456, [hep-th/0512181].

[216] P. R. Anderson, W. A. Hiscock, and D. J. Loranz, *Semiclassical stability of the extreme reissner-nordström black hole*, *Phys. Rev. Lett.* **74** (May, 1995) 4365–4368.

[217] D. M. DeTurck, *Deforming metrics in the direction of their Ricci tensors*, *Journal of Differential Geometry* **18** (1983) 157–162.

[218] R. Gregory, *Black string instabilities in Anti-de Sitter space*, *Class.Quant.Grav.* **17** (2000) L125–L132, [hep-th/0004101].

[219] E. Poisson and W. Israel, *Internal structure of black holes*, *Phys. Rev. D* **41** (Mar, 1990) 1796–1809.

[220] C. Holzhey, F. Larsen, and F. Wilczek, *Geometric and renormalized entropy in conformal field theory*, *Nucl.Phys.* **B424** (1994) 443–467, [hep-th/9403108].

[221] P. Calabrese and J. L. Cardy, *Entanglement entropy and quantum field theory*, *J.Stat.Mech.* **0406** (2004) P06002, [hep-th/0405152].

[222] J. M. Maldacena, *Eternal black holes in anti-de Sitter*, *JHEP* **0304** (2003) 021, [hep-th/0106112].

[223] M. Van Raamsdonk, *Comments on quantum gravity and entanglement*, arXiv:0907.2939.

[224] M. Van Raamsdonk, *Building up spacetime with quantum entanglement*, *Gen.Rel.Grav.* **42** (2010) 2323–2329, [arXiv:1005.3035].

[225] J. Maldacena and L. Susskind, *Cool horizons for entangled black holes*, arXiv:1306.0533.

[226] I. A. Morrison and M. M. Roberts, *Mutual information between thermo-field doubles and disconnected holographic boundaries*, arXiv:1211.2887.

[227] D. Brecher, J. He, and M. Rozali, *On charged black holes in anti-de Sitter space*, *JHEP* **0504** (2005) 004, [hep-th/0410214].

[228] G. Festuccia and H. Liu, *Excursions beyond the horizon: Black hole singularities in Yang-Mills theories. I.*, *JHEP* **0604** (2006) 044, [hep-th/0506202].

[229] T. Hartman and J. Maldacena, *Time Evolution of Entanglement Entropy from Black Hole Interiors*, *JHEP* **1305** (2013) 014, [arXiv:1303.1080].

[230] M. Edalati, J. F. Pedraza, and W. Tangarife Garcia, *Quantum Fluctuations in Holographic Theories with Hyperscaling Violation*, *Phys.Rev.* **D87** (2013), no. 4 046001, [arXiv:1210.6993].

[231] W. Fischler and S. Kundu, *Strongly Coupled Gauge Theories: High and Low Temperature Behavior of Non-local Observables*, *JHEP* **1305** (2013) 098, [arXiv:1212.2643].

[232] W. Fischler, A. Kundu, and S. Kundu, *Holographic Mutual Information at Finite Temperature*, *Phys.Rev.* **D87** (2013) 126012, [arXiv:1212.4764].

[233] S. S. Gubser, *Breaking an Abelian gauge symmetry near a black hole horizon*, *Phys.Rev.* **D78** (2008) 065034, [arXiv:0801.2977].

[234] S. S. Gubser and A. Nellore, *Low-temperature behavior of the Abelian Higgs model in anti-de Sitter space*, *JHEP* **0904** (2009) 008, [arXiv:0810.4554].

[235] S. A. Hartnoll, C. P. Herzog, and G. T. Horowitz, *Building a Holographic Superconductor*, *Phys.Rev.Lett.* **101** (2008) 031601, [arXiv:0803.3295].

[236] S. A. Hartnoll, C. P. Herzog, and G. T. Horowitz, *Holographic Superconductors*, *JHEP* **0812** (2008) 015, [arXiv:0810.1563].

[237] F. Denef and S. A. Hartnoll, *Landscape of superconducting membranes*, *Phys.Rev.* **D79** (2009) 126008, [arXiv:0901.1160].

[238] S.-S. Lee, *A Non-Fermi Liquid from a Charged Black Hole: A Critical Fermi Ball*, *Phys.Rev.* **D79** (2009) 086006, [arXiv:0809.3402].

[239] H. Liu, J. McGreevy, and D. Vegh, *Non-Fermi liquids from holography*, *Phys.Rev.* **D83** (2011) 065029, [arXiv:0903.2477].

[240] M. Cubrovic, J. Zaanen, and K. Schalm, *String Theory, Quantum Phase Transitions and the Emergent Fermi-Liquid*, *Science* **325** (2009) 439–444, [arXiv:0904.1993].

[241] T. Faulkner, H. Liu, J. McGreevy, and D. Vegh, *Emergent quantum criticality, Fermi surfaces, and AdS(2)*, *Phys.Rev.* **D83** (2011) 125002, [arXiv:0907.2694].

[242] J. S. Schwinger, *On gauge invariance and vacuum polarization*, *Phys.Rev.* **82** (1951) 664–679.

[243] G. Gibbons, *Vacuum Polarization and the Spontaneous Loss of Charge by Black Holes*, *Commun.Math.Phys.* **44** (1975) 245–264.

[244] S. A. Hartnoll, J. Polchinski, E. Silverstein, and D. Tong, *Towards strange metallic holography*, *JHEP* **1004** (2010) 120, [arXiv:0912.1061].

[245] S. D. Mathur, *The Fuzzball proposal for black holes: An Elementary review*, *Fortsch.Phys.* **53** (2005) 793–827, [hep-th/0502050].

[246] A. Sen, *State Operator Correspondence and Entanglement in AdS_2/CFT_1*, *Entropy* **13** (2011) 1305–1323, [arXiv:1101.4254].

[247] K. Jensen, S. Kachru, A. Karch, J. Polchinski, and E. Silverstein, *Towards a holographic marginal Fermi liquid*, *Phys.Rev.* **D84** (2011) 126002, [arXiv:1105.1772].

[248] V. A. Kostelecky and M. J. Perry, *Solitonic black holes in gauged N=2 supergravity*, *Phys.Lett.* **B371** (1996) 191–198, [hep-th/9512222].

[249] J. B. Gutowski and H. S. Reall, *Supersymmetric AdS(5) black holes*, *JHEP* **0402** (2004) 006, [hep-th/0401042].

[250] S. D. Mathur, *The Information paradox: A Pedagogical introduction*, *Class.Quant.Grav.* **26** (2009) 224001, [arXiv:0909.1038].

[251] B. Groisman, S. Popescu, and A. Winter, *Quantum, classical, and total amount of correlations in a quantum state*, *Phys.Rev.A* **72** (Sept., 2005) 032317, [quant-ph/0410091].

[252] M. M. Wolf, F. Verstraete, M. B. Hastings, and J. I. Cirac, *Area Laws in Quantum Systems: Mutual Information and Correlations*, *Physical Review Letters* **100** (Feb., 2008) 070502, [arXiv:0704.3906].

[253] E. H. Lieb and M. B. Ruskai, *A Fundamental Property of Quantum-Mechanical Entropy*, *Phys.Rev.Lett.* **30** (1973) 434–436.

[254] E. Lieb and M. Ruskai, *Proof of the strong subadditivity of quantum-mechanical entropy*, *J.Math.Phys.* **14** (1973) 1938–1941.

[255] M. Headrick and T. Takayanagi, *A Holographic proof of the strong subadditivity of entanglement entropy*, *Phys.Rev.* **D76** (2007) 106013, [arXiv:0704.3719].

[256] V. E. Hubeny, *Extremal surfaces as bulk probes in AdS/CFT*, *JHEP* **1207** (2012) 093, [arXiv:1203.1044].

[257] P. Calabrese and J. Cardy, *Entanglement entropy and conformal field theory*, *J.Phys.* **A42** (2009) 504005, [arXiv:0905.4013].

[258] D. P. Divincenzo, M. Horodecki, D. W. Leung, J. A. Smolin, and B. M. Terhal, *Locking Classical Correlations in Quantum States*, *Physical Review Letters* **92** (Feb., 2004) 067902, [quant-ph/0303088].

[259] P. Hayden, D. Leund, P. W. Shor, and A. Winter, *Randomizing Quantum States: Constructions and Applications* , *Communications in Mathematical Physics* **250** (Sept., 2004) 371–391.

[260] I. R. Klebanov and E. Witten, *AdS / CFT correspondence and symmetry breaking*, *Nucl.Phys.* **B556** (1999) 89–114, [hep-th/9905104].

[261] J. Louko, D. Marolf, and S. F. Ross, *On geodesic propagators and black hole holography*, *Phys.Rev.* **D62** (2000) 044041, [hep-th/0002111].

[262] B. Wang, C.-Y. Lin, and C. Molina, *Quasinormal behavior of massless scalar field perturbation in Reissner-Nordstrom anti-de Sitter spacetimes*, *Phys.Rev.* **D70** (2004) 064025, [hep-th/0407024].

[263] A. Belin, L.-Y. Hung, A. Maloney, S. Matsuura, R. C. Myers, *et. al.*, *Holographic Charged Renyi Entropies*, arXiv:1310.4180.

[264] S. Östlund and S. Rommer, *Thermodynamic Limit of Density Matrix Renormalization*, *Physical Review Letters* **75** (Nov., 1995) 3537–3540, [cond-mat/9503107].

[265] F. Verstraete and J. I. Cirac, *Renormalization algorithms for Quantum-Many Body Systems in two and higher dimensions*, *eprint arXiv:cond-mat/0407066* (July, 2004) [cond-mat/0407066].

[266] G. Vidal, *Class of Quantum Many-Body States That Can Be Efficiently Simulated*, *Physical Review Letters* **101** (Sept., 2008) 110501, [quant-ph/0610099].

[267] G. Vidal, *Entanglement Renormalization: an introduction*, *ArXiv e-prints* (Dec., 2009) [arXiv:0912.1651].

[268] U. Schollwöck, *The density-matrix renormalization group in the age of matrix product states*, *Annals of Physics* **326** (Jan., 2011) 96–192, [arXiv:1008.3477].

[269] J. Abajo-Arrastia, J. Aparicio, and E. Lopez, *Holographic Evolution of Entanglement Entropy*, *JHEP* **1011** (2010) 149, [arXiv:1006.4090].

[270] T. Albash and C. V. Johnson, *Evolution of Holographic Entanglement Entropy after Thermal and Electromagnetic Quenches*, *New J.Phys.* **13** (2011) 045017, [arXiv:1008.3027].

[271] V. Balasubramanian, A. Bernamonti, J. de Boer, N. Copland, B. Craps, *et. al.*, *Thermalization of Strongly Coupled Field Theories*, *Phys.Rev.Lett.* **106** (2011) 191601, [arXiv:1012.4753].

[272] C. T. Asplund and S. G. Avery, *Evolution of Entanglement Entropy in the D1-D5 Brane System*, *Phys.Rev.* **D84** (2011) 124053, [arXiv:1108.2510].

[273] J. Aparicio and E. Lopez, *Evolution of Two-Point Functions from Holography*, *JHEP* **1112** (2011) 082, [arXiv:1109.3571].

[274] P. Basu and S. R. Das, *Quantum Quench across a Holographic Critical Point*, *JHEP* **1201** (2012) 103, [arXiv:1109.3909].

[275] V. Balasubramanian, A. Bernamonti, N. Copland, B. Craps, and F. Galli, *Thermalization of mutual and tripartite information in strongly coupled two dimensional conformal field theories*, *Phys.Rev.* **D84** (2011) 105017, [arXiv:1110.0488].

[276] A. Allais and E. Tonni, *Holographic evolution of the mutual information*, *JHEP* **1201** (2012) 102, [arXiv:1110.1607].

[277] P. Basu, D. Das, S. R. Das, and T. Nishioka, *Quantum Quench Across a Zero Temperature Holographic Superfluid Transition*, *JHEP* **1303** (2013) 146, [arXiv:1211.7076].

[278] A. Buchel, L. Lehner, R. C. Myers, and A. van Niekerk, *Quantum quenches of holographic plasmas*, *JHEP* **1305** (2013) 067, [arXiv:1302.2924].

[279] D. Marolf, M. Rangamani, and T. Wiseman, *Holographic thermal field theory on curved spacetimes*, arXiv:1312.0612.

[280] S. Ryu and T. Takayanagi, *Aspects of Holographic Entanglement Entropy*, *JHEP* **0608** (2006) 045, [hep-th/0605073].

[281] S. H. Shenker and D. Stanford, *Multiple Shocks*, *JHEP* **1412** (2014) 046, [arXiv:1312.3296].

[282] S. Leichenauer, *Disrupting Entanglement of Black Holes*, *Phys.Rev.* **D90** (2014) 046009, [arXiv:1405.7365].

[283] B. Freivogel, V. E. Hubeny, A. Maloney, R. C. Myers, M. Rangamani, *et. al.*, *Inflation in AdS/CFT*, *JHEP* **0603** (2006) 007, [hep-th/0510046].

[284] M. Alishahiha, A. Karch, E. Silverstein, and D. Tong, *The dS/dS correspondence*, *AIP Conf.Proc.* **743** (2005) 393–409, [hep-th/0407125].

[285] M. Alishahiha, A. Karch, and E. Silverstein, *Hologravity*, *JHEP* **0506** (2005) 028, [hep-th/0504056].

[286] X. Dong, B. Horn, S. Matsuura, E. Silverstein, and G. Torroba, *FRW solutions and holography from uplifted AdS/CFT*, *Phys.Rev.* **D85** (2012) 104035, [arXiv:1108.5732].

[287] E. Farhi and A. H. Guth, *An Obstacle to Creating a Universe in the Laboratory*, *Phys.Lett.* **B183** (1987) 149.

[288] D. V. Fursaev, *Proof of the holographic formula for entanglement entropy*, *JHEP* **0609** (2006) 018, [hep-th/0606184].

[289] T. Faulkner, *The Entanglement Renyi Entropies of Disjoint Intervals in AdS/CFT*, arXiv:1303.7221.

[290] T. Hartman, *Entanglement Entropy at Large Central Charge*, arXiv:1303.6955.

[291] D. Fursaev, *Notes on Derivation of 'Generalized Gravitational Entropy'*, arXiv:1406.5635.

[292] J. L. Friedman, K. Schleich, and D. M. Witt, *Topological censorship*, *Phys.Rev.Lett.* **71** (1993) 1486–1489, [gr-qc/9305017].

[293] G. Galloway, K. Schleich, D. Witt, and E. Woolgar, *The AdS / CFT correspondence conjecture and topological censorship*, *Phys.Lett.* **B505** (2001) 255–262, [hep-th/9912119].

[294] A. C. Wall, *The Generalized Second Law implies a Quantum Singularity Theorem*, *Class.Quant.Grav.* **30** (2013) 165003, [arXiv:1010.5513].

[295] H. Firouzjahi and F. Leblond, *The Clash between de Sitter and anti-de Sitter space*, *JCAP* **0306** (2003) 003, [hep-th/0209248].

[296] D. Das, S. R. Das, and K. Narayan, *dS/CFT at uniform energy density and a de Sitter 'bluewall'*, *JHEP* **1404** (2014) 116, [arXiv:1312.1625].

[297] E. Poisson and W. Israel, *Internal structure of black holes*, *Phys.Rev.* **D41** (1990) 1796–1809.

[298] A. Ori, *Inner structure of a charged black hole: An exact mass-inflation solution*, *Phys.Rev.Lett.* **67** (1991) 789–792.

[299] M. Dafermos, *The Interior of charged black holes and the problem of uniqueness in general relativity*, *Commun.Pure Appl.Math.* **58** (2005) 0445–0504, [gr-qc/0307013].

[300] P. Vaidya, *The External Field of a Radiating Star in Relativity*, *Curr. Sci.* **12** (1943) 183. republished as Gen.Rel.Grav. **31** 119-120.

[301] P. Vaidya, *The Gravitational Field of a Radiating Star*, *Proc.Indian Acad.Sci.* **A33** (1951) 264. republished as Gen.Rel.Grav. **31** 121-135.

[302] E. Poisson, *A Relativist's Toolkit: The Mathematics of Black-Hole Mechanics*. Cambridge University Press, 2004.

[303] A. C. Wall, *Maximin Surfaces, and the Strong Subadditivity of the Covariant Holographic Entanglement Entropy*, *Class.Quant.Grav.* **31** (2014), no. 22 225007, [arXiv:1211.3494].

[304] S. Hawking, *Gravitational radiation from colliding black holes*, *Phys.Rev.Lett.* **26** (1971) 1344–1346.

[305] P. T. Chrusciel, E. Delay, G. J. Galloway, and R. Howard, *The Area theorem*, *Annales Henri Poincare* **2** (2001) 109–178, [gr-qc/0001003].

[306] B. Czech, J. L. Karczmarek, F. Nogueira, and M. Van Raamsdonk, *The Gravity Dual of a Density Matrix*, *Class.Quant.Grav.* **29** (2012) 155009, [arXiv:1204.1330].

[307] R. Bousso, S. Leichenauer, and V. Rosenhaus, *Light-sheets and AdS/CFT*, *Phys.Rev.* **D86** (2012) 046009, [arXiv:1203.6619].

[308] V. E. Hubeny and M. Rangamani, *Causal Holographic Information*, *JHEP* **1206** (2012) 114, [arXiv:1204.1698].

[309] H. Araki, *Relative Entropy of States of Von Neumann Algebras*, *Publ.Res.Inst.Math.Sci.Kyoto* **1976** (1976) 809–833.

[310] V. Balasubramanian, A. Bernamonti, B. Craps, V. Kernen, E. Keski-Vakkuri, *et. al.*, *Thermalization of the spectral function in strongly coupled two dimensional conformal field theories*, *JHEP* **1304** (2013) 069, [arXiv:1212.6066].

[311] O. M. A.P. Prudnikov, Yu.A. Brychkov, *Integrals and Series*, vol. 3. Gordon and Breach Science Publishers, 1986.

[312] T. Faulkner, A. Lewkowycz, and J. Maldacena, *Quantum corrections to holographic entanglement entropy*, *JHEP* **1311** (2013) 074, [arXiv:1307.2892].

[313] N. Engelhardt and A. C. Wall, *Quantum Extremal Surfaces: Holographic Entanglement Entropy beyond the Classical Regime*, *JHEP* **1501** (2015) 073, [arXiv:1408.3203].

[314] S. Kachru, R. Kallosh, A. D. Linde, and S. P. Trivedi, *De Sitter vacua in string theory*, *Phys.Rev.* **D68** (2003) 046005, [hep-th/0301240].

[315] T. Nishioka, S. Ryu, and T. Takayanagi, *Holographic Entanglement Entropy: An Overview*, *J.Phys.* **A42** (2009) 504008, [arXiv:0905.0932].

[316] M. Nozaki, T. Numasawa, A. Prudenziati, and T. Takayanagi, *Dynamics of Entanglement Entropy from Einstein Equation*, *Phys.Rev.* **D88** (2013), no. 2 026012, [arXiv:1304.7100].

[317] N. Lashkari, M. B. McDermott, and M. Van Raamsdonk, *Gravitational Dynamics From Entanglement "Thermodynamics"*, *JHEP* **1404** (2014) 195, [arXiv:1308.3716].

[318] T. Faulkner, M. Guica, T. Hartman, R. C. Myers, and M. Van Raamsdonk, *Gravitation from Entanglement in Holographic CFTs*, *JHEP* **1403** (2014) 051, [arXiv:1312.7856].

[319] B. Swingle and M. Van Raamsdonk, *Universality of Gravity from Entanglement*, arXiv:1405.2933.

[320] V. Balasubramanian, P. Hayden, A. Maloney, D. Marolf, and S. F. Ross, *Multiboundary Wormholes and Holographic Entanglement*, arXiv:1406.2663.

[321] V. Balasubramanian and S. F. Ross, *Holographic particle detection*, *Phys.Rev.* **D61** (2000) 044007, [hep-th/9906226].

[322] M. Taylor, *Non-relativistic holography*, arXiv:0812.0530.

[323] M. Headrick, "Entanglement entropy." Talk at KITP Conference: Quantum Fields beyond Perturbation Theory, 2014.

[324] R. C. Myers Private discussion, May, 2013.

[325] D. R. Brill, *Multi-black-hole geometries in (2+ 1)-dimensional gravity*, *Physical Review D* **53** (1996), no. 8 R4133, [gr-qc/9511022].

[326] D. Brill, *Black holes and wormholes in 2+ 1 dimensions*, in *Mathematical and quantum aspects of relativity and cosmology*, pp. 143–179. Springer, 2000. gr-qc/9904083.

[327] S. Aminneborg, I. Bengtsson, D. Brill, S. Holst, and P. Peldan, *Black holes and wormholes in (2+1)-dimensions*, *Class. Quant. Grav.* **15** (1998) 627–644, [gr-qc/9707036].

[328] S. Aminneborg, I. Bengtsson, and S. Holst, *A spinning anti-de Sitter wormhole*, *Class. Quant. Grav.* **16** (1999) 363–382, [gr-qc/9805028].

[329] J. Louko and D. Marolf, *Single exterior black holes and the AdS / CFT conjecture*, *Phys.Rev.* **D59** (1999) 066002, [hep-th/9808081].

[330] K. Skenderis and B. C. van Rees, *Holography and wormholes in 2+ 1 dimensions*, *Communications in Mathematical Physics* **301** (2011), no. 3 583–626, [arXiv:0912.2090].

[331] D. Marolf, *Path integrals and instantons in quantum gravity: Minisuperspace models*, *Phys.Rev.* **D53** (1996) 6979–6990, [gr-qc/9602019].

[332] G. Festuccia and H. Liu, *A Bohr-Sommerfeld quantization formula for quasinormal frequencies of AdS black holes*, *Adv.Sci.Lett.* **2** (2009) 221–235, [arXiv:0811.1033].

[333] S. Kachru, X. Liu, and M. Mulligan, *Gravity duals of Lifshitz-like fixed points*, *Phys.Rev.* **D78** (2008) 106005, [arXiv:0808.1725].

[334] C. Hoyos and P. Koroteev, *On the Null Energy Condition and Causality in Lifshitz Holography*, *Phys.Rev.* **D82** (2010) 084002, [arXiv:1007.1428].

[335] M. Alishahiha, A. F. Astaneh, and M. R. M. Mozaffar, *Thermalization in backgrounds with hyperscaling violating factor*, *Phys.Rev.* **D90** (2014), no. 4 046004, [arXiv:1401.2807].

[336] N. Engelhardt and A. C. Wall, *Extremal Surface Barriers*, *JHEP* **1403** (2014) 068, [arXiv:1312.3699].

[337] B. Czech and L. Lamprou, *Holographic definition of points and distances*, *Phys.Rev.* **D90** (2014), no. 10 106005, [arXiv:1409.4473].

[338] B. Czech, L. Lamprou, S. McCandlish, and J. Sully, *Integral Geometry and Holography*, 1505.05515.

[339] V. Balasubramanian, B. Czech, B. D. Chowdhury, and J. de Boer, *The entropy of a hole in spacetime*, *JHEP* **1310** (2013) 220, [arXiv:1305.0856].

[340] V. Balasubramanian, B. D. Chowdhury, B. Czech, J. de Boer, and M. P. Heller, *Bulk curves from boundary data in holography*, *Phys.Rev.* **D89** (2014), no. 8 086004, [arXiv:1310.4204].

[341] B. Czech, X. Dong, and J. Sully, *Holographic Reconstruction of General Bulk Surfaces*, *JHEP* **1411** (2014) 015, [arXiv:1406.4889].

[342] M. Headrick, R. C. Myers, and J. Wien, *Holographic Holes and Differential Entropy*, *JHEP* **1410** (2014) 149, [arXiv:1408.4770].

[343] R. C. Myers, J. Rao, and S. Sugishita, *Holographic Holes in Higher Dimensions*, *JHEP* **1406** (2014) 044, [arXiv:1403.3416].

[344] R. Bousso, *Holography in general space-times*, *JHEP* **9906** (1999) 028, [hep-th/9906022].

[345] B. Swingle, *Entanglement Renormalization and Holography*, *Phys.Rev.* **D86** (2012) 065007, [arXiv:0905.1317].

[346] B. Swingle, *Constructing holographic spacetimes using entanglement renormalization*, arXiv:1209.3304.

[347] B. Freivogel, R. A. Jefferson, L. Kabir, B. Mosk, and I.-S. Yang, *Casting Shadows on Holographic Reconstruction*, *Phys.Rev.* **D91** (2015), no. 8 086013, [arXiv:1412.5175].

[348] A. Ashtekar and B. Krishnan, *Dynamical horizons: Energy, angular momentum, fluxes and balance laws*, *Phys.Rev.Lett.* **89** (2002) 261101, [gr-qc/0207080].

[349] S. Hayward, *General laws of black hole dynamics*, *Phys.Rev.* **D49** (1994) 6467–6474.

[350] R. Bousso and N. Engelhardt, *A New Area Law in General Relativity*, arXiv:1504.0762.

[351] R. Bousso and N. Engelhardt, *Proof of a New Area Law in General Relativity*, arXiv:1504.0766.

[352] R. Bousso, *A Covariant entropy conjecture*, *JHEP* **9907** (1999) 004, [hep-th/9905177].

[353] S. Fischetti, W. Kelly, and D. Marolf, *Conserved Charges in Asymptotically (Locally) AdS Spacetimes*, arXiv:1211.6347.

[354] V. E. Hubeny and H. Maxfield, *Holographic probes of collapsing black holes*, *JHEP* **1403** (2014) 097, [arXiv:1312.6887].

[355] V. Balasubramanian, B. D. Chowdhury, B. Czech, and J. de Boer, *Entwinement and the emergence of spacetime*, *JHEP* **1501** (2015) 048, [arXiv:1406.5859].

[356] R. Bousso, Z. Fisher, S. Leichenauer, and A. C. Wall, *A Quantum Focussing Conjecture*, arXiv:1506.0266.

[357] R. Bousso and N. Engelhardt. To appear.

[358] A. Chamblin and G. Gibbons, *Supergravity on the brane*, *Phys.Rev.Lett.* **84** (2000) 1090–1093, [hep-th/9909130].

[359] N. Engelhardt and G. T. Horowitz, *Entanglement Entropy Near Cosmological Singularities*, *JHEP* **1306** (2013) 041, [arXiv:1303.4442].

[360] F. M. Haehl, *The Schwarzschild-Black String AdS Soliton: Instability and Holographic Heat Transport*, *Class.Quant.Grav.* **30** (2013) 055002, [arXiv:1210.5763].

[361] M. Cvetic, H. Lu, and C. Pope, *Brane world Kaluza-Klein reductions and branes on the brane*, *J.Math.Phys.* **42** (2001) 3048–3070, [hep-th/0009183].

[362] H. Lu and C. Pope, *Branes on the brane*, *Nucl.Phys.* **B598** (2001) 492–508, [hep-th/0008050].

[363] I. Park, C. Pope, and A. Sadrzadeh, *AdS brane world Kaluza-Klein reduction*, *Class.Quant.Grav.* **19** (2002) 6237–6258, [hep-th/0110238].

[364] S. R. Das, J. Michelson, K. Narayan, and S. P. Trivedi, *Cosmologies with Null Singularities and their Gauge Theory Duals*, *Phys.Rev.* **D75** (2007) 026002, [hep-th/0610053].

[365] A. Awad, S. R. Das, K. Narayan, and S. P. Trivedi, *Gauge theory duals of cosmological backgrounds and their energy momentum tensors*, *Phys.Rev.* **D77** (2008) 046008, [arXiv:0711.2994].

[366] K. Koyama and J. Soda, *Strongly coupled CFT in FRW universe from AdS / CFT correspondence*, *JHEP* **0105** (2001) 027, [hep-th/0101164].

[367] W. Fischler, S. Kundu, and J. F. Pedraza, *Entanglement and out-of-equilibrium dynamics in holographic models of de Sitter QFTs*, *JHEP* **1407** (2014) 021, [arXiv:1311.5519].

[368] J. E. Lidsey, *Holographic Cosmology from the First Law of Thermodynamics and the Generalized Uncertainty Principle*, *Phys.Rev.* **D88** (2013) 103519, [arXiv:0911.3286].

[369] J. Erdmenger, K. Ghoroku, R. Meyer, and I. Papadimitriou, *Holographic Cosmological Backgrounds, Wilson Loop (De)confinement and Dilaton Singularities*, *Fortsch.Phys.* **60** (2012) 991–997, [arXiv:1205.0677].

[370] K. Ghoroku and A. Nakamura, *Holographic Friedmann equation and N=4 supersymmetric Yang-Mills theory*, *Phys.Rev.* **D87** (2013), no. 6 063507, [arXiv:1212.2304].

[371] S. Banerjee, S. Bhowmick, A. Sahay, and G. Siopsis, *Generalized Holographic Cosmology*, *Class.Quant.Grav.* **30** (2013) 075022, [arXiv:1207.2983].

[372] P. Binetruy, C. Deffayet, U. Ellwanger, and D. Langlois, *Brane cosmological evolution in a bulk with cosmological constant*, *Phys.Lett.* **B477** (2000) 285–291, [hep-th/9910219].

[373] K. Kajantie, J. Louko, and T. Tahkokallio, *Isotropic AdS/CFT fireball*, *Phys.Rev.* **D78** (2008) 126011, [arXiv:0809.4875].

[374] P. S. Apostolopoulos, G. Siopsis, and N. Tetradis, *Cosmology from an AdS Schwarzschild black hole via holography*, *Phys.Rev.Lett.* **102** (2009) 151301, [arXiv:0809.3505].

[375] R. A. Janik, *Viscous plasma evolution from gravity using AdS/CFT*, *Phys.Rev.Lett.* **98** (2007) 022302, [hep-th/0610144].

[376] K. Kajantie, J. Louko, and T. Tahkokallio, *Casimir energy in the gauge/gravity description of Bjorken flow?*, *Phys.Rev.* **D78** (2008) 126012, [arXiv:0809.5033].

[377] H. Culetu, *Bjorken expansion in the isotropic Kasner spacetime*, *Eur.Phys.J.Plus* **126** (2011) 126, [arXiv:0902.0916].

[378] J. F. Pedraza, *Evolution of nonlocal observables in an expanding boost-invariant plasma*, *Phys.Rev.* **D90** (2014), no. 4 046010, [arXiv:1405.1724].

[379] R. A. Janik, *The Dynamics of Quark-Gluon Plasma and AdS/CFT*, *Lect.Notes Phys.* **828** (2011) 147–181, [arXiv:1003.3291].

[380] N. Lamprou, S. Nonis, and N. Tetradis, *The BTZ black hole with a time-dependent boundary*, *Class.Quant.Grav.* **29** (2012) 025002, [arXiv:1106.1533].

[381] P. Figueras, V. E. Hubeny, M. Rangamani, and S. F. Ross, *Dynamical black holes and expanding plasmas*, *JHEP* **0904** (2009) 137, [arXiv:0902.4696].

[382] N. Tetradis, *The Temperature and entropy of CFT on time-dependent backgrounds*, *JHEP* **1003** (2010) 040, [arXiv:0905.2763].

[383] G. Beuf, M. P. Heller, R. A. Janik, and R. Peschanski, *Boost-invariant early time dynamics from AdS/CFT*, *JHEP* **0910** (2009) 043, [arXiv:0906.4423].

[384] D. Kastor and J. H. Traschen, *Cosmological multi - black hole solutions*, *Phys.Rev.* **D47** (1993) 5370–5375, [hep-th/9212035].

[385] D. Mateos, *String Theory and Quantum Chromodynamics*, *Class.Quant.Grav.* **24** (2007) S713–S740, [arXiv:0709.1523].

[386] B. Mahmoud El-Menoufi, B. Ett, D. Kastor, and J. Traschen, *Gravitational Tension and Thermodynamics of Planar AdS Spacetimes*, *Class.Quant.Grav.* **30** (2013) 155003, [arXiv:1302.6980].

[387] B. M. El-Menoufi, B. Ett, D. Kastor, and J. Traschen, *Sum Rule for the ADM Mass and Tensions in Planar AdS Spacetimes*, *Class.Quant.Grav.* **30** (2013) 205006, [arXiv:1305.1913].

[388] R. C. Myers, *Stress tensors and Casimir energies in the AdS / CFT correspondence*, *Phys.Rev.* **D60** (1999) 046002, [hep-th/9903203].

[389] J. H. Traschen, *A Positivity theorem for gravitational tension in brane space-times*, *Class.Quant.Grav.* **21** (2004) 1343–1350, [hep-th/0308173].

[390] E. Caceres and A. Kundu, *Holographic Thermalization with Chemical Potential*, *JHEP* **1209** (2012) 055, [arXiv:1205.2354].

[391] M. Alishahiha, M. R. M. Mozaffar, and M. R. Tanhayi, *Evolution of Holographic n-partite Information*, arXiv:1406.7677.

[392] S. Carlip, *The (2+1)-Dimensional black hole*, *Class.Quant.Grav.* **12** (1995) 2853–2880, [gr-qc/9506079].

[393] P. F. Byrd and M. D. Friedman, *Handbook of Elliptic Integrals for Engineers and Physicists*. Springer-Verlag, 1954.

[394] C. Schomblond and P. Spindel, *Unicity Conditions of the Scalar Field Propagator Delta(1) (x,y) in de Sitter Universe*, *Annales Poincare Phys.Theor.* **25** (1976) 67–78.

[395] T. Bunch and P. Davies, *Quantum Field Theory in de Sitter Space: Renormalization by Point Splitting*, *Proc.Roy.Soc.Lond.* **A360** (1978) 117–134.